Synthesis of Resveratrol Natural Products and Evaluation of their Antioxidant Properties

by

Matthew Galliher

A dissertation submitted in partial fulfillment
of the requirements for the degree of
Doctor of Philosophy
(Chemistry)
in The University of Michigan
2022

Doctoral Committee:

Professor Corey R. J. Stephenson, Chair
Professor Pavel Nagorny
Professor Nouri Neamati
Professor Corinna S. Schindler

Matthew S. Galliher

mgallihe@umich.edu

ORCiD: 0000-0002-5597-3526

DEDICATION

To Paul, Elizabeth, Amy, Jillian, Michelle and Bryn – for making me the person that I am today

ACKNOWLEDGEMENTS

The training and inspiration that I received from my undergraduate advisor, Professor Clifford Berkman, was paramount in my pursuit of my Ph.D. in chemistry. I was always interested in biology but my undergraduate research helped me to realize that synthetic chemistry was another thing for which I had passion. My experience in the Berkman lab helped me to realize that one does not need to decide do chemistry or biology and that pursuing organic synthetic chemistry presents endless ways in which I could make an impact in the biological field. He ultimately helped me in making my decision to come to University of Michigan for my graduate studies. I thank my dissertation committee members Professors Corinna Schindler, Pavel Nagorny, and Nouri Neamati — you have each been generous with your time and mentorship during my time at the University of Michigan. I would also like to thank the incredble administrative support here at UM — specifically that of Liz Oxford, Katie Foster, Heather Hanosh, and Emma Houle — you have truly made my integration into this department as seamless as possible and have provided me with all of the administrative information that I would need. Finally, I would like to thank the excellent technical support here at UM, including that of Eugenio Alvarado (NMR), Jim Windak, Paul Lennon, and Russell Bornschein (Mass Spectrometry) and Roy Wentz (glass shop).

I have benefited immensely from the good fortune of working with a group of incredibly talented and hard-working individuals throughout my time in the Stephenson lab. I would like to specifically thank Kevin Romero for his steadfast mentorship and friendship, Daryl Staveness for his endless wisdom and constant encouragement, and Haley Albright for her early mentorship and friendship.

I would also like to directly mention other contributors to the project. Mark Raycroft was my mentor while I was at University of Ottawa for the first time conducting the kinetics work for this dissertation. He was not only an effective mentor but a great friend and helped me integrate into the Pratt group. I want to thank Markus Griesser for his important contributions (along with Mark's) to this collaborative work. A special thanks to Mel Mallais for her friendship outside the lab and mentorship within. If it were not for the guidance by Zijun Wu and Omkar Zilka, I would not have been able to successfully execute the cell experiments. Lastly, I want to give a special thanks to Derek Pratt. He was a second advisor to me and helped me along every step of the way with his expertise in radical chemistry and wisdom. His group's expertise in the study of free radical oxidation chemistry has been of tremendous value for helping to re-shape the thinking about the biological role of resveratrol-derived natural products and analogues through their systematic evaluation of the physical and biological properties of these compounds. Their skillful characterization of these systems extends far beyond what we would have been able to accomplish in lieu of their assistance.

A special thanks to Edward McClain, Gabe Magallanes, Taylor Sodano, James Collins, Anthony Allen, Annika Tharp, Cheng Yang, and Alexander Harmata for always being a friend an ear to which to vent and for their camaraderie and to the Schindler group — for always keeping things interesting, with special mention of Mark Becker, Rebecca Watson, Ahlam Armaly, Christopher McAtee, and Lara Alvarez.

TABLE OF CONTENTS

LIST OF FIGURES

LIST OF TABLES

LIST OF ABBREVIATIONS

°C degrees Celsius
δ chemical shift in parts per million
μL microliters
μM micromolar
α-TOH alpha-tocopherol
5-LOX arachidonate 5-lipoxygenase
abs absorbance
Ac acetyl
ACE angiotensin converting enzyme
AChE acetylcholinesterase
AIBN azobisisobutyronitrile
Akt protein kinase B
APPH 2,2'-azobis-(2-amidinopropane)-dihydrochloride
ARE antioxidant response element
ATRA atom transfer radical addition
Aβ amyloid-β
aq. aqueous
Ar aryl
BAD BCL-2-associated death promoter
BAX BCL-2-associated X protein
BCL-2 B-cell lymphoma 2
BCL-XL B-cell lymphoma-extra large
BDE bond dissociation energy
BHT 2,6-di-tert-butyl-4-hydroxytoluene
Bn benzyl
Boc tert-butyloxycarbonyl
Bu n-butyl
bpy 2,2’-bipyridine
bpz 2,2’-bipyrazine
caspase cysteine-dependent aspartate-directed proteases
cm centimeters
COX-1 cyclooxygenase-1
Cp cyclopentadienyl
Cys cysteine
d doublet
DBU 1,8-diazabicyclo[5.4.0]undec-7-ene
dd doublet of doublets
DDQ 2,3-dichloro-5,6-dicyano-1,4-benzoquinone
dF(CF3)ppy 2-(2,4-difluorophenyl)-5-(trifluoromethyl)pyridine
DFT density functional theory

DHB dihydrobenzofuran
DIBAL-H diisobutylaluminum hydride
DISC death-inducing signaling complex
DMF dimethylformamide
DMP Dess-Martin periodinane
DMSO dimethylsulfoxide
DNA deoxyribonucleic acid
DP dirigent protein
DPPH 2,2-diphenyl-1-picrylhydrazyl
dr diastereomeric ratio
dtbbpy 4,4'-di-tert-butyl-2,2'-bipyridine
EC50 half maximal effective concentration
EDG electron-donating group
ee enantiomeric excess
Eoxp standard oxidation potential
EPR electron paramagnetic resonance
eq. equation
equiv molar equivalents
ERK extracellular-signal-regulated kinases
ESI electrospray ionization
Et ethyl
EtOH ethanol
EWG electron-withdrawing group
fac facial
FADD Fas-Associated protein with Death Domain
FTIR Fourier transform infrared spectroscopy
g grams
GPCR G-protein-coupled receptors
GPx glutathione peroxidase
GSH glutathione
GSK GlaxoSmithKline
h hours
H2B-PMHC BODIPY-2,2,5,7,8-pentamethyl-6-hydroxy-chromane
HAT hydrogen atom transfer
HCV hepatitis c virus
HIF-1 hypoxia-inducible factor 1
HMDS hexamethyldisilazide
HO-1 heme oxygenase-1
HPLC high performance liquid chromatography
HRMS high resolution mass spectrometry
HRP horseradish peroxidase
Hz Hertz
IC50 half maximal inhibitory concentration
IFN interferon
IL interleukin
iNOS inducible nitric oxide synthase

IκB	inhibitor of κB
IR	infrared
J	coupling constant in units of Hertz
Keap1	Kelch-like ECH-associated protein 1
L	liters
LFP	laser flash photolysis
LPS	lipopolysaccharide
m	multiplet
M	molar concentration
MAPK	mitogen-activated protein kinases
Me	methyl
MeCN	acetonitrile
MeOAMVN	2,2'-azobis(4-methoxy-2,4-dimethylvaleronitrile)
MeOH	methanol
mg	milligrams
MHz	megahertz
min	minutes
mL	milliliters
MLCT	metal to ligand charge transfer
mm	millimeters
mmol	millimoles
MMP-1	matrix metalloproteinase-1
mol	moles
MRP1	multidrug resistance-associated protein 1
NBS	N-bromosuccinimide
n-BuOH	n-butanol
NF-κB	nuclear factor kappa-light-chain-enhancer of activated B cells
nM	nanomolar
nm	nanometers
NMR	nuclear magnetic resonance
Nrf2	nuclear transcription factor erythroid 2-related factor 2
[O]	oxidant
PARP1	poly(ADP-ribose) polymerase 1
PC	photocatalyst
PET	photoinduced electron transfer
PI3K	phosphatidylinositol 3-kinase
PIDA	[diacetoxyiodo]benzene
PIFA	[bis(trifluoroacetoxy)iodo]benzene
PG	protecting group
PKC	protein kinase C
PMB	para-methoxybenzyl protecting group
PPAR	peroxisome proliferator-activated receptors
ppm	parts per million
ppy	2-phenylpyridine
q	quartet
ROS	reactive oxygen species

RT room temperature
RTA radical trapping antioxidant
s singlet
SAR structure activity relationship
SCE saturated calomel electrode
SPLET sequential proton loss electron transfer
STAT-1 Signal transducer and activator of transcription 1
t triplet
T3SS type III secretion system
TBAF tetra-n-butyl ammonium fluoride
TBS tert-butyl-dimethylsilyl
tBu tert-butyl
THF tetrahydrofuran
TLC thin layer chromatography
TMS trimethylsilyl
Topo II topoisomerase II
tRNA transfer ribonucleic acid
TXN thioredoxin
TYR tyrosinase
TyrRS tyrosyl transfer-RNA (tRNA) synthetase
UV ultraviolet
V volts

ABSTRACT

Numerous reports exist for the biological properties of resveratrol natural products and many clinical trials have been initiated based on promising preliminary evidence that these compounds have promising therapeutic potential. Many of these clinical trials end with inconclusive results and evidence of side effects that may hinder future clinical trials. There is much that is unknown about this class of natural products which underscores the need to develop new methodologies of the synthesis of these compounds in scalable quantities that will fuel future research studies. This dissertation discloses the advancements made for the synthesis of natural products and their analogues as well as the radical trapping antioxidant properties of those synthesized. The syntheses of natural products and analogues will help serve future structure activity relationship (SAR) studies to make unequivocal conclusions regarding the biological properties of resveratrol natural products. Chapter 1 describes the biosynthetic pathway for resveratrol synthesis and the proposed radical-based oligomerization strategy that could produce higher order oligomers. An introduction of radical-based methods in total synthesis as well as the persistent radical effect is provided. The biological properties of resveratrol natural products are also described therein. Chapter 2 describes an electrochemical methodology that was developed for the synthesis of C8 – C8' *bis*-quinone methide dimers and tetramers and C3 – C8' dihydrobenzofuran resveratrol dimers. The results of this methodology created a library of quadrangularin A analogs that were evaluated for the radical trapping antioxidant properties. Chapter 3 presents that the C8 – C8' bis quinone methide dimers were found to be persistent radicals that were able to undergo intermolecular coupling to produce

dihydrobenzofuran motieties found in numerous resveratrol-derived natural products. This synthetic strategy has helped drive the synthesis of resveratrol trimer analogs. Chapter 4 presents the efforts made to evaluate the radical-trapping antioxidant properties of synthesized natural products as well as their synthetic precursors. Through collaboration, these natural products, natural product analogs, and commercially purchased phenols and polyphenols were also evaluated for their radical trapping antioxidant activities. The results from this study are as follows: C8 – C8 bisquinone methide dimers are good antioxidants in organic solutions but fail to inhibit autoxidation in liposomes due to their mechanism of action (via dissociation). The antioxidant potential of phenols is reliant on lipophilicity and substitutions that stabilize the resulting phenoxy radical. The antioxidant potential of resveratrol natural products is also reliant on lipophilicity and alkylated natural product precursors behave as better antioxidants. Surprisingly, analogs containing hindered phenols on substituted dihydrofurans about an unprotected resorcinol have increased radical trapping activities and trap more equivalents than those that lack the sterically encumbering alkylations or have protected resorcinols. Cell studies performed to ascertain the ability of these antioxidants to prevent ferroptosis in cells generated results that were parallel to the liposome studies indicating that the substitutions and structural motifs that permit good activity in liposomes are needed to rescue cells from ferroptosis. Preliminary data shows that hindered phenols can work synergistically with resorcinols in the same way that occurs between vitamin E and vitamin C. These results support that resveratrol antioxidants could work in a similar synergistic manner.

Chapter 1: Resveratrol Oligomer Biosynthetic Pathway, Overview of Radicals, and their Relation to Resveratrol Oligomer Synthesis and Biological Activities

*Portions of this chapter have been published in: Matthew S. Galliher, Bec J. Roldan, and Corey R. J. Stephenson. *Chem. Soc. Rev.* **2021**, *50*, 10044-10057.;[1] Kevin J. Romero, Matthew S. Galliher, Derek A. Pratt, and Corey R. J. Stephenson. *Chem. Soc. Rev.* **2018**, *47*, 7851.[2]

1.1 Introduction

Antioxidant compounds have long retained the interest of the chemical and biological communities for decades as a result of various reports of their antioxidant activities as well as other biological activities. It is believed that this class of compounds are able to treat or prevent oxidative stress-related diseases, such as cardiovascular diseases, cancer, ageing, diabetes mellitus and neurodegenerative diseases. As a result, there is a societal emphasis on including certain foods that contain larger quantities of these small molecules in order to promote longevity and overall human health. Numerous foods and dietary supplements are marketed as being healthy options to include in ones dietary intake.[3] While cells are equipped with a set of endogenous antioxidants (*e.g.* glutathione and coenzyme Q) and antioxidant enzymatic pathways (Nrf2-Keap1) to maintain homeostasis and a relatively reducing environment needed by the cell to perform normal cellular processes, the amount of reactive oxygen species (ROS) (byproducts of cellular metabolic pathways) can inundate the cell and cause undesired oxidation of cellular components and eventually lead to the aforementioned ailments. As such, exogenous antioxidant (*e.g.* vitamin E)

intake is needed which is entirely dietary in nature.[4]

Polyphenolic compounds are abundant in nature and have long been purported to possess antioxidant activities. Specifically, they are believed to act as radical-trapping chemicals that disrupt and inhibit the propagation of radical chain reactions within the cell. Of this class of compounds, resveratrol (**1.1**) and its oligomers have maintained the curiosity of the scientific community. This is in part due to resveratrol having a well-defined biosynthetic pathway, sharing key enzymatic transformations with other phenylpropanoid compounds while the biosynthesis of its congeners remains enigmatic and enzymes responsible for their syntheses remain elusive. Additionally, it was reported that resveratrol and oligomers are found in red wine with high abundance and provided a timely, possible explanation of the "French paradox" – the observation that societies (namely the French) report lower incidences of cardiovascular diseases although they are subjected to higher risk factors as a result of a high-fat diet and other risky lifestyle choices.[5, 6] Similarly, the Mediterranean diet, which is high in polyunsaturated fatty acids, has also been marketed to be preventative for cardiovascular health disease (CHD). However, red wine consumption is also associated with regions sharing this diet. Ultimately, the debate regarding whether red wine consumption offsets the rate of CHD remains contentious as other explanations are offered (*e.g.* better societal healthcare). Regardless, the resveratrol nutraceutical and red wine industries are ever expanding. The resveratrol nutraceutical market was valued at $71.9 million in 2020 and is estimated to be valued at $131.0 million by 2030.[7]

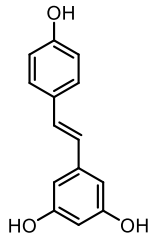

resveratrol (1.1)

Given the worldwide attention of resveratrol, many clinical trials have been conducted with resveratrol supplementation. As of Sept. 2022, there are 191 clinical trials involving the use of resveratrol for various ailments.[8] Although the results from preliminary studies are encouraging,

the results of the clinical trials are inconsistent. These trials investigated the metabolomics and pharmacokinetics of resveratrol. It is recommended for future clinical trials to not exceed dosages >1.0 gram/day of resveratrol. There have been several reports of mild to moderate side effects of taking resveratrol which may limit future studies.[9]

The oligomers of resveratrol have not been subject to *in vivo* testing as resveratrol has despite the *in vitro* data that suggests this expansive collection of congeners possess a myriad of activities to specific protein targets.[10] This is most likely due to the low abundance of these materials in natural sources. The limitation in natural supplies of resveratrol oligomers underscores the need for the development of synthetic routes to meet the demand of these materials in order to interrogate their purported biological activities and subsequently their clinical applications. This dissertation will highlight the numerous synthetic developments towards the syntheses of resveratrol natural products and analogues from the Stephenson group and the collaborative efforts made to remark on the radical-trapping antioxidant activities of these compounds. This chapter will outline what is known regarding the biosynthetic routes of resveratrol and similar classes of molecules, discuss the biological properties of these molecules, introduce the reader to concepts in free-radical chemistry as well as give context for the radical-trapping antioxidant potential of this structurally diverse class of molecules. Later chapters will focus on methods for accessing key bonds in the targeted natural products and the progress that has been made to evaluate these molecules as radical-trapping antioxidants in a pre-clinical setting.

1.2 Resveratrol oligomer biosynthesis

The phenylpropanoid family of molecules stems from the same biosynthetic route, the phenylpropanoid polymalonate pathway, and is responsible for the synthesis of resveratrol in

addition to cinnamic acid, coumarin, and the lignin family of molecules.[11] The starting precursor to all of these natural products is phenylalanine (1.2), a naturally occurring amino acid that is synthesized from the shikimate pathway in plants. This pathway converts phenylalanine to coumaroyl-CoA and following condensation with malonyl-CoA, the common intermediate (1.5),

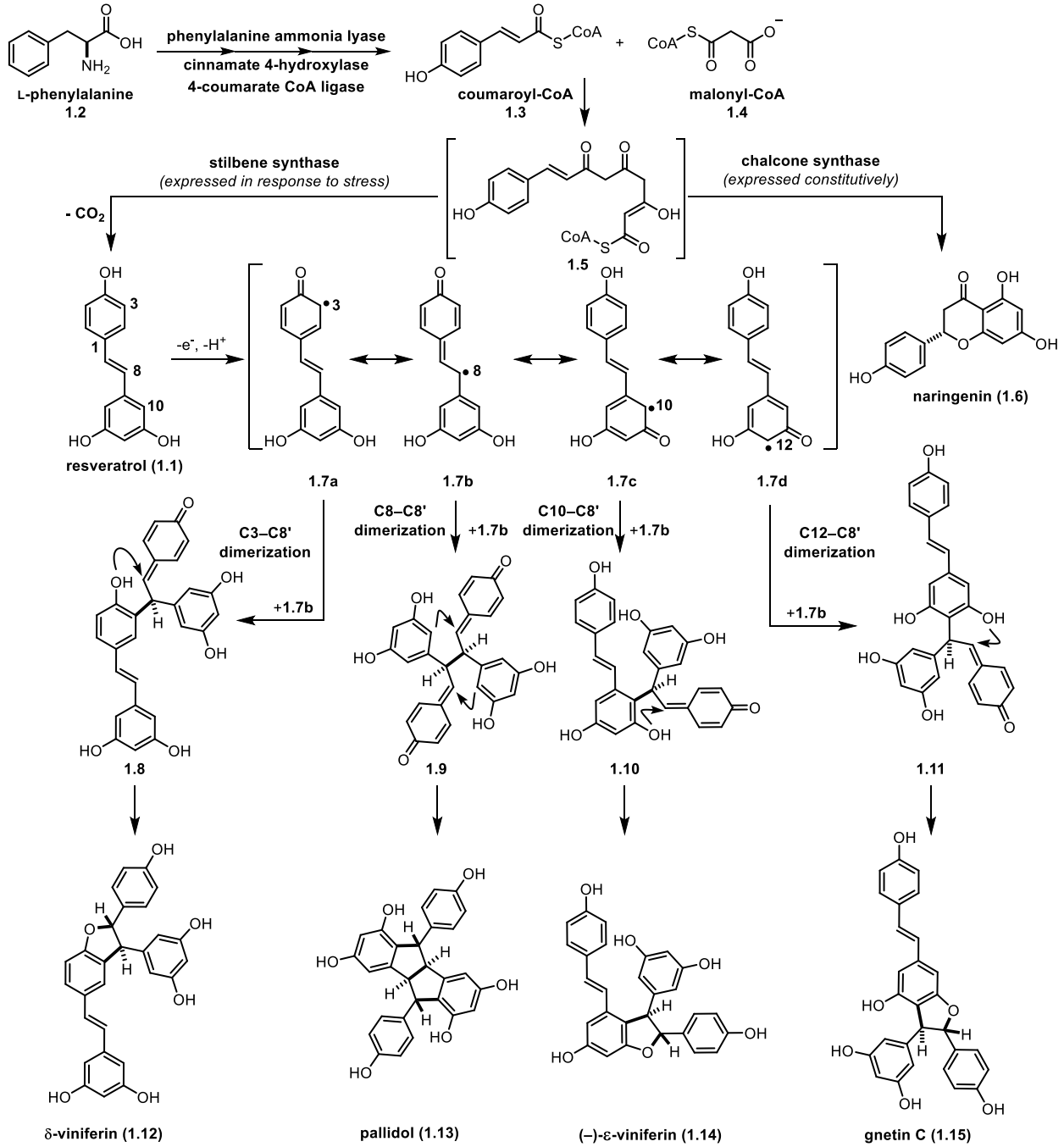

Figure 1.1. The phenylpropanoid polymalonate pathway-dependent synthesis of naringenin, resveratrol and its proposed radical-based oligomeization to form dimers.

a linear tetraketide, is synthesized. In times of normal homeostasis, chalcone synthase is constitutively expressed (type III polyketide synthase) and converts this linear tetraketide to naringenin as well as other flavonoid natural products. When oxidative stress or fungal infection wreak havoc on the plant, stilbene synthase is expressed and diverts linear tetraketide (1.5) to the synthesis of resveratrol.[12, 13] Because of the oxidative stress or UV light needed to activate the expression of stilbene synthase, resveratrol (1.1) was originally proposed to be a phytoalexin, a secondary metabolite made by plants in response to infection or stress. Further work by Langcake and Pryce suggests that resveratrol may rather be a precursor to phytoalexins. It was found to be the major blue fluorescent molecule at the sight of botritsed infection in Vitaceae grapes. Interestingly, resveratrol itself offers no potency to combat the fungal infection, but other oligomers such as α-viniferin (not depicted) and ε-viniferin (**1.9**) were found to be more potent at rescuing the plant (**Figure 1.1**).[14]

Resveratrol is able to undergo numerous transformations and modifications within biological systems. For instance, glycosylation and methylation are common modifications that influence the physical properties of the resveratrol scaffold. The impacts of methylation of resveratrol can enhance its antifungal properties,[15] presumably by enhancing the lipophilicity at the target. Glycosylation of resveratrol can have several impacts effecting how the molecule is stored within or translocated out of the cell. Additionally, glycosylation can affect its ability to undergo enzymatic ocidation.[15, 16] How these oligomers form from the monomeric resveratrol is uncertain as the enzymes that are responsible for their stereo-selective have been elusive to isolation attempts. But the reactivity of the C6-hydroxy group in conjugation with the stilbene is suspected to play a role in oligomerization in biological systems. Due to the electron rich nature of the resveratrol aromatic system and the extended conjugation of the phenol with the rest of the

aromatic system, resveratrol is easily oxidizable (E^{ox}_P = +1.14 V vs SCE in MeCN).[17] Following single electron oxidation and deprotonation, **1.1** reacts to form the phenoxyl radical (**1.7a-d**). This

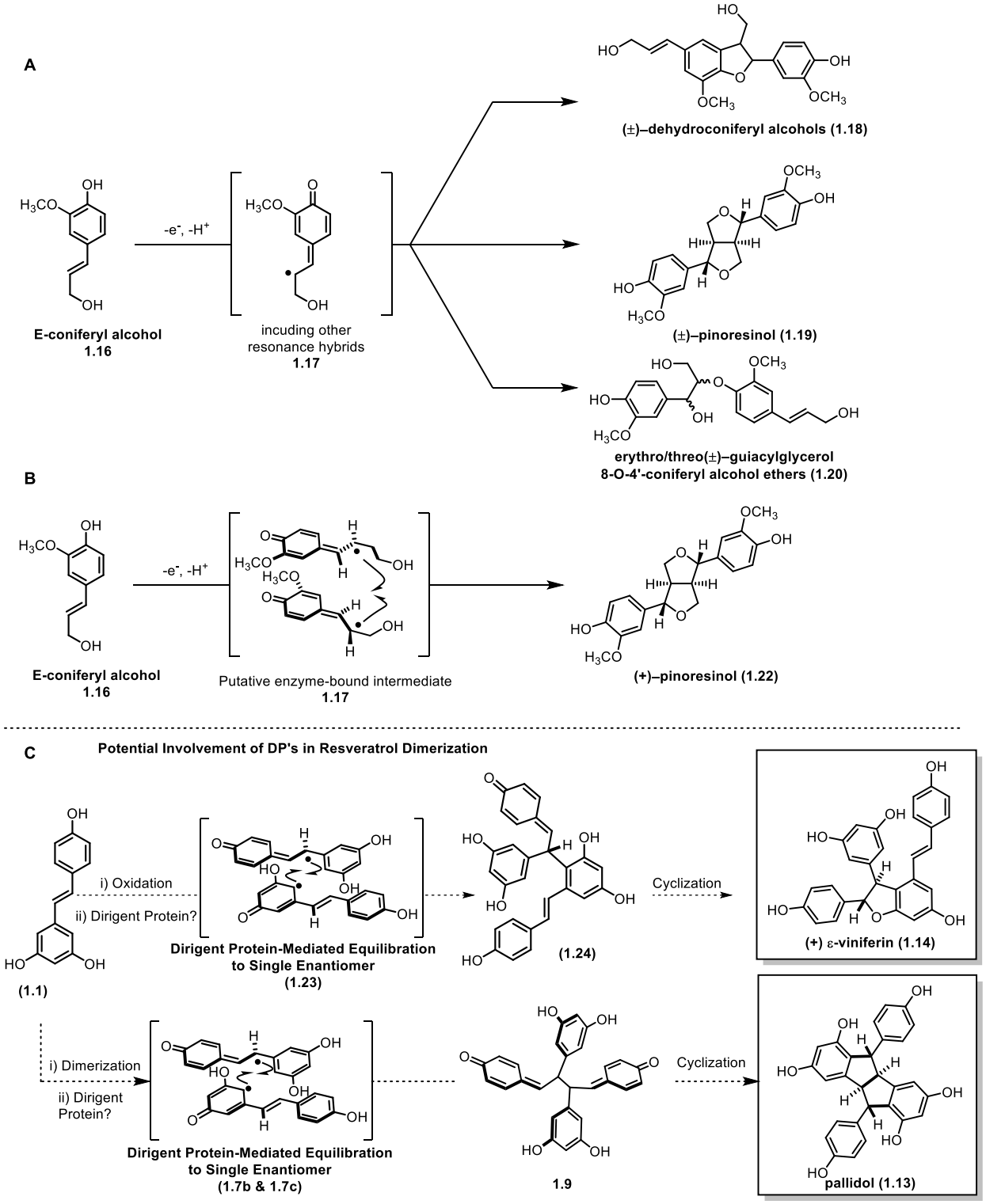

Figure 1.2. Stereo- and regio- control of oxidation of coniferyl alcohol (A) without dirigent protein (B) and with dirigent protein (C) and the potential involvement of dirigent proteins in resveratrol oligomer synthesis.

is possibly facilitated by an oxidase such as laccase or peroxidase within the plant cell or using fungal enzymatic machinery during infection of the plant.[18-26] Radical-radical combination between **1.7a** and **1.7b** furnishes the C3 – C8' dimerized adduct. Radical-radical combination between two equivalents of **1.7b** furnishes the C8 – C8' dimerized adduct. Radical-radical combination between **1.7c** and **1.7b** furnishes the C10 – C8' dimerized adduct. Lastly, radical-radical combination between **1.7d** and **1.7b** furnishes the C12 – C8' dimerized adduct. Each of these dimer intermediates (**1.8**-**1.11**) contain an electrophilic quinone methide that easily undergoes Friedel-Crafts cyclization by the electron rich aromatic system forming an additional new C – C bonds in the product (**1.13**) or cyclization by the phenol results in additional C – O bonds forming dihydrobenzofurans moieties (**1.12**, **1.14**, **1.15**). The presence of ROS within the cell can increase the local concentrations of these reactive phenoxyl radicals as they oxidize resveratrol which would allow for dimerization in the absence of an oxidizing enzyme.[27]

While random dimerization of resveratrol within the cell is possible, it does not account for the specific regio- and stereo- configurations found within the dimers as racemic mixtures of isomers result when performed *in vitro*. This suggests that small molecule-aiding chaperone-like proteins may be present within the cellular environment to dictate the regiochemical and stereochemical outcomes in the product. The lignan class of natural products have been found to be synthesized by similar single electron oxidation reactions with the regio- and stereo- control of the reaction being facilitated by dirigent proteins. In 1997, the Lewis group isolated lignan dirigent

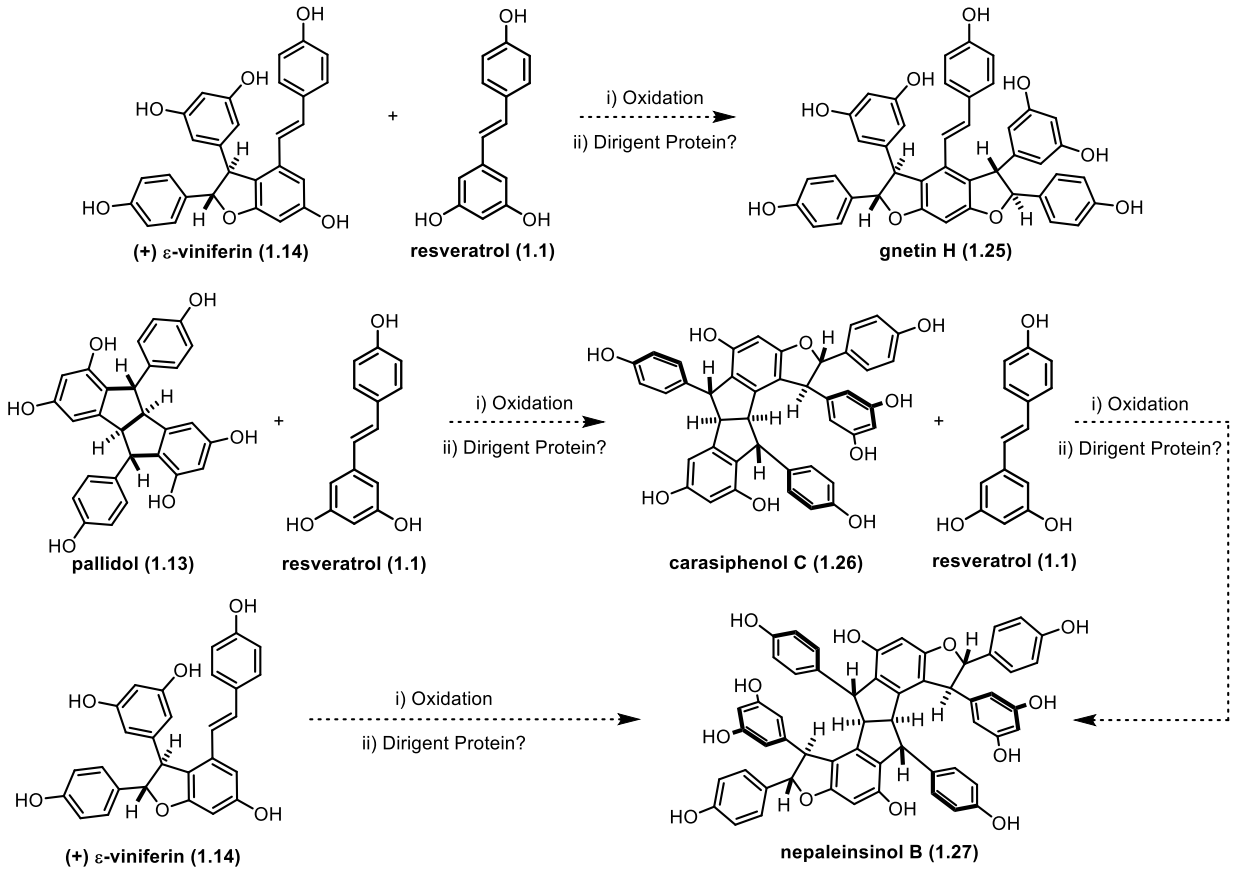

Figure 1.3. Proposed radical-based oligomerization for the synthesis of higher order oligmers. (Top) Trimerization be radical monomer-dimer combination, (Middle) Sequential monomer addition to dimers for tetramer synthesis, (Bottom) homodimerization of dimer to form tetramers.

protein. When performing the oxidative coupling of coniferyl alcohol (1.16) a racemic mixture of regioisomers was formed (1.18, 1.19, 1.20). Following the isolation of dirigent protein and subsequently using it in the oxidation coniferyl alcohol, the stero- and regio-specific oxidative coupling formed (+)-pinoresinol (1.22) (**Figure 1.2**).[28] This dirigent protein was later characterized to reveal the enzyme exists as a trimer possessing two binding sites that are spatially separated for monomer binding thus allowing for the facial and regio-selectivity in coupling.[29] Given the similarities in the hydroxystilbene core and that both natural product families stem from the same biosynthetic pathway, it is reasonable to speculate that an analogous class of enzymes exist to control the radical dimerization coupling with specific stereoselectivity.

The synthesis of the higher order oligomers of resveratrol are believed to occur through a similar radical mechanism in which the monomer phenoxyl radical combines with a dimer-derived radical to form trimers and tetramers from two subsequent additions of radical monomer or combination of two radical dimers (**Figure 1.3**).[10] Again, this is likely due to the propensity of phenols to oxidize to the phenoxyl radical with possible regioselectivity guided by dirigent proteins. The following section will provide a general overview of the physical characteristics of radicals and their application to complex molecule synthesis.

1.3 Overview of radicals and their application in total Synthesis

The existence of carbon-centered radicals has been known for 120 years, but it was not until the latter half of the 20th century that their potential as intermediates in complex molecule synthesis was realized.[30] In the last several decades, the use of radical methodologies has surged and radical intermediates are now an integral part of many synthetic pathways towards complex natural products. The analytical and synthetic methods used to characterize, generate, and utilize radicals in organic synthesis have evolved since the discovery of the triphenylmethyl radical by Moses Gomberg in 1900 at the University of Michigan.[30] This discovery, which was made while attempting to prepare the

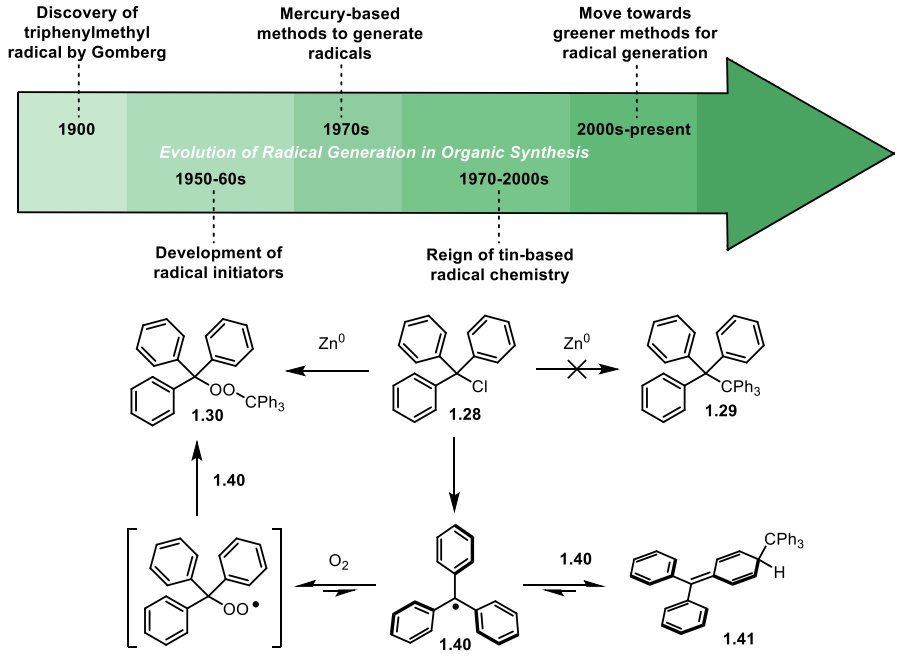

Figure 1.4. History of carbon-cenetered radicals beginning from Gomberg's discovery of the tripheny lmethyl radical.

compound hexaphenylethane by the Zn-mediated Wurtz coupling of triphenylmethyl chloride **1.28**, paved the way for the new field of radical chemistry (**Figure 1.4**).

radical	k_r ($M^{-1}s^{-1}$)	$t_{1/2}$ (s)[a]	RSE (kcal/mol)
1.42	1.1×10^{10}	9.1×10^{-6}	0.0
1.43	8.5×10^{9}	1.2×10^{-5}	17
1.44	2.3×10^{9}	4.3×10^{-5}	15
1.45	8.1×10^{9}	1.2×10^{-5}	9
1.46	2.5×10^{8}	4.0×10^{-4}	17[b]
1.47	2.0×10^{2}	5.0×10^{2}	9[b]
1.48	n/a	days	11[b]
1.49	6.9×10^{7}	1.5×10^{-3}	25[c]

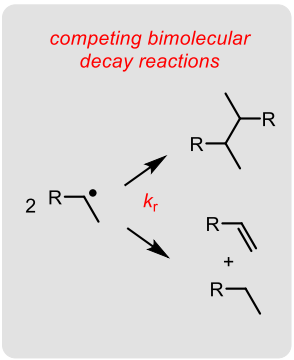

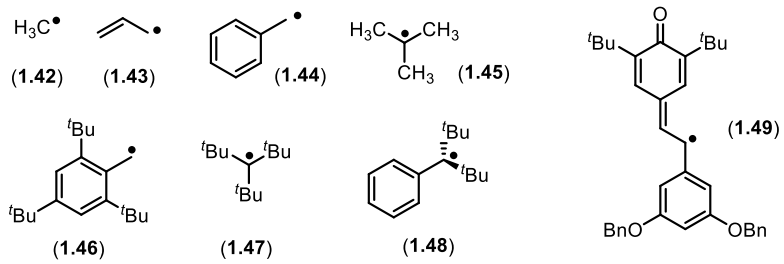

Figure 1.5. Selected kinetic and thermodynamic parameters of some C-centred radicals. a. Lifetimes are based upon a radical concentration of 10-5 M. b. Calculated using CBS-QB3.9 c. This RSE is derived from the BDE of the phenolic tautomer that gives rise to **1.49**.

Griller and Ingold proposed that the adjective persistent be used "to describe a radical that has a lifetime significantly greater than methyl under the same conditions." In contrast, methyl and other short-lived radicals are described as transient. These definitions are based upon the kinetics with which the radicals decay when generated in dilute solutions, which are characterized by the recombination rate constant k_r (this despite the fact that radical recombination[‡] is often competitive with disproportionation). Illustrative kinetic parameters of selected carbon-centered radicals are given in **Figure 1.5**.

Griller and Ingold also suggested "that 'stabilized' should be used to describe a carbon-centered radical, R•, when the R–H bond strength is less than the appropriate C–H bond strength in an alkane".[31] The difference of the C-H BDE of a given hydrocarbon from methane is often used as a measure of the so-called 'radical stabilization energy (RSE)' afforded by the substituent(s) attached to the central carbon atom, so these are also included in Figure 1. Although radical stability and persistence are often used interchangeably, it is evident from the data collected in Figure 1 that they should not. For example, while introduction of a vinyl or phenyl substituent

on methyl significantly increases its stability, its lifetime in solution is essentially unchanged.[32, 33] However, introduction of substituents that hinder dimerization and/or disproportionation of the radicals increase their persistence – even if they do not increase the stability of the radical.[3] In fact, substitutions that increase persistence often decrease the stability of the radical by localizing the electron spin (e.g. **1.48**).[34, 35]

Another consideration in evaluating the persistence of a radical (which is not included in Ingold and Griller's definition) is the reversibility of the radical (re)combination reaction. A radical with a relatively short lifetime in solution can be highly persistent if the reaction that limits its lifetime is readily reversible.

The triphenylmethyl radical **1.40** provides a good starting point to introduce the concepts of radical stability and radical persistence, which were first clearly delineated by Griller and Ingold.[31] The triphenylmethyl radical is relatively stable; the C-H bond strength in triphenylmethane (81 kcal/mol) is significantly lower than that in methane (105 kcal/mol), reflecting the stabilizing interactions between the unpaired electron on the central carbon atom and the π orbitals of the three attached phenyl rings which serve to delocalize it.[36, 37] The triphenylmethyl radical can also be persistent; in the absence of O_2, it makes up roughly 0.01% of a sample of **1.41**. However, in the presence of O_2, the triphenylmethyl radical is not persistent. Since persistence is a kinetic characteristic, it depends on reaction conditions. Stability, which is a thermodynamic characteristic, is inherent to the electronic structure of the radical.

Of the persistent radicals utilized in organic chemistry, (2,2,6,6-tetramethylpiperidin-1-oxyl), or TEMPO (not depicted), is most prevalent. TEMPO is a stable radical that exists as a red-orange solid at room temperature. It was first prepared by Lebedev and Kazarnowskii in 1960 by oxidizing

2,2,6,6-tetramethylpiperidine with hydrogen peroxide.[38] The stability of TEMPO can be attributed largely to resonance, while its persistence, largely to sterics. The stability is evident upon consideration of the O-H BDE of the corresponding hydroxylamine, which has been reported to be 69 kcal/mol – approx. 35 kcal/mol lower than a typical O–H bond.[37, 39] The four methyl groups flanking the aminoxyl radical prevent dimerization, and the lack of adjacent C-H bonds prevents disproportionation to nitrone and hydroxylamine.

The selectivity observed in many of the reactions which utilize TEMPO is governed by the persistent radical effect (PRE). Fischer and Ingold were among the first to observe and characterize this intriguing phenomenon in which systems containing both persistent and transient radicals afforded remarkably selective product distributions.[40] There are two main criteria necessary for the persistent radical effect to be operative: a) of the radical intermediates formed in a given reaction, one is more persistent than the other(s), meaning it has a significantly slower termination rate, and b) the radical intermediates are generated in effectively equivalent rates. When such

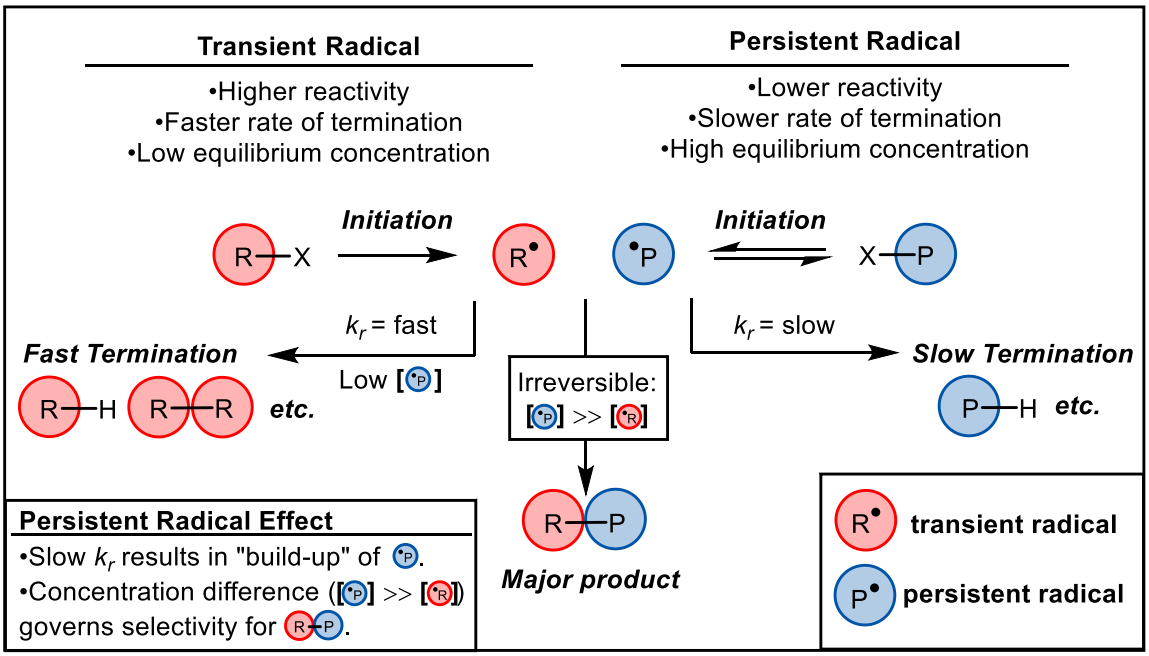

Figure 1.6. Generic depiction of the persistent radical effect.

criteria are met, the initial rapid termination of transient radicals in solution results in a system in which the persistent radical has a significantly larger concentration than any transient radical. Such

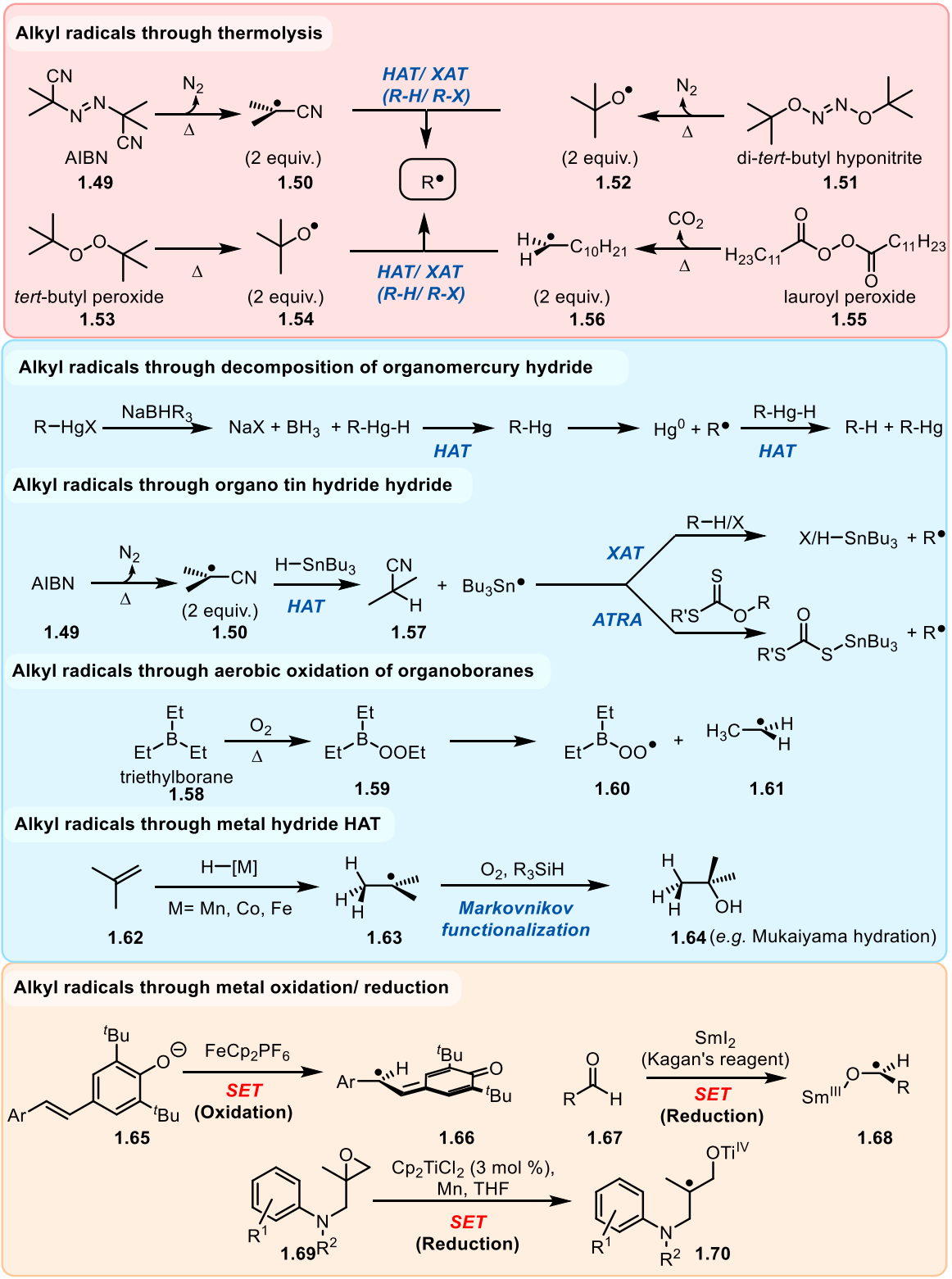

Figure 1.7. Common "classical" techniques for the generation of radical intermediates.

an excess of the persistent radical serves to drive the reaction forward in a selective fashion.[41] Figure 2 provides a generic example of this scenario. A radical initiation event creates a system in which both the transient radical R$^{\bullet}$ (red) and the persistent radical P$^{\bullet}$ (blue) are present in solution. R$^{\bullet}$ rapidly undergoes termination events, therefore its concentration in solution remains relatively low. On the contrary, P$^{\bullet}$ maintains a relatively high concentration in solution due to its persistence, thereby resulting in a system in which [P$^{\bullet}$]>>[R$^{\bullet}$]. This "buildup" in [P$^{\bullet}$] increases the favorability of coupling to R$^{\bullet}$, and the irreversible formation of the R–P heterocoupled product ultimately drives the reaction. In other words, the persistent radical effect favors the formation of R–P due to the persistence of P$^{\bullet}$ in solution. The following section will highlight how TEMPO has been utilized to leverage the PRE for the synthesis of natural products (**Figure 1.6**).

An appreciation for the relationship between radical structure and persistence is vital to the successful use of radical-based transformations in complex molecule synthesis. Persistent radicals, which by definition have higher barriers to reaction, are generally more selective in the reactions they undergo, whereas transient radicals, which by definition have lower barriers to reaction, generally prove to be less selective. As such, careful selection of reaction conditions becomes all the more important in the use of transient radicals in synthesis as compared to persistent radicals.

Radical chain reactions, which include initiation, propagation, and termination steps, offer a way in which to utilize promiscuous radicals in complexity-building reactions in a selective manner (**Figure 1.8**).[42, 43] The initiation stage often uses radical initiators (*i.e*. metals, one electron oxidants/ reductants, photolabile initiators, etc). Dialkylazo compounds (**1.49**), dialkylhyponitrites (**1.51**), and peroxides (**1.53, 1.55**) are classes of molecules that are commonly used to thermally initiate radical processes via homolysis and loss of N_2 or CO_2 (**Figure 1.7,** top).[44] Azobisisobutylnitrile (AIBN, **1.49**) is one of the most common and well-studied aza-based radical

initiators. Once the radical is generated, a variety of propagation steps can occur including: radical-radical couplings, β-eliminations, inter- and intramolecular C–C bond formations, and more. Radical chain reactions can be terminated in a number of ways including reduction, fragmentation, or a reaction of the final radical with the initial radical precursor.[45]

The evolution of the use of radicals in the synthesis of complex molecules can be characterized into several phases. The first began in the late 1970's with Bernd Giese's development of the mercury hydride method to generate radicals for the coupling of organomercurials and olefins. This was the first form of the reaction we know today as the Giese reaction.[46] The reductive demercuration conditions responsible for the generation of carbon-centered radicals have been known for some time, but this method was employed almost exclusively to reduce the radical to the alkane. The Giese reaction differs in that it forms C–C bonds intermolecularly.[47] These conditions were greatly surpassed in popularity by the use of tin hydride in the presence of an

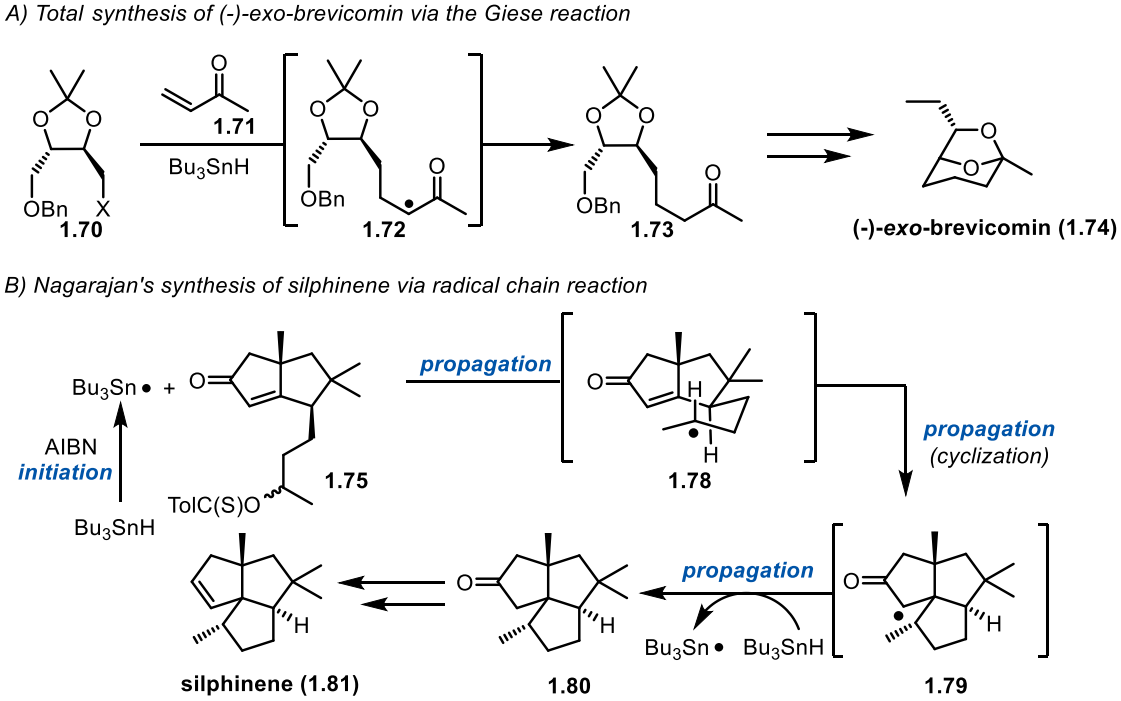

Figure 1.8. A) Giese's synthesis of (-)-*exo*-brevicomin (**1.74**); B) Nagarajan's synthesis of silphinene (**1.81**)

initiator. This could be attributed to the benefits in reactivity that tin hydride offers and perhaps due to these conditions being less toxic than organomercury salts. The use of tin hydride in current Giese reactions is still encountered in modern total synthesis. This reaction was utilized by Giese and co-workers in the total synthesis of (–)-*exo*-brevicomin (**1.74**, **Figure 1.8A**).[42] Another early example of the use of radical chain reactions in total synthesis is Nagarajan's synthesis of silphinene (**1.81**), which relies on the use of tin hydride and AIBN as the radical initiator, followed by an intermolecular cyclization as the propagation step (**Figure 1.8B**).[43] Concurrently, metal hydrides as MH HAT (metal-hydride hydrogen atom transfer) reagents for the Markovnikov radical functionalization of olefins were being developed. Other developments included using samarium diiodide (SmI_2) for the generation of radicals from carbonyl reduction were also being made at the time. Both of these methods remain steadfast in total synthesis.[48, 49]

Over time, synthetic chemistry has witnessed a shift in attitude regarding the means of radical initiation. Since the development of the principles of green chemistry, chemists have looked to incorporate these tenets into new and long-established methods. The principles of green chemistry advocate for limiting the use of toxic or hazardous reagents as well as minimize the generation of waste products due to bulk solvent use and poor atom economy.[50] Although less toxic than mercury, organotin reagents have an associated toxicity to humans and aquatic life that has driven the field to find alternative techniques for radical genesis.[51] Organotin byproducts are sometimes challenging to remove by chromatography as they coelute with desired products. This has necessitated the development of chromatography techniques that utilize alternative stationary phases.[51] Generally, these "classical" means of radical genesis require either stoichiometric metal reagents or stoichiometric reductants and oxidants to regenerate reactive metal species at substoichiometric loadings.

The development of milder methods for radical generation over the last 15 years, taking the form of electrochemical and photoredox catalysis approaches, has fueled a resurgence of interest in radical chemistry. These new radical strategies have been applied to total synthesis. Electrochemistry has historically been used for bulk chemical production.[52] Improvements to chemoselectivity have permitted the use of electrochemistry in the synthesis of complex molecules, where chemoselectivity is often a challenge. Additionally, electrodes act as both a source and sink of electrons in an electrochemical reaction which circumvents the need for stoichiometric quantities of reagents. Similarly, developments and improvements to photoredox catalysis has allowed its use in total synthesis. When applied to net-redox neutral transformations, stoichiometric reductants and oxidants can be avoided. Both of these fields offer new ways to generate radicals in simpler, milder, and greener ways that differ from the classical methods mentioned above. To provide context for the development of these greener methods, this review highlights the application of "classical" radical methodologies in modern total synthesis. Then this review will highlight the use of greener electrochemical and photoredox-mediated catalytic strategies for generating radical intermediates in total synthesis.

1.3.1. Classical methods for radical synthesis

Some of the earliest examples of radical reactions have been performed with organomercurials, a class of stable compounds known since 1852.[53] Organomercurials (R-HgX) can be decomposed to the alkyl radical in several ways (reductive demercuration, halogen cleavage, etc). Most common to organic synthesis is the treatment of the organomercurial salt with a reducing agent such as a borohydride. The hydride performs ligand substitutions yielding the mercuric hydride (R–HgH) intermediate. Mercuric hydrides contain an extremely labile Hg–H bond (BDE= 9.5 kcal/mol) and decompose readily to the carbon-centered radical (R•) forming

mercury metal as a stoichiometric byproduct (**Figure 1.7**, middle).[54] Though challenging, the resulting alkyl radical can undergo intermolecular chemistry. However, the rate of HAT termination via mercuric hydride is fast and often unavoidable making the mercury hydride method for radical generation less ideal for intermolecular chemistry. Due to this shortcoming of poor chemoselectivity coupled with the associated toxicities of these intermediates and the generated waste, mercury has been largely replaced by tin.

The use of tin hydrides (especially Bu_3SnH) in radical transformations have been used for several decades and continues to persist despite the push to find greener alternatives.[55] In addition to being "safer" than mercury, tin hydrides are especially advantageous due to the breadth of reactivity they offer in comparison to mercury (**Figure 1.7**, middle).[56] Due to the stability and longevity of the tin-centered radical generated following initiation via HAT (Sn–H BDE= 64 kcal/mol) from an initiator, they are used to propagate radical chain reactions.[55] Propagation can occur when $Bu_3Sn\bullet$ performs HAT or XAT (halogen atom transfer) on labile C–H or C–X bonds, or when performing atom transfer radical additions (ATRA) that form carbon-centered radicals that can then undergo intra- or intermolecular reactions. Due to the affinity of tin towards sulfur and forming Sn–S bonds, thiocarbonyl-containing functional groups such as a xanthates have been employed with tin hydrides to serve as carbon-centered radical precursors (**Figure 1.7**, middle).[57] In this process, the addition of tin radical to sulfur triggers a fragmentation event resulting in the carbon centered radical. This process is central for the mechanisms of the Barton-McCombie deoxygenation and Barton decarboxylation reactions.[58] Organosilanes (*e.g.* tris(trimethylsilyl)silane) have become an invaluable tool for mediating radical processes as they can act as H-atom sources.

Organoboranes are a class of molecules used frequently as initiators upon reaction with oxygen (**Figure 1.7**, middle).[59] Though this chemistry has been known for over 150 years, it was not until the late 1960's that intensive mechanistic studies were performed and concluded the involvement of radical intermediates. Triethyl borane (**1.58**) is most commonly used. Initial reaction between triethyl borane and oxygen yields the autooxidation product, a peroxyboronate ester (**1.59**) which can decompose to the peroxy radical (**1.60**) and alkyl radical (**1.61**) species. This method of initiation is useful as it permits radical generation at low temperatures. However, as the presence of oxygen is required, chain processes become less efficient due to autooxidaiton of radical intermediates.

Techniques involving metal hydrides in radical processes have evolved such that transition metals (*e.g.,* Fe, Co, and Mn) can be used in catalytic systems requiring substoichiometric quantities of metal and stoichiometric quantities of reductant (typically organosilanes).[60] These developments have greatly reduced metal waste that is typically generated, although waste associated with the stoichiometric reductants and oxidants is challenging to avoid. In these systems, olefins (**1.62**) undergo MH HAT which results in a carbon-centered radical intermediate (**1.63**) that then undergoes reaction with a radical acceptor or termination by HAT or oxygen (Mukaiyama hydration) (**Figure 1.7**, middle).

Metals can generate radical intermediates simply by performing single-electron redox processes (Figure 3, bottom).[61, 62] Ferrocenium, Mn(III), and Ce(IV) reagents have been useful as single electron oxidants.[63, 64] Samarium diiodide (SmI_2) is frequently used as a stoichiometric reductant to generate carbon-centered radicals by single-electron reduction of ketone and aldehyde carbonyls (**1.67**, **Figure 1.7**, bottom).[65] Ti^{III} reagents are able to reductively open epoxides (**1.69**, via inner sphere SET) to give the more substituted carbon-centered radicals (**1.70**).[66, 67]

1.3.2. Electrochemistry in radical synthesis

Although the field of electrochemistry has been well-established since the late 18th century, its synthetic use was largely grounded in the process-scale generation of bulk chemicals rather than the synthesis of fine chemicals and complex molecules.[52] In recent decades, there has been a shift in interest toward the use of electrochemistry for total synthesis. Due to the number of parameters

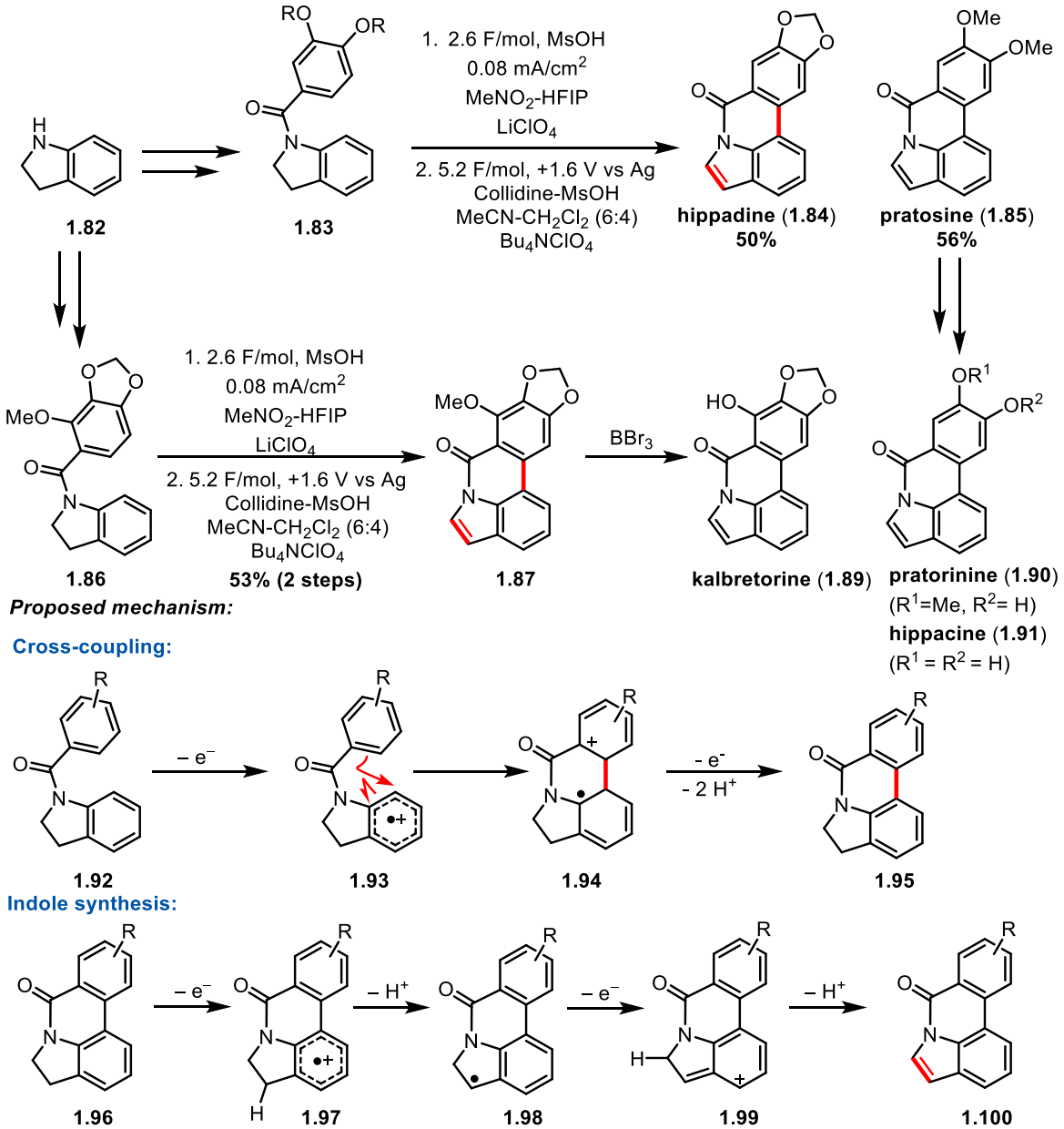

Figure 1.9. Chiba's 2020 electrochemical total synthesis of pyrrolophenanthridone natural products via $C(sp^2)$–$C(sp^2)$ cross coupling and indoline oxidation.

that can be adjusted (applied potential, electrode composite, electrolyte, divided vs. undivided cells, etc), desired chemoselectivity can be fine-tuned, making electrochemistry well-suited for complex molecule synthesis. Electrochemistry is particularly advantageous for single-electron processes that generate radical intermediates. Kärkäs and co-workers have published a recent review on advances in electrochemistry in organic synthesis.[68]

Electrochemical strategies for radical transformations can be performed under oxidizing or reducing conditions. Further control can be instilled by performing reactions with constant potential or a constant current. Performing an electrochemical reaction with a constant potential imparts greater chemoselectivity whereas doing so with a constant current imparts operational simplicity.[69] Electron transfers are typically achieved at the double layer, the characterized stacking of charged molecules that forms around the electrode due to Coulombic interactions.[70] These electron exchanges can occur between the electrode and substrate. In some instances, electrochemistry can be used to generate an active oxidant or reductant *in situ* that performs the electron transfer to or from the substrate. In these instances, regeneration of the active redox reagent is permitted without the need for exogenous, stoichiometric oxidants and reductants.[69]

An example of electrochemistry in radical-mediated total synthesis is the 2020 total synthesis of pyrrolophenanthridone alkaloids by the Chiba group which demonstrates the utility of electrochemistry to generate radical intermediates in order to accomplish an intramolecular C(sp^2)–C(sp^2) cross-coupling and indoline oxidations (**Figure 1.9**).[71] In this method, the indoline **1.92** is first oxidized to the arene radical cation **1.93**. Subsequent coupling of the neighboring arene to the radical cation forms tertiary radical **1.94**. Subsequent re-aromatization and oxidation delivers coupled indoline (**1.95**). The authors suggest that HFIP is critical to increase the electrophilicity of radical cation **1.93** in the presence of ClO_4^- electrolyte. Following the synthesis of cross-coupled

indoline **1.95**, constant current oxidation is utilized to oxidize the indoline to the indole (**1.100**). In this step, the indoline is oxidized to the radical cation **1.97**. Deprotonation of **1.97** generates benzylic radical intermediate **1.98** which then undergoes a subsequent anodic oxidation to form cation **1.99**. This is ultimately deprotonated by collidine to give the indole product **1.100**. Several pyrrolophenanthridone natural products (**1.89-1.91**) were accessed from the coupled products following protecting group manipulation.

1.3.3. Generation of radicals by photoredox catalysis

Photoredox catalysis has had widespread use in the chemistry field over the last decade, it has only been recently applied to generating radical intermediates for natural product synthesis. Photoredox catalysts can take several forms including ligand-bound metal complexes or organic molecules which can permit redox chemistry using visible light. Using these catalysts provides a milder alternative to high energy UV light utilized in photochemistry of the previous century.[72] Once excited with visible light, catalysts are able to perform single-electron transfer (SET) oxidation and/or reduction processes.[73] There have been more comprehensive reviews on advances in photoredox-based methodology and applications in organic synthesis than what is covered in this review.[72, 74] Photoredox catalysis has the ability to generate radicals for reductive couplings, photocycloadditions, intermolecular C—H functionalization reactions, and more. This provides multiple avenues to access natural product cores through complexity-building reactions. Net-neutral redox catalytic cycles offer a "green" means to generate reactive radical intermediates for total synthesis applications while reducing the generation of excess waste. Net-neutral redox cycles circumvent the need to handle toxic reagents as substoichiometric loadings of catalyst is achievable without relying on exogenous stoichiometric oxidants or reductants to regenerate the reactive oxidation state of the catalyst.

A noteworthy example of photoredox catalysis replacing stoichiometric metal oxidants in total synthesis is the synthetic endeavors made for the synthesis of Catharanthine (**1.101**). **1.101** is a polycyclic natural product that has been utilized as a starting point for several semisynthetic efforts to access a variety of structurally related alkaloid natural products. It contains an indole and an isoquinuclidine ring, and these fragments are connected by the seven-membered C ring. Catharanthine is easily accessed from cell

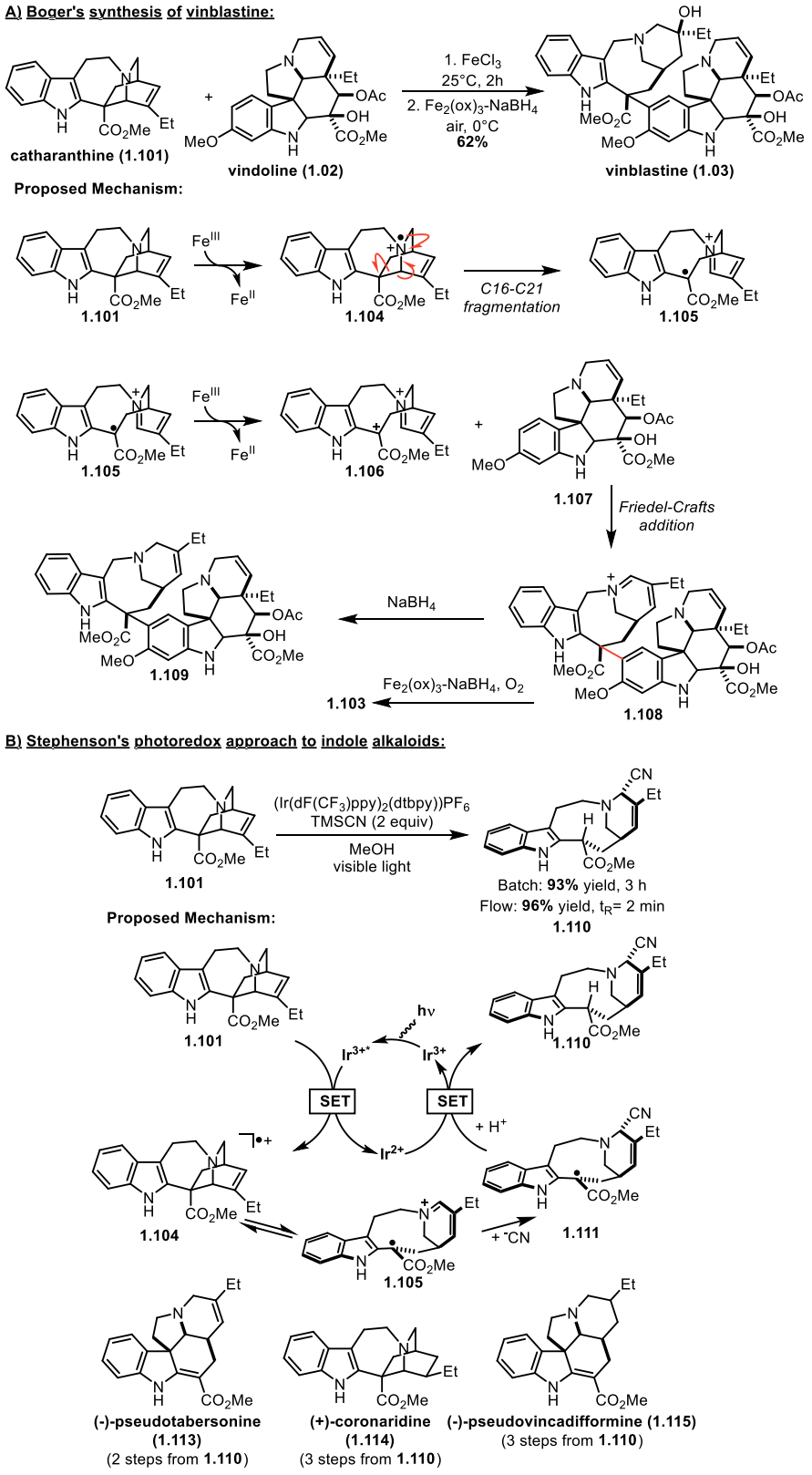

Figure 1.10. Approaches leveraging the fragmentation of catharanthine (**1.101**) to access indole alkaloid natural products.

cultures in synthetically useful quantities; thus, its abundance and resulting commercial availability has fuelled multiple semisynthetic efforts. The utility of **1.101** as a synthetic precursor for related alkaloids is enabled by the ease with which the C16-C21 bond undergoes oxidative fragmentation to the benzylic radical intermediate **1.105** (**Figure 1.10**).

The Boger group published a remarkable total synthesis of vinblastine (**1.103**) in 2008 in which the key step involved the coupling of catharanthine (**1.101**) and vindoline (**1.102**) via the radical-induced fragmentation of **1.101** (**Figure 1.10A**).[75] Vinblastine (**1.103**) is a potent inhibitor of microtubule formation and mitosis and is a key anticancer drug target. In Boger's synthesis of vinblastine, catharanthine (**1.101**) is treated with $FeCl_3$ to form the amine radical cation **1.104**. This intermediate presumably undergoes rapid C16–C21 fragmentation, affording benzyl radical **1.105**. Subsequent oxidation of **1.105** gives intermediate **1.106**, which acts as the electrophile in a Friedel-Crafts coupling reaction with vindoline (**1.102**) to give **1.108**. This fragmentation and coupling sequence to was originally developed by Kutney and co-workers in 1988 to access 3'-4'-anhydrovinblastine (**1.109**), which was obtained by reduction of **1.108** with $NaBH_4$.[76] Boger and co-workers instead leveraged conditions ($Fe_2(ox)_3$-$NaBH_4/O_2$) that enabled reduction of the iminium and stereoselective oxidation of the C15'–C20' double bond in a single pot. This decisive step affords the C20' tertiary alcohol of vinblastine (**1.103**) in 43% yield under optimized conditions.

While Boger demonstrated that alkaloid natural products can be accessed through the $FeCl_3$-mediated single electron oxidation and fragmentation of catharanthine, we were able to show this can also be accomplished with photoredox catalysis. In 2014, we reported the syntheses of (-)-pseudotabersonine (**1.113**), (+)-coronaridine (**1.114**), and (-)-pseudovincadifformine (**1.115**) (**Figure 1.10B**).[77] The key step to the syntheses of **1.113-1.115** involved the formation of a

common intermediate (**1.110**) by the photoredox-mediated fragmentation of catharanthine (**1.101**). Excitation of the photocatalyst and reductive quench with **1.101** yields amine radical cation **1.104**. Fragmentation of the C16–C21 bond occurs in the same way as discussed in Boger's synthesis of vinblastine, generating the stabilized benzyl radical **1.105**. This stabilized radical survives the addition of cyanide to the iminium group before being ultimately reduced by the photocatalyst and subsequently protonated to give **1.110**. This transformation was achieved via batch reaction (93% yield) as well as by utilizing flow chemistry (96% yield), demonstrating the versatility of photoredox catalysis for natural product synthesis. From **1.110**, the desired natural products (**1.113-1.115**) were synthesized in 1 or 2 additional steps.

1.4 Biological activities of resveratrol natural products

The resveratrol class of natural products has an abundance of potential biological activities that compliments this natural product family's structural diversity.[10] Despite the numerous aromatic motifs within these molecules, they are anything but flat which is a characteristic of many important drugs. [78] The lack of planarity is a due to the C – C coupling modes discussed earlier in which these bridging points are often sp^3 hybridized, imparting them with three-dimensional architecture. The increase in saturation opens up more modes of selective binding with protein target of interest.[78]

For example, resveratrol itself has been shown to be a sirtuin activating compound in several cell model systems. This is significant because sirtuins are a class of deacetylases that have been proposed to be activated in times of caloric restriction which can extend longevity. ε-viniferin and α-viniferin are potential cytotoxic agents to numerous cancer cell lines of varying tissue types. Nepalensinol B, a resveratrol tetramer (discussed in Chapters 2 & 3), has been shown to be a topoisomerase type II inhibitor (IC_{50} = 11 nM) making it a potential target as an anticancer drug.

Vitisin B, another resveratrol tetramer (mentioned in chapter 3), has been shown to have potent activity against NS3 helicase (IC_{50} = 3nM) which makes it a valuable target for combating hepatitis C. Of all the alleged biological properties that the resveratrol class of compounds has to offer, the scientific community is often fixated on their potential antioxidant activities, which is a hallmark of their polyphenol nature. This specific biological activity will be the focus for the duration of this dissertation.[10]

1.5 Autoxidation and radical trapping antioxidant properties of resveratrol and polyphenols

Hydrocarbon autoxidation is the oxidative breakdown of organic materials. It is a chemical reaction in which molecular oxygen formally is inserted within a C – H bond. In the scope of

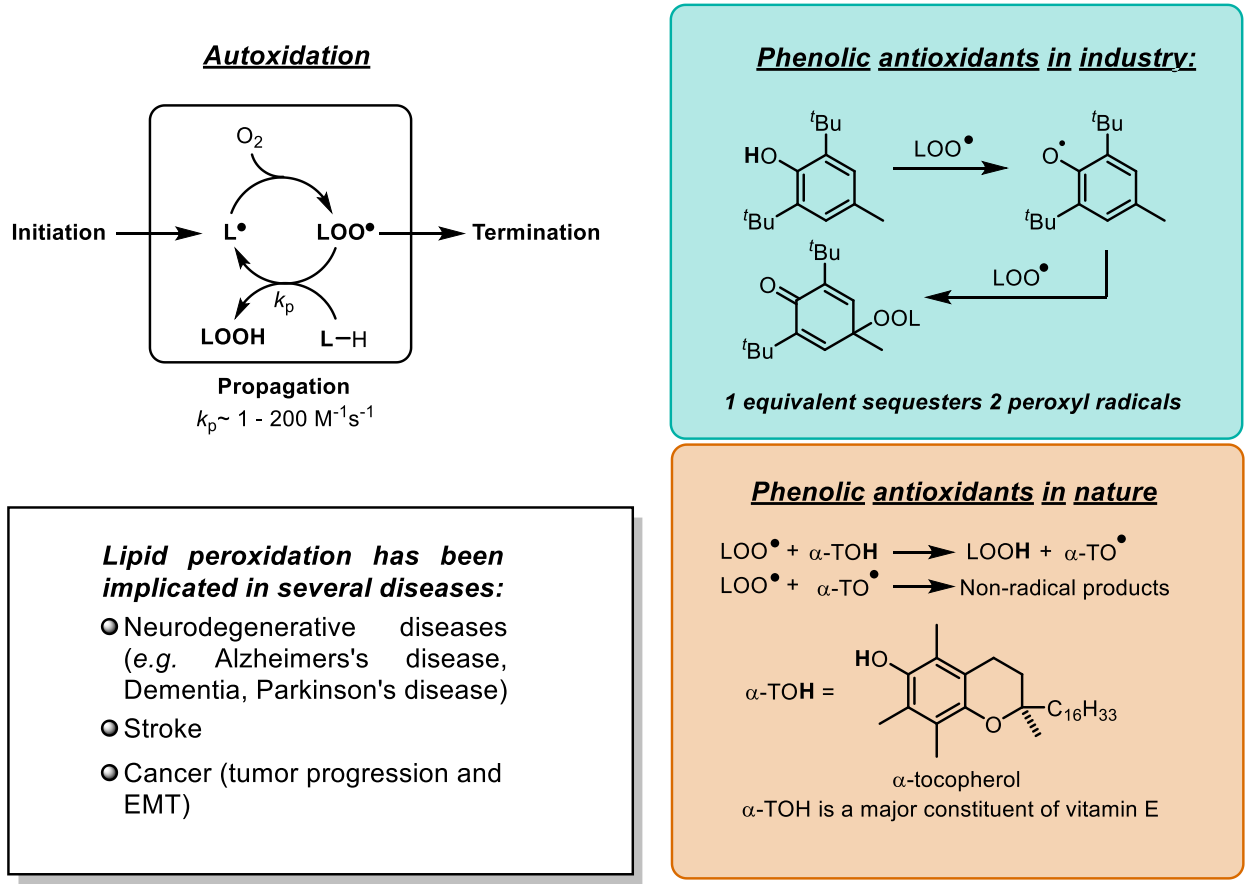

Figure 1.11: This presents an overview of autoxidation, industrial applications of antixodants, biological antioxidants, and the pathogenic impact of autoxidation.

industrial petroleum-based materials (*e.g.* oils, fuels, rubbers, lubricants, and polymers), this process results in the decomposition of the material which negatively impacts its properties resulting in its degradation and fouling. Biological materials are not immune to this process as the macromolecules that comprise cells, tissues and organs are hydrocarbon-based. Macromolecules that are most susceptible to this decomposition pathway are lipids that comprise biological membranes and lipoproteins. There is an abundance of research in academic and industrial labs that aim to find chemical additives that mitigate/retard or completely inhibit this spontaneous chemical reaction. The impacts of synthesizing, discovering, and applying molecules to mitigate autoxidation include the development of new material formulations that impart longer lifetimes for the material in use as well as the potential to prevent oxidative damage to living systems that could ultimately lead to preventative treatments for certain neurological and cardiovascular diseases, cancer, and potentially increase the longevity of living beings.[79, 80]

More labile C – H bonds (lower BDE) are where this reaction occurs spontaneously. The mechanism for this reaction begins with the initiation of a radical chain reaction. The resulting radical species can perform HAT on the labile position of an oxidizable substrate to give the reduced product and a new radical species (oxidized substrate). This newformed carbon-centered radical undergoes reaction with oxygen at (or close to) the rate of diffusion (k_D) to form a peroxyl radical (ROO•). This peroxyl radical species is then able to perform HAT on another oxidizable substrate to produce a hydrogen peroxide (ROOH) and a new carbon-centered radical thus propagating the radical chain reaction. This sequence of steps can repeat until the chain reaction is terminated. Termination of the radical chain reaction occurs either by radical-radical dimerization or disproportionation, both being bimolecular processes that result in non-radical products. For example, the dimerization of two peroxyl radicals leads to the formation of a ketone, alcohol, and

O2. This mechanism is responsible for the autoxidation of cumene to form acetone and phenol. This mechanism was first proposed and supported with deuterium labeling experiments in which the kinetics of HAT from an oxidizable substrate (Specifically cumene and ethylbenzene) to peroxyl radical were measured. The high kinetic isotope effect ($k_H/k_D = 5.5$) indicated that this step was rate-limiting.[81]

Antioxidants are chemical compounds that have the ability to inhibit or slow the rate of autoxidation. Depending on the mechanism in which they slow autoxidation, antioxidants are generally divided into two categories: preventative antioxidants and radical-trapping antioxidants.[82, 83] Preventative antioxidants decrease the rate at which autoxidation is initiated. This is accomplished by the breakdown and decomposition of alkyl peroxides and hydrogen peroxides which in turn prevents the initiation of radical chain reactions and formation of hydroxyl radicals via Fenton chemistry. In a cellular environment, preventative antioxidants include enzymes such as catalase and glutathione peroxidase. Organophosphines and organosulfur compounds are often used preventative antioxidants within industrial settings. Radical trapping antioxidants, on the other hand, are chain-breaking antioxidants in that they sequester chain propagating radical species such as peroxyl radicals. This is accomplished by the labile X – H bond of a phenol (X=O)(or biaryl amine, X=N) which can undergo HAT by a reactive radical species resulting in the reduced chain propagator and the phenoxyl radical. Due the phenoxyl radicals inability to react with an oxidized substrate or O2, they are effectively persistent radicals which eventually react with another equivalent of peroxyl radical forming non-radical peroxyl adducts.[84] Common radical-trapping antioxidants that are used as industrial additives for materials include derivatives of 2,6-di-*tert*-butyl-4-methylphenol/ *bis*-*tert*-butyl hydroxytoluene (BHT) and ring-alkylated phenylamines. α-tocopherol, the major isomer of vitamin E that is absorbed by

humans, is the quintessential phenolic-based radical-trapping antioxidant in biological systems that breaks radical chain reactions involving poly-unsaturated fatty acids, sterols, and lipoproteins in cellular membranes. [79, 85-87]

Thermodynamics and kinetics are factors responsible for the inherent reactivity of phenols (and diarylamines) as peroxyl radical-trapping antioxidants. The labile O – H bond of phenol has a bond dissociation energy of 87 kcal/mol – similar to that of hydroperoxide. This suggests that there is not a thermodynamic driving force for HAT to occur between the phenol and peroxyl radical but in actuality this process occurs with a measured rate constant (k_{inh}) of ~10^3 $M^{-1}s^{-1}$ indicating that there is a relatively low energy barrier in the transition state.[88] This low transition state energy is a result of the pre-complexation of the electron rich phenol HOMO and the electron-poor LUMO of the peroxyl radical that promotes the transfer of an electron and simultaneous proton transfer.[84] This process can be further improved by changing the substitution on the phenol to have more electron-donating groups which lowers the BDE of the O – H bond. This change effectively raises the HOMO of the phenol and reduces the energy gap with the electron-deficient peroxyl radical LUMO. The k_{inh} increases as a result.[89] For this reason, α-tocopherol is able to perform HAT at a rate (k_{inh}) of 3x10^6 $M^{-1}s^{-1}$, a 3 fold increase in order of magnitude compared to phenol (~10^3 $M^{-1}s^{-1}$).[85] Some substitutions that lower the phenol BDE can actually hinder the ability for the phenol to sequester a peroxyl radical. Comparing BHT to 2,4,6-trimethylphenol, BHT has a BDE that is 1.7 kcal/mol lower than 2,4,6-trimethylphenol but has a k_{inh} that is 6-fold less reactive than the latter. This supports that the RTA potential of the phenol is sensitive to the steric environment that surrounds it.[90]

Due to the given interest in antioxidants and the potential health benefits attributed to their dietary intake, many assays have been developed for the characterization of total antioxidant

content of a given molecule with developments dating back to the 1950s.[79] The most popular assays involve colorimetric or fluorescent reagents that have signal intensities that are reliant on the potency of the antioxidant in question to inhibit autoxidation or sequester free radicals. There are three types of antioxidant assays: single electron transfer (SET), metal chelation-based assays, and HAT-based assays. In SET assays, an antioxidant is evaluated based on its ability to reduce a radical probe (via SET) in order to stabilize it. This results in a color change (from the radical) that corresponds to the end point concentration of the antioxidant. As its name suggests, metal chelation assays evaluate an antioxidant based on its ability to chelate metals such as Zn^{2+}, Fe^{2+}, or Cu^{2+} which have been shown to be involved in the pathogenesis of various diseases and neurological diseases (*e.g.* Alzheimer's and Parkinson's diseases). HAT-based assays measure the ability of antioxidants to transfer a hydrogen atom to a radical.

Chapter 2: Development of an Electrochemical Dimerization to Access C3 – C8 Dihydrobenzofurans and C8 – C8' Quinone Methide Dimers

*Portions of this chapter have been published in:

Romero, K. J.; Galliher, M. S.; Raycroft, M. A. R.; Chauvin, J.-P. R.; Bosque, I.; Pratt, D. A.; Stephenson, C. R. J., *Angewandte Chemie International Edition* **2018,** *57* (52), 17125-17129.;[91] Matthew S. Galliher, Bec J. Roldan, and Corey R. J. Stephenson. *Chem. Soc. Rev.* **2021**, *50*, 10044-10057.;[1] Kevin J. Romero, Matthew S. Galliher, Derek A. Pratt, and Corey R. J. Stephenson. *Chem. Soc. Rev.* **2018**, *47*, 7851.[2]

2.1 Introduction

Strategies in forming the key C8 – C8' and C3 – C8' bonds of resveratrol derived oligomers are numerous. The most notable is the early work contributed to the field by Hou and Li in the use of various oxidation techniques including enzymatic and metal-mediated oxidations to access resveratrol oligomers[26, 92-94] as well as Stephenson's use of metal oxidants in a regio-controlled fashion[64] and the *de novo* strategies employed by Snyder.[95-100] The use of electrochemistry to generate the resveratrol-derived phenoxyl radical, although relatively new, has become powerful

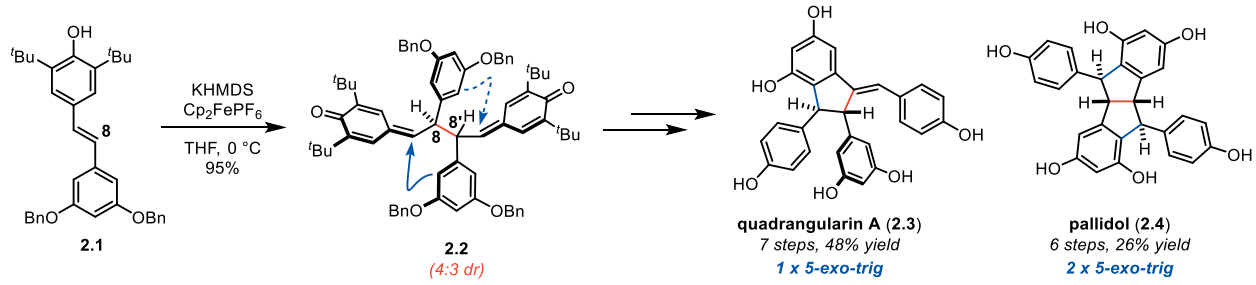

Figure 2.1. Stephenson's biomimetic synthesis of quadrangularin A (**2.3**) and pallidol (**2.4**).

technique in resveratrol oligomer synthesis. Our previous work for achieving the regiocontrolled C8 – C8' dimerization of **2.1** was realized in the synthesis of quadrangularin A and pallidol (**Figure 2.1**) which utilized quinone methide dimer (QMD) **2.3**.[2, 101]

2.2 Development of an electrochemical method of C8 – C8 and C3 – C8 dimerization

The biomimetic strategies for the C8 – C8 and C3 – C8 bonds of resveratrol oligomers utilize the resveratrol derived phenoxyl radical. The biosynthesis of these oligomers is hypothesized to proceed via the regio- and stereoselective coupling of phenoxyl radicals of form **2.5a**–**2.5c** to generate products such as hierochin D (**2.6**) via C3–C8' coupling and quadrangularin A (**2.3**) via C8–C8' coupling (**Figure 2.2A**).[102, 103] Several of the synthetic efforts to recapitulate this strategy, including our own, have used enzymatic catalysis or single-electron oxidants, while others have targeted these molecules through *de novo* routes.[63, 64, 92-94, 96-99, 104-111] Our previous approaches employed ferrocenium hexafluorophosphate as a mild stoichiometric oxidant to promote dimerization of protected resveratrol derivatives, which ultimately enabled the total synthesis of several dimeric and tetrameric resveratrol natural

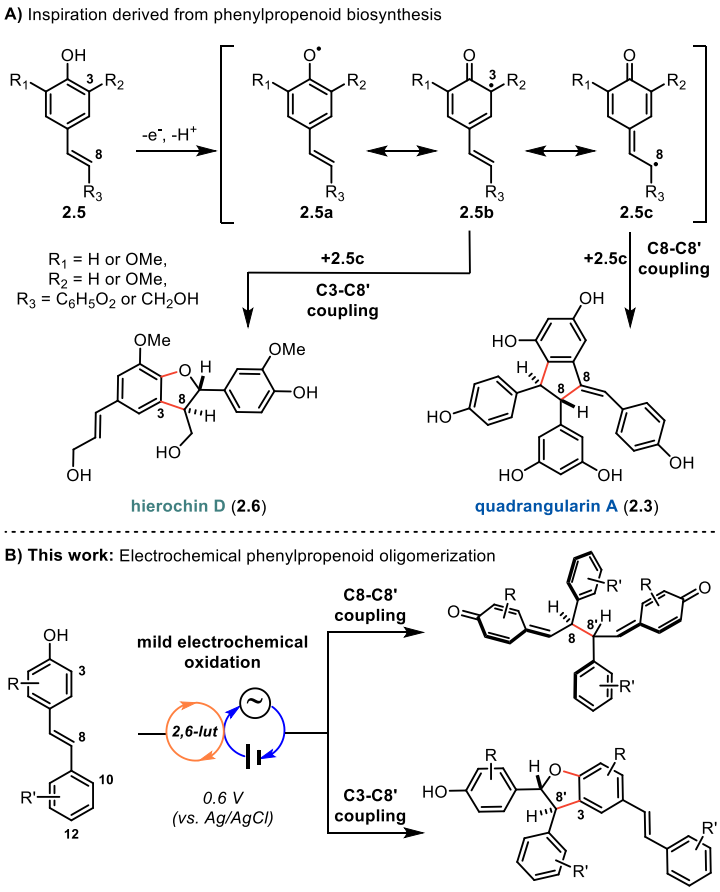

Figure 2.2. A) Phenylpropenoid oligomerization occurs via phenoxyl radical coupling. B) Our electrochemical approach to the oligomerization of phenylpropenoid scaffolds.To determine whether the desired dimerization would be feasible under anodic oxidation conditions, we interrogated the oxidation potential of various 4-hydroxystilbene substrates using cyclic voltammetry (see page S38 of the Supporting Information).

products.[63, 64] While these conditions were high-yielding and afforded excellent regioselectivity, we sought to develop a catalytic method that would translate more readily to other systems, especially those that may be prone to overoxidation. We previously investigated the use of photocatalysis to achieve this goal.[64] Unfortunately, competing energy transfer pathways resulted in stilbene isomerization, while stoichiometric terminal oxidants led to decomposition of the products and/or starting materials. Therefore, an alternative method for catalytic phenol oxidation was desired.

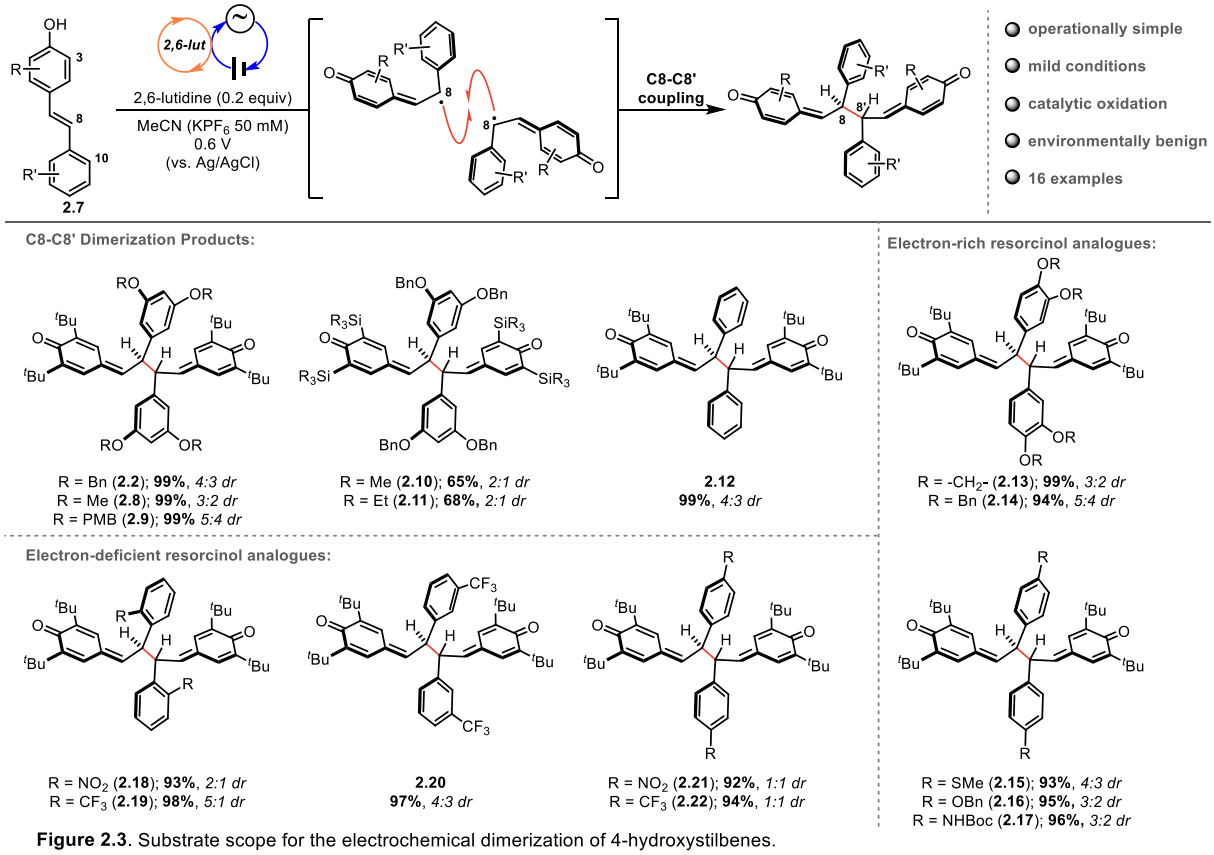

Figure 2.3. Substrate scope for the electrochemical dimerization of 4-hydroxystilbenes.

Several reports have demonstrated the utility of anodic oxidation in total synthesis,[112-120] but efforts to apply this approach in the context of phenylpropenoid natural product total synthesis have been limited by low yields and lack of regiocontrol.[121-124] Here, we present an electrochemical method for the regioselective dimerization of various hydroxystilbene derivatives (**Figure 2.2B**). The anodic oxidation reactions proceed at low potential and deliver the corresponding quinone

methide dimers (QMDs) in good to excellent yields, providing rapid access to multiple natural product scaffolds in a selective fashion.

In all cases, direct oxidation of the substrate occurred above +0.8 V, however in the presence of 2,6-lutidine oxidation occurred below +0.6 V in all cases. With this information in hand (see page S43 of the Supporting Information for complete details), we developed conditions where anodic oxidation in the presence of 2,6-lutidine enables phenoxyl radical dimerization (**Figure 2.3**). The scope of this reaction was investigated by first varying the substituents of the resorcinol ring. A range of 3,5-di-*tert*-butyl-4-hydroxystilbene substrates were prepared from commercially available starting materials in 2-3 steps (see Supporting Information). Various protecting groups were tolerated on the resorcinol ring without diminishing the yield (**2.2, 2.8, 2.9**). When the *tert*-butyl substituents at C3 were exchanged with trialkylsilyl groups (**2.10, 2.11**), the yield diminished due to the decreased stability of the QMDs, which we have reported on previously.[63] It was apparent that both electron-withdrawing and electron-donating groups were tolerated at each position of this aromatic ring as reactions proceeded with a wide-variety of electronically distinct substrates in excellent yields (**2.12**–**2.22**). The scope of this chemistry was extended to include dimerization of the ε-viniferin analogue (**2.23**/**2.24**), whose QMD product is the key intermediate in our recently reported syntheses of the natural products nepalensinol B and vateriaphenol C.[63] As observed in the preparation of **2.5** and **2.10**, the electrochemical yields of **2.25** and **2.26** were comparable to those obtained using a stoichiometric chemical oxidant, demonstrating the generality of this method for selective biomimetic synthesis of C8–C8' resveratrol oligomers (Figure 3A). Regarding the observed diastereoselectivities in the synthesis of these QMD products, we presume that these dimers are in dynamic equilibrium with the corresponding phenoxyl radical monomers via C8–C8' homolysis as we have previously characterized for QMDs **2.5, 2.10, 2.25**

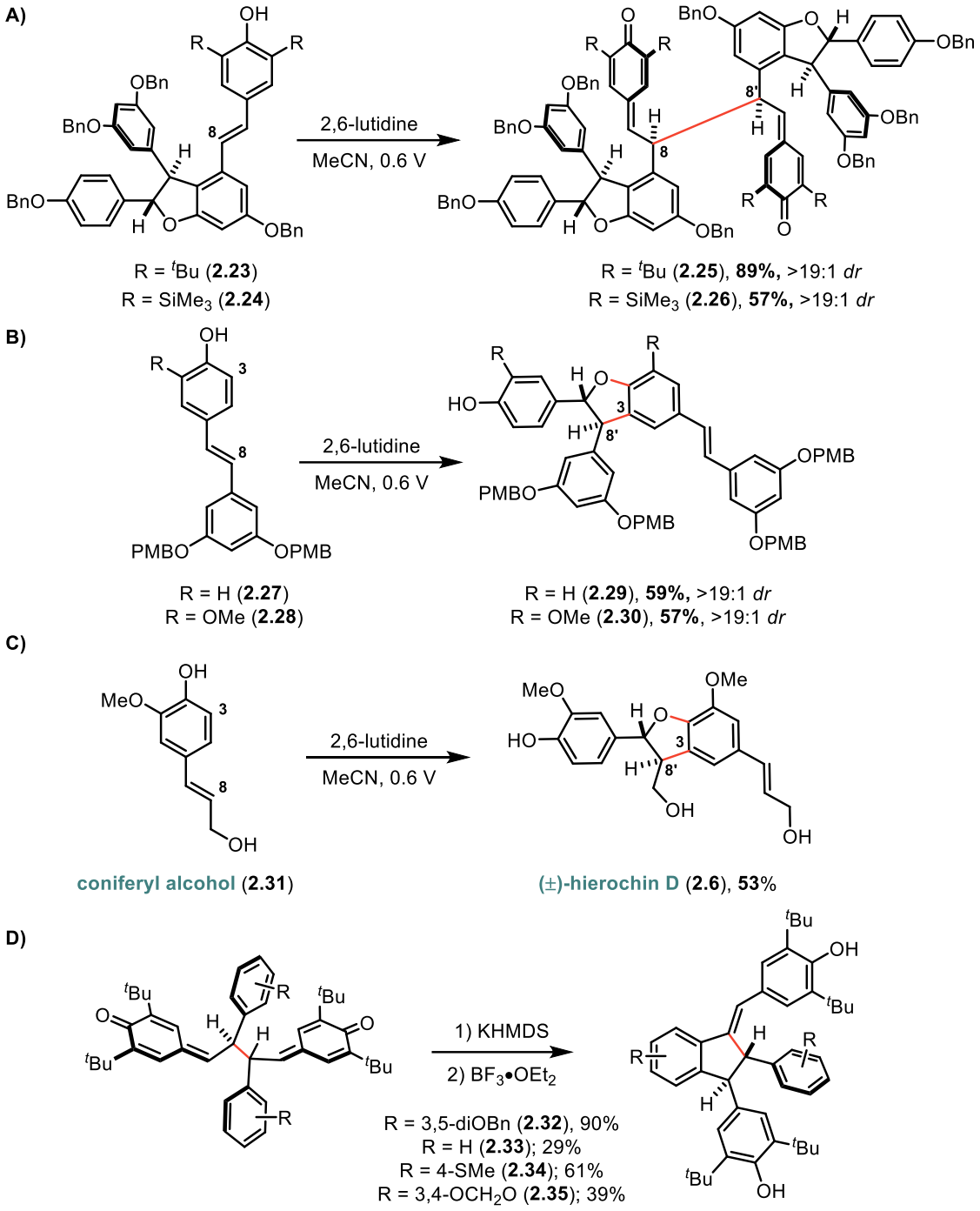

Figure 2.4. A) Electrochemical dimerization delivers the key intermediate for the synthesis of resveratrol tetramers. 2,6-lut. = 20 mol%, Electrolyte = KPF6 (50 mM), Reference Electrode = Ag/AgCl. B) The removal of the C3-substituent results in a direct C3–C8' dimerization, affording dihydrobenzofuran products. 2,6-lut. = 20 mol%, Electrolyte = KPF6 (50 mM), Reference Electrode = Ag/AgCl. C) Electrochemical synthesis of (±)-hierochin D. 2,6-lut. = 50 mol%, Electrolyte = KPF6 (50 mM), Reference Electrode = Ag/AgCl. D) Preparation of natural product analogue cores from QMDs.

and **2.26**.[63] Therefore, the minimal diastereoselectivity observed for **2.2, 2.8**–**2.22** is in agreement

with prior methods for preparing these materials, as is the excellent diastereoselectivity observed for **2.25** and **2.26**. The influence of additional stereocenters present in **2.25**/**2.26** presumably has a greater impact on the orientation in which the persistent radicals recombine, resulting in an increase in diastereoselectivity when moving from the dimer to the tetramer system.[2] Importantly, the preparation of *tert*-butylated dimers (**5-7**, **10-20**, **23**) did not require chromatographic purification, which is highly advantageous for multi-step syntheses and provides an attractive alternative to stoichiometric dimerization methods.

The scalability of this reaction was later demonstrated after the publication of this manuscript.[91] In efforts to produce QMD for the synthesis of oligomers, the electrochemical dimerization was demonstrated to work on a 100 gram scale. This was accomplished in a batch reaction format and as such the amount of RVC electrode material was scaled up as the rate of this reaction is reliant on the available surface area of the electrode. Additionally, superstoichiometric quantities of 2,6-lutidine were used to mitigate the reaction time. In less than 24 hours, the reaction was completed. This batch of material was purified via silica chromatography to remove electrolyte to yield a semi-crude mixture which was later triterated in acetone to produce 90 grams of pure, yellow QMD powder (90% yield after triteration in acetone).

The removal of one of the C3 blocking groups resulted in C3–C8’ dimerization, enabling access to the cores of the natural products δ-viniferin (**2.29**) and shegansu B (**2.30**) exclusively as the *trans*-diastereomers (**Figure 2.4B**), consistent with prior biomimetic dimerization studies of these types of hydroxystilbenes.[102] As a result, the regioselectivity for this transformation is controlled exclusively by the presence or absence of a C3-blocking group. As described in Figure 1B, the analogous biosyntheses of the lignan class of natural products prompted us to investigate an extension of this electrochemical dimerization strategy. Subjection of coniferyl alcohol (**2.31**)

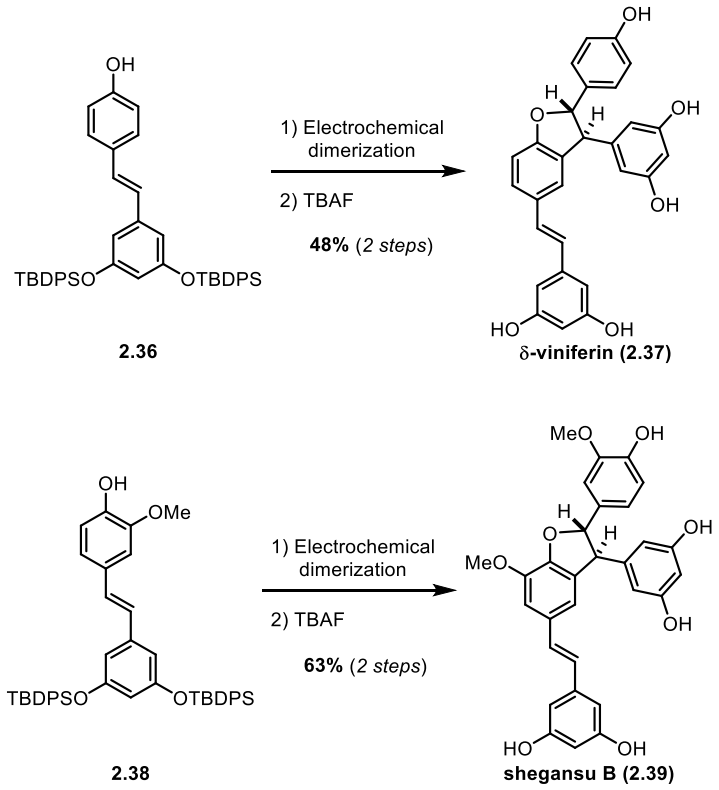

Figure 2.5. Total syntheses of δ-viniferin (top) and shegansu B (bottom) accomplished by electrochemical dimerization of stilbene precursors.

to anodic oxidation under our optimized conditions afforded moderate conversion of the starting material; gratifyingly, a simple increase in the concentration of 2,6-lutidine from 20 mol% to 50 mol% afforded the neolignan natural product (±)-hierochin D in 53% yield (**2.6**, **Figure 2.4C**).

Following the successful synthesis of the natural product cores, the total syntheses of shegansu B and δ-viniferin was targeted. Previous syntheses of these natural products have been performed previously which utilized the oxidative dimerization of the corresponding stilbenes via horseradish peroxidase and hydrogen peroxide conditions.[125] The syntheses were successfully carried out using the TBDPS-protected stilbene precursors. Following the electrochemical dimerization and TBAF-mediated desilylation, shegansu B and δ-viniferin were isolated (63% and 48% respectively over 2 steps) (**Figure 2.5**).

To explore the utility of the electrochemically-synthesized quinone methide dimers for the preparation of natural product-like indane and diquinane scaffolds, the QMDs described in **Figure 2.2** were exposed to Lewis acids that promote intramolecular Friedel-Crafts cyclizations. While direct, double cyclization of **2.2** was successful in our previous synthesis of the resveratrol dimer pallidol,[64] QMDs lacking the resorcinol moiety present in **2.2** did not react in this fashion. Instead,

substrates with electron-donating groups at C12 (and their corresponding phenoxyl radicals) were susceptible to redox disproportionation conditions, returning half of the material as the stilbene precursor (reduction product) with loss of the remaining mass to oxidative decomposition (See Figure S1 on page S85 of the Supporting Information). The QMDs depicted in Figure 2 were, however, found to be suitable intermediates for the preparation of analogues of quadrangularin A (**2.3**). Base-mediated isomerization of one quinone methide followed by Lewis acid activation and Friedel-Crafts cyclization onto the remaining quinone methide forged a series of *tert*-butylated quadrangularin A analogues (**2.32**–**2.35**), Figure 3D). Only QMDs containing the resorcinol oxygen substitution pattern were able to undergo the double cyclization forming the [3.3.0] bicyclooctane and as such, pallidol derivatives were inaccessible by the rest of the substrates. It must be mentioned that the electronically-deficient QMDs were unable to undergo the Lewis acid-mediated Friedel-Crafts cyclization as they were too poor of a nucleophile to complete this transformation.

2.3 Experimental

General Procedures:

Unless specifically noted otherwise, all glassware was flame-dried under vacuum (~0.5 Torr) and cooled under inert atmosphere (N_2 or Ar) prior to use. Each reaction container was charged with a Teflon/PTFE-coated magnetic stir bar and sealed with a rubber septum to maintain a positive pressure of inert atmosphere (N_2 or Ar). Reagents sensitive to the atmosphere were transferred via syringe or cannula as necessary. Reaction conversion was evaluated using analytical thin-layer chromatography (TLC) using Merck silica gel 60 F254 TLC plates. TLC plates were visualized under a dual short wave/long wave UV lamp and/or stained using solutions of *p*-anisaldehyde or potassium permanganate or ceric ammonium molybdate. Stained plates were developed over a heat gun as needed. Reactions were purified via flash column chromatography either with Redi*Sep*®*R*$_F$ Gold silica columns using a Teledyne Isco CombiFlash R_F automated purification system or manually using 230-400 mesh silica gel. Either sodium sulfate or magnesium sulfate were utilized to exclude water from worked up reactions, and the solvent was removed on Büchi rotary evaporators and/or a Welch vacuum pump. All electrochemical experiments were acquired using either a CH1620E electrochemical analyzer (from CH Instruments) or a uSTAT4000 4-Channel Potentiostat/Galvanostat (from Metrohm USA). Cyclic voltammetry measurements were performed in five-neck cells (3 mL) using a three-electrode set-up in which the working electrode was glassy carbon (3 mm diameter), the counter/auxiliary electrode was a platinum wire, and the reference electrode was Ag/AgCl (3 M KCl, from CHInstruments). Bulk electrolysis experiments were performed on discovery scale in open 10-mL vials and in a beaker of the appropriate size (15 – 40 mL) for the subsequent scale-up experiments. These reactions used RVC panels (reticulated vitreous carbon, 100 ppi, 0.25 inch thickness, 3%

relative density, from McMaster Carr) as the working or counter/auxiliary electrodes and a Ag/AgCl (3 M KCl) reference electrode.

Reaction Materials:

Commercially available reagents were used without further purification unless specified. Organic solvents (acetonitrile, dichloromethane, diethyl ether, dimethylformamide, dimethyl sulfoxide, methanol, tetrahydrofuran, and toluene) and amine bases (triethylamine, pyridine, N,N-diisopropylethylamine, and diisopropylamine) were purified prior to use with a Phoenix Solvent Drying System from JC-Meyer Solvent Systems and PureSolv Micro amine drying columns from Innovative Technology, respectively, and kept under a pressure of argon. Solutions of organolithium reagents and Grignard reagents were purchased from Acros Organics and titrated prior to use.

Product Analysis:

Product names were obtained using ChemDraw Professional 16.0 from Perkin Elmer. For racemic compounds, the name corresponds to the depicted structure. Nuclear magnetic resonance (NMR) spectra were obtained using an internal deuterium lock on Varian Inova 500 or Varian VNMR 500 and 700 spectrometers. For ^{1}H spectra, chemical shifts were referenced to the center line of the residual solvent signal ($CDCl_3$: δ 7.26; acetone-d_6: δ 2.05) and are reported in parts per million (ppm). Signal multiplicity is reported as follows: (br = broad, s = singlet, d = doublet, t = triplet, dd = doublet of doublets, ddd = doublet of doublet of doublets, m = multiplet), and the associated coupling constants are given in Hertz. For ^{13}C spectra, experiments were completely heterodecoupled (broadband) and chemical shifts are reported as ppm using the center line of the solvent signal as reference ($CDCl_3$: δ 77.16; acetone-d_6: δ 29.92). The following resveratrol numbering scheme was used for the

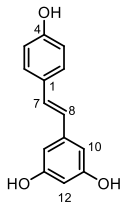

assignment of ^{1}H and ^{13}C NMR signals. High-resolution mass spectra (HRMS) were acquired using a Micromass AutoSpec Ultima Magnetic Sector mass spectrometer using electrospray ionization (ESI), positive ion mode. We thank James Windak and Paul Lennon at the University of Michigan, Department of Chemistry Instrumentation Facility for conducting the HRMS experiments. Infrared spectra were acquired using a Perkin-Elmer Spectrum BX FT-IR spectrophotometer using an ATR mount with a ZnSe crystal.

General Stilbene preparation:

Unless otherwise specified, stilbene substrates were prepared from the benzyl alcohol or benzyl bromide via a Wittig olefination with one of the following aldehydes:

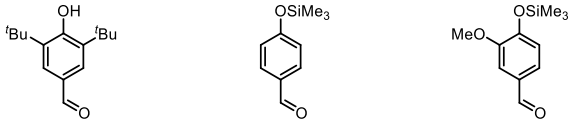

Aldehyde A Aldehyde B Aldehyde C

3,5-di-*tert*-butyl-4-hydroxybenzaldehyde (aldehyde A), commercially available;

4-((trimethylsilyl)oxy)benzaldehyde (aldehyde B), from silyl protection of 4-hydroxybenzaldehyde;

3-methoxy-4-((trimethylsilyl)oxy)benzaldehyde (aldehyde C), from silyl protection of vanillin.

Starting from the benzyl alcohol:

A solution of triphenylphosphine (0.97 g, 3.71 mmol) in dry THF (2.5 mL) was sparged with N_2 (18G needle, 5 min) and was added dropwise to a solution of (benzyl) alcohol (2.97 mmol) and carbon tetrabromide (1.31 3.71 mmol) in dry THF (4.5 mL) that had been previously sparged (18G needle, 5 min.) in a 50 mL flame-dried round bottom flask and chilled to 0 °C. The mixture was stirred at room temperature for 16 h followed by dropwise addition of methanol (1 mL). The mixture was diluted with EtOAc (100 mL) and added to a separatory funnel and the organic phase was washed with a 1:1:1 mixture of 10% bicarbonate solution, saturated $Na_2S_2O_3$, and DI water solution (100mL). The organic phase was washed with brine and dried over Na_2SO_4. The organic phase was then concentrated under reduced pressure and purified by silica gel (pre-neutralized) column chromatography and eluted with 10:1 (hexane/ ethyl acetate) to afford the brominated product.

Starting from the benzyl bromide:

The benzyl bromide was added to a flame-dried round bottom flask charged with a stir bar and fitted with a reflux condenser and dissolved in toluene (0.15 – 0.20 M). To the stirring solution was added triphenylphosphine (1.5 equiv.), and the reaction was heated to 100 °C for 12 hours. After cooling the reaction mixture to room temperature, the white phosphonium salt was collected via vacuum filtration, and any excess triphenylphosphine was rinsed away with hexanes. The phosphonium salt was dried under vacuum for >24 hours prior to use in the Wittig olefination to ensure full removal of residual solvent and water.

The phosphonium salt was added to a flame-dried, 3-neck, round bottom flask charged with stir bar and fitted with a reflux condenser. The salt was suspended in solvent (toluene or THF, 0.1 M), and to the stirring mixture was added *n*BuLi (1.6 or 2.5 M, 1.00 equiv.). After 30 minutes, the reaction mixture had become a brilliant red, clear solution, at which point the aldehyde was added under a stream of nitrogen, and the reaction was heated at reflux for 12 hours. After cooling the reaction mixture to room temperature, the reaction was quenched with saturated aqueous ammonium chloride, diluted with ethyl acetate, and added to a separatory funnel containing additional aqueous ammonium chloride. The layers were separated, and the aqueous layer was extracted with additional ethyl acetate. The combined organic layers were washed with brine, dried over magnesium sulfate, and concentrated under reduced pressure. The crude stilbene products were purified via flash column chromatography (see characterization data for specific chromatography conditions).

The following substrates were acquired from previous investigations reported by our group.[1,2]

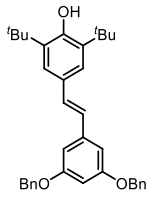

(S0) (*E*)-4-(3,5-bis(benzyloxy)styryl)-2,6-di-*tert*-butylphenol

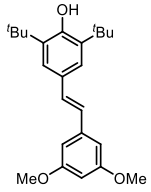

(S1) (*E*)-2,6-di-*tert*-butyl-4-(3,5-dimethoxystyryl)phenol

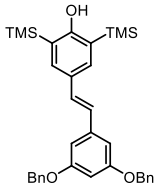

(S2) (*E*)-2,6-di-*tert*-butyl-4-(3,5-dimethoxystyryl)phenol

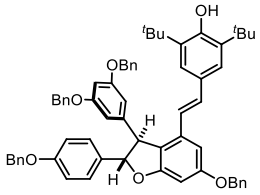

(21) 4-((*E*)-2-((2*S*,3*S*)-6-(benzyloxy)-2-(4-(benzyloxy)phenyl)-3-(3,5-bis(benzyloxy)phenyl)-2,3-dihydrobenzofuran-4-yl)vinyl)-2,6-di-*tert*-butylphenol

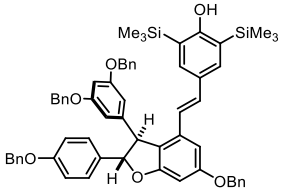

(22) 4-((*E*)-2-((2*S*,3*S*)-6-(benzyloxy)-2-(4-(benzyloxy)phenyl)-3-(3,5-bis(benzyloxy)phenyl)-2,3-dihydrobenzofuran-4-yl)vinyl)-2,6-bis(trimethylsilyl)phenol

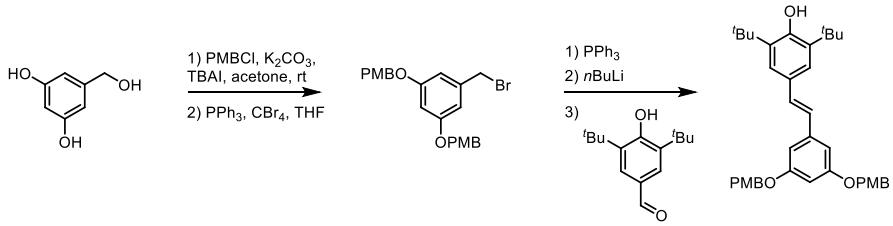

(S3) (*E*)-4-(3,5-bis((4-methoxybenzyl)oxy)styryl)-2,6-di-*tert*-butylphenol

Commercially available 3,5-dihydroxybenzyl alcohol (2.0 g, 14.3 mmol) was added to flask charged with potassium carbonate (2.25 equiv., 4.44 g) and tetrabutylammonium iodide (0.2 equiv., 1.05 g), and the solids were dissolved/suspended in acetone (42 mL). To the stirring reaction mixture was added 4-methoxybenzyl chloride (2.20 equiv., 4.26 mL), and the reaction was allowed to stir at room temperature for 16 hours. Upon completion, the reaction was diluted with ethyl acetate and poured into a separatory funnel containing deionized water. The layers were separated, and the aqueous layer was extracted with additional portions of ethyl acetate. The combined organic layer was washed with brine, dried over magnesium sulfate, and concentrated under reduced pressure to afford the crude product, which was carried forward without further purification. The PMB-protected material (2.18g, 5.72 mmol) was subjected to the general procedure using toluene as the solvent for the olefination with aldehyde A. The product was purified by column chromatography (4% to 28% ethyl acetate in hexanes) to afford (*E*)-4-(3,5-bis((4-methoxybenzyl)oxy)styryl)-2,6-di-*tert*-butylphenol (2.06g, 62% yield).

R_f = 0.22 (ethyl acetate/hexanes 1:9; UV)

^{1}H NMR (500 MHz, Chloroform-*d*) δ 7.37 (d, *J* = 8.6 Hz, 4H), 7.33 (s, 2H), 7.04 (d, *J* = 16.1 Hz, 1H), 6.93 (d, *J* = 8.6 Hz, 4H), 6.87 (d, *J* = 16.1 Hz, 1H), 6.76 (d, *J* = 2.2 Hz, 2H), 6.51 (t, *J* = 2.2 Hz, 1H), 5.29 (s, 1H), 5.00 (s, 4H), 3.83 (s, 6H), 1.48 (s, 18H).

^{13}C NMR (126 MHz, Chloroform-*d*) δ 160.32, 159.61, 154.08, 140.13, 136.29, 130.26, 129.44, 129.17, 128.56, 125.92, 123.66, 114.15, 105.56, 101.24, 70.04, 55.47, 34.53, 30.43.

IR (Neat): 3606, 2965, 1577, 1515, 1439, 1245, 1147, 1046, 1026, 967, 858 cm^{-1};

HRMS (ESI) *m/z* calculated for $C_{38}H_{45}O_5^+$ ([M+H]$^+$) 581.3262, found 581.3267.

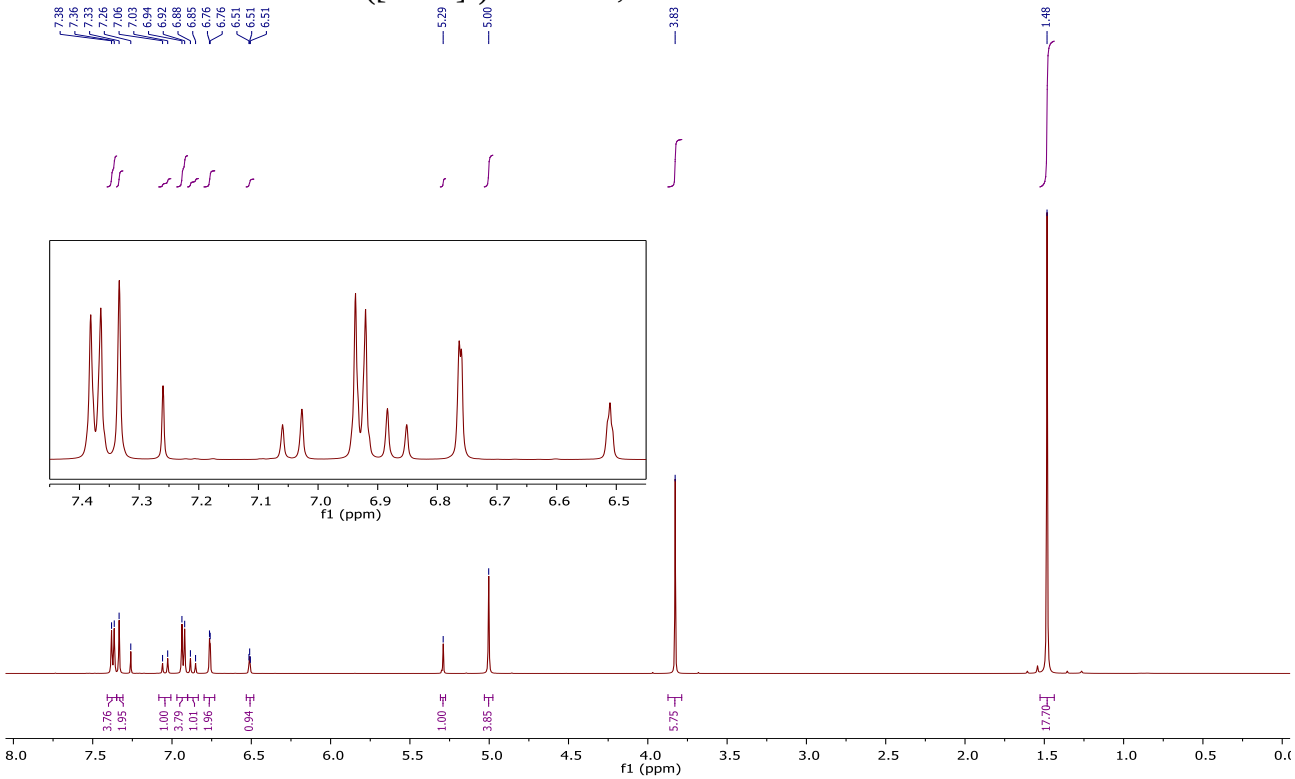

^{13}C NMR, 126 MHz, Chloroform-*d*, Stilbene **S3**

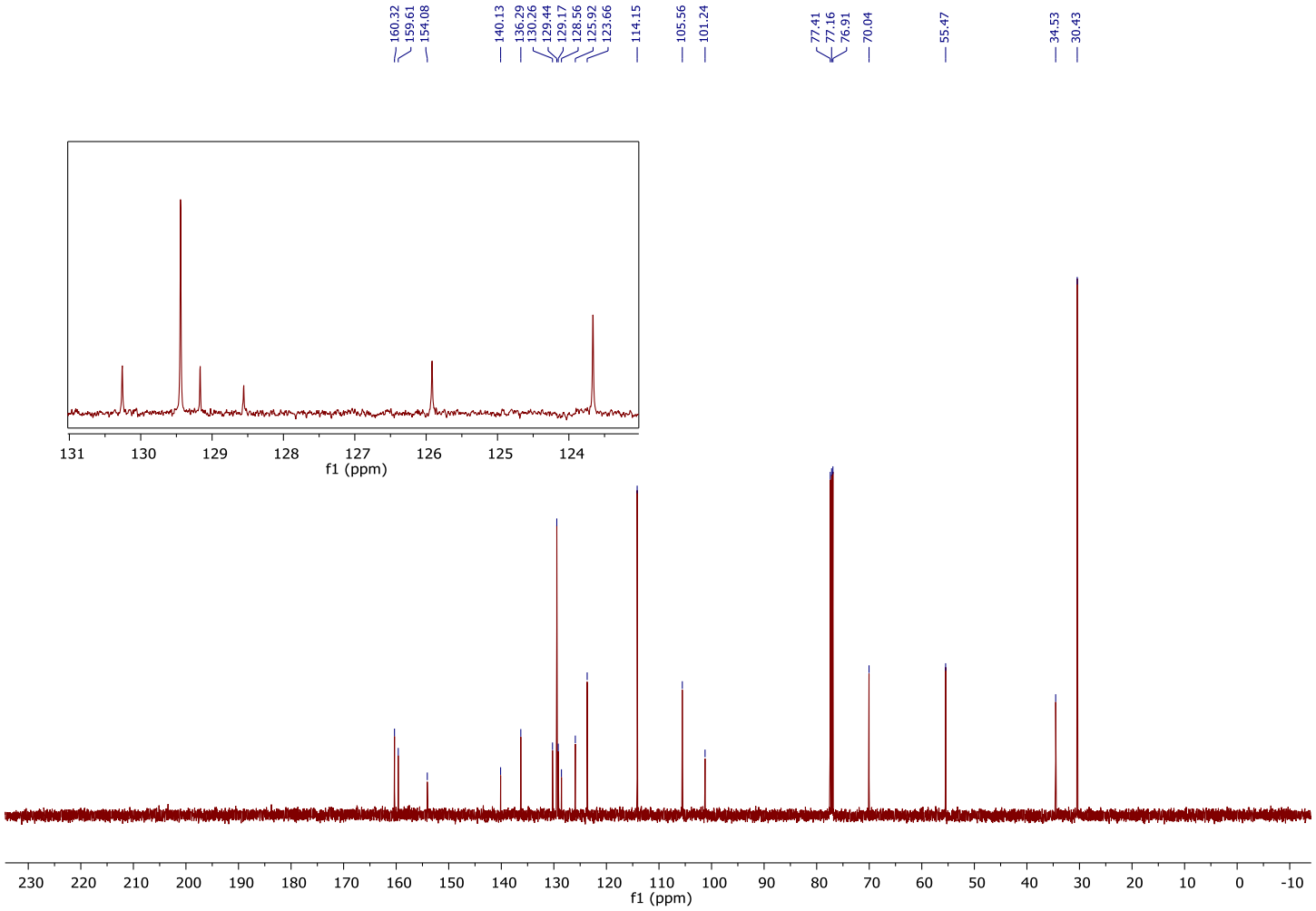

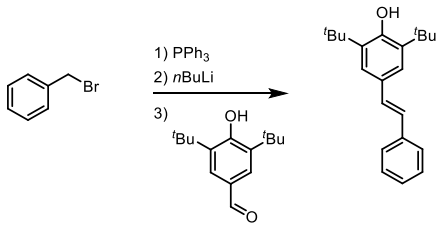

(S4) (*E*)-2,6-di-*tert*-butyl-4-styrylphenol

Commercially available benzyl bromide ((bromomethyl)benzene, 1.1 g, 6.4 mmol) was subjected to the general procedure using toluene as the solvent for the olefination with aldehyde A. The product was purified by column chromatography (2% to 12% ethyl acetate in hexanes) to afford (*E*)-2,6-di-*tert*-butyl-4-styrylphenol (1.64 g, 83% yield). The acquired ^{1}H and ^{13}C NMR spectra were consistent with those reported in the literature.

R_f = 0.31 (ethyl acetate/hexanes 1:9; UV)

^{1}H NMR (500 MHz, Chloroform-*d*) δ 7.50 (d, *J* = 7.6 Hz, 2H), 7.35 (s, 2H), 7.34 (t, *J* = 7.5 Hz, 1H), 7.23 (t, *J* = 7.3 Hz, 1H), 7.08 (d, *J* = 16.3 Hz, 1H), 6.95 (d, *J* = 16.2 Hz, 1H), 5.28 (s, 1H), 1.49 (s, 18H).

^{13}C NMR (126 MHz, Chloroform-*d*) δ 153.99, 138.09, 136.28, 129.70, 128.73, 127.11, 126.33, 126.00, 123.57, 34.53, 30.44.

IR (Neat): 3616, 2953, 1470, 1235, 1137, 1118, 957 cm^{-1};

HRMS (ESI) *m/z* calculated for $C_{22}H_{29}O^{+}$ ($[M+H]^{+}$) 309.2213, found 309.2206.

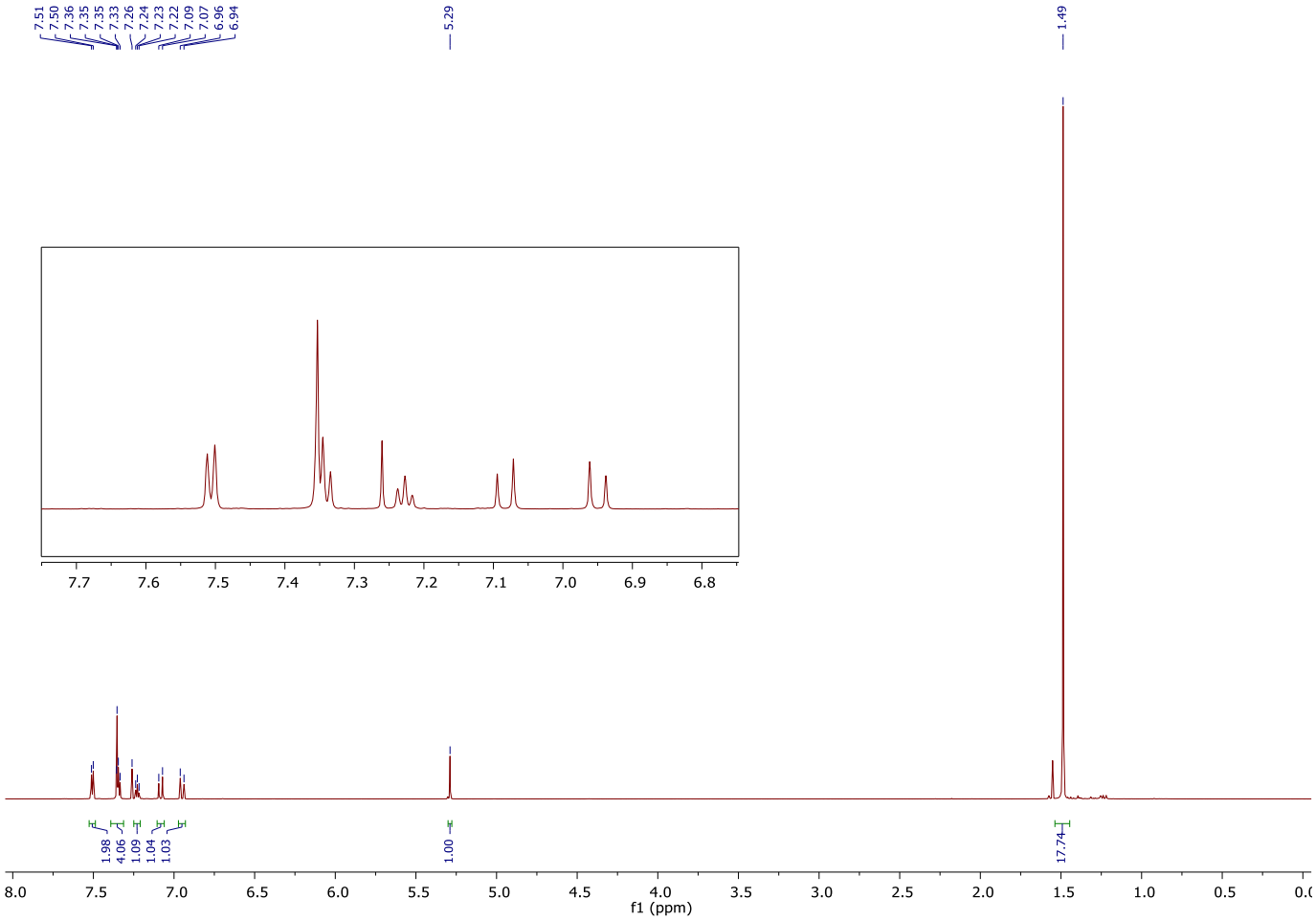
7.51
7.50
7.36
7.35
7.35
7.33
7.26
7.24
7.23
7.22
7.09
7.07
6.96
6.94
5.29
1.49
7.7
7.6
7.5
7.4
7.3
7.2
7.1
7.0
6.9
6.8
1.98
4.06
1.09
1.04
1.03
1.00
17.74
8.0
7.5
7.0
6.5
6.0
5.5
5.0
4.5
4.0
3.5
3.0
2.5
2.0
1.5
1.0
0.5
f1 (ppm)

^{13}C NMR, 126 MHz, Chloroform-*d*, Stilbene **S4**

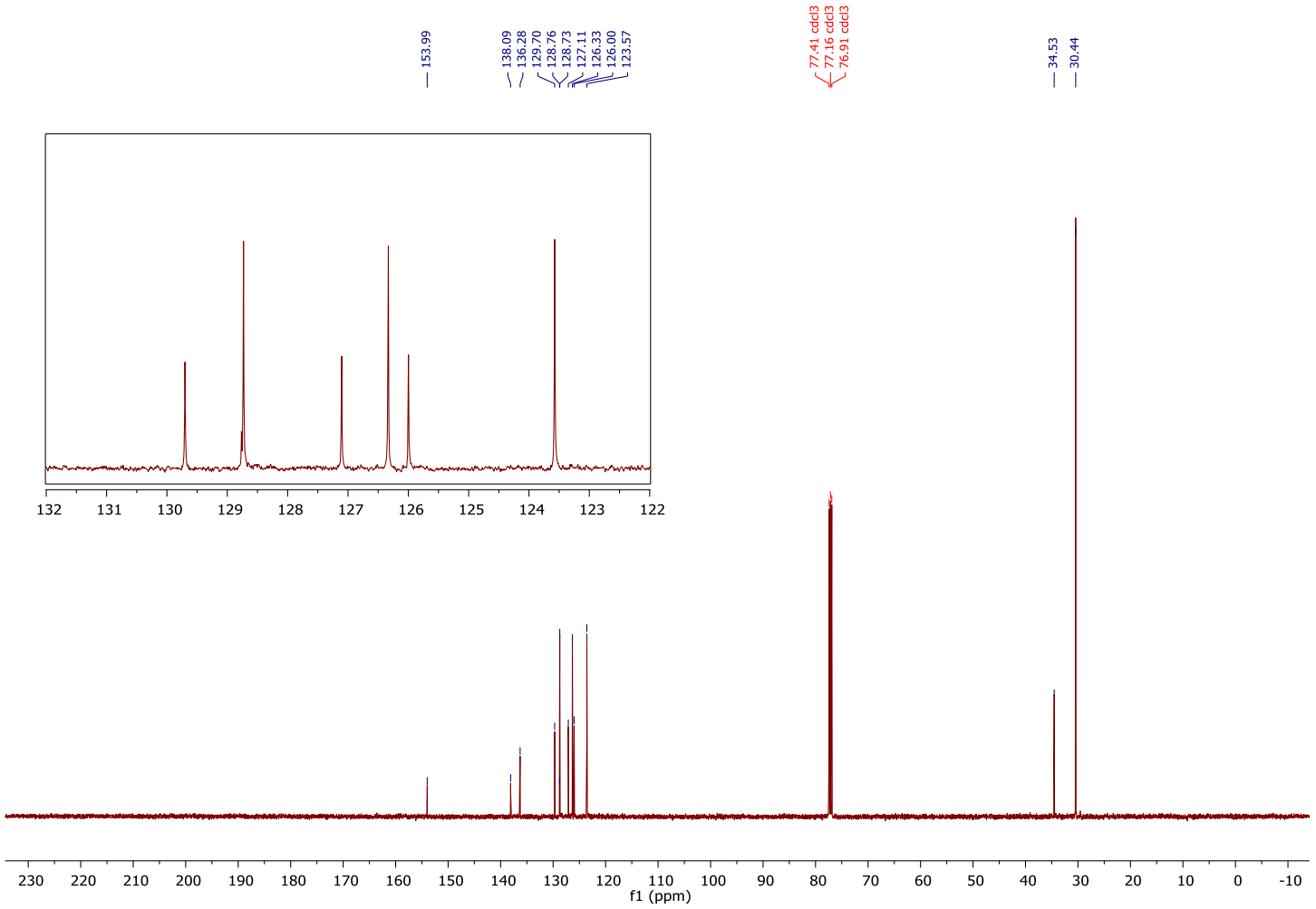

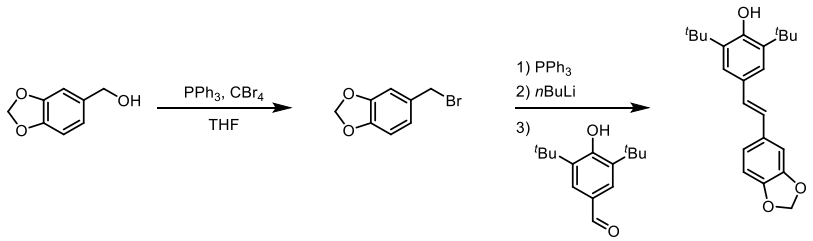

(S5) (*E*)-4-(2-(benzo[*d*][1,3]dioxol-5-yl)vinyl)-2,6-di-*tert*-butylphenol

Commercially available benzyl alcohol (benzo[*d*][1,3]dioxol-5-ylmethanol, 1.00g, 6.6 mmol) was subjected to the general procedure using toluene as the solvent for the olefination with aldehyde A. The product was purified by column chromatography (2% to 12% ethyl acetate in hexanes) to afford (*E*)-4-(2-(benzo[*d*][1,3]dioxol-5-yl)vinyl)-2,6-di-*tert*-butylphenol (1.72 g, 74% yield).

R_f = 0.26 (ethyl acetate/hexanes 1:9; UV)

^{1}H NMR (700 MHz, Chloroform-*d*) δ 7.31 (s, 2H), 7.06 (s, 1H), 6.92 (d, *J* = 8.0 Hz, 1H), 6.91 (d, *J* = 16.2 Hz, 1H), 6.86 (d, *J* = 16.2 Hz, 1H), 6.79 (d, *J* = 8.0 Hz, 1H), 5.97 (s, 2H), 5.26 (s, 1H), 1.48 (s, 18H).

^{13}C NMR (126 MHz, Chloroform-*d*) δ 153.79, 148.22, 146.94, 136.28, 132.69, 128.82, 128.10, 125.71, 123.36, 121.03, 108.50, 105.52, 101.16, 34.53, 30.44.

IR (Neat): 3625, 2955, 1486, 1435, 1249, 1135, 1036, 950 cm^{-1};

HRMS (ESI) *m/z* calculated for $C_{23}H_{29}O_3^+$ ($[M+H]^+$) 353.2111, found 353.2107.

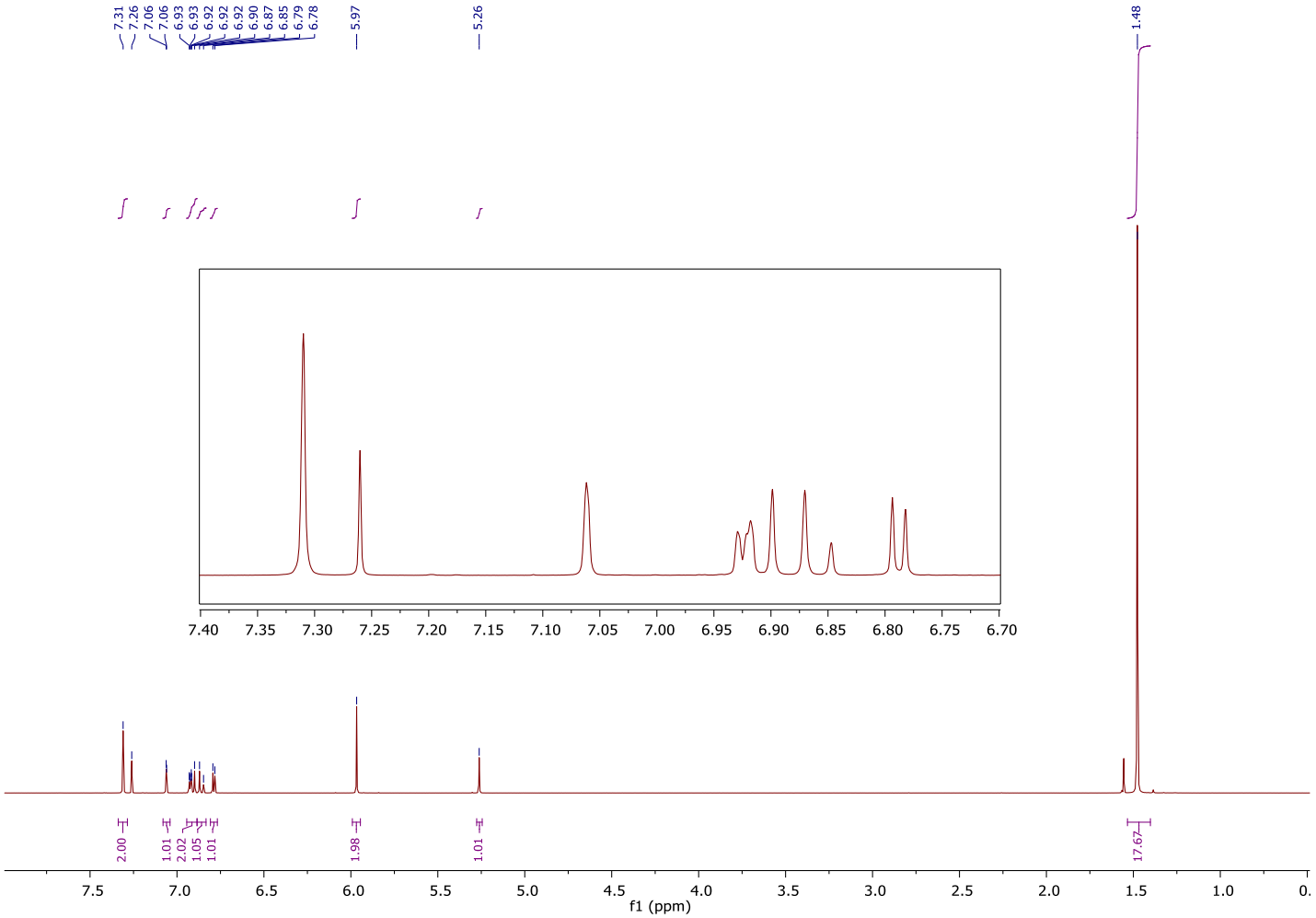
7.31
7.26
7.06
7.06
6.93
6.93
6.92
6.92
6.92
6.90
6.87
6.85
6.79
6.78
5.97
5.26
1.48
7.40 7.35 7.30 7.25 7.20 7.15 7.10 7.05 7.00 6.95 6.90 6.85 6.80 6.75 6.70
2.00
1.01
2.02
1.05
1.01
1.98
1.01
17.67
7.5 7.0 6.5 6.0 5.5 5.0 4.5 4.0 3.5 3.0 2.5 2.0 1.5 1.0 0.
f1 (ppm)

^{13}C NMR, 126 MHz, Chloroform-*d*, Stilbene **S5**

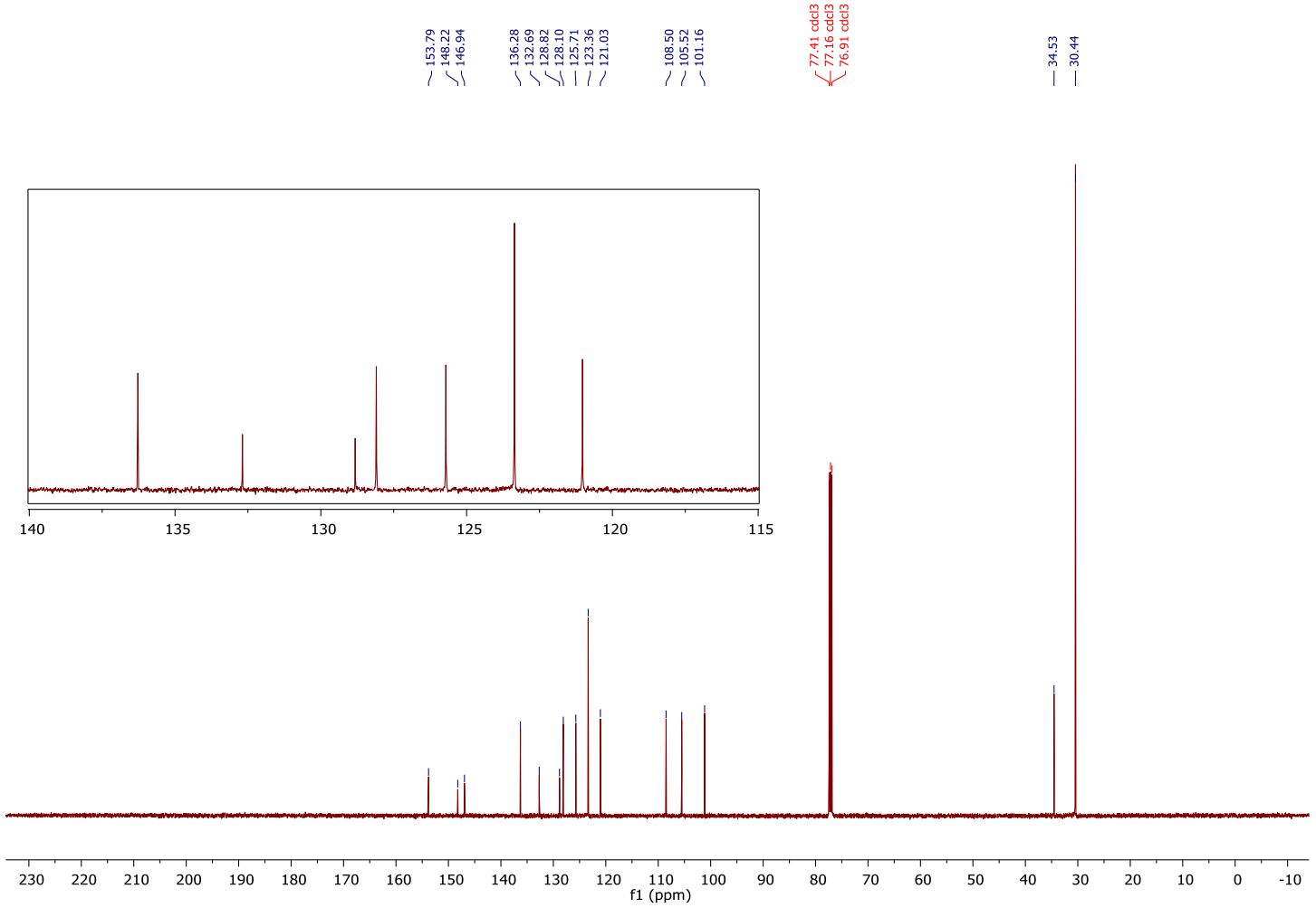

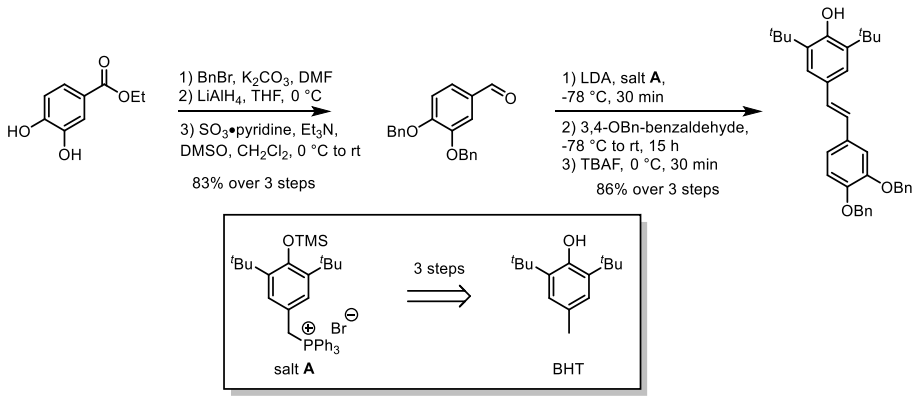

(S6) (*E*)-4-(3,4-bis(benzyloxy)styryl)-2,6-di-*tert*-butylphenol

Freshly distilled diisopropylamine (1.04 mmol, 146 μL) was added to a flame-dried heart-shaped flask, dissolved in freshly distilled THF (2 mL), and cooled to -78 °C. To the stirring solution was added *n*BuLi (1.00 mmol, 400 μL, 2.5 M), and the solution was allowed to stir at the same temperature for 30 min. Meanwhile, in a 3-neck round bottom flask, the phosphonium salt **A** (1.00 mmol, 634 mg, available in 3 steps[2]) was suspended in freshly distilled THF (10 mL) and cooled to -78 °C. The freshly prepared LDA solution was added to the phosphonium salt suspension via cannula, and the ylid was allowed to form at the same temperature for 30 min, turning the solution deep red. To a flame-dried heart-shaped flask was added 3,4-benzyloxybenzaldehyde (0.80 mmol, 255 mg, available in 3 steps via alkylation, reduction, and oxidation), and the solid was dissolved in THF (5 mL). The aldehyde solution was added to the ylid via cannula, and the reaction was allowed to warm to room temperature overnight (~15 hours). The reaction was subsequently cooled to 0 °C, and a solution of TBAF (1.00 mmol, 1.00 mL, 1.0 M) was added. The desilylation was allowed to occur for 30 min, at which point the reaction was quenched via the addition of saturated ammonium chloride, diluted with EtOAc, and added to a separatory funnel containing deionized water. The layers were separated, and the aqueous layer was extracted with additional portions of EtOAc. The combined organic layers were washed with brine, dried over magnesium sulfate, and concentrated under reduced pressure. The crude product was purified by flash column chromatography (10% to 60% CH_2Cl_2 in Hexanes) to afford the stilbene product (360 mg, 86% yield).

R_f = 0.30 (CH_2Cl_2/hexanes 1:1; UV)

^{1}H NMR (700 MHz, Chloroform-*d*) δ 7.49 (d, *J* = 7.5 Hz, 2H), 7.45 (d, *J* = 7.5 Hz, 2H), 7.40 – 7.37 (m, 2H), 7.37 – 7.35 (m, 2H), 7.34 – 7.30 (m, 2H), 7.30 (s, 2H), 7.14 (d, *J* = 2.0 Hz, 1H), 7.01 (dd, *J* = 8.3, 2.0 Hz, 1H), 6.91 (d, *J* = 8.3 Hz, 1H), 6.89 (d, *J* = 16.2 Hz, 1H), 6.83 (d, *J* = 16.2 Hz, 1H), 5.25 (s, 1H), 5.21 (s, 2H), 5.17 (s, 2H), 1.48 (s, 18H).

^{13}C NMR (176 MHz, Chloroform-*d*) δ 153.77, 149.34, 148.56, 137.52, 137.49, 136.26, 132.10, 128.90, 128.63, 128.61, 128.28, 127.95, 127.91, 127.58, 127.45, 125.64, 123.36, 120.14, 115.39, 112.86, 71.62, 71.55, 34.53, 30.45.

IR (Neat): 3617, 2951, 1680, 1595, 1504, 1255, 1133, 1016, 729, 695 cm^{-1};

HRMS (ESI) *m/z* calculated for $NaC_{36}H_{40}O_3^+$ ($[M+Na]^+$) 543.2870, found 543.2873.

^{1}H NMR, 700 MHz, Chloroform-*d*, Stilbene **S6**

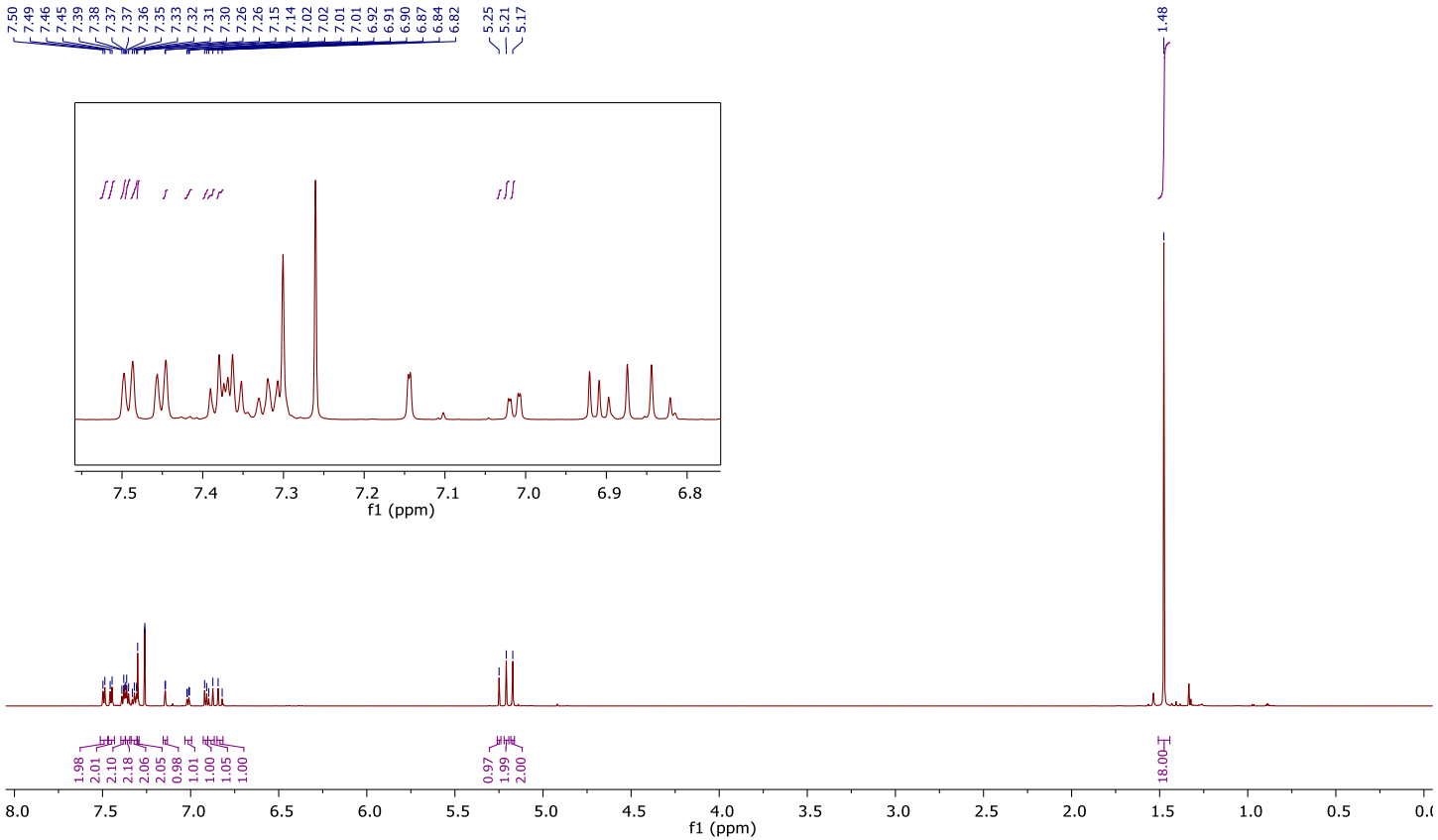

^{13}C NMR, 176 MHz, Chloroform-*d*, Stilbene **S6**

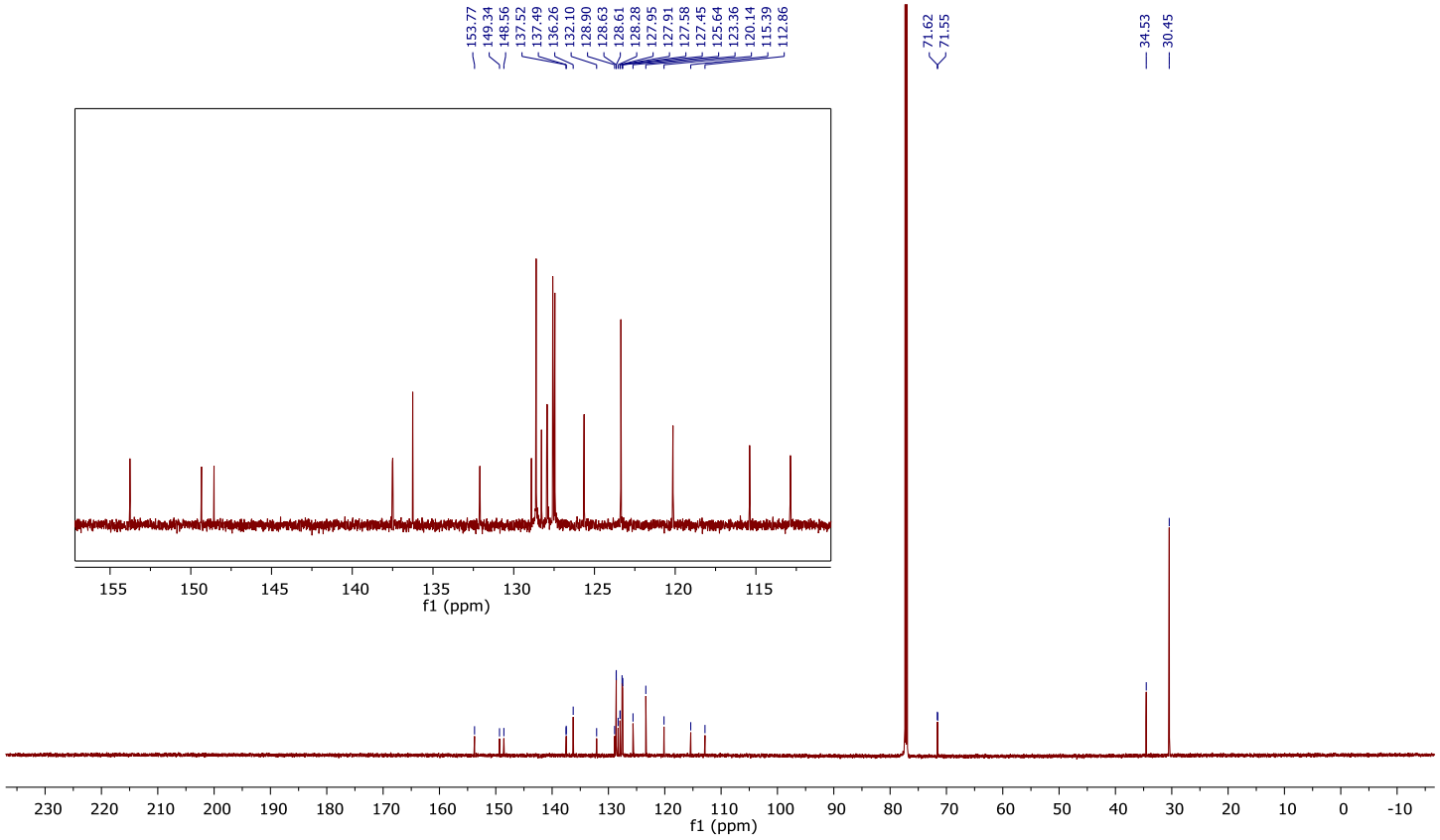

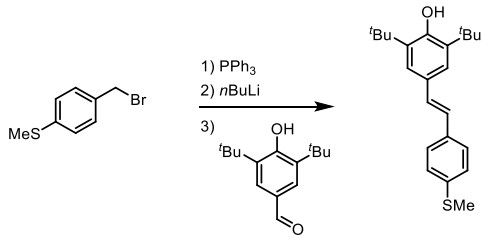

(S7) (*E*)-2,6-di-*tert*-butyl-4-(4-(methylthio)styryl)phenol

Commercially available benzyl bromide ((4-(bromomethyl)phenyl)(methyl)sulfane, 1.0 g, 4.6 mmol) was subjected to the general procedure using toluene as the solvent for the olefination with aldehyde A. The product was purified by column chromatography (2% to 12% ethyl acetate in hexanes) to afford (*E*)-2,6-di-*tert*-butyl-4-(4-(methylthio)styryl)phenol (1.35 g, 82% yield).

R_f = 0.34 (ethyl acetate/hexanes 1:9; UV)

^{1}H NMR (500 MHz, Chloroform-*d*) δ 7.42 (d, *J* = 8.1 Hz, 2H), 7.33 (s, 2H), 7.24 (d, *J* = 8.4 Hz, 2H), 7.04 (d, *J* = 16.2 Hz, 1H), 6.89 (d, *J* = 16.2 Hz, 1H), 5.28 (s, 1H), 2.50 (s, 3H), 1.48 (s, 18H).

^{13}C NMR (126 MHz, Chloroform-*d*) δ 153.96, 137.00, 136.30, 135.20, 129.18, 128.73, 127.04, 126.72, 125.31, 123.50, 34.53, 30.44, 16.18.

IR (Neat): 3616, 2955, 1435, 1249, 1184, 962, 800 cm^{-1};

HRMS (ESI) *m/z* calculated for $C_{23}H_{31}OS^+$ ($[M+H]^+$) 355.2090, found 355.2087.

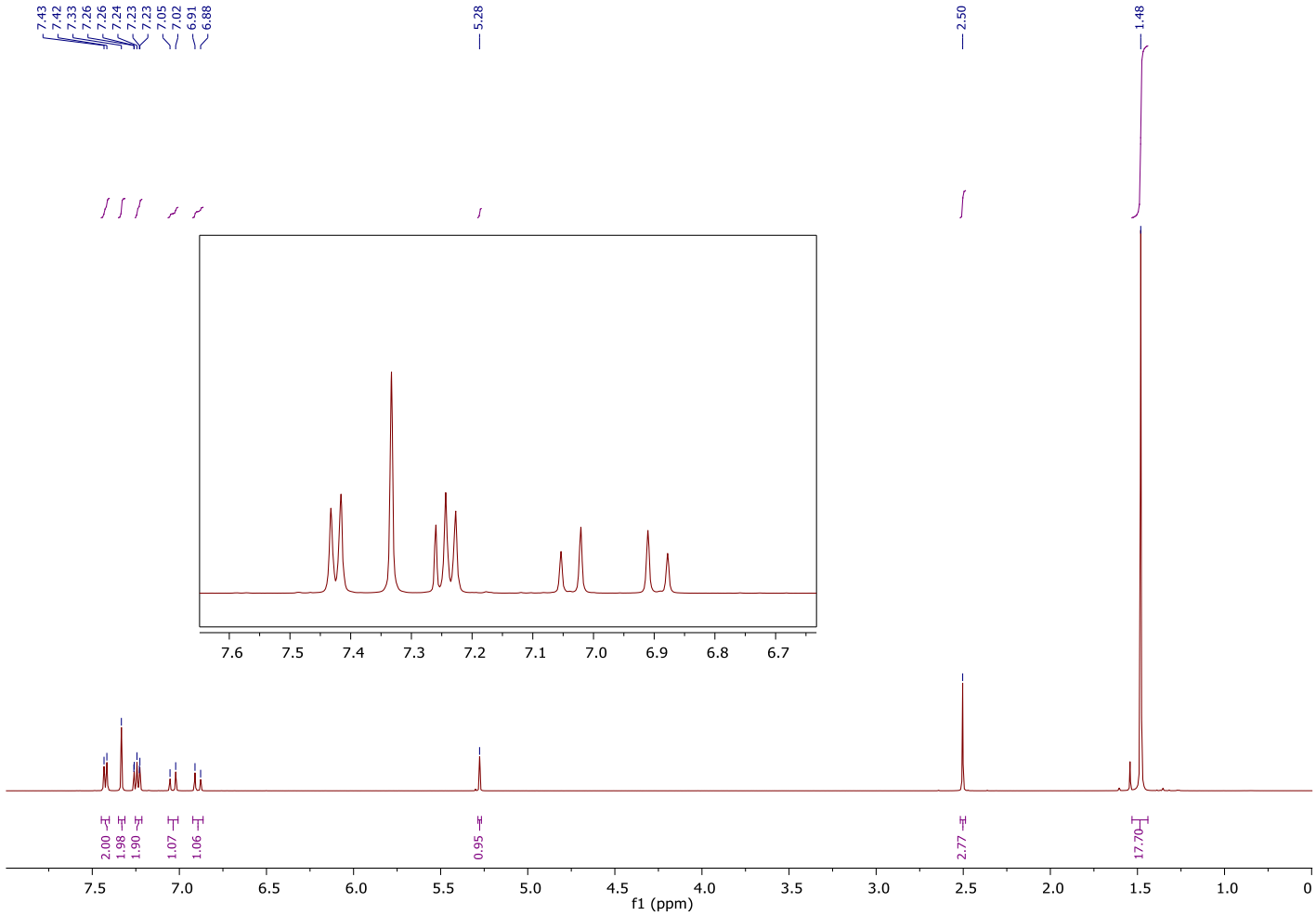
7.43
7.42
7.33
7.26
7.24
7.23
7.23
7.05
7.02
6.91
6.88
5.28
2.50
1.48
7.6
7.5
7.4
7.3
7.2
7.1
7.0
6.9
6.8
6.7
2.00
1.98
1.90
1.07
1.06
0.95
2.77
17.70
7.5
7.0
6.5
6.0
5.5
5.0
4.5
4.0
3.5
3.0
2.5
2.0
1.5
1.0
0
f1 (ppm)

^{13}C NMR, 126 MHz, Chloroform-*d*, Stilbene **S7**

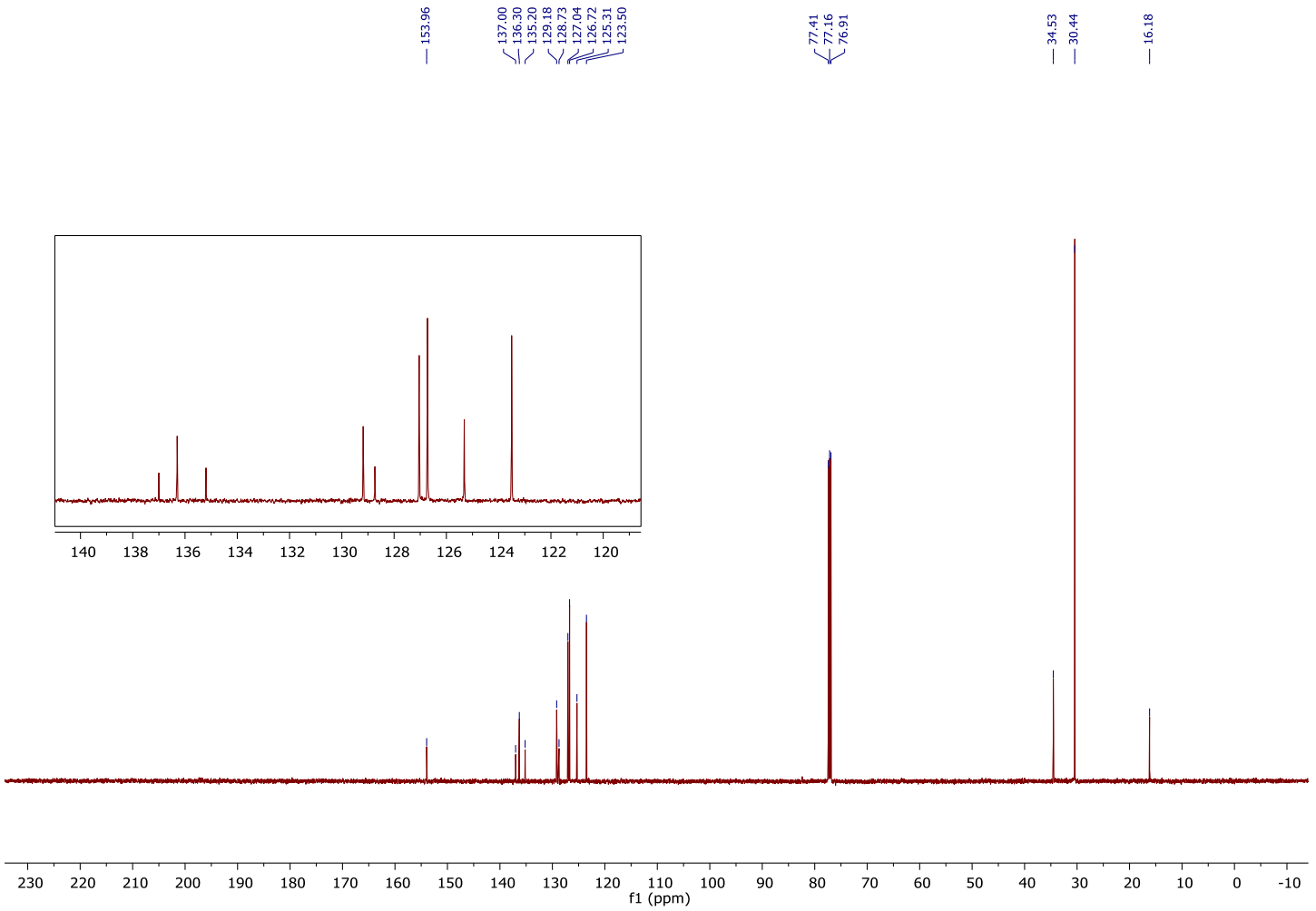

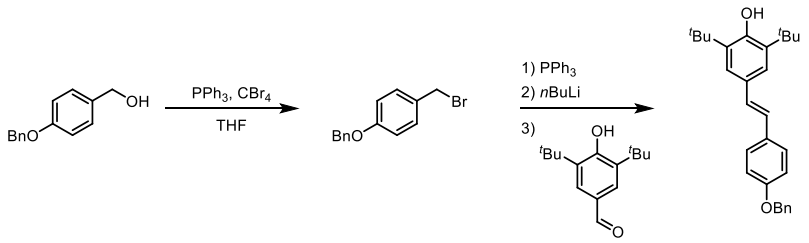

(S8) (*E*)-4-(4-(benzyloxy)styryl)-2,6-di-*tert*-butylphenol

Commercially available benzyl alcohol ((4-(benzyloxy)phenyl)methanol, 1.00g, 4.7 mmol) was subjected to the general procedure using toluene as the solvent for the olefination with aldehyde A. The product was purified by column chromatography (2% to 12% ethyl acetate in hexanes) to afford (*E*)-4-(4-(benzyloxy)styryl)-2,6-di-*tert*-butylphenol (1.52g, 78% yield).

R_f = 0.28(ethyl acetate/hexanes 1:9; UV)

^{1}H NMR (500 MHz, Chloroform-*d*) δ 7.44 (d, *J* = 7.1 Hz, 2H), 7.44 (d, *J* = 8.6 Hz, 2H), 7.40 (t, *J* = 7.6 Hz, 2H), 7.33 (t, *J* = 7.3 Hz, 1H), 7.32 (s, 2H), 6.96 (d, *J* = 8.6 Hz, 2H), 6.95 (d, *J* = 16.2 Hz, 1H), 6.89 (d, *J* = 16.3 Hz, 1H), 5.25 (s, 1H), 5.09 (s, 2H), 1.48 (s, 18H).

^{13}C NMR (126 MHz, Chloroform-*d*) δ 158.20, 153.69, 137.16, 136.24, 131.21, 129.05, 128.73, 128.11, 127.83, 127.63, 127.48, 125.53, 123.30, 115.17, 70.22, 34.53, 30.45.

IR (Neat): 3628, 2953, 1606, 1510, 1465, 1233, 1175, 1010, 954, 745 cm^{-1};

HRMS (ESI) *m/z* calculated for $C_{29}H_{35}O_2^+$ ([M+H]$^+$) 415.2632, found 415.2632.

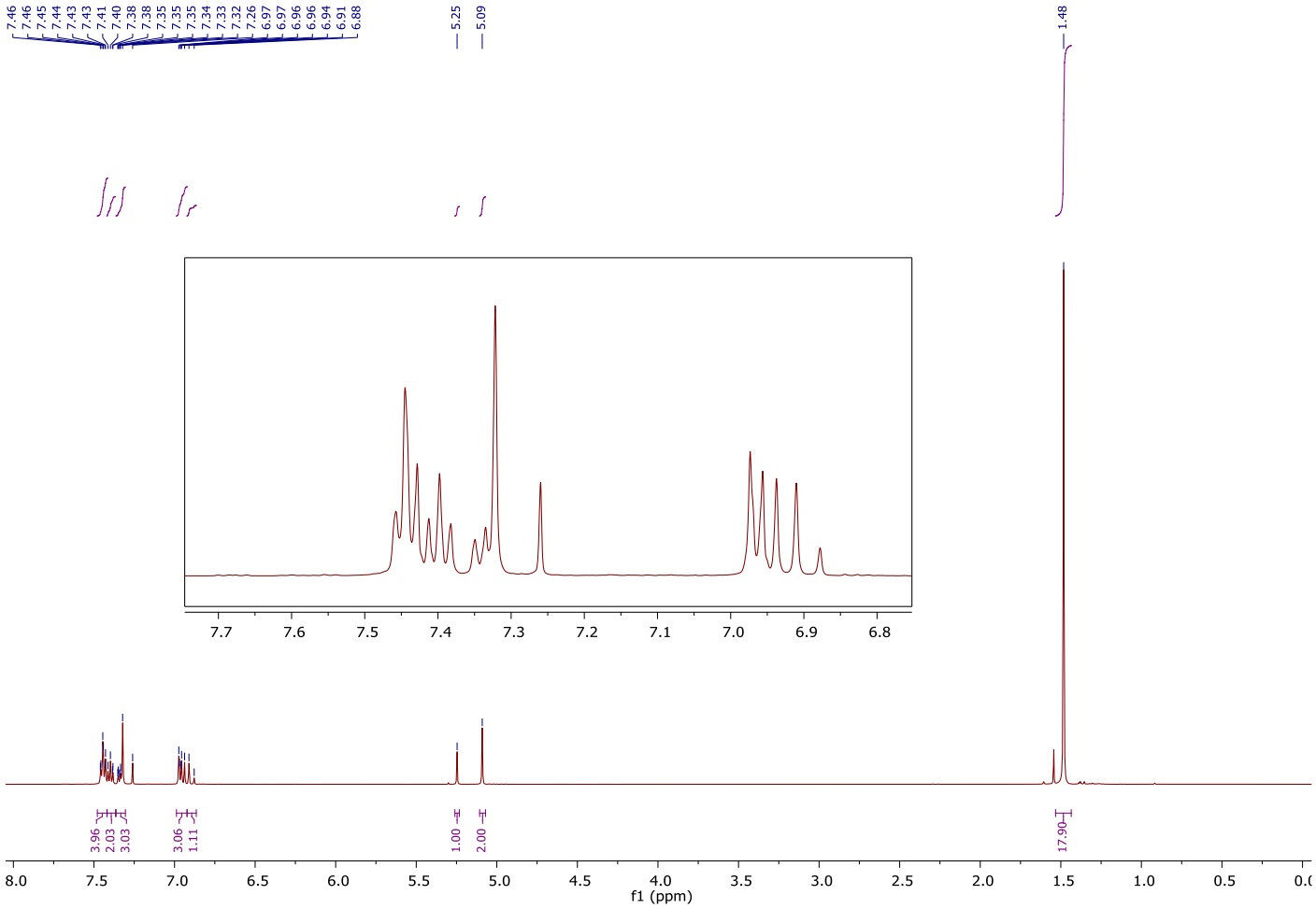
7.46
7.46
7.45
7.44
7.43
7.43
7.41
7.40
7.38
7.38
7.35
7.35
7.35
7.34
7.33
7.32
7.26
6.97
6.97
6.96
6.96
6.94
6.91
6.88
5.25
5.09
1.48
7.7
7.6
7.5
7.4
7.3
7.2
7.1
7.0
6.9
6.8
3.96
2.03
3.03
3.06
1.11
1.00
2.00
17.90
8.0
7.5
7.0
6.5
6.0
5.5
5.0
4.5
4.0
3.5
3.0
2.5
2.0
1.5
1.0
0.5
f1 (ppm)

^{13}C NMR, 126 MHz, Chloroform-*d*, Stilbene **S8**

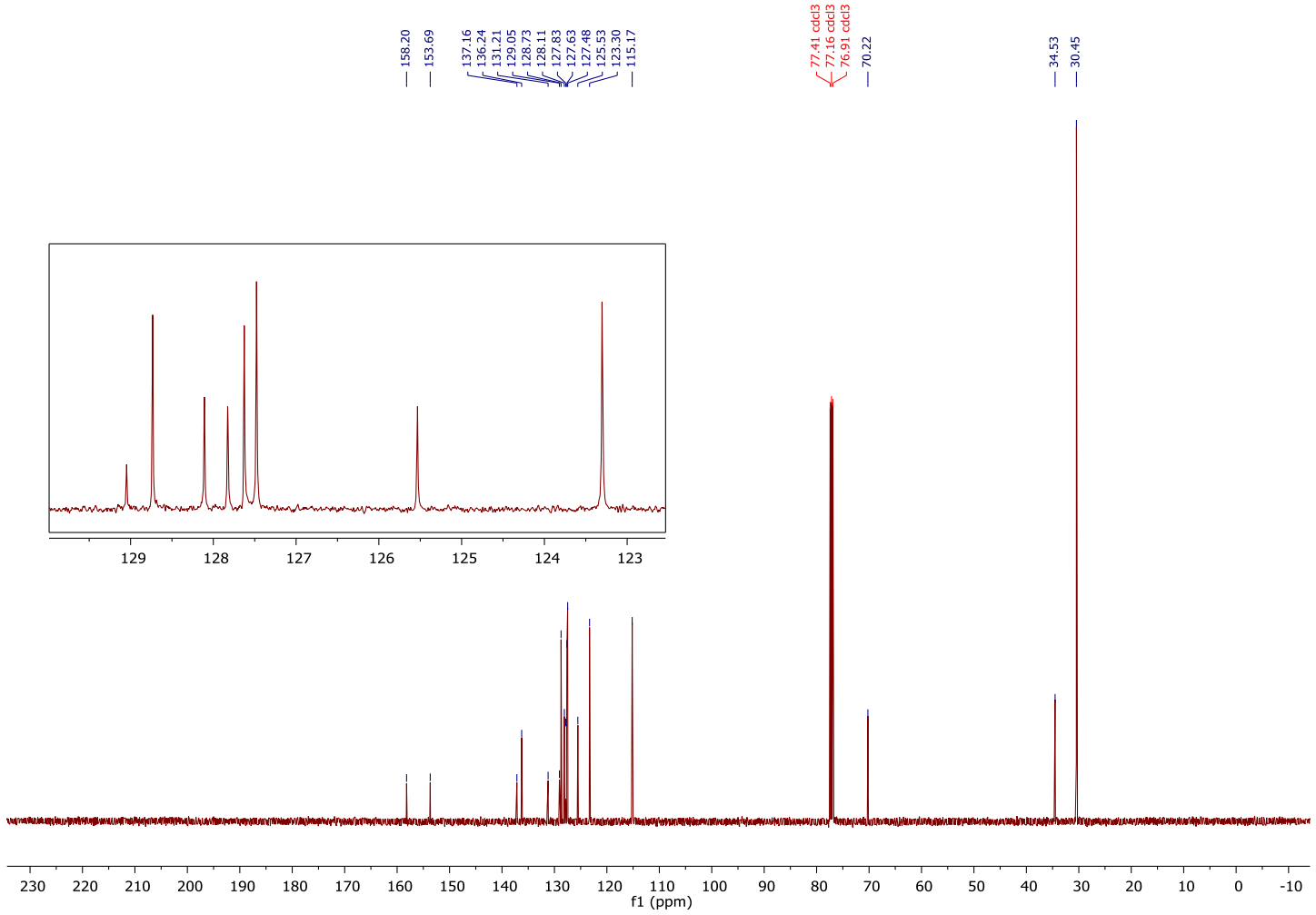

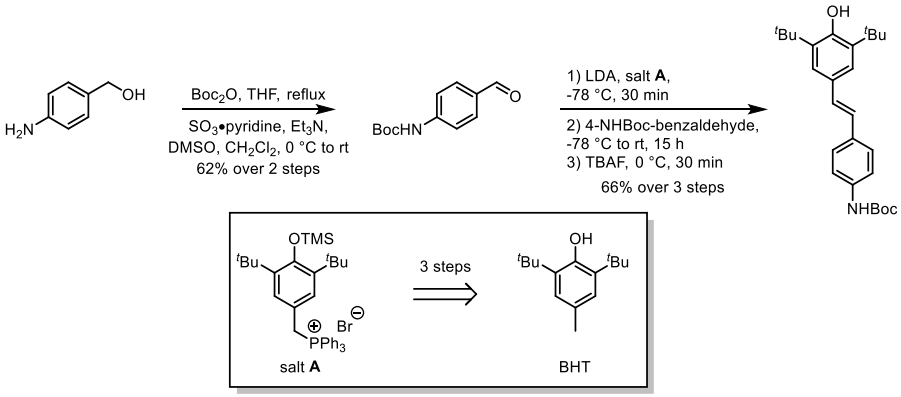

(S9) *tert*-butyl (*E*)-(4-(3,5-di-*tert*-butyl-4-hydroxystyryl)phenyl)carbamate

Freshly distilled diisopropylamine (3.41 mmol, 478 μL) was added to a flame-dried heart-shaped flask, dissolved in freshly distilled THF (10 mL), and cooled to -78 °C. To the stirring solution was added *n*BuLi (3.28 mmol, 1.31 mL, 2.5 M), and the solution was allowed to stir at the same temperature for 30 min. Meanwhile, in a 3-neck round bottom flask, the phosphonium salt **A** (3.28 mmol, 2.08 g) was suspended in freshly distilled THF (25 mL) and cooled to -78 °C. The freshly prepared LDA solution was added to the phosphonium salt suspension via cannula, and the ylid was allowed to form at the same temperature for 30 min, turning the solution deep red. To a flame-dried heart-shaped flask was added 4-NHBoc-benzaldehyde (2.62 mmol, 580 mg, available in 2 steps via Boc protection and oxidation), and the solid was dissolved in THF (10 mL). The aldehyde solution was added to the ylid via cannula, and the reaction was allowed to warm to room temperature overnight (~15 hours). The reaction was subsequently cooled to 0 °C, and a solution of TBAF (3.28 mmol, 3.28 mL, 1.0 M) was added. The desilylation was allowed to occur for 30 min, at which point the reaction was quenched via the addition of saturated ammonium chloride, diluted with EtOAc, and added to a separatory funnel containing deionized water. The layers were separated, and the aqueous layer was extracted with additional portions of EtOAc. The combined organic layers were washed with brine, dried over magnesium sulfate, and concentrated under reduced pressure. The crude product was purified by flash column chromatography (20% to 100% CH_2Cl_2 in Hexanes) to afford the stilbene product (1.00 g, 90% yield).

R_f = 0.30 (CH_2Cl_2/hexanes 3:1; UV)

^{1}H NMR (700 MHz, Chloroform-*d*) δ 7.43 (d, *J* = 8.4 Hz, 2H), 7.34 (d, *J* = 8.3 Hz, 2H), 7.32 (s, 2H), 6.98 (d, *J* = 16.2 Hz, 1H), 6.89 (d, *J* = 16.2 Hz, 1H), 6.47 (s, 1H), 5.26 (s, 1H), 1.53 (s, 9H), 1.47 (s, 18H).

^{13}C NMR (176 MHz, Chloroform-*d*) δ 153.79, 152.77, 137.31, 136.22, 133.06, 128.87, 128.36, 126.93, 125.42, 123.39, 118.69, 80.71, 34.52, 30.43, 28.50.

IR (Neat): 3623, 3325, 2957, 1709, 1600, 1521, 1234, 1153, 1051, 740 cm^{-1};

HRMS (ESI) *m/z* calculated for $NaC_{27}H_{37}NO_3^+$ ($[M+Na]^+$) 446.2666, found 446.2660.

^{1}H NMR, 700 MHz, Chloroform-*d*, Stilbene **S9**

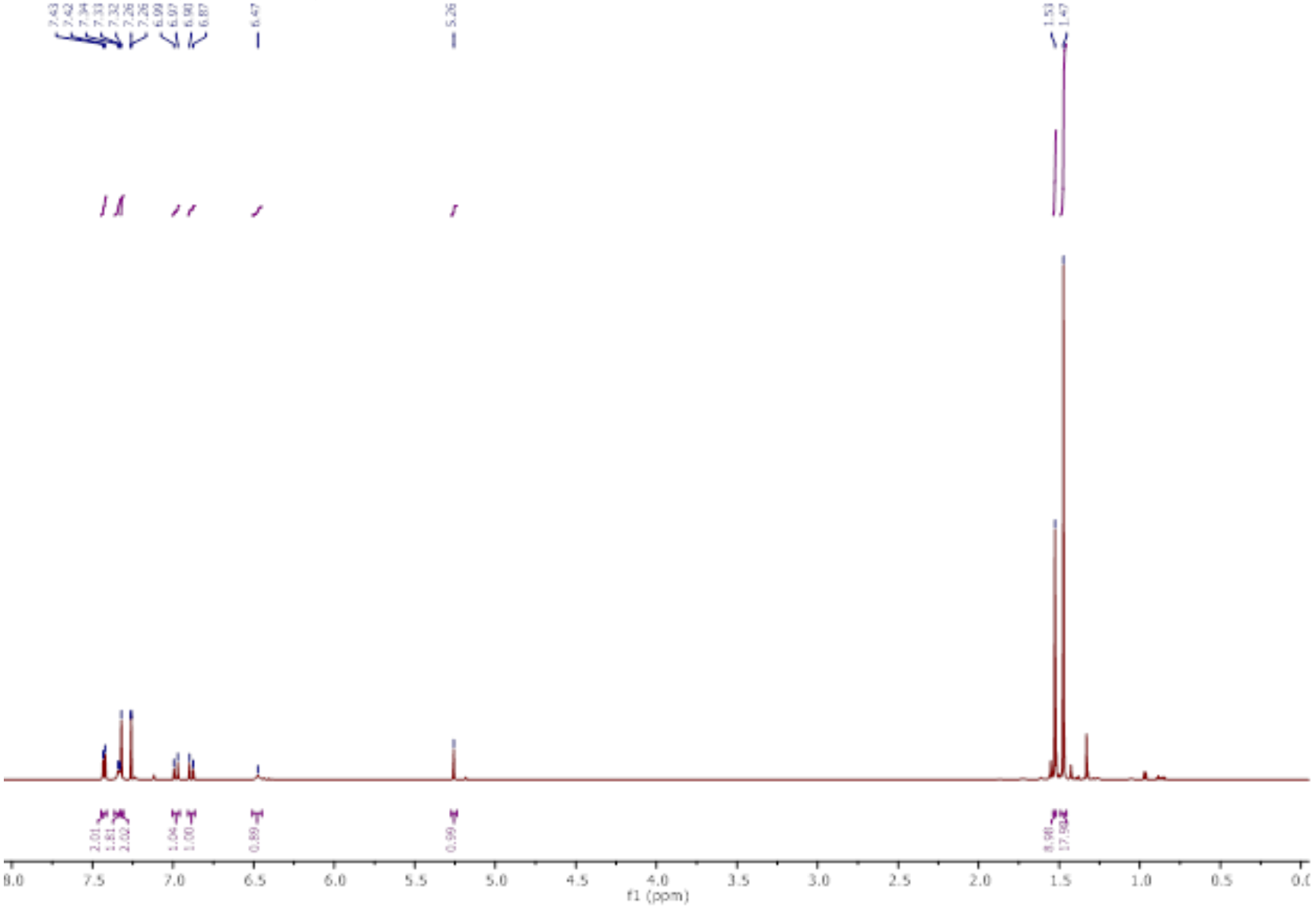

^{13}C NMR, 176 MHz, Chloroform-*d*, Stilbene **S9**

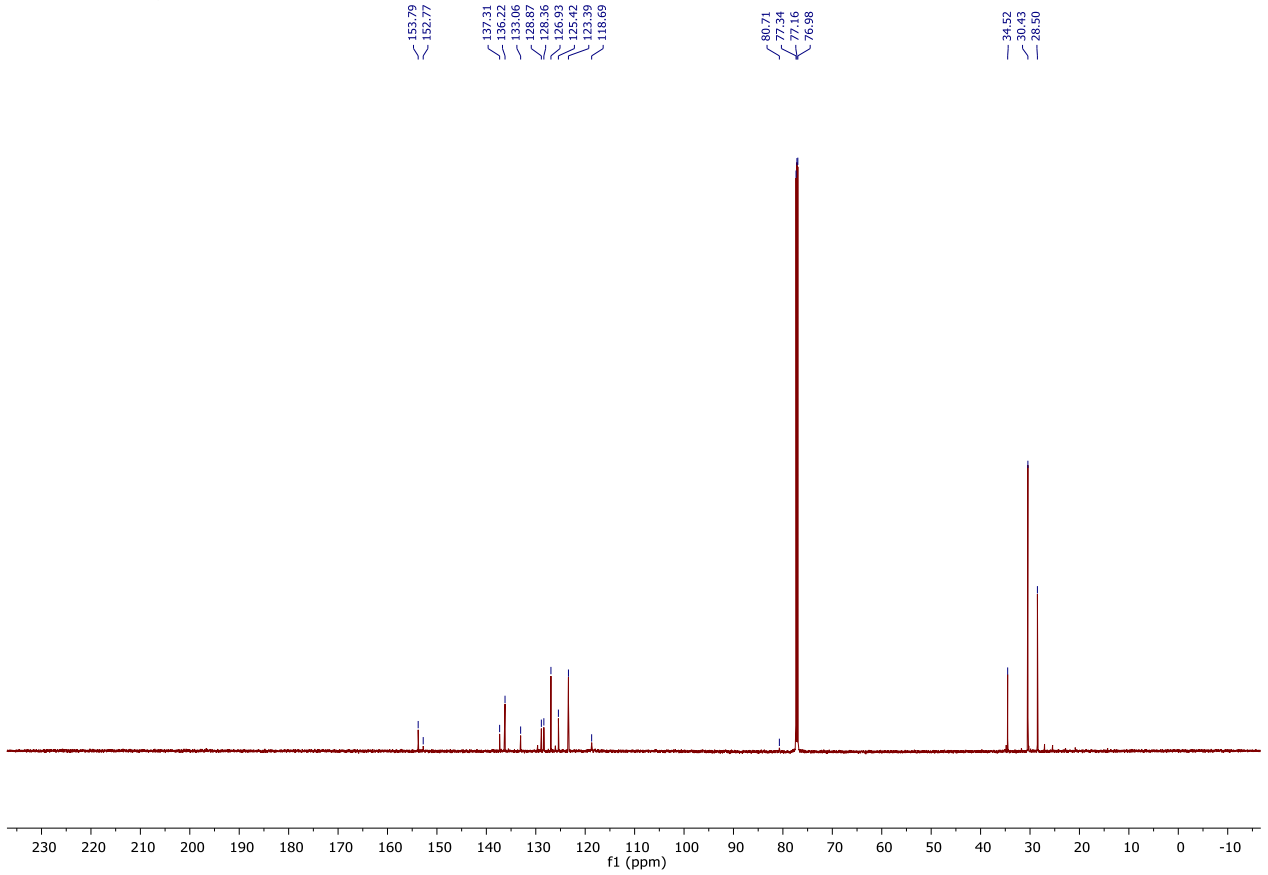

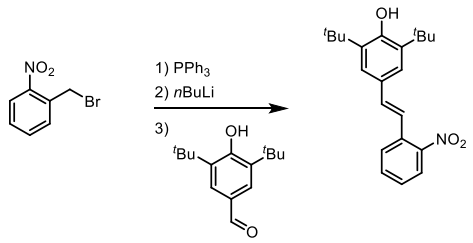

(S10) (*E*)-2,6-di-*tert*-butyl-4-(2-nitrostyryl)phenol

Commercially available benzyl bromide (1-(bromomethyl)-2-nitrobenzene, 1.0 g, 4.6 mmol) was subjected to the general procedure using toluene as the solvent for the olefination. The product was purified by column chromatography (2% to 12% ethyl acetate in hexanes) to afford (*E*)-2,6-di-*tert*-butyl-4-(2-nitrostyryl)phenol (927 mg, 57% yield).

R_f = 0.38 (ethyl acetate/hexanes 1:9; UV)

^{1}H NMR (700 MHz, Chloroform-*d*) δ 7.94 (d, *J* = 8.1 Hz, 1H), 7.76 (d, *J* = 7.9 Hz, 1H), 7.57 (t, *J* = 7.6 Hz, 1H), 7.44 (d, *J* = 16.0 Hz, 1H), 7.37 (s, 3H), 7.36 (t, *J* = 7.7 Hz, 3H), 7.07 (d, *J* = 16.0 Hz, 1H), 5.38 (s, 1H), 1.48 (s, 18H).

^{13}C NMR (176 MHz, Chloroform-*d*) δ 154.83, 147.95, 136.44, 135.03, 133.80, 133.07, 128.09, 128.05, 127.40, 124.91, 124.29, 120.65, 34.52, 30.38.

IR (Neat): 3626, 2961, 1626, 1603, 1515, 1348, 1233, 1150, 965, 742 cm^{-1};

HRMS (ESI) *m/z* calculated for $C_{22}H_{28}NO_3^+$ ($[M+H]^+$) 354.2064, found 354.2064.

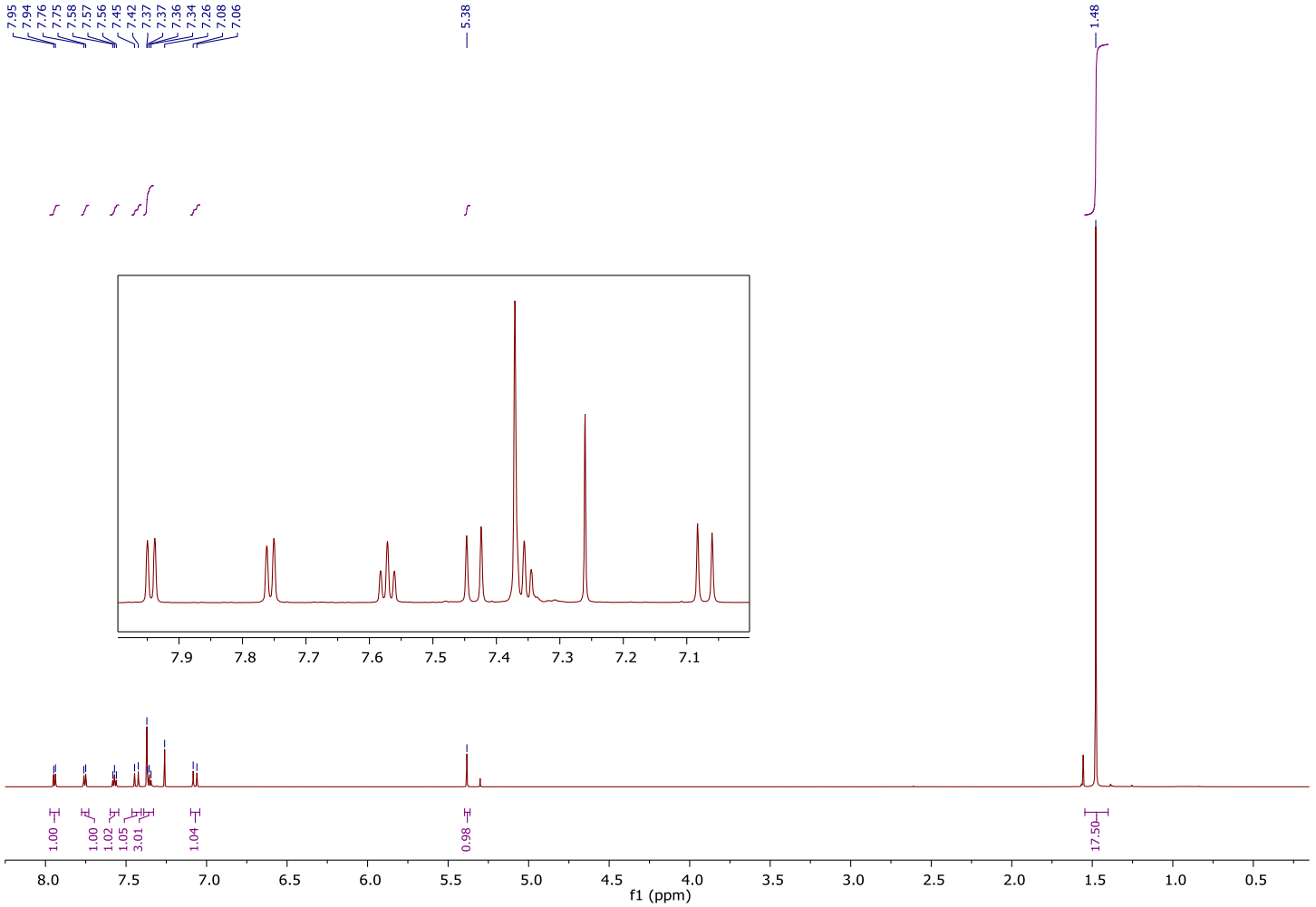
7.95
7.94
7.76
7.75
7.58
7.57
7.56
7.45
7.42
7.37
7.37
7.36
7.34
7.26
7.08
7.06
5.38
1.48
7.9
7.8
7.7
7.6
7.5
7.4
7.3
7.2
7.1
1.00
1.00
1.02
1.05
3.01
1.04
0.98
17.50
8.0
7.5
7.0
6.5
6.0
5.5
5.0
4.5
4.0
3.5
3.0
2.5
2.0
1.5
1.0
0.5
f1 (ppm)

^{13}C NMR, 176 MHz, Chloroform-*d*, Stilbene **S10**

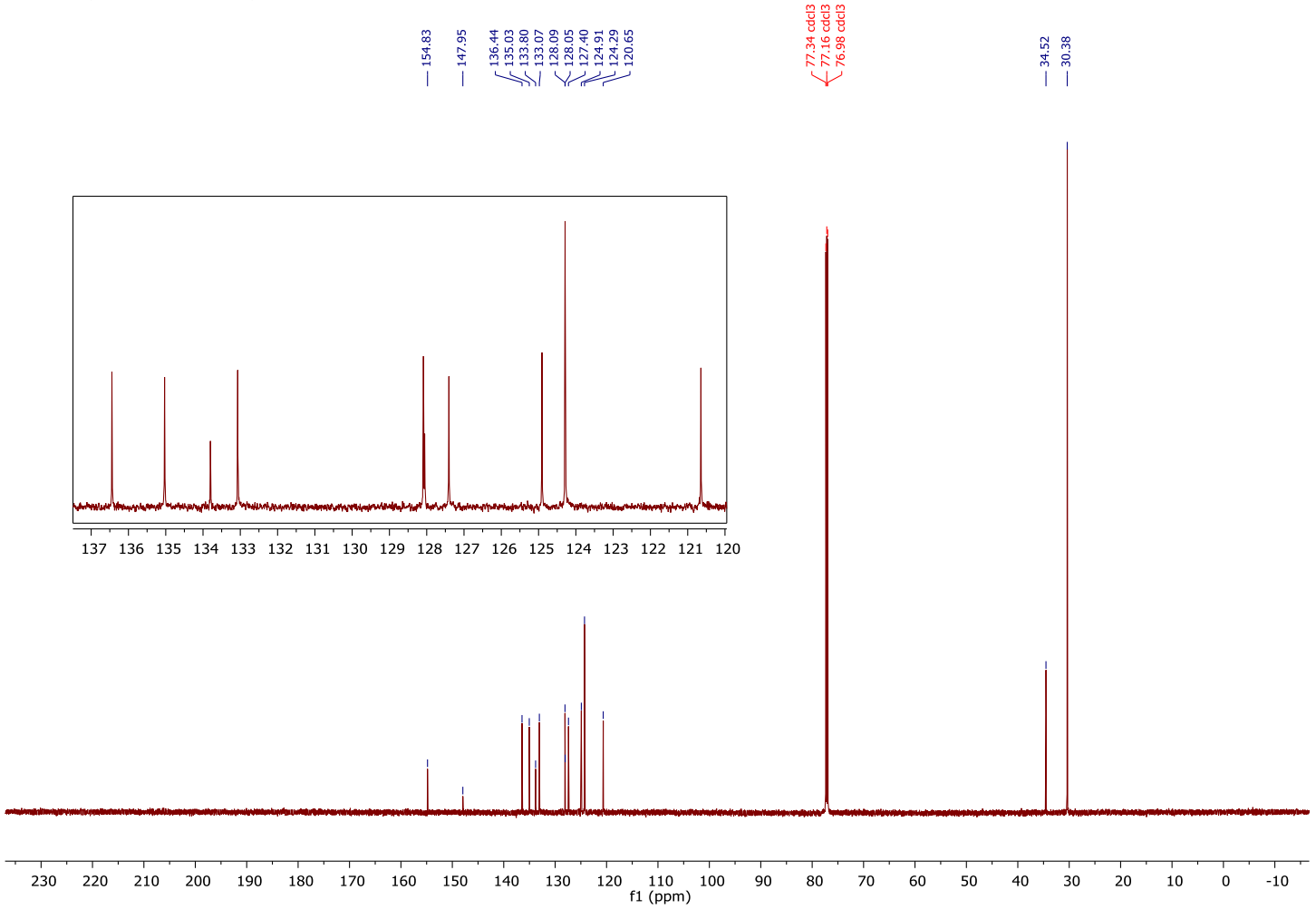

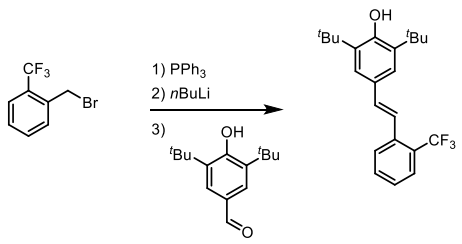

(S11) (*E*)-2,6-di-*tert*-butyl-4-(2-(trifluoromethyl)styryl)phenol

Commercially available benzyl bromide (1-(bromomethyl)-2-(trifluoromethyl)benzene, 0.79 g, 3.29 mmol) was subjected to the general procedure using THF as the solvent for the olefination. The product was purified by column chromatography (2% to 12% ethyl acetate in hexanes) to afford (*E*)-2,6-di-*tert*-butyl-4-(2-(trifluoromethyl)styryl)phenol (989 mg, 73% yield).

R_f = 0.40 (ethyl acetate/hexanes 1:9; UV)

^{1}H NMR (700 MHz, Chloroform-*d*) δ 7.76 (d, *J* = 7.9 Hz, 1H), 7.66 – 7.63 (m, 1H), 7.51 (t, *J* = 7.6 Hz, 1H), 7.37 (s, 2H), 7.33 – 7.28 (m, 2H), 7.04 (d, *J* = 16.0 Hz, 1H), 5.34 (s, 1H), 1.48 (s, 18H).

^{13}C NMR (176 MHz, Chloroform-*d*) δ 154.48, 137.16, 136.34, 133.57, 131.92, 128.37, 127.32 (q, $J_{C\text{-}F}$ = 29 Hz), 126.90, 126.71, 125.99 (q, $J_{C\text{-}F}$ = 6.2 Hz), 124.66 (q, $J_{C\text{-}F}$ = 275 Hz), 124.03, 121.71, 34.50, 30.36.

IR (Neat): 3636, 2956, 1435, 1422, 1308, 1122, 1035, 960, 753 cm^{-1};

HRMS (ESI) *m/z* calculated for $C_{23}H_{28}F_3O^+$ ($[M+H]^+$) 377.2087, found 377.2084.

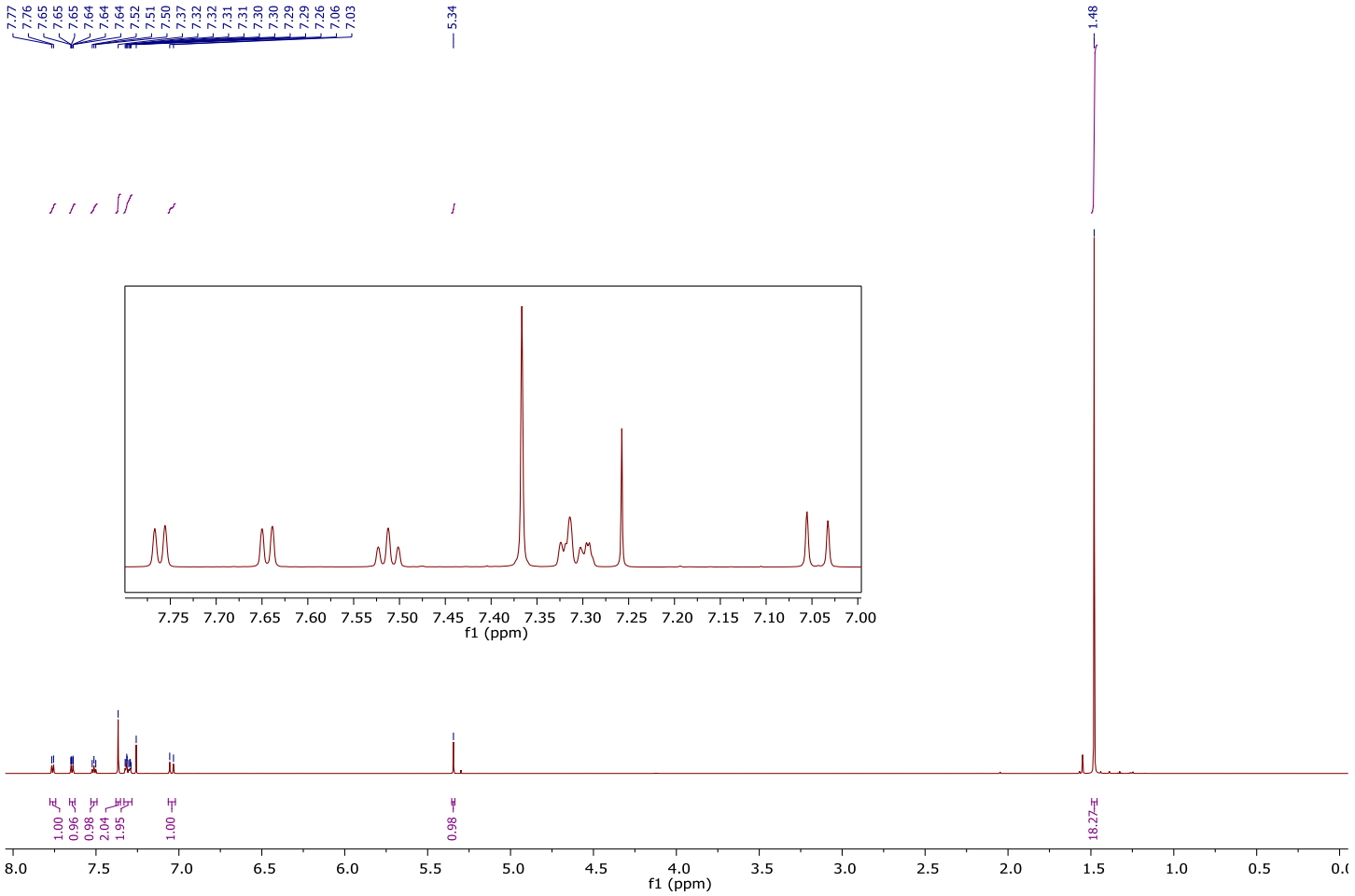
7.77
7.76
7.65
7.65
7.65
7.64
7.64
7.64
7.52
7.51
7.50
7.37
7.32
7.32
7.31
7.31
7.30
7.30
7.29
7.29
7.26
7.06
7.03
5.34
1.48
7.75 7.70 7.65 7.60 7.55 7.50 7.45 7.40 7.35 7.30 7.25 7.20 7.15 7.10 7.05 7.00
f1 (ppm)
1.00
0.96
0.98
2.04
1.95
1.00
0.98
18.27
8.0 7.5 7.0 6.5 6.0 5.5 5.0 4.5 4.0 3.5 3.0 2.5 2.0 1.5 1.0 0.5
f1 (ppm)

^{13}C NMR, 176 MHz, Chloroform-*d*, Stilbene **S11**

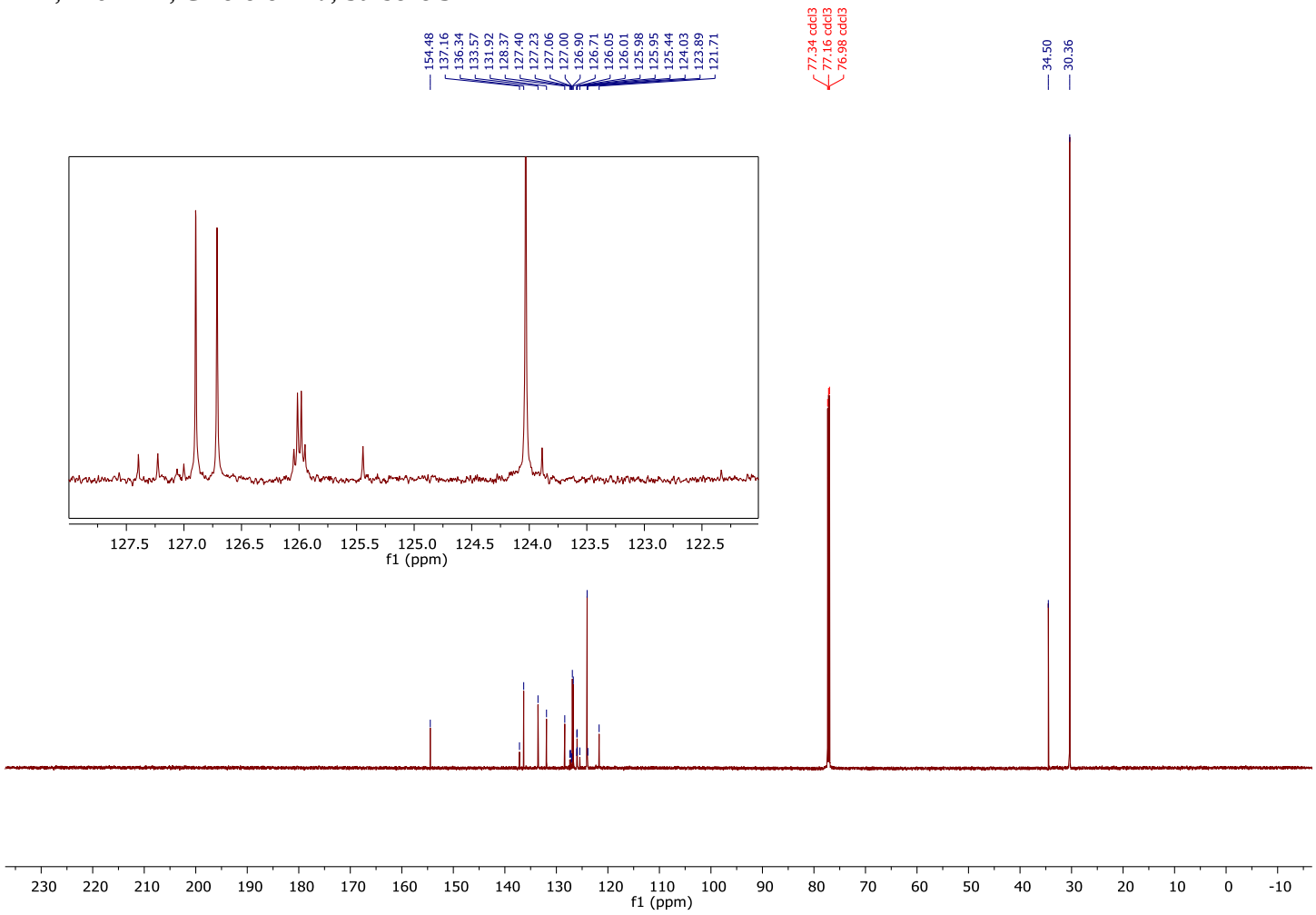

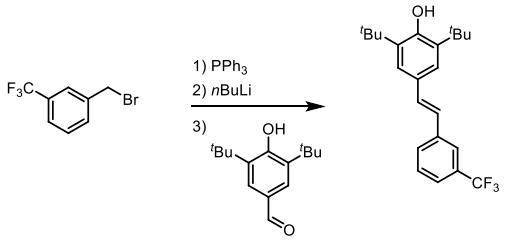

(S12) (*E*)-2,6-di-*tert*-butyl-4-(3-(trifluoromethyl)styryl)phenol

Commercially available benzyl bromide (1-(bromomethyl)-3-(trifluoromethyl)benzene, 0.78 g, 3.25 mmol) was subjected to the general procedure using THF as the solvent for the olefination. The product was purified by column chromatography (2% to 12% ethyl acetate in hexanes) to afford (*E*)-2,6-di-*tert*-butyl-4-(3-(trifluoromethyl)styryl)phenol (1.06 g, 87% yield).

R_f = 0.40 (ethyl acetate/hexanes 1:9; UV)

^{1}H NMR (700 MHz, Chloroform-*d*) δ 7.73 (s, 1H), 7.66 (dd, *J* = 7.0, 1.9 Hz, 1H), 7.48 – 7.42 (m, 2H), 7.36 (s, 2H), 7.14 (d, *J* = 16.2 Hz, 1H), 6.95 (d, *J* = 16.2 Hz, 1H), 5.34 (s, 1H), 1.48 (s, 18H).

^{13}C NMR (176 MHz, Chloroform-*d*) δ 154.42, 138.85, 136.38, 131.48, 131.13 (q, J_{C-F} = 32 Hz), 129.33, 129.14, 128.11, 124.37 (q, J_{C-F} = 273 Hz), 124.33, 123.82, 123.51 (q, J_{C-F} = 3.5 Hz), 122.88 (q, J_{C-F} = 3.5 Hz), 34.54, 30.41.

IR (Neat): 3639, 2957, 1655, 1437, 1328, 1163, 1121, 1073 cm^{-1};

HRMS (ESI) *m/z* calculated for $C_{23}H_{28}F_3O^+$ ($[M+H]^+$) 377.2087, found 377.2093.

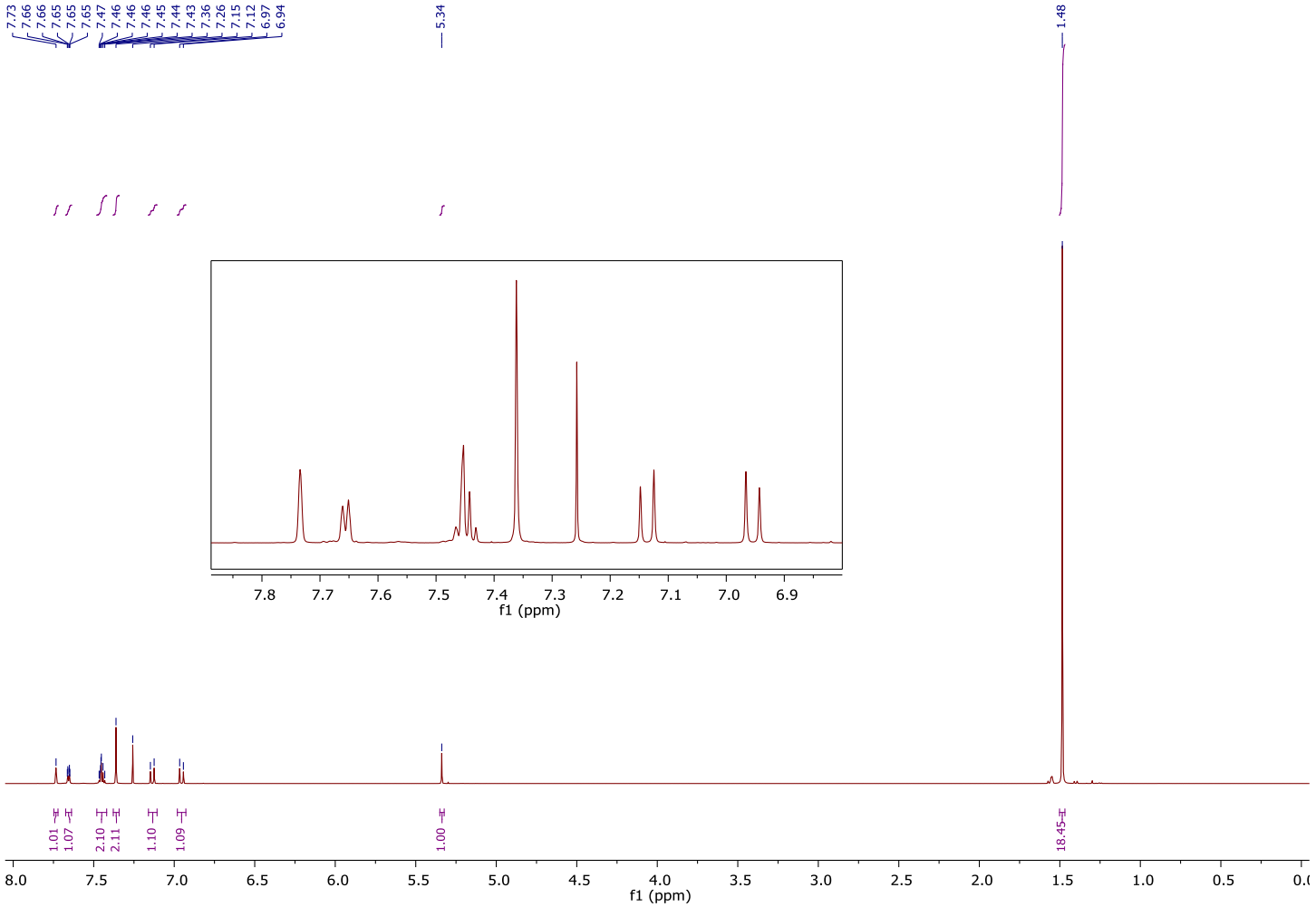
7.73
7.66
7.66
7.65
7.65
7.65
7.47
7.46
7.46
7.46
7.45
7.44
7.43
7.36
7.26
7.15
7.12
6.97
6.94
5.34
1.48
7.8
7.7
7.6
7.5
7.4
7.3
7.2
7.1
7.0
6.9
f1 (ppm)
1.01
1.07
2.10
2.11
1.10
1.09
1.00
18.45
8.0
7.5
7.0
6.5
6.0
5.5
5.0
4.5
4.0
3.5
3.0
2.5
2.0
1.5
1.0
0.5
f1 (ppm)

^{13}C NMR, 176 MHz, Chloroform-*d*, Stilbene **S12**

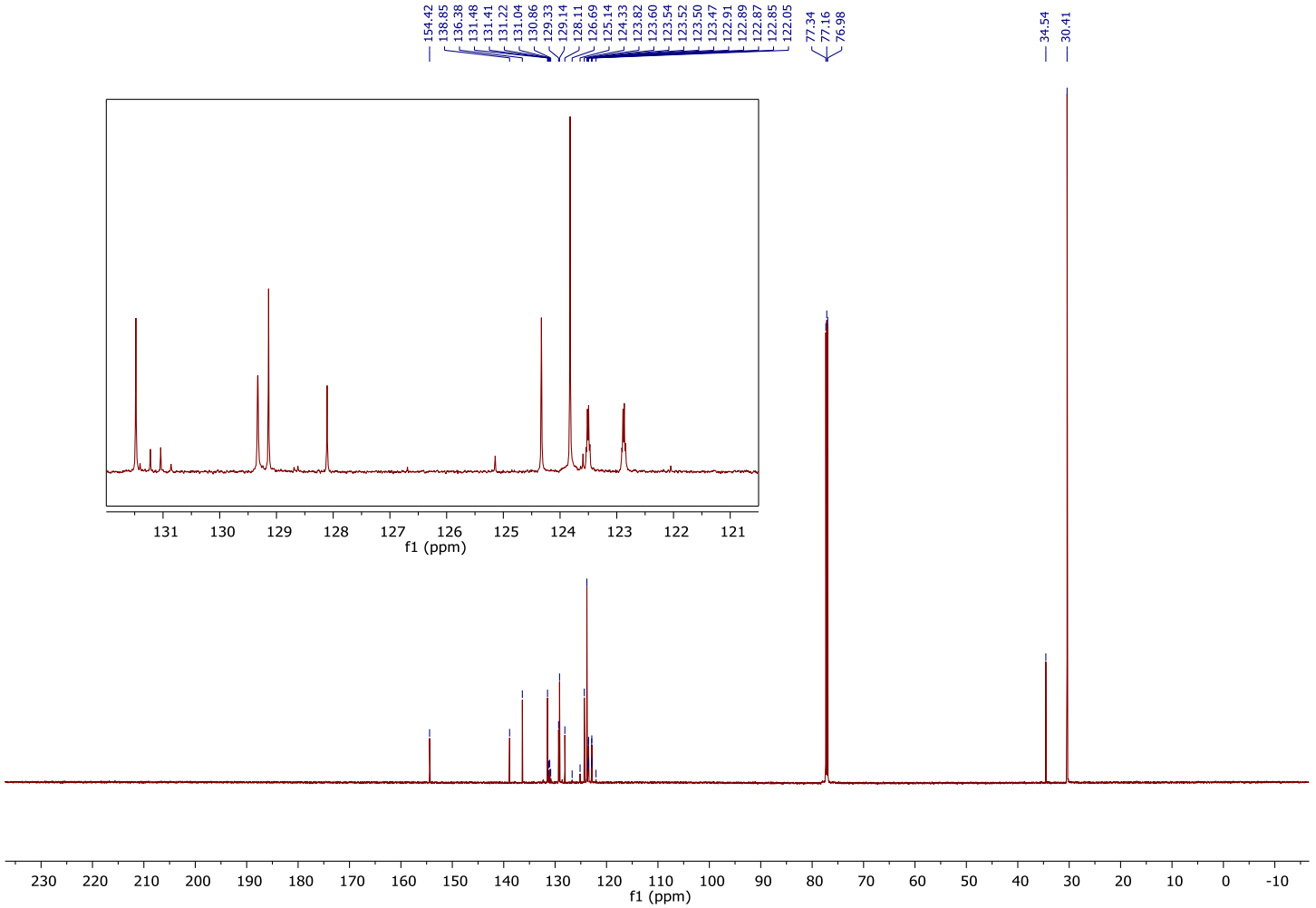

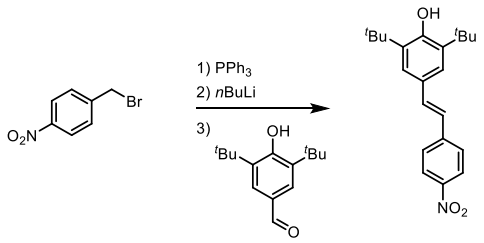

(S13) (*E*)-2,6-di-*tert*-butyl-4-(4-nitrostyryl)phenol

Commercially available benzyl bromide (1-(bromomethyl)-4-nitrobenzene, 1.0 g, 4.6 mmol) was subjected to the general procedure using toluene as the solvent for the olefination with aldehyde A. The product was purified by column chromatography (2% to 12% ethyl acetate in hexanes) to afford (*E*)-2,6-di-*tert*-butyl-4-(4-nitrostyryl)phenol (990 mg, 61% yield).

R_f = 0.38 (ethyl acetate/hexanes 1:9; UV)

^{1}H NMR (500 MHz, Chloroform-*d*) δ 8.20 (d, *J* = 8.5 Hz, 2H), 7.60 (d, *J* = 8.6 Hz, 2H), 7.38 (s, 2H), 7.24 (d, *J* = 16.1 Hz, 2H), 6.97 (d, *J* = 16.2 Hz, 1H), 5.41 (s, 1H), 1.48 (s, 18H).

^{13}C NMR (126 MHz, Chloroform-*d*) δ 155.07, 146.40, 144.77, 136.56, 134.49, 127.69, 126.53, 124.29, 123.44, 34.56, 30.39.

IR (Neat) 3618, 2955, 1629, 1595, 1505, 1428, 1332, 1117, 973, 861, 748 cm^{-1};

HRMS (ESI) *m/z* calculated for $C_{22}H_{28}NO_3^+$ ($[M+H]^+$) 354.2064, found 354.2068.

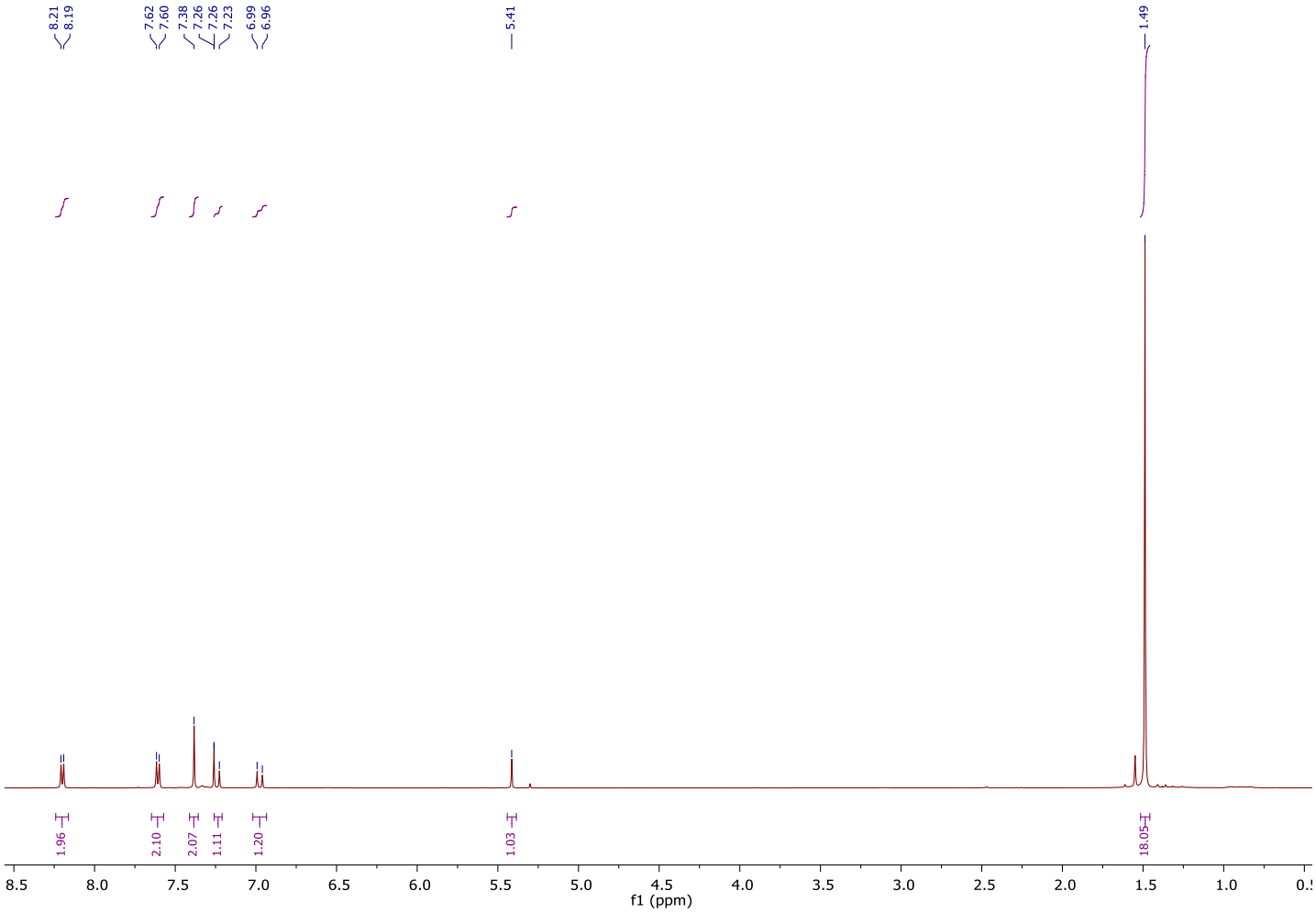
8.21
8.19
7.62
7.60
7.38
7.26
7.26
7.23
6.99
6.96
5.41
1.49
1.96
2.10
2.07
1.11
1.20
1.03
18.05
8.5
8.0
7.5
7.0
6.5
6.0
5.5
5.0
4.5
4.0
3.5
3.0
2.5
2.0
1.5
1.0
f1 (ppm)

^{13}C NMR, 126 MHz, Chloroform-*d*, Stilbene **S13**

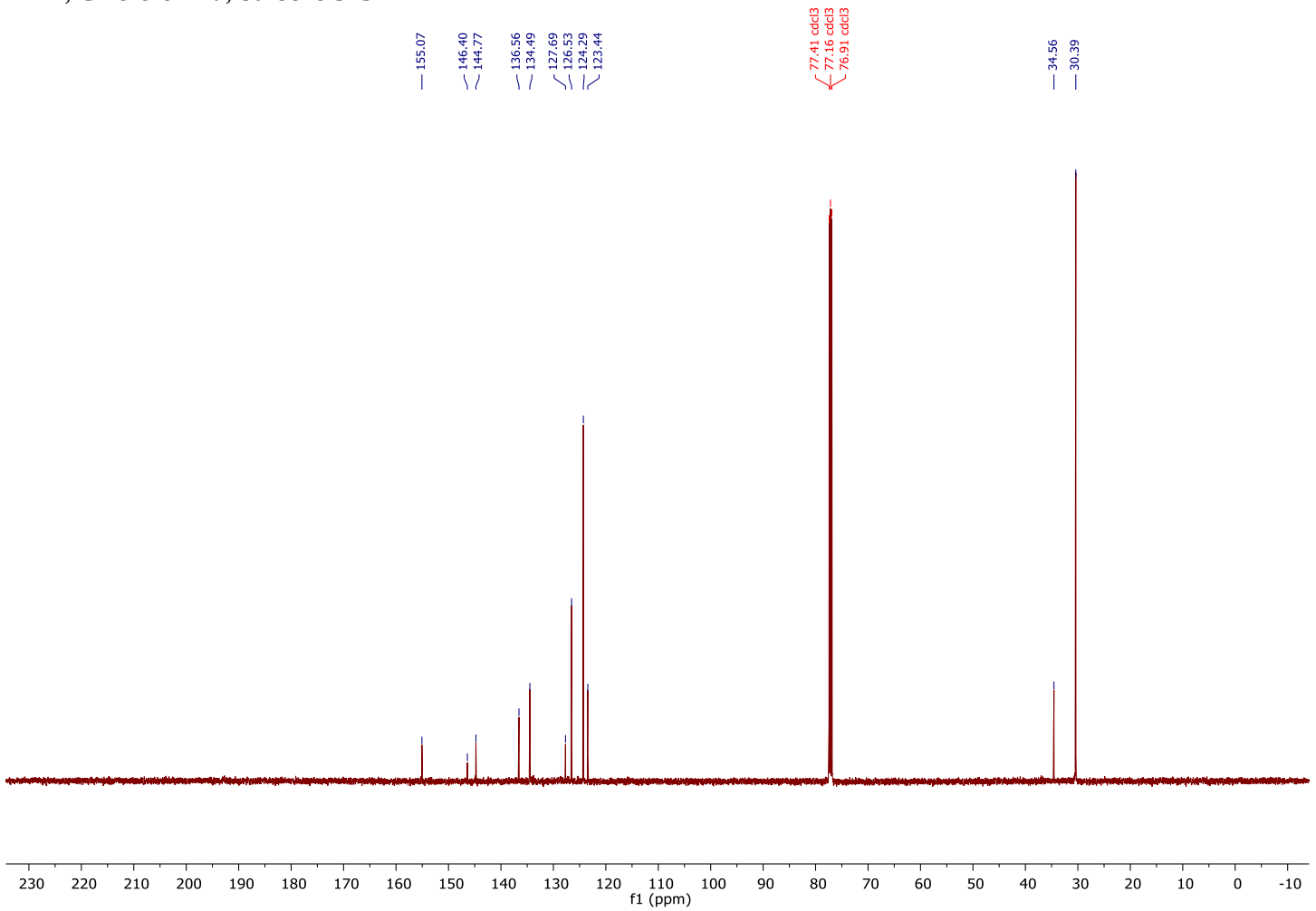

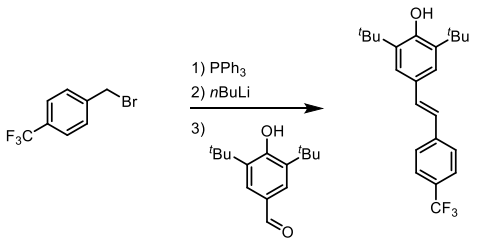

(S14) (*E*)-2,6-di-*tert*-butyl-4-(4-(trifluoromethyl)styryl)phenol

Commercially available benzyl bromide (1-(bromomethyl)-4-(trifluoromethyl)benzene, 1.0 g, 4.18 mmol) was subjected to the general procedure using THF as the solvent for the olefination. The product was purified by column chromatography (2% to 12% ethyl acetate in hexanes) to afford (*E*)-2,6-di-*tert*-butyl-4-(4-(trifluoromethyl)styryl)phenol (1.15 g, 77% yield).

R_f = 0.40 (ethyl acetate/hexanes 1:9; UV)

^{1}H NMR (700 MHz, Chloroform-*d*) δ 7.58 (s, 4H), 7.36 (s, 2H), 7.16 (d, *J* = 16.3 Hz, 1H), 6.95 (d, *J* = 16.2 Hz, 1H), 5.35 (s, 1H), 1.49 (s, 18H).

^{13}C NMR (176 MHz, Chloroform-*d*) δ 154.56, 141.63, 136.43, 132.26, 128.71 (q, *J* = 32 Hz), 128.11, 126.33, 125.68 (q, *J* = 3.5 Hz), 124.52 (q, *J* = 271 Hz), 124.32, 123.93, 34.54, 30.41.

IR (Neat): 3636, 2955, 1435, 1422, 1308, 1122, 1035, 960, 753 cm^{-1};

HRMS (ESI) *m/z* calculated for $C_{23}H_{28}F_3O^+$ ([M+H]$^+$) 377.2087, found 377.2084.

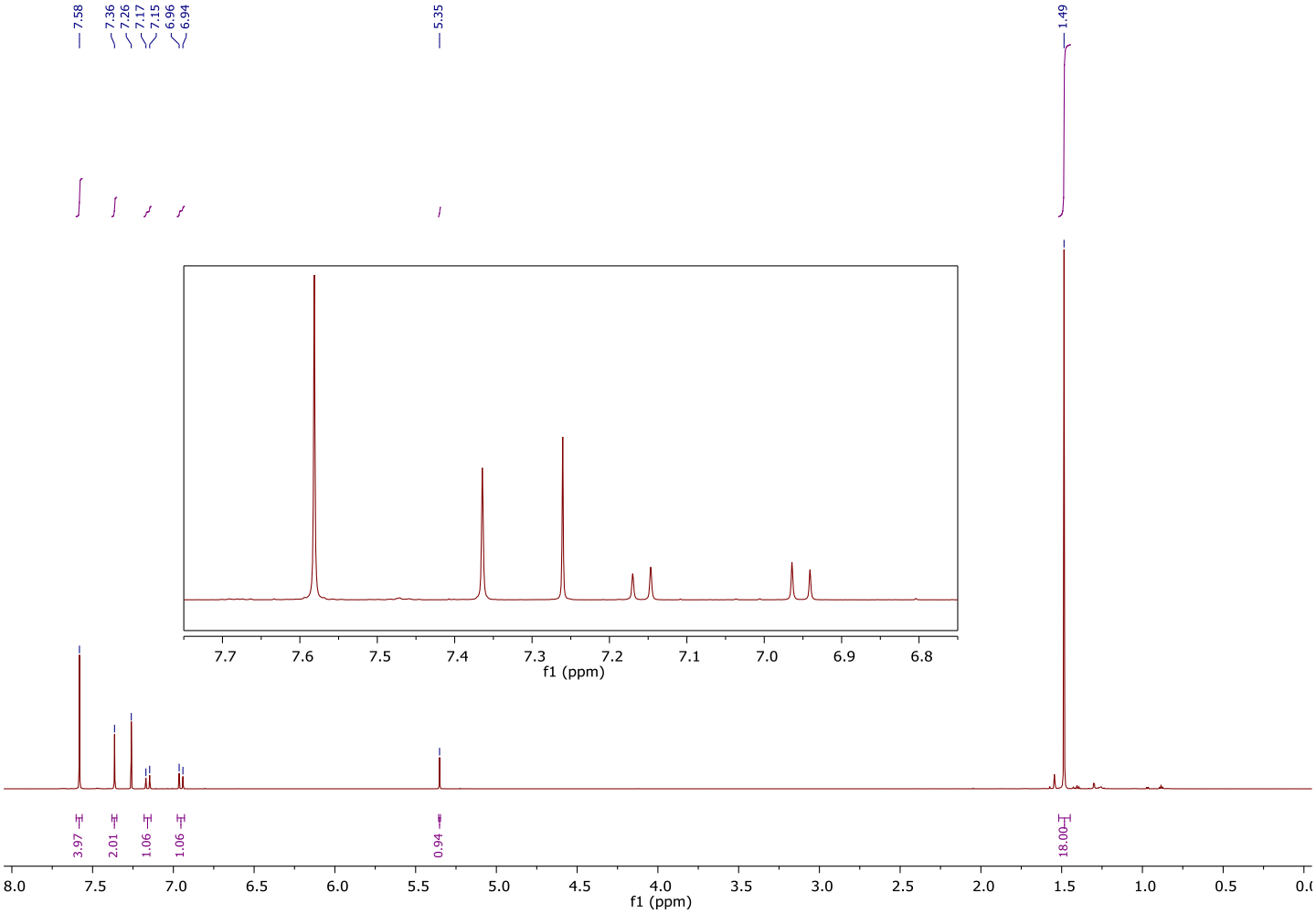
7.58
7.36
7.26
7.17
7.15
6.96
6.94
5.35
1.49
7.7
7.6
7.5
7.4
7.3
7.2
7.1
7.0
6.9
6.8
f1 (ppm)
3.97
2.01
1.06
1.06
0.94
18.00
8.0
7.5
7.0
6.5
6.0
5.5
5.0
4.5
4.0
3.5
3.0
2.5
2.0
1.5
1.0
0.5
f1 (ppm)

^{13}C NMR, 176 MHz, Chloroform-*d*, Stilbene **S14**

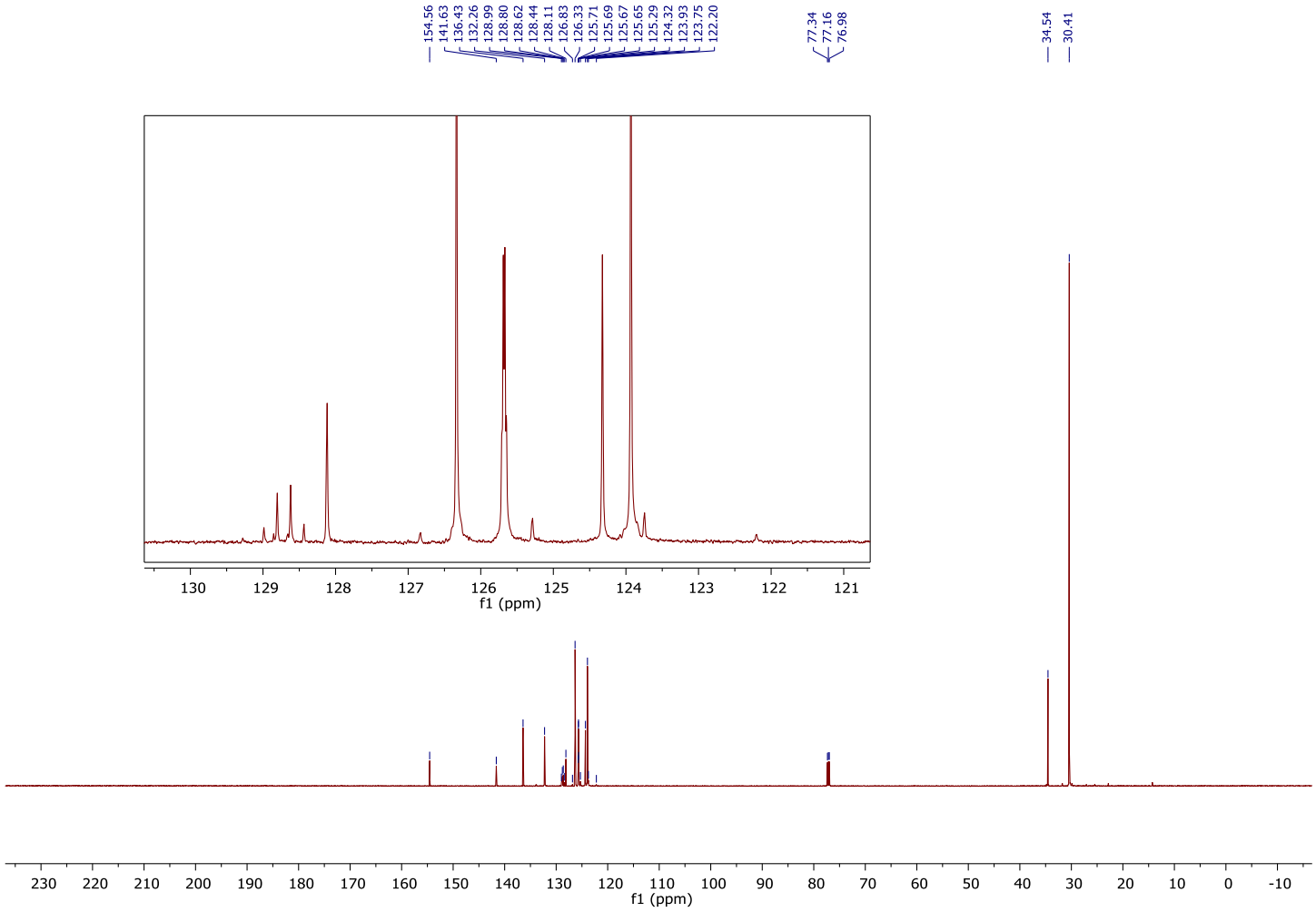

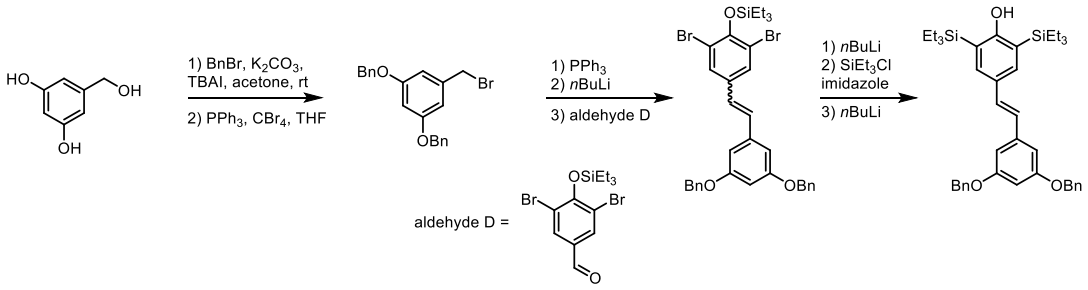

(S15) (*E*)-4-(3,5-bis(benzyloxy)styryl)-2,6-bis(triethylsilyl)phenol

Commercially available 3,5-dihydroxybenzyl alcohol (2.0 g, 14.3 mmol) was added to flask charged with potassium carbonate (2.25 equiv., 4.44 g) and tetrabutylammonium iodide (0.2 equiv., 1.05 g), and the solids were dissolved/suspended in acetone (42 mL). To the stirring reaction mixture was added 4-methoxybenzyl chloride (2.20 equiv., 3.74 mL), and the reaction was allowed to stir at room temperature for 16 hours. Upon completion, the reaction was diluted with ethyl acetate and poured into a separatory funnel containing deionized water. The layers were separated, and the aqueous layer was extracted with additional portions of ethyl acetate. The combined organic layer was washed with brine, dried over magnesium sulfate, and concentrated under reduced pressure to afford the crude product, which was carried forward without further purification. The benzyl-protected material (2.22 g, 5.79 mmol) was subjected to the general procedure using THF as the solvent for the olefination with aldehyde D, which is available from silyl protection of commercially available 3,5-dibromo-4-hydroxybenzaldehyde. The product was purified by column chromatography (2% to 12% ethyl acetate in hexanes, 2% increments, 2 column volumes each, then 2 column volumes at both 16% and 20%) to afford both olefin isomers in a ~1:1 ratio (2.26 g, 69% yield combined). The E-isomer (900 mg, 1.59 mmol) was carried forward and dissolved in THF, and the reaction mixture was cooled to -78 °C. *n*BuLi (1.0 equiv, 1.6 M in hexanes, 993 μL) was added dropwise to the stirring solution, and the reaction was held

at temperature for 15 min prior to being allowed to warm to room temperature. The retro-Brook rearrangement was quenched and worked up following the general procedure. The resulting product was silyl protected following standard conditions, then subjected to the same retro-Brook reaction to afford the product (*E*)-4-(3,5-bis(benzyloxy)styryl)-2,6-bis(triethylsilyl)phenol (861 mg, 85% yield).

R_f = 0.37 (ethyl acetate/hexanes 1:9; UV)

^{1}H NMR (700 MHz, Chloroform-*d*) δ 7.48 (d, *J* = 3.5 Hz, 4H), 7.46 (s, 2H), 7.41 (t, *J* = 7.5 Hz, 4H), 7.35 (t, *J* = 7.2 Hz, 2H), 7.07 (d, *J* = 16.1 Hz, 1H), 6.88 (d, *J* = 16.2 Hz, 1H), 6.80 (t, *J* = 1.8 Hz, 2H), 6.55 (q, *J* = 2.0 Hz, 1H), 5.10 (s, 4H), 5.06 (s, 1H), 1.02 (t, *J* = 8.0 Hz, 18H), 0.91 (q, *J* = 7.7 Hz, 12H).

^{13}C NMR (176 MHz, Chloroform-*d*) δ 166.04, 160.27, 140.16, 137.07, 136.01, 129.77, 129.09, 128.72, 128.12, 127.72, 125.88, 121.44, 105.62, 101.18, 70.25, 7.70, 3.98.

IR (Neat): 3592, 2951, 2870, 1591, 1453, 1397, 1161, 1144, 1060, 1004, 953, 723, 692 cm^{-1};

HRMS (ESI) *m/z* calculated for $C_{40}H_{53}O_3Si_2^+$ ($[M+H]^+$) 637.3528, found 637.3535.

^{1}H NMR, 700 MHz, Chloroform-*d*, Stilbene **S15**

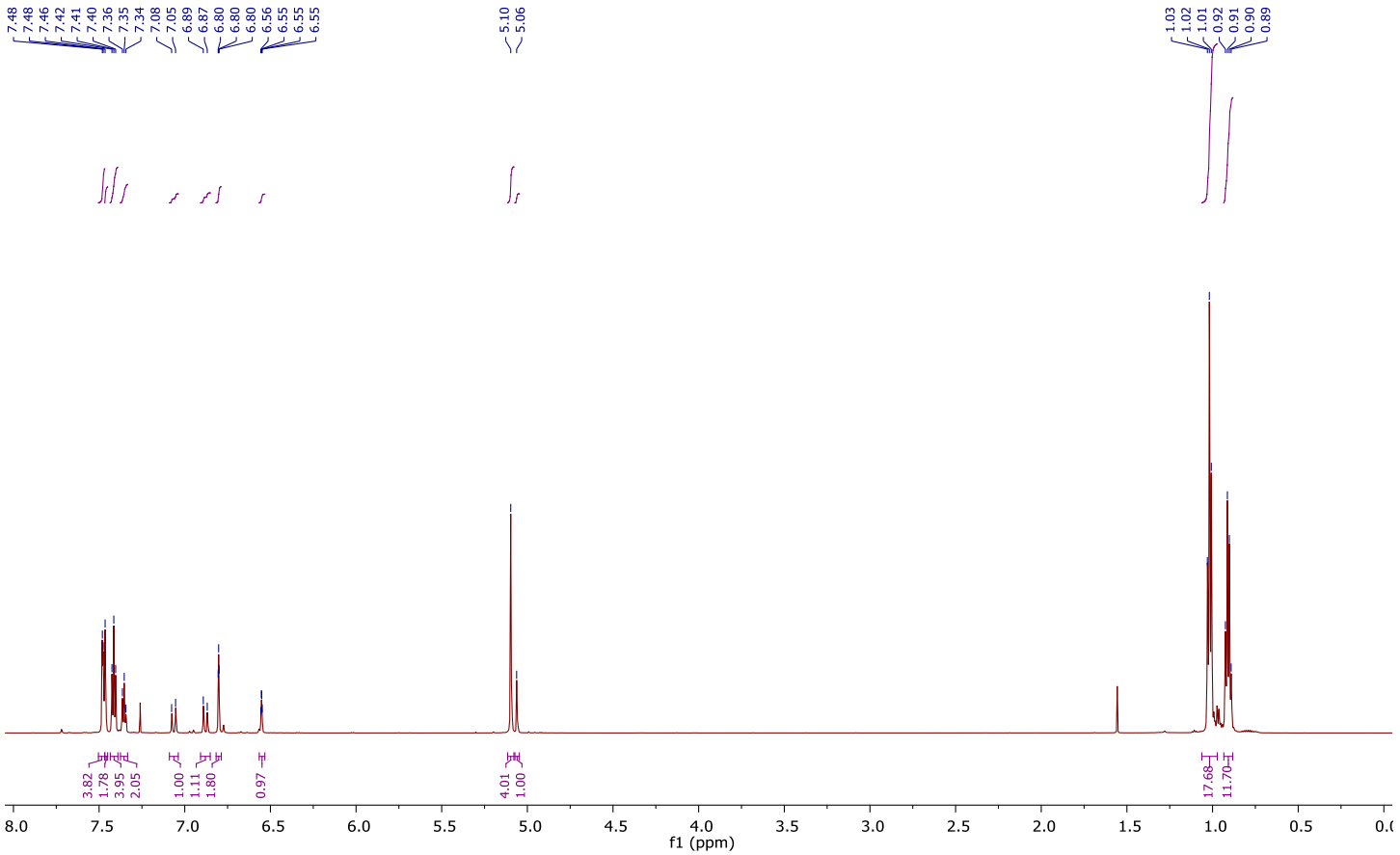

^{3}C NMR, 176 MHz, Chloroform-*d*, Stilbene **S15**

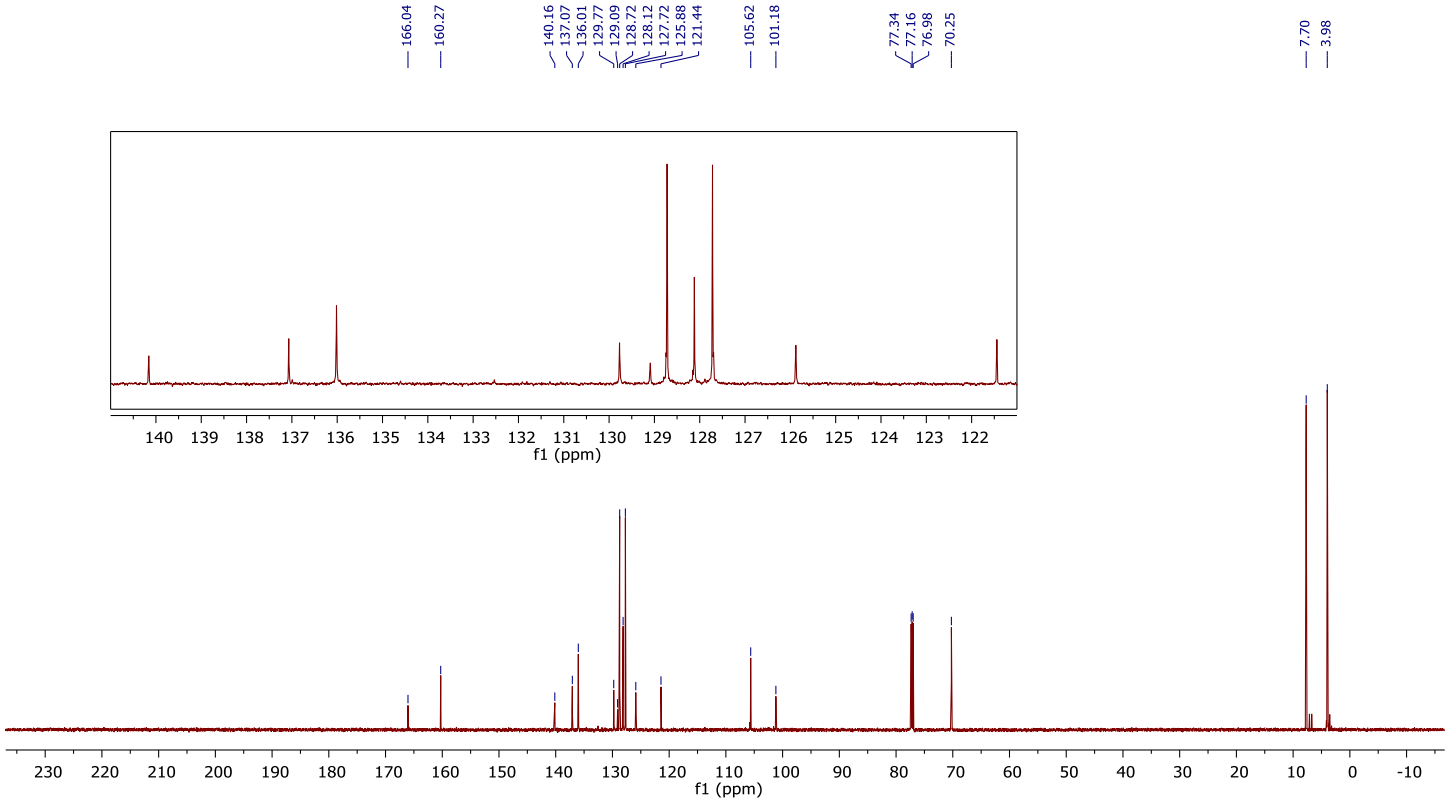

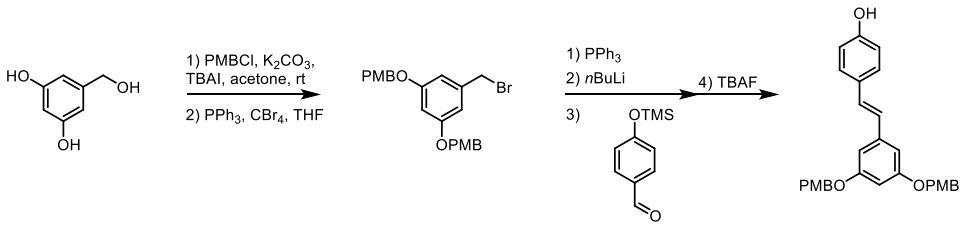

(25) (*E*)-4-(3,5-bis((4-methoxybenzyl)oxy)styryl)phenol

Commercially available 3,5-dihydroxybenzyl alcohol (2.0 g, 14.3 mmol) was added to flask charged with potassium carbonate (2.25 equiv., 4.44 g) and tetrabutylammonium iodide (0.2 equiv., 1.05 g), and the solids were dissolved/suspended in acetone (42 mL). To the stirring reaction mixture was added 4-methoxybenzyl chloride (2.20 equiv., 4.26 mL), and the reaction was allowed to stir at room temperature for 16 hours. Upon completion, the reaction was diluted with ethyl acetate and poured into a separatory funnel containing deionized water. The layers were separated, and the aqueous layer was extracted with additional portions of ethyl acetate. The combined organic layer was washed with brine, dried over magnesium sulfate, and concentrated under reduced pressure to afford the crude product, which was carried forward without further purification. A portion of the PMB-protected benzyl alcohol (783 mg, 2.06 mmol) was subjected to the general procedure using toluene as the solvent for the olefination with aldehyde B. Upon completion of the olefination, the reaction was cooled to 0 °C, and TBAF (1.0 equiv., 1.0 M in THF, 2.06 mL) was added dropwise. The reaction was allowed to stir for 30 min, at which point it was quenched and worked up following the general procedure. The product was purified by column chromatography (8% to 40% ethyl acetate in hexanes) to afford the desired product (478 mg, 49% yield).

R_f = 0.30 (ethyl acetate/hexanes 3:7; UV)

^{1}H NMR (500 MHz, Chloroform-*d*) δ 7.38 (d, *J* = 8.3 Hz, 2H), 7.37 (d, *J* = 8.5 Hz, 4H) 7.01 (d, *J* = 16.2 Hz, 1H), 6.93 (d, *J* = 8.6 Hz, 4H), 6.88 (d, *J* = 16.2 Hz, 1H), 6.81 (d, *J* = 8.3 Hz, 2H), 6.74 (d, *J* = 2.2 Hz, 2H), 6.53 (d, *J* = 2.3 Hz, 1H), 5.23 (s, 1H), 5.00 (s, 4H), 3.83 (s, 6H).

^{13}C NMR (126 MHz, Chloroform-*d*) δ 160.14, 159.45, 155.45, 139.65, 130.02, 129.33, 128.95, 128.73, 127.99, 126.52, 115.63, 114.03, 105.57, 101.24, 69.92, 55.32.

IR (Neat): 3608, 2953, 1611, 1580, 1514, 1436, 1245, 1144, 1030 cm^{-1};

HRMS (ESI) *m/z* calculated for $C_{30}H_{29}O_5^+$ ($[M+H]^+$) 469.2010, found 469.2007.

^{1}H NMR, 500 MHz, Chloroform-*d*, Stilbene **25**

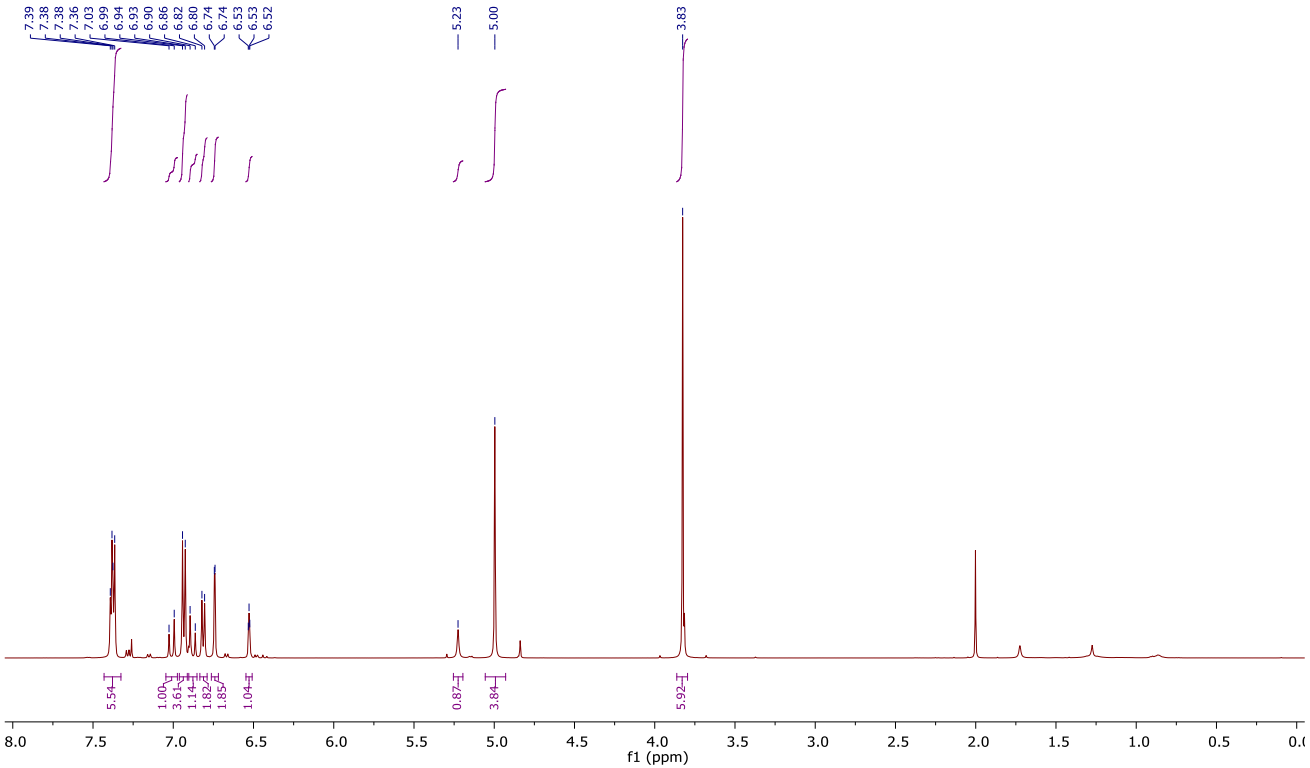

^{13}C NMR, 126 MHz, Chloroform-*d*, Stilbene **25**

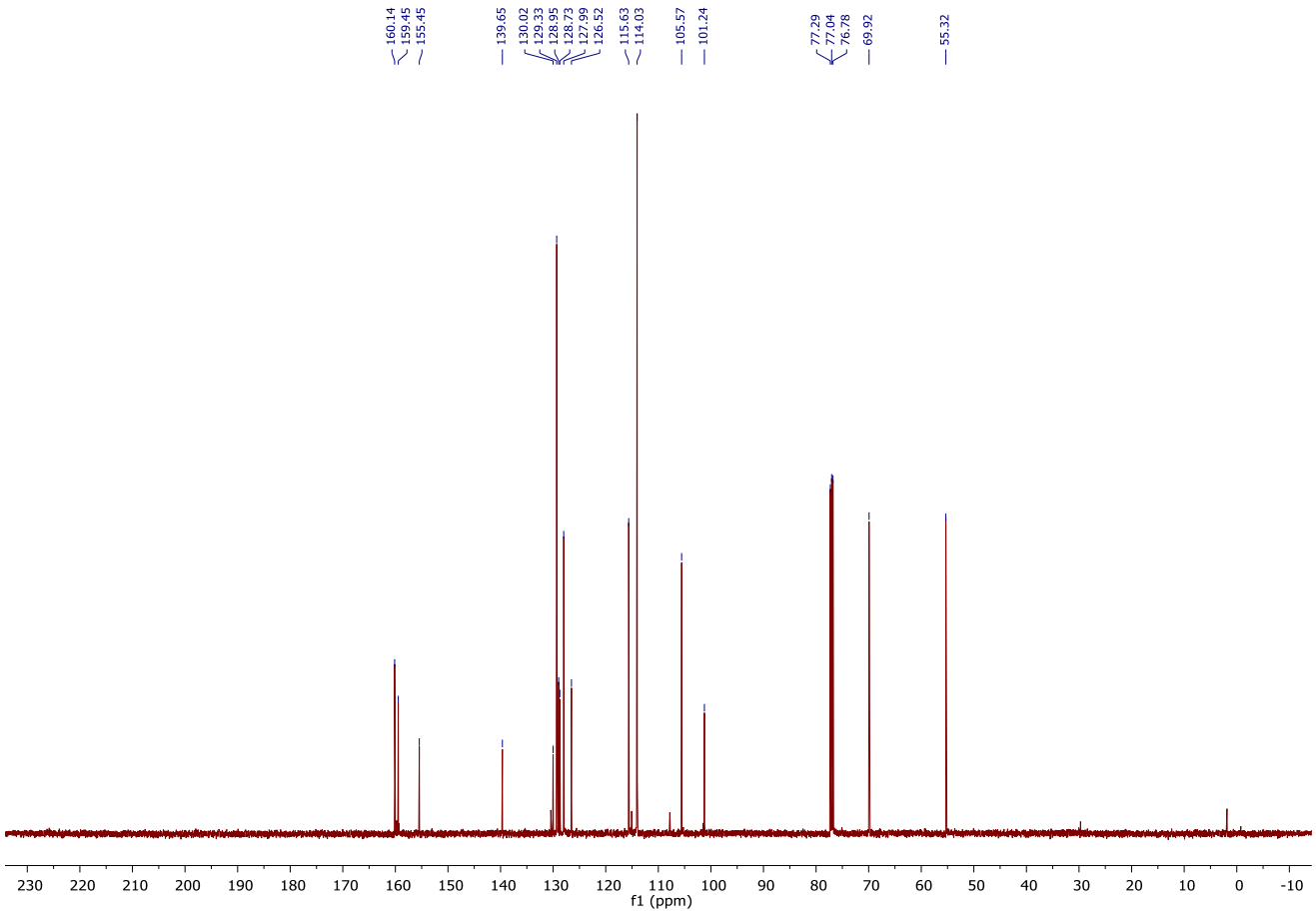

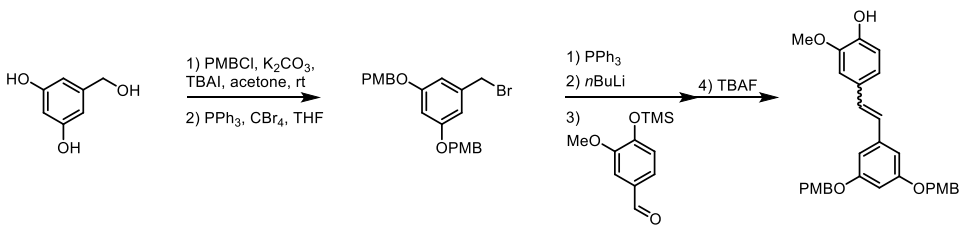

(26) (*E*)-4-(3,5-bis((4-methoxybenzyl)oxy)styryl)-2-methoxyphenol

Commercially available 3,5-dihydroxybenzyl alcohol (2.0 g, 14.3 mmol) was added to flask charged with potassium carbonate (2.25 equiv., 4.44 g) and tetrabutylammonium iodide (0.2 equiv., 1.05 g), and the solids were dissolved/suspended in acetone (42 mL). To the stirring reaction mixture was added 4-methoxybenzyl chloride (2.20 equiv., 4.26 mL), and the reaction was allowed to stir at room temperature for 16 hours. Upon completion, the reaction was diluted with ethyl acetate and poured into a separatory funnel containing deionized water. The layers were separated, and the aqueous layer was extracted with additional portions of ethyl acetate. The combined organic layer was washed with brine, dried over magnesium sulfate, and concentrated under reduced pressure to afford the crude product, which was carried forward without further purification. A portion of the PMB-protected material (734 mg, 1.93 mmol) was subjected to the general procedure using toluene as the solvent for the olefination with aldehyde C. Upon completion of the olefination, the reaction was cooled to 0 °C, and TBAF (1.0 equiv., 1.0 M in THF, 1.93 mL) was added dropwise. The reaction was allowed to stir for 30 min, at which point it was quenched and worked up following the general procedure. The product was purified by column chromatography (8% to 40% ethyl acetate in hexanes) to afford the desired product as a ~3.6:1 E:Z mixture (762 mg, 79% yield).

R_f = 0.32 (ethyl acetate/hexanes 3:7; UV)

E-isomer:

^{1}H NMR (700 MHz, Chloroform-*d*) δ 7.37 (d, *J* = 8.4 Hz, 4H), 7.03 (d, *J* = 1.8 Hz, 1H), 7.01 (dd, *J* = 8.2, 1.8 Hz, 1H), 7.00 (d, *J* = 15.9 Hz, 1H), 6.93 (d, *J* = 8.4 Hz, 4H), 6.91 (d, *J* = 8.1 Hz, 1H), 6.87 (d, *J* = 15.9 Hz, 1H), 6.52 (t, *J* = 2.5 Hz, 1H), 5.67 (s, 1H), 5.00 (s, 4H), 3.95 (s, 3H), 3.83 (s, 6H).

^{13}C NMR (126 MHz, Acetone-d_6) δ 160.30, 159.58, 146.83, 145.82, 139.70, 129.90, 129.40, 129.28, 129.06, 126.55, 120.71, 114.69, 114.13, 108.42, 105.63, 101.38, 70.01, 56.03, 55.42.

Z-isomer:

^{1}H NMR (700 MHz, Chloroform-*d*) δ 7.28 (d, *J* = 8.6 Hz, 4H), 6.88 (d, *J* = 8.6 Hz, 4H), 6.80 (dd, *J* = 7.6, 1.8 Hz, 1H), 6.79 (d, *J* = 7.6 Hz, 1H), 6.77 (d, *J* = 1.5 Hz, 1H), 6.54 (d, *J* = 2.2 Hz, 2H), 6.48 (d, *J* = 12.1 Hz, 1H), 6.46 (t, *J* = 2.3 Hz, 1H), 6.44 (d, *J* = 12.1 Hz, 1H), 5.57 (s, 1H), 4.84 (s, 4H), 3.81 (s, 6H), 3.62 (s, 3H).

^{13}C NMR (126 MHz, Acetone-d_6) δ 159.95, 159.51, 146.08, 145.08, 139.74, 130.53, 129.90, 128.61, 124.41, 122.87, 121.77, 114.07, 112.30, 111.42, 107.93, 101.44, 69.88, 55.75, 55.42.

Mixture of isomers:

IR (Neat): 3522, 2954, 2869, 1592, 1454, 1353, 1287, 1212, 1194, 1157, 1149, 1056, 1037, 963, 828, 732, 695, 634 cm^{-1};

HRMS (ESI) *m/z* calculated for $C_{31}H_{31}O_6^+$ ($[M+H]^+$) 499.2115, found 499.2111.

^{1}H NMR, 700 MHz, Chloroform-*d*, Stilbene **26** (~3.6:1 mixture of isomers)

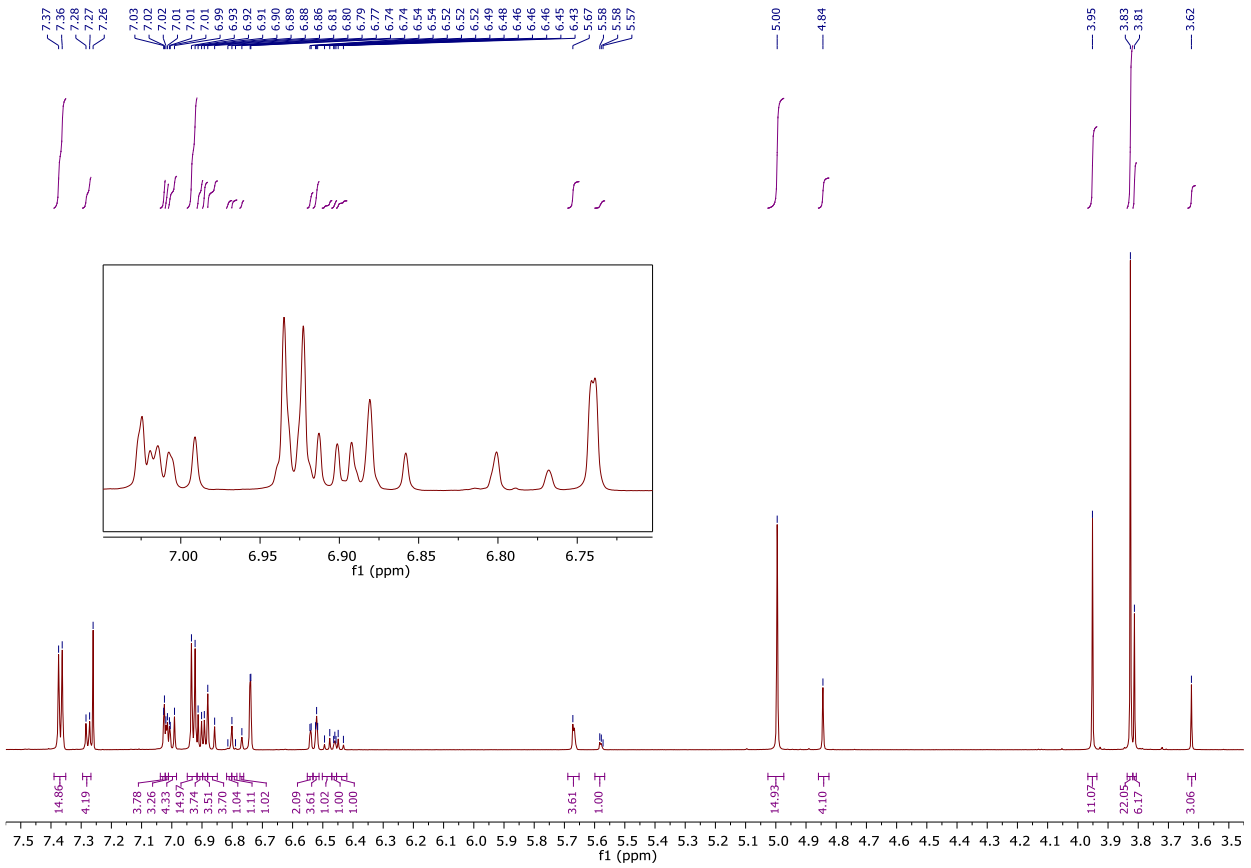

^{1}H NMR, 700 MHz, Chloroform-*d*, Stilbene **26** (Z isomer)

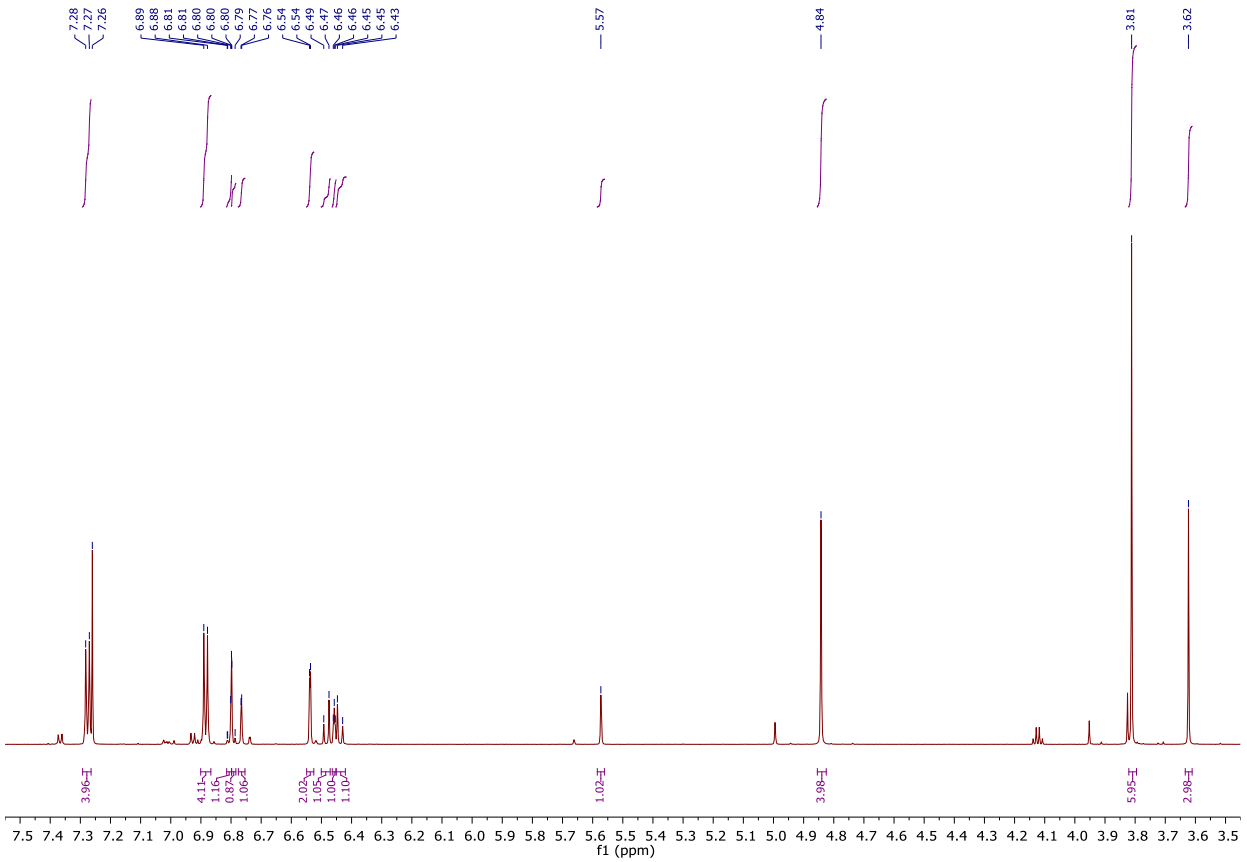

^{13}C NMR, 126 MHz, Chloroform-*d*, Stilbene **26** (~3.6:1 mixture of isomers)

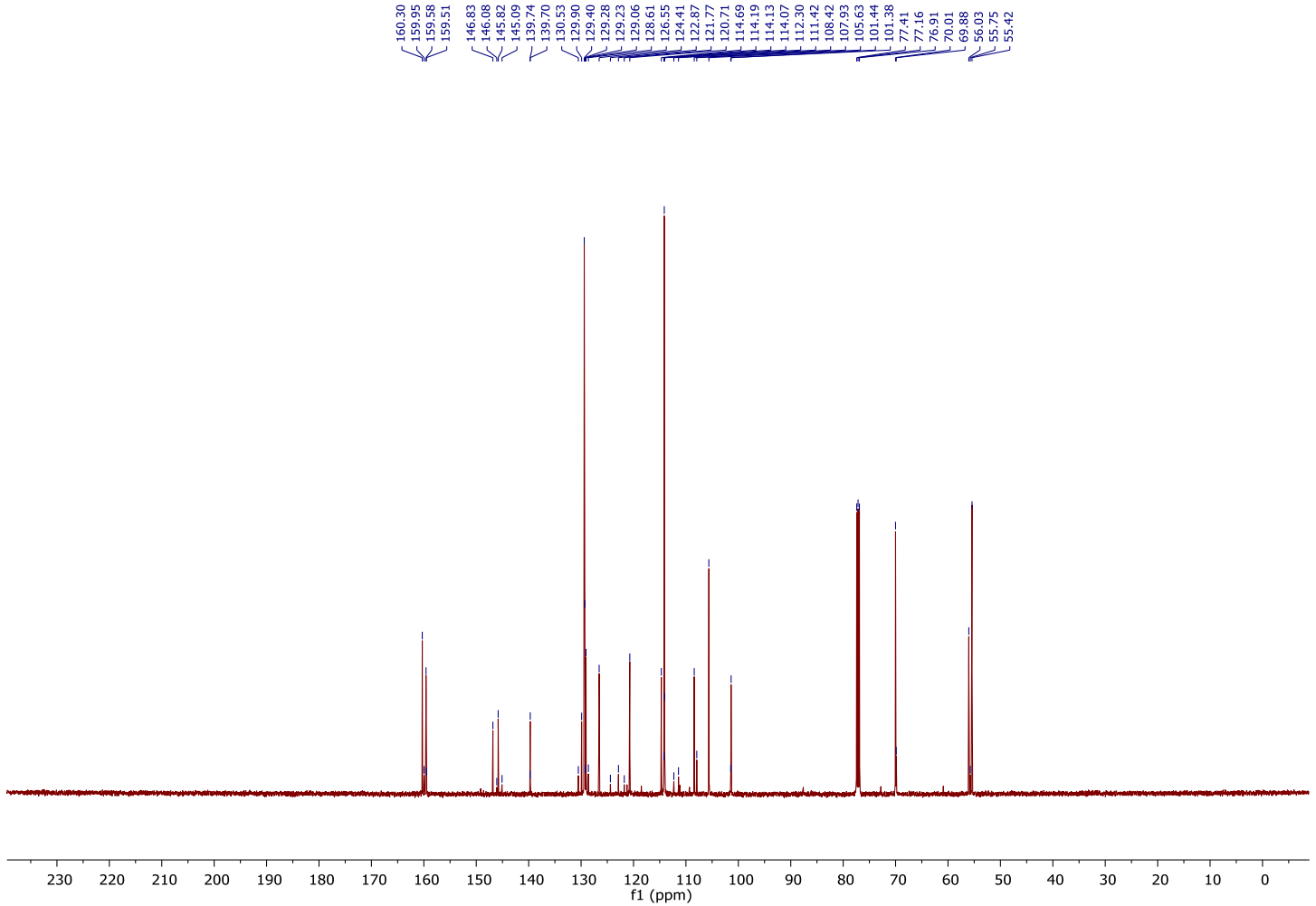

Cyclic Voltammetry Experimental Procedure:

For each stilbene substrate, two cyclic voltammetry experiments were conducted. The first was to measure oxidation of the substrate (green or blue curve), while the second was to measure oxidation in the presence of 2,6-lutidine (orange curve). The stilbene substrate (0.03 mmol) and the electrolyte (Bu_4NPF_6, 0.3 mmol, 116 mg) were dissolved in acetonitrile (3 mL). For the experiments with base, 2,6-lutidine (0.03 mmol, 3.5 μL) was added. The solution was transferred to a 5-neck electrochemical cell, which was outfitted with a working electrode (glassy carbon, 3 mm diameter, surface area = 0.0707 cm^2), reference electrode (Ag/AgCl, 3 M aq. KCl), and counter/auxiliary electrode (platinum wire). The electrochemical cell was connected to the CH1620E electrochemical analyzer, and the potential was swept from 0.0 V to +1.0 V in two sweep segments at a scan rate of 100 mV/s to afford the observed cyclic voltammograms. It can be seen in the data below that direct oxidation of the electron rich substrates occurs between +0.8 to +1.0 V, however direct oxidation of electron deficient substrates occurs beyond +1.0 V. In the presence of 2,6-lutidine, oxidation occurs below +0.6 V in all cases, suggesting that +0.6 V is a sufficient potential to attain the desired reactivity.

Cyclic Voltammetry Data:

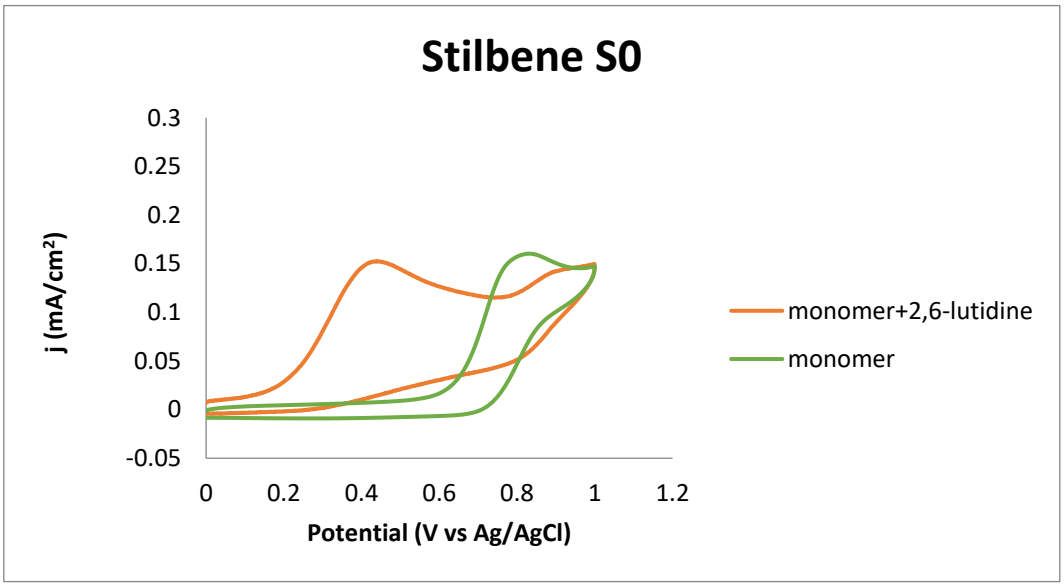

Figure S1. Cyclic voltammogram for stilbene S1.

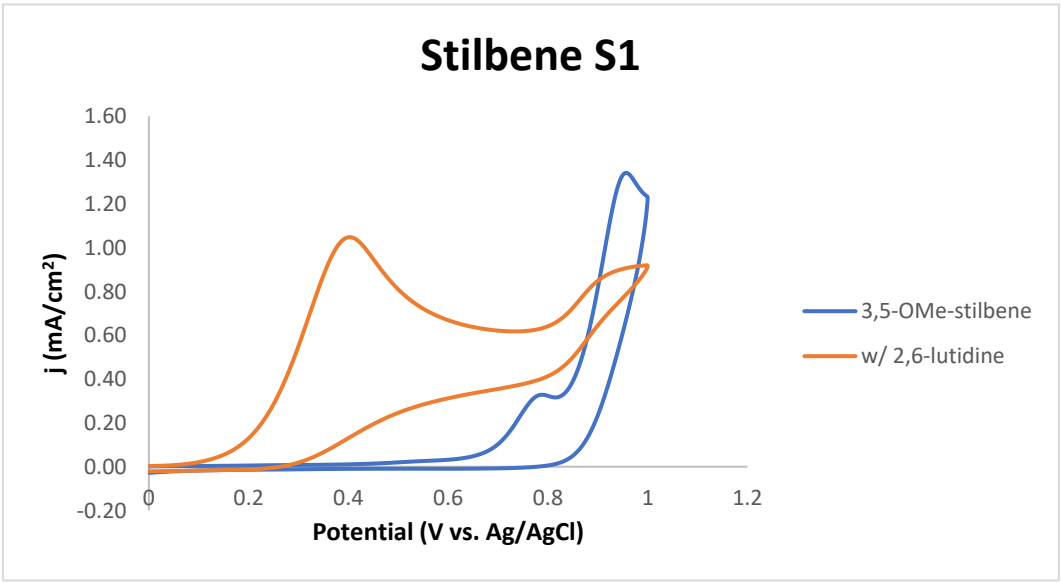

Figure S2. Cyclic voltammogram for stilbene S2.

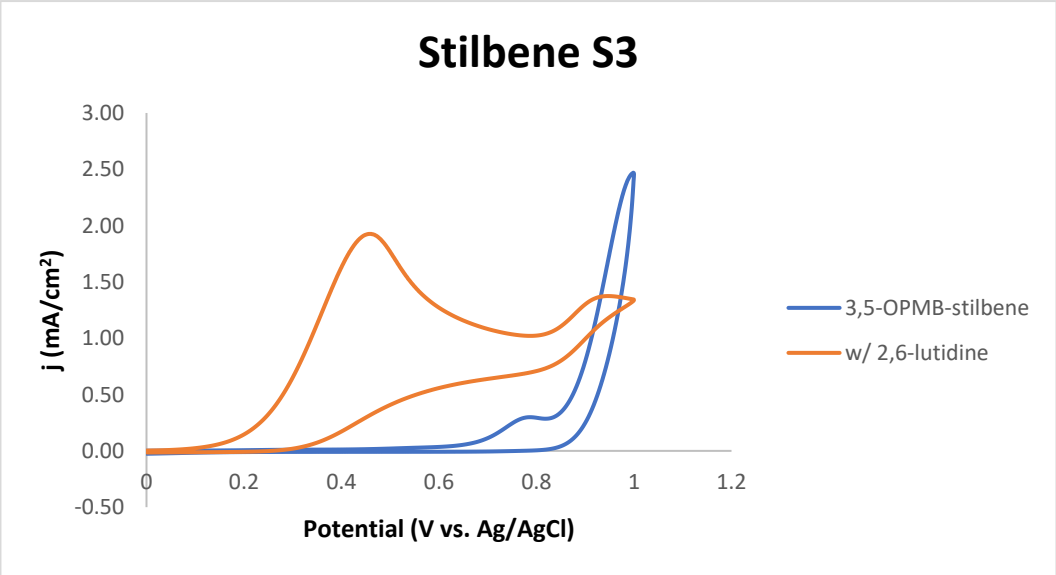

Figure S3. Cyclic voltammogram for stilbene S3.

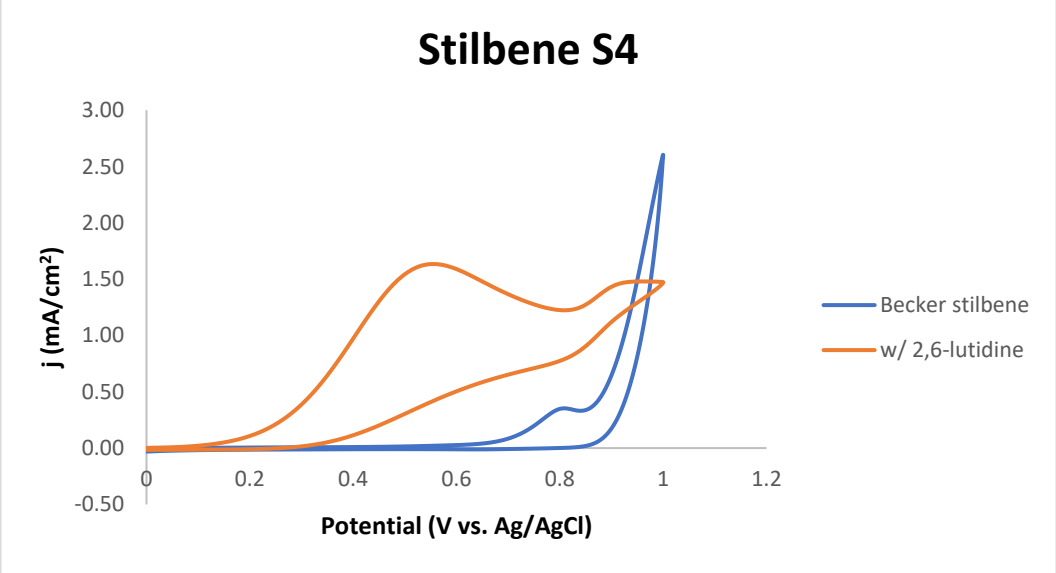

Figure S4. Cyclic voltammogram for stilbene S4.

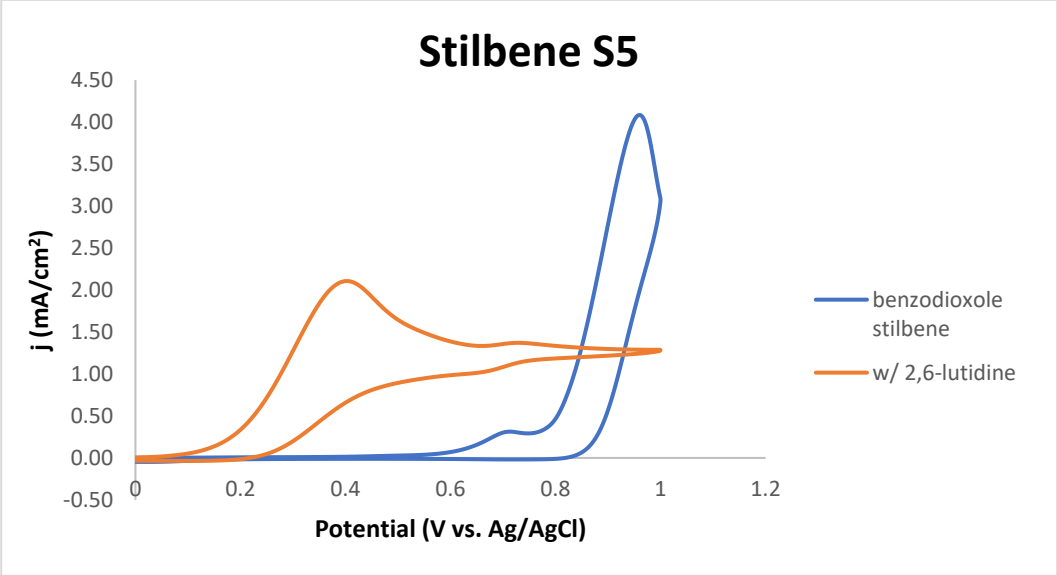

Figure S5. Cyclic voltammogram for stilbene S5.

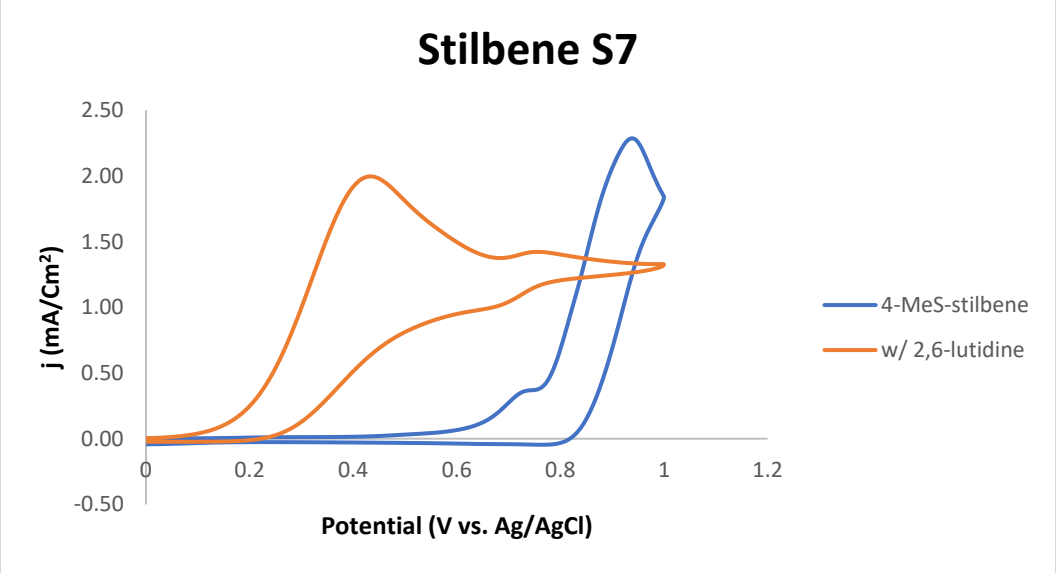

Figure S6. Cyclic voltammogram for stilbene S7.

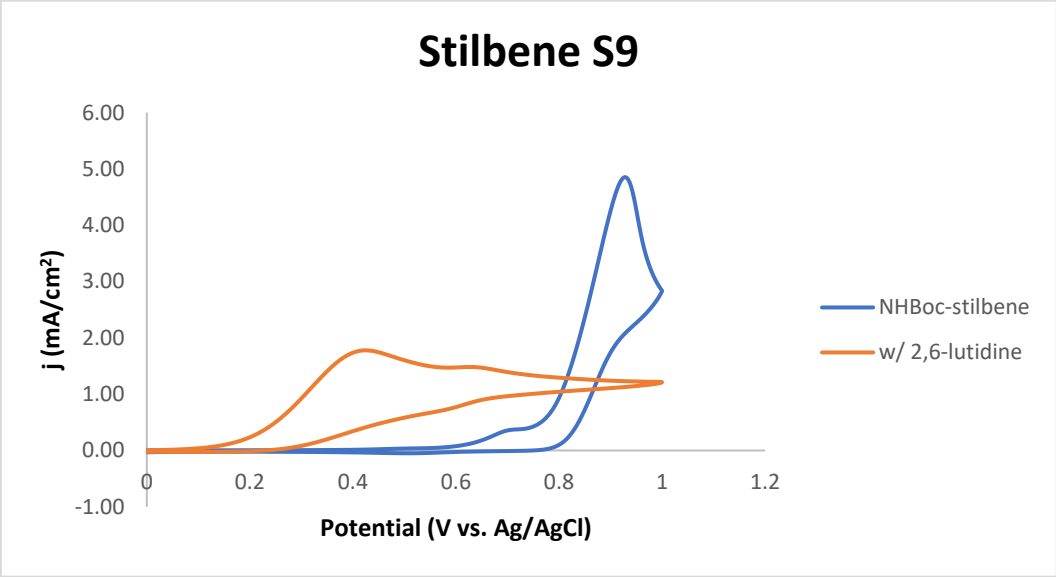

Figure S7. Cyclic voltammogram for stilbene S9.

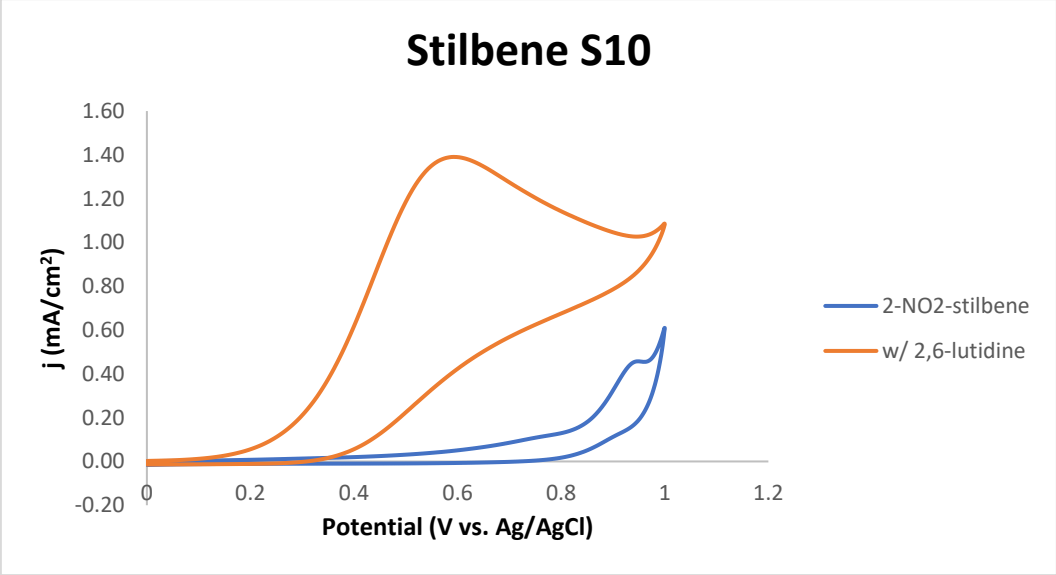

Figure S8. Cyclic voltammogram for stilbene S10.

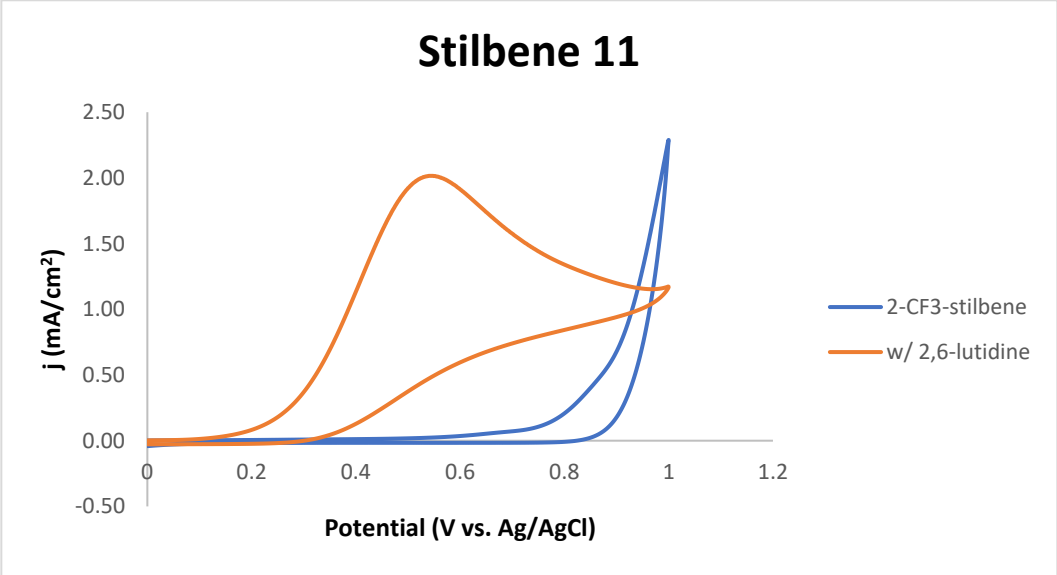

Figure S9. Cyclic voltammogram for stilbene S11.

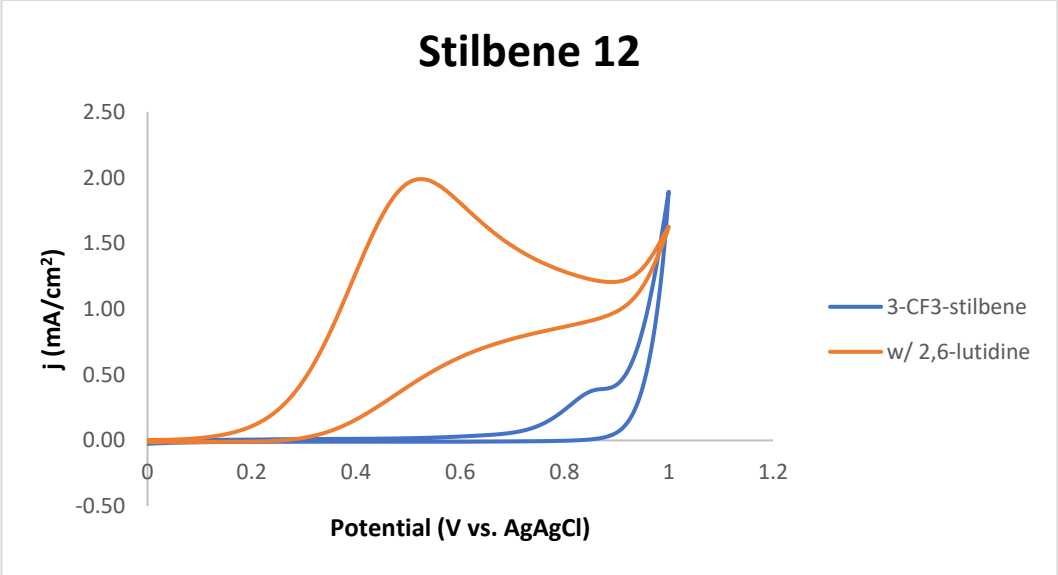

Figure S10. Cyclic voltammogram for stilbene S12.

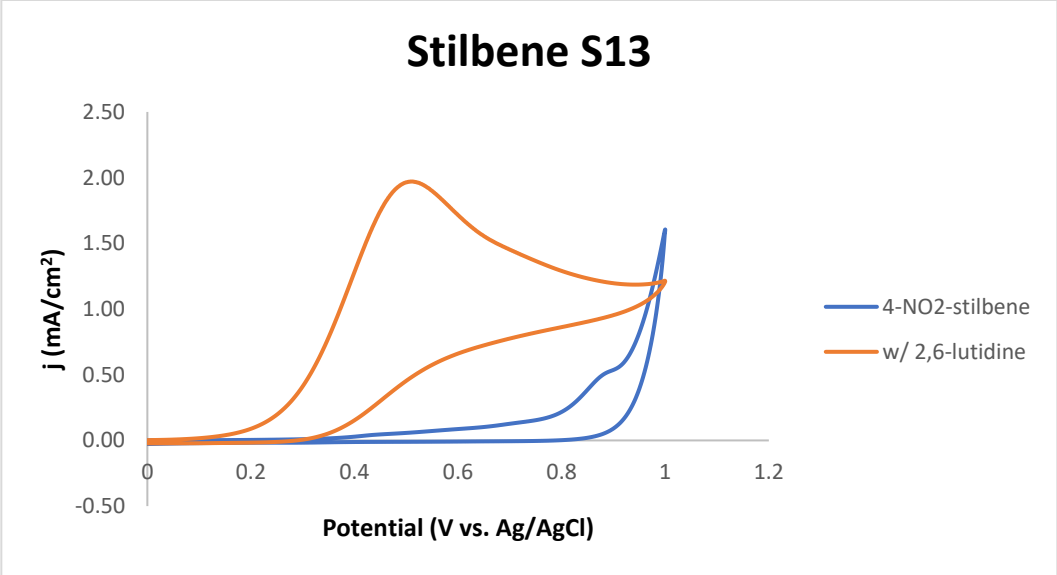

Figure S11. Cyclic voltammogram for stilbene S13.

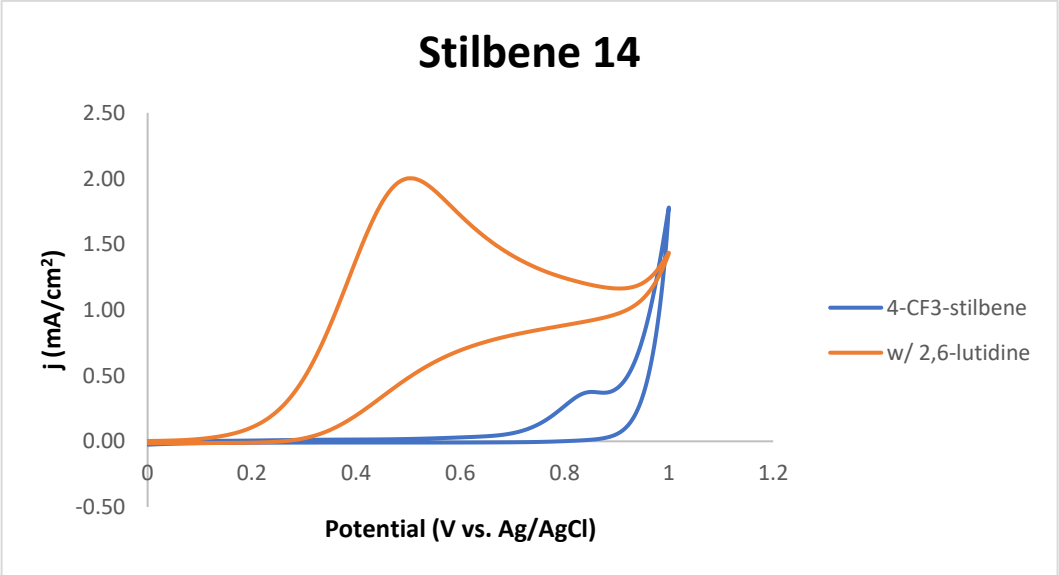

Figure S12. Cyclic voltammogram for stilbene S14.

General Dimerization Procedure[3]:

The starting phenol (0.1 mmol) was added to a reaction vial with KPF_6 (74 mg, 0.4 mmol) and 2,6-lutidine (2.3 μL, 0.02 mmol) and dissolved in acetonitrile (8 mL). Two pieces of 0.25 x 2-inch RVC panel (0.25 inch thickness) were cut. To each, a hole was made near one end, and copper wire was placed through the hole and wrapped around the top of each electrode. One end of the wire was left free in to connect to the alligator clips. These electrodes were carefully placed into the reaction vial along with the reference electrode (Ag/AgCl in 3 M KCl) and a divider (**see image**). The alligator clips were connected such that the reference and working electrodes were adjacent to each other, while the counter electrode was opposite the divider. Care was taken to ensure the copper wire was not submerged in solvent, nor the active components of the alligator clips touching each other. The reaction was stirred at 750 rpm for 1-2 h at a constant voltage of 0.6 V. A chronoampergram was recorded to follow the course of the reaction. Upon completion of the reaction, the electrodes were removed and rinsed into a collection flask with DCM (~40 mL). The contents of the reaction vial were also rinsed into the collection flask. The solvent was removed on the rotovap, the crude material was resuspended in DCM, and the electrolyte was filtered away with a plug of Celite. The filtrate was then concentrated to afford the product, which did not require further purification. The diastereomeric ratios were determined by integration of the aryl protons on the quinone methide. When these were overlapping with other aryl signals, the δ-protons of the quinone methide were integrated to determine dr.

Optimization and Scalability of Dimerization

Table S1. Optimization of Electrochemical Dimerization

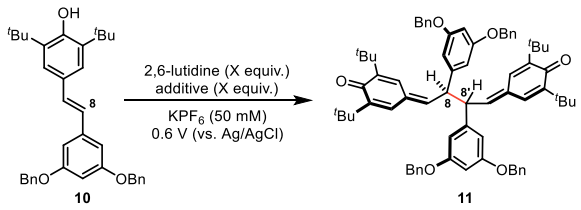

Entry	Scale (mmol)	Additive (equiv.)	2,6-lut. (equiv.)	Solvent (ratio)	Time (h)	Yield (%)[a]
1	0.1	Fc (0.1)	2.0	A	0.5	94
2	0.1	-	2.0	A	0.5	99
3	0.1	-	0.2	A	0.5	99
4	0.1	-	0	A	0.5	0
5	0.3	-	0.2	A	1	90
6	0.3	-	0.2	A:B (2:1)	1	95
7	0.9	-	0.2	A:B (2:1)	5	99
8	3.6	-	0.2	A:B (2:1)	12	95

[a]Isolated yields. Fc = ferrocene. A = MeCN. B = CH_2Cl_2.

The investigation of this electrochemical dimerization strategy began with protected resveratrol analogue **10**, mimicking the key transformation in our prior syntheses of pallidol and quadrangularin A.[1] Initial attempts sought to recapitulate the ferrocenium-mediated conditions, positing that the well-known, low and reversible oxidation potential of ferrocene (E1/2 (Fc+/Fc) = 0.40 V vs SCE) would allow for the use of sub-stoichiometric equivalents of the oxidant.[4] Gratifyingly, an excellent yield was achieved using only 10 mol% of ferrocene and 2 equivalents of 2,6-lutidine (Table S1, Entry 1). It was speculated that the oxidative dimerization of **10** could occur without the need for a metal catalyst, given the apparent selectivity window that existed between the oxidation potential of the starting material (Ep/2 = +0.81 V vs Ag/AgCl) and the desired product **11** (Ep/2 = +1.23 vs Ag/AgCl, see page S37 for voltammetry data). This selectivity could be further enhanced by lowering the oxidation potential through the addition of base, an effect demonstrated by Corduneanu et al. in their investigation of the effect of pH on the oxidation potential of resveratrol.[5] Indeed, we observed a dramatic decrease in the oxidation potential of **10**

upon adding 2,6-lutidine (Ep/2 = +0.44 V (vs Ag/AgCl)), while the bis-quinone methide (BQM) product **11** was unaffected. Employing these metal-free conditions for the bulk electro-chemical processing of monomer **10** proved highly effective (Table S1, entry 2), generating the desired product in near quantitative yield after just 30 min at +0.6 V. Furthermore, it was observed that only a sub-stoichiometric amount of base was needed (Table S1, Entry 3), and the reaction did not occur at the same set potential when base was excluded (Table S1, Entry 4). Upon increasing the scale of the reaction (from 0.1 mmol to 0.3 mmol), deposition of insoluble dimeric products on the surface of the electrodes was found to inhibit the reaction (Table S1, Entry 5), an issue that was ameliorated through the addition of dichloromethane as a co-solvent. Importantly, these optimized conditions proved readily-scalable (Table S1, Entries 6-8), including operation on multi-gram scale while still maintaining high yields (≥95%). In addition to the efficiency, the operational simplicity of this method is viewed as a definitive benefit, as it is carried out on the benchtop, open to atmosphere, and only requires the addition of an electrolyte and a single, readily-available reagent. Furthermore, column chromatography is generally not required, increasing the attractiveness of this method for multi-step synthetic routes.

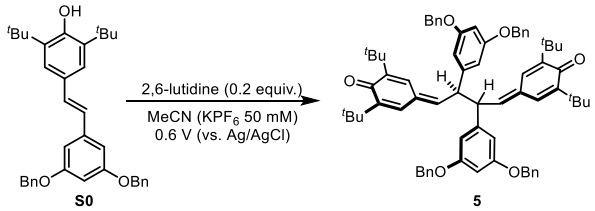

(5) 4,4'-((2R,3R)-2,3-bis(3,5-bis(benzyloxy)phenyl)butane-1,4-diylidene)bis(2,6-di-tert-butylcyclohexa-2,5-dien-1-one)

Stilbene **S0** (0.1 mmol, 52.1 mg) was subjected to the general dimerization procedure, affording bis-quinone methide **5** (51.7 mg, 99% yield, 4:3 dr). The ^{1}H NMR spectrum was identical to the previous report for this compound.[1]

^{1}H NMR (CDCl3, 500 MHz): δ 7.40 – 7.30 (m, 20H), β-H's of quinone methides: 7.12 (major diastereomer, d, *J* = 2.2 Hz, 2H), 7.02 (minor diastereomer, d, *J* = 2.0 Hz, 2H), 6.82 (minor diastereomer, d, *J* = 2.2 Hz, 2H), 6.72 (major diastereomer, d, *J* = 2.0 Hz, 2H); δ-H's of quinone methides: 6.41 – 6.37 (minor diastereomer, m, 2H), 6.33 – 6.29 (major diastereomer, m, 2H); 6.48 (major diastereomer, t, *J* = 2.1 Hz, 2H), 6.47 (minor diastereomer, t, *J* = 2.2 Hz, 2H), 6.45 (major diastereomer, d, *J* = 2.1 Hz, 4H), 6.38 (minor diastereomer, d, *J* = 2.2 Hz, 4H), 4.96 (major diastereomer, d, *J* = 11.5 Hz, 4H), 4.94 (major diastereomer, d, *J* = 11.5 Hz, 4H), 4.91 (minor diastereomer, d, *J* = 11.5 Hz, 4H), 4.89 (minor diastereomer, d, *J* = 11.5 Hz, 4H), 4.28 (m, overlap, sp^3 methines of both diastereomers, 4H), 1.26 (minor diastereomer *t*Bu's, s, 18H), 1.24 (major diastereomer *t*Bu's, s, 36H), 1.23 (minor diastereomer *t*Bu's, s, 18H).

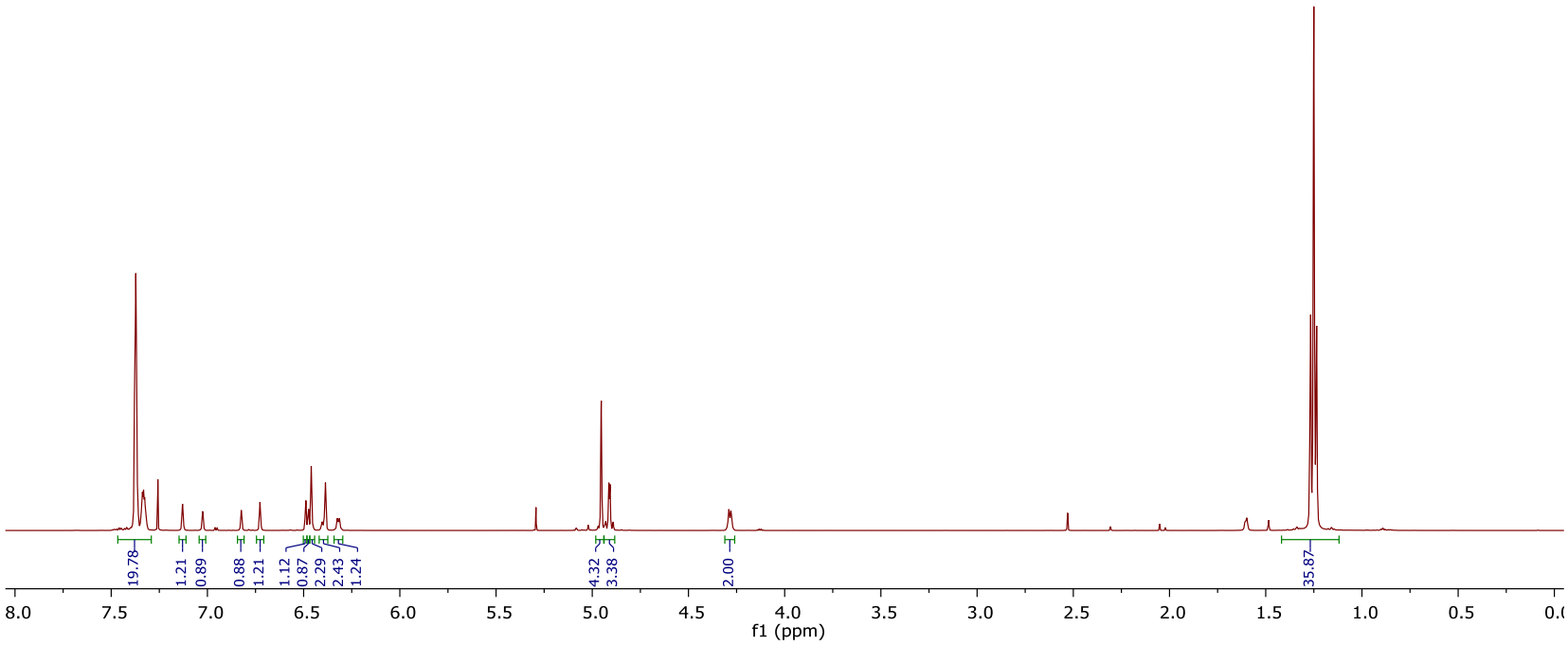
19.78
1.21
0.89
0.88
1.21
1.12
0.87
2.29
2.43
1.24
4.32
3.38
2.00
35.87
8.0
7.5
7.0
6.5
6.0
5.5
5.0
4.5
4.0
3.5
3.0
2.5
2.0
1.5
1.0
0.5
f1 (ppm)

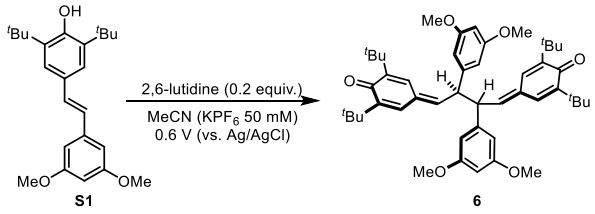

(6) 4,4'-((2*R*,3*R*)-2,3-bis(3,5-dimethoxyphenyl)butane-1,4-diylidene)bis(2,6-di-*tert*-butylcyclohexa-2,5-dien-1-one)

Stilbene **S1** (0.1 mmol, 36.9 mg) was subjected to the general dimerization procedure, affording bis-quinone methide **6** (36.5mg, 99% yield, 3:2 dr). The ^{1}H NMR spectrum was identical to the previous report for this compound.[1]

^{1}H NMR (CDCl3, 700 MHz): δ β-H's of quinone methides: 7.13 (major diastereomer, d, *J* = 1.9 Hz, 2H), 7.09 (minor diastereomer, d, *J* = 2.0 Hz, 2H), 6.82 (minor diastereomer, d, *J* = 2.2 Hz, 2H), 6.71 (major diastereomer, d, *J* = 2.2 Hz, 2H); δ-H's of quinone methides: 6.43 (minor diastereomer, m, 2H), 6.33 (major diastereomer, m, 2H); 6.35 (Ar-H major diastereomer, d, *J* = 2.1 Hz, 4H), 6.31 (Ar-H major diastereomer, t, *J* = 2.1 Hz, 2H), 6.29-6.27 (Ar-H's minor diastereomer, overlap, 6H), 4.34 – 4.30 (minor diastereomer sp^3 methines, m, 2H), 4.30 – 4.26 (major diastereomer sp^3 methines, m, 2H), 3.74 (major diastereomer –OMe's, s, 12H), 3.70 (minor diastereomer –OMe's, s, 12H), 1.25 (minor diastereomer *t*Bu's, s, 18H), 1.24 (major diastereomer *t*Bu's, s, 18H), 1.23 (minor diastereomer *t*Bu's, s, 18H), 1.22 (major diastereomer *t*Bu's, s, 18H).

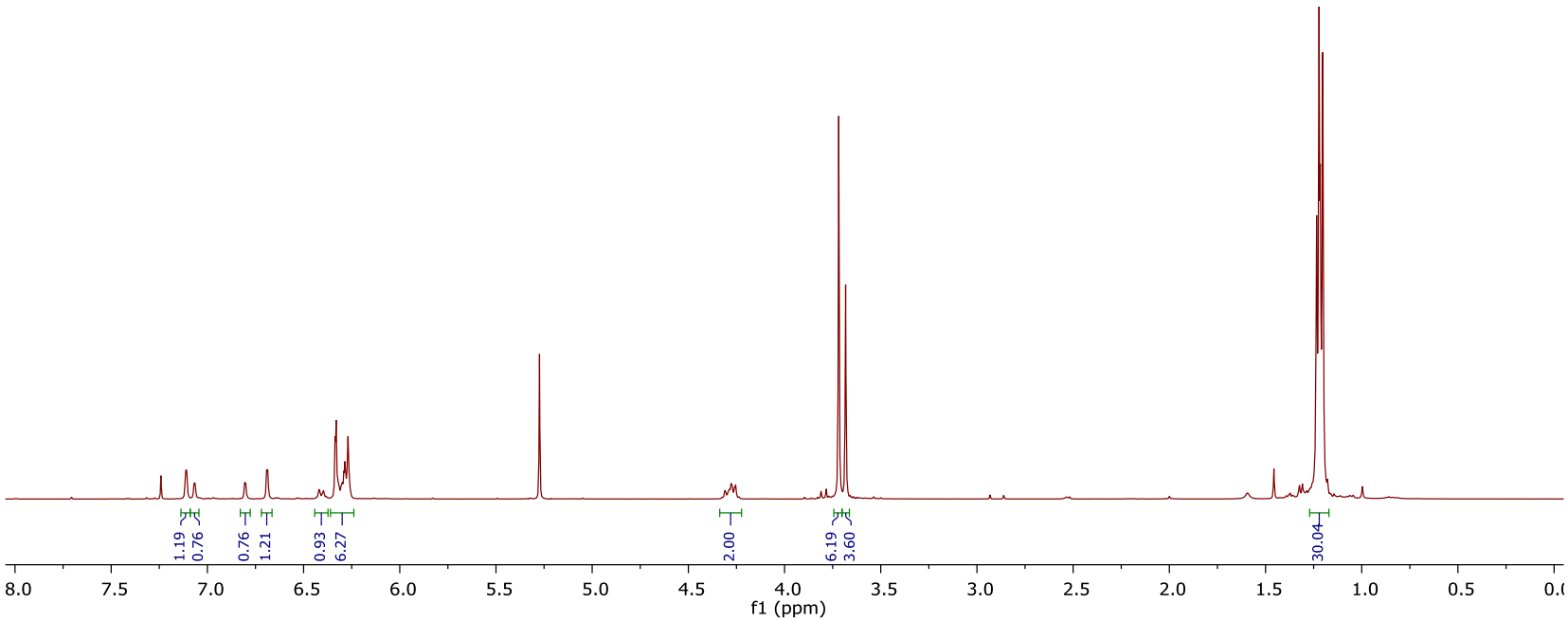
1.19
0.76
0.76
1.21
0.93
6.27
2.00
6.19
3.60
30.04
8.0
7.5
7.0
6.5
6.0
5.5
5.0
4.5
4.0
3.5
3.0
2.5
2.0
1.5
1.0
0.5
f1 (ppm)

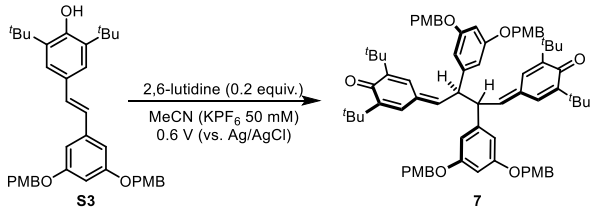

(7) 4,4'-((2*R*,3*R*)-2,3-bis(3,5-bis((4-methoxybenzyl)oxy)phenyl)butane-1,4-diylidene)bis(2,6-di-*tert*-butylcyclohexa-2,5-dien-1-one)

Stilbene **S3** (0.1 mmol, 58.1 mg) was subjected to the general dimerization procedure, affording bis-quinone methide **7** (57.8 mg, 99% yield, 5:4 dr).

^{1}H NMR (700 MHz, Chloroform-*d*) δ 7.30 (m, 16H), 7.13 (β-H, major diastereomer, d, *J* = 2.4 Hz, 2H), 7.03 (β-H, minor diastereomer, d, *J* = 2.4 Hz, 2H), 6.90 (m, 16H), 6.83 (β-H, minor diastereomer, d, *J* = 2.4 Hz, 2H), 6.74 (β-H, major diastereomer, d, *J* = 2.4 Hz, 2H), 6.46 (m, 8H), 6.43 (δ-H, minor diastereomer, d, *J* = 8.8 Hz, 2H), 6.39 (minor diastereomer, d, *J* = 2.2 Hz, 4H), 6.35 (δ-H, major diastereomer, dd, *J* = 7.2, 2.5 Hz, 2H), 4.87 (d, *J* = 2.6 Hz, 8H), 4.83 (q, *J* = 10.6 Hz, 8H), 4.30 (m, sp^3 methines of both diastereomers, 4H), 3.81 (s, 12H), 3.80 (s, 12H), ^{t}Bu signals: 1.26 (s, 18 H), 1.25 (s, 18H), 1.24 (s, 18 H), 1.23 (s, 18 H).

^{13}C NMR (176 MHz, Chloroform-*d*) δ 186.66, 186.61, 160.44, 160.31, 159.72, 159.71, 149.02, 148.93, 147.58, 147.27, 145.28, 143.91, 143.12, 142.79, 134.86, 134.71, 133.08, 132.03, 129.55, 129.53, 128.59, 128.54, 126.13, 125.97, 114.17, 107.95, 107.75, 100.33, 100.31, 70.15, 70.13, 55.44, 55.42, 51.78, 51.14, 35.49, 35.47, 35.03, 34.97, 29.62, 29.56, 29.54.

IR (Neat): 2955, 2929, 1611, 1577, 1515, 1439, 1245, 1147, 1046, 1026, 967, 858 cm^{-1};

HRMS (ESI) *m/z* calculated for $C_{76}H_{87}O_{10}^{+}$ ([M+H]$^{+}$) 1159.6294, found 1159.6278.

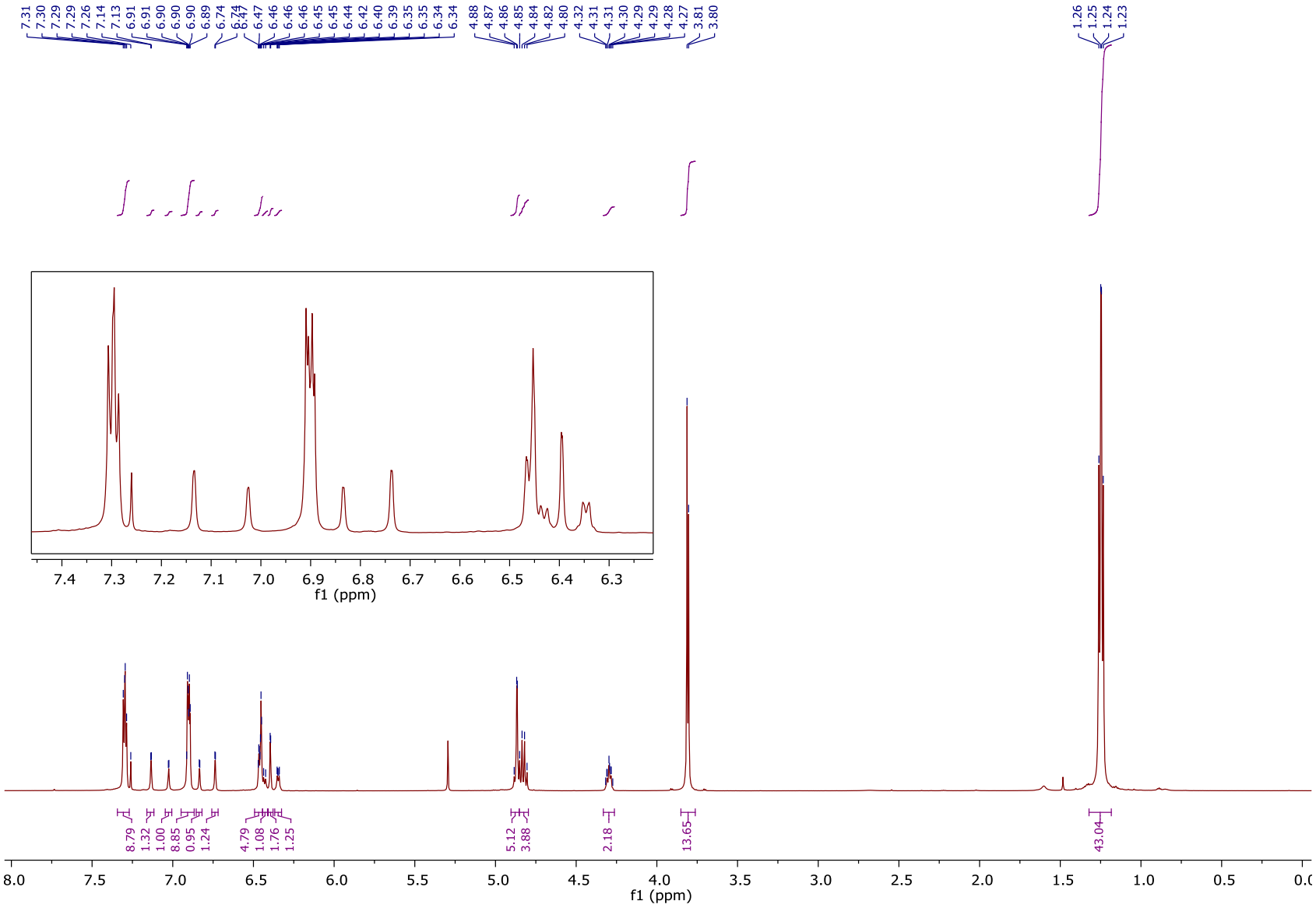
7.31 7.30 7.29 7.29 7.26 7.14 7.13 6.91 6.91 6.90 6.90 6.90 6.89 6.74 6.74 6.47 6.47 6.46 6.46 6.46 6.45 6.45 6.44 6.42 6.40 6.39 6.35 6.35 6.34 6.34
4.88 4.87 4.86 4.85 4.84 4.82 4.80 4.32 4.31 4.31 4.30 4.29 4.29 4.28 4.27 3.81 3.80
1.26 1.25 1.24 1.23
7.4 7.3 7.2 7.1 7.0 6.9 6.8 6.7 6.6 6.5 6.4 6.3
f1 (ppm)
8.79 1.32 1.00 8.85 0.95 1.24 4.79 1.08 1.76 1.25 5.12 3.88 2.18 13.65 43.04
8.0 7.5 7.0 6.5 6.0 5.5 5.0 4.5 4.0 3.5 3.0 2.5 2.0 1.5 1.0 0.5
f1 (ppm)

^{13}C NMR, 176 MHz, Chloroform-*d*, Dimer **7**

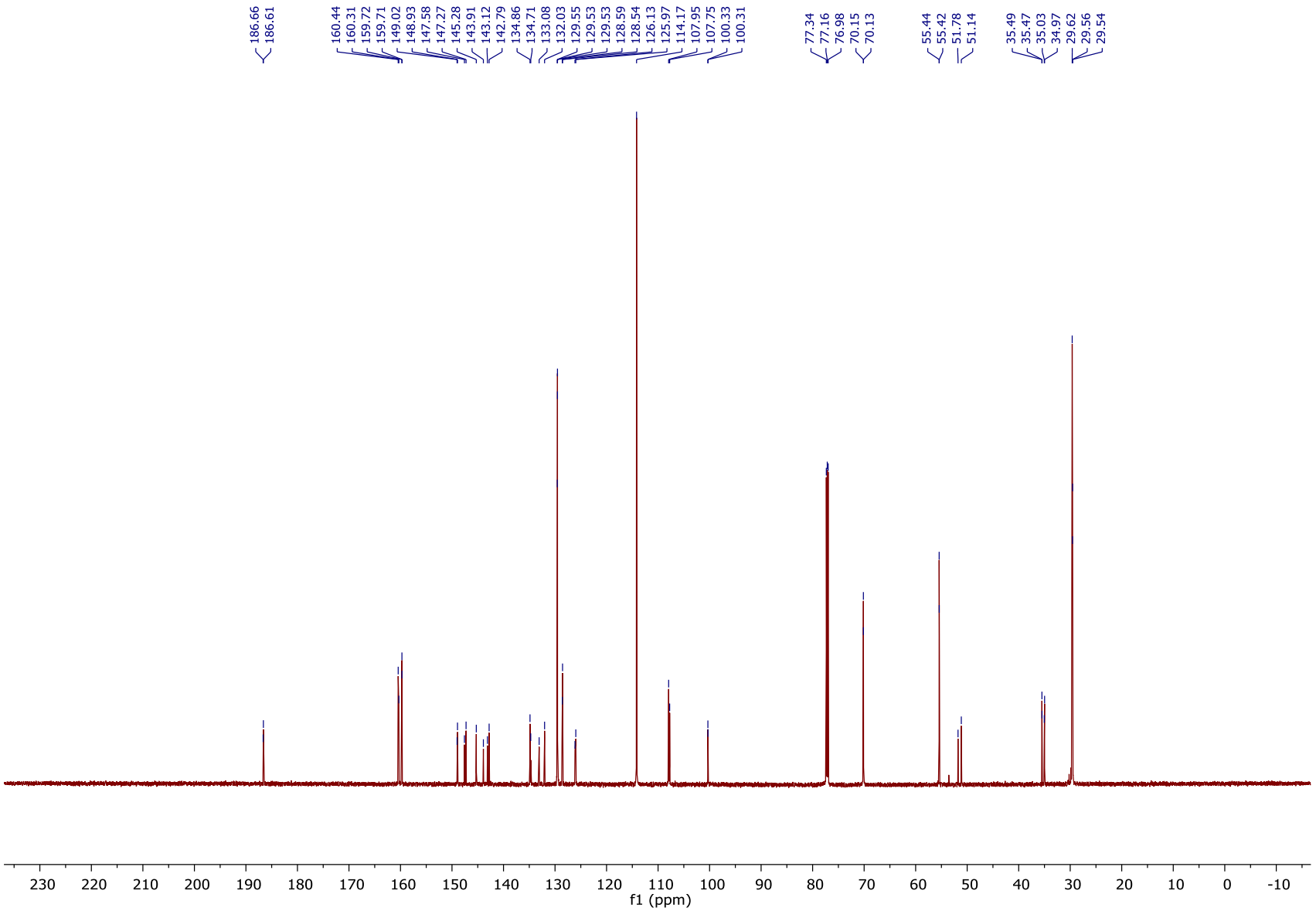

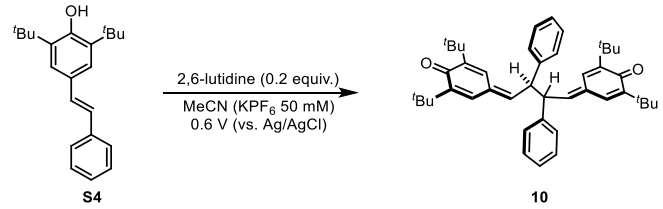

(10) 4,4'-((2*R*,3*R*)-2,3-diphenylbutane-1,4-diylidene)bis(2,6-di-*tert*-butylcyclohexa-2,5-dien-1-one)

Stilbene **S4** (0.1 mmol, 33 mg) was subjected to the general dimerization procedure, affording bis-quinone methide **10** (32.6 mg, 99% yield, 4:3 dr).

^{1}H NMR (500 MHz, Chloroform-*d*) δ 7.31 (t, *J* = 7.5 Hz, 4H), 7.25 – 7.08 (m, 20H), β-H's of quinone methides: 6.82 (minor diastereomer, d, *J* = 2.4 Hz, 2H), 6.70 (major diastereomer, d, *J* = 2.4 Hz, 2H), δ-H's of quinone methides: 6.52 – 6.47 (minor diastereomer, m, 2H), 6.42 – 6.35 (major diastereomers, m, 2H), 4.42 (m, sp^3 methines of both diastereomers, 4H), ^{t}Bu signals: 1.25 (s, 18 H), 1.25 (s, 18H), 1.23 (s, 18 H), 1.22 (s, 18 H).

^{13}C NMR (126 MHz, Chloroform-*d*) δ 186.59, 186.55, 149.11, 148.91, 147.61, 147.32, 145.47, 144.98, 141.14, 140.63, 134.67, 132.76, 132.02, 129.17, 128.97, 128.47, 128.27, 127.55, 127.23, 126.07, 125.94, 51.68, 51.31, 35.52, 35.49, 35.03, 34.95, 29.60, 29.56, 29.52.

IR (Neat): 2951, 2915, 1614, 1577, 1453, 1358, 1257, 917, 883, 759, 697 cm^{-1};

HRMS (ESI) *m/z* calculated for $NaC_{44}H_{54}O_2^+$ ([M+Na]$^+$) 637.4016, found 637.4012.

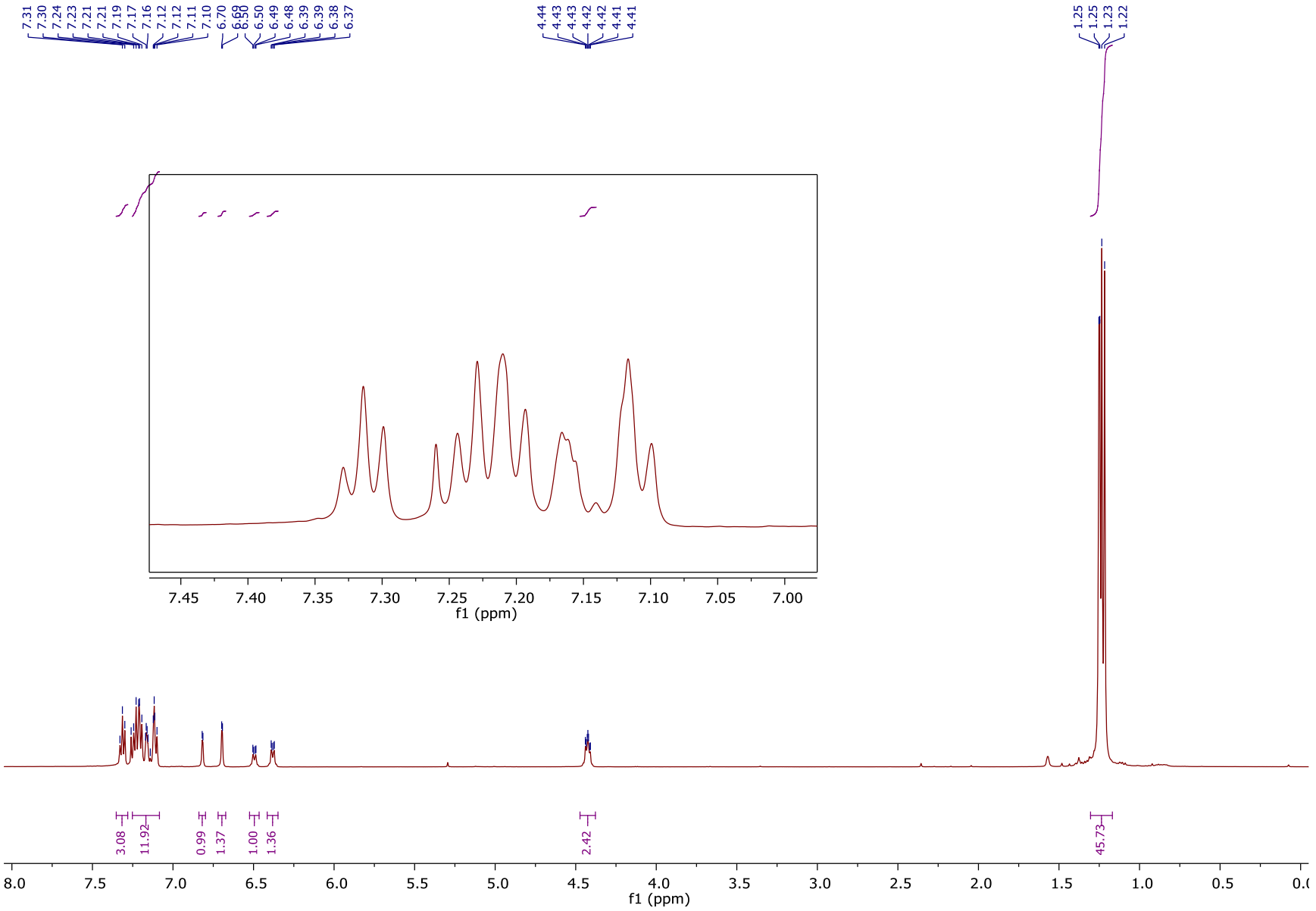
7.31
7.30
7.24
7.23
7.21
7.21
7.19
7.17
7.16
7.12
7.12
7.11
7.10
6.70
6.69
6.50
6.50
6.49
6.48
6.39
6.39
6.38
6.37
4.44
4.43
4.43
4.42
4.42
4.41
4.41
1.25
1.25
1.23
1.22
7.45
7.40
7.35
7.30
7.25
7.20
7.15
7.10
7.05
7.00
f1 (ppm)
3.08
11.92
0.99
1.37
1.00
1.36
2.42
45.73
8.0
7.5
7.0
6.5
6.0
5.5
5.0
4.5
4.0
3.5
3.0
2.5
2.0
1.5
1.0
0.5
f1 (ppm)

^{13}C NMR, 126 MHz, Chloroform-*d*, Dimer **10**

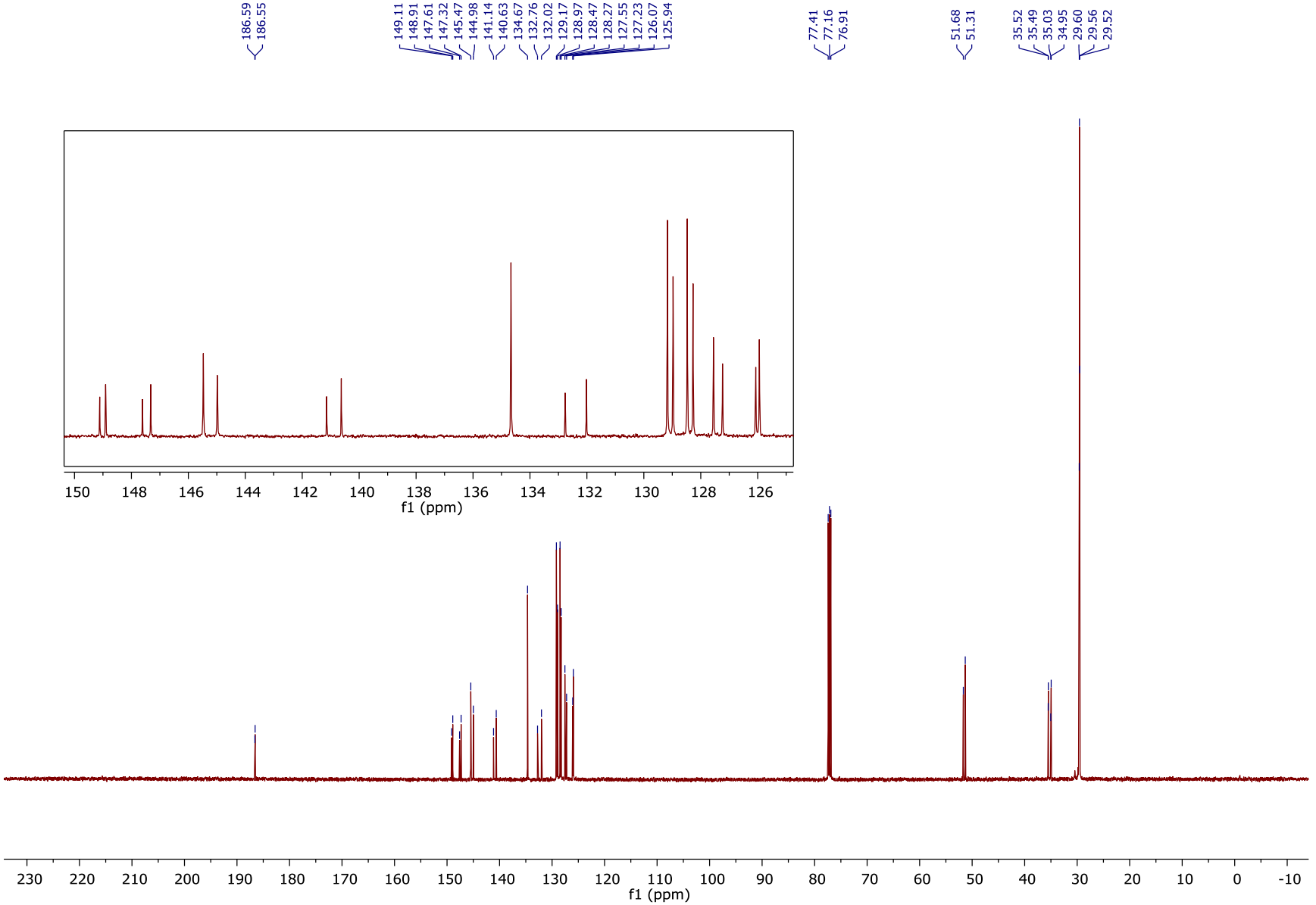

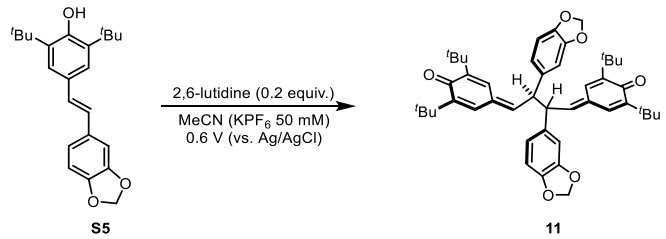

(11) 4,4'-((2*R*,3*R*)-2,3-bis(benzo[*d*][1,3]dioxol-5-yl)butane-1,4-diylidene)bis(2,6-di-*tert*-butylcyclohexa-2,5-dien-1-one)

Stilbene **S5** (0.1 mmol, 35.2 mg) was subjected to the general dimerization procedure, affording bis-quinone methide **11** (34.7 mg, 99% yield, 3:2 dr).

^{1}H NMR (500 MHz, Chloroform-*d*) δ 7.16 (minor diastereomer, d, *J* = 2.4 Hz, 2H), 7.10 (major diastereomer, d, *J* = 2.4 Hz, 2H), 6.79 (minor diastereomer, d, *J* = 2.3 Hz, 2H), 6.73 (minor diastereomer, d, *J* = 7.9 Hz, 2H), 6.69 (d, *J* = 1.6 Hz, 4H), 6.68 – 6.64 (m, 4H), 6.62 (d, *J* = 1.7 Hz, 2H), 6.55 (dd, *J* = 8.0, 1.7 Hz, 2H), 6.36 (δ-H, minor diastereomer, dt, *J* = 8.7, 4.4 Hz, 2H), 6.32 – 6.26 (δ-H, minor diastereomer, m, 2H), 5.93 (d, *J* = 2.3 Hz, 4H), 5.91 (d, *J* = 2.1 Hz, 4H), 4.30 – 4.21 (sp^3 methines of both diastereomers, m, 4H), ^{t}Bu signals: 1.26 (s, 18 H), 1.25 (s, 36 H), 1.23 (s, 18 H).

^{13}C NMR (126 MHz, Chloroform-*d*) δ 186.58, 186.56, 149.21, 148.97, 148.36, 148.15, 147.67, 147.36, 146.94, 146.67, 145.39, 144.85, 134.91, 134.68, 134.63, 134.52, 132.60, 131.90, 125.96, 125.93, 121.74, 121.61, 108.80, 108.70, 108.32, 108.27, 101.37, 101.29, 51.25, 50.95, 35.55, 35.50, 35.04, 34.98, 29.63, 29.58, 29.55, 29.53.

IR (Neat): 2954, 2914, 2361, 2336, 1616, 1539, 1362, 1243, 1034, 924, 808 cm^{-1};

HRMS (ESI) *m/z* calculated for $NaC_{46}H_{54}O_6^+$ ($[M+Na]^+$) 725.3813, found 725.3817.

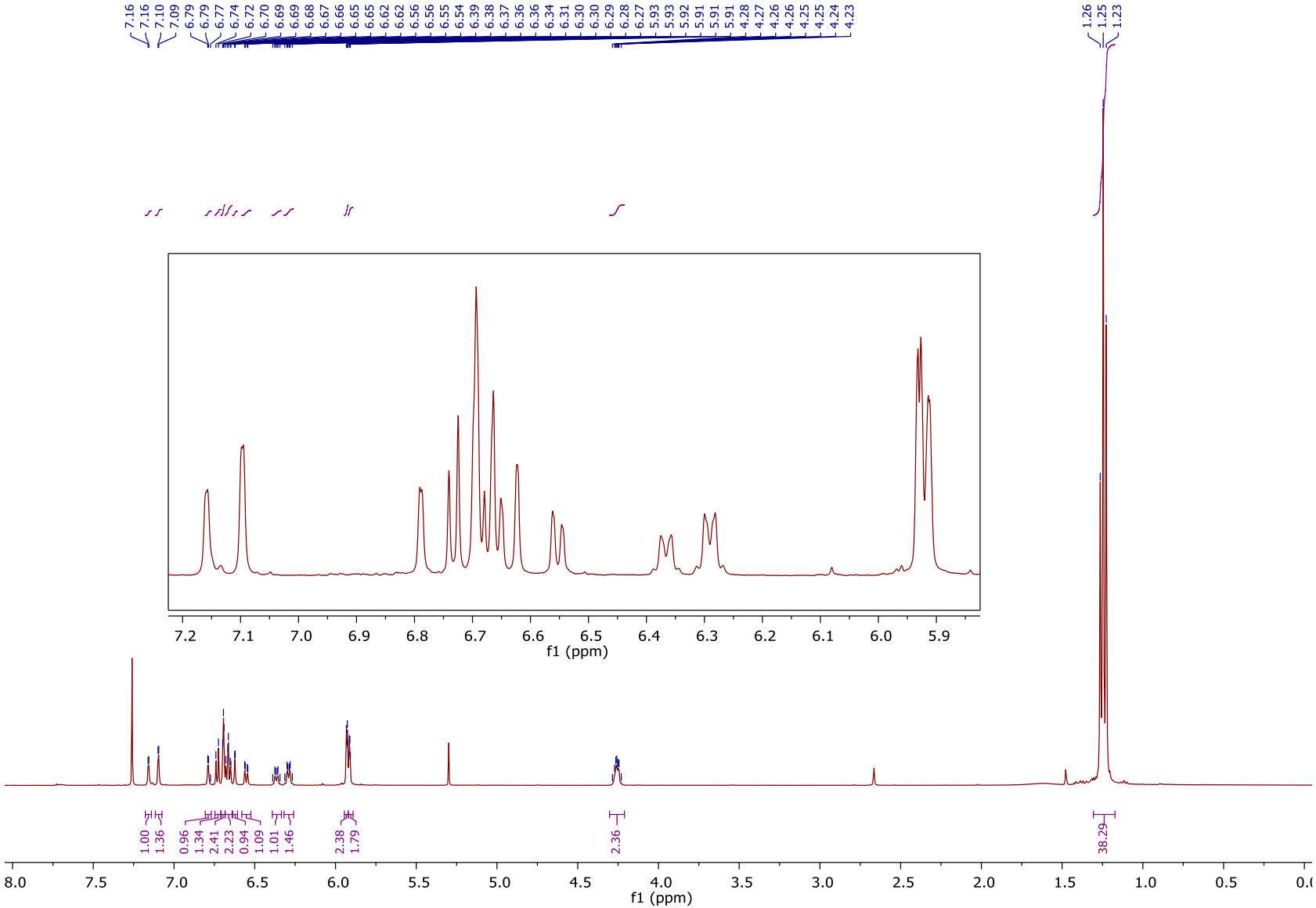
7.16 7.16 7.10 7.09 6.79 6.79 6.77 6.74 6.72 6.70 6.69 6.69 6.68 6.67 6.66 6.65 6.65 6.62 6.62 6.56 6.56 6.55 6.54 6.39 6.38 6.37 6.36 6.36 6.34 6.31 6.30 6.30 6.29 6.28 6.27 5.93 5.93 5.92 5.91 5.91 5.91 4.28 4.27 4.26 4.26 4.25 4.25 4.24 4.23
1.26 1.25 1.23
7.2 7.1 7.0 6.9 6.8 6.7 6.6 6.5 6.4 6.3 6.2 6.1 6.0 5.9
f1 (ppm)
1.00 1.36 0.96 1.34 2.41 2.23 0.94 1.09 1.01 1.46 2.38 1.79 2.36 38.29
8.0 7.5 7.0 6.5 6.0 5.5 5.0 4.5 4.0 3.5 3.0 2.5 2.0 1.5 1.0 0.5
f1 (ppm)

^{13}C NMR, 126 MHz, Chloroform-*d*, Dimer **11**

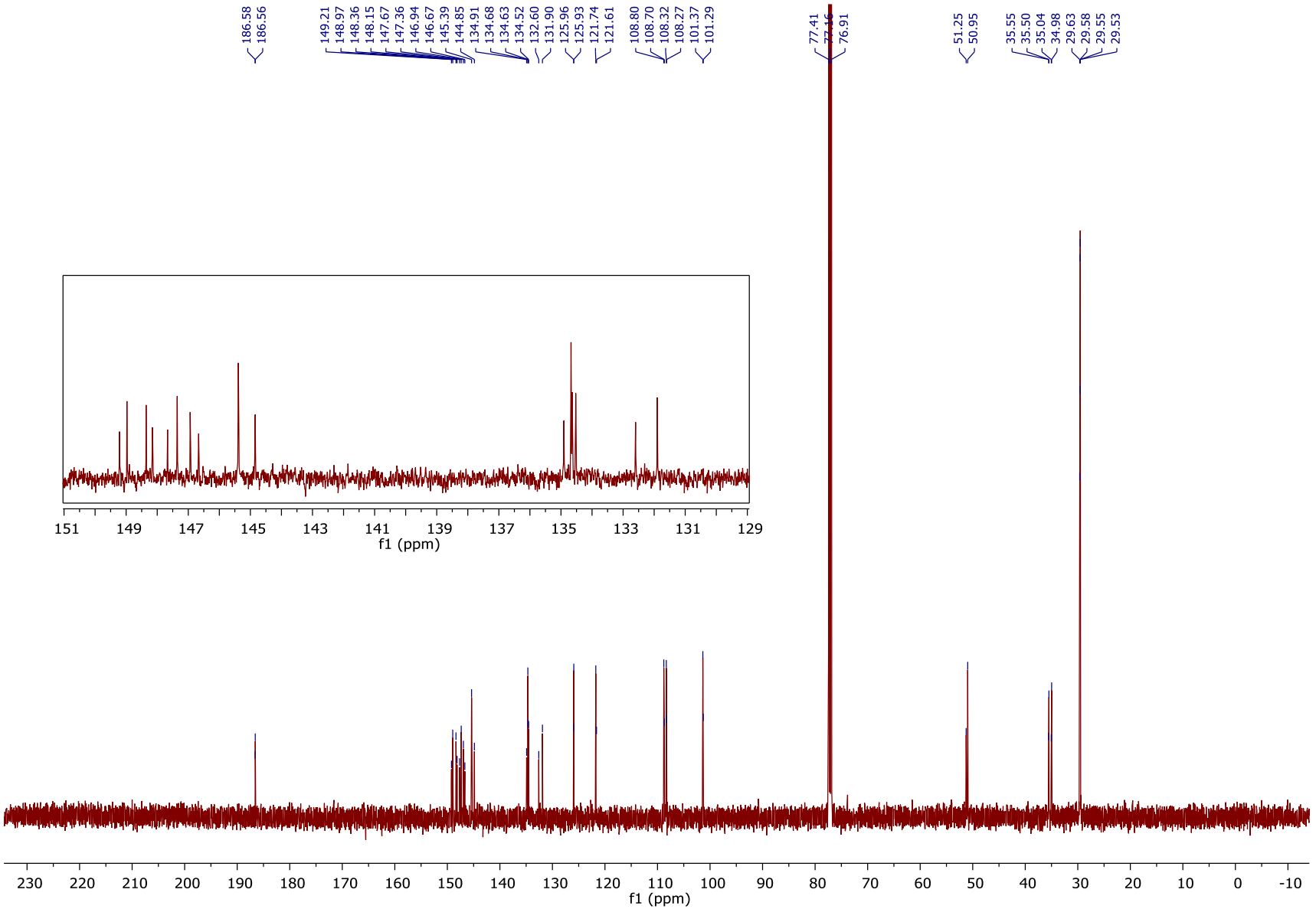

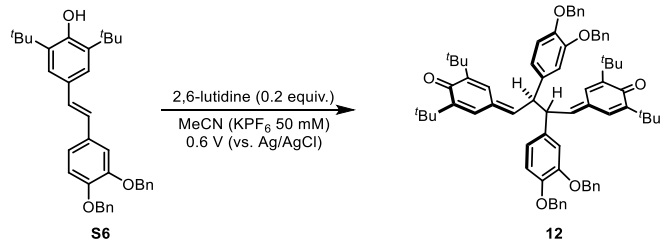

(12) 4,4'-((2*R*,3*R*)-2,3-bis(3,4-bis(benzyloxy)phenyl)butane-1,4-diylidene)bis(2,6-di-*tert*-butylcyclohexa-2,5-dien-1-one)

Stilbene **S6** (0.1 mmol, 52.1 mg) was subjected to the general dimerization procedure, affording bis-quinone methide **12** (48.9 mg, 94% yield, 5:4 dr).

^{1}H NMR (500 MHz, Chloroform-*d*) δ 7.40 (t, *J* = 6.5 Hz, 4H), 7.37 – 7.27 (m, 16H), 7.10 (major diastereomer, d, *J* = 2.3 Hz, 1H), 7.01 (minor diastereomer, d, *J* = 2.1 Hz, 1H), 6.86 (major diastereomer, d, *J* = 8.2 Hz, 1H), 6.77 (s, 1H), 6.76 (d, *J* = 8.0 Hz, 1H), 6.68 (m, 2H), 6.67 – 6.63 (m, 2H), 6.56 (minor diastereomer, d, *J* = 2.0 Hz, 1H), 6.49 (minor diastereomer, dd, *J* = 8.3, 2.0 Hz, 1H), 6.29 (minor diastereomer, d, *J* = 8.2 Hz, 1H), 6.22 (major diastereomer, d, *J* = 8.4 Hz, 1H), 5.11 (major diastereomer, s, 2H), 5.08 (minor diastereomer, s, 2H), 5.04 (major diastereomer, d, *J* = 11.9 Hz, 1H), 5.00 (major diastereomer, d, *J* = 11.9 Hz, 1H), 4.98 (minor diastereomer, s, 2H), 4.23 (major diastereomer, d, *J* = 8.2 Hz, 1H), 4.12 (minor diastereomer, d, *J* = 8.0 Hz, 1H), 1.26 (s, 9H), 1.25 (s, 9H), 1.23 (s, 9H), 1.22 (s, 9H).

^{13}C NMR (126 MHz, Chloroform-*d*) δ 186.53, 186.49, 149.08, 149.00, 148.99, 148.83, 148.49, 148.26, 147.54, 147.39, 145.58, 144.90, 137.23, 137.17, 137.12, 137.06, 136.94, 134.75, 134.66, 133.98, 133.33, 132.52, 131.72, 128.63, 128.61, 128.03, 128.01, 128.00, 127.98, 127.47, 127.41, 127.35 (2C), 126.10, 125.86, 121.69, 121.55, 120.41, 115.98, 115.69, 115.06, 114.95, 71.81, 71.75, 71.31, 71.27, 51.17, 50.76, 35.50, 35.47, 35.02, 34.99, 29.61 (2C), 29.56, 29.54.

IR (Neat): 2960, 2867, 1616, 1510, 1453, 1358, 1262, 1136, 1021, 734, 697 cm^{-1};

HRMS (ESI) *m/z* calculated for $NaC_{72}H_{78}O_6^+$ ($[M+Na]^+$) 1061.5691, found 1061.5672.

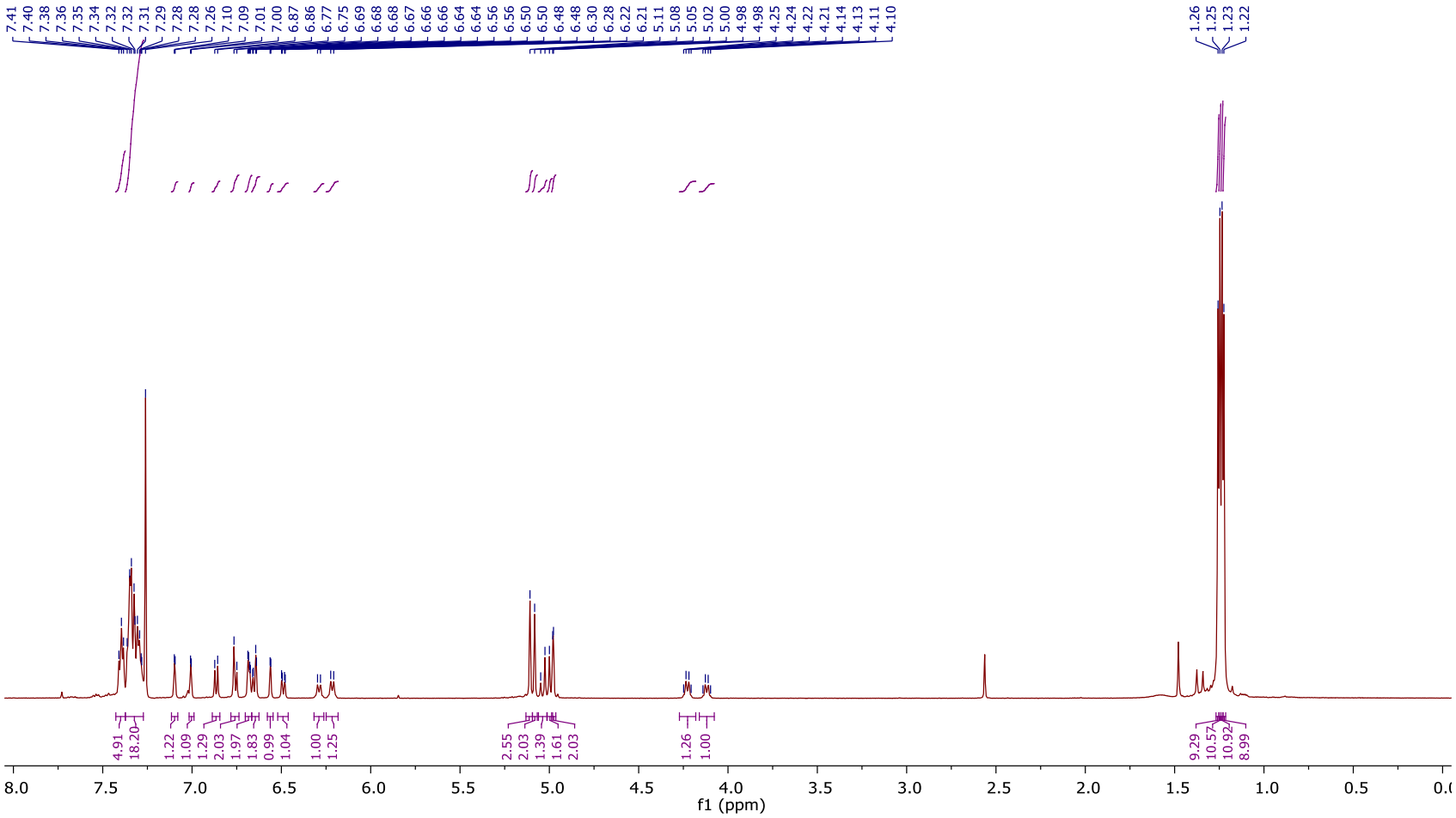
7.41 7.40 7.38 7.36 7.35 7.34 7.32 7.32 7.31 7.29 7.28 7.28 7.26 7.10 7.09 7.01 7.00 6.87 6.86 6.77 6.75 6.69 6.68 6.68 6.67 6.66 6.66 6.64 6.64 6.56 6.56 6.50 6.50 6.48 6.48 6.30 6.28 6.22 6.21 5.11 5.08 5.05 5.02 5.00 4.98 4.98 4.25 4.24 4.22 4.21 4.14 4.13 4.11 4.10
1.26 1.25 1.23 1.22
4.91 18.20 1.22 1.09 1.29 2.03 1.97 1.83 0.99 1.04 1.00 1.25 2.55 2.03 1.39 1.61 2.03 1.26 1.00 9.29 10.57 10.92 8.99
8.0 7.5 7.0 6.5 6.0 5.5 5.0 4.5 4.0 3.5 3.0 2.5 2.0 1.5 1.0 0.5
f1 (ppm)

^{13}C NMR, 126 MHz, Chloroform-*d*, Dimer **12**

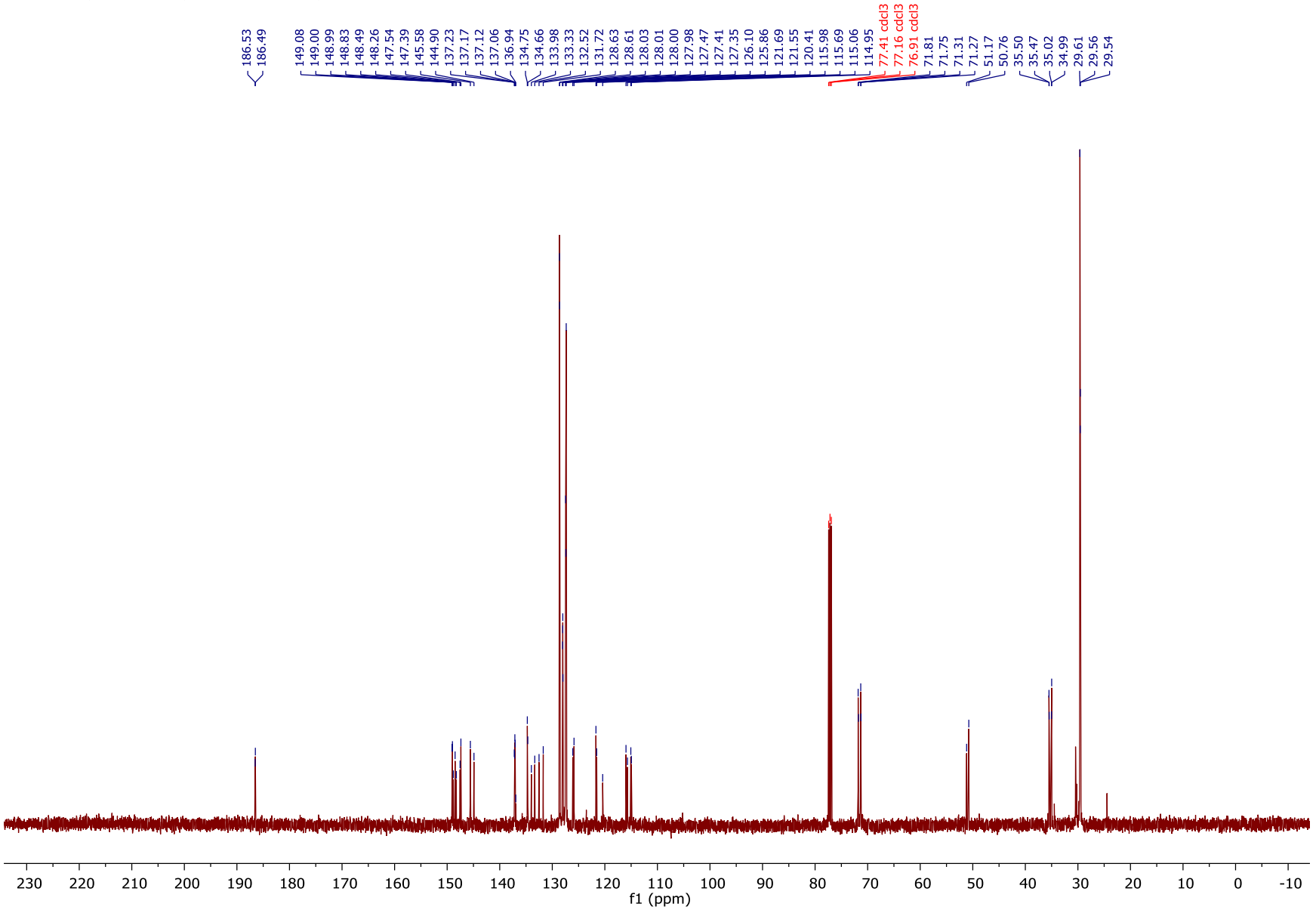

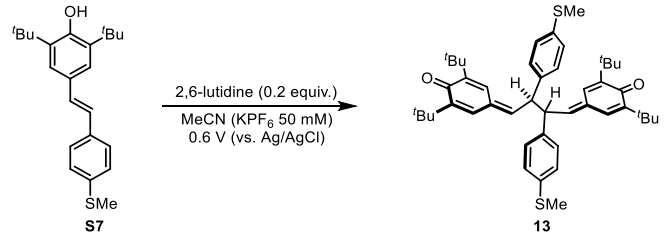

(13) 4,4'-((2*R*,3*R*)-2,3-bis(4-(methylthio)phenyl)butane-1,4-diylidene)bis(2,6-di-*tert*-butylcyclohexa-2,5-dien-1-one)

Stilbene **S7** (0.1 mmol, 35.5 mg) was subjected to the general dimerization procedure, affording bis-quinone methide **13** (32.9 mg, 93% yield, 4:3 dr).

^{1}H NMR (500 MHz, Chloroform-*d*) δ 7.19 (major diastereomer, d, *J* = 8.0 Hz, 4H), 7.12 (m, 12H), 7.02 (minor diastereomer, d, *J* = 8.0 Hz, 4H), β-H's of quinone methides: 6.80 (minor diastereomer, d, *J* = 2.4 Hz, 2H), 6.70 (major diastereomer, d, *J* = 2.4 Hz, 2H), δ-H's of quinone methides: 6.42 (minor diastereomer, dd, *J* = 7.2, 2.4 Hz, 2H), 6.36 – 6.29 (major diastereomer, m, 2H), 4.43 – 4.30 (sp^3 methines of both diastereomers, m, 4H), 2.44 (s, 3H), 2.42 (s, 3H), ^{t}Bu signals: 1.25 (s, 18 H), 1.25 (s, 18H), 1.24 (s, 18 H), 1.22 (s, 18 H).

^{13}C NMR (126 MHz, Chloroform-*d*) δ 186.56, 186.51, 149.25, 149.13, 147.71, 147.47, 145.03, 144.63, 137.93, 137.68, 137.59, 137.21, 134.62, 132.65, 132.02, 128.88, 128.70, 127.11, 126.98, 125.92, 125.79, 50.91, 50.64, 35.54, 35.53, 35.05, 34.99, 29.60, 29.58, 29.55, 29.52, 15.83, 15.80.

IR (Neat): 2960, 2906, 1698, 1591, 1437, 1358, 1262, 1096, 1023, 846, 815, 740 cm^{-1};

HRMS (ESI) *m/z* calculated for $NaC_{46}H_{58}O_2S_2^+$ ($[M+Na]^+$) 729.3770, found 729.3773.

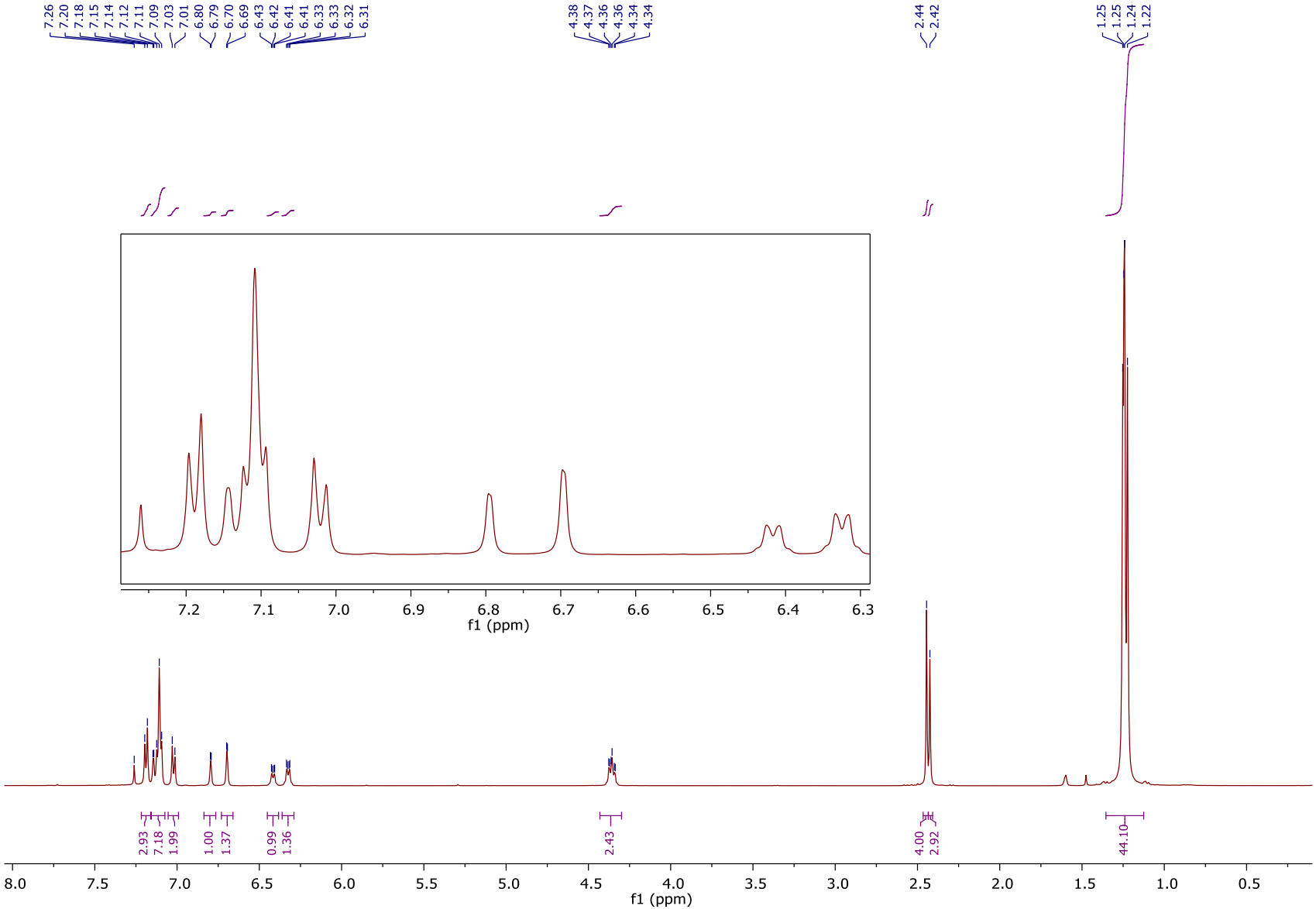
7.26
7.20
7.18
7.15
7.14
7.12
7.11
7.09
7.03
7.01
6.80
6.79
6.70
6.69
6.43
6.42
6.41
6.41
6.33
6.33
6.32
6.31
4.38
4.37
4.36
4.36
4.34
4.34
2.44
2.42
1.25
1.25
1.24
1.22
7.2
7.1
7.0
6.9
6.8
6.7
6.6
6.5
6.4
6.3
f1 (ppm)
2.93
7.18
1.99
1.00
1.37
0.99
1.36
2.43
4.00
2.92
44.10
8.0
7.5
7.0
6.5
6.0
5.5
5.0
4.5
4.0
3.5
3.0
2.5
2.0
1.5
1.0
0.5
f1 (ppm)

^{13}C NMR, 126 MHz, Chloroform-*d*, Dimer **13**

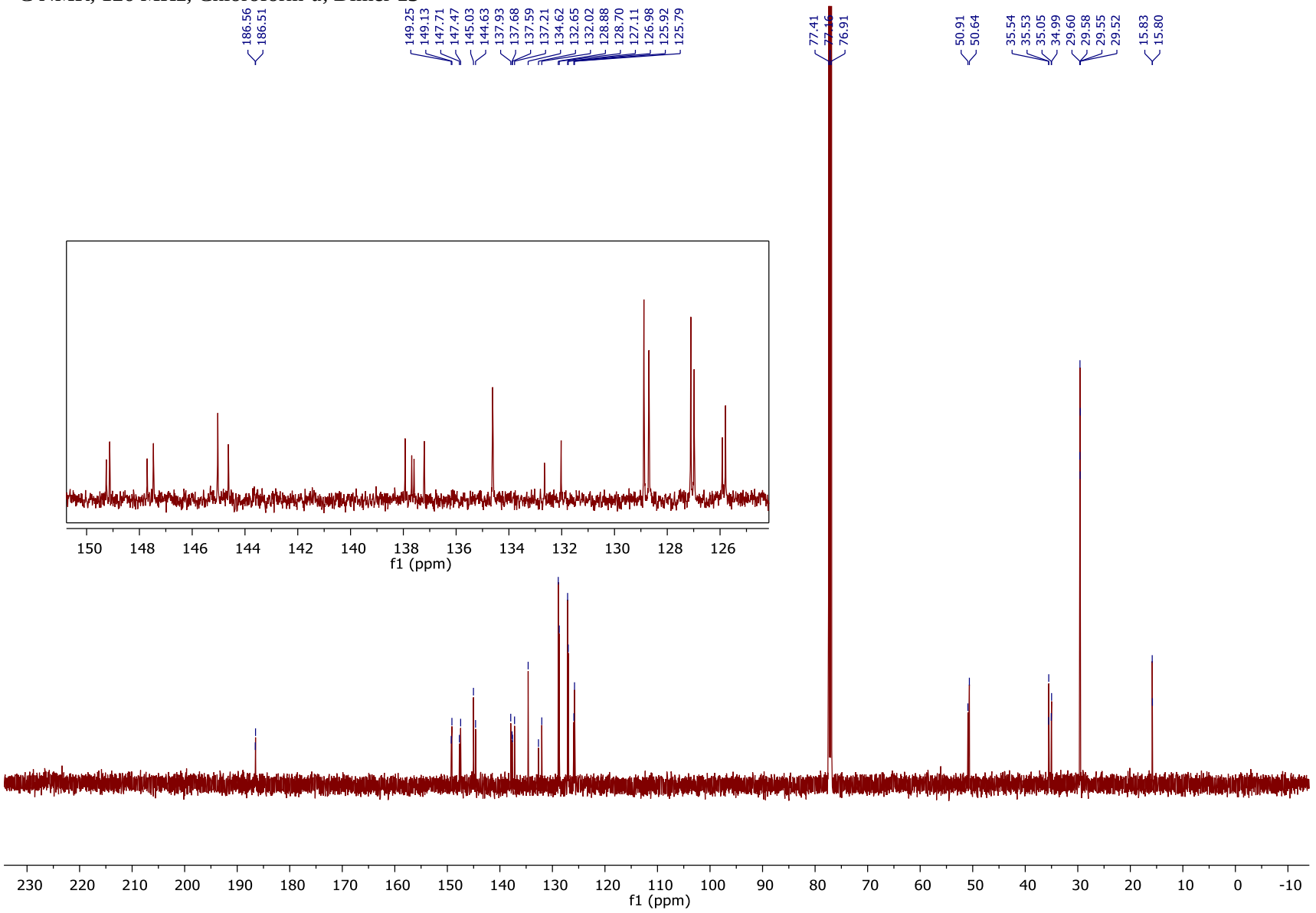

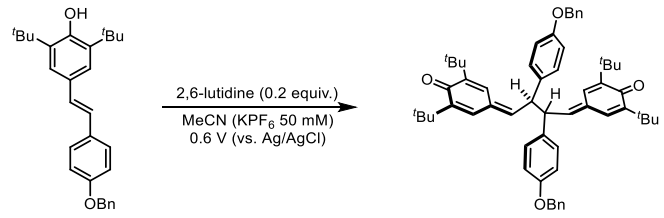

(14) 4,4'-((2*R*,3*R*)-2,3-bis(4-(benzyloxy)phenyl)butane-1,4-diylidene)bis(2,6-di-*tert*-butylcyclohexa-2,5-dien-1-one)

Stilbene **S8** (0.1 mmol, 41.5 mg) was subjected to the general dimerization procedure, affording bis-quinone methide **14** (39.3 mg, 95% yield, 3:2 dr).

^{1}H NMR (700 MHz, Chloroform-*d*) δ 7.43 – 7.35 (m, 16H), 7.34 – 7.31 (m, 4H), 7.14 (β-H, minor diastereomer, d, *J* = 2.4 Hz, 2H), 7.12 (β-H, major diastereomer, d, *J* = 2.4 Hz, 2H), 7.09 (major diastereomer, d, *J* = 8.7 Hz, 4H), 7.02 (minor diastereomer, d, *J* = 8.7 Hz, 4H), 6.91 (major diastereomer, d, *J* = 8.7 Hz, 4H), 6.85 (minor diastereomer, d, *J* = 8.7 Hz, 4H), 6.80 (β-H, minor diastereomer, d, *J* = 2.4 Hz, 2H), 6.70 (β-H, major diastereomer, d, *J* = 2.4 Hz, 2H), 6.44 (δ-H, minor diastereomer, d, *J* = 8.2 Hz, 2H), 6.35 (δ-H, major diastereomer, d, *J* = 8.4 Hz, 2H), 5.01 (major diastereomer, s, 4H), 4.99 (minor diastereomer, s, 4H), 4.31 (sp^3 methines of both diastereomers, m, 4H), ^{t}Bu signals: 1.25 (s, 36H), 1.24 (s, 18H), 1.23 (s, 18H).

^{13}C NMR (176 MHz, Chloroform-*d*) δ 186.62, 186.58, 158.08, 157.85, 149.02, 148.88, 147.52, 147.25, 146.02, 145.41, 136.92, 136.87, 134.80, 134.75, 133.43, 132.95, 132.40, 131.70, 129.49, 129.31, 128.75, 128.74, 128.21, 128.18, 127.64, 127.48, 126.11, 126.03, 123.30, 115.44, 115.30, 70.22, 70.16, 50.87, 50.57, 35.51, 35.02, 34.97, 34.53, 30.45, 29.86, 29.62, 29.60, 29.56, 29.54.

IR (Neat): 2954, 2918, 1608, 1569, 1510, 1358, 1245, 1018, 824, 740, 695 cm^{-1};

HRMS (ESI) *m/z* calculated for $C_{58}H_{67}O_4^+$ ($[M+H]^+$) 827.5034, found 827.5040.

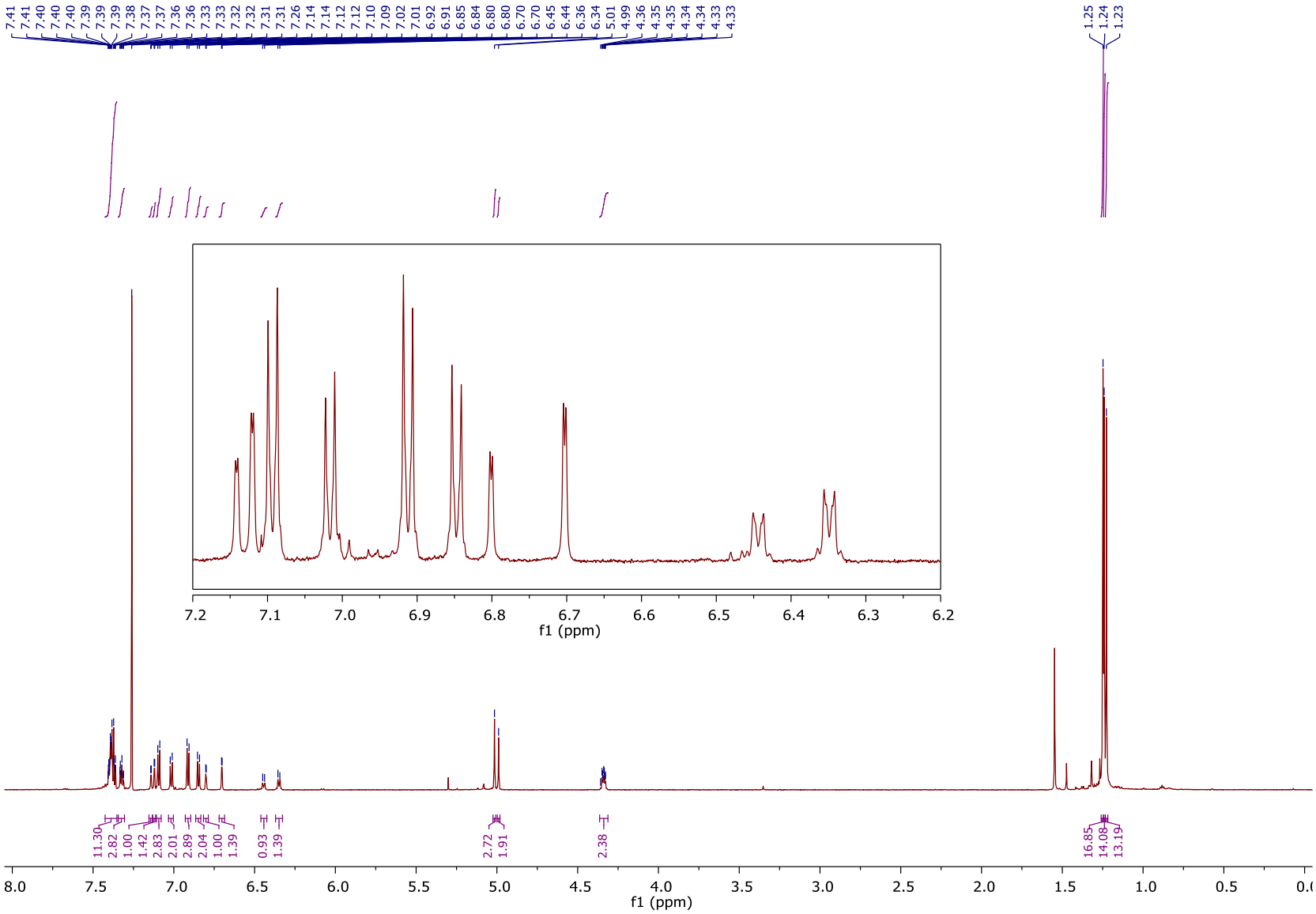
7.41 7.41 7.40 7.40 7.40 7.39 7.39 7.39 7.38 7.37 7.37 7.36 7.36 7.33 7.33 7.32 7.32 7.31 7.31 7.26 7.14 7.14 7.12 7.12 7.10 7.09 7.02 7.01 6.92 6.91 6.85 6.84 6.80 6.80 6.70 6.70 6.45 6.44 6.36 6.34 5.01 4.99 4.36 4.35 4.35 4.34 4.34 4.33 4.33
1.25 1.24 1.23
7.2 7.1 7.0 6.9 6.8 6.7 6.6 6.5 6.4 6.3 6.2
f1 (ppm)
11.30 2.82 1.00 1.42 2.83 2.01 2.89 2.04 1.00 1.39 0.93 1.39 2.72 1.91 2.38 16.85 14.08 13.19
8.0 7.5 7.0 6.5 6.0 5.5 5.0 4.5 4.0 3.5 3.0 2.5 2.0 1.5 1.0 0.5
f1 (ppm)

^{13}C NMR, 176 MHz, Chloroform-*d*, Dimer **14**

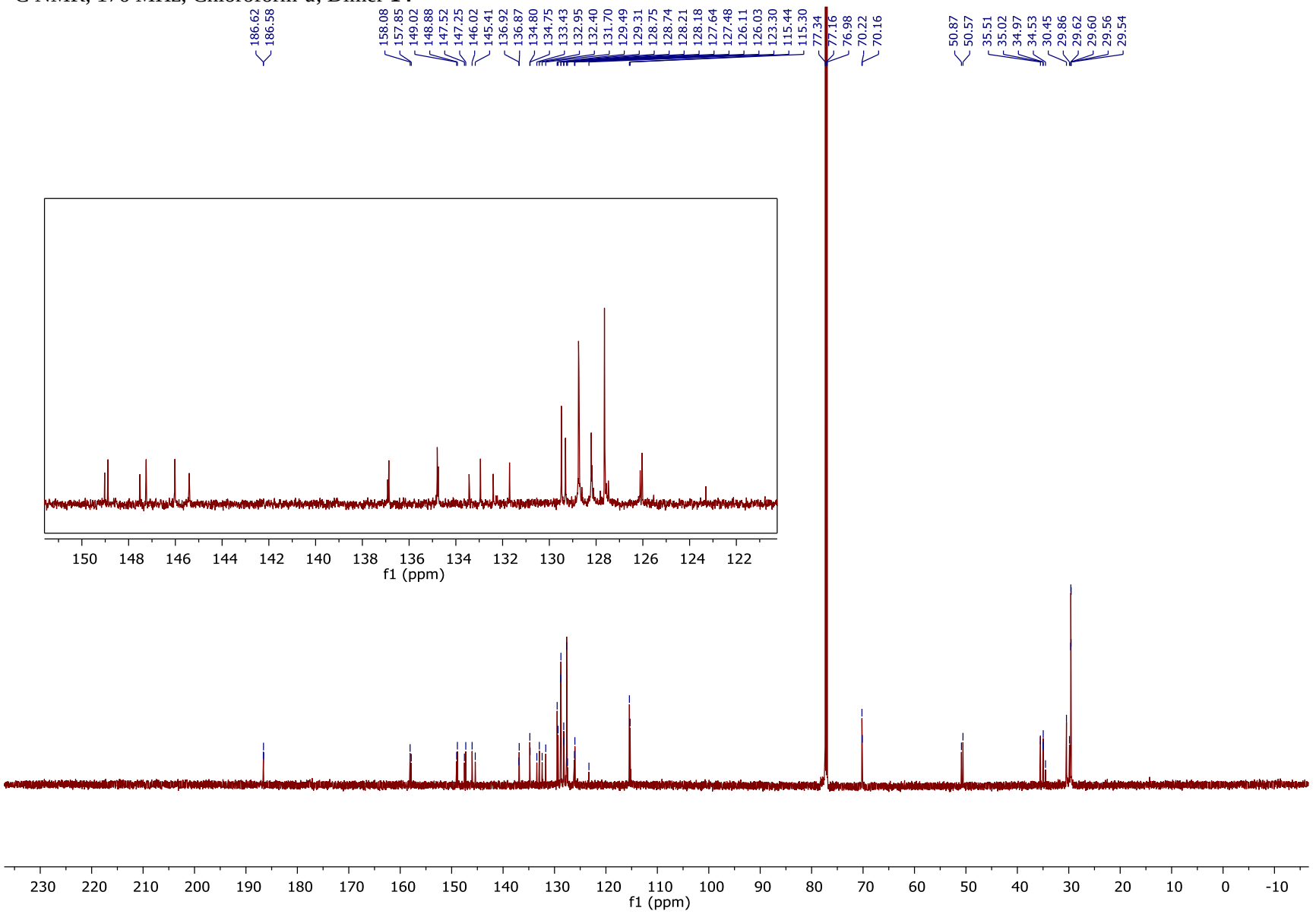

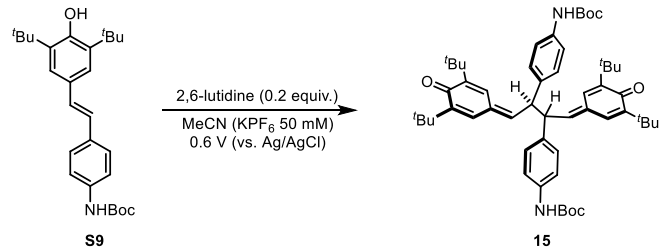

(15) Di-*tert*-butyl (((2*R*,3*R*)-1,4-bis(3,5-di-*tert*-butyl-4-oxocyclohexa-2,5-dien-1-ylidene)butane-2,3-diyl)bis(4,1-phenylene))dicarbamate

Stilbene **S9** (0.1 mmol, 42.4 mg) was subjected to the general dimerization procedure, affording bis-quinone methide **15** (40.7 mg, 95% yield, 3:2 dr).

^{1}H NMR (500 MHz, Chloroform-*d*) δ 7.31 (major diastereomer, d, *J* = 8.2 Hz, 2H), 7.23 (minor diastereomer, d, *J* = 8.1 Hz, 2H), 7.16 (minor diastereomer, d, *J* = 2.3 Hz, 1H), 7.13 (major diastereomer, d, *J* = 2.3 Hz, 2H), 7.09 (major diastereomer, d, *J* = 8.2 Hz, 2H), 7.00 (minor diastereomer, d, *J* = 8.1 Hz, 2H), 6.79 (minor diastereomer, d, *J* = 2.3 Hz, 1H), 6.69 (major diastereomer, d, *J* = 2.3 Hz, 1H), 6.45 (major diastereomer, s, 1H), 6.42 (minor diastereomer, d, *J* = 9.2 Hz, 1H), 6.40 (minor diastereomer, s, 1H), 6.34 (major diastereomer, d, *J* = 8.9 Hz, 1H), 4.35 (major diastereomer, dd, *J* = 7.3, 2.4 Hz, 1H), 4.33 (minor diastereomer, dd, *J* = 7.4, 2.3 Hz, 1H), 1.50 (major diastereomer, s, 9H), 1.49 (minor diastereomer, s, 9H), 1.25 (minor diastereomer, s, 9H), 1.24 (minor diastereomer, s, 9H), 1.24 (major diastereomer, s, 9H), 1.22 (major diastereomer, s, 9H).

^{13}C NMR (126 MHz, Chloroform-*d*) δ 186.60, 186.59, 152.74, 152.69, 149.10, 148.99, 147.56, 147.29, 145.64, 145.21, 137.68, 137.43, 135.41, 134.98, 134.78, 134.71, 132.46, 131.81, 128.99, 128.86, 126.04, 125.94, 118.95, 118.79, 80.88, 80.80, 50.86, 50.59, 35.51, 35.50, 35.02, 34.97, 29.60, 29.58, 29.55, 29.52, 28.45 (2C).

IR (Neat): 3333, 2954, 2864, 1715, 1611, 1521, 1361, 1231, 1153, 1049, 818 cm^{-1};

HRMS (ESI) *m/z* calculated for $NaC_{54}H_{72}N_2O_6^+$ ([M+Na]$^+$) 867.5283, found 867.5276.

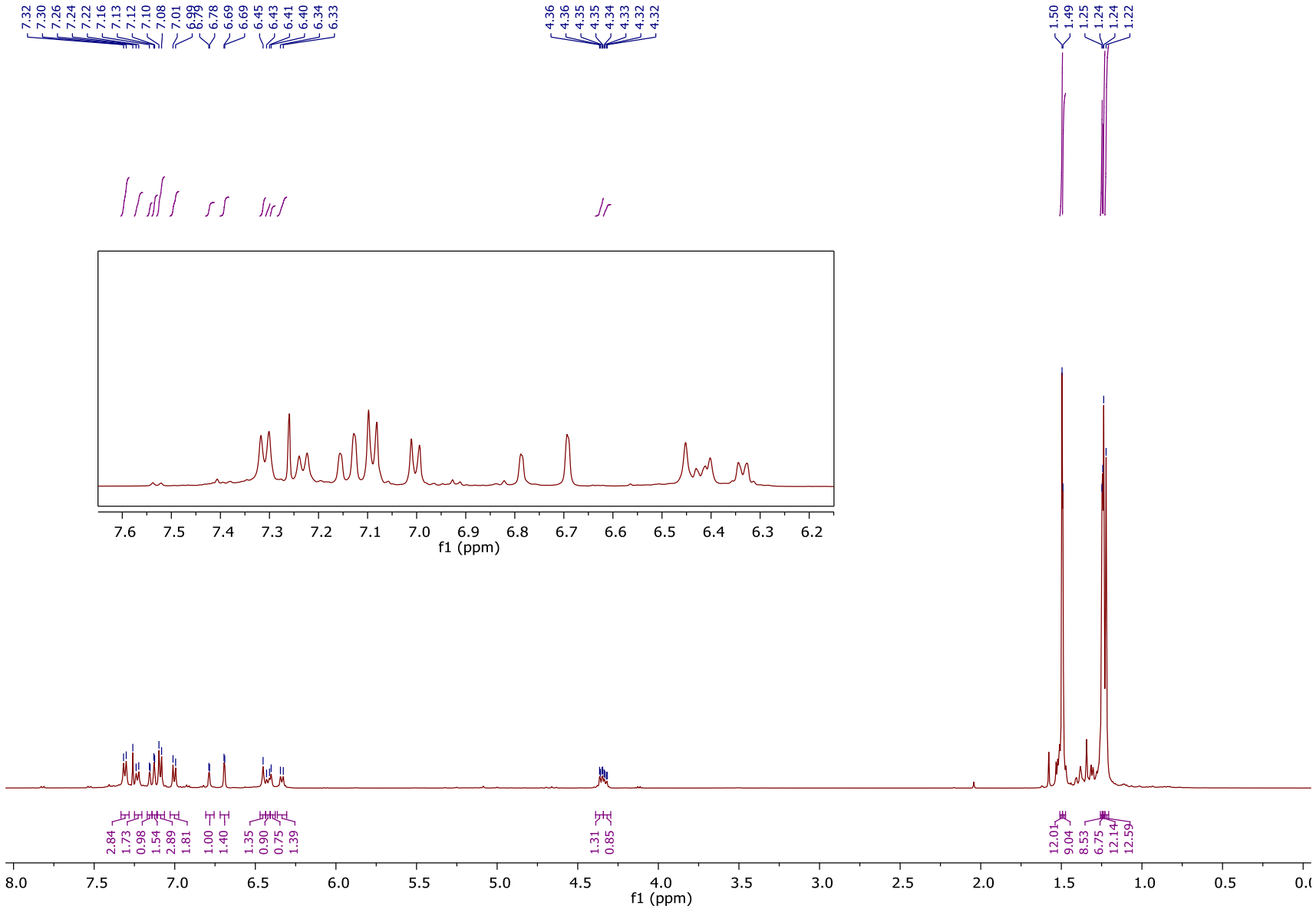
7.32
7.30
7.26
7.24
7.22
7.16
7.13
7.12
7.10
7.08
7.01
6.99
6.78
6.69
6.69
6.45
6.43
6.41
6.40
6.34
6.33
4.36
4.36
4.35
4.35
4.34
4.33
4.32
4.32
1.50
1.49
1.25
1.24
1.24
1.22
7.6 7.5 7.4 7.3 7.2 7.1 7.0 6.9 6.8 6.7 6.6 6.5 6.4 6.3 6.2
f1 (ppm)
2.84 1.73 0.98 1.54 2.89 1.81 1.00 1.40 1.35 0.90 0.75 1.39 1.31 0.85 12.01 9.04 8.53 6.75 12.14 12.59
8.0 7.5 7.0 6.5 6.0 5.5 5.0 4.5 4.0 3.5 3.0 2.5 2.0 1.5 1.0 0.5
f1 (ppm)

^{13}C NMR, 176 MHz, Chloroform-*d*, Dimer **15**

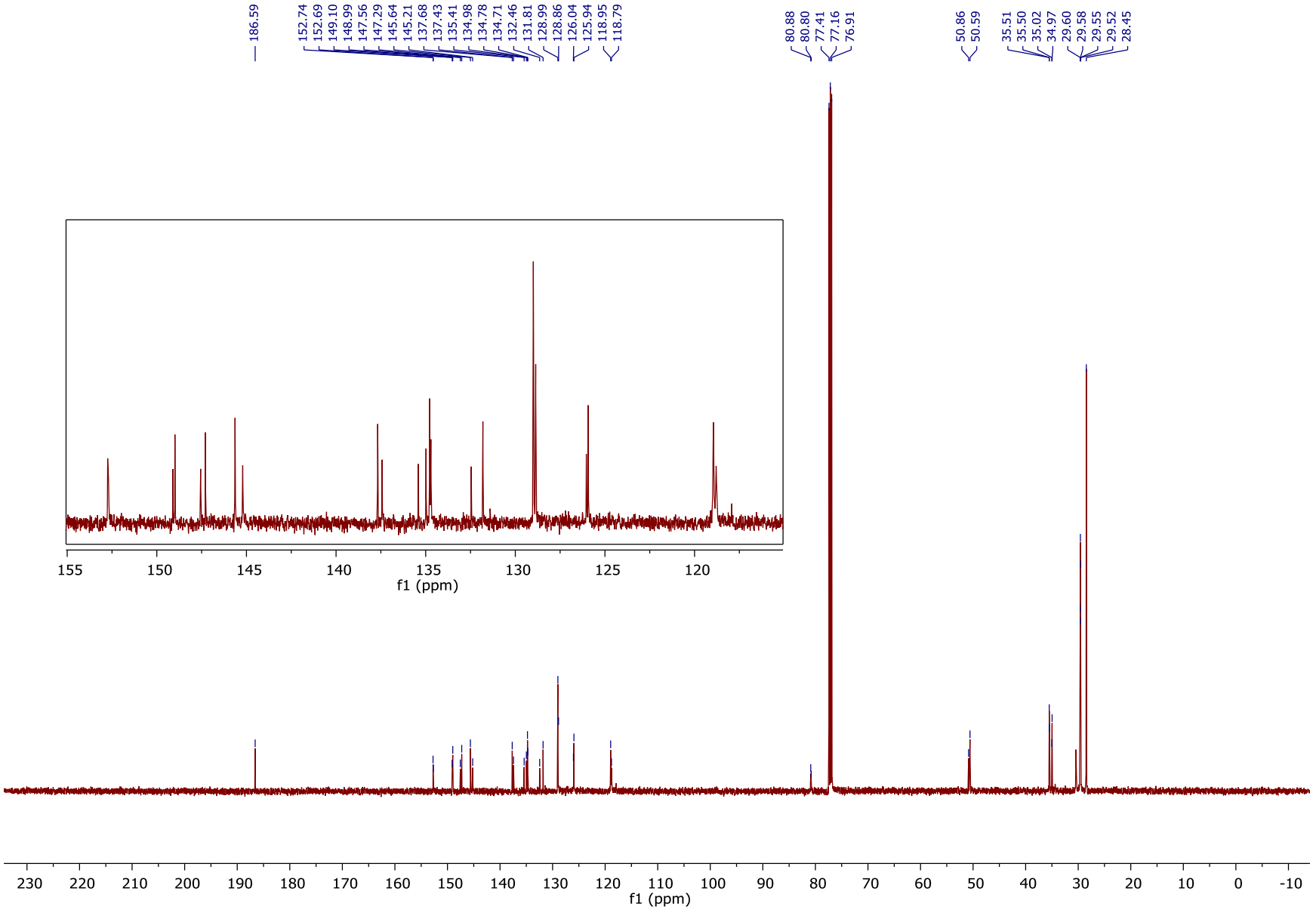

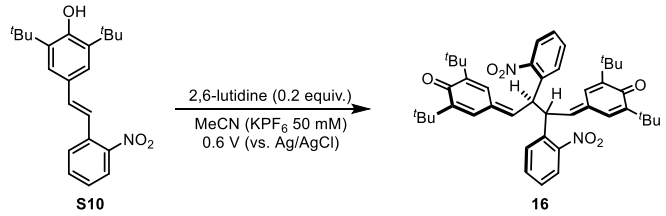

(16) 4,4'-((2*R*,3*R*)-2,3-bis(2-nitrophenyl)butane-1,4-diylidene)bis(2,6-di-*tert*-butylcyclohexa-2,5-dien-1-one)

Stilbene **S10** (0.1 mmol, 35.3 mg) was subjected to the general dimerization procedure, affording bis-quinone methide **16** (32.8 mg, 93% yield, 2:1 dr).

^{1}H NMR (500 MHz, Chloroform-*d*) δ 7.80 (d, *J* = 8.1 Hz, 2H), 7.64 (d, *J* = 4.3 Hz, 4H), 7.61 – 7.57 (m, 2H), 7.56 (dd, *J* = 7.5, 1.4 Hz, 2H), 7.50 (dd, *J* = 8.0, 1.4 Hz, 2H), 7.44 (d, *J* = 2.2 Hz, 2H), 7.38 (dt, *J* = 8.4, 4.3 Hz, 2H), 7.35 – 7.30 (m, 2H), 7.00 (β-H, major diastereomer, d, *J* = 2.4 Hz, 2H), 6.82 (β-H, major diastereomer, d, *J* = 2.3 Hz, 2H), 6.62 (β-H, major diastereomer, d, *J* = 2.3 Hz, 2H), 6.36 (δ-H, minor diastereomer, dd, *J* = 6.5, 2.6 Hz, 2H), 6.25 (δ-H, major diastereomer, dd, *J* = 7.1, 2.8 Hz, 2H), 5.49 – 5.41 (m, 4H), ^{t}Bu signals: 1.27 (s, 18 H), 1.25 (s, 18H), 1.20 (s, 18 H), 1.20 (s, 18 H).

^{13}C NMR (126 MHz, Chloroform-*d*) δ 186.56, 186.47, 150.22, 149.82, 149.71, 148.86, 148.37, 148.00, 141.92, 140.99, 135.23, 135.07, 134.52, 134.07, 133.99, 133.95, 133.91, 133.89, 130.09, 129.76, 128.54, 128.45, 126.22, 125.35, 125.16, 125.05, 44.58, 44.36, 35.76, 35.53, 35.12, 35.01, 29.66, 29.55, 29.50, 29.48.

IR (Neat): 2956, 2917, 1616, 1520, 1345, 1255, 918, 886, 822, 782, 729 cm^{-1};

HRMS (ESI) *m/z* calculated for $C_{44}H_{53}N_2O_6^+$ ([M+H]$^+$) 705.3898, found 705.3893.

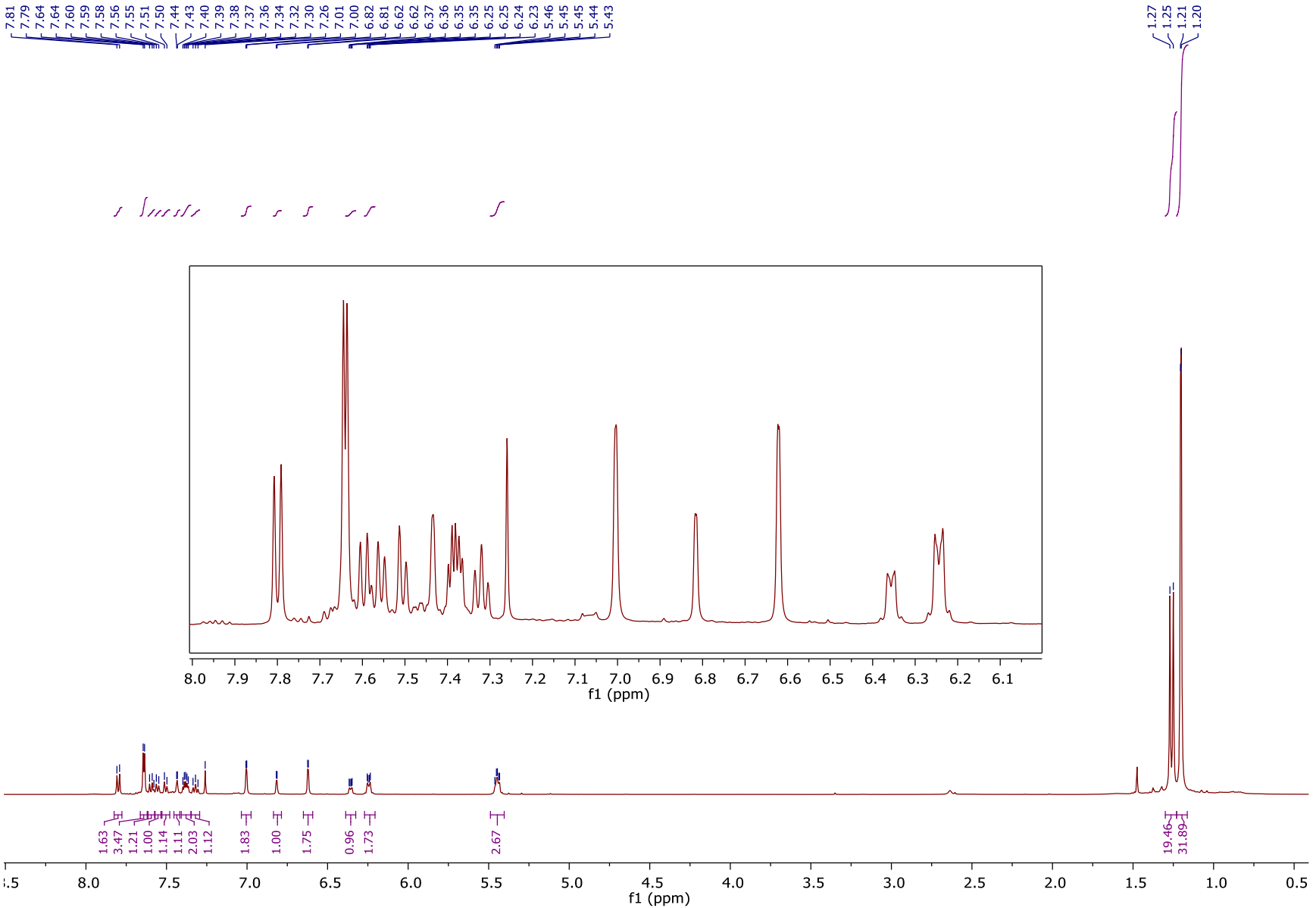
7.81 7.79 7.64 7.64 7.60 7.59 7.58 7.56 7.55 7.51 7.50 7.44 7.43 7.40 7.39 7.38 7.37 7.36 7.34 7.32 7.30 7.26 7.01 7.00 6.82 6.81 6.62 6.62 6.37 6.36 6.35 6.35 6.25 6.25 6.24 6.23 5.46 5.45 5.45 5.44 5.43
1.27 1.25 1.21 1.20
8.0 7.9 7.8 7.7 7.6 7.5 7.4 7.3 7.2 7.1 7.0 6.9 6.8 6.7 6.6 6.5 6.4 6.3 6.2 6.1
f1 (ppm)
1.63 3.47 1.21 1.00 1.14 1.11 2.03 1.12 1.83 1.00 1.75 0.96 1.73 2.67 19.46 31.89
8.5 8.0 7.5 7.0 6.5 6.0 5.5 5.0 4.5 4.0 3.5 3.0 2.5 2.0 1.5 1.0 0.5
f1 (ppm)

^{13}C NMR, 126 MHz, Chloroform-*d*, Dimer **16**

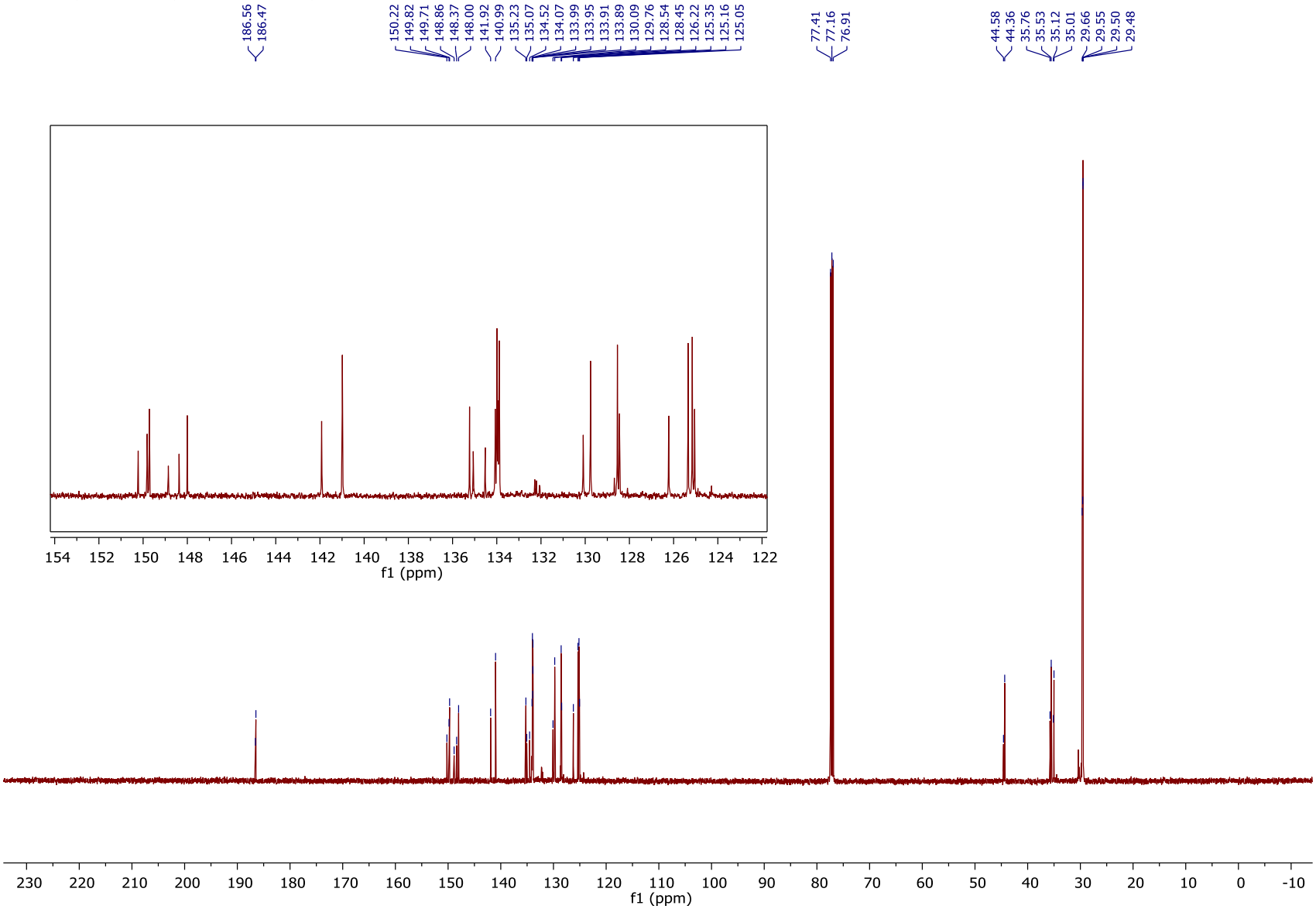

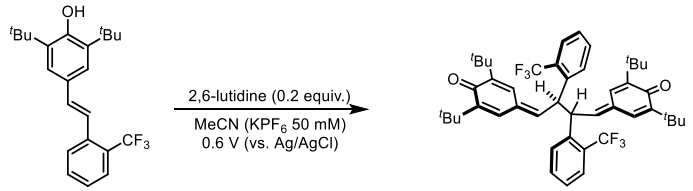

S11 17

(17) 4,4'-((2*R*,3*R*)-2,3-bis(2-(trifluoromethyl)phenyl)butane-1,4-diylidene)bis(2,6-di-*tert*-butylcyclohexa-2,5-dien-1-one)

Stilbene **S11** (0.1 mmol, 37.6 mg) was subjected to the general dimerization procedure, affording bis-quinone methide **17** (36.8 mg, 98% yield, 5:1 dr).

^{1}H NMR (500 MHz, Chloroform-*d*) δ 7.73 (major diastereomer, d, *J* = 7.9 Hz, 2H), 7.62 (major diastereomer, d, *J* = 8.0 Hz, 2H), 7.59 (major diastereomer, t, *J* = 7.7 Hz, 2H), 7.53 (minor diastereomer, d, *J* = 8.0 Hz, 2H), 7.42 (minor diastereomer, t, *J* = 7.7 Hz, 2H), 7.32 (major diastereomer, t, *J* = 7.7 Hz, 2H), 7.24 (minor diastereomer, t, *J* = 7.7 Hz, 2H), β-H's of quinone methides: 7.17 (minor diastereomer, d, *J* = 2.3 Hz, 2H), 7.12 (major diastereomer, d, *J* = 2.5 Hz, 2H), 6.70 (minor diastereomer, d, *J* = 2.4 Hz, 2H), 6.58 (major diastereomer, d, *J* = 2.3 Hz, 2H), δ-H's of quinone methides: 6.25 (major diastereomer, d, *J* = 8.6 Hz, 2H), 6.20 (minor diastereomer, d, *J* = 8.8 Hz, 2H), 5.03 (sp^3 methines of both diastereomers, m, 4H), ^{t}Bu signals: 1.27 (minor diastereomer, s, 18H), 1.25 (major diastereomer, s, 18H), 1.20 (minor diastereomer, s, 18H), 1.17 (major diastereomer, s, 18H),

^{13}C NMR (176 MHz, Chloroform-*d*) δ 186.54, 186.41, 149.07, 148.80, 148.03, 147.56, 143.23, 143.05, 138.97, 138.65, 134.40, 134.06, 132.74, 132.56, 132.40, 132.15, 129.51, 129.21, 128.50 (major diastereomer, q, *J* = 28 Hz), 128.44 (minor diastereomer, q, *J* = 28 Hz), 127.69, 127.29, 126.80 (major diastereomer, q, *J* = 5.3 Hz), 126.62 (minor diastereomer, q, *J* = 5.3 Hz), 126.17, 125.81, 124.50 (major diastereomer, q, *J* = 273 Hz), 124.43 (minor diastereomer, q, *J* = 273 Hz), 46.40, 45.18, 35.48, 35.00, 34.91, 29.70, 29.51, 29.46.

IR (Neat): 3005, 2957, 2918, 1614, 1569, 1453, 1363, 1310, 1155, 1111, 1032, 931, 765 cm^{-1};

HRMS (ESI) *m/z* calculated for $NaC_{46}H_{52}F_6O_2^+$ ($[M+Na]^+$) 773.3764, found 773.3772.

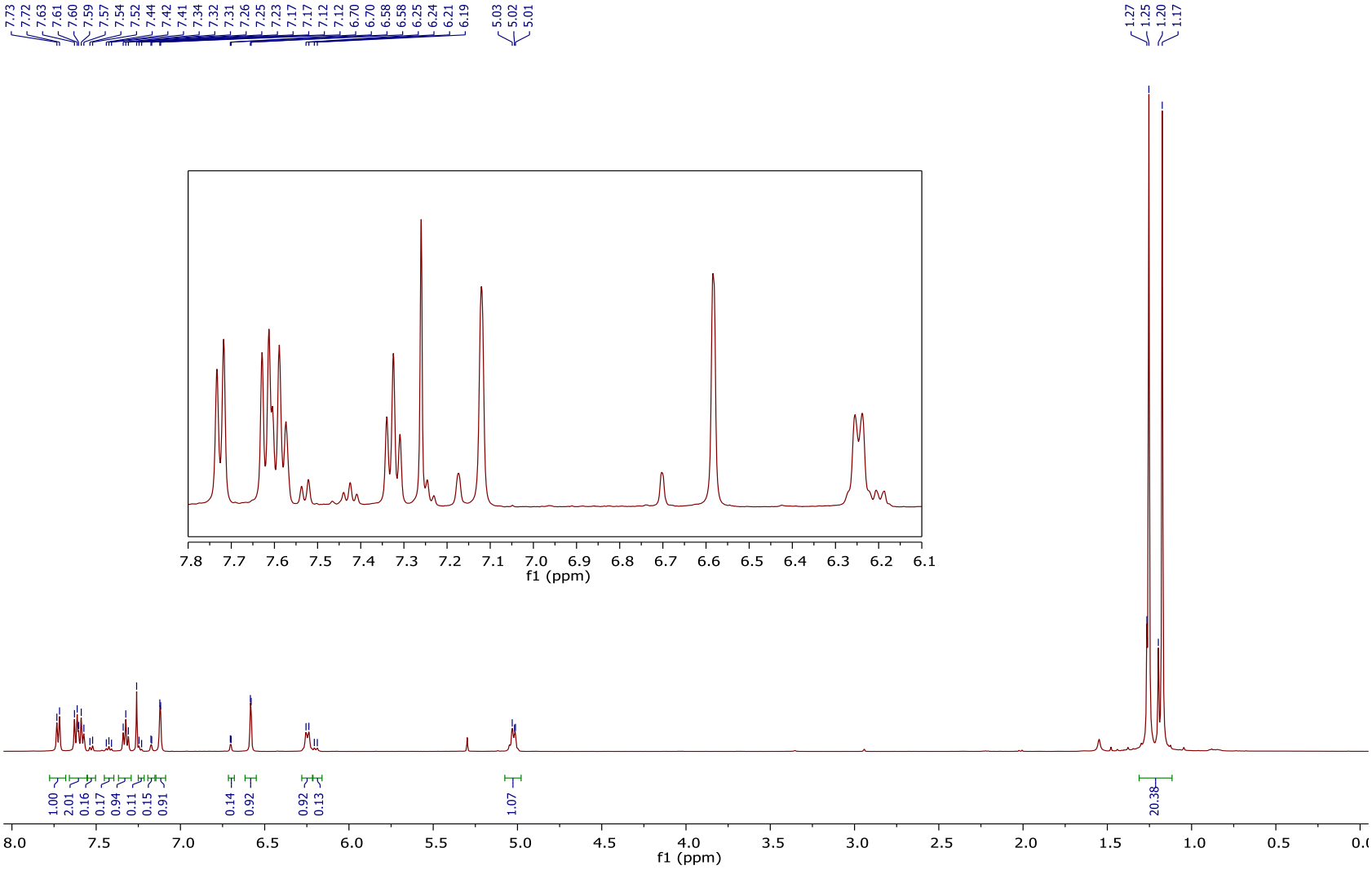
7.73
7.72
7.63
7.61
7.60
7.59
7.57
7.54
7.52
7.44
7.42
7.41
7.34
7.32
7.31
7.26
7.25
7.23
7.17
7.17
7.12
7.12
6.70
6.70
6.58
6.58
6.25
6.24
6.21
6.19
5.03
5.02
5.01
1.27
1.25
1.20
1.17
7.8 7.7 7.6 7.5 7.4 7.3 7.2 7.1 7.0 6.9 6.8 6.7 6.6 6.5 6.4 6.3 6.2 6.1
f1 (ppm)
1.00
2.01
0.16
0.17
0.94
0.11
0.15
0.91
0.14
0.92
0.92
0.13
1.07
20.38
8.0 7.5 7.0 6.5 6.0 5.5 5.0 4.5 4.0 3.5 3.0 2.5 2.0 1.5 1.0 0.5
f1 (ppm)

^{13}C NMR, 176 MHz, Chloroform-*d*, Dimer **17**

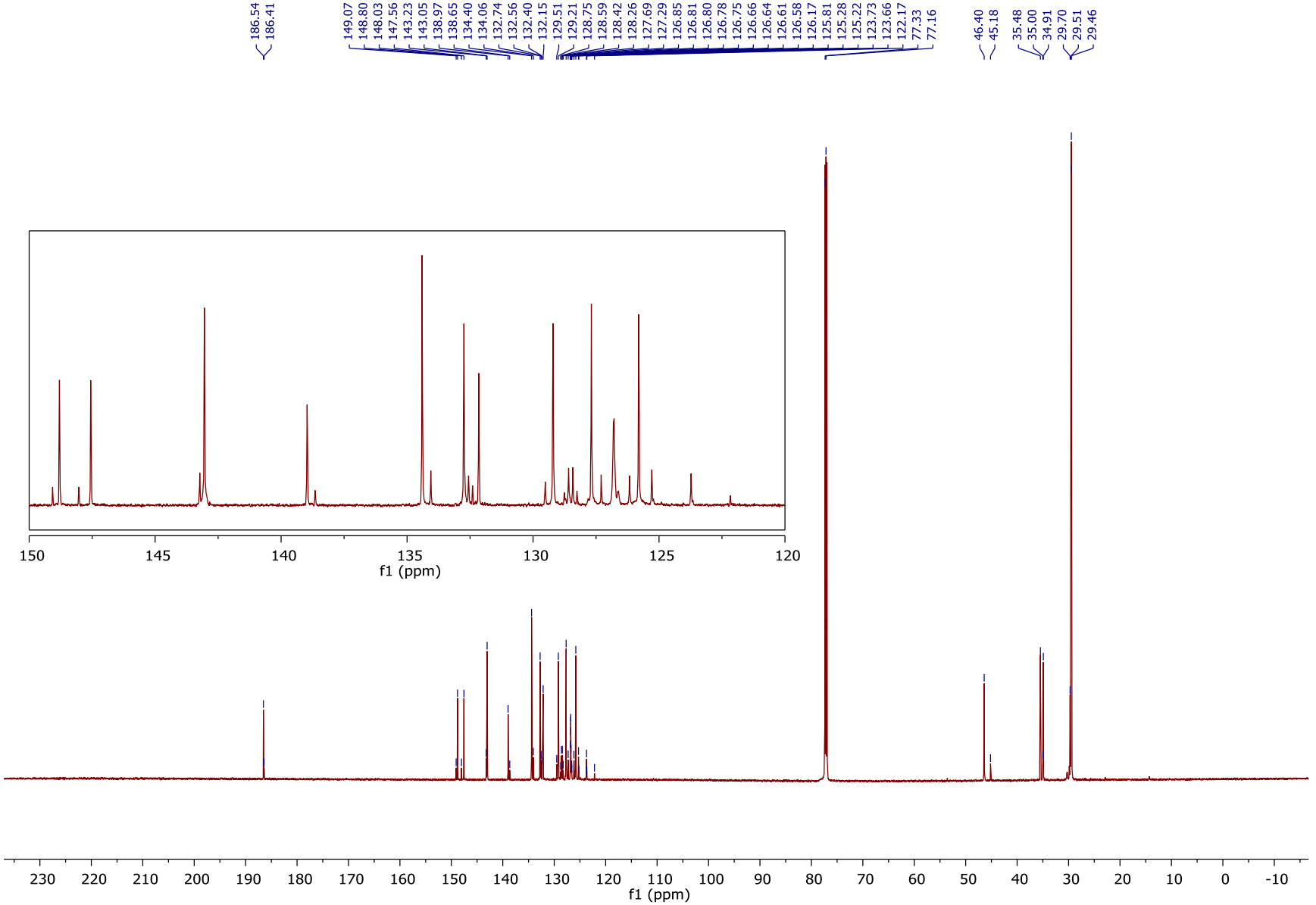

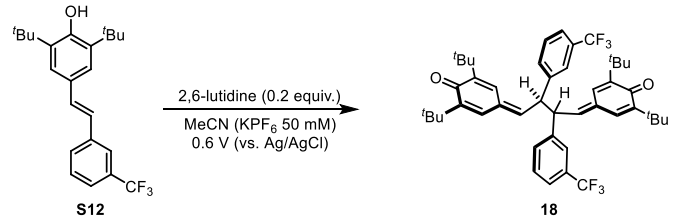

(18) 4,4'-((2*R*,3*R*)-2,3-bis(3-(trifluoromethyl)phenyl)butane-1,4-diylidene)bis(2,6-di-*tert*-butylcyclohexa-2,5-dien-1-one)

Stilbene **S12** (0.1 mmol, 37.6 mg) was subjected to the general dimerization procedure, affording bis-quinone methide **18** (36.4 mg, 97% yield, 4:3 dr).

^{1}H NMR (500 MHz, Chloroform-*d*) δ 7.52 (major diastereomer, d, *J* = 7.8 Hz, 2H), 7.46 (m, 4H), 7.43 – 7.35 (m, 6H), 7.32 (minor diastereomer, d, *J* = 7.8 Hz, 2H), 7.26 (minor diastereomer, s, 2H), β-H's of quinone methides: 7.01 (major diastereomer, d, *J* = 2.4 Hz, 2H), 6.98 (minor diastereomer, d, *J* = 2.4 Hz, 2H), 6.85 (minor diastereomer ,d, *J* = 2.4 Hz, 2H), 6.72 (major diastereomer, d, *J* = 2.4 Hz, 2H), δ-H's of quinone methides: 6.45 (minor diastereomer, d, *J* = 9.5 Hz, 1H), 6.30 (major diastereomer, d, *J* = 9.9 Hz, 1H), 4.46 (sp^3 methine of major diastereomer, d, *J* = 10.0 Hz, 1H), 4.42 (sp^3 methine of minor diastereomer, d, *J* = 9.6 Hz, 1H), ^{t}Bu signals: 1.26 (minor diastereomer, s, 18H), 1.22 (major diastereomer, s, 18H), 1.22 (major diastereomer, s, 18H), 1.21 (minor diastereomer, s, 18H),

^{13}C NMR (126 MHz, Chloroform-*d*) δ 186.41, 186.34, 149.80, 148.26, 148.07, 142.29, 141.68, 141.64, 141.04, 134.15, 134.12, 133.92, 132.96, 132.29, 132.21, 131.59, 131.52, 131.51 (q, *J* = 32 Hz), 131.39 (q, *J* = 32 Hz), 129.81, 129.65, 128.70, 128.61, 125.33, 125.31 (q, *J* = 3.8 Hz), 125.09 (q, *J* = 3.8 Hz), 125.01, 124.65 (q, *J* = 3.8 Hz), 124.34 (q, *J* = 3.8 Hz), 123.90 (q, *J* = 271 Hz), 123.83 (q, *J* = 271 Hz), 51.60, 51.02, 35.54, 35.12, 35.04, 29.55, 29.52, 29.48.

IR (Neat): 2959, 1617, 1571, 1448, 1390, 1324, 1252, 1162, 1124, 1069, 883, 813 cm^{-1};

HRMS (ESI) *m/z* calculated for $NaC_{46}H_{52}F_6O_2^+$ ($[M+Na]^+$) 773.3764, found 773.3762.

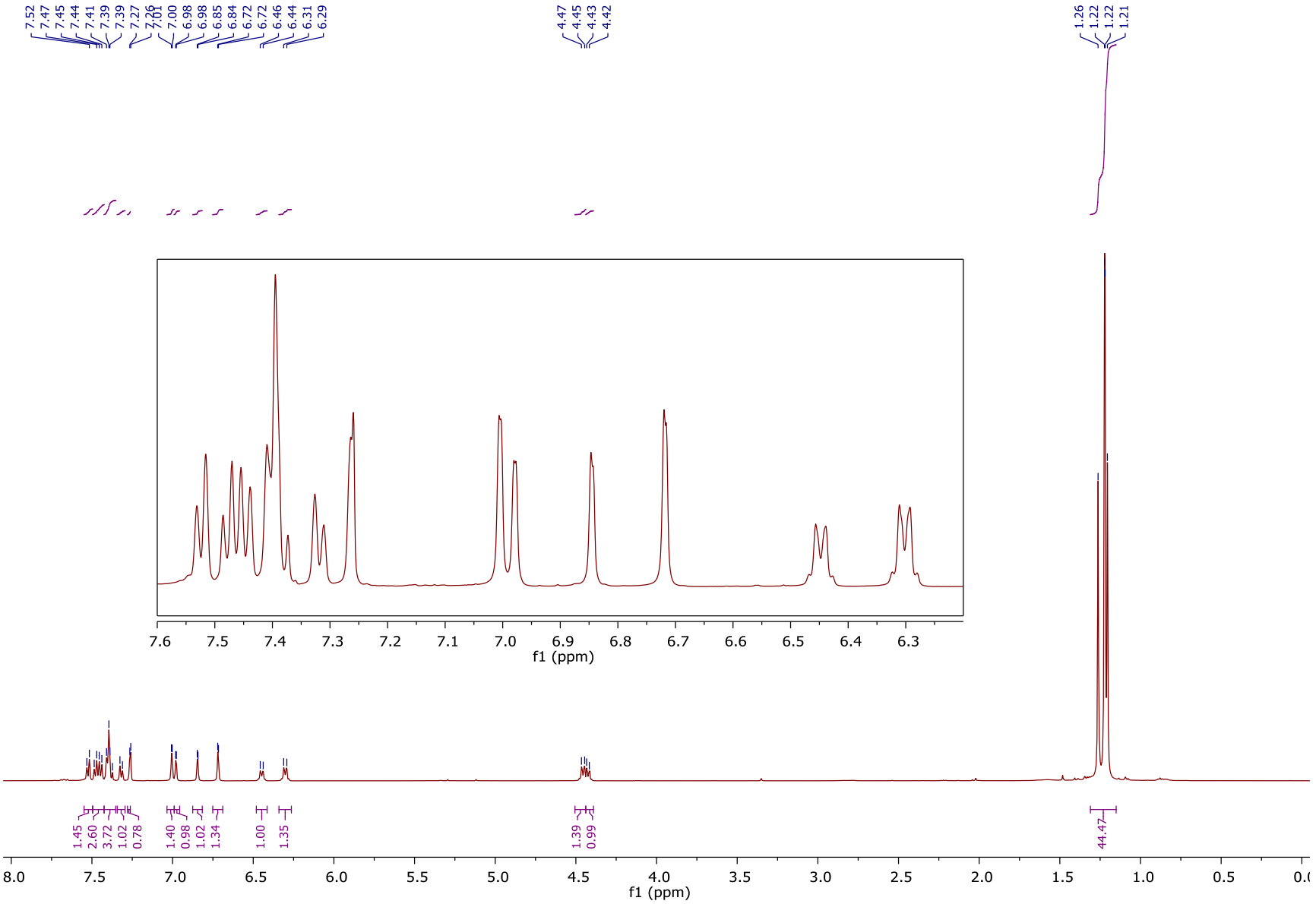
7.52
7.47
7.45
7.44
7.41
7.39
7.39
7.27
7.26
7.01
7.00
6.98
6.98
6.85
6.84
6.72
6.72
6.46
6.44
6.31
6.29
4.47
4.45
4.43
4.42
1.26
1.22
1.22
1.21
7.6 7.5 7.4 7.3 7.2 7.1 7.0 6.9 6.8 6.7 6.6 6.5 6.4 6.3
f1 (ppm)
1.45
2.60
3.72
1.02
0.78
1.40
0.98
1.02
1.34
1.00
1.35
1.39
0.99
44.47
8.0 7.5 7.0 6.5 6.0 5.5 5.0 4.5 4.0 3.5 3.0 2.5 2.0 1.5 1.0 0.5
f1 (ppm)

^{13}C NMR, 126 MHz, Chloroform-*d*, Dimer **18**

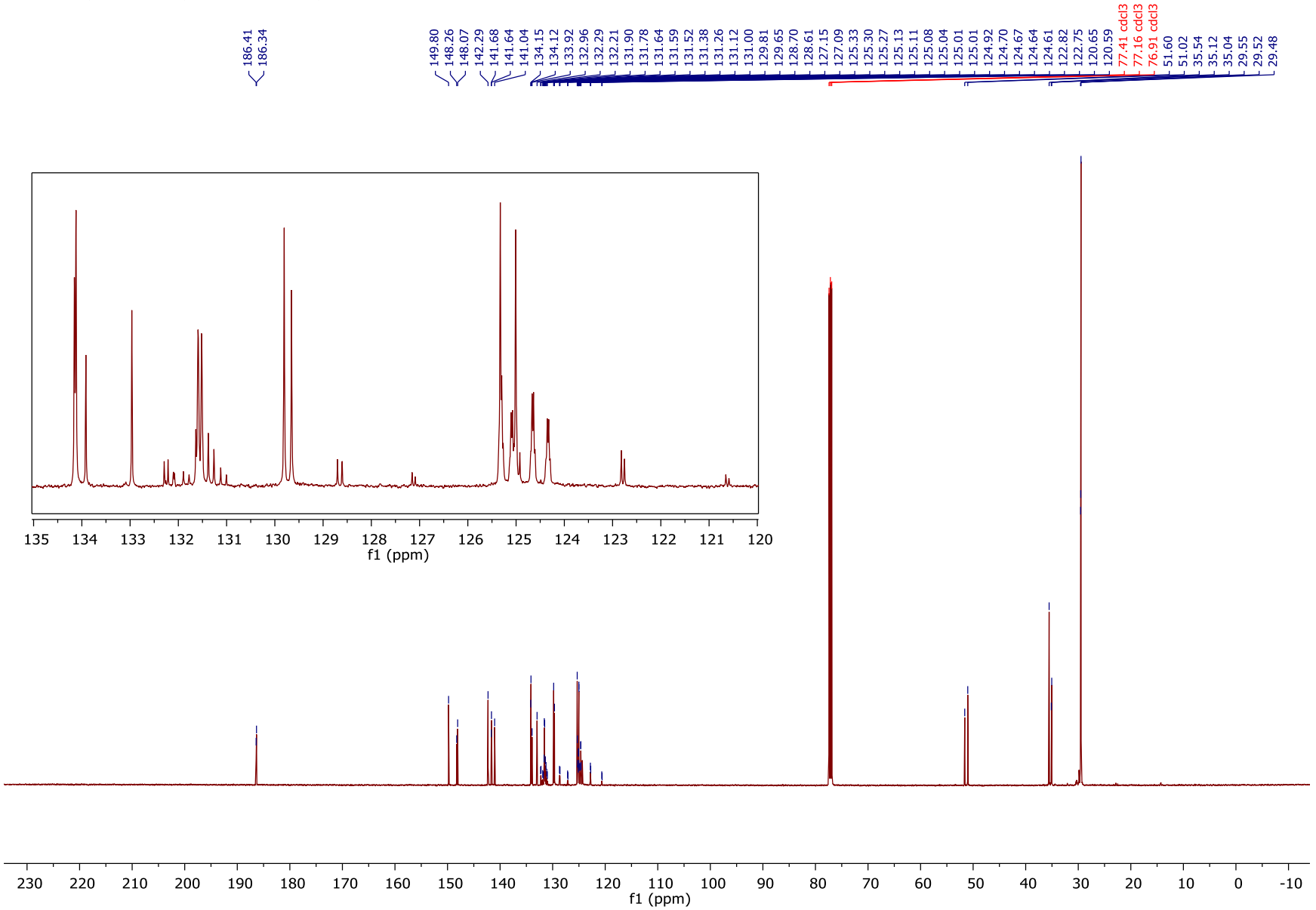

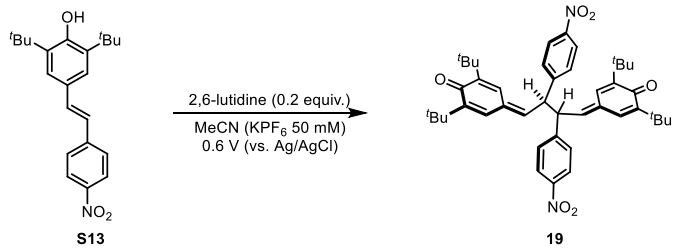

(19) 4,4'-((2*R*,3*R*)-2,3-bis(4-nitrophenyl)butane-1,4-diylidene)bis(2,6-di-*tert*-butylcyclohexa-2,5-dien-1-one)

Stilbene **S13** (0.1 mmol, 35.3 mg) was subjected to the general dimerization procedure, affording bis-quinone methide **19** (32.5 mg, 92% yield, 1:1 dr).

^{1}H NMR (500 MHz, Chloroform-*d*) δ 8.22 (d, *J* = 8.4 Hz, 4H), 8.12 (d, *J* = 8.4 Hz, 4H), 7.39 (d, *J* = 8.3 Hz, 4H), 7.27 (d, *J* = 8.4 Hz, 4H), β-H's of quinone methides: 7.06 (d, *J* = 2.4 Hz, 2H), 7.00 (d, *J* = 2.4 Hz, 2H), 6.81 (d, *J* = 2.4 Hz, 2H), 6.68 (d, *J* = 2.4 Hz, 2H), δ-H's of quinone methides: 6.36 (d, *J* = 8.5 Hz, 2H), 6.24 (d, *J* = 8.8 Hz, 2H), sp^3 methines: 4.60 – 4.53 (m, 2H), 4.53 – 4.46 (m, 2H), 1.25 (s, 18H), 1.24 (s, 18H), 1.22 (s, 18H), 1.22 (s, 18H).

^{13}C NMR (126 MHz, Chloroform-*d*) δ 186.24, 186.15, 150.31, 148.64, 148.54, 147.96, 147.45, 147.33, 147.19, 140.74, 140.57, 134.16, 133.86, 133.74, 133.46, 129.26, 128.99, 124.98, 124.63, 124.58, 124.51, 51.16, 50.57, 35.67, 35.64, 35.17, 35.11, 29.59, 29.55, 29.52, 29.48.

IR (Neat): 2953, 1613, 1518, 1344, 1254, 913, 857, 706 cm^{-1};

HRMS (ESI) *m/z* calculated for $C_{44}H_{52}N_2O_6^+$ ($[M+Na]^+$) 727.3718, found 727.3723.

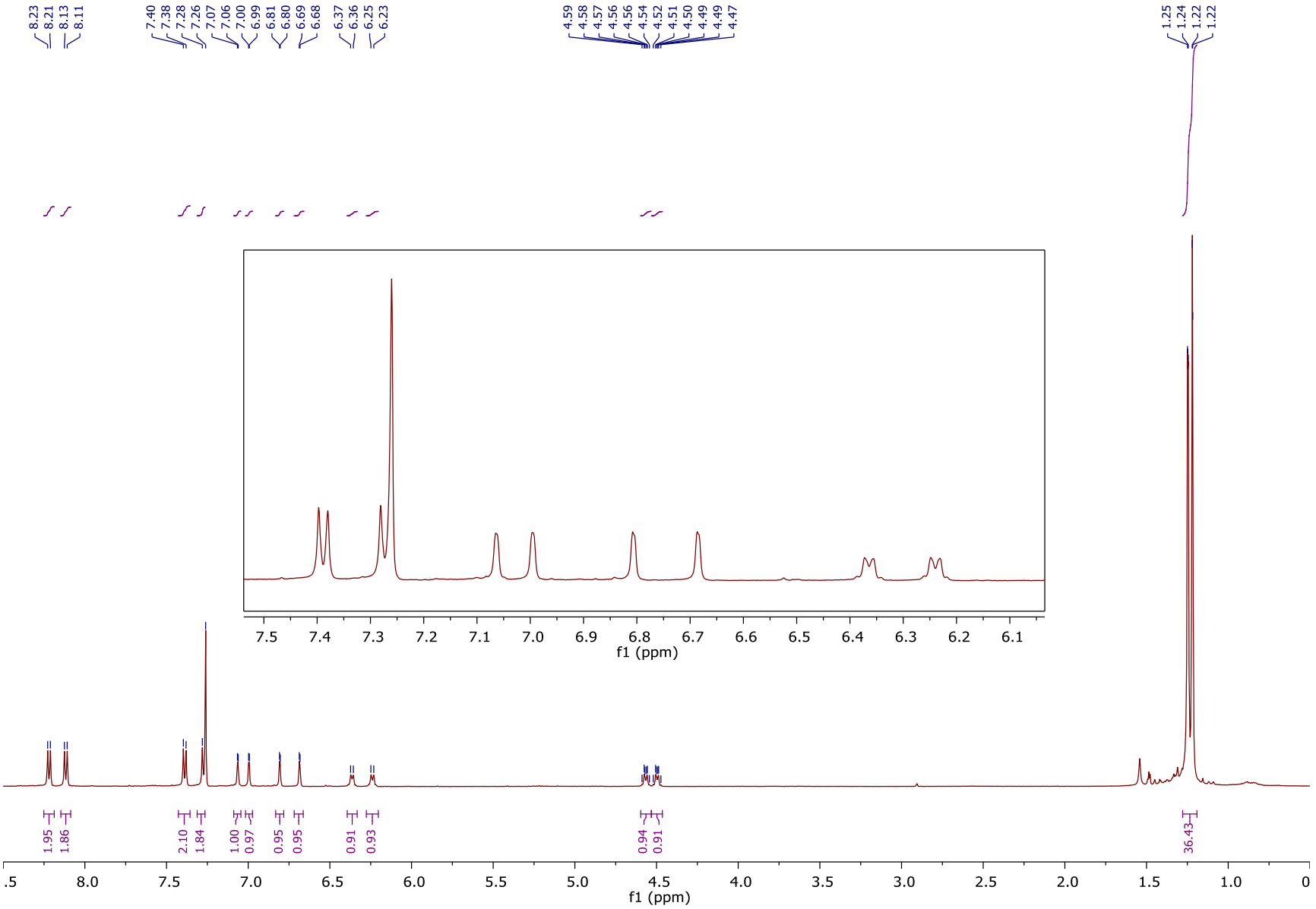
8.23
8.21
8.13
8.11
7.40
7.38
7.28
7.26
7.07
7.06
7.00
6.99
6.81
6.80
6.69
6.68
6.37
6.36
6.25
6.23
4.59
4.58
4.57
4.56
4.56
4.54
4.52
4.51
4.50
4.49
4.49
4.47
1.25
1.24
1.22
1.22
7.5 7.4 7.3 7.2 7.1 7.0 6.9 6.8 6.7 6.6 6.5 6.4 6.3 6.2 6.1
f1 (ppm)
1.95
1.86
2.10
1.84
1.00
0.97
0.95
0.95
0.91
0.93
0.94
0.91
36.43
.5 8.0 7.5 7.0 6.5 6.0 5.5 5.0 4.5 4.0 3.5 3.0 2.5 2.0 1.5 1.0 0
f1 (ppm)

^{13}C NMR, 126 MHz, Chloroform-*d*, Dimer **19**

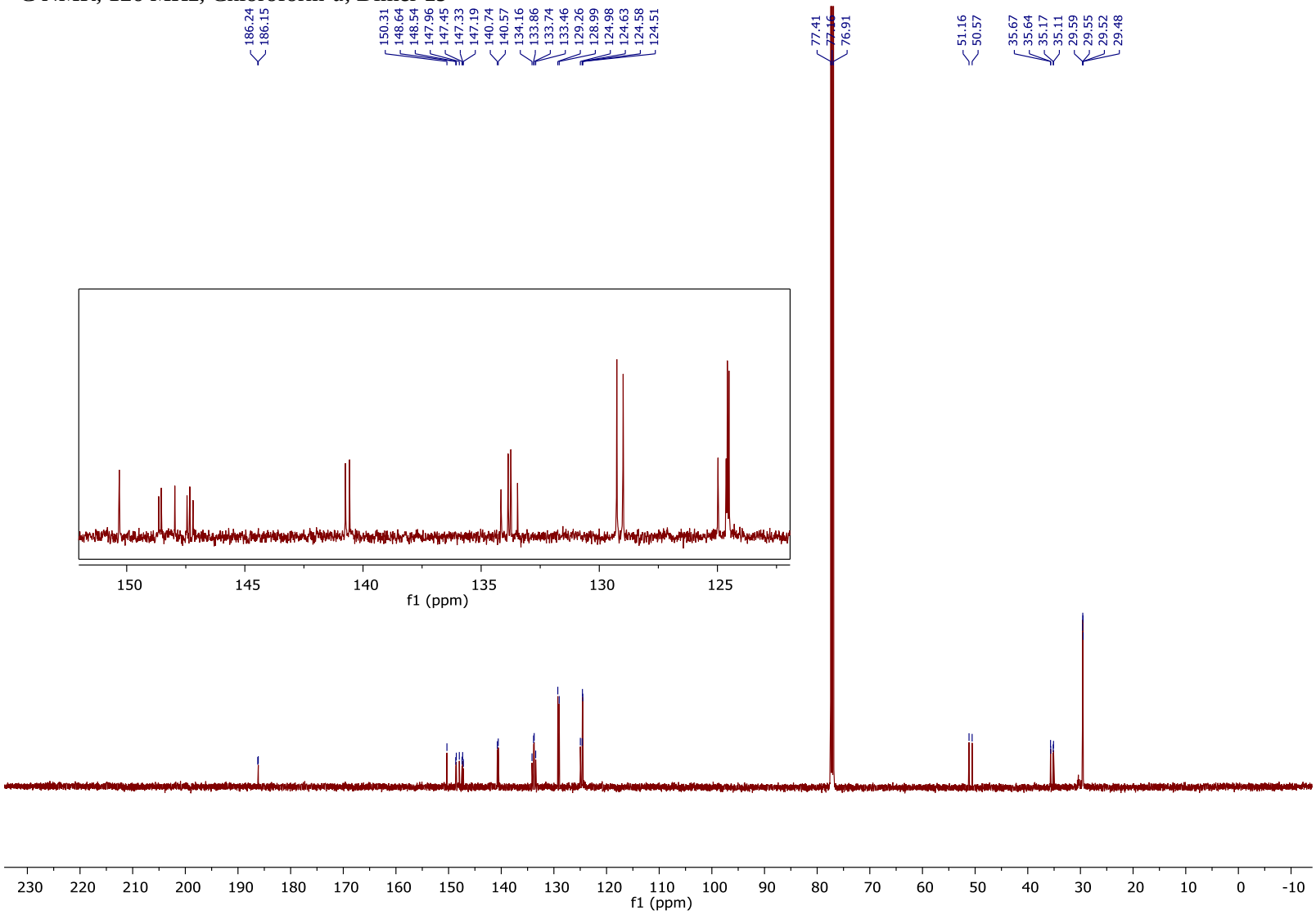

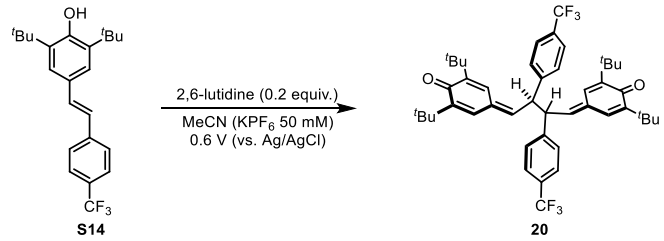

(20) 4,4'-((2*R*,3*R*)-2,3-bis(4-(trifluoromethyl)phenyl)butane-1,4-diylidene)bis(2,6-di-*tert*-butylcyclohexa-2,5-dien-1-one)

Stilbene **S14** (0.1 mmol, 37.6 mg) was subjected to the general dimerization procedure, affording bis-quinone methide **20** (33.8 mg, 90% yield, 1:1 dr).

^{1}H NMR (500 MHz, Chloroform-*d*) δ 7.60 (d, *J* = 8.1 Hz, 4H), 7.51 (d, *J* = 8.1 Hz, 4H), 7.31 (d, *J* = 8.0 Hz, 4H), 7.22 (d, *J* = 8.1 Hz, 4H), 7.07 (d, *J* = 2.4 Hz, 2H), 7.03 (d, *J* = 2.4 Hz, 2H), 6.82 (d, *J* = 2.4 Hz, 2H), 6.70 (d, *J* = 2.4 Hz, 2H), 6.46 – 6.39 (m, 2H), 6.33 – 6.26 (m, 2H), 4.50 (dd, *J* = 7.4, 2.4 Hz, 2H), 4.46 (dt, *J* = 8.7, 6.3 Hz, 2H), 1.25 (s, 18H), 1.23 (s, 18H), 1.22 (s, 36H).

^{13}C NMR (176 MHz, Chloroform-*d*) δ 186.40, 186.30, 149.82, 149.76, 148.20, 148.04, 144.87, 144.25, 142.48, 142.30, 134.20, 134.13, 133.56, 132.87, 130.04 (q, *J* = 33 Hz), 129.80 (q, *J* = 32 Hz), 128.85, 128.54, 126.21 (q, *J* = 3.5 Hz), 126.12 (q, *J* = 3.5 Hz), 125.39, 125.13, 123.96 (q, *J* = 273 Hz), 123.92 (q, *J* = 273 Hz), 51.21, 50.74, 35.58, 35.56, 35.10, 35.04, 29.54, 29.52, 29.51, 29.48.

IR (Neat): 2955, 1612, 1571, 1361, 1322, 1165, 1105, 1067, 883, 834 cm^{-1};

HRMS (ESI) *m/z* calculated for $NaC_{46}H_{52}F_6O_2^+$ ($[M+H]^+$) 773.3764, found 773.3769.

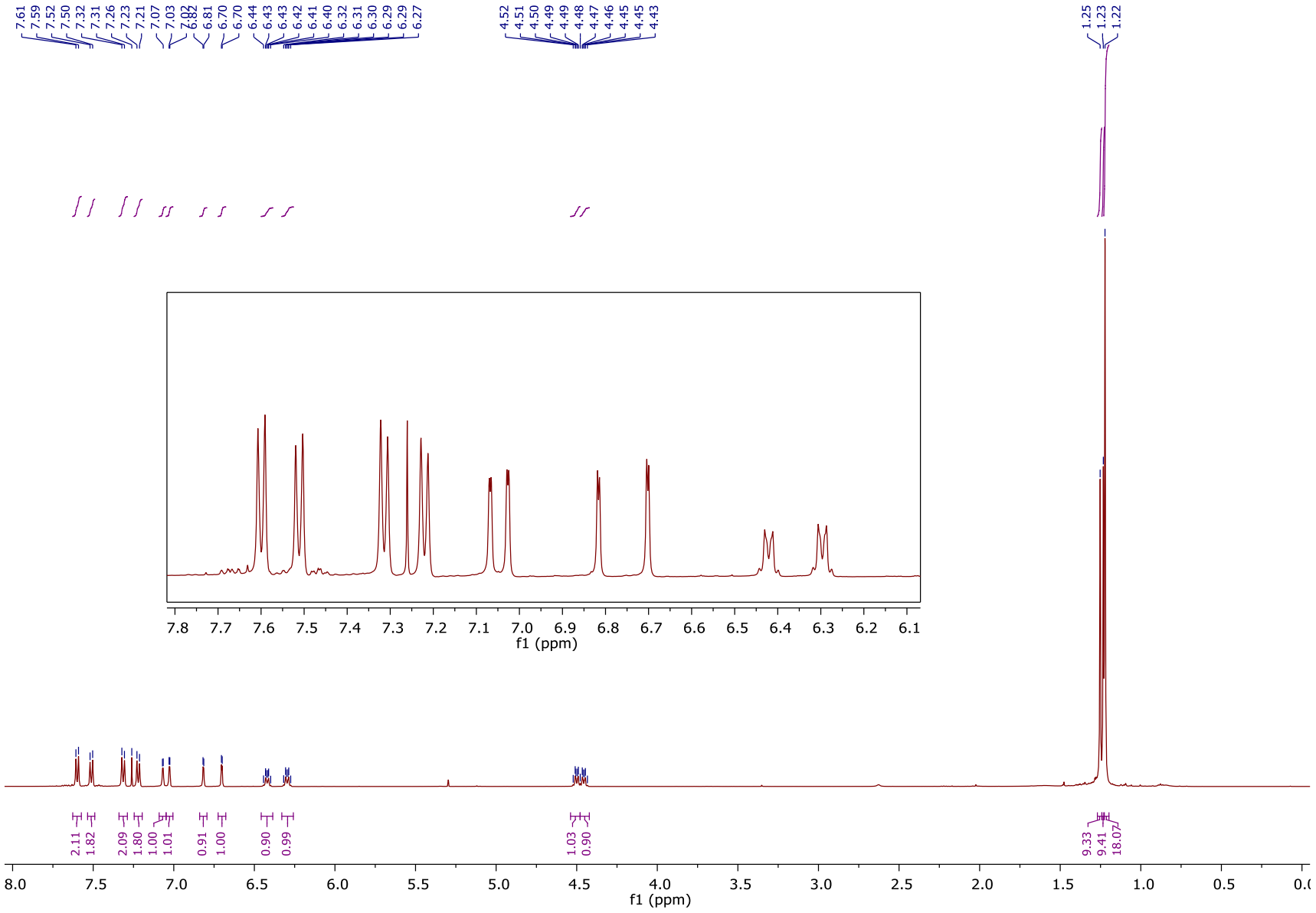
7.61
7.59
7.52
7.50
7.32
7.31
7.26
7.23
7.21
7.07
7.03
6.82
6.81
6.70
6.70
6.44
6.43
6.43
6.42
6.41
6.40
6.32
6.31
6.30
6.29
6.29
6.27
4.52
4.51
4.50
4.49
4.49
4.48
4.47
4.46
4.45
4.45
4.43
1.25
1.23
1.22
7.8 7.7 7.6 7.5 7.4 7.3 7.2 7.1 7.0 6.9 6.8 6.7 6.6 6.5 6.4 6.3 6.2 6.1
f1 (ppm)
2.11
1.82
2.09
1.80
1.00
1.01
0.91
1.00
0.90
0.99
1.03
0.90
9.33
9.41
18.07
8.0 7.5 7.0 6.5 6.0 5.5 5.0 4.5 4.0 3.5 3.0 2.5 2.0 1.5 1.0 0.5
f1 (ppm)

^{13}C NMR, 176 MHz, Chloroform-*d*, Dimer **20**

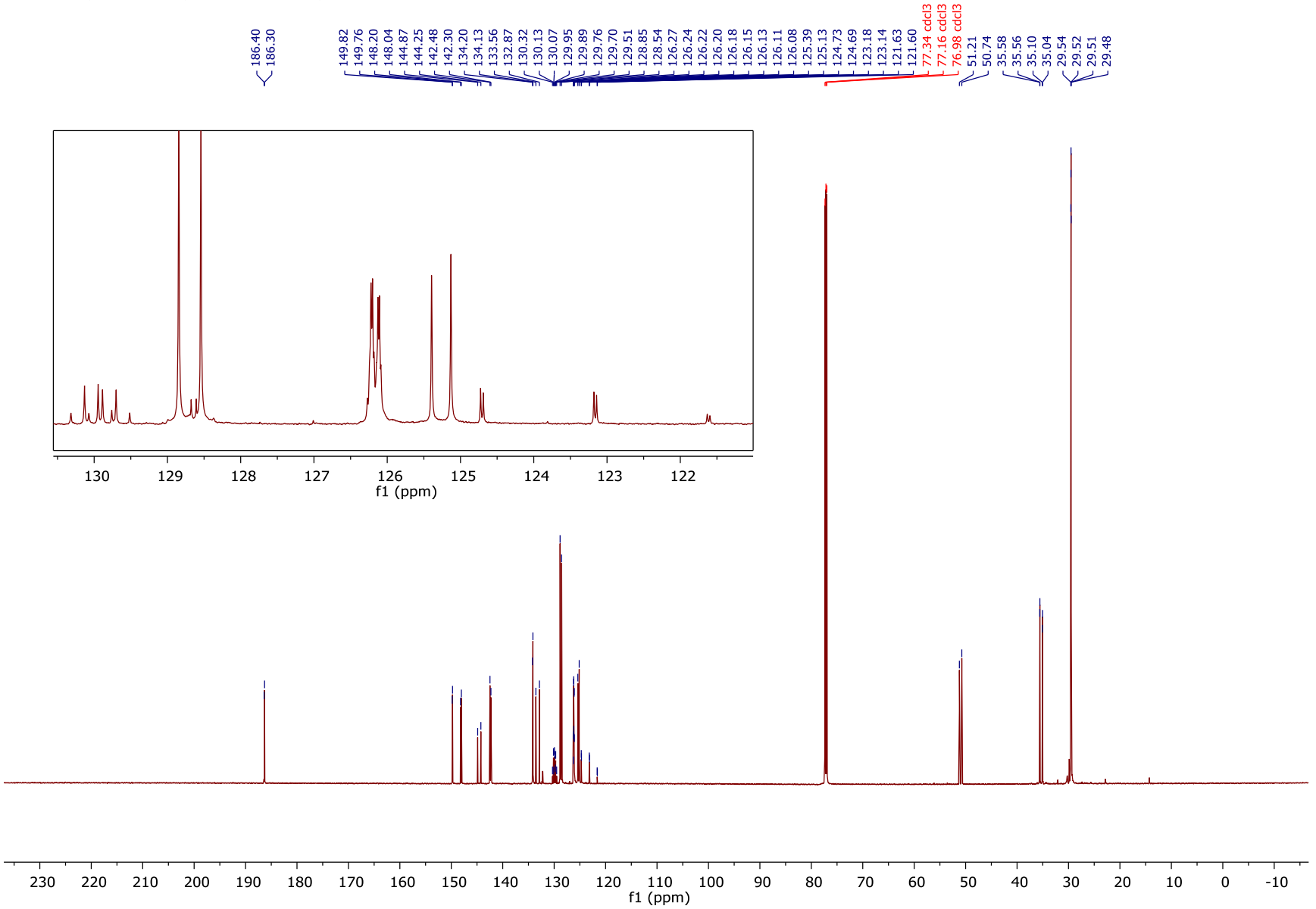

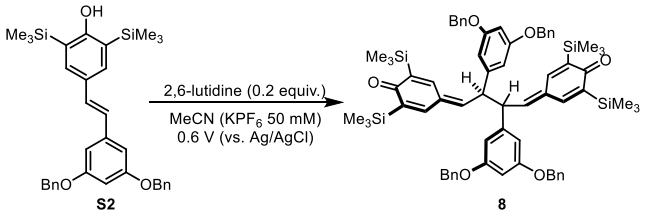

(8) 4,4'-((2*R*,3*R*)-2,3-bis(3,5-bis(benzyloxy)phenyl)butane-1,4-diylidene)bis(2,6-bis(trimethylsilyl)cyclohexa-2,5-dien-1-one)

Stilbene **S2** (0.1 mmol, 55 mg) was subjected to the general dimerization procedure, and the crude reaction mixture was purified by flash column chromatography (0 to 15% EtOAc in Hexanes) to afford bis-quinone methide **8** (35.8 mg, 65% yield, 2:1 dr). The ^{1}H NMR spectrum was identical to the previous report for this compound.[2]

^{1}H NMR (500 MHz, CDCl3, 25 °C) δ: 7.47 (d, J = 2.5 Hz, 2H, major), 7.45 – 7.28 (m, 32H), 7.15 (d, J = 2.5 Hz, 2H, minor), 7.04 (d, J = 2.5 Hz, 2H, major), 6.50 – 6.47 (m, overlap, 4H), 6.45 (d, J = 2.2 Hz, 4H, major), 6.38 (m, 4H), 6.37 (d, J = 2.2 Hz, 4H, minor), 5.07 (d, J = 9.3 Hz, 2H, minor), 4.99 (d, J = 9.3 Hz, 2H, minor), 4.96 (s, 8H, major/minor overlap), 4.91 (d, J = 11.2 Hz, 2H, major), 4.89 (d, J = 11.2 Hz, 2H, major), 4.36 – 4.28 (m, overlap, 4H, major/minor), 0.20 (s, 18H, minor), 0.19 (s, 18H, minor), 0.18 (s, 36H, major)

^{1}H NMR, 500 MHz, Chloroform-*d*, Dimer **8**

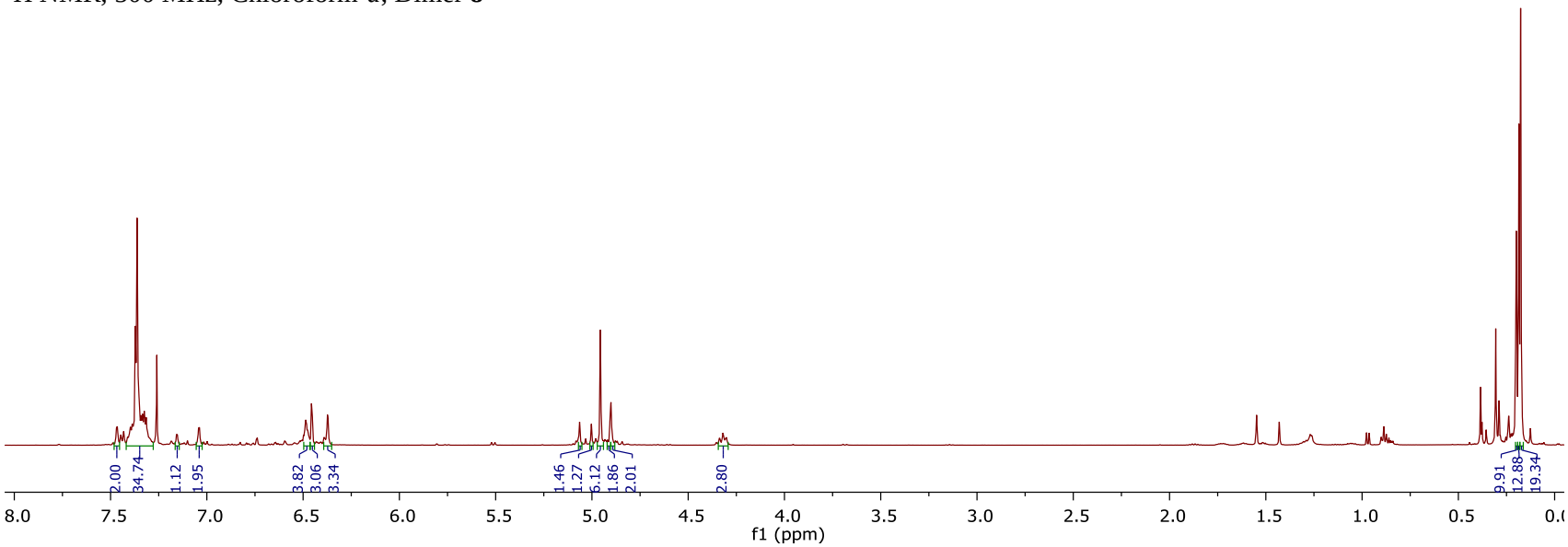

^{1}H NMR, 500 MHz, Chloroform-*d*, Compound **4b**[2]

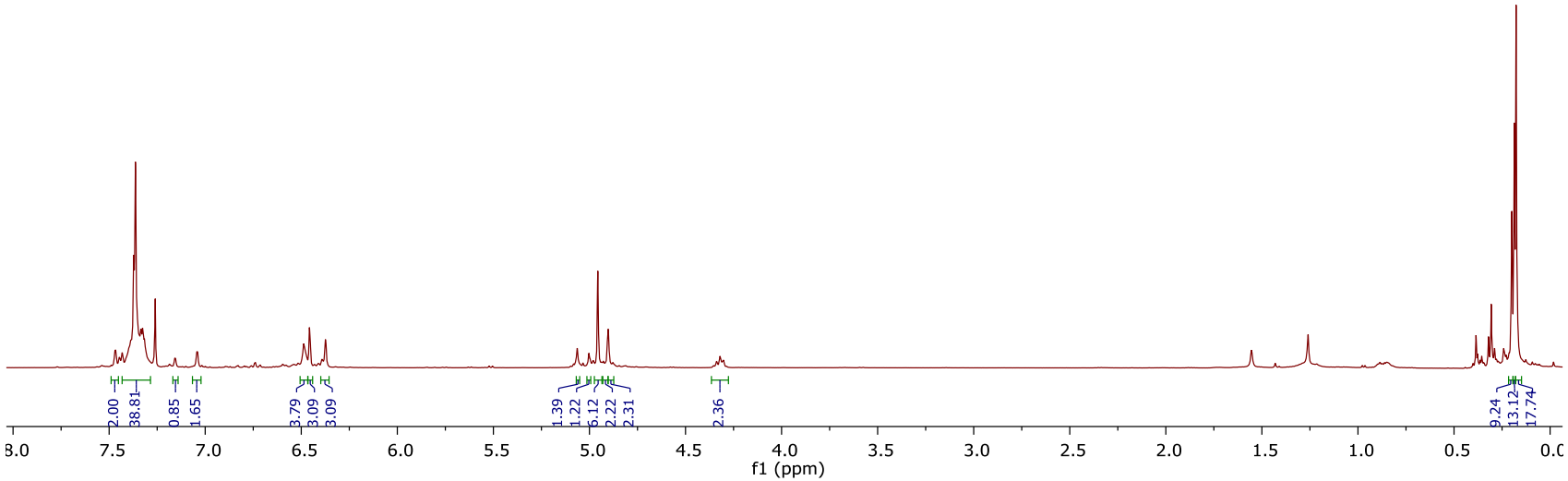

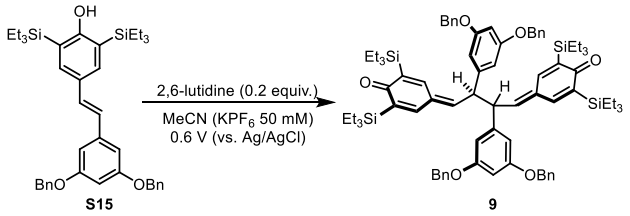

(9) 4,4'-((2*R*,3*R*)-2,3-bis(3,5-bis(benzyloxy)phenyl)butane-1,4-diylidene)bis(2,6-bis(triethylsilyl)cyclohexa-2,5-dien-1-one)

Stilbene **S15** (0.1 mmol, 63.7 mg) was subjected to the general dimerization procedure, and the crude reaction mixture was purified by flash column chromatography (0 to 15% EtOAc in Hexanes) to afford bis-quinone methide **9** (43.4 mg, 68% yield, 2:1 dr).

^{1}H NMR (700 MHz, Chloroform-*d*) δ 7.47 (d, *J* = 2.6 Hz, 2H), 7.45 (d, *J* = 7.8 Hz, 4H), 7.44 (d, *J* = 2.6 Hz, 2H), 7.42 – 7.28 (m, 30H), 7.11 (d, *J* = 2.6 Hz, 1H), 7.04 (d, *J* = 2.6 Hz, 2H), 6.50 – 6.47 (m, 4H), 6.47 (s, 4H), 6.44 (d, *J* = 6.8 Hz, 1H), 6.39 (s, 3H), 6.38 (d, *J* = 9.6 Hz, 3H), 5.08 (d, *J* = 3.1 Hz, 1H), 5.00 (s, 1H), 4.95 (s, 6H), 4.92 (s, 4H), 4.32 (td, *J* = 8.5, 7.1, 4.5 Hz, 2H), 0.88 (q, *J* = 8.1 Hz, 46H), 0.76 – 0.70 (m, 30H).

^{13}C NMR (176 MHz, Chloroform-*d*) δ 193.51, 150.13, 149.94, 145.83, 144.64, 142.70, 142.56, 141.40, 141.15, 141.12, 141.10, 139.41, 139.01, 136.56, 136.49, 132.42, 131.56, 128.79, 128.77, 128.33, 128.32, 127.73, 127.69, 107.93, 107.86, 100.47, 70.38, 70.37, 51.55, 51.04, 7.74, 7.71, 7.70, 7.66, 3.22, 3.17, 3.15, 3.11.

IR (Neat): 2957, 2898, 1588, 1456, 1248, 1158, 1051, 841, 734, 695, 619 cm^{-1};

HRMS (ESI) *m/z* calculated for $C_{80}H_{103}O_6Si_4^+$ ($[M+H]^+$) 1271.6826, found 1271.6816.

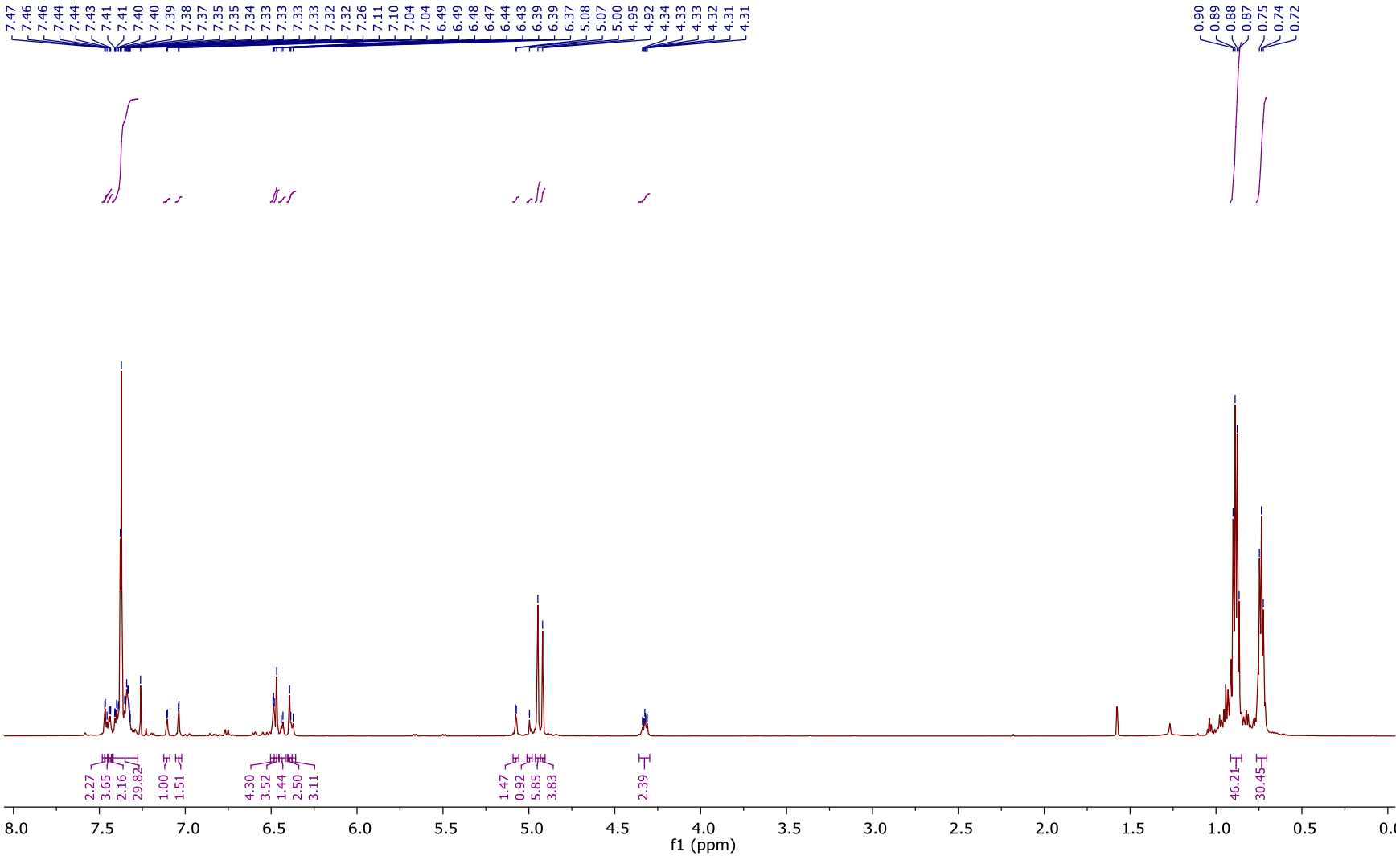
7.47 7.46 7.46 7.44 7.44 7.43 7.41 7.41 7.40 7.40 7.39 7.38 7.37 7.35 7.34 7.33 7.33 7.33 7.33 7.32 7.32 7.26 7.11 7.10 7.04 7.04 6.49 6.49 6.48 6.47 6.44 6.43 6.39 6.39 6.37 5.08 5.07 5.00 4.95 4.92 4.34 4.33 4.33 4.32 4.31 4.31
0.90 0.89 0.88 0.87 0.75 0.74 0.72
2.27 3.65 2.16 29.82 1.00 1.51 4.30 3.52 1.44 2.50 3.11 1.47 0.92 5.85 3.83 2.39 46.21 30.45
8.0 7.5 7.0 6.5 6.0 5.5 5.0 4.5 4.0 3.5 3.0 2.5 2.0 1.5 1.0 0.5
f1 (ppm)

^{13}C NMR, 176 MHz, Chloroform-*d*, Dimer **9**

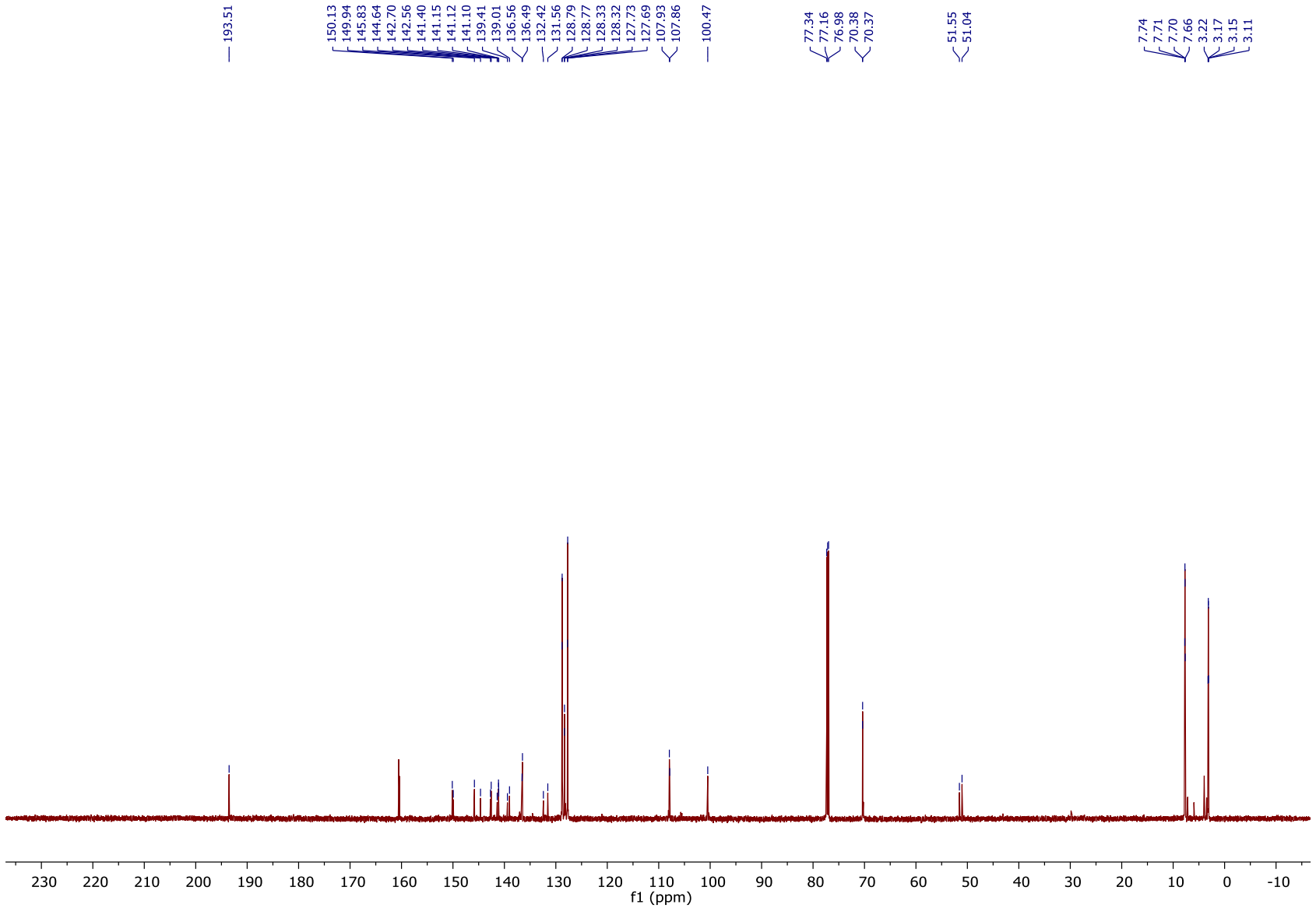

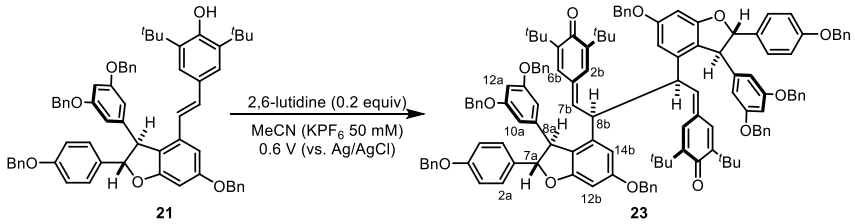

(23) 4,4'-((2*S*,3*S*)-2,3-bis((2*S*,3*S*)-6-(benzyloxy)-2-(4-(benzyloxy)phenyl)-3-(3,5-bis(benzyloxy)phenyl)-2,3-dihydrobenzofuran-4-yl)butane-1,4-diylidene)bis(2,6-di-*tert*-butylcyclohexa-2,5-dien-1-one)

Stilbene **21** (0.05 mmol, 45 mg) was subjected to the general dimerization procedure, affording bis-quinone methide **23** (40 mg, 89% yield, >19:1 dr). The ^{1}H NMR spectrum was identical to the previous report for this compound.[2]

^{1}H NMR (700 MHz, CDCl3, 50 °C) δ: 7.52 – 7.12 (m, 40H, –OCH2C6H5), 7.10 (d, *J*= 8.5 Hz, 4H, C2a–H), 7.01 (d, *J* = 8.5 Hz, 4H, C3a–H), 6.70 (s, 2H, C14b–H), 6.42 (s, 2H, C2/6b–H), 6.39 (s, 2H, C12b–H), 6.37 (s, 2H, C12a–H), 6.23 (s, 2H, C2/6b–H), 6.16 (s, 4H, C10a–H), 6.11 (dd, br, *J* = 7.3, 9.2 Hz, 2H, C7b–H), 5.11 (d, *J* = 8.1 Hz, 2H, C7a–H), 5.04 (d, *J* = 12.5 Hz, 2H, C4a–OCH2C6H5), 5.02 (d, *J* = 12.5 Hz, 2H, C4a–OCH2C6H5), 4.83 (d, *J* = 10.8 Hz, 2H, C13b–OCH2C6H5), 4.77 (d, *J* = 10.8 Hz, 2H, C13b–OCH2C6H5), 4.62 (d, *J* = 11.1 Hz, 4H, C11a–OCH2C6H5), 4.56 (d, *J* = 11.1 Hz, 4H, C11a–OCH2C6H5), 4.06 (dd, br, *J* = 7.9, 9.2 Hz, 2H, C8b–H), 3.87 (d, *J* = 8.1 Hz, 2H, C8a–H), 1.17 (s, 18H, C3/5b–C(CH3)3), 1.00 (s, 18H, C3/5b–C(CH3)3).

^{1}H NMR, 400 MHz, Chloroform-*d*, Dimer **23**

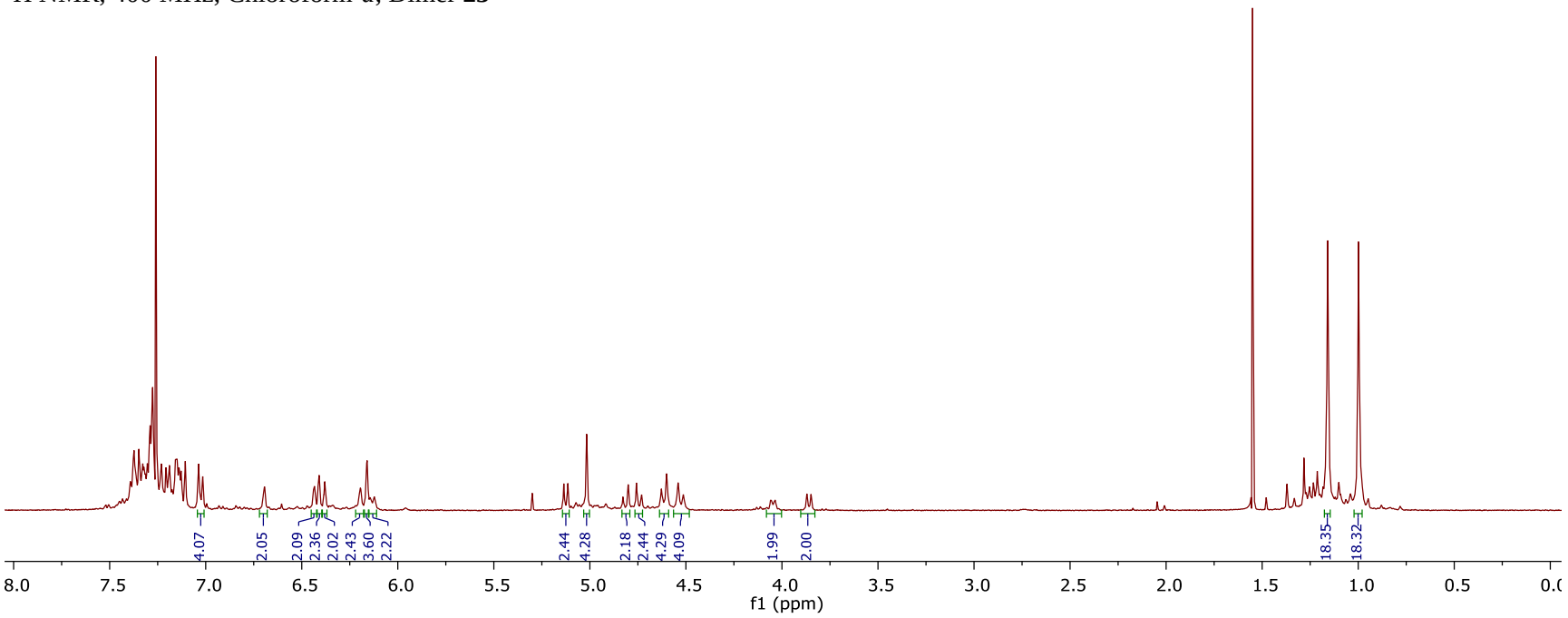

^{1}H NMR, 500 MHz, Chloroform-*d*, Compound **(±)-5a**[2]

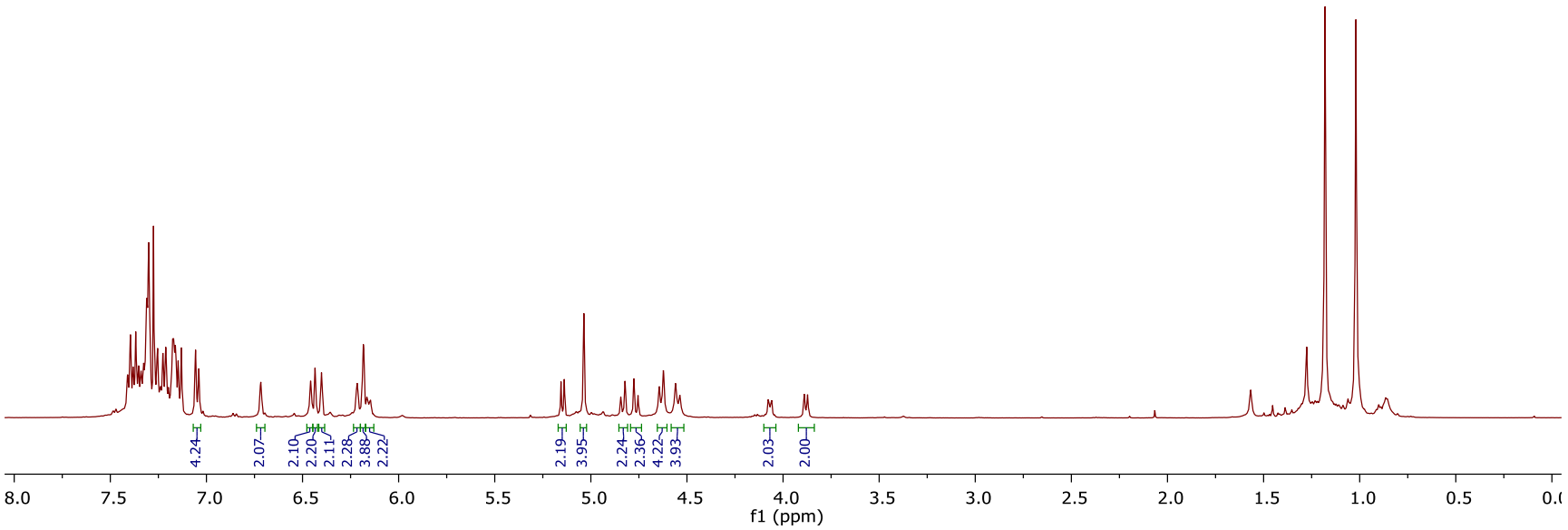

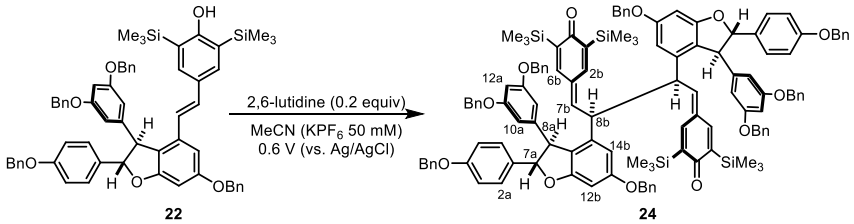

(24) 4,4'-((2*S*,3*S*)-2,3-bis((2*S*,3*S*)-6-(benzyloxy)-2-(4-(benzyloxy)phenyl)-3-(3,5-bis(benzyloxy)phenyl)-2,3-dihydrobenzofuran-4-yl)butane-1,4-diylidene)bis(2,6-bis(trimethylsilyl)cyclohexa-2,5-dien-1-one)

Stilbene **22** (0.039 mmol, 37 mg) was subjected to the general dimerization procedure, affording bis-quinone methide **24** (21 mg, 57% yield, >19:1). The ^{1}H NMR spectrum was identical to the previous report for this compound.[2]

^{1}H NMR (500 MHz, CDCl3, 25 °C) δ: 7.44 – 7.10 (m, 40H, –OCH2C6H5), 7.11 (d, *J* = 8.6 Hz, 4H, C2a–H), 7.03 (d, *J* = 8.6 Hz, 4H, C3a–H), 6.80 (d, *J* = 2.2 Hz, 2H, C2/6b–H), 6.69 (s, br, 2H, C14b–H), 6.51 (d, br, *J* = 2.2 Hz, 2H, C2/6b–H), 6.44 (d, *J* = 2.2 Hz, 2H, C12b–H), 6.34 (t, *J* = 2.0 Hz, 2H, C12a–H), 6.21 (dd, *J* = 7.7, 9.9 Hz, 2H, C7b–H), 6.15 (d, *J* = 2.0 Hz, 4H, C10a–H), 5.14 (d, *J* = 8.6 Hz, 2H, C7a–H), 5.01 (s, 4H, C4a–OCH2C6H5), 4.85 (d, *J* = 11.0 Hz, 2H, C13b–OCH2C6H5), 4.77 (d, *J* = 11.0 Hz, 2H, C13b–OCH2C6H5), 4.56 (d, *J* = 11.0 Hz, 4H, C11a–OCH2C6H5), 4.51 (d, *J* = 11.0 Hz, 4H, C11a– OCH2C6H5), 4.11 (dd, *J* = 7.7, 9.9 Hz, 2H, C8b–H), 3.99 (d, *J* = 8.6 Hz, 2H, C8a– H), 0.14 (s, 18H, C3/5b–Si(CH3)3), −0.02 (s, 18H, C3/5b–Si(CH3)3).

^{1}H NMR, 500 MHz, Chloroform-*d*, Dimer **24**

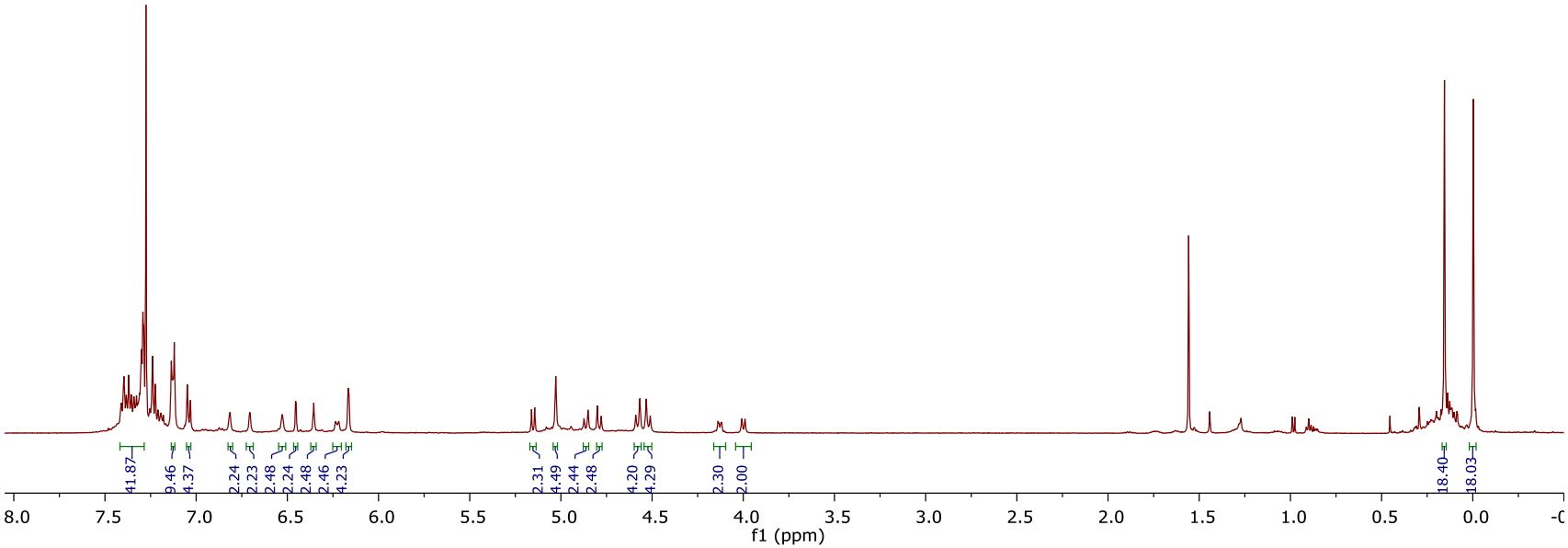

^{1}H NMR, 500 MHz, Chloroform-*d*, Compound **(±)-5b**[2]

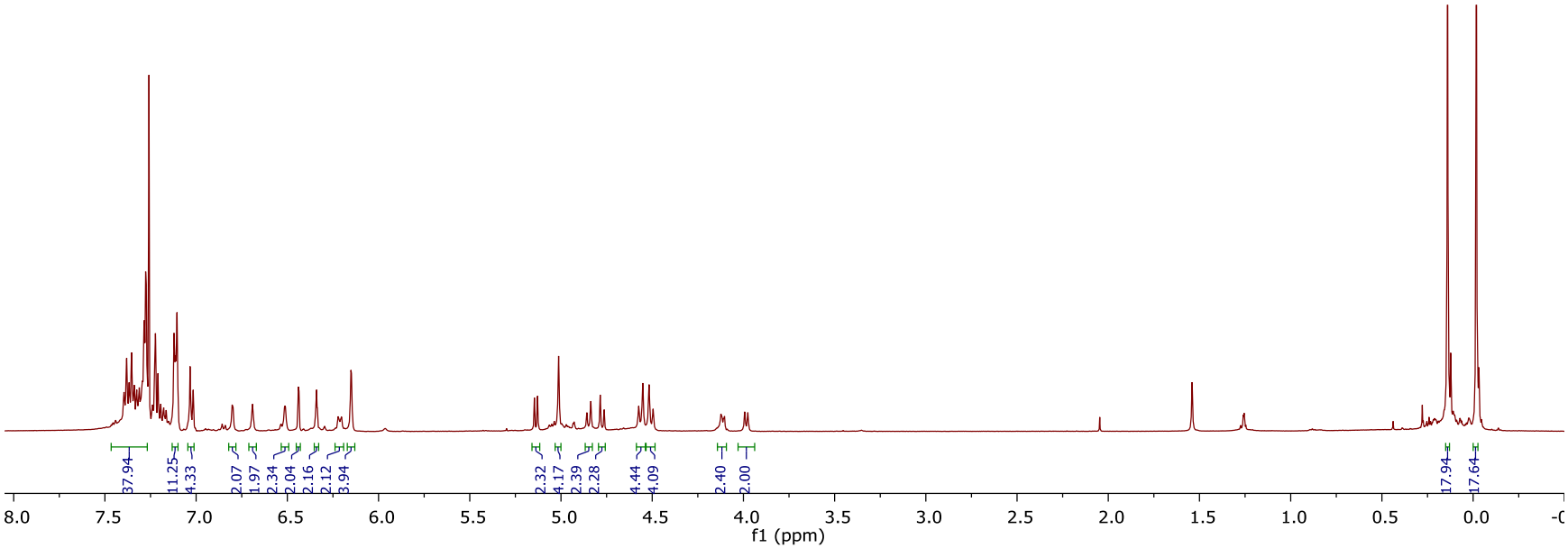

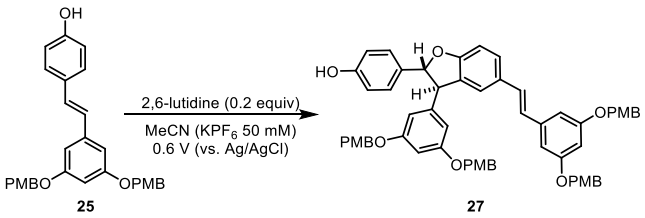

(27) 4-((2*R*,3*R*)-3-(3,5-bis((4-methoxybenzyl)oxy)phenyl)-5-((*E*)-3,5-bis((4-methoxybenzyl)oxy)styryl)-2,3-dihydrobenzofuran-2-yl)phenol

Stilbene **25** (0.1 mmol, 46.9 mg) was subjected to the general dimerization procedure. The crude product was purified via flash column chromatography (1% to 5% Acetone in CH_2Cl_2) to afford the dihydrobenzofuran **27** (27.5 mg, 59% yield, >19:1 dr).

^{1}H NMR (700 MHz, Chloroform-*d*) δ 7.36 (d, *J* = 8.4 Hz, 4H), 7.31 (d, *J* = 8.6 Hz, 4H), 7.19 (d, *J* = 8.5 Hz, 2H), 7.17 (d, *J* = 1.7 Hz, 1H), 7.00 (d, *J* = 16.2 Hz, 1H), 6.92 (d, *J* = 8.3, 4H), 6.91 (d, *J* = 8.5, 2H), 6.89 (d, *J* = 8.5 Hz, 4H), 6.83 (d, *J* = 16.2 Hz, 1H), 6.80 (d, *J* = 8.6 Hz, 2H), 6.71 (dd, *J* = 2.3, 1.2 Hz, 2H), 6.55 (td, *J* = 2.3, 1.0 Hz, 1H), 6.50 (td, *J* = 2.2, 1.2 Hz, 1H), 6.42 (t, *J* = 1.9 Hz, 2H), 5.49 (d, *J* = 8.2 Hz, 1H), 4.98 (s, 4H), 4.93 – 4.88 (m, 4H), 4.46 (d, *J* = 8.2 Hz, 1H), 3.82 (s, 6H), 3.79 (s, 6H).

^{13}C NMR (176 MHz, Chloroform-*d*) δ 160.38, 160.26, 159.80, 159.59, 159.57, 155.78, 144.03, 139.80, 132.88, 130.93, 130.77, 129.52, 129.46, 129.44, 129.17, 129.07, 128.81, 128.15, 127.67, 126.38, 123.30, 115.63, 114.14, 109.84, 107.62, 105.53, 101.38, 100.89, 93.11, 69.99, 57.92, 55.45, 55.44.

IR (Neat): 3391, 2932, 2835, 1585, 1512, 1440, 1301, 1244, 1146, 1030, 818 cm^{-1};

HRMS (ESI) m/z calculated for $C_{60}H_{55}O_{10}^+$ ([M+H]+) 935.3790, found 935.3800.

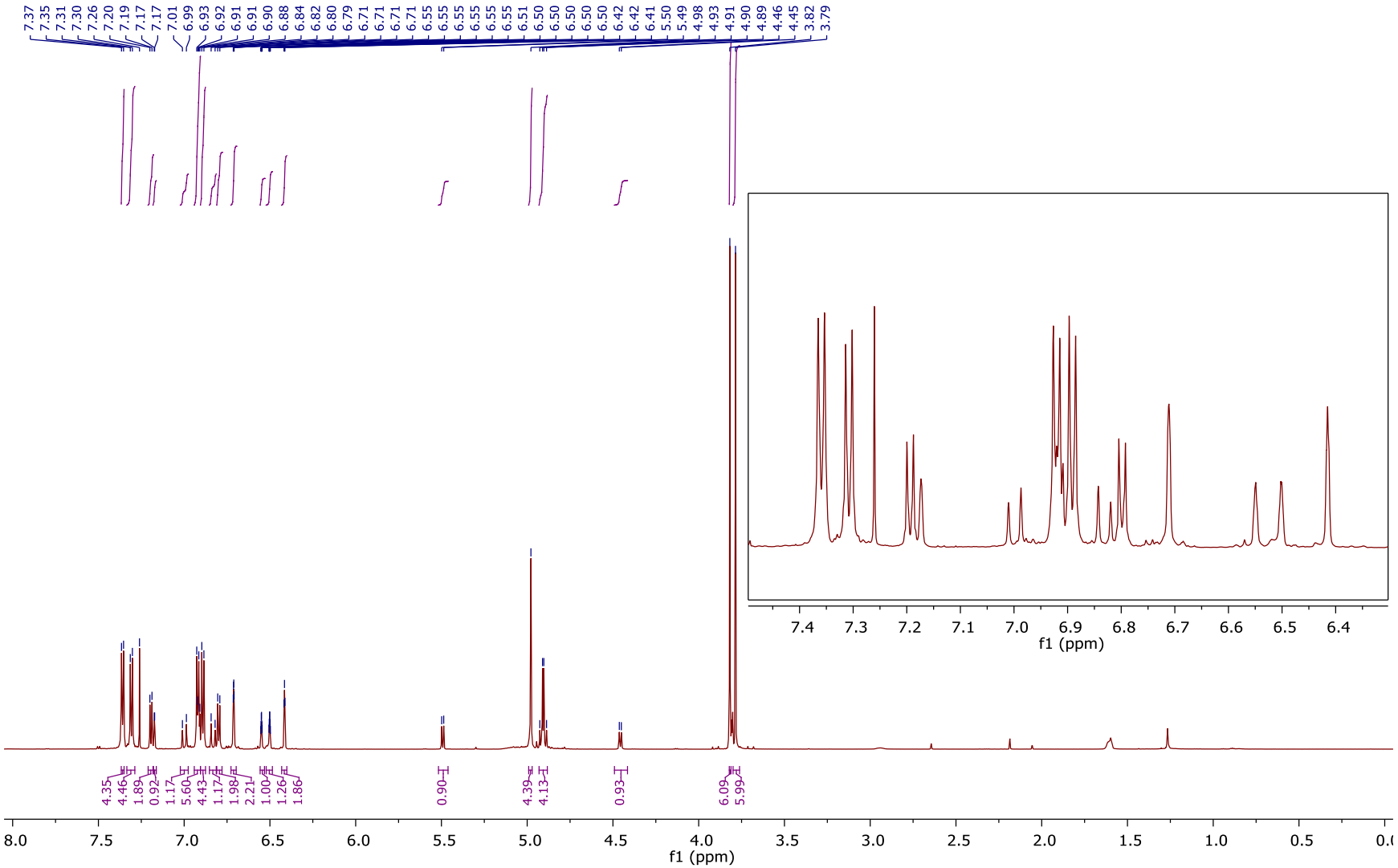
7.37 7.35 7.31 7.30 7.26 7.20 7.19 7.17 7.17 7.01 6.99 6.93 6.92 6.91 6.91 6.90 6.88 6.84 6.82 6.80 6.79 6.71 6.71 6.71 6.55 6.55 6.55 6.55 6.55 6.51 6.50 6.50 6.50 6.50 6.50 6.42 6.42 6.41 5.50 5.49 4.98 4.93 4.91 4.90 4.89 4.46 4.45 3.82 3.79
4.35 4.46 1.89 0.92 1.17 5.60 4.43 1.17 1.98 2.21 1.00 1.26 1.86 0.90 4.39 4.13 0.93 6.09 5.99
8.0 7.5 7.0 6.5 6.0 5.5 5.0 4.5 4.0 3.5 3.0 2.5 2.0 1.5 1.0 0.5
f1 (ppm)
7.4 7.3 7.2 7.1 7.0 6.9 6.8 6.7 6.6 6.5 6.4
f1 (ppm)

^{13}C NMR, 176 MHz, Chloroform-*d*, Dimer **27**

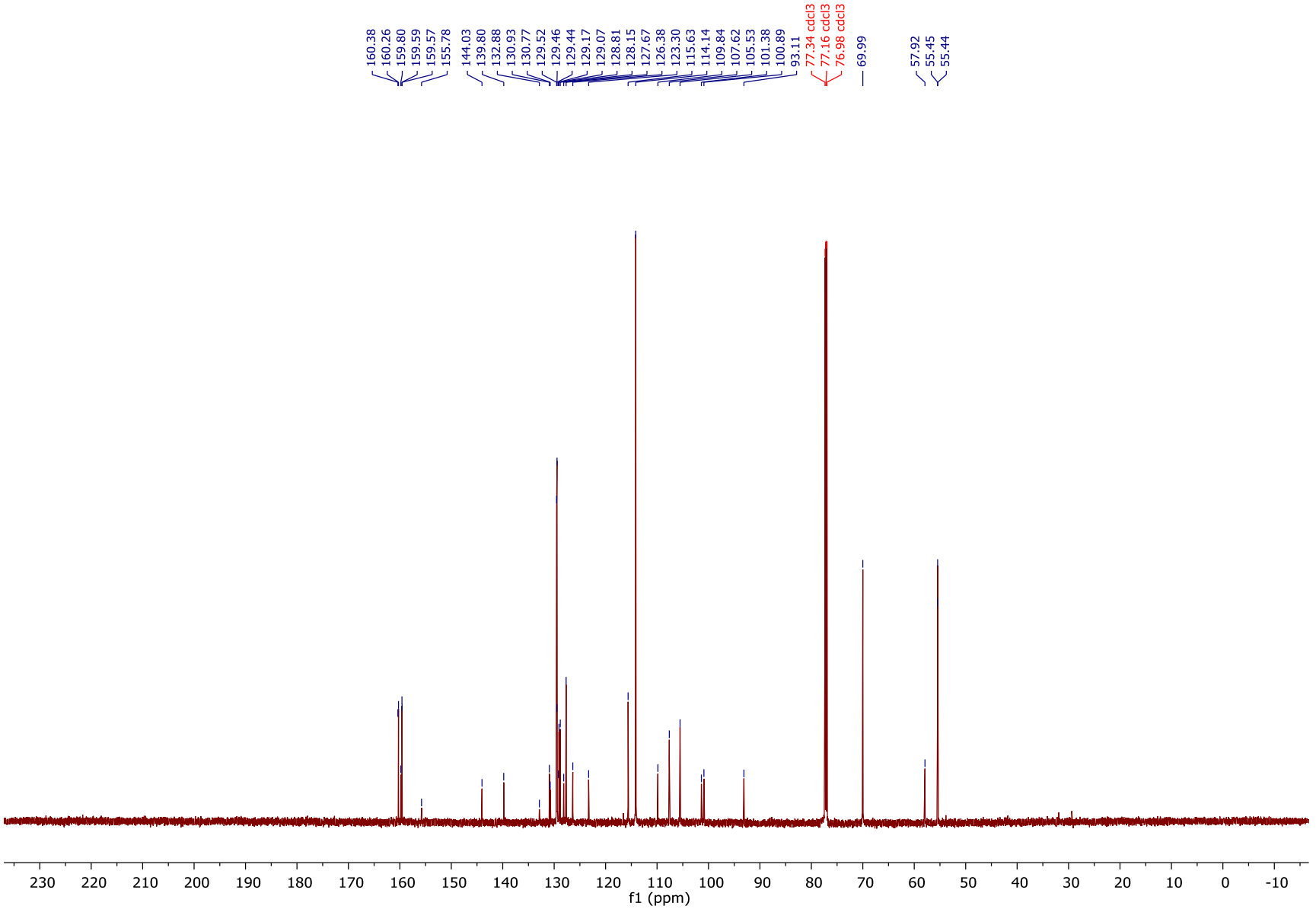

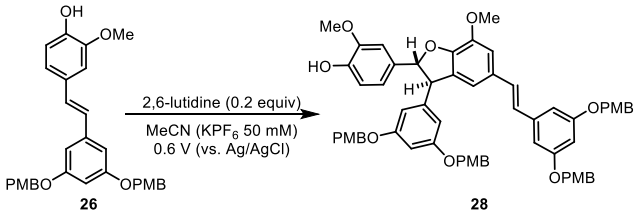

(28) 4-((2*R*,3*R*)-3-(3,5-bis((4-methoxybenzyl)oxy)phenyl)-5-((*E*)-3,5-bis((4-methoxybenzyl)oxy)styryl)-7-methoxy-2,3-dihydrobenzofuran-2-yl)-2-methoxyphenol

Stilbene **26** (0.1 mmol, 49.9 mg) was subjected to the general dimerization procedure. The crude product was purified via flash column chromatography (1% to 5% Acetone in CH_2Cl_2) to afford the dihydrobenzofuran **28** (28.4 mg, 57% yield, >19:1 dr).

^{1}H NMR (700 MHz, Chloroform-*d*) δ 7.37 (d, *J* = 8.1 Hz, 4H), 7.31 (d, *J* = 8.3 Hz, 4H), 7.00 (d, *J* = 15.0 Hz, 2H), 6.93 (d, *J* = 8.2 Hz, 5H), 6.90 (d, *J* = 7.8 Hz, 6H), 6.88 – 6.84 (m, 3H), 6.81 (d, *J* = 4.1 Hz, 2H), 6.74 – 6.71 (m, 2H), 6.55 (s, 1H), 6.52 (s, 1H), 6.45 – 6.42 (m, 2H), 5.67 (s, 1H), 5.54 (d, *J* = 8.8 Hz, 1H), 4.99 (s, 4H), 4.91 (d, *J* = 11.2 Hz, 2H), 4.89 (d, *J* = 11.0 Hz, 2H), 4.54 (d, *J* = 8.8 Hz, 1H), 3.99 (s, 3H), 3.85 (s, 3H), 3.82 (s, 6H), 3.79 (s, 6H).

^{13}C NMR (176 MHz, Chloroform-*d*) δ 160.35, 160.27, 159.60, 159.57, 148.34, 146.72, 145.86, 144.53, 143.70, 139.66, 132.07, 131.73, 131.51, 129.50, 129.43, 129.41, 129.36, 129.03, 128.77, 126.68, 119.79, 116.08, 114.34, 114.12, 114.11, 114.10, 110.18, 108.80, 107.66, 105.61, 105.53, 101.47, 100.92, 94.19, 69.98, 58.28, 56.18, 56.10, 55.43, 55.40.

IR (Neat): 3395, 2999, 2934, 2833, 1585, 1512, 1439, 1302, 1245, 1150, 1032, 824, 734 cm^{-1};

HRMS (ESI) m/z calculated for $C_{62}H_{59}O_{12}^+$ ([M+H]+) 995.4001, found 995.3979.

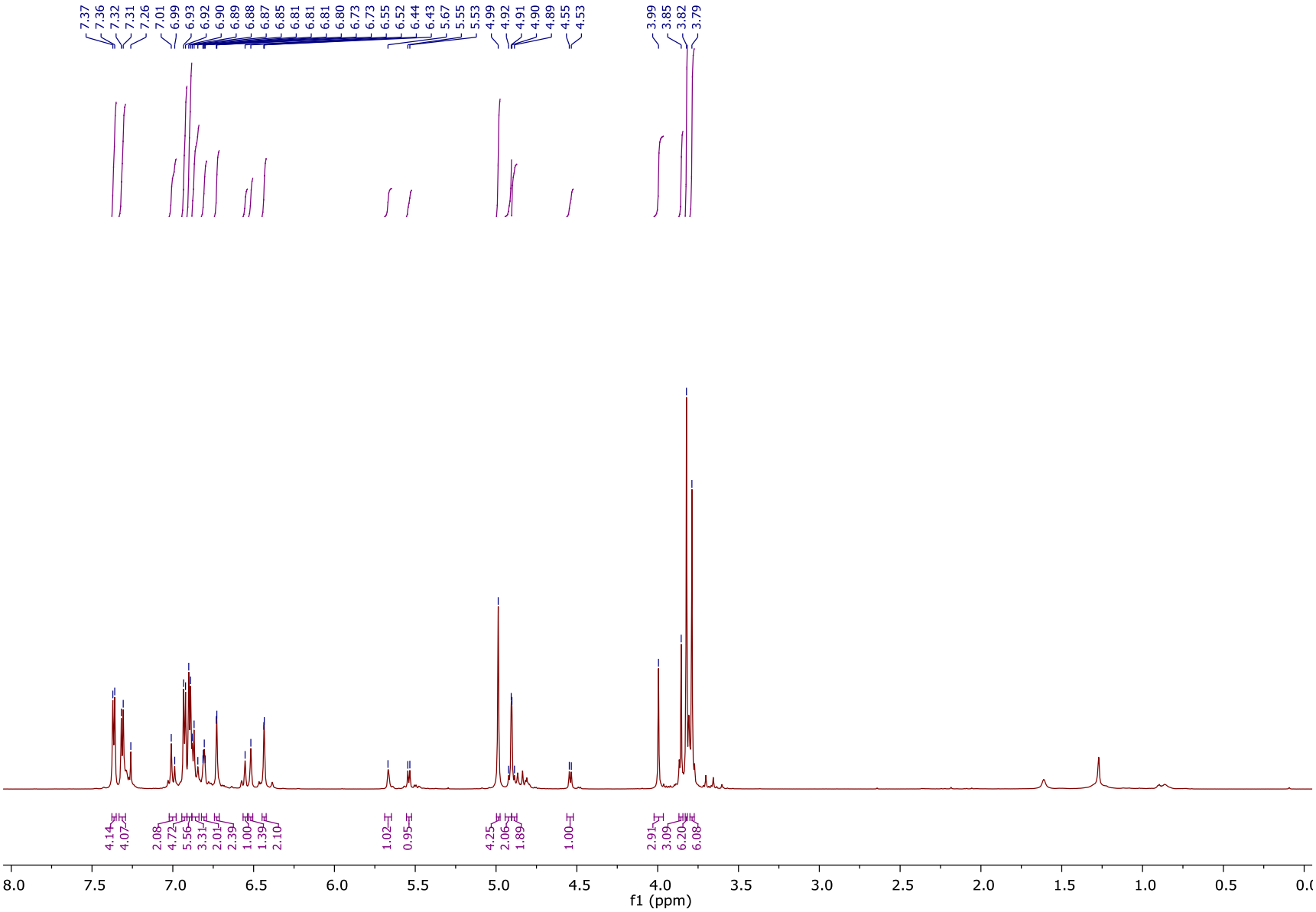
7.37
7.36
7.32
7.31
7.26
7.01
6.99
6.93
6.92
6.90
6.89
6.88
6.87
6.85
6.81
6.81
6.81
6.80
6.73
6.73
6.55
6.52
6.44
6.43
5.67
5.55
5.53
4.99
4.92
4.91
4.90
4.89
4.55
4.53
3.99
3.85
3.82
3.79
4.14
4.07
2.08
4.72
5.56
3.31
2.01
2.39
1.00
1.39
2.10
1.02
0.95
4.25
2.06
1.89
1.00
2.91
3.09
6.20
6.08
8.0
7.5
7.0
6.5
6.0
5.5
5.0
4.5
4.0
3.5
3.0
2.5
2.0
1.5
1.0
0.5
f1 (ppm)

^{13}C NMR, 176 MHz, Chloroform-*d*, Dimer **28**

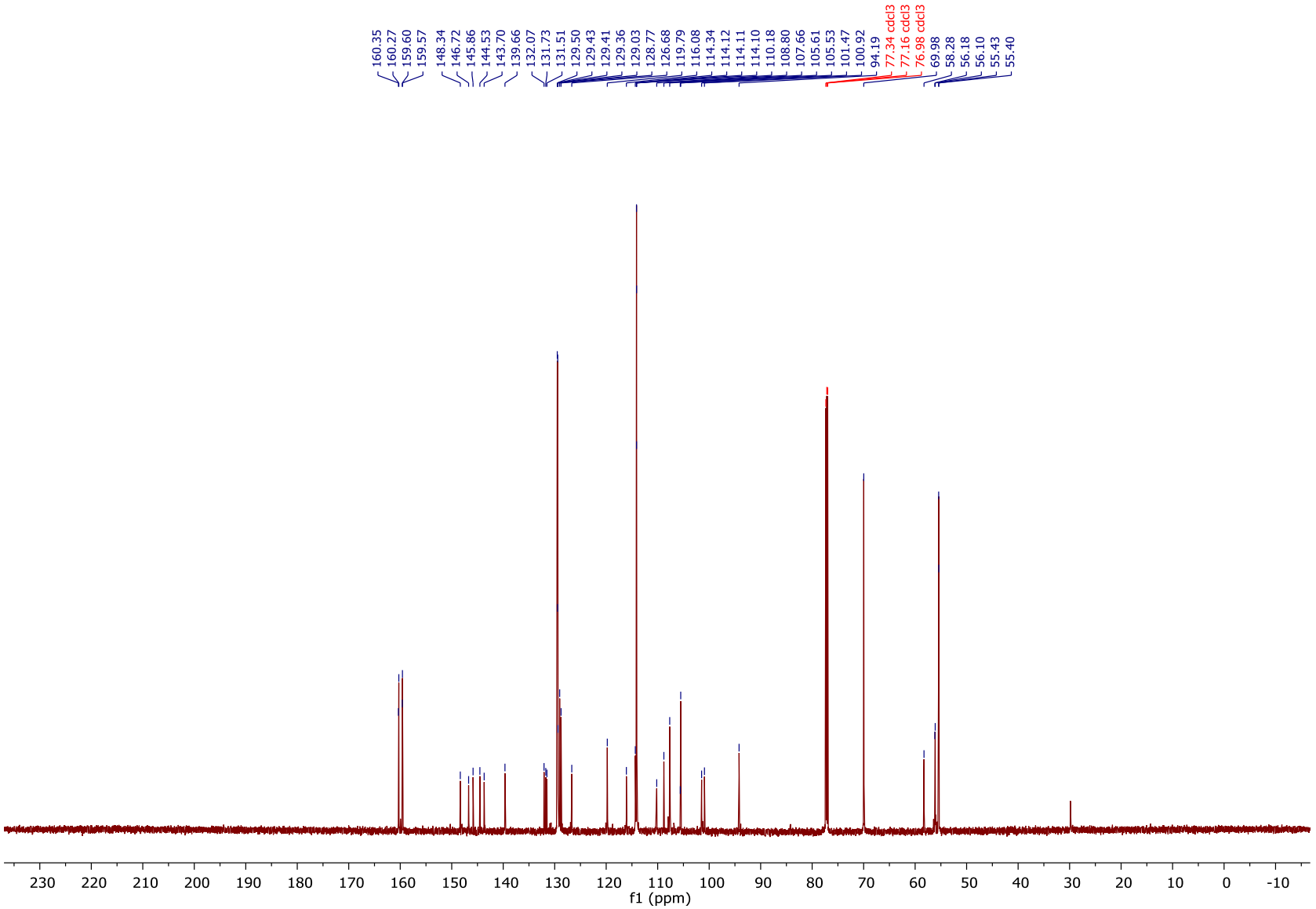

Total Synthesis of (±)-hierochin D

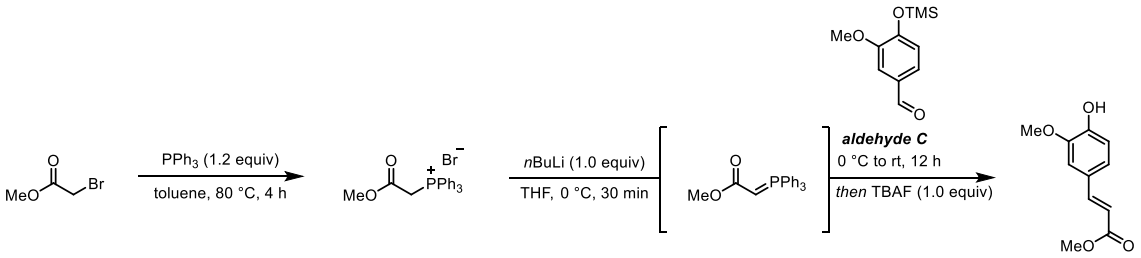

(S16) methyl (*E*)-3-(4-hydroxy-3-methoxyphenyl)acrylate

Commercially available methyl bromoacetate (1.42 mL, 15 mmol) was dissolved in toluene (60 mL) in a flame-dried round bottom flask. To the stirring solution was added triphenylphosphine (18 mmol, 4.72g), and the reaction was heated to 80 °C for 4 hours. Upon cooling the reaction mixture to room temperature, the white solid product was collected via vacuum filtration, and any excess triphenylphosphine was rinsed away with hexanes. The product was dried under vacuum for >24 hours to ensure full removal of solvent and water prior to use in the subsequent olefination.

To a flame-dried, three-neck, round bottom flask was added methyl acetophosphonium bromide (5.35 mmol, 2.22 g), which was subsequently suspended in THF (15 mL) and cooled on ice to 0 °C. To the stirring suspension was added *n*BuLi (5.35 mmol, 2.14 mL, 2.5 M in hexanes), and the reaction mixture was allowed to stir at temperature for 30 minutes to form the ylid. In a separate flame-dried, heart-shaped flask, TMS-vanillin (aldehyde C, 5.35 mmol, 1.20 g) was dissolved in THF (20 mL). The aldehyde was added to the ylide solution via cannula, and the reaction was allowed to warm to room temperature over 12 hours. The reaction was subsequently cooled on ice to 0 °C, and TBAF (5.35 mmol, 5.35 mL, 1.0 M in THF) was added. The reaction was allowed to warm to room temperature over 1 hour, at which point it was quenched by the addition of saturated ammonium chloride, diluted with EtOAc, then transferred to a separatory funnel containing additional saturated ammonium chloride. The layers were separated, and the aqueous layer was extracted with additional EtOAc. The combined organic layers were washed with brine, dried over magnesium sulfate, and concentrated under reduced pressure. The crude product was purified via flash column chromatography (6-42% EtOAc in Hexanes, 7-step gradient, 2 column volumes per step) to afford the product **S16** as a clear, colorless, oil (857 mg, 77% yield). The ^{1}H and ^{13}C NMR spectra of the product was consistent with the data previously reported in the literature.[6]

^{1}H NMR (700 MHz, Chloroform-*d*) δ 7.62 (d, *J* = 15.9 Hz, 1H), 7.07 (dd, *J* = 8.3, 1.9 Hz, 1H), 7.02 (d, *J* = 1.9 Hz, 1H), 6.92 (d, *J* = 8.2 Hz, 1H), 6.29 (d, *J* = 15.9 Hz, 1H), 5.93 (s, 1H), 3.92 (s, 3H), 3.79 (s, 3H).

^{13}C NMR (176 MHz, Chloroform-*d*) δ 167.87, 148.09, 146.88, 145.09, 127.05, 123.16, 115.26, 114.85, 109.46, 56.05, 51.76.

^{1}H NMR, 700 MHz, Chloroform-*d*, **S16**

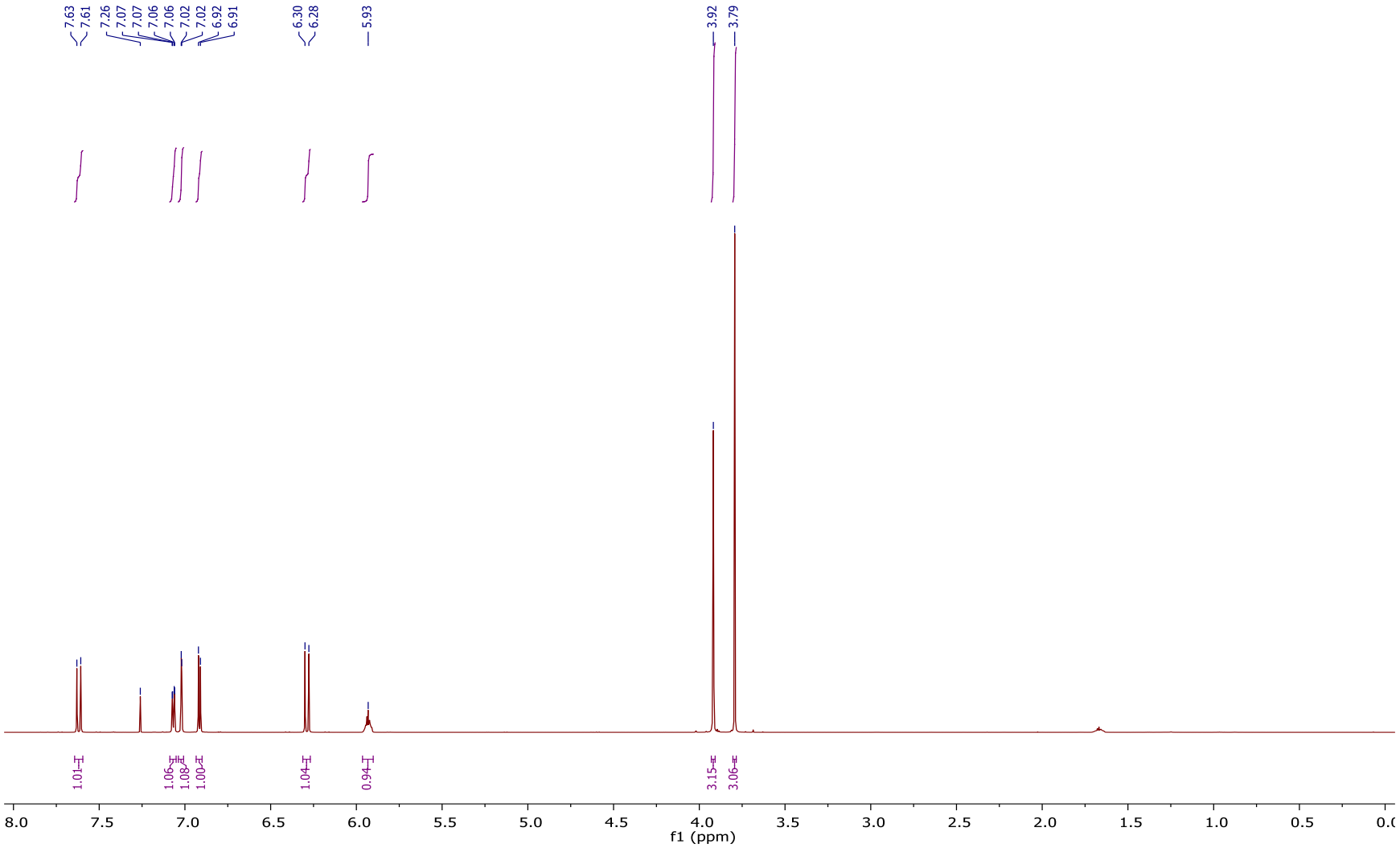

^{13}C NMR, 176 MHz, Chloroform-*d*, **S16**

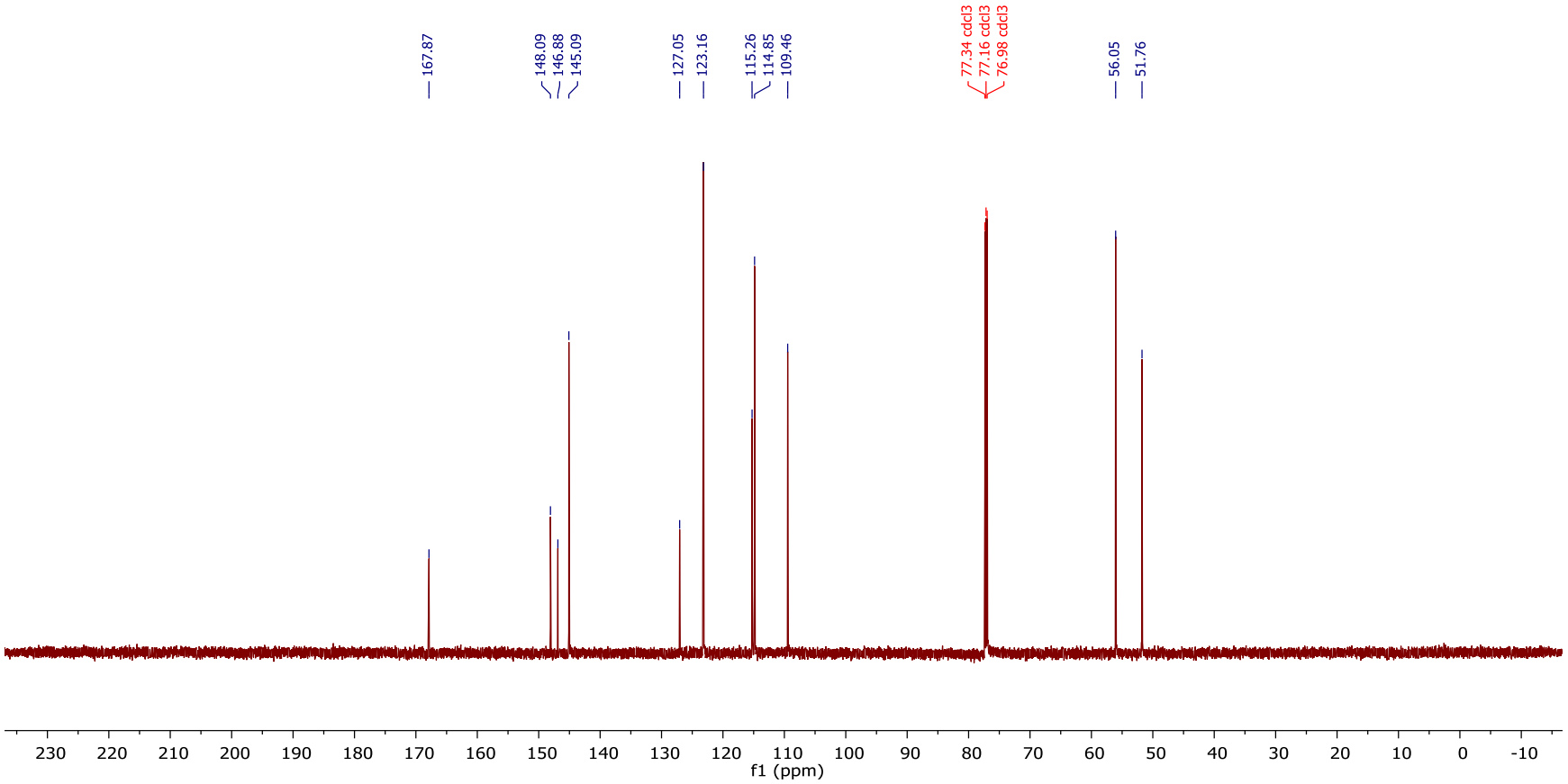

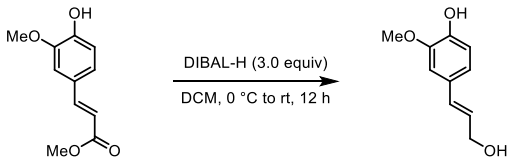

coniferyl alcohol (29) ((*E*)-4-(3-hydroxyprop-1-en-1-yl)-2-methoxyphenol)

Compound **S16** (1.12 mmol, 233 mg) was dissolved in DCM under inert atmosphere, and the stirring solution was cooled to 0 °C on ice. A solution of diisobutylaluminum hydride (3.36 mmol, 3.36 mL, 1.0 M in DCM) was added dropwise to the stirring solution, causing the reaction to change from colorless to slightly yellow. The reaction mixture was held at 0 °C for 10 minutes, at which point it was allowed to warm to room temperature over 12 hours. The reaction was quenched slowly with 4mL of Rochelle's salt, turning the mixture cloudy. The mixture was let to stir at room temperature for >6 hours, at which point it was diluted with DI water and transferred to a separatory funnel. The layers were separated, and the aqueous layer was washed with multiple portions of DCM. The combined organic layers were washed with brine, dried over magnesium sulfate, and concentrated under reduced pressure. The crude product was purified via flash column chromatography (28-98% EtOAc in Hexanes, 5 step gradient, 2 column volumes per step) to afford the product **35** as a white solid (167 mg, 83% yield). The ^{1}H and ^{13}C NMR spectra of the product was consistent with the data previously reported in the literature.[7]

^{1}H NMR (500 MHz, Chloroform-*d*) δ 6.92 (d, *J* = 1.8 Hz, 1H), 6.90 (dd, *J* = 8.1, 1.8 Hz, 1H), 6.87 (d, *J* = 8.1 Hz, 1H), 6.54 (dt, *J* = 15.8, 1.6 Hz, 1H), 6.23 (dt, *J* = 15.8, 6.0 Hz, 1H), 5.63 (d, *J* = 2.8 Hz, 1H), 4.30 (d, *J* = 5.9 Hz, 2H), 3.91 (s, 3H), 1.41 (s, 1H).

^{13}C NMR (126 MHz, Chloroform-*d*) δ 146.76, 145.74, 131.55, 129.38, 126.30, 120.47, 114.58, 108.44, 64.04, 56.03.

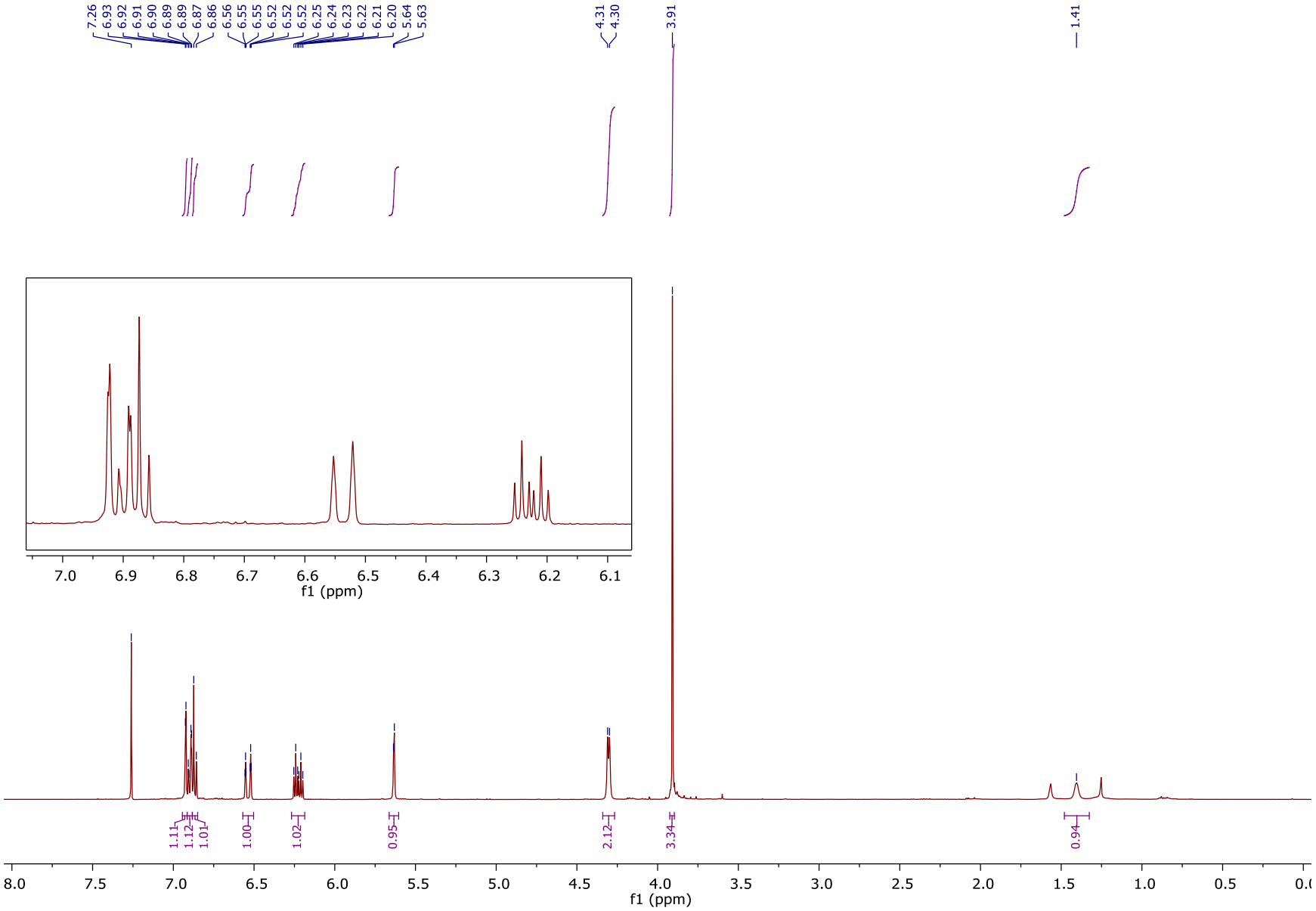
7.26
6.93
6.92
6.91
6.90
6.89
6.89
6.87
6.86
6.56
6.55
6.55
6.52
6.52
6.52
6.25
6.24
6.23
6.22
6.21
6.20
5.64
5.63
4.31
4.30
3.91
1.41
7.0
6.9
6.8
6.7
6.6
6.5
6.4
6.3
6.2
6.1
f1 (ppm)
1.11
1.12
1.01
1.00
1.02
0.95
2.12
3.34
0.94
8.0
7.5
7.0
6.5
6.0
5.5
5.0
4.5
4.0
3.5
3.0
2.5
2.0
1.5
1.0
0.5
f1 (ppm)

^{13}C NMR, 126 MHz, Chloroform-*d*, **29**

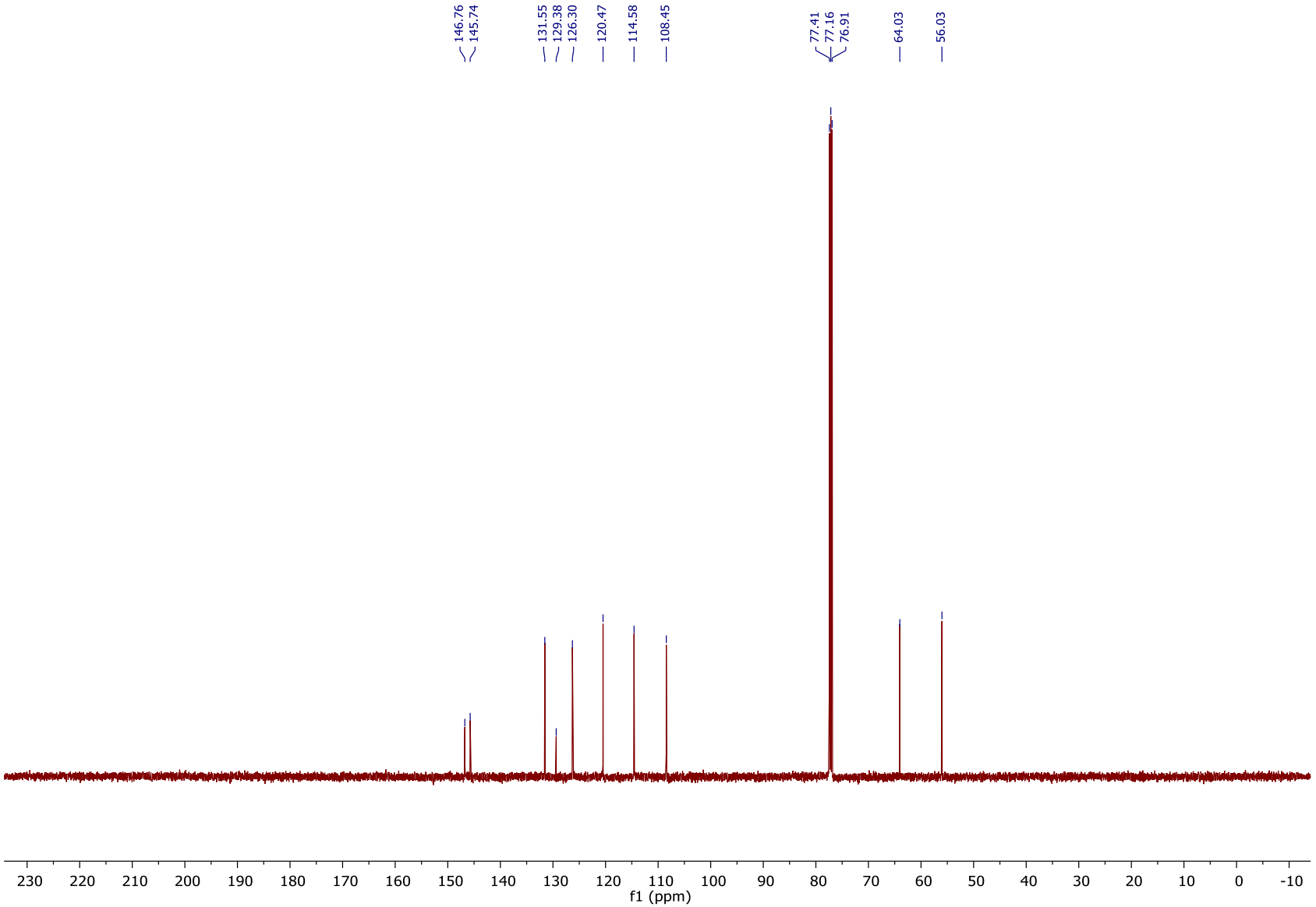

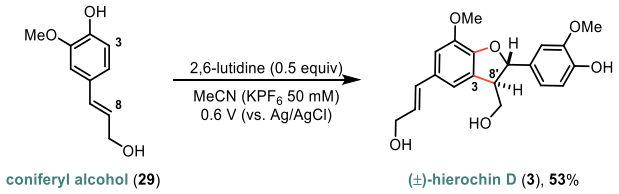

coniferyl alcohol (**29**) (±)-hierochin D (**3**), **53**%

(±)-hierochin D (3) (4-((2*S*,3*R*)-3-(hydroxymethyl)-5-((*E*)-3-hydroxyprop-1-en-1-yl)-7-methoxy-2,3-dihydrobenzofuran-2-yl)-2-methoxyphenol)

Coniferyl alcohol (**29**, 0.1 mmol, 18 mg) was subjected to the general dimerization conditions (see page S42), with the only variation being the amount of 2,6-lutidine (5.8 μL, 0.05 mmol). The crude reaction material was purified via flash column chromatography to afford (±)-hierochin D (**3**) as a colorless oil (9.4 mg, 53% yield). The ^{13}C NMR was consistent with the previous report for this compound.[8]

^{13}C NMR (126 MHz, Acetone-d_6) δ 148.97, 148.38, 147.29, 145.18, 134.40, 131.93, 130.54, 130.42, 128.38, 119.60, 116.09, 115.68, 111.70, 110.47, 88.54, 64.63, 63.43, 56.39, 56.28, 54.79.

^{13}C NMR, 126 MHz, Chloroform-*d*, **3**

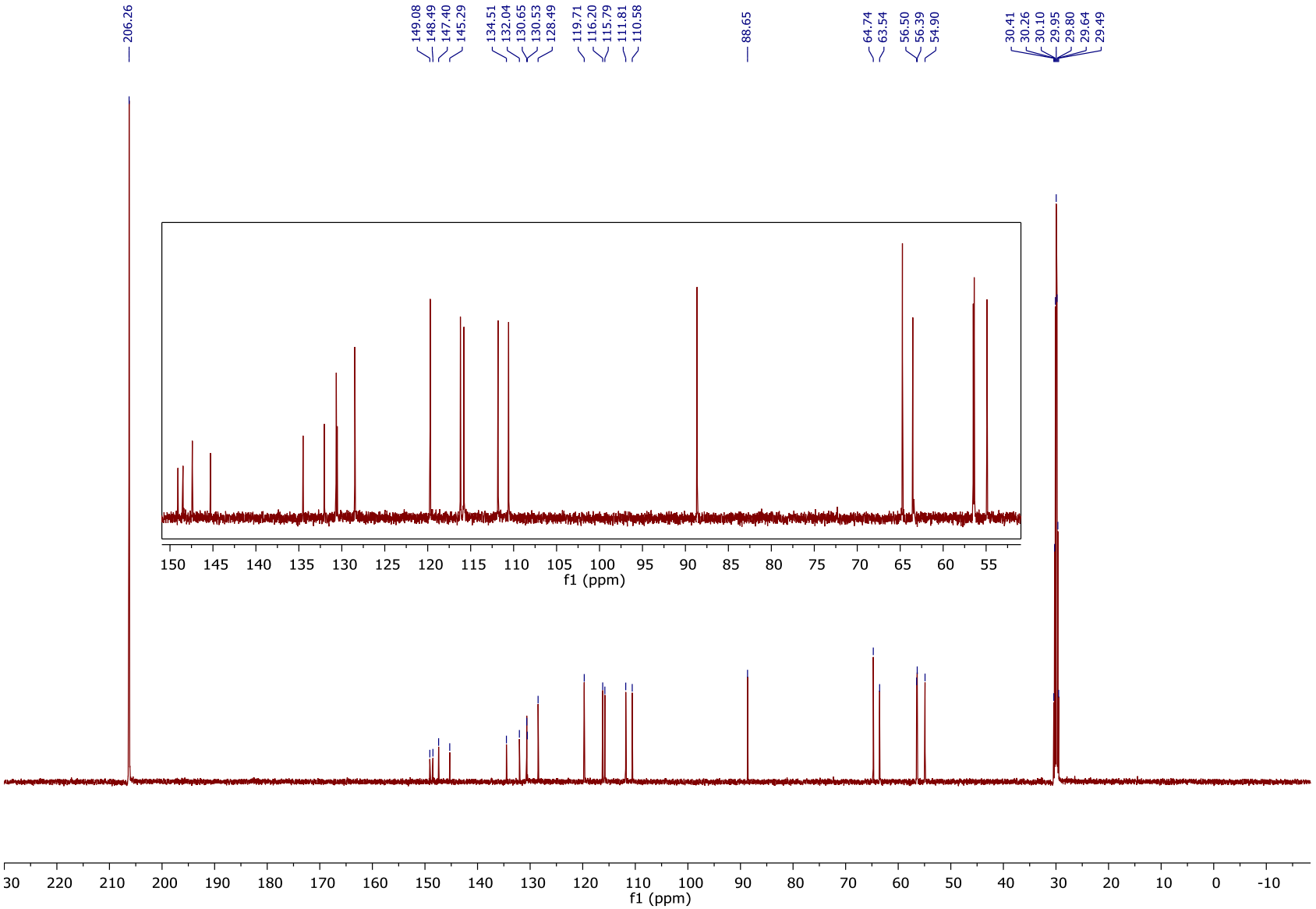

Attempted Direct Cyclization of QMD products:

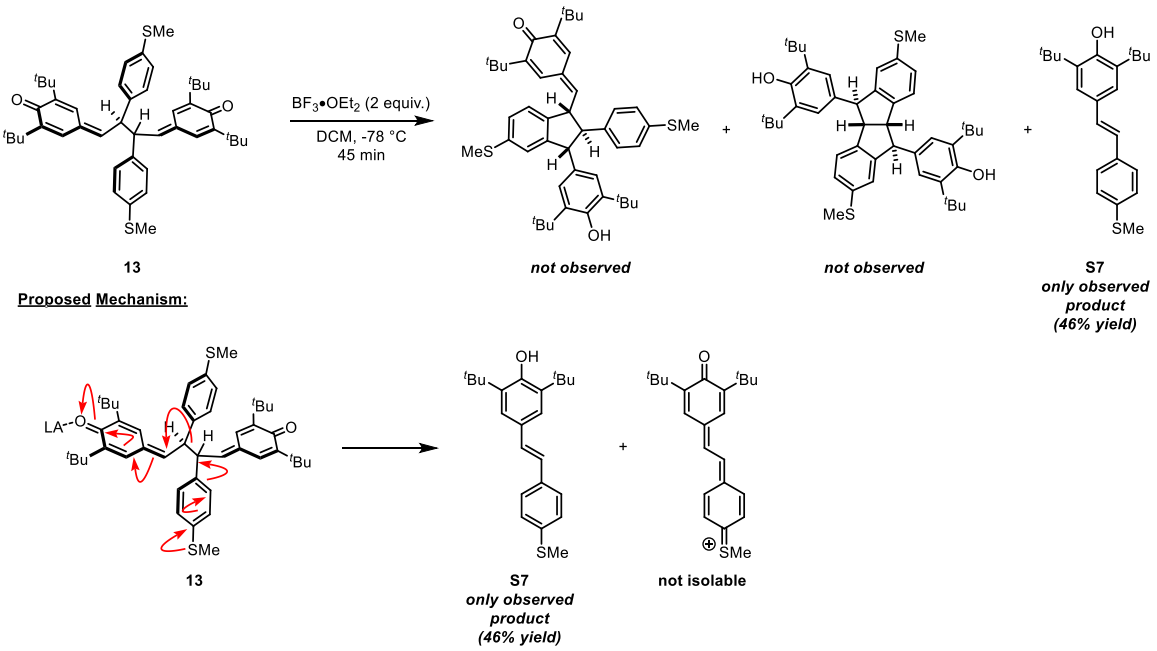

Figure S1. Attempted direct cyclization of QMDs containing electron-donating substituents at C12 results in disproportionation back to the stilbene precursor. Note that 46% yield is relative to the mass of **13**, therefore the fragmentation has a theoretical yield for **S7** of 50%.

Natural Product Analog Synthesis:

Tautomerization of BQM dimer to MQM dimer – General Procedure:

The starting BQM dimer was added to a reaction vial charged with a stir bar. The atmosphere was evacuated and replaced with nitrogen, and the starting material was dissolved in THF. The reaction solution was cooled in an ice bath to 0 °C, and potassium bis(trimethylsilyl)amide (KHMDS) was added as a solution (1.25 equiv., 0.7 M in toluene). The reaction was allowed to stir until the starting material consumed based on TLC analysis. The reaction was quenched by the addition of aqueous saturated ammonium chloride, diluted with EtOAc, and transferred to a separatory funnel containing additional aq. sat. NH_4Cl. The layers were separated, and the aqueous layer was extracted with additional portions of ethyl acetate. The combined organic layers were washed with brine, dried over magnesium sulfate, and concentrated under reduced pressure. The crude product was further purified by flash column chromatography.

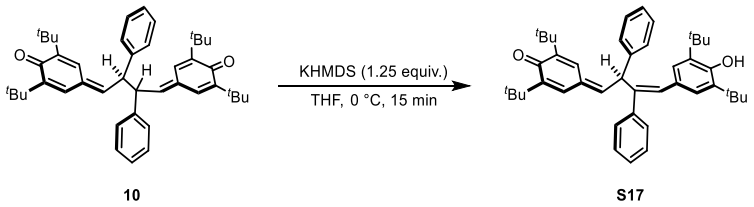

10 **S17**

(S17) (*S*,*Z*)-2,6-di-*tert*-butyl-4-(4-(3,5-di-*tert*-butyl-4-hydroxyphenyl)-2,3-diphenylbut-3-en-1-ylidene)cyclohexa-2,5-dien-1-one

Dimer **10** (0.026 mmol, 16 mg) was subjected to the tautomerization conditions, and the crude product was purified by flash column chromatography (10–50% DCM/Hexanes) to afford MQM **S17** (10 mg, 62% yield).

^{1}H NMR (500 MHz, Chloroform-*d*) δ 7.34 (d, *J* = 7.0 Hz, 2H), 7.25 – 7.14 (m, 7H), 7.12 (t, *J* = 6.8 Hz, 1H), 6.95 (s, 2H), 6.74 (d, *J* = 2.7 Hz, 1H), 6.27 (d, *J* = 2.7 Hz, 1H), 5.83 (d, *J* = 1.9 Hz, 1H), 5.10 (dd, *J* = 9.5, 2.0 Hz, 1H), 5.01 (s, 1H), 3.67 (d, *J* = 9.5 Hz, 1H), 1.38 (s, 18H), 1.30 (s, 9H), 0.92 (s, 9H).

^{13}C NMR (126 MHz, Chloroform-*d*) δ 186.41, 152.63, 147.21, 146.57, 145.86, 144.46, 143.44, 141.60, 135.28, 135.20, 130.05, 128.51, 128.24, 128.18, 127.76, 127.47, 126.68, 126.39, 123.82, 65.46, 56.53, 54.16, 34.78, 34.58, 34.23, 30.28, 29.77, 29.06.

IR (Neat): 3623, 2954, 2912, 1653, 1437, 1366, 1192, 1116, 886, 734, 700 cm^{-1};

HRMS (ESI) m/z calculated for $C_{44}H_{55}O_2^+$ ([M+H]+) 615.4197, found 615.4194.

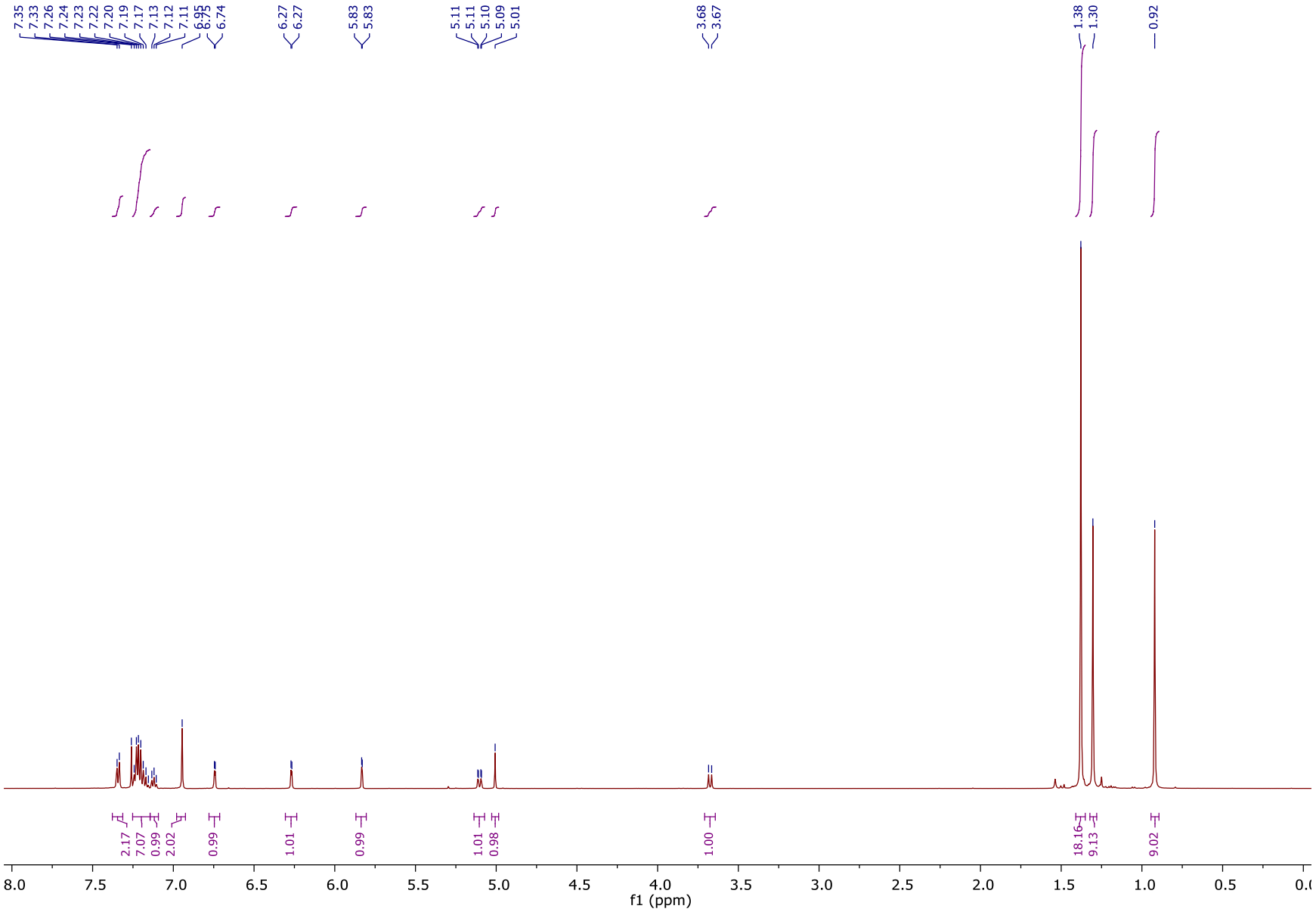
7.35
7.33
7.26
7.24
7.23
7.22
7.20
7.19
7.17
7.13
7.12
7.11
6.95
6.75
6.74
6.27
6.27
5.83
5.83
5.11
5.11
5.10
5.09
5.01
3.68
3.67
1.38
1.30
0.92
2.17
7.07
0.99
2.02
0.99
1.01
0.99
1.01
0.98
1.00
18.16
9.13
9.02
8.0
7.5
7.0
6.5
6.0
5.5
5.0
4.5
4.0
3.5
3.0
2.5
2.0
1.5
1.0
0.5
f1 (ppm)

^{13}C NMR, 126 MHz, Chloroform-*d*, Tautomer **S17**

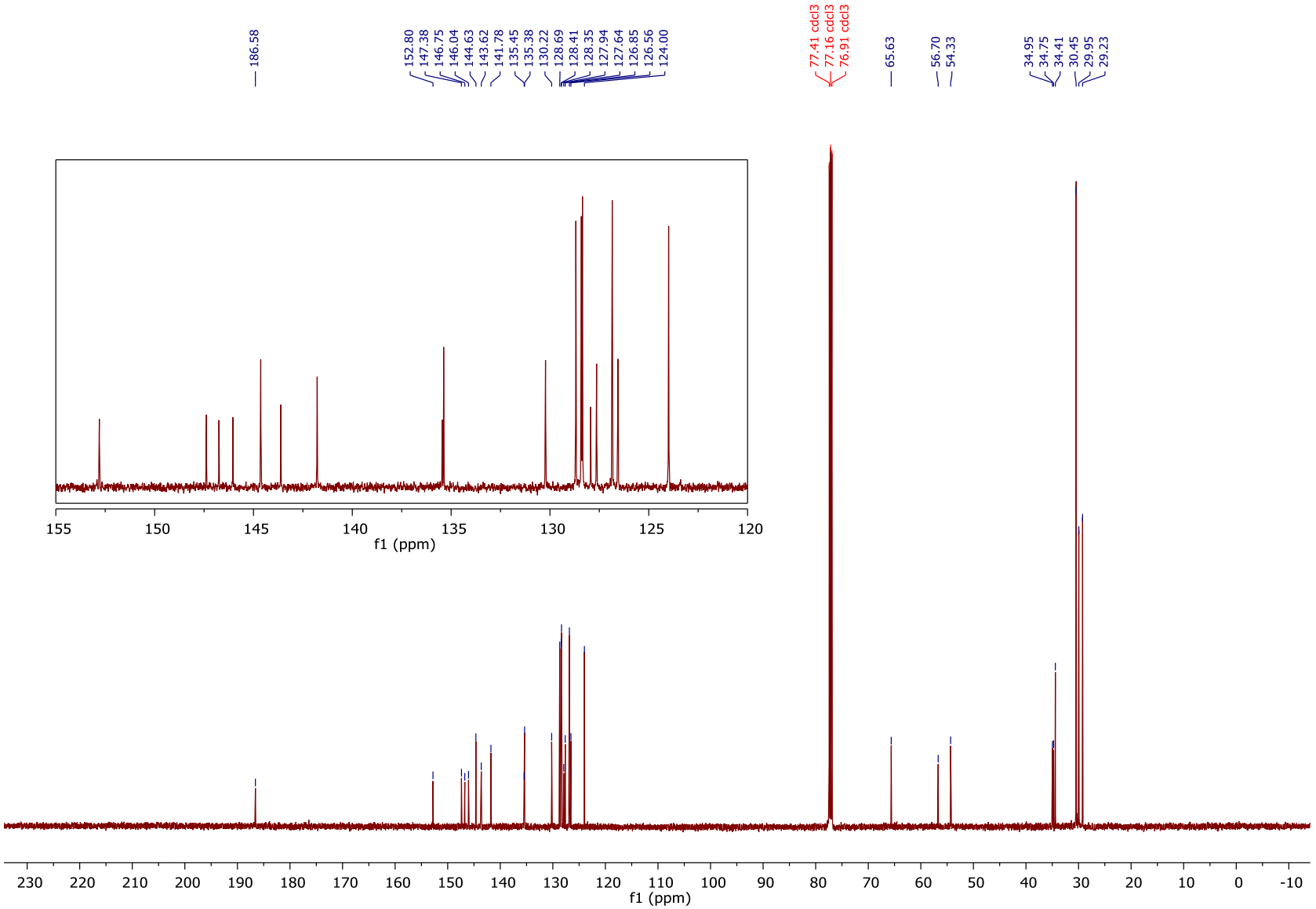

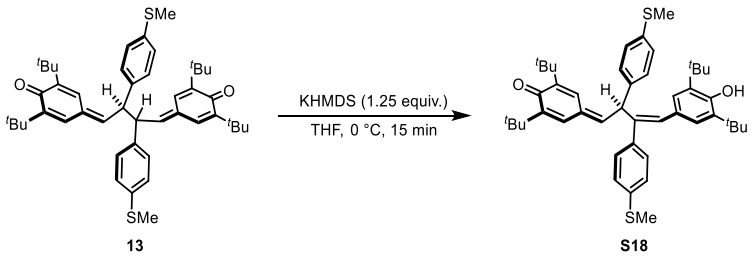

(S18) (*S*,*Z*)-2,6-di-*tert*-butyl-4-(4-(3,5-di-*tert*-butyl-4-hydroxyphenyl)-2,3-bis(4-(methylthio)phenyl)but-3-en-1-ylidene)cyclohexa-2,5-dien-1-one

Dimer **13** (0.021 mmol, 15 mg) was subjected to the tautomerization conditions, and the crude product was purified by flash column chromatography (10-50% DCM/Hexanes) to afford MQM **S18** (14.8 mg, 99% yield).

^{1}H NMR (500 MHz, Chloroform-*d*) δ 7.24 (d, *J* = 8.2 Hz, 2H), 7.13 (d, *J* = 8.2 Hz, 2H), 7.10 (d, *J* = 8.2 Hz, 2H), 7.09 (d, *J* = 8.2 Hz, 2H), 6.91 (s, 2H), 6.71 (d, *J* = 2.7 Hz, 1H), 6.24 (d, *J* = 2.7 Hz, 1H), 5.79 (d, *J* = 1.9 Hz, 1H), 5.02 (dd, *J* = 9.2, 2.0 Hz, 1H), 5.01 (s, 1H), 3.60 (d, *J* = 9.6 Hz, 1H), 2.44 (s, 3H), 2.41 (s, 3H), 1.38 (s, 18H), 1.30 (s, 9H), 0.91 (s, 9H).

^{13}C NMR (126 MHz, Chloroform-*d*) δ 186.52, 152.83, 147.44, 146.09, 145.94, 144.52, 141.58, 140.43, 138.06, 136.31, 135.41, 132.09, 129.66, 128.82, 127.70, 127.25, 126.90, 126.22, 123.97, 65.73, 56.60, 53.73, 34.95, 34.75, 34.40, 30.45, 29.94, 29.22, 15.85, 15.72.

IR (Neat): 3645, 2960, 1659, 1496, 1439, 1363, 1316, 1237, 1150, 1094, 891, 814, 728 cm^{-1};

HRMS (ESI) m/z calculated for $C_{46}H_{59}O_2S_2^+$ ([M+H]+) 707.3951, found 707.3940.

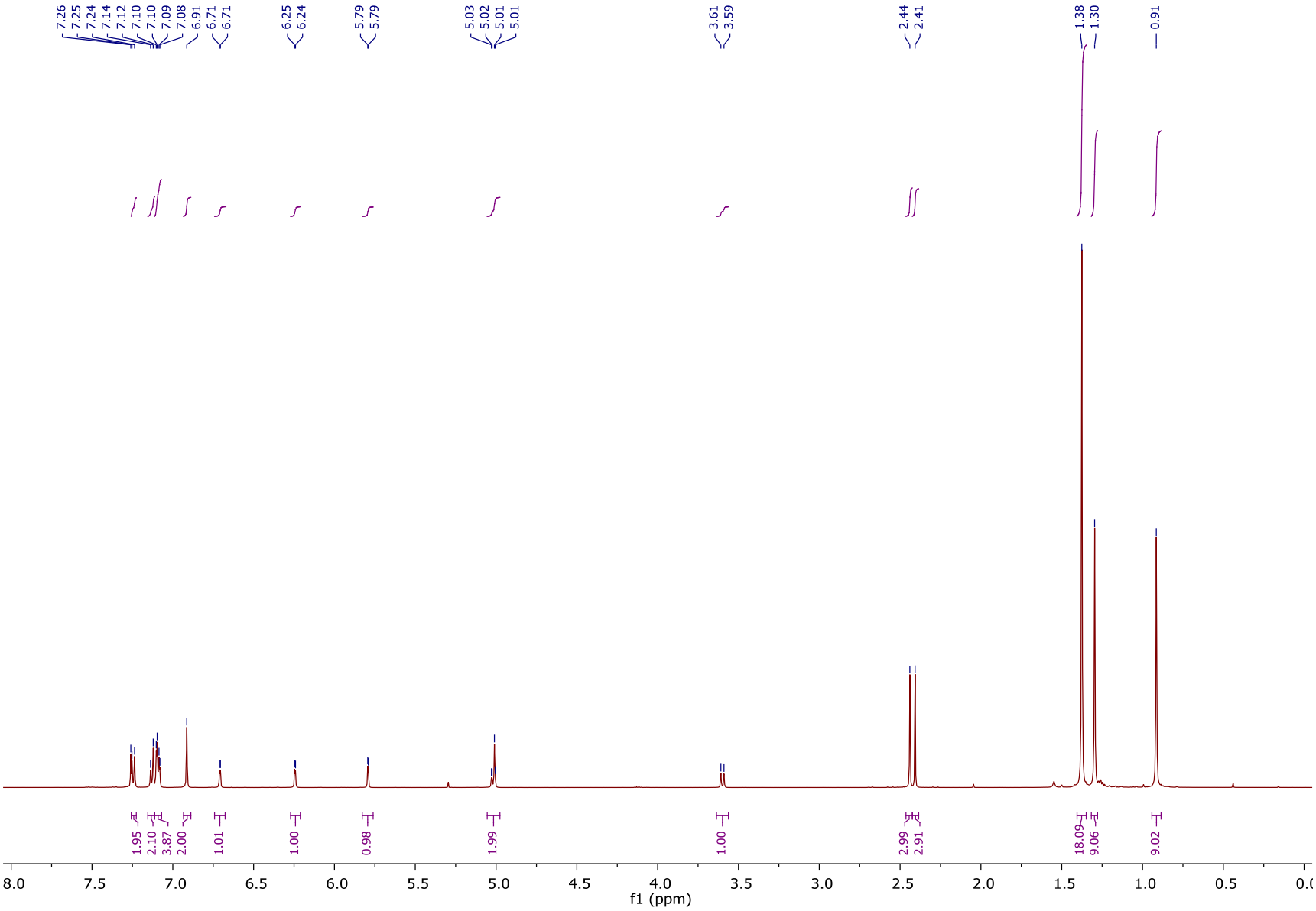
7.26
7.25
7.24
7.14
7.12
7.10
7.10
7.09
7.08
6.91
6.71
6.71
6.25
6.24
5.79
5.79
5.03
5.02
5.01
5.01
3.61
3.59
2.44
2.41
1.38
1.30
0.91
1.95
2.10
3.87
2.00
1.01
1.00
0.98
1.99
1.00
2.99
2.91
18.09
9.06
9.02
8.0
7.5
7.0
6.5
6.0
5.5
5.0
4.5
4.0
3.5
3.0
2.5
2.0
1.5
1.0
0.5
f1 (ppm)

^{13}C NMR, 126 MHz, Chloroform-*d*, Tautomer **S18**

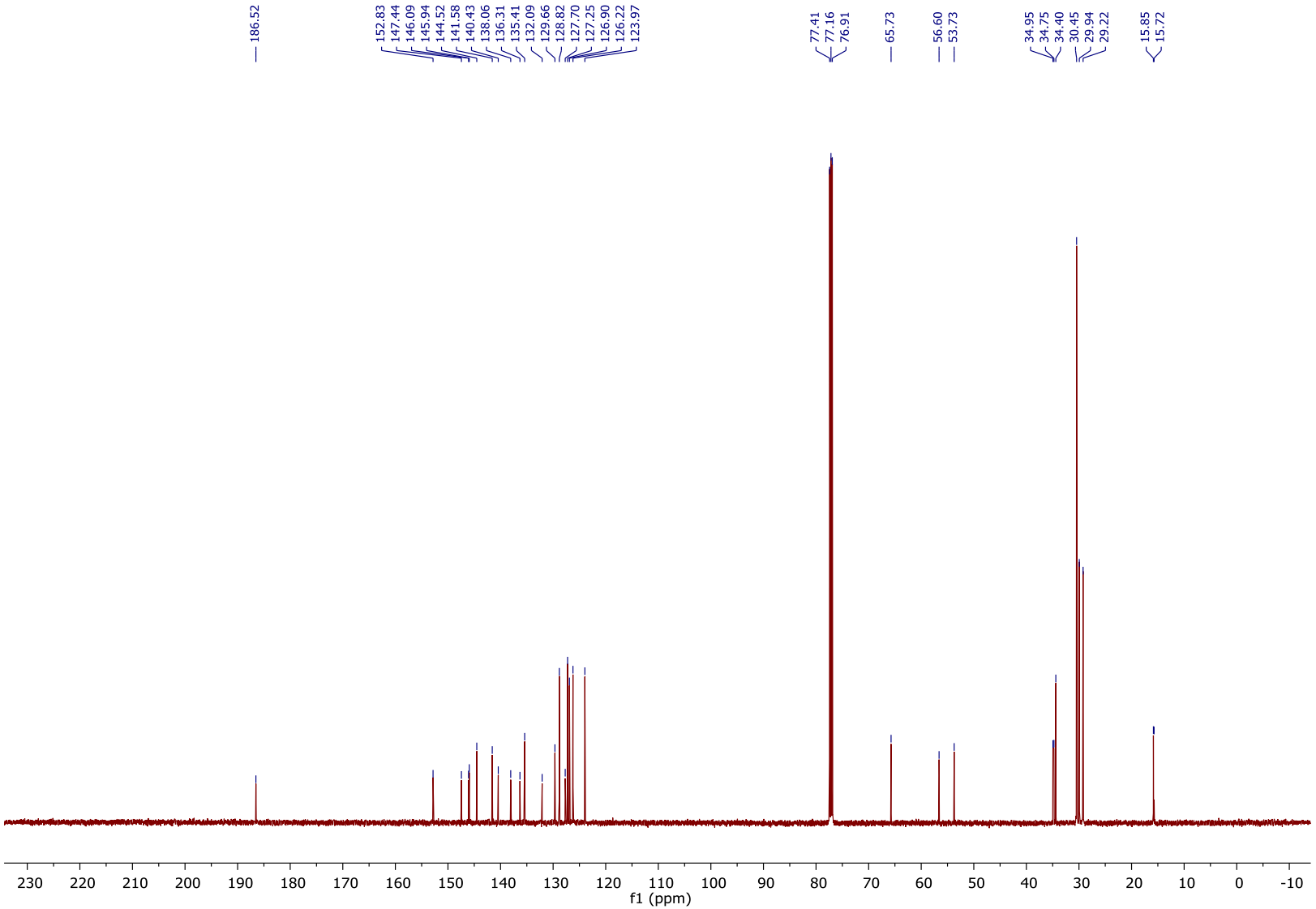

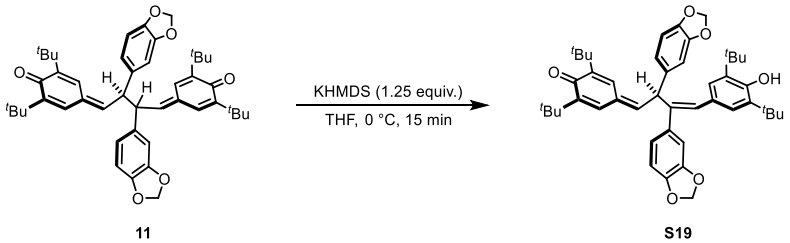

(S19) (*S*,*Z*)-4-(2,3-bis(benzo[*d*][1,3]dioxol-5-yl)-4-(3,5-di-*tert*-butyl-4-hydroxyphenyl)but-3-en-1-ylidene)-2,6-di-*tert*-butylcyclohexa-2,5-dien-1-one

Dimer **11** (0.021 mmol, 14.7 mg) was subjected to the tautomerization conditions, and the crude product was purified by flash column chromatography (10–50% DCM/Hexanes) to afford MQM **S19** (9 mg, 61% yield).

^{1}H NMR (700 MHz, Chloroform-*d*) δ 6.90 (s, 2H), 6.88 (d, *J* = 1.8 Hz, 1H), 6.81 (dd, *J* = 8.1, 1.8 Hz, 1H), 6.70 – 6.66 (m, 4H), 6.65 (d, *J* = 7.8 Hz, 1H), 6.21 (d, *J* = 2.7 Hz, 1H), 5.93 – 5.89 (m, 2H), 5.89 – 5.84 (m, 2H), 5.65 (d, *J* = 1.9 Hz, 1H), 5.01 (s, 1H), 4.94 (dd, *J* = 9.5, 2.0 Hz, 1H), 3.59 (d, *J* = 9.5 Hz, 1H), 1.37 (s, 18H), 1.29 (s, 9H), 0.90 (s, 9H).

^{13}C NMR (176 MHz, Chloroform-*d*) δ 186.54, 152.80, 147.88, 147.74, 147.31, 147.16, 146.24, 146.23, 145.91, 144.70, 141.82, 137.52, 135.37, 129.74, 128.76, 127.84, 123.90, 121.69, 120.77, 108.43, 108.40, 108.19, 107.19, 101.17, 100.99, 65.65, 56.40, 54.12, 34.93, 34.72, 34.39, 30.44, 29.94, 29.20.

IR (Neat): 3628, 2955, 2905, 1653, 1635, 1503, 1436, 1363, 1235, 1038, 933, 809, 729 cm^{-1};

HRMS (ESI) m/z calculated for $C_{46}H_{55}O_6^+$ ([M+H]+) 703.3993, found 703.3985.

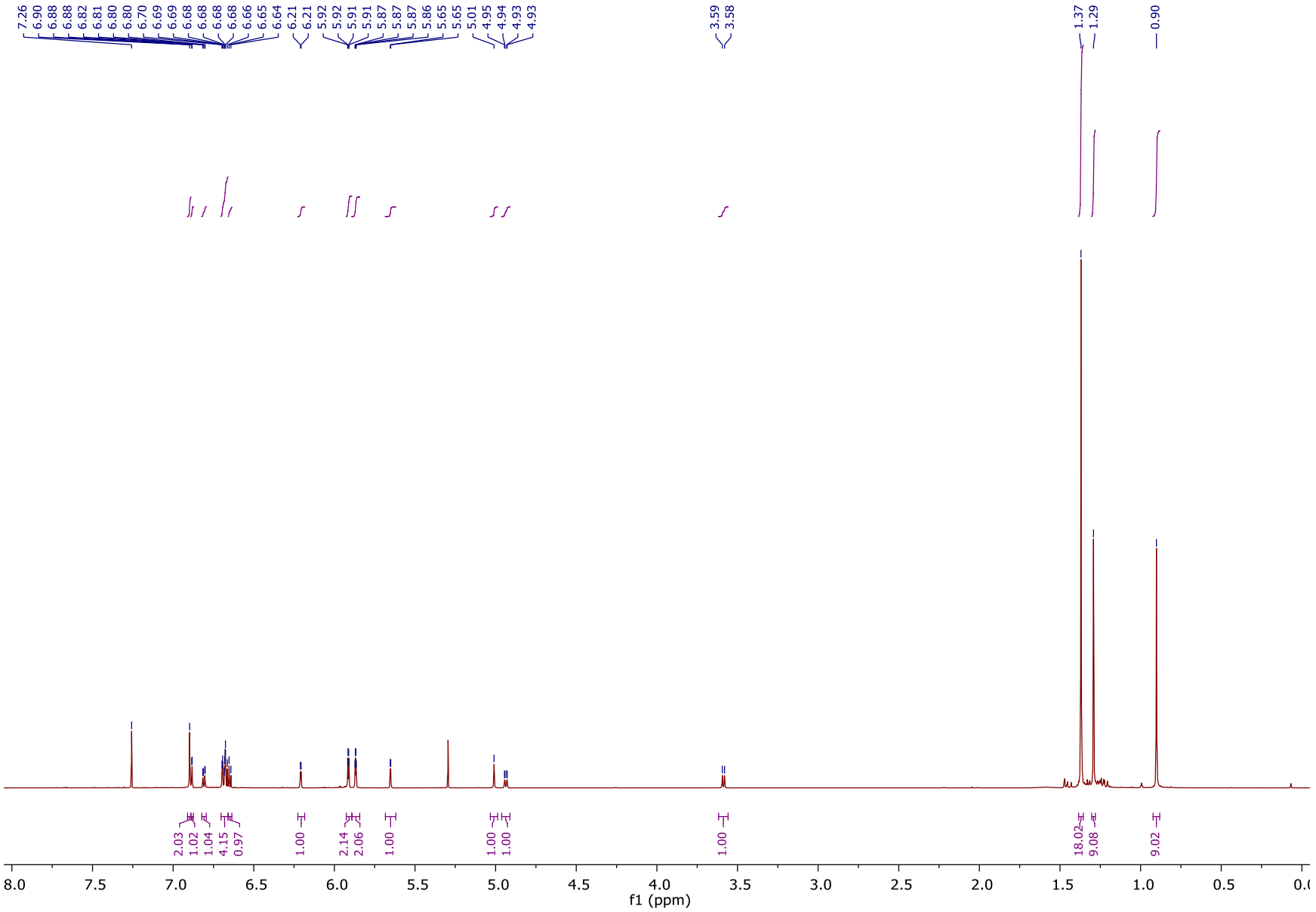
7.26
6.90
6.88
6.88
6.82
6.81
6.80
6.80
6.70
6.69
6.69
6.68
6.68
6.68
6.68
6.66
6.65
6.64
6.21
6.21
5.92
5.92
5.91
5.91
5.87
5.87
5.87
5.86
5.65
5.65
5.01
4.95
4.94
4.93
4.93
3.59
3.58
1.37
1.29
0.90
2.03
1.02
1.04
4.15
0.97
1.00
2.14
2.06
1.00
1.00
1.00
1.00
1.00
18.02
9.08
9.02
8.0
7.5
7.0
6.5
6.0
5.5
5.0
4.5
4.0
3.5
3.0
2.5
2.0
1.5
1.0
0.5
f1 (ppm)

^{13}C NMR, 176 MHz, Chloroform-*d*, Tautomer **S19**

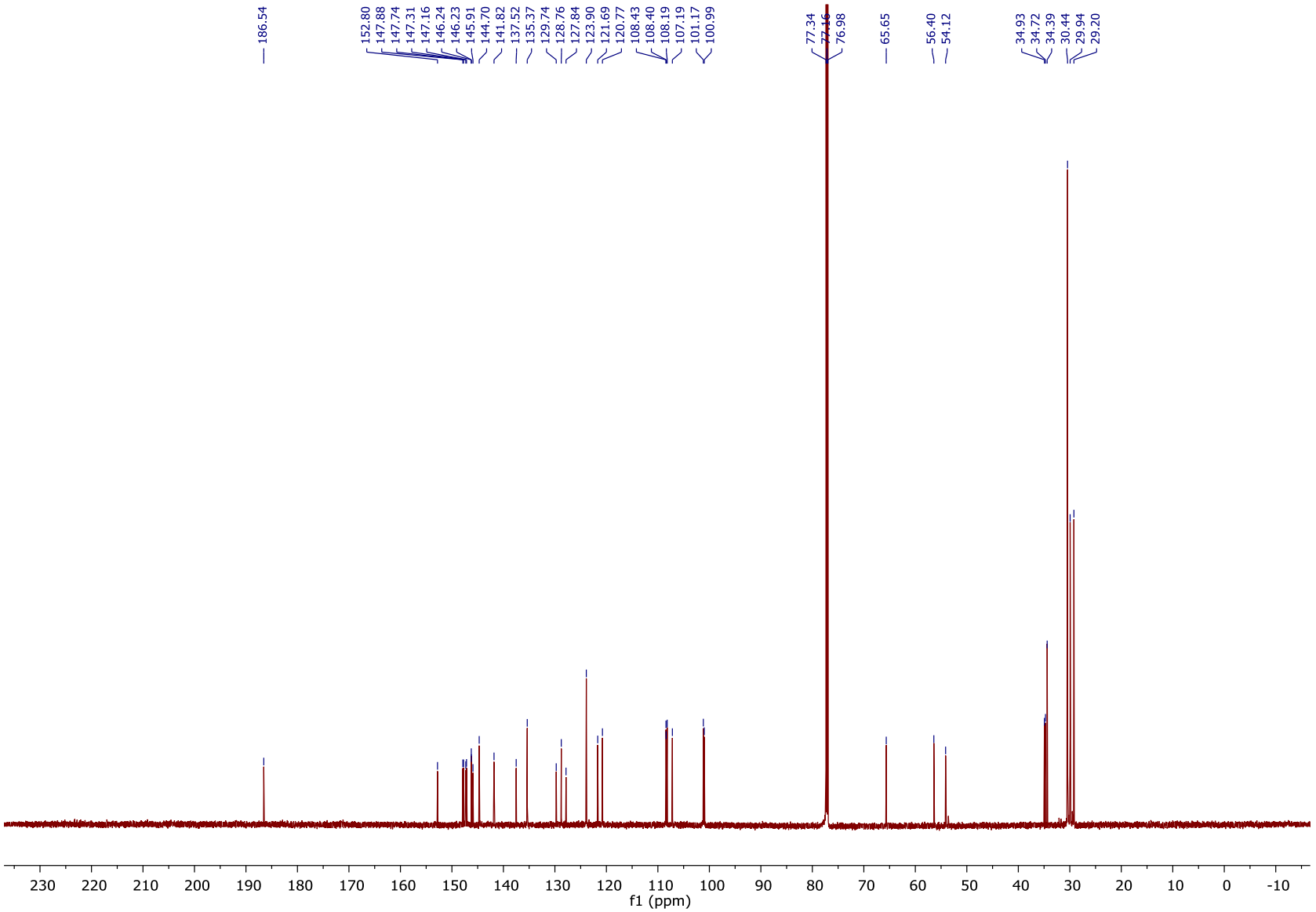

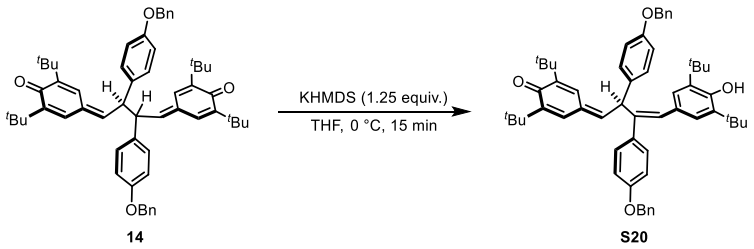

(S20) (*S*,*Z*)-4-(2,3-bis(4-(benzyloxy)phenyl)-4-(3,5-di-*tert*-butyl-4-hydroxyphenyl)but-3-en-1-ylidene)-2,6-di-*tert*-butylcyclohexa-2,5-dien-1-one

Dimer **14** (0.087 mmol, 72 mg) was subjected to the tautomerization conditions, and the crude product was purified by flash column chromatography (5–35% DCM/Hexanes) to afford MQM **S20** (50 mg, 69% yield).

^{1}H NMR (500 MHz, Chloroform-*d*) δ 7.38 (m, 8H), 7.32 (m, 2H), 7.28 (m, 2H), 7.14 (d, *J* = 8.3 Hz, 2H), 6.92 (s, 2H), 6.83 (d, *J* = 8.3 Hz, 4H), 6.72 (d, *J* = 2.6 Hz, 1H), 6.24 (d, *J* = 2.6 Hz, 1H), 5.69 (d, *J* = 1.9 Hz, 1H), 5.01 (m, 4H), 4.96 (s, 2H), 3.61 (d, *J* = 9.5 Hz, 1H), 1.37 (s, 18H), 1.29 (s, 9H), 0.90 (s, 9H).

^{13}C NMR (126 MHz, Chloroform-*d*) δ 186.64, 158.28, 157.48, 152.73, 147.14, 146.16, 145.73, 145.03, 142.15, 137.16, 136.96, 136.14, 135.30, 135.27, 129.35, 128.73, 128.69, 128.38, 128.36, 128.15, 128.09, 127.92, 127.67, 127.59, 123.96, 114.97, 114.64, 70.06 (2C), 65.65, 56.53, 53.57, 34.92, 34.71, 34.39, 30.44, 29.95, 29.22.

IR (Neat): 3635, 2959, 2869, 1656, 1507, 1454, 1433, 1364, 1228, 1178, 1120, 1027, 886, 732, 695 cm^{-1};

HRMS (ESI) *m/z* calculated for $C_{58}H_{67}O_4^+$ ($[M+H]^+$) 827.5034, found 827.5010.

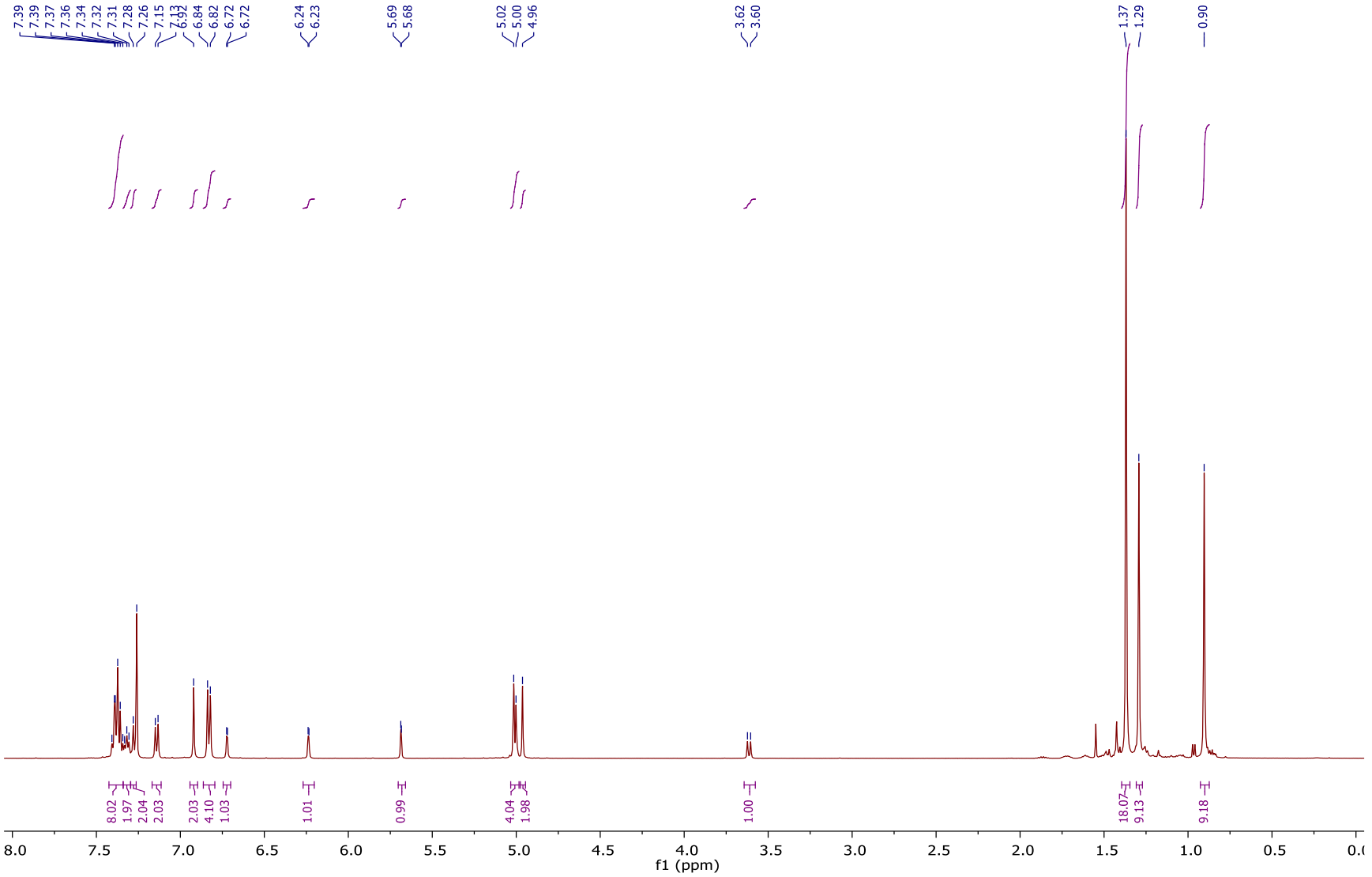
7.39
7.39
7.37
7.36
7.34
7.32
7.31
7.28
7.26
7.15
7.13
7.12
6.84
6.82
6.72
6.72
6.24
6.23
5.69
5.68
5.02
5.00
4.96
3.62
3.60
1.37
1.29
0.90
8.02
1.97
2.04
2.03
2.03
4.10
1.03
1.01
0.99
4.04
1.98
1.00
18.07
9.13
9.18
8.0
7.5
7.0
6.5
6.0
5.5
5.0
4.5
4.0
3.5
3.0
2.5
2.0
1.5
1.0
0.5
f1 (ppm)

^{13}C NMR, 176 MHz, Chloroform-*d*, Tautomer **S20**

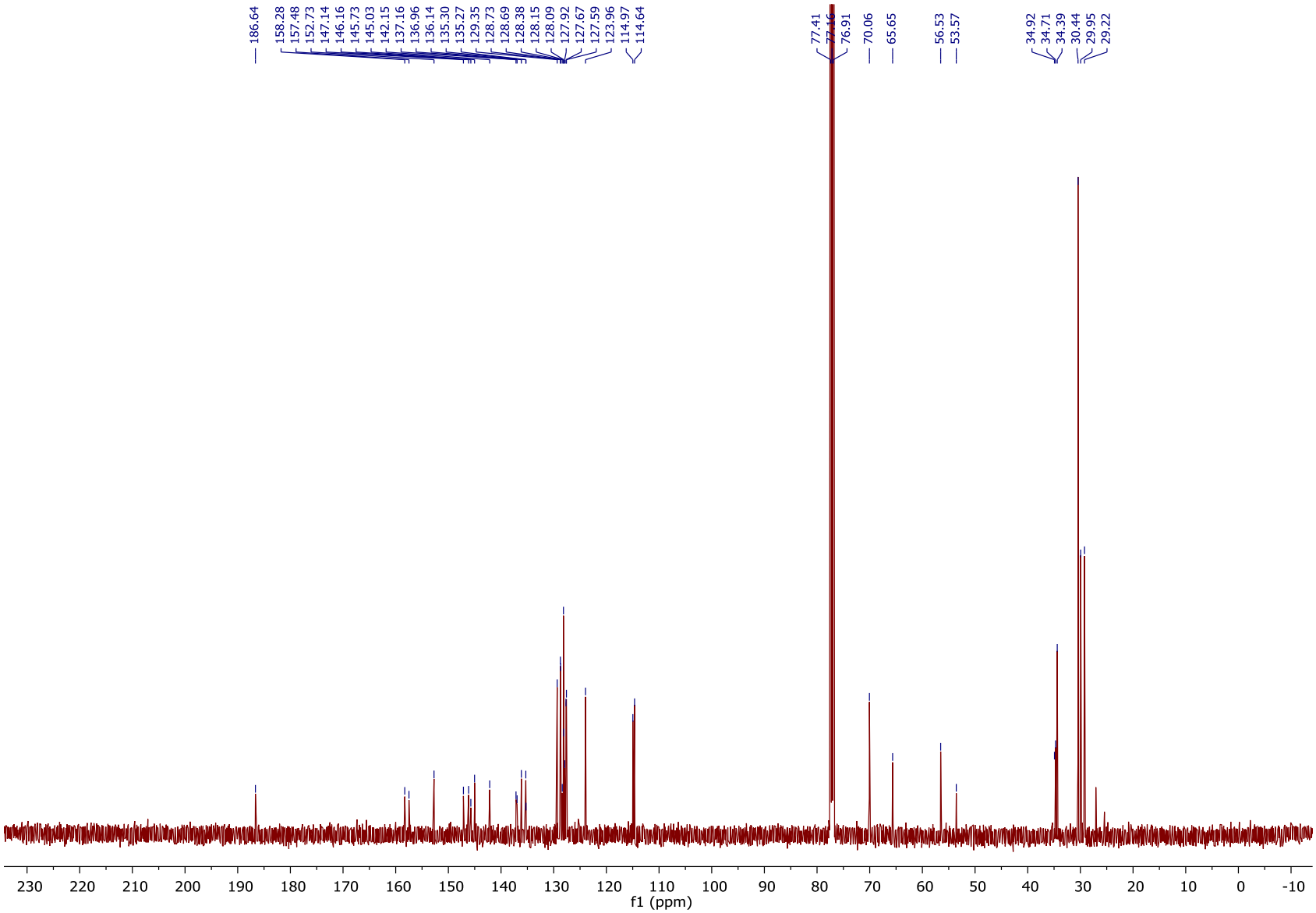

Cyclization of MQM dimer to quadrangularin A core:

The starting material was dried down into a flame-dried round bottom flask charged with stir bar. The atmosphere was evacuated and replaced with N_2, and the starting material was dissolved in CH_2Cl_2 (0.01 M reaction concentration). The solution was cooled to the reaction temperature, and $BF_3{\bullet}OEt_2$ (2 equiv.) was added dropwise. The reaction was allowed to stir for 3 hours, at which point it was raised from the ice bath and quenched via the addition of saturated $NaHCO_3$. Once the reaction had thawed, it was poured into a separatory funnel, and the layers were separated. The aqueous layer was extracted with additional portions of CH_2Cl_2, and the combined organic layers were washed with brine, dried over magnesium sulfate, and concentrated under reduced pressure. The crude product was purified by column chromatography.

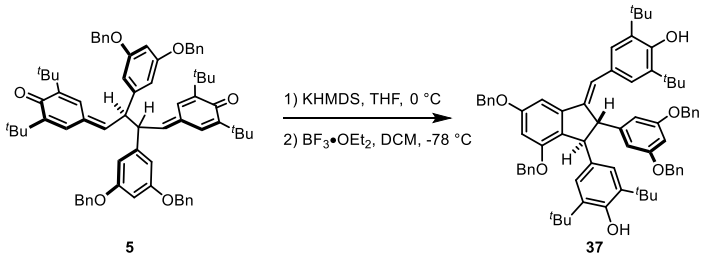

(30) 4-((1S,2S)-5,7-bis(benzyloxy)-2-(3,5-bis(benzyloxy)phenyl)-3-((E)-3,5-di-tert-butyl-4-hydroxybenzylidene)-2,3-dihydro-1H-inden-1-yl)-2,6-di-tert-butylphenol

BQM **5** (500 mg, 0.481 mmol) was subjected to the standard tautomerization conditions, and the crude product was subjected to the cyclization conditions at -78 °C with $BF_3{\bullet}OEt_2$ (128 μL, 0.962 mmol, 2.0 equiv.). The product was purified by column chromatography (0% to 20% EtOAc in Hexanes) to afford compound **37** (452 mg, 90% yield). The ^{1}H NMR spectrum was consistent with the prior report for this compound.[1]

^{1}H NMR (500 MHz, Chloroform-*d*) δ 7.55 – 7.49 (m, 2H), 7.45 – 7.33 (m, 13H), 7.33 – 7.28 (m, 3H), 7.24 (t, *J* = 2.8 Hz, 3H), 7.19 – 7.16 (m, 1H), 7.08 (d, *J* = 1.8 Hz, 2H), 7.05 (dd, *J* = 7.2, 2.7 Hz, 4H), 6.98 (t, *J* = 1.9 Hz, 1H), 6.62 (d, *J* = 2.1 Hz, 2H), 6.45 (dt, *J* = 5.4, 2.0 Hz, 2H), 5.19 (s, 1H), 5.18 (s, 2H), 5.02 (d, *J* = 1.6 Hz, 1H), 4.97 (s, 4H), 4.93 (d, *J* = 12.4 Hz, 1H), 4.86 (d, *J* = 12.0 Hz, 1H), 4.43 (s, 1H), 4.35 (s, 1H), 1.34 (s, 18H), 1.32 (s, 18H).

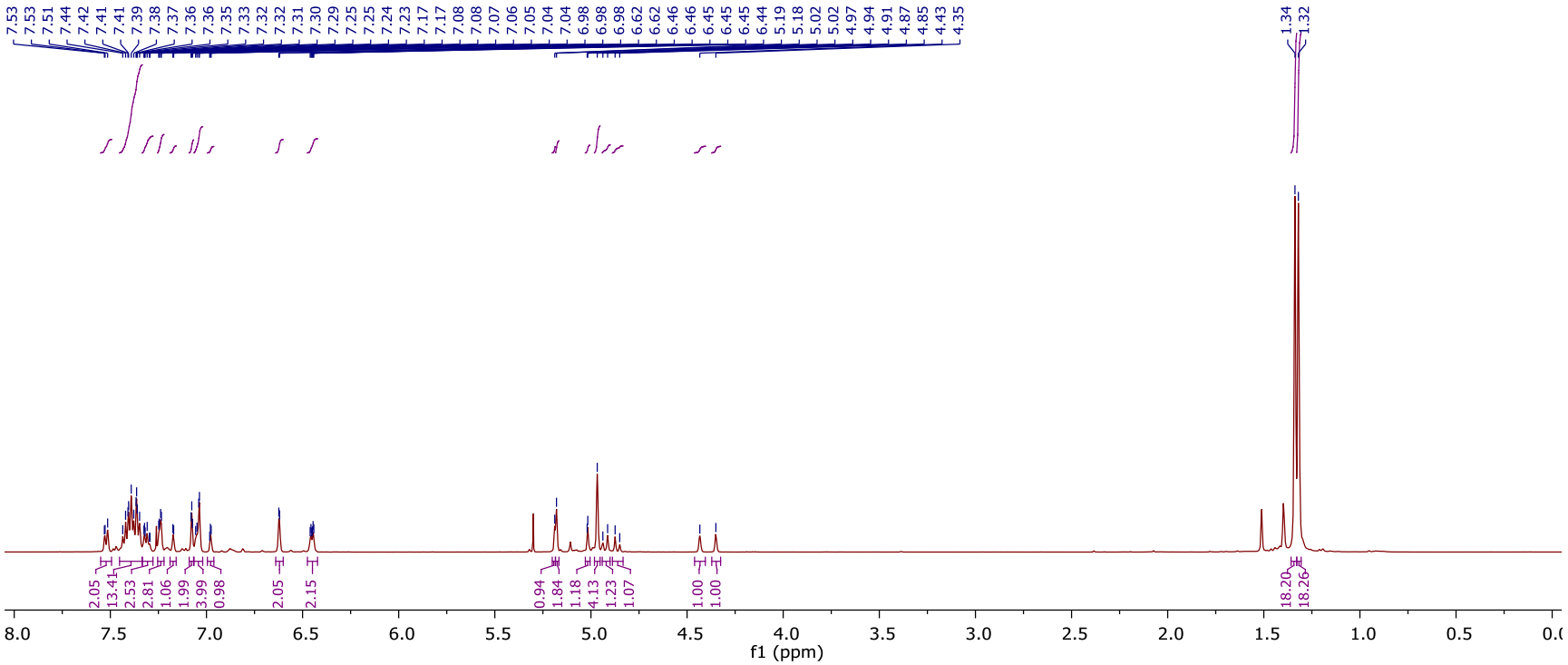
7.53 7.53 7.51 7.44 7.42 7.41 7.41 7.39 7.38 7.37 7.36 7.36 7.35 7.33 7.32 7.32 7.31 7.30 7.29 7.25 7.25 7.24 7.23 7.17 7.17 7.08 7.08 7.07 7.06 7.05 7.04 7.04 6.98 6.98 6.98 6.62 6.62 6.46 6.46 6.45 6.45 6.45 6.44 5.19 5.18 5.02 5.02 4.97 4.94 4.91 4.87 4.85 4.43 4.35
1.34 1.32
2.05 13.41 2.53 2.81 1.06 1.99 3.99 0.98 2.05 2.15 0.94 1.84 1.18 4.13 1.23 1.07 1.00 1.00 18.20 18.26
8.0 7.5 7.0 6.5 6.0 5.5 5.0 4.5 4.0 3.5 3.0 2.5 2.0 1.5 1.0 0.5
f1 (ppm)

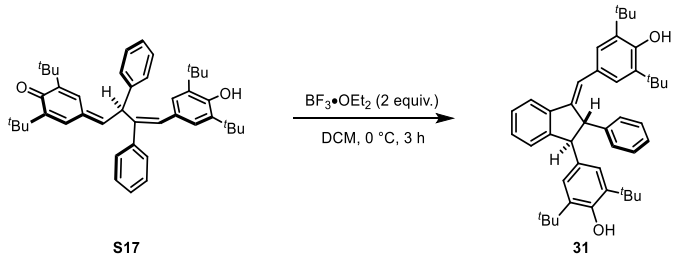

S17 31

(31) 2,6-di-*tert*-butyl-4-((1*S*,2*S*)-3-((*E*)-3,5-di-*tert*-butyl-4-hydroxybenzylidene)-2-phenyl-2,3-dihydro-1H-inden-1-yl)phenol

Compound **S17** (330 mg, 0.537 mmol) was subjected to the standard cyclization conditions at 0 °C with BF_3●OEt_2 (0.132 mL, 1.07 mmol), and the crude product was purified by column chromatography (3%, 6%, 9%, 12%, 17%, 26%, 37%, 51%, DCM/Hexanes, 2 CV per step) to afford compound **31** (154 mg, 47% yield).

^{1}H NMR (500 MHz, Chloroform-*d*) δ 7.75 (d, *J* = 7.7 Hz, 1H), 7.31 (m, 3H), 7.24 (d, *J* = 7.9 Hz, 2H), 7.18 (d, *J* = 7.9 Hz, 1H), 7.15 (d, *J* = 7.9 Hz, 1H), 7.10 (d, *J* = 7.5 Hz, 1H), 7.03 (s, 2H), 6.94 (s, 2H), 5.16 (s, 1H), 5.04 (s, 1H), 4.47 (s, 1H), 4.28 (s, 1H), 1.35 (s, 18H), 1.25 (s, 18H).

^{13}C NMR (126 MHz, Chloroform-*d*) δ 153.00, 152.30, 146.24, 145.16, 143.23, 141.47, 136.98, 135.75, 135.66, 128.82, 128.78, 128.30, 127.69, 127.39, 126.33, 126.26, 125.84, 123.88, 123.83, 119.87, 61.23, 58.11, 34.45, 34.32, 30.38, 30.23.

IR (Neat): 3616, 2953, 1470, 1311, 1235, 1137, 957, 767, 694 cm^{-1};

HRMS (ESI) *m/z* calculated for $NaC_{44}H_{54}O_2^+$ ($[M+Na]^+$) 637.3965, found 637.3965.

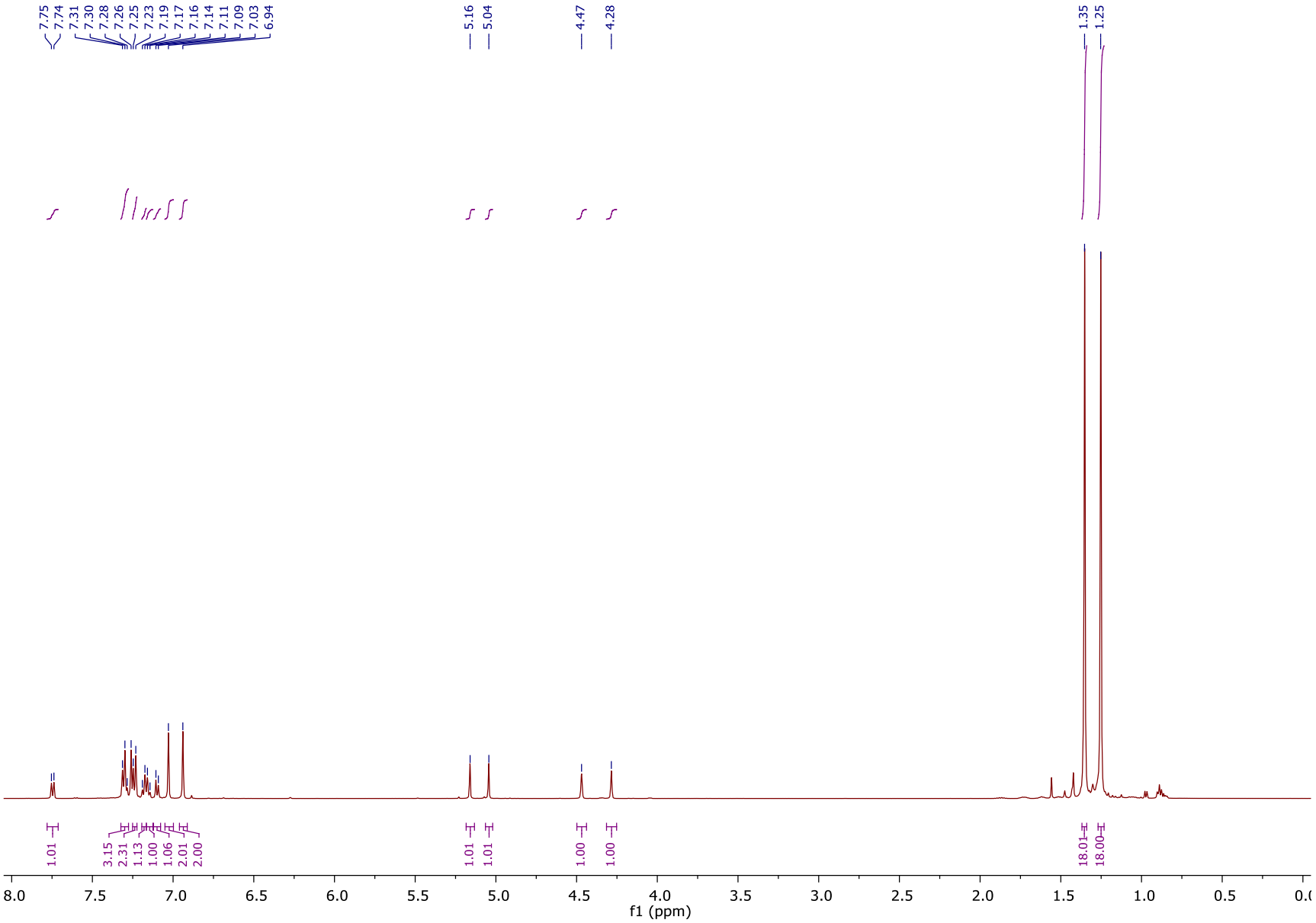
7.75
7.74
7.31
7.30
7.28
7.26
7.25
7.23
7.19
7.17
7.16
7.14
7.11
7.09
7.03
6.94
5.16
5.04
4.47
4.28
1.35
1.25
1.01
3.15
2.31
1.13
1.00
1.06
2.01
2.00
1.01
1.01
1.00
1.00
18.01
18.00
8.0
7.5
7.0
6.5
6.0
5.5
5.0
4.5
4.0
3.5
3.0
2.5
2.0
1.5
1.0
0.5
f1 (ppm)

^{13}C NMR, 176 MHz, Chloroform-*d*, Analog Core **31**

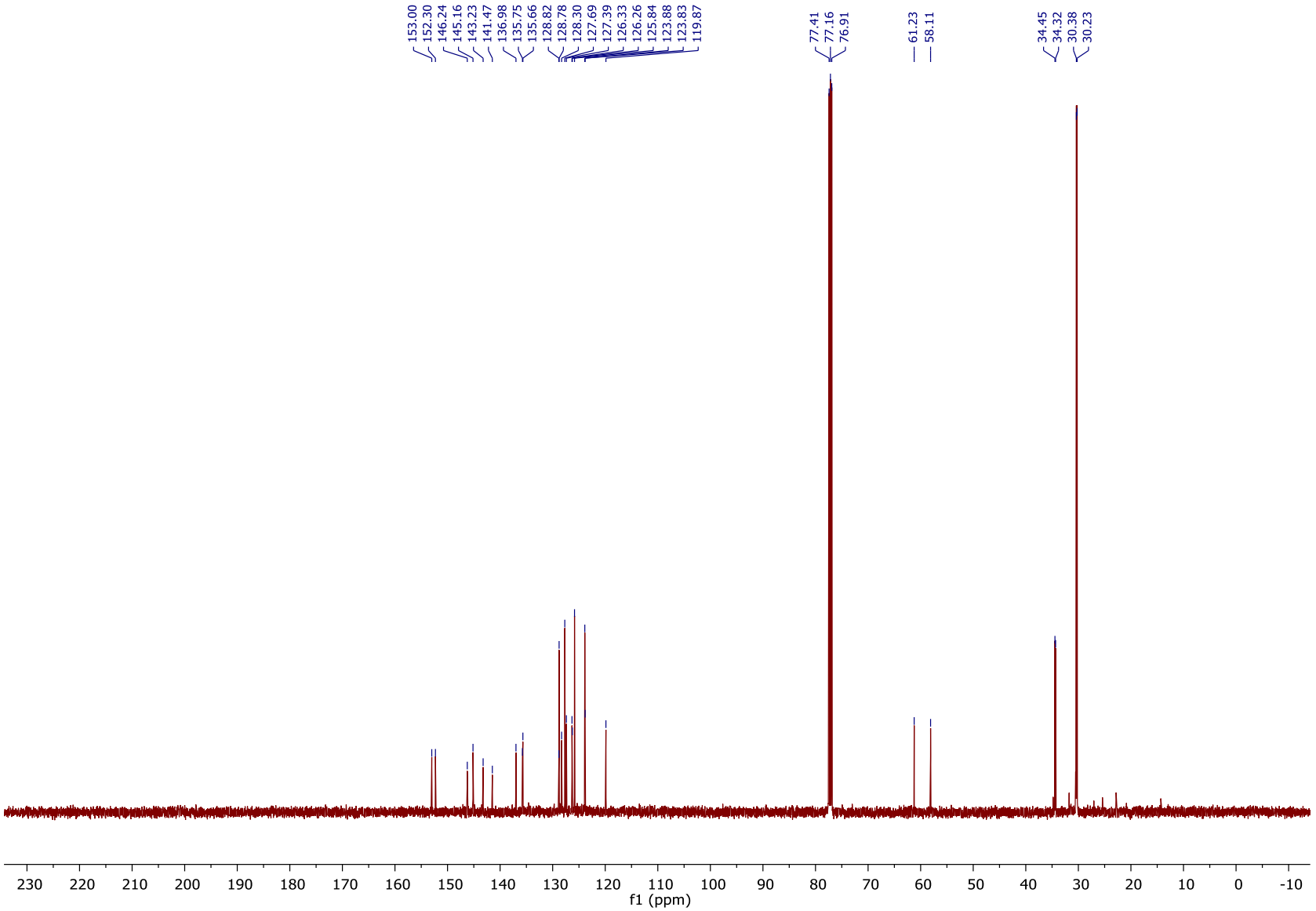

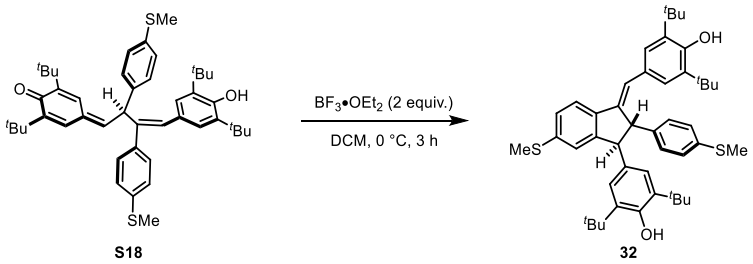

(32) 2,6-di-*tert*-butyl-4-((1*S*,2*S*)-3-((*E*)-3,5-di-*tert*-butyl-4-hydroxybenzylidene)-6-(methylthio)-2-(4-(methylthio)phenyl)-2,3-dihydro-1H-inden-1-yl)phenol

Compound **S18** (96 mg, 0.136 mmol) was subjected to the standard cyclization conditions at 0 °C with BF_3●OEt_2 (0.034 mL, 0.27 mmol), and the crude product was purified by column chromatography (10% to 50% DCM/Hexanes) to afford compound **32** (59 mg, 62% yield).

^{1}H NMR (500 MHz, Chloroform-*d*) δ 7.37 (d, *J* = 8.1 Hz, 2H), 7.16 (m, 3H), 7.11 (s, 2H), 7.07 (d, *J* = 7.9 Hz, 1H), 7.05 (s, 1H), 7.01 (s, 1H), 6.98 (s, 2H), 5.01 (s, 1H), 4.98 (s, 1H), 4.15 (s, 1H), 4.06 (s, 1H), 2.45 (s, 3H), 2.42 (s, 3H), 1.33 (s, 18H), 1.29 (s, 18H).

^{13}C NMR (126 MHz, Chloroform-*d*) δ 152.49, 152.40, 138.90, 138.15, 137.34, 137.20, 136.43, 135.73, 135.65, 133.50, 131.60, 127.92, 126.99, 126.51, 126.47, 125.25, 124.10, 123.97, 123.88, 53.25, 50.27, 34.52, 34.47, 30.43, 30.41, 16.23, 15.99.

IR (Neat): 3614, 2957, 2920, 1597, 1434, 1240, 1150, 1119, 883, 821, 790, 765 cm^{-1};

HRMS (ESI) *m/z* calculated for $C_{46}H_{58}O_2S_2^+$ ($[M]^+$) 706.3873, found 706.3872.

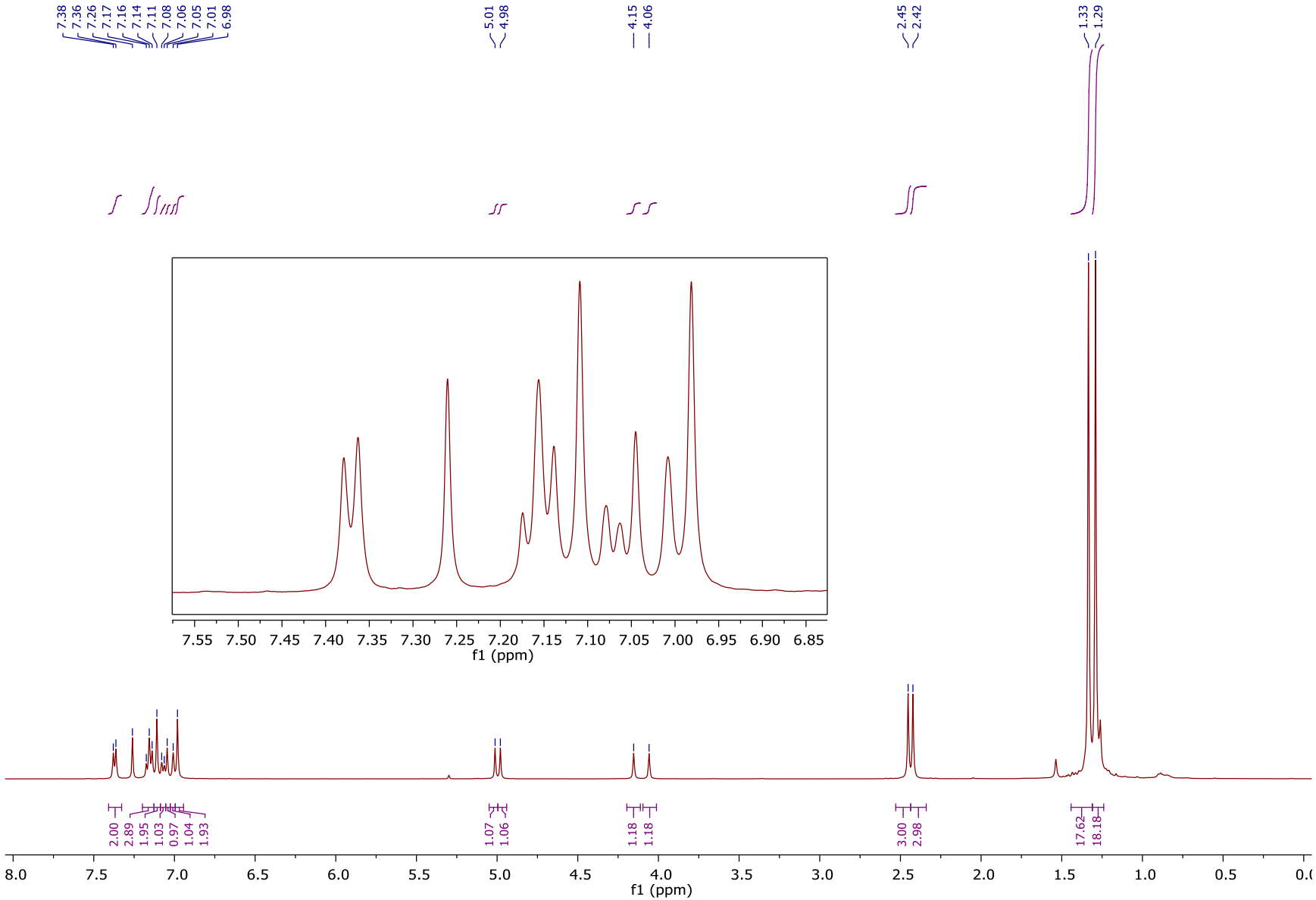
7.38
7.36
7.26
7.17
7.16
7.14
7.11
7.08
7.06
7.05
7.01
6.98
5.01
4.98
4.15
4.06
2.45
2.42
1.33
1.29
7.55 7.50 7.45 7.40 7.35 7.30 7.25 7.20 7.15 7.10 7.05 7.00 6.95 6.90 6.85
f1 (ppm)
2.00
2.89
1.95
1.03
0.97
1.04
1.93
1.07
1.06
1.18
1.18
3.00
2.98
17.62
18.18
8.0 7.5 7.0 6.5 6.0 5.5 5.0 4.5 4.0 3.5 3.0 2.5 2.0 1.5 1.0 0.5
f1 (ppm)

^{13}C NMR, 126 MHz, Chloroform-*d*, Analog Core **32**

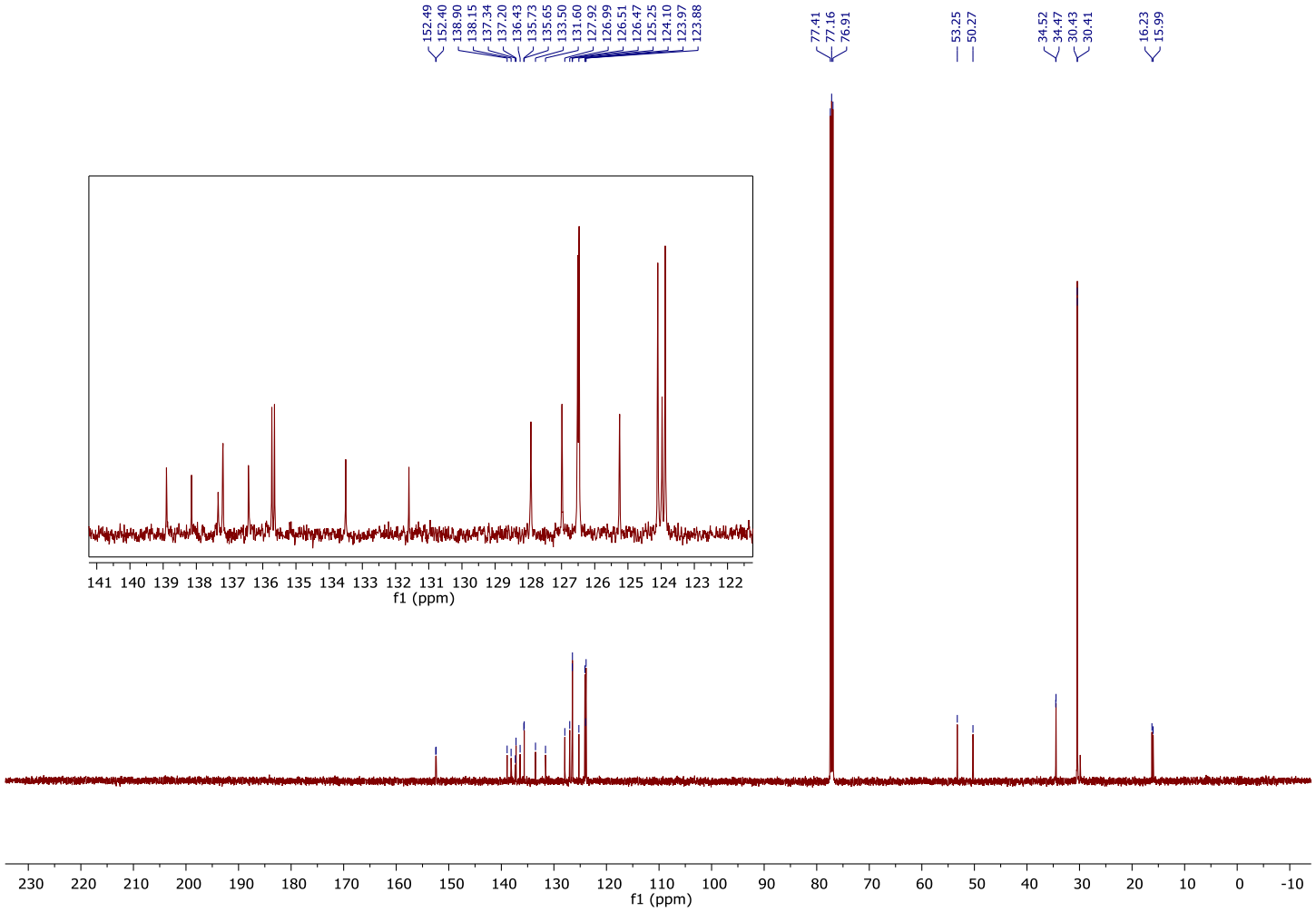

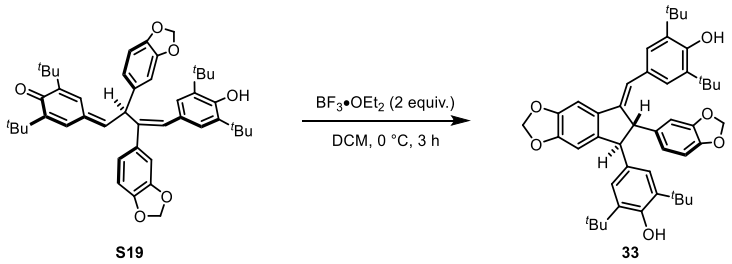

(33) 4-((1*S*,2*S*)-6-(benzyloxy)-2-(4-(benzyloxy)phenyl)-3-((*E*)-3,5-di-*tert*-butyl-4-hydroxybenzylidene)-2,3-dihydro-1H-inden-1-yl)-2,6-di-*tert*-butylphenol

Compound **S19** (102 mg, 0.145 mmol) was subjected to the standard cyclization conditions at 0 °C with $BF_3{\bullet}OEt_2$ (0.036 mL, 0.29 mmol), and the crude product was purified by column chromatography (10% to 50% DCM/Hexanes) to afford compound **33** (65 mg, 64% yield).

^{1}H NMR (500 MHz, Chloroform-*d*) δ 7.14 (s, 1H), 7.01 (s, 2H), 6.97 (d, *J* = 1.4 Hz, 1H), 6.91 (s, 2H), 6.76 (s, 1H), 6.75 (d, *J* = 4.6 Hz, 1H), 6.70 (d, *J* = 8.4 Hz, 1H), 6.52 (s, 1H), 5.95 (s, 2H), 5.88 (dd, *J* = 5.2, 3.7 Hz, 2H), 5.13 (s, 1H), 5.03 (s, 1H), 4.34 (s, 1H), 4.07 (s, 1H), 1.36 (s, 18H), 1.28 (s, 18H).

^{13}C NMR (176 MHz, Chloroform-*d*) δ 152.81, 152.38, 148.46, 147.95, 147.79, 145.86, 141.64, 140.57, 139.39, 136.91, 136.82, 135.87, 135.68, 128.94, 125.60, 123.72, 121.85, 120.70, 108.46, 108.28, 106.21, 101.35, 100.86, 99.99, 61.17, 58.31, 34.47, 34.37, 30.41, 30.29.

IR (Neat): 3634, 2957, 2912, 1476, 1431, 1231, 1150, 1035, 936, 737 cm^{-1};

HRMS (ESI) *m/z* calculated for $C_{46}H_{54}O_6^+$ ($[M]^+$) 702.3915, found 702.3900.

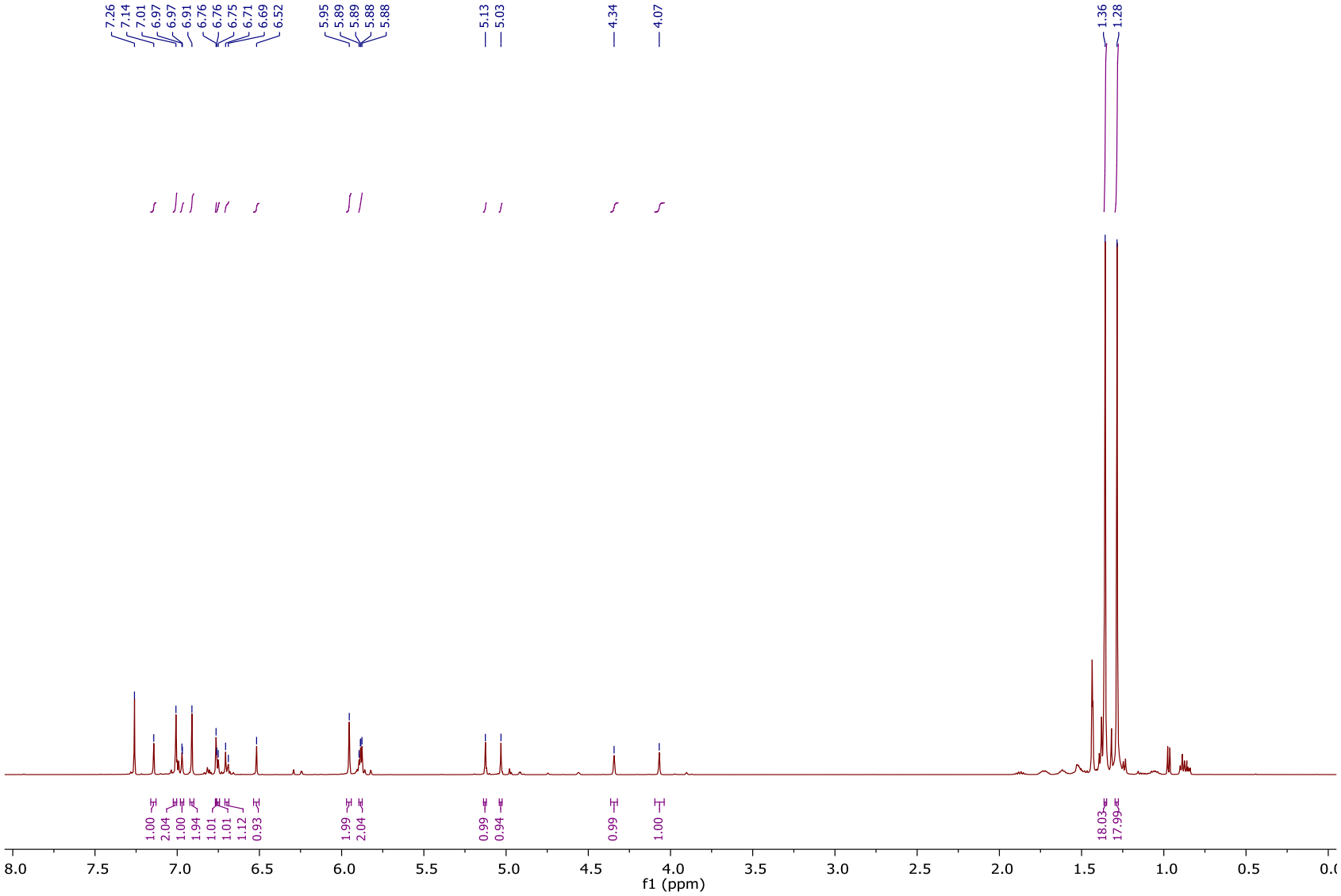
7.26
7.14
7.01
6.97
6.97
6.91
6.76
6.76
6.75
6.71
6.69
6.52
5.95
5.89
5.89
5.88
5.88
5.13
5.03
4.34
4.07
1.36
1.28
1.00
2.04
1.00
1.94
1.01
1.01
1.12
0.93
1.99
2.04
0.99
0.94
0.99
1.00
18.03
17.99
8.0
7.5
7.0
6.5
6.0
5.5
5.0
4.5
4.0
3.5
3.0
2.5
2.0
1.5
1.0
0.5
f1 (ppm)

^{13}C NMR, 176 MHz, Chloroform-*d*, Analog Core **33**

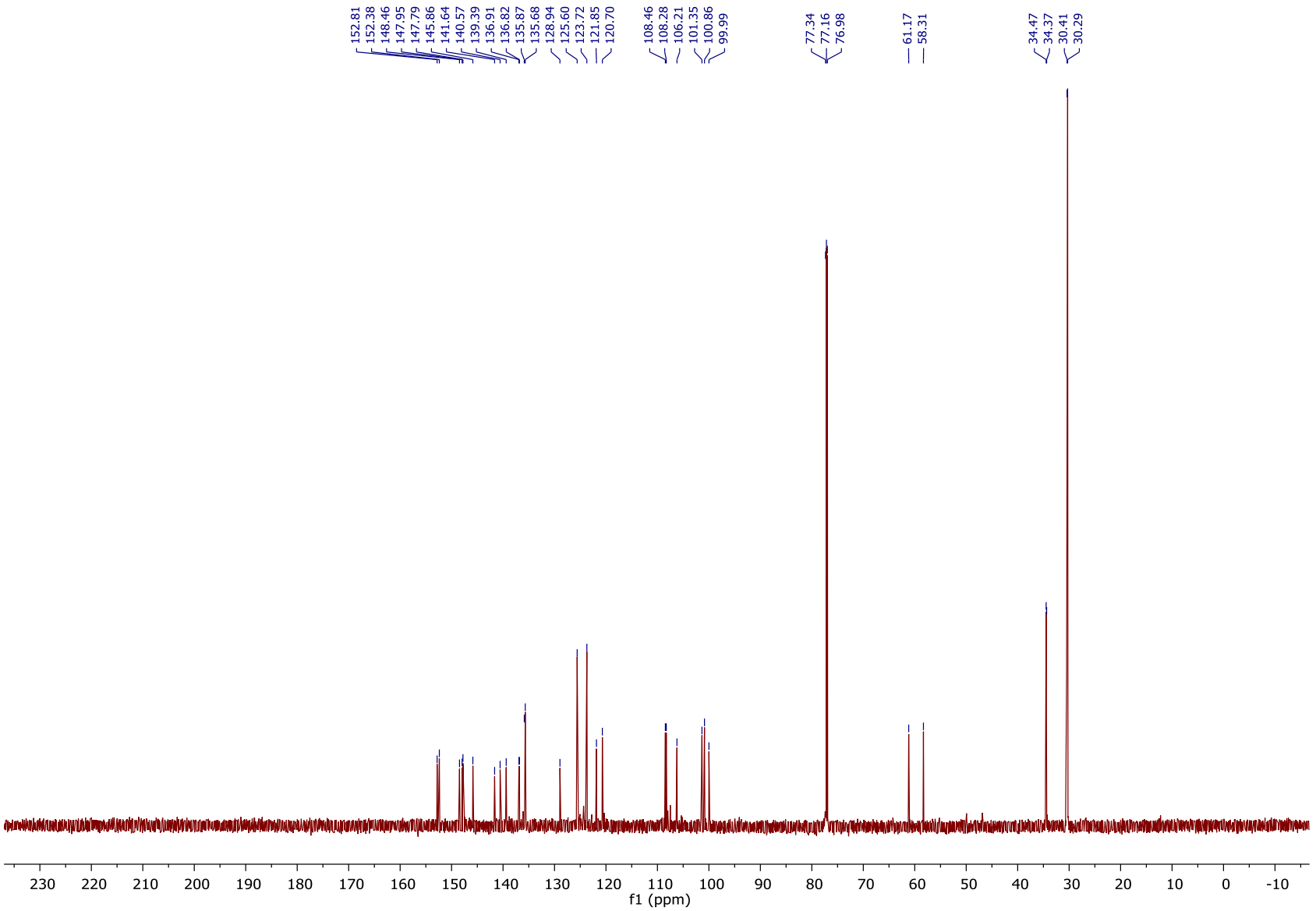

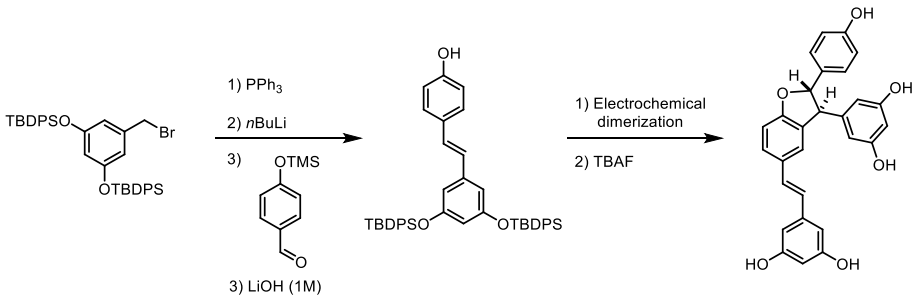

5-(€-2-((2S,3S)-3-(3,5-dihydroxyphenyl)-2-(4-hydroxyphenyl)-2,3-dihydrobenzofuran-5-yl)vinyl)benzene-1,3-diol (δ-viniferin)

Benzyl bromide was dissolved in toluene in a 500mL round bottom flask and charged with triphenylphosphine. The reaction mixture was heated to 100°C for 24 h. The resulting white precipitate was filtered and washed with hexanes and dried under vacuum. The resulting white phosphonium bromide salt (4.82 g, 5.12 mmol, 1.25 eq) was dissolved in THF (40 mL) within a flame-dried round bottom flask (100mL). nBuLi (1.25M in hexanes, 2.05mL, 1.25 eq) was added dropwise to the solution. After 30 minutes, benzaldehyde (0.80 g, 4.1 mmol, 1 eq) was added as a solution in THF (2mL) and the reaction was left at room temperature overnight (12h). Freshly prepared aqueous LiOH (1M,10mL) was added and the reaction was left at room temperature for 2 h. The crude reaction was extracted with ethyl acetate and washed with aqueous bicarbonate, aqueous ammonium chloride, and brine then dried over sodium sulfate and concentrated under vacuum. The stilbene was isolated by column chromatography (DCM/hexanes, 10% to 50%). The stilbene (3.19 g) was then subjected to the general electrochemical dimerization conditions to afford the silylated δ-viniferin (89.2% yield over two steps). δ-viniferin (O-TBDPS) (0.95 g) was dissolved in THF (6.75 mL) and treated with TBAF (1M in THF, 2.77mL, 4.1 eq) and the reaction was left for 12 h. The crude was extracted with ethyl acetate and washed with aqueous ammonium chloride, aqueous bicarbonate, and brine then dried over sodium sulfate and concentrated under vacuum. The δ-viniferin was isolated by column chromatography (Acetone/DCM, 1% to 20%) (81.9% yield).

1H NMR (300 MHz, Acetone) δ 8.46 (s, 1H), 8.20 (d, J = 12.1 Hz, 5H), 7.42 (s, 2H), 7.24 (d, J = 8.5 Hz, 6H), 7.07 (d, J = 16.4 Hz, 2H), 6.95 – 6.83 (m, 8H), 6.54 (d, J = 2.1 Hz, 4H), 6.27 (dt, J = 6.7, 2.2 Hz, 4H), 6.19 (d, J = 2.2 Hz, 4H), 5.45 (d, J = 8.0 Hz, 2H), 4.47 (d, J = 8.4 Hz, 2H).

13C NMR (126 MHz, Acetone) δ 160.44, 159.57, 159.36, 158.23, 145.05, 140.61, 132.37, 131.95, 131.55, 128.93, 128.46, 128.42, 127.02, 123.74, 115.97, 109.96, 107.23, 105.52, 102.51, 102.18, 93.87, 57.64.

IR: 3285.90 cm^{-1}, 1594.68 cm^{-1}, 1458.81 cm^{-1}, 1232.33 cm^{-1}, 1143.24 cm^{-1}, 992.72 cm^{-1}, 958.12 cm^{-1}, 827.87 cm^{-1}, 679.25 cm^{-1}

HRMS (APCI+): *m/z* calculated for $C_{28}H_{22}O_6$ $[M+H]^+$: 455.1489, found 455.1499.

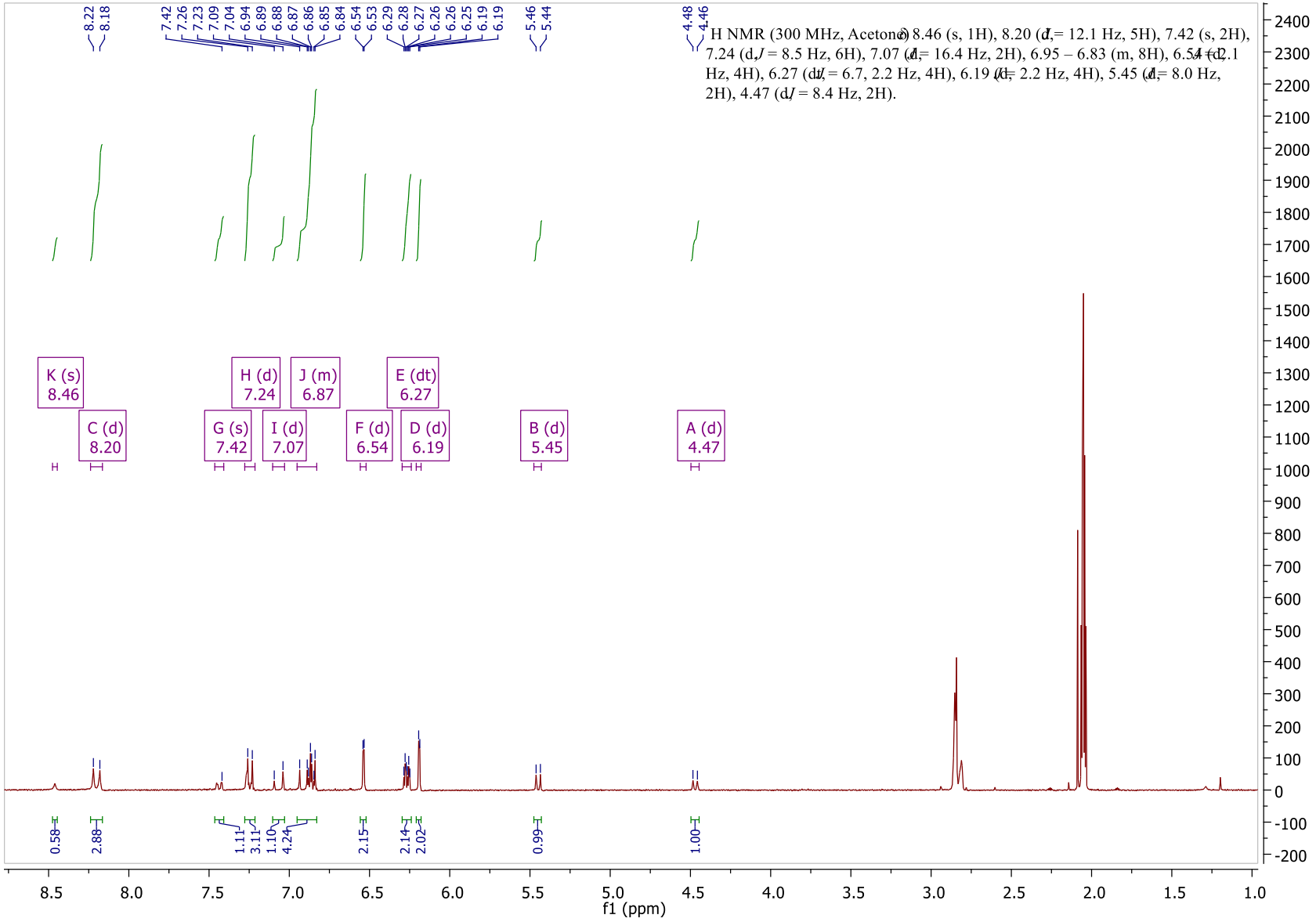
8.22
8.18
7.42
7.26
7.23
7.09
7.04
6.94
6.89
6.88
6.87
6.86
6.85
6.84
6.54
6.53
6.29
6.28
6.27
6.26
6.26
6.25
6.19
6.19
5.46
5.44
4.48
4.46
K (s) 8.46
C (d) 8.20
H (d) 7.24
G (s) 7.42
J (m) 6.87
I (d) 7.07
E (dt) 6.27
F (d) 6.54
D (d) 6.19
B (d) 5.45
A (d) 4.47
0.58
2.88
1.11
3.11
1.10
4.24
2.15
2.14
2.02
0.99
1.00
f1 (ppm)

199

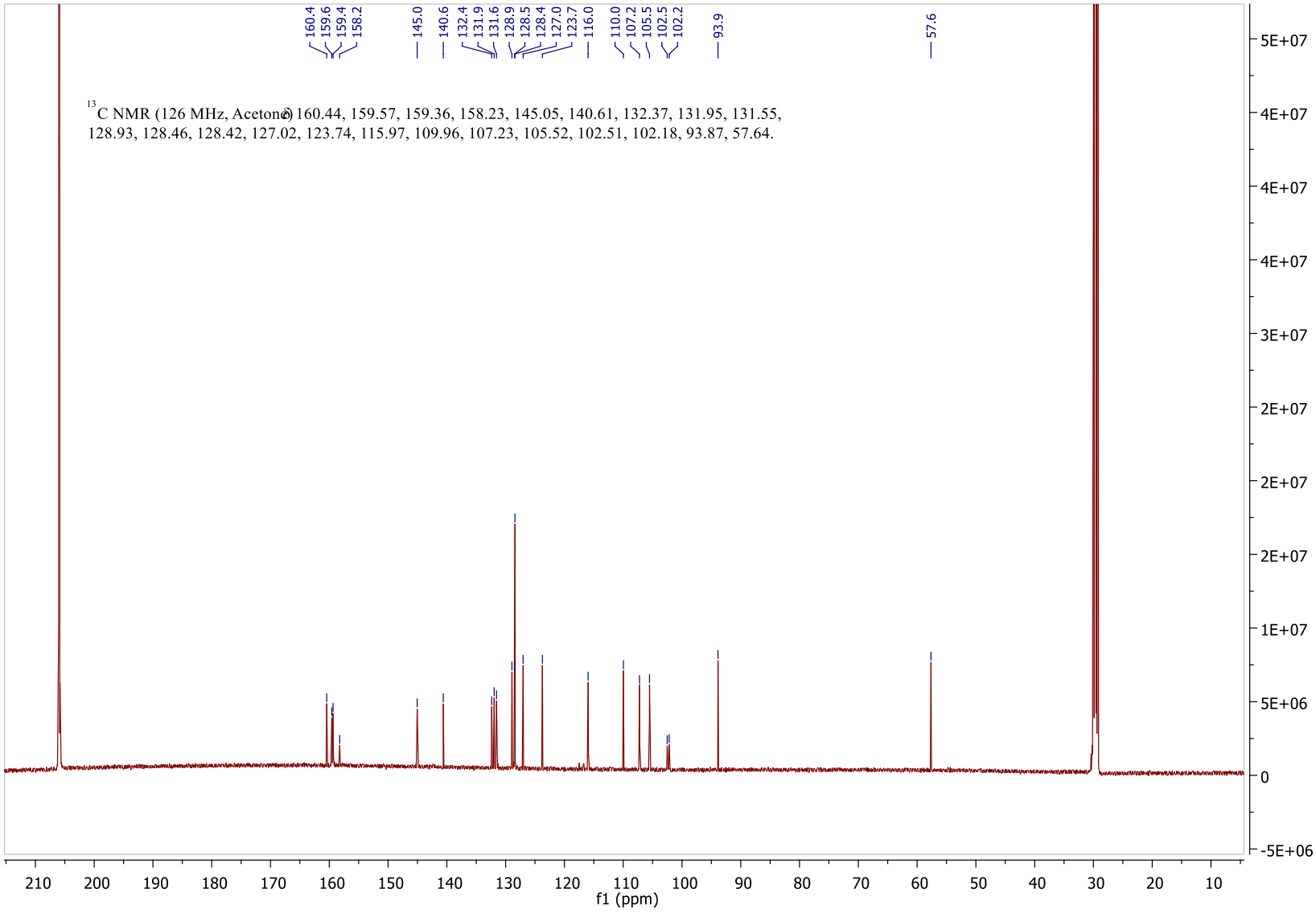
160.4
159.6
159.4
158.2
145.0
140.6
132.4
131.9
131.6
128.9
128.5
128.4
127.0
123.7
116.0
110.0
107.2
105.5
102.5
102.2
93.9
57.6
13C NMR (126 MHz, Acetone) δ 160.44, 159.57, 159.36, 158.23, 145.05, 140.61, 132.37, 131.95, 131.55, 128.93, 128.46, 128.42, 127.02, 123.74, 115.97, 109.96, 107.23, 105.52, 102.51, 102.18, 93.87, 57.64.
5E+07
4E+07
4E+07
4E+07
3E+07
2E+07
2E+07
2E+07
1E+07
5E+06
0
-5E+06
210 200 190 180 170 160 150 140 130 120 110 100 90 80 70 60 50 40 30 20 10
f1 (ppm)

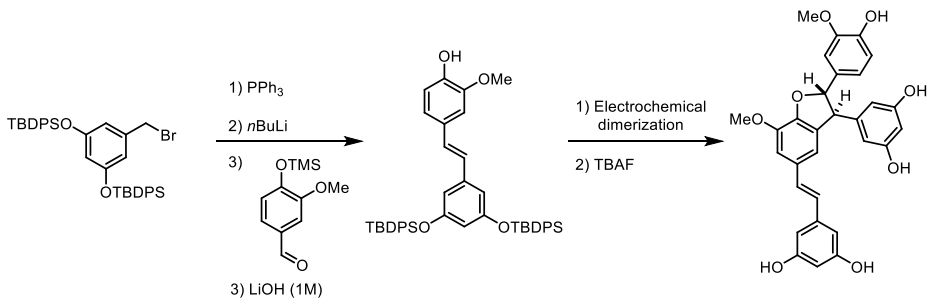

5-((E)-2-((2S,3S)-3-(3,5-dihydroxyphenyl)-2-(4-hydroxy-3-methoxyphenyl)-7-methoxy-2,3-dihydrobenzofuran-5-yl)vinyl)benzene-1,3-diol (Shegansu B)

Phosphonium bromide salt (3.87 g, 4.11 mmol, 1.25 eq) was dissolved in THF (32.1 mL) within a flame-dried round bottom flask (100mL). nBuLi (1.25 M in hexanes, 1.64 mL, 1.25 eq) was added dropwise to the solution. After 30 minutes, benzaldehyde (0.74 g, 3.29 mmol, 1 eq) was added as a solution in THF (2mL) and the reaction was left at room temperature overnight (12h). Freshly prepared aqueous LiOH (1M,10mL) was added and the reaction was left at room temperature for 2 h. The crude reaction was extracted with ethyl acetate and washed with aqueous bicarbonate, aqueous ammonium chloride, and brine then dried over sodium sulfate and concentrated under vacuum. The stilbene was isolated by column chromatography (DCM/hexanes, 10% to 50%) (69.2% yield). The stilbene was then subjected to the general electrochemical dimerization conditions to afford the silylated shegansu B (64.2% yield). Shegansu B (O-TBDPS) (0.715 g, 0.49 mmol) was dissolved in THF (4.9 mL) and treated with TBAF (1M in THF, 0.98 mL, 4.1 eq) and the reaction was left for 12 h. The crude was extracted with ethyl acetate and washed with aqueous ammonium chloride, aqueous bicarbonate, and brine then dried over sodium sulfate and concentrated under vacuum. Shegansu B was isolated by column chromatography (Acetone/DCM, 1% to 20%) (90.8 % yield).

1H NMR (500 MHz, acetone) δ 8.2 (s, exchangeable, 2H), 8.1 (s, exchangeable, 2H), 7.66 (s, 1H), 7.18 (s, 1H), 7.05 (dd, J = 9.0, 7.3 Hz, 2H), 6.94 (d, J = 16.3 Hz, 1H), 6.87 – 6.81 (m, 3H), 6.54 (d, J = 2.1 Hz, 2H), 6.27 (dt, J = 8.1, 2.1 Hz, 2H), 6.20 (d, J = 2.2 Hz, 2H), 5.44 (d, J = 8.5 Hz, 1H), 4.52 (d, J = 8.5 Hz, 1H), 3.93 (s, 3H), 3.84 (s, 3H).

13C NMR (126 MHz, Acetone) δ 158.85, 158.68, 158.58, 148.36, 144.59, 144.11, 139.93, 132.00, 131.84, 131.67, 128.53, 126.56, 119.41, 115.83, 114.79, 114.71, 110.73, 109.93, 106.64, 106.55, 104.85, 104.76, 101.76, 101.41, 93.71, 57.23, 55.54, 55.39.

IR: 3350.15 cm-1, 1695.12 cm-1,1596.47 cm-1, 1493.17 cm-1, 1138.51 cm-1, 1005.82 cm-1, 835.20 cm-1, 682.02 cm-1

HRMS (APCI+): *m/z* calculated for $C_{30}H_{26}O_8$ $[M+H]^+$: 515.17, found 515.1723.

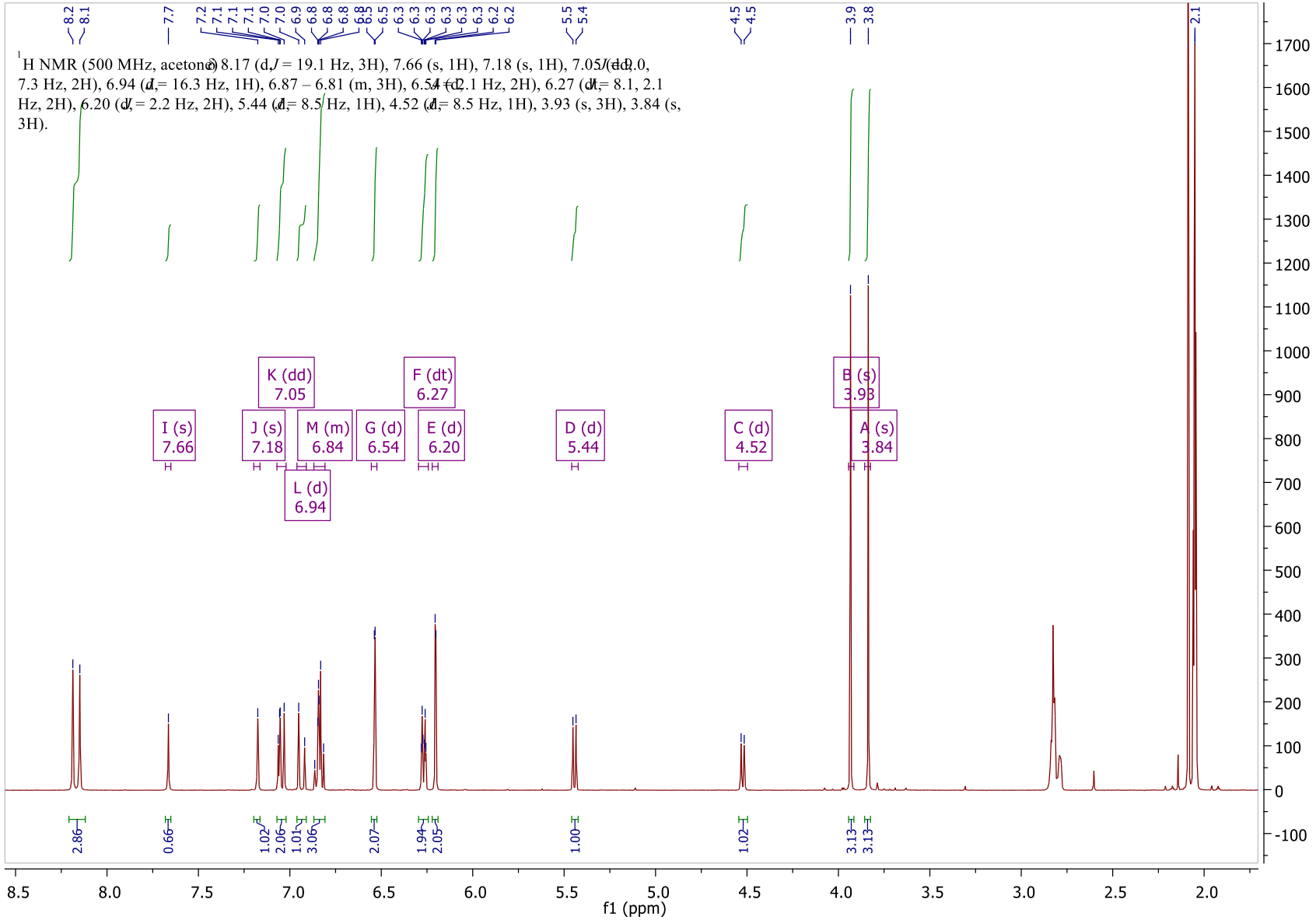
1H NMR (500 MHz, acetone-d6) δ 8.17 (d, J = 19.1 Hz, 3H), 7.66 (s, 1H), 7.18 (s, 1H), 7.05 (dd, J = 12.0, 7.3 Hz, 2H), 6.94 (d, J = 16.3 Hz, 1H), 6.87 – 6.81 (m, 3H), 6.54 (d, J = 2.1 Hz, 2H), 6.27 (dt, J = 8.1, 2.1 Hz, 2H), 6.20 (d, J = 2.2 Hz, 2H), 5.44 (d, J = 8.5 Hz, 1H), 4.52 (d, J = 8.5 Hz, 1H), 3.93 (s, 3H), 3.84 (s, 3H).
K (dd) 7.05
F (dt) 6.27
B (s) 3.93
I (s) 7.66
J (s) 7.18
M (m) 6.84
G (d) 6.54
E (d) 6.20
D (d) 5.44
C (d) 4.52
A (s) 3.84
L (d) 6.94
f1 (ppm)

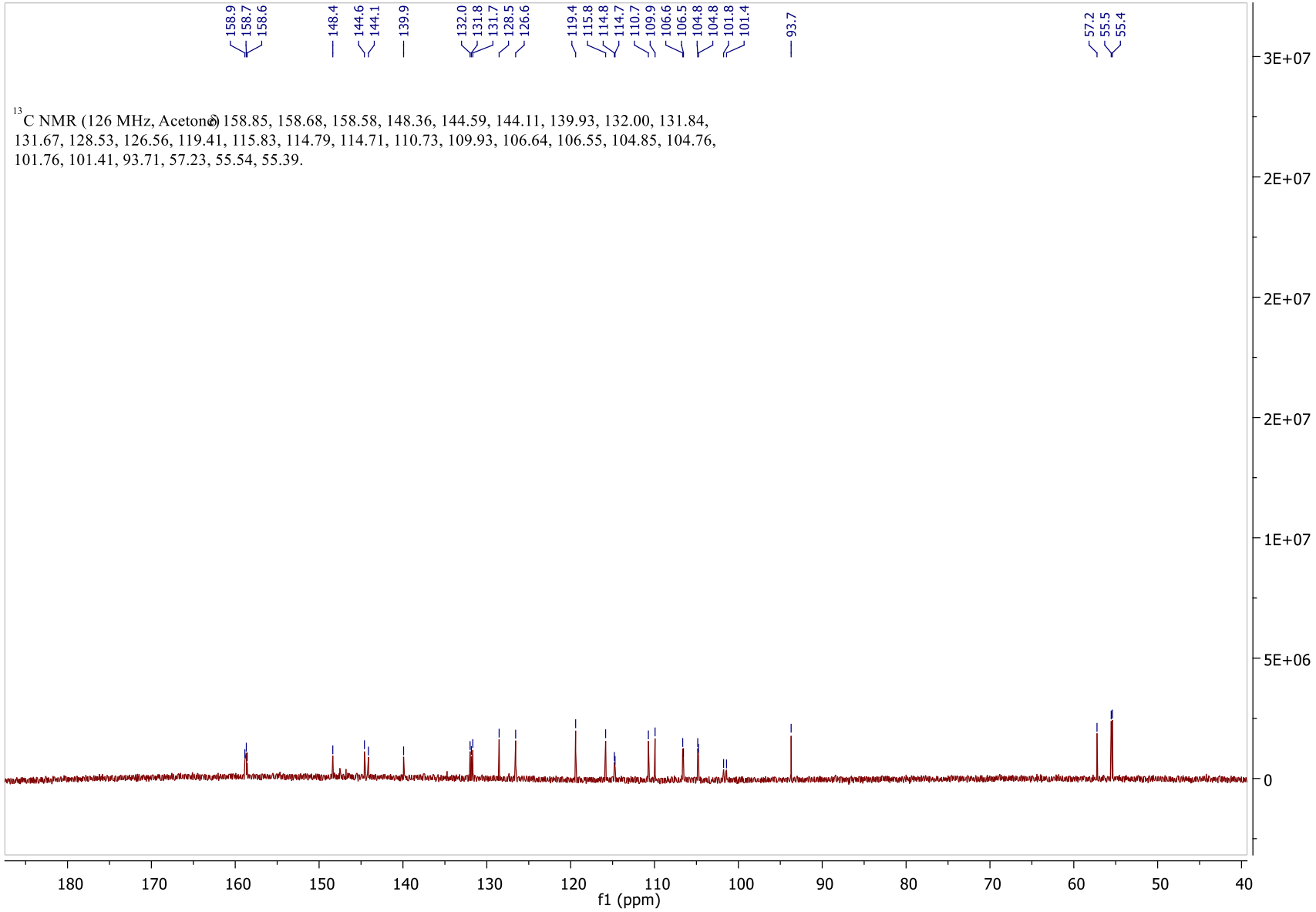

^{13}C NMR (126 MHz, Acetone) δ 158.85, 158.68, 158.58, 148.36, 144.59, 144.11, 139.93, 132.00, 131.84, 131.67, 128.53, 126.56, 119.41, 115.83, 114.79, 114.71, 110.73, 109.93, 106.64, 106.55, 104.85, 104.76, 101.76, 101.41, 93.71, 57.23, 55.54, 55.39.

Chapter 3: Leveraging the Persistent Radical Effect for the Accessing the C8 – C10 and C8 – C12 Bond of Resveratrol Oligomers

*Portions of this chapter have been published in: Matthew S. Galliher, Bec J. Roldan, and Corey R. J. Stephenson. *Chem. Soc. Rev.* **2021**, *50*, 10044-10057.;[1] Kevin J. Romero, Matthew S. Galliher, Derek A. Pratt, and Corey R. J. Stephenson. *Chem. Soc. Rev.* **2018**, *47*, 7851.[2] Romero, K. J.; Galliher, M. S.; Raycroft, M. A. R.; Chauvin, J.-P. R.; Bosque, I.; Pratt, D. A.; Stephenson, C. R. J., *Angewandte Chemie International Edition* **2018,** *57* (52), 17125-17129.;[91]

3.1 Introduction

The C8 – C10' bond of resveratrol derived natural products are very abundant in this family of natural products. They often take the form of a benzofuran or dihydrobenzofuran functional motif but there are also examples of C8 – C10 bonds that are part of an all-carbon framework. There has been considerable work generated by the Snyder group for the synthesis of resveratrol-derived natural products with examples containing the C8 – C10 bond.

3.2 Prior work to synthesize C8 – C10' bonds in resveratrol oligomers

In 2007, the Snyder group published the syntheses of ampelopsin D (not depicted), isoampelopsin D (**3.5**), ampelopsin F (not depicted), and paucifloral F (not depicted) – examples of resveratrol-derived natural products containing C8 – C10 bonds in an all-carbon skeleton that were formed with a *de novo* strategy.[104] The syntheses of paucifloral F ampelopsin D (**3.4**), and

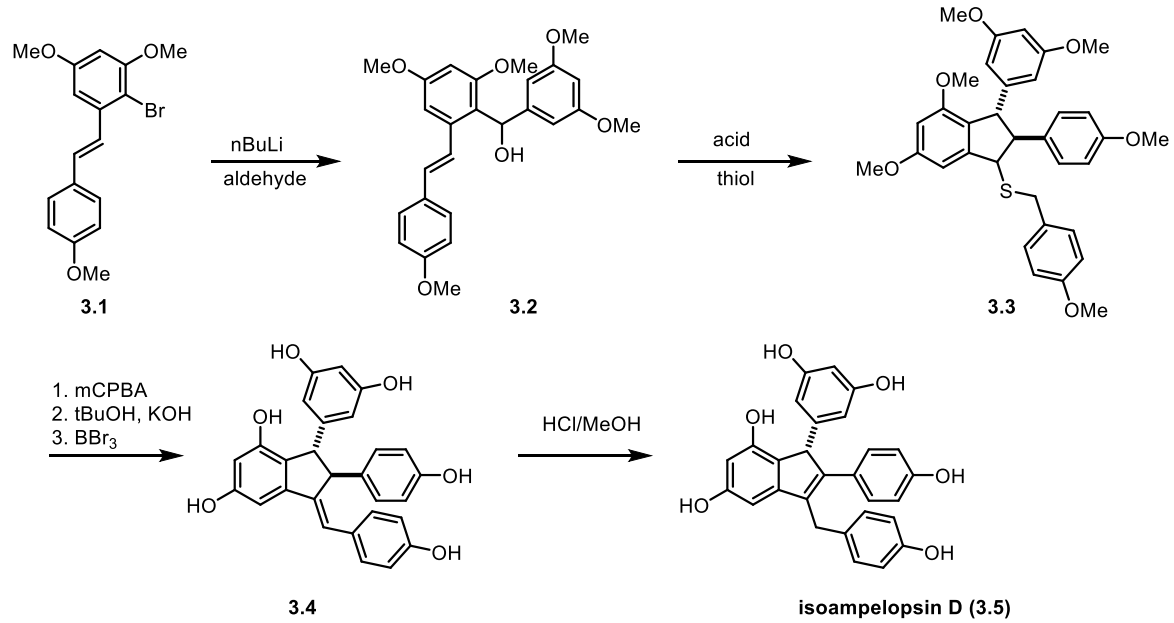

Figure 3.1. Snyder's 2007 synthesis of isoampelopsin D.

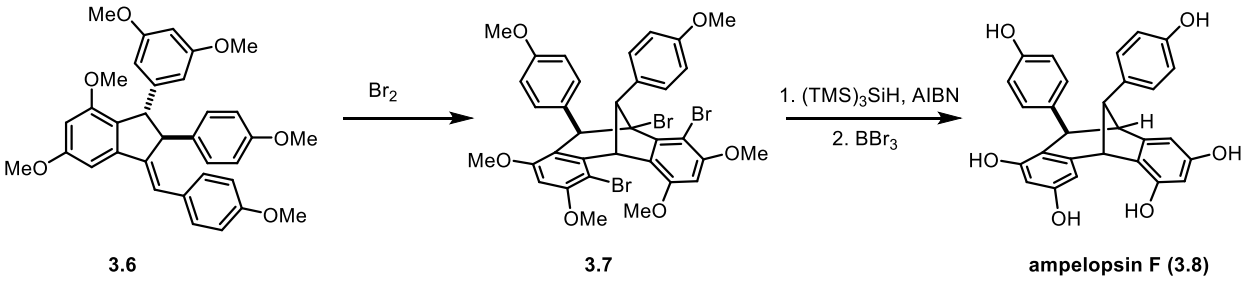

Figure 3.2. Snyder's 2007 synthesis of ampelopsin F.

isoampelopsin D (**3.5**) begin from the C10-bromo resveratrol analog (**3.1**). Lithium/halogen exchange of (**3.1**) with nBuLi followed by the addition of 3,5-dimethoxy benzadehyde forms alcohol (**3.2**) by 1,2-addition. This effectively forms the key C8 – C10 bond. Treatment of alcohol (**3.2**) with TFA results in the loss of water of the benzylic alcohol that undergoes cyclization and subsequent addition of trifluoroacetate and eventual basic quench to produce the alcohol. This alcohol is then oxidized by Dess-Martin periodane to the ketone and demethylated by BBr_3 to produce paucifloral F. When alcohol (**3.2**) was treated with toluenesulfonic acid and quenched with *p*-methoxy-α-toluenethiol, sulfide (**3.3**) is produced. (**3.3**) was then oxidized with *m*CPBA to the sulphone and undergoes a selective Ramberg-Backlund reaction with modified Meyer's

conditions[126] to furnish the desired olefin that was then demethylated with BBr_3 to produce ampelopsin D (**3.4**). The olefin of ampelopsin D (**3.4**) was then isomerized under acidic conditions to form isoampelopsin D (**3.5**). The bromination of ampelopsin D resulted in the Friedel-Crafts alkylation to form [3.2.1] bicyclooctane (**3.7**). The bromine substitutions were further reduced under radical conditions and the intermediate demethylated to furnish ampelopsin F (**3.8**).

In addition to forming C8 – C10 all-carbon skeletons for several resveratrol derived natural products, Snyder has also explored the *de novo* syntheses of resveratrol natural products containing the C8 – C10 dihydrobenzofuran for carasiphenol C, nepalensinol B, ampelopsin H, ampelopsin G, and carasiphenol B.[97] Generally, the strategy employed by the Snyder group involved regioselective halogenations that were used for site specific homologations. The synthesis of carasiphenol C began with the bromination and Friedel-Crafts cyclization of protected quadrangularin A (**3.9**). The [2.2.0] bicycle (**3.9**) was then converted to the dibrominated intermediate with differentially substituted C10 positions. The extension sequence was accomplished by lithiation of (**3.10**) and addition of 3,5-dimethoxybenzaldehyde, followed by DMP oxidation. After a swapping protecting groups, the homologation sequence was accomplished by Corey Chaykovsky epoxidation and ZnI_2-mediated Meinwald rearrangement to give the homologated aldehyde (**3.12**). Addition of 4-benzyloxyphenylmagnesium bromide to the aldehyde, Pd-mediated debenzylation, and Lewis acid-mediated cyclization of the resorcinol produced the key C8 – C10 dihydrobenzofuran thus completing the synthesis of carasiphenol C (**3.13**). This strategy was repeated using protected pallidol (**3.14)** as a scaffold for carrying out the homologation/extension strategy for the syntheses of ampelopsin H and an unnatural diastereomer of ampelopsin H and nepalensniol B. Dibromination of the protected pallidol produced dibromo (**3.15**). The extension sequence was initiated by the lithiation of (**3.15**) and addition of 3,5-

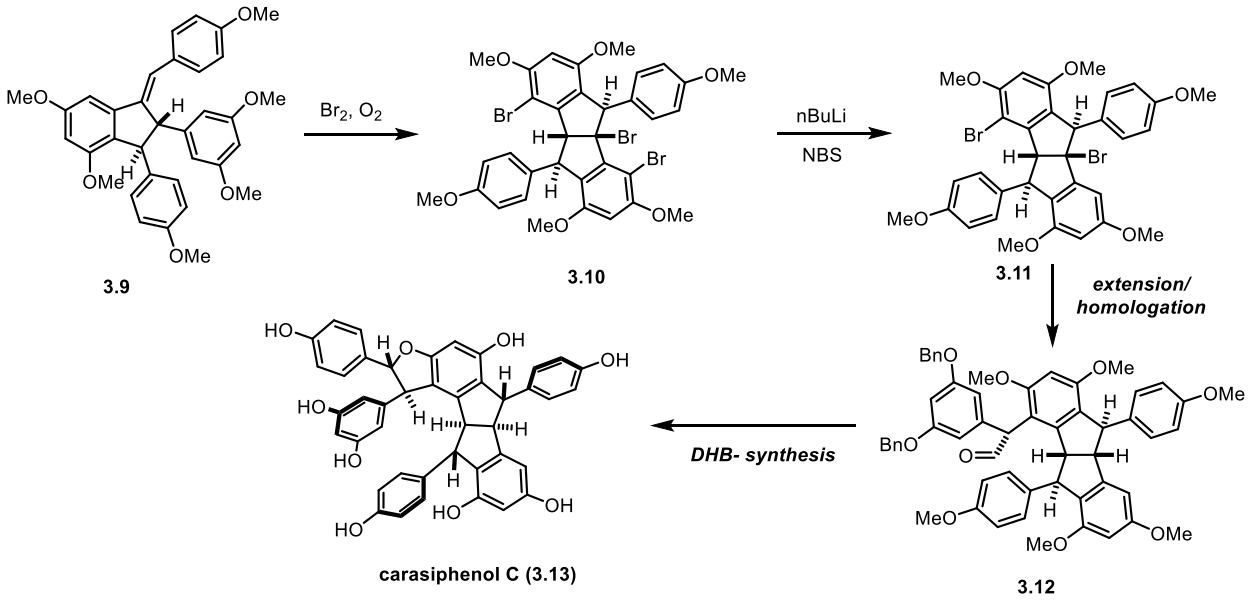

Figure 3.3. Snyder's 2007 synthesis of carasiphenol C.

dimethoxybenzaldehyde and subsequently oxidized with DMP to furnish extended aldehyde. In a similar fashion as with carasiphenol C **(3.13**), the swapping of the protecting groups was followed by initiation of the homologation sequence. This was accomplished by Corey Chaykovsky epoxidation and ZnI_2-mediated Meinwald rearrangement to give the homologated unsymmetric dialdehyde (**3.16**). The unsymmetric dialdehyde (**3.16**) then underwent addition of 4-benzyloxyphenylmagnesium bromide to both aldehydes, Pd-mediated debenzylation, and Lewis acid-mediated cyclization of the resorcinol to produce both key C8 – C10 dihydrobenzofuran thus completing the synthesis of the unnatural diastereomer of ampelopsin H (**3.19**). The Unsymmetric dialdehyde (**3.16**) was epimerized to the symmetric dialdehyde (**3.17**). Following the same sequence of Grignard addition, debenzylation, and Lewis acid mediated cyclization allowed for the successful synthesis of the C8 – C10 dihydrobenzofuran thus furnishing ampelopsin H (**3.18**). For the syntheses of carasiphenol B, protected ampelopsin F (**3.20**) underwent monobromination with a variety of brominating reagents to produce (**3.21**), indicating this was the most reactive position. The regioselectivity made it perfectly poised to undergo extension/homologation and C8 – C10 dihydrobenzofuran synthesis for the successful production of carasiphenol B (**3.23**). The

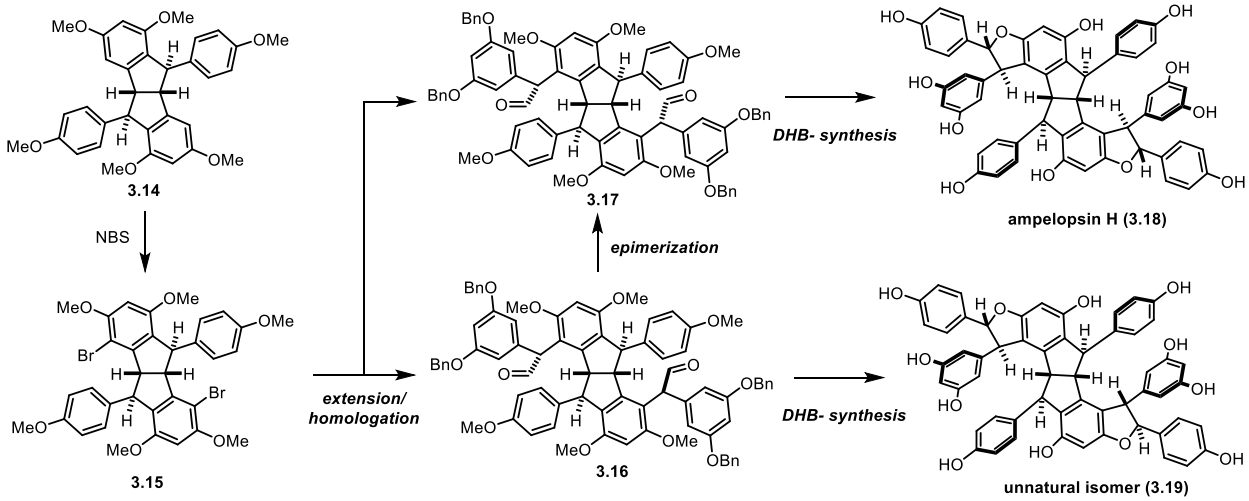

Figure 3.4. Snyder's 2007 synthesis of ampelopsin H.

regioselectivity made it perfectly poised to undergo extension/homologation and C8 – C10 dihydrobenzofuran synthesis for the successful production of carasiphenol B. When treated with NBS, the protected ampelopsin F (**3.20**) underwent dibromoination at both resorcinol positions. Following the extension/homologation and C8 – C10 dihydrobenzofuran-forming sequence, vaticanol C (**3.26**) was formed containing the two *de novo* oligomerized dihydrobenzofuran motifs. Lastly, with the change of brominating conditions to BDSB, the regioselectivity was toggled to the opposite resorcinol as for the carasiphenol B intermediate thus allowing for the successful synthesis of ampelopsin G (**3.26**) following the extension/homologation and C8 – C10 dihydrobenzofuran-forming sequence.

3.3 Discovery of the persistent radical equilibrium of *bis*-quinone methide dimers

While examples of polar, *de novo* strategies for constructing this key connection are abundant, radical approaches are relatively unexplored. Work from the Stephenson group hopefully provides a seeding point for new methodologies. We first accomplished the syntheses of pallidol (**2.4**) and quadrangularin A (**2.3**) from common bis-quinone methide (BQM) intermediate **2.2** (**Figure 2.1, Chapter 2**).[64] In the bio-inspired dimerization step, protected resveratrol analogue **2.5** was

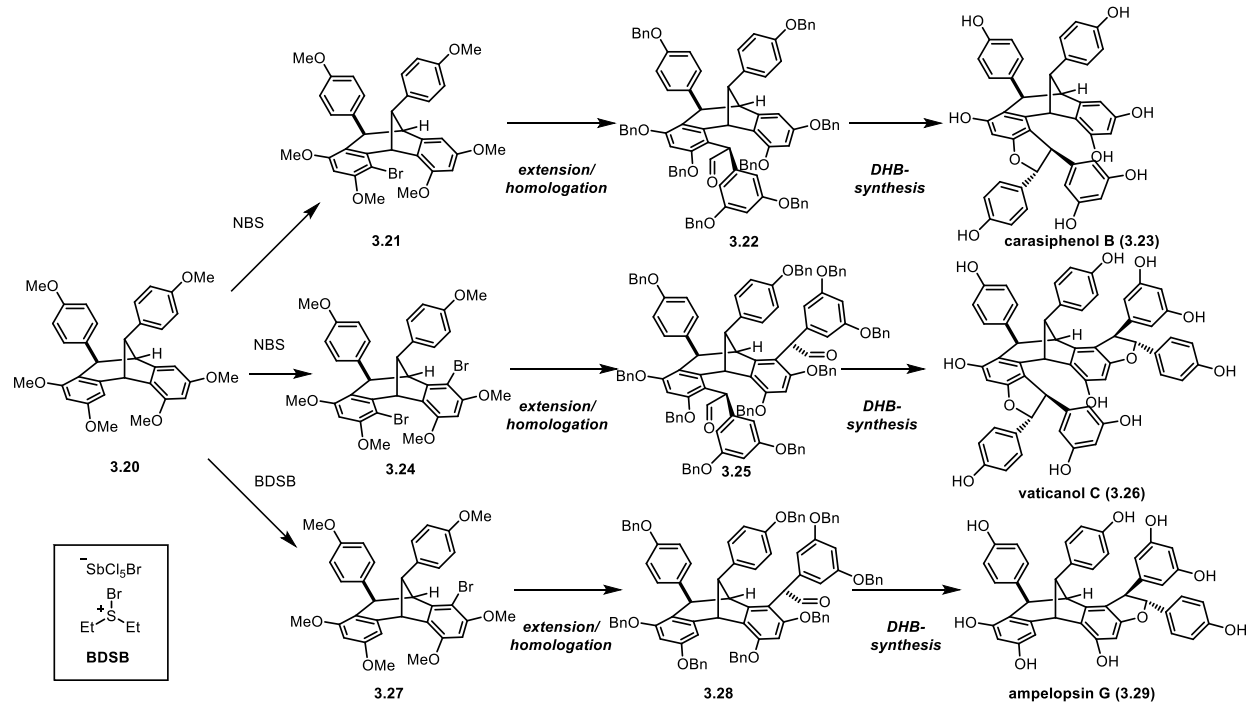

Figure 3.5. Snyder's 2011 synthesis of carasiphenol B, vaticanol C, and ampelopsin G.

oxidized under basic conditions to yield the key intermediate. Subsequent Lewis-acid mediated cyclizations and deprotections of afforded pallidol (**2.4**) and quadrangularin A (**2.3**) with good synthetic efficiency.

Upon further investigation of the cyclization conditions for **2.2**, we found that treatment of BQM **2.2** with 10 mol% of trifluoroacetic acid afforded the cyclized quinone methide **3.30** as a single diastereomer in 93% yield (Scheme 20). The conversion of **2.2** (as a 4:3 mixture of diastereomers) to the *trans,trans*–indane product **2.30** was confirmed by X-ray crystallography (**Figure 3.6**). It was hypothesized that only the *meso* diastereomer of **2.2** (**3.31**) could undergo this cyclization. It was believed that this product could only arise through the meso diastereomer of QMD (X) however both diastereomers converge to the

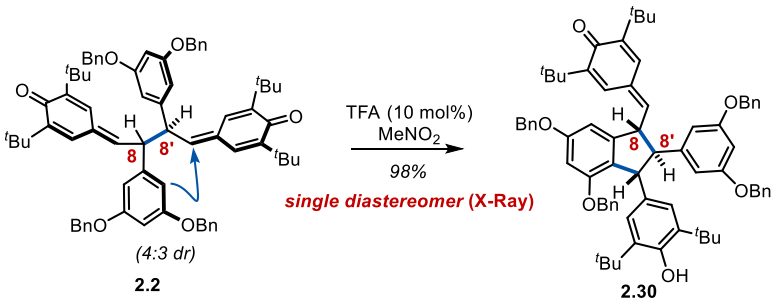

Figure 3.6. TFA-mediated cyclization of tBu-QMD **2.2** yields a single diasteroemer confirmed by X-ray crystallography

single diastereomer product. The reaction mechanism was further probed. One hypothesis was that (**3.30**) arises from indene containing quadrangularin A core (**3.36**) via a vinylogous protonation but the diastereomer was not produced upon subjection of the olefin to the reaction conditions. Secondly, it was hypothesized that QMD (**2.2**) undergoes a tautomerization to form intermediate quinone methide tautomer (**3.37**) and then undergoes protonation/epimerization before cyclization occurs. This hypothesis was rejected after subjection of the tautomer to the reaction conditions failed to produce indane (**3.30**) (**Figure 3.7**). we hypothesized that a radical mechanism was responsible for the observed reactivity.[127] Quinone methide dimers have been shown to have intrinsic persistent radical properties in solution. Becker first published on the persistent radical equilibrium of QMD (**2.12**) in chloroform. At 25 °C, K_{eq} for the dissociation of the dimer to the radical monomers was found to be $K_{eq} = 1x10^{-7}$.[127]

Based on the work contributed by Becker and the discovery of persistent carbon-centered radicals by Gomberg, we decided to interrogate the possibility of a radical-based mechanism. A thermal crossover experiment (**Figure 3.8**) was the first piece of evidence that QMD (**2.2**) was in equilibrium with its persistent radical monomer. A mixture of differentially substituted QMDs (**2.2** and **3.38**) were mixed in a sealed vial and subjected to heating in $CDCl_3$. The solution of both QMDs started off yellow but then changed green after heating. HRMS and NMR analysis determined a statistical mixture of products was formed with the crossover heterodimer being the major component. This was consistent with the proposed radical mechanism (**Figure 3.8**). The mechanistic explanation for this crossover is thermolysis of the QMDs and then recombination to

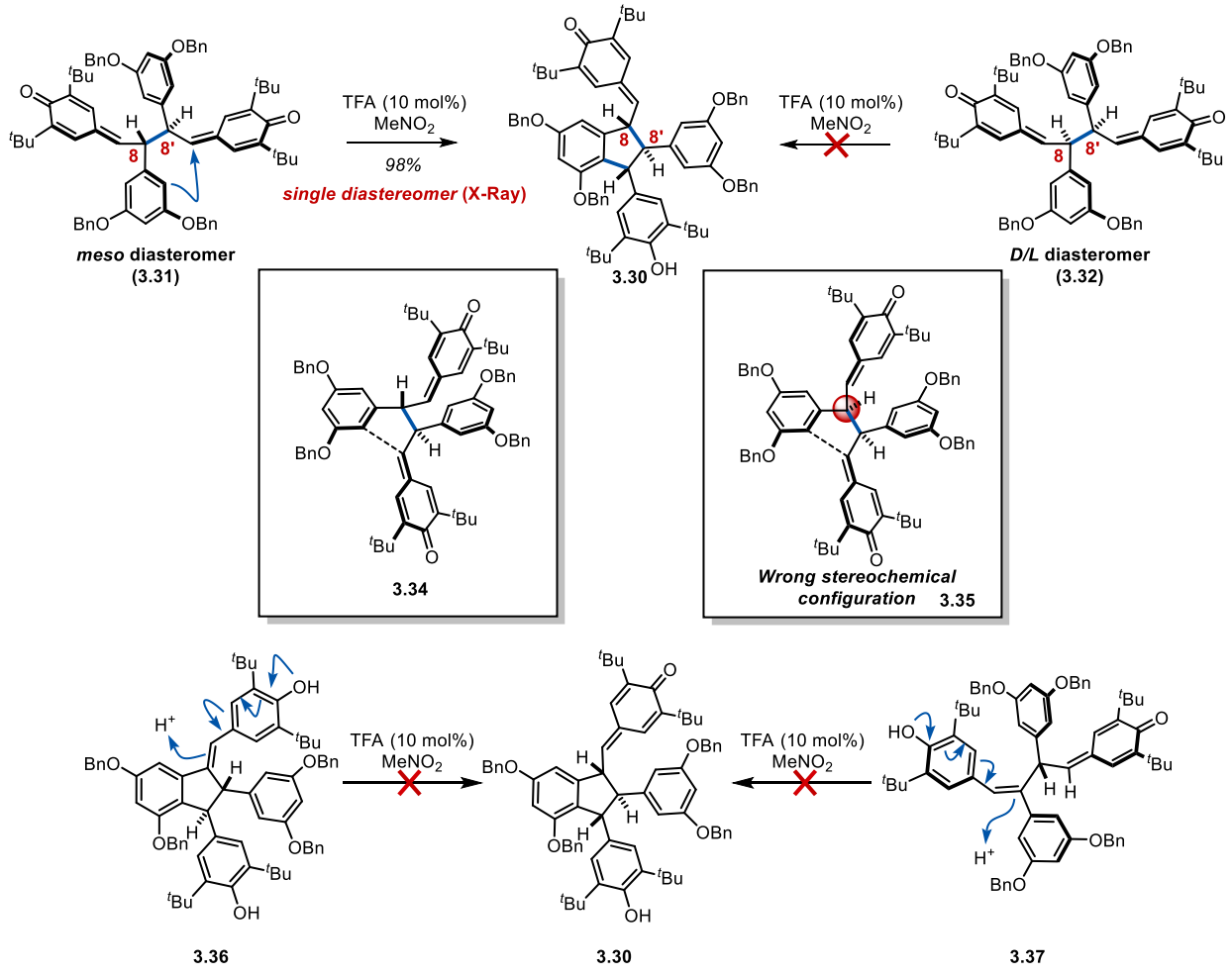

Figure 3.7. Mechanistic interrogation of the the converging diastereoselective acid-mediated cyclization

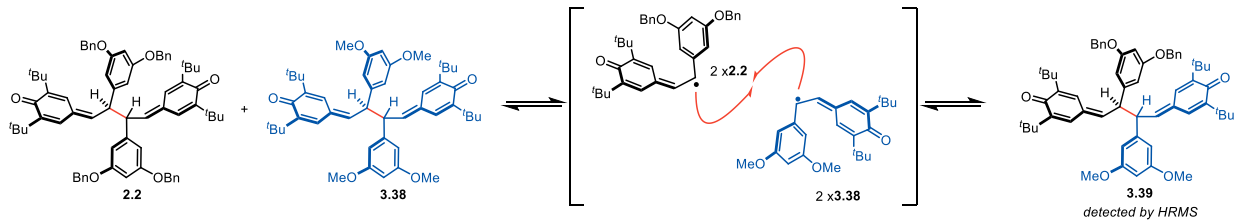

Figure 3.8. Thermal crossover experiments concluded that QMDs behave as peristent radicals.

form the statistical mixture. In collaboration with the Pratt group, the radical properties of QMD (X) were interrogated. Van't Hoff analysis was first used to calculate the BDE of the C8–C8' bond. The bond was found to be astoundingly weak with a BDE measured at 17.0 ± 0.7 kcal/mol. This is comparable to Gomberg's trityl dimer (BDE= 10.7 ± 0.2 kcal/mol) a known persistent radical. Further, EPR analysis determined radical localization on the persistent radical monomer is concentrated at the C8 position and to a lesser extent the C10 and C12 positions. This observation tracts with C3 silyl resveratrol as well as the tetrameric silyl QMD (**2.26**).

The persistent radical effect subsequently applied to the synthesis of higher-order resveratrol oligomers (**Figure 3.10**).[63] In the synthesis of these compounds the key C8 – C10' bond was first constructed by a multi-step *de novo* process originally accomplished by Snyder in the examples above.[95-97, 99, 100, 104] In the first portion of this route, the multi-substituted brominated

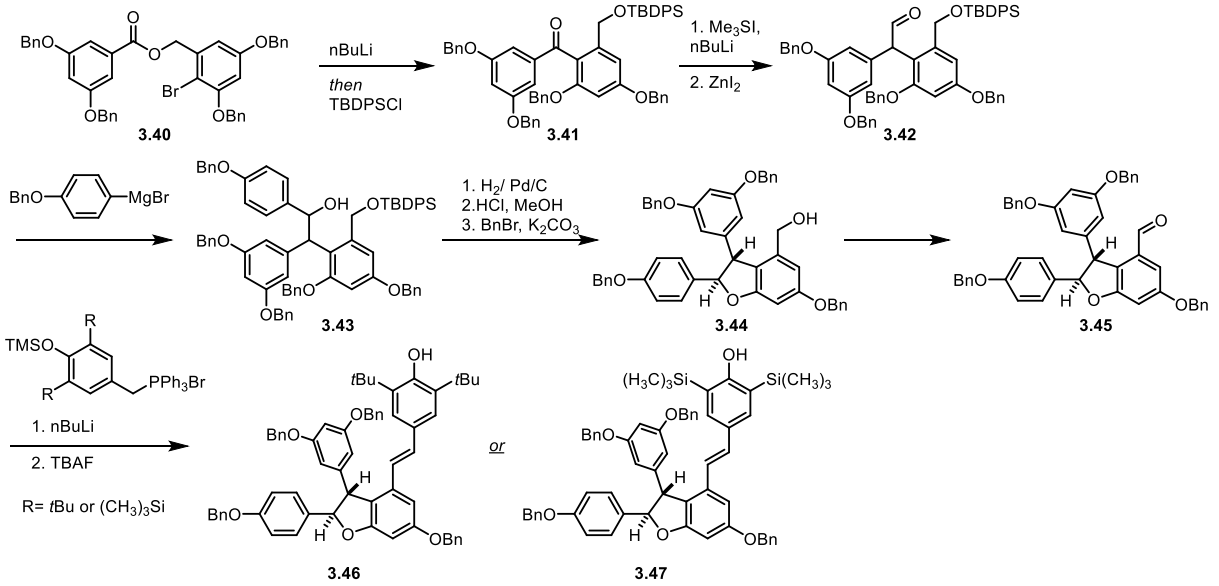

Figure 3.9. Synthesis of ε-viniferin analogs for the synthesis of nepalensinol B and vateriaphenol C

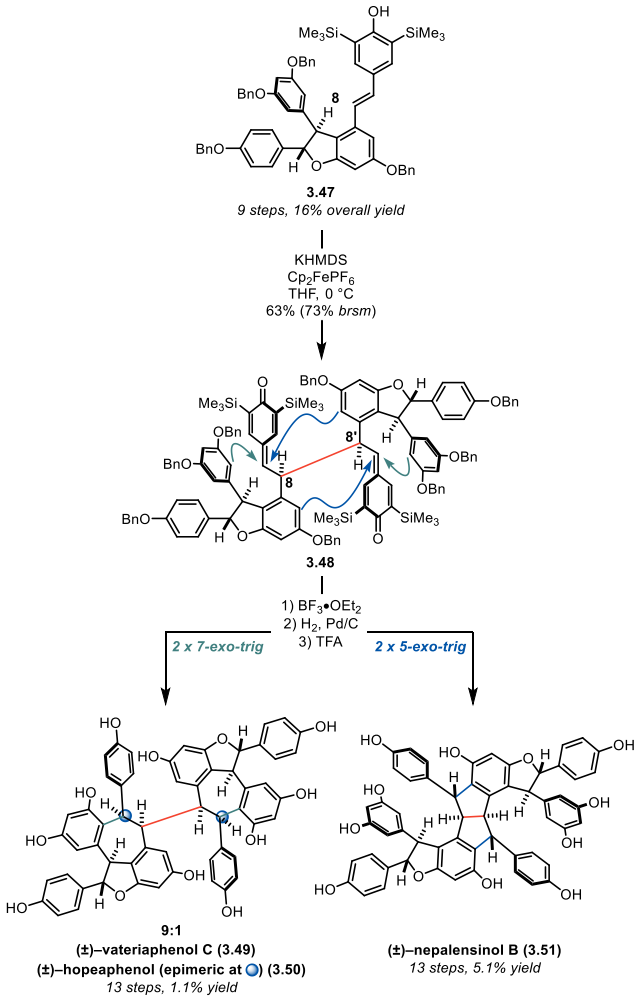

Figure 3.10. Biomimetic synthesis of vateriaphenol C (And diastereomer hopeaphenol) and nepalensinol B

benzyl ester (**3.40**) was subjected to ortho lithiation which induced the anionic Fries rearrangement and furnished bis-aryl ketone (**3.41**). **3.41** was then subjected to a Corey-Chaykovsky epoxidation, ZnI_2-mediated Meinwald rearrangement and subsequent aryl Grignard addition to deliver tri aryl species (**3.43**). Following debenzylation via hydrogenolysis, the key C8 – C10 fused dihydrobenzofuran (**3.44**) was produced by an acid-mediated cyclization. Several additional steps produced the epsilon-viniferin analog (**3.46**). Upon preparing racemic alkylated ε-viniferin analogue (**3.46**), subjection of this material to the same dimerization conditions afforded **2.25** as a single diastereomer. This BQM tetramer was found to have a slightly weaker C8–C8' BDE of just 16.4 ± 0.5 kcal/mol, and it is believed that the highly reversible homolysis and recombination of the radicals contributes to the observed diastereoselectivity. The assignment of the relative configuration of **2.25** was based largely upon the outcome of the subsequent cyclization. It is possible that the isolated isomer of **2.25** is of a different configuration than the one that reacts due to the dynamic homolysis-recombination equilibrium. Lewis-acid mediated cyclization afforded two reaction modes – the double 5-*exo-trig* and double 7-*exo-trig* reactions. Subsequent hydrogenolysis of the benzyl ethers produced the alkylated tetramer precursors.

Attempts to remove the alkyl groups by Lewis-acid mediated retro-Friedel-Crafts dealkylation unfortunately did not produced the desired natural products. Instead, decomposition results, presumably due to the lability of the dihydrobenzofuran. Switching the C3 blocking groups to trialkyl silyl groups was the solution. The corresponding ε-viniferin analogue **3.47** (9 steps, 16% yield), was dimerized and cyclized in a similar fashion as with the tert-butyl groups and subsequent protodesilylation to remove the C3-silyl substituents afforded resveratrol tetramers nepalensinol B (**3.43**) and vateriaphenol C (**3.41**) in just 13 steps and 5.1% and 1.1% overall yield, respectively (**Figure 3.9**). The persistent radical effect was critical to the selective outcome of these syntheses, as we were able to successfully dimerize racemic, prochiral material to a single diastereomer in good yield, enabling the first syntheses of these two resveratrol tetramers.

3.4 Leveraging the persistent radical effect for the synthesis of the vitisins

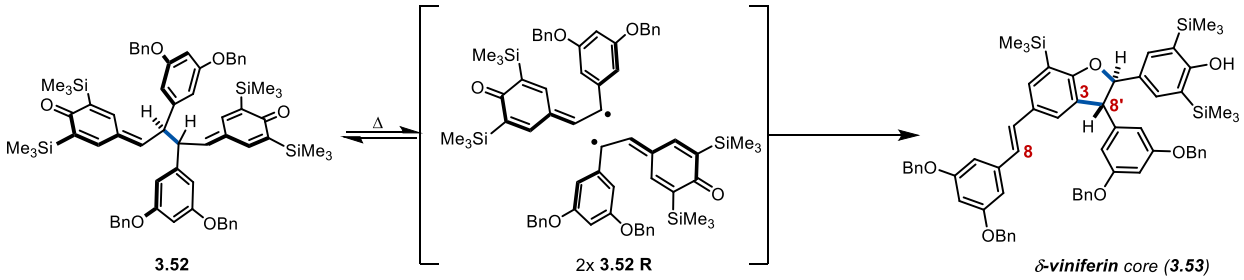

Figure 3.11. Thermolysis-induced rearrangemnt of C3 silylated QMDs.

Although the QMD radical monomer has a high energy barrier for undergoing bimolecular processes thus giving the radical persistence – the kinetic property, the QMD (**2.2**) can undergo both unimolecular and bimolecular reactions. The extension of the Van't Hoff investigation to the silyl analog in order to determine the BDE, it was found that the persistent radical equilibrium becomes irreversible when heating beyond 60 °C. Rather than recombining with the other C8 centered radical, a rearrangement occurs in which the C8 radical adds to the C3 silylated position.

Following radical addition, desilylation and rearomatization occurs to furnish a dihydrobenzofuran product with C3–C8' connectivity (**Figure 3.11**). This persistent radical effect presented an opportunity for the synthesis of vitisin tetramers.

In Stephenson's synthesis of vitisin A and vitisin D, a *de novo* strategy was employed to construct the C8 – C10 bond by the Lewis acid-mediated cyclization to produce a benzofuran (**3.54**). The ε-viniferin analog was completed and then subjected to electrochemical dimerization to produce the tetrameric QMD. When heated, the expected C3 – C8 persistent radical rearrangement furnished the C3 – C8 dihydrobenzofuran intermediate (**3.56**). Fluoride-mediated desilylation and subsequent acid-mediated rearrangement then afforded vitisin A (**3.57**). Intermediate (**3.58**) was used for an acid-mediated (HCl generated *in situ*) cyclization/desilylation to form vitisin D (**3.59**). Attempts to convert intermediate (**3.56**) to vitisin B was unsuccessful as the remaining C5 TMS group proved impervious to several desilylation conditions, presumably due its steric inaccessibility.[101]

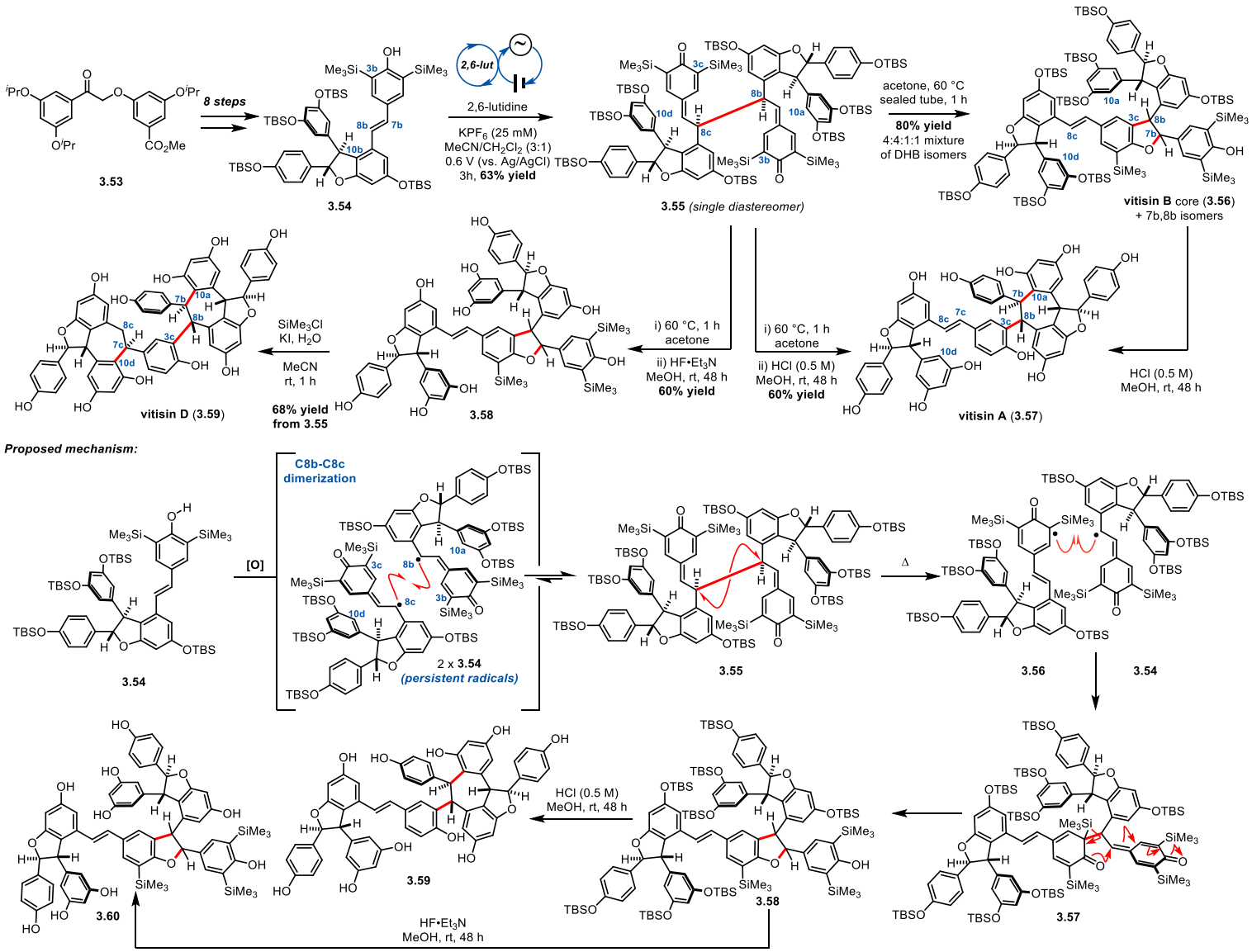

Figure 3.12. Stephenson's 2020 total synthesis of vitisins A & D that utilized an electrochemical oxidation to form the key *bis*-quinonemethide intermediate. The persistent radical nature of **3.55** was then leveraged to thermally induce the C3–C8' reaarrangement to access the vitisin B core. Acid-mediated rearrangements furnished vitisins A & D.

3.5 Leveraging the persistent radical effect for intermolecular coupling of trimers

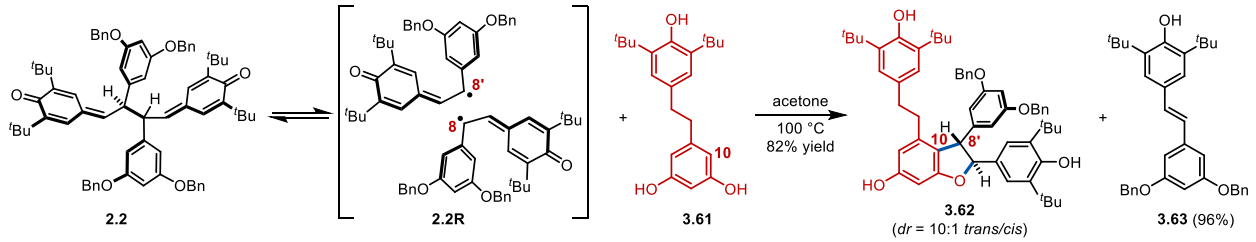

Figure 3.13. Intermolecular coupling of QMD to free resorcinols results in dyhydrobenzofuran products.

Surprisingly, the persistent radical of the tert-butyl QMD (**2.2**) is capable of intermolecular coupling (**Figure 3.13**). When **2.2** was heated in the presence of reduced tBu resveratrol (**3.61**), a C8 – C10' dihydrobenzofuran product (**3.62**) is observed in addition to a single equivalent of protected resveratrol with the intact olefin (**3.63.**). This is indicative that the second equivalent of radical from the QMD is either reduced and protonated or abstracts a hydrogen atom during the course of the reaction. This observation has direct application to the biomimetic syntheses of resveratrol trimers by means of the persistent radical effect.

There have been developments in obtaining mechanistic insight into how this transformation proceeds (**Figure 3.14/ Figure 3.15**). Initially it was speculated that the mechanism of this persistent radical oligomerization was occurring as summarized in **Figure 3.15** whereby the radical initially adds into the C10 position of the resorcinol arene **3.61** following thermolysis of QMD (**2.2**). Addition of the radical into the arene would generate a dearomamtized radical arene species **3.64**. This has a drastic effect on the pKa of the proton at C10 in that it is reduced and further deprotonated to generate radical anion **3.65**. This radical anion can then be oxidized by the

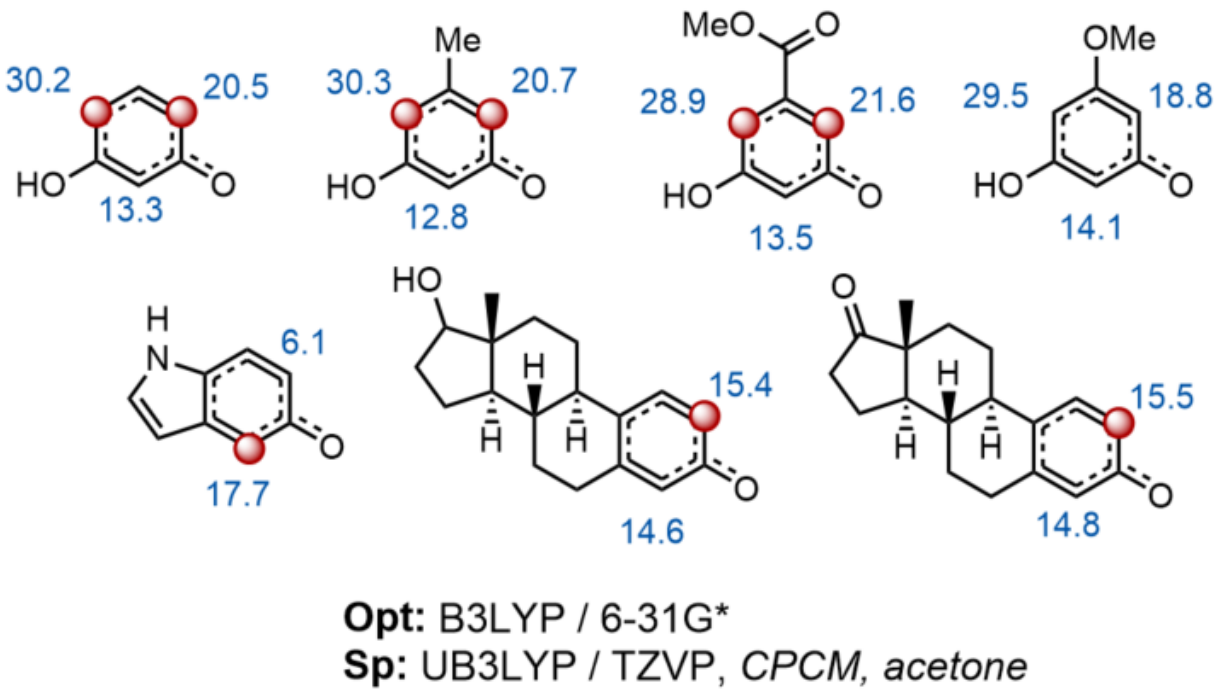

Figure 3.14. Computational results of radical stabilization for oligomerization

other radical equivalent (from the QMD) thus forming the stilbene containing phenoxide and the rearomatized adduct **3.66**. Intramolecular cyclization (5-*exo*-trig) of the phenol onto the quinone methide and proton shuffling results in the observed trans-substituted dihydrobenzofuran product **3.68** and one equivalent of stilbene (**2.1**). This originally proposed mechanism has been precedented through the work of Studer.[128] However, evidence has been obtained that suggests another mechanism may be at play (**Figure 3.16**). When QMD is heated in the presence of tBu_2-resveratrol (**3.69**), a cross over C8 – C8' cyclized dimer (**3.70**) is obtained whereas it was expected to produce the ε-viniferin core containing the dihydrobenzofuran motif (similar to **3.62**). This product can only be achieved following the loss of a proton and electron (or H atom) from the starting stilbene species. This has resulted in speculation that the radical monomer if capable of performing H atom abstraction rather than radical addition. With these results in hand, it is possible that HAT from the resorcinol to the radical monomer happens first. This would generate a radical

intermediate with localization of the radical on C10 and C12. Computational analysis shows that radical intermediates with localization at C10 and C12 have lower energies than radical

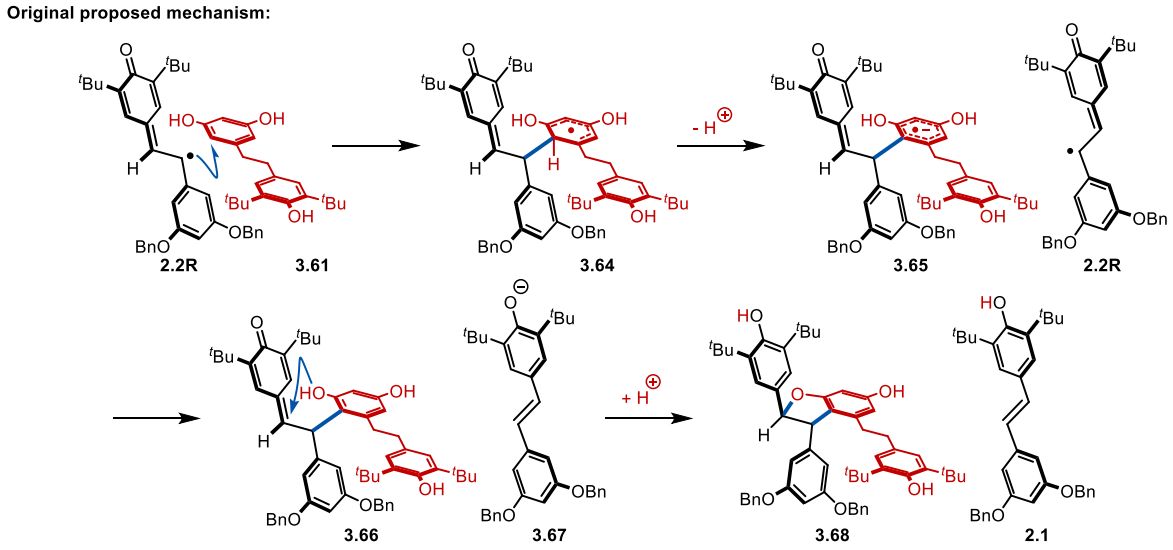

Figure 3.15. Initially proposed mechanistic hypotheses for the intermolecular radical coupling.

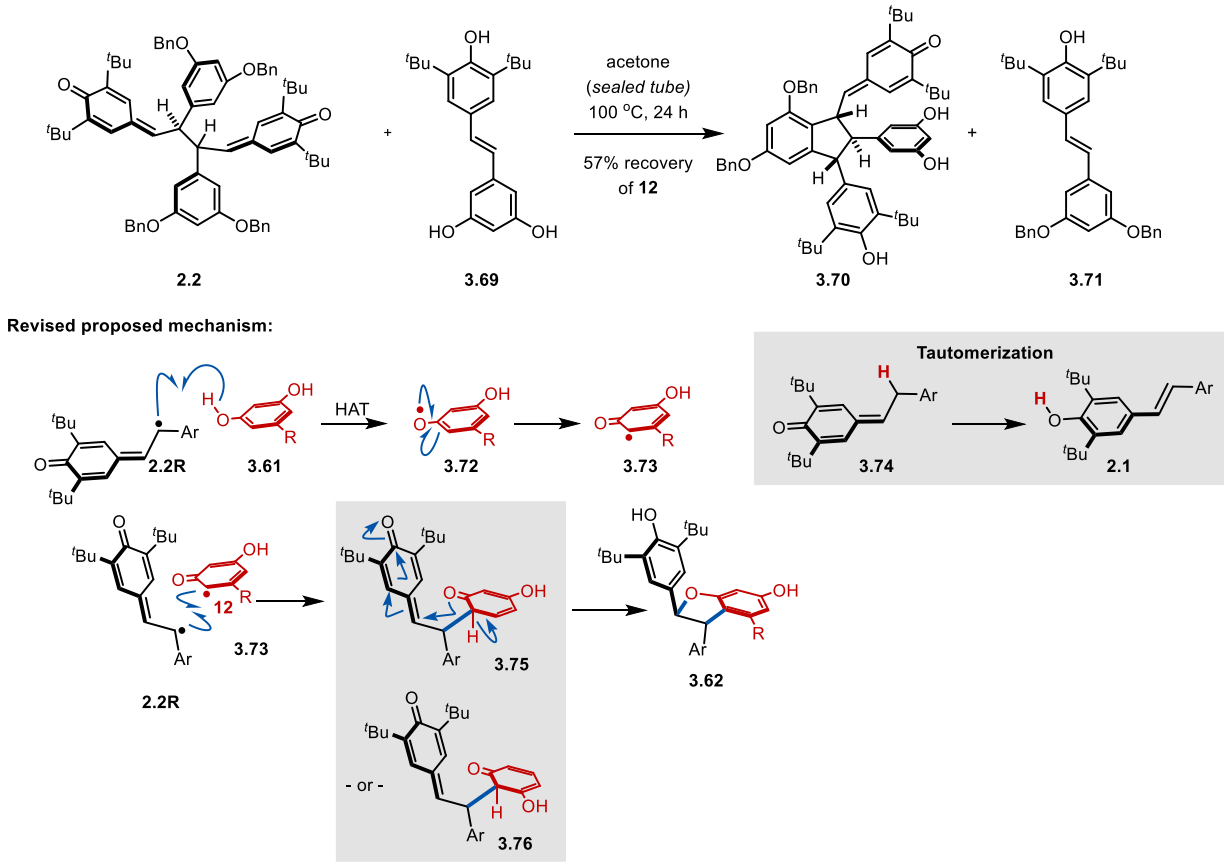

Figure 3.16. Revised mechanistic hypotheses for the intermolecular radical coupling. (Top) experimental evidence for revised mechanism. (Bottom) Revised hypotheses made with experiemntal and computational data.

localization occurring at C14 (**Figure 3.14**). The differences in radical localization energies between C10 and C12 may also have implications for the regioselectivity of the radical oligomerization and will be discussed later. Currently, it is hypothesized that the mechanism of this oligomerization occurs as presented in **Figure 3.16**. In this proposed mechanism, HAT from the resorcinol to the radical monomer happens first. This results in the resonance-stabilized radical of the resorcinol. This C10 (or C12, dependent on the preferred energy level)-centered radical undergoes direct radical combination with the second radical equivalent forming the neutral adduct. The now reduced equivalent half (from the QMD) can undergo tautomerization to furnish the stilbene equivalent that is observed. The neutral oligomerized adduct can then rearomatize (by deprotonation), undergo 5-exo-trig cyclization from the phenol to the quinone methide forming the dihydrobenzofuran, and then protonation of the phenoxide produces the neutral product. A substrate scope analysis of this reaction was performed with various phenols containing simple aromatic substitutions as well as complex aromatic systems (*e.g.* indoles, steroids, etc.).

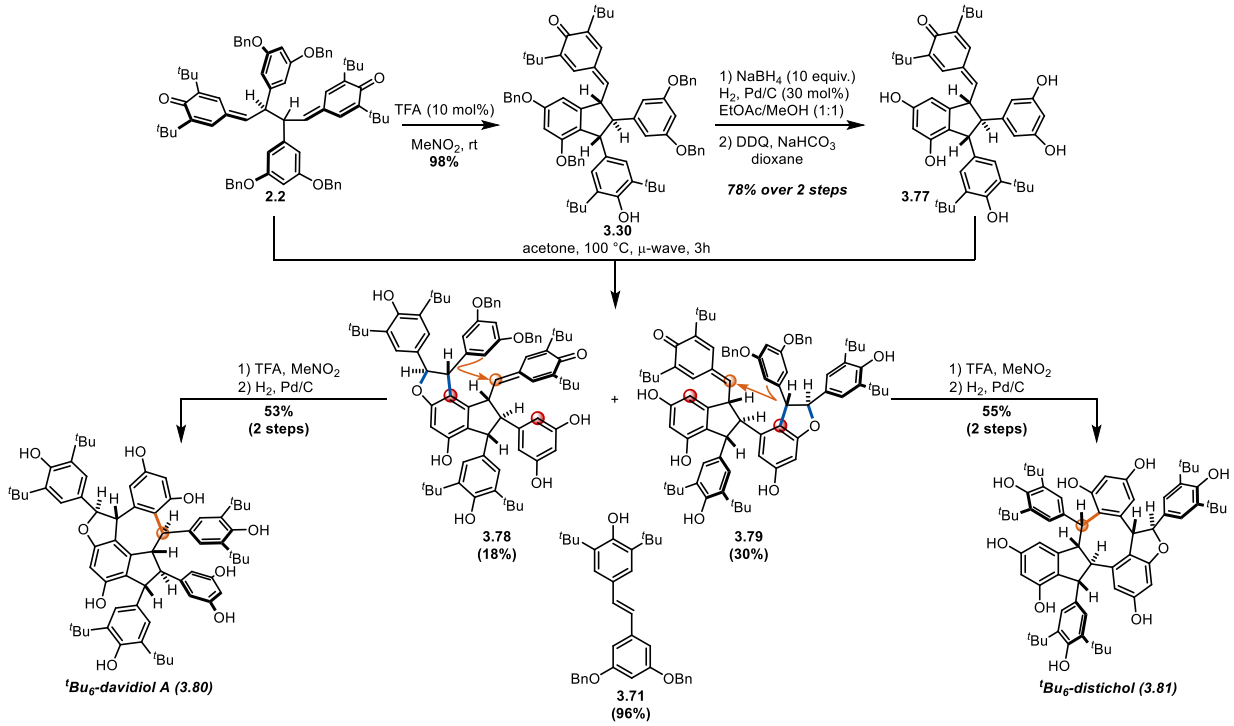

Figure 3.17. Overview of the radical oligomerization to access tBu_6-davidiol A and tBu_6-distichol.

Interestingly, it was found that the site of radical addition (C10 or C12) was dependent on the substrate. This can be explained by the relative energies of the C10 or C12 centered radical as divulged earlier (**Figure 3.14**). The scope of this oligomerization is currently being investigated.

With this newfound reactivity of QMDs we next sought to apply this towards a biomimetic strategy for accessing resveratrol trimeric natural products. Generally, for the formation of trimers, oligomerization would need to occur onto a dimer scaffold. Davidiol A and distichol were chosen as they have no prior reported total syntheses and can be made from the same dimer scaffold (**3.77**). This scaffold was synthesized from **2.2** via the outline route **Figure 3.17**. First **2.2** was subjected to the TFA-mediated cyclization to afford single diastereomer **3.30**. The intermediate quinone methide was then reduced by $NaBH_4$ reduction and then debenzylated through standard Pd-mediated hydrogenolysis conditions. It was found that stoichiometric quantities of Pd/C were required as substoichiometric amounts did not result in complete conversion. This is thought to be due to semi-debenzylated intermediate poisoning the catalyst. After debenzylation, the quinone methide was restored by DDQ oxidation (**3.77**). This resulted in a red material after column chromatography and was later triturated in DCM to form an off white solid. When subjected to the persistent radical oligomerization via microwave heating, a mixture of two regioisomers was observed wherein both contained the C8 – C10 fused dihydrobenzofuran at both resorcinol rings.

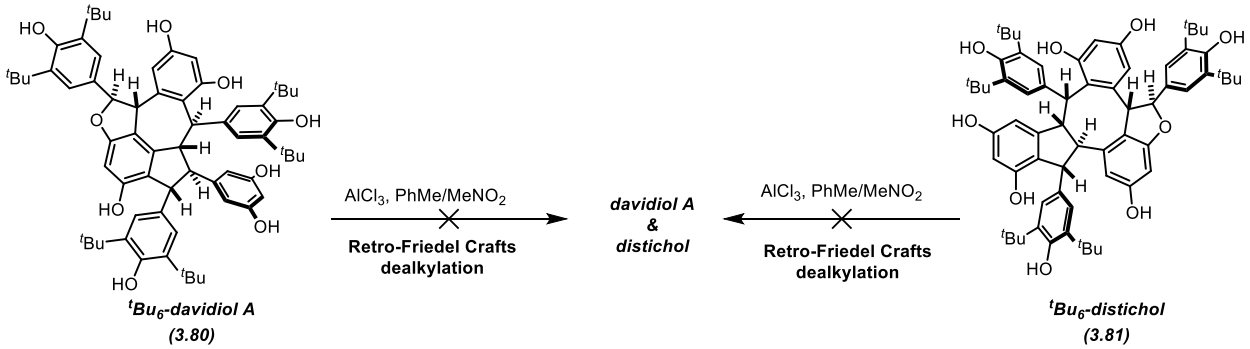

Figure 3.18. Attempts to perform dealkylation of the natural product precursors for davidiol A and distichol.

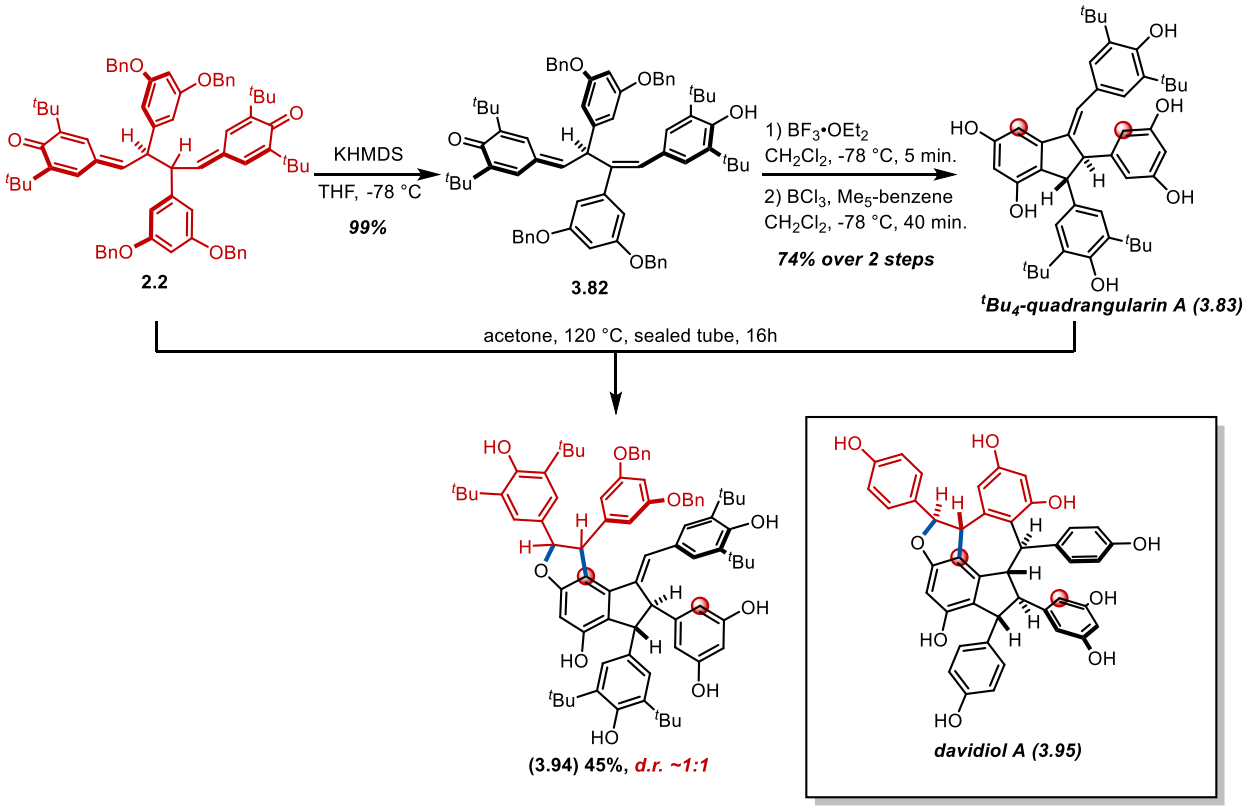

Figure 3.19. Regioselectivity achieved for the potential synthesis of davidiol A.

Regioisomer (**3.79**) has the connectivity needed for distichol (**3.81**) whereas regioisomer (**3.78**) has the connectivity needed for davidiol A (**3.80**). These regioisomers were then treated with TFA to induce EAS cyclization to form the fused cores. Regioisomer **3.78** underwent 7-exo-trig needed for davidiol A and regioisomer **3.79** underwent 8-*exo*-trig needed for distichol. These two intermediates were then subjected to hydrogenolysis to afford the debenzylated alkylated natural product precursors corresponding to davidiol A (**3.80)** and distichol (**3.81**). Removal of the tert-butyl groups at C3 proved to be unfruitful with classic retro-Friedel-Crafts conditions ($AlCl_3$ in $PhMe/MeNO_2$) and instead resulted in decomposition of the starting materials. This is believed to be due to the acid-sensitivity of the dihydrobenzofuran as has been observed in the previous syntheses of nepalensinol B, vateriaphenol C, and hopeaphenol.

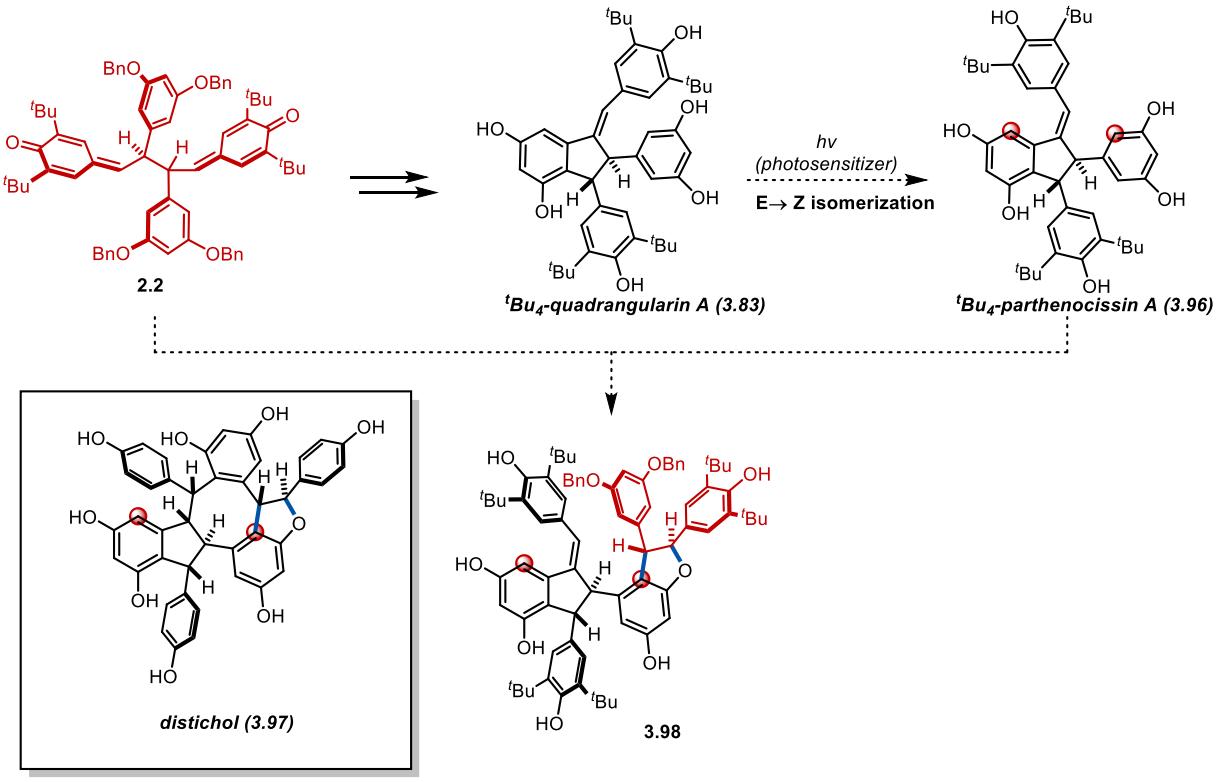

Figure 3.20. Proposed regioselective route for accessing distichol connectivity selectively.

It is desirable to be able to control the regioselectivity of oligomerization for selective syntheses of either distichol or davidiol A. In exploring the scope of dimer scaffolds that can undergo oligomerization, alkylated quadragularin A (**3.83**) was subjected to the conditions and resulted in a single regioisomer product as a mixture of diastereomers (*dr* 1:1) (**3.94**). The resulting product contains the C8 – C10 connectivity that is specific to davidiol A (**Figure 3.19**). It is speculated that the regiospecificity is a result of the diastereomeric configuration of the olefin wherein the trans side of the olefin is less sterically incumbered by the bis-butyl phenol. From this intermediate (**3.94**), it is required to manipulate the oxidation state of the olefin to form the quinone methide such that the acid-mediated 7-exo-trig cyclization can form the desired carbon skeleton. Currently, efforts are being made to isomerize the olefin of tBu4-quadrangularin A (**3.83**) to form tBu4-parthenocissin A (**3.96**) to redirect the oligomerization to the other resorcinol that would result in the C8 – C10 connectivity of distichol (**3.97**) (**Figure 3.20**). Preliminary efforts have been

done made to accomplish the isomerization through a photochemical approach. In this strategy, a photocatalyst has been used to attempt to sensitize the olefin to the triplet state which would then isomerize to the opposite diastereomer. If successful, oligomerization would take place to afford the other regioisomer that has connectivity for distichol followed by a similar oxidation state manipulative strategy as outlined for the regioselective synthesis of davidiol A (**3.95**).

Carasiphenol C (**3.13**) (and its diastereomer wilsonol A) are other desirable targets to demonstrate the utility of the persistent radical oligomerization to form key C8 – C10 fused dihydrobenzofuran-containing resveratrol trimeric oligomers. The rationale for pursuing these natural products is that the core contains pallidol which has been previously synthesized by the Stephenson group and the C8 – C10 dihydrobenzofuran-fused motif that can be accessed by the persistent radical oligomerization (**Figure 3.21**). The synthetic sequence begins from QMD (**2.2**) which resulted from the developed electrochemical dimerization method. The QMD was then subjected to BF3•OEt2-mediated cyclization to form the desired [3.3.0] bicyclooctane product (**3.99**) (40% yield) that occurs by two sequential EAS cyclizations that only the *D/L* isomer can

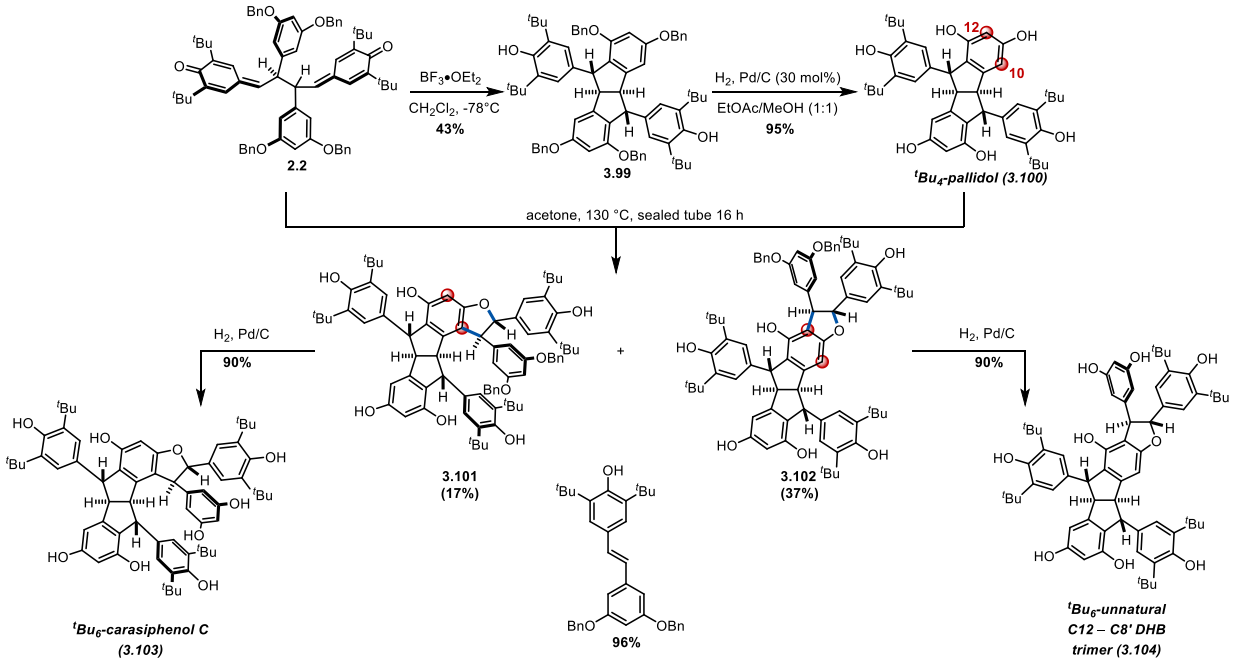

Figure 3.21. Outlined route for the radical oligomerization of tBu4-pallidol to access tBu6-carasiphenol C

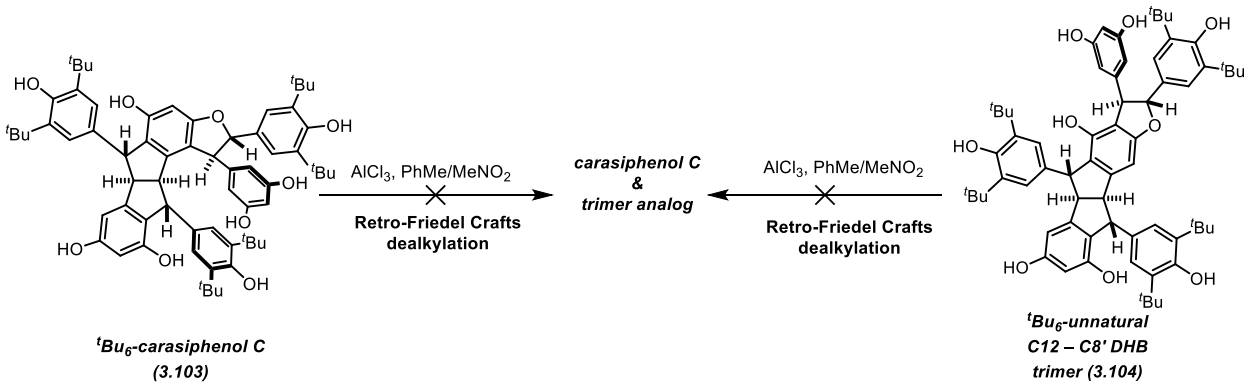

Figure 3.22. Attempts to perform dealkylation of the natural product precursors for carasiphenol C and the unnatural trimer.

undergo. In addition to the desired intermediate, monocyclized monoquinone methide is formed (60% yield) that comes from the *meso* isomer. The [3.3.0] bicylooctane was then debenzylated to give (**3.100**) now having the free resorcinols needed for oligomerization. Subjection of tBu4 pallidol to the radical oligomerization with excess QMD furnished the desired C8 – C10 fused dihydrobenzofuran product (**3.101**) as a mixture of diastereomers (17% yield, 1:1 *d.r.*). Surprisingly, the C8 – C12 regioisomer (**3.102**) was produced as the favored isomer as a single diasereomer (37% yield). Initially it was hypothesized that this C8 – C12 regioisomer was favored as the C12 position is most distal to the [3.3.0] core and is more accessible in terms of sterics. In light of the computational evidence, it may also be favored as the radical localization at C12 presents a lower energy resonance structure. It is uncertain which factor is at play and can be a combination of both steric and electronic favorability. Separation of the this regioisomer mixture into the individually purified isomers proved to be ineffective by column chromatography and preperative TLC. It was rationalized that telescoping the mixture through the debenzylation would allow for separation of the isomers. This was indeed fruitful as the debenzylated isomers had a substantial difference in Rf by silica chromatography. The desired C8 – C10-containing tBu_6-carasiphenol was much less polar in comparison to the unnatural C8 – C12 alkylated trimer and came as a surprise that the difference in polarities would be as stark as observed. Attempts to

remove the C3 tert-butyl groups through the aforementioned retro-Friedel-Crafts conditions ($AlCl_3$, toluene/$MeNO_2$) proved to be ineffective as previously observed with products containing the dihydrobenzofuran motif. Due to the ease of synthesis of these natural product precursors, and the favorability in producing the C8 – C12 isomer, it was used as a model system in screening dealkylation conditions.

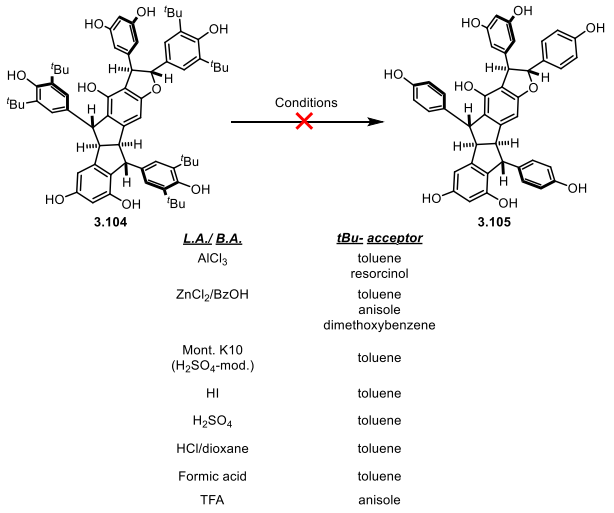

Figure 3.23. Attempted conditions for retro-Friedel-Crafts dealkylation.

3.6 Exploring strategies for the removal of C3 blocking groups

In exploring alternative conditions for the retro-Friedel-Crafts dealkylation, the C8 – C12 isomer was used as a model substrate for the desired C8 – C10 natural product precursor due to it being the major isomer that forms in the persistent radical oligomerization. First it was hypothesized that using a different *tert*-butyl cation acceptor would allow for the reaction to proceed at a faster rate than decomposition of the dihydrobenzofuran. To this end, resorcinol was used in excess as it is more electronically rich and can act as a more potent nucleophile for the EAS substitution. Unfortunately, this too resulted in decomposition and returned a complex mixture in which no major product or starting material could be isolated. This is indicative that a different Lewis acid would be needed as it is too strong and promotes dihydrobenzofuran opening

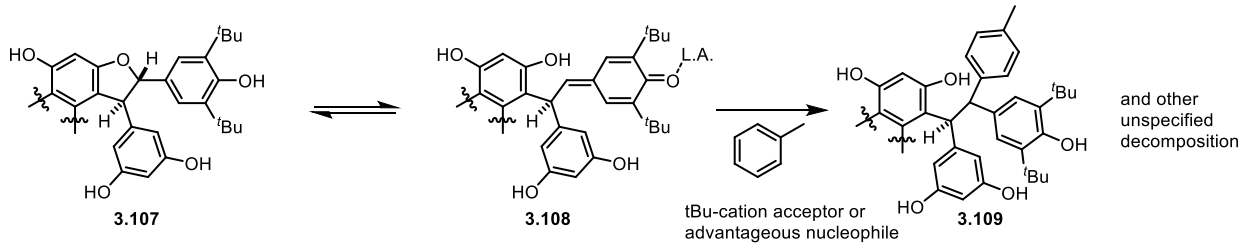

Figure 3.24. Potential decomposition pathway for dihydrobenzofuran under acidic conditions.

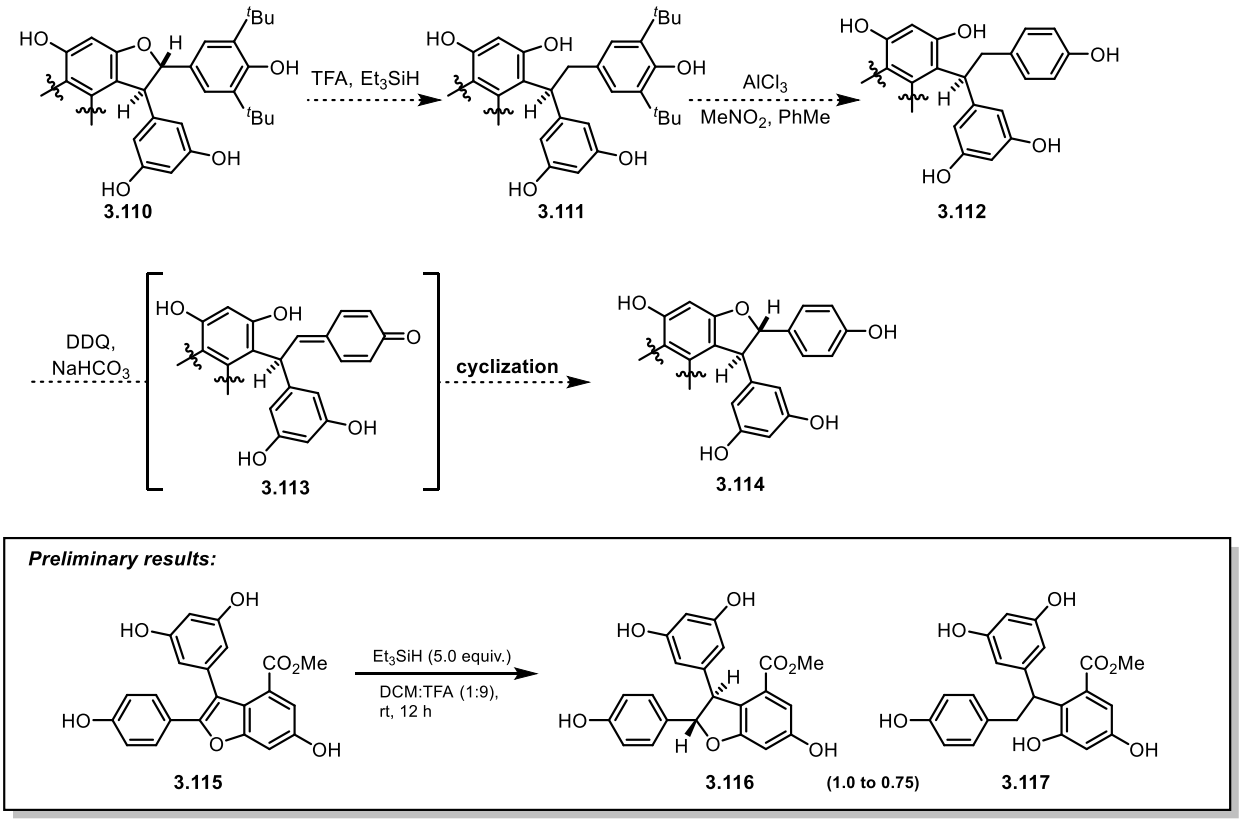

Figure 3.25. (Top) Alternative strategy for dealkylation involving reductive cleavage of the dihydrobenzofuran prior to retro-Friedel-Crafts dealkylation. (Bottom) preliminary results for reductive ckeavage of dihydrobenzofurans.

and decomposition. The softer Lewis acid $ZnCl_2$ in combination with benzoic acid was used to help promote the retro-Friedel Crafts but this too returned a similar decomposition profile as previously observed. Literature precedence for using montmorillonite K10, a mineral clay solid acid catalyst, was found to be successful in promoting Friedel-Crafts tert-butyl alkylation of resorcinol. In this prior work, the montmorillonite clay was activated by pretreating with sulfuric acid.[129] However, these conditions also proved to be too harsh and ultimately resulted in loss of the dihydrobenzofuran motif. Bronsted acids were then explored wherein the concentration of the active Lewis acid (H^+) could be controlled by pK_a. It was found through the screening of Bronsted acids that the dihydrobenzofuran is unstable in acidic conditions with a range of Bronsted acids with varying pK_as (H_2SO_4, HI, HCl in dioxane, formic acid, and TFA) (**Figure 3.23**). It is presumed that the dihydrobenzofuran is decomposing through the proposed mechanism (**Figure**

3.24). In this mechanism, the dihydrobenzofuran oxygen is able to be activated for ring opening via protonation. The alkylated phenol is in conjugation with the C7 position allowing the dihydrobenzofuran ring to cleave forming the free phenol and quinone methide. This acidic environment increases the electrophilicity of the quinone methide which can undergo addition by aromatic electrophilic substitution by solvent quantities of toluene that is required as a tert-butyl cation acceptor.

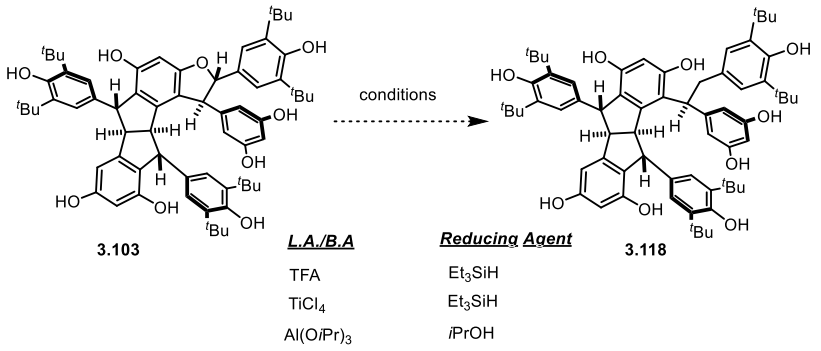

Figure 3.26. Attempted Kishi reduction and similar L.A-mediated hydride reductions of tBu6-carasiphenol.

The presented incompatibility of the dihydrobenzofuran and the acidic conditions required for the retro-Friedel-Crafts dealkylation of the C3 tert-butyl groups presented the need for alternative strategy. Initially, it was speculated that oxidation of the dihydrobenzofuran ring to the benzofuran would make it unlikely for the phenol to be released with ring cleavage under the acidic conditions required for retro-Friedel crafts dealkylation. However, the oxidative sensitivity of the butylated phenols would make such an approach unlikely to succeed. Instead, it was deemed more feasible to reductively cleave the dihydrobenzofuran ring to the reduced benzylic phenol. Previous studies for the synthesis of the vitisins made this a promising strategy **Figure 3.25**. This preliminary result was presented when attempting to reduce the benzofuran of intermediate (**3.115**) to the trans-fused dihydrobenzofuran (**3.116**) but also produced the reductively cleaved side byproduct (**3.117**). Kishi conditions were first explored to accomplish this task. Screening of equivalents of triethyl silane and reaction temperatures and reaction time did no afford the desired product but rather a complex mixture. Mass spectrometry analysis of the resulting mixture did not

show the formation of detectable amounts of product but showed unspecified dealkylation had accord. Unfortunately, the screen presented no conditions that would allow for dealkylation without decomposition. Again, this decomposition is most likely due to the TFA needed for the Kishi reaction in that the acid activates the dihydrobenzofuran for hydride addition in the same way that leads to decomposition. Evidently the hydride transfer is not fast enough to outcompete decomposition. $TiCl_4$ was also employed in place of TFA to see if a milder Lewis acid with enable the desired reactivity. This not only did not result in reductive cleavage but the Titanium proved challenging to remove from the starting material due to the free phenols. The Meerwein-Ponndorf-Verley reaction was attempted to transfer a hydride equivalent from isopropyl alcohol to the quinone methide that was reasoned to form when the dihydrobenzofuran is heated in the presence of $Al(O^iPr)_3$. This failed to convert starting material to the intended product. It is reasoned that this failed as the quinone methide is too far away from the phenol being coordinated by the aluminum catalyst so the intramolecular hydride transfer is improbable. Attempting this reaction at a higher concentration for an intermolecular hydride transfer was also unsuccessful (**Figure 3.26)**. Basic conditions were then explored for the reductive cleavage.

The rationale for performing this transformation using a basic hydride reagent is outline in **Figure 3.25** in which deprotonation of the phenol in conjugation with the dihydrobenzofuran would induce the ring opening and present the quinone methide that can be reduced by addition of hydride ultimately forming the phenol. It has already been demonstrated that sodium borohydride is able to reduce a quinone methide in a similar fashion. Lithium aluminum hydride was first screened with various equivalents and reaction temperature but failed to convert starting material to product. To prevent the loss of more precious trimer material, a simpler model substrate was employed for continuing the investigation of the reductive cleavage using basic conditions. This

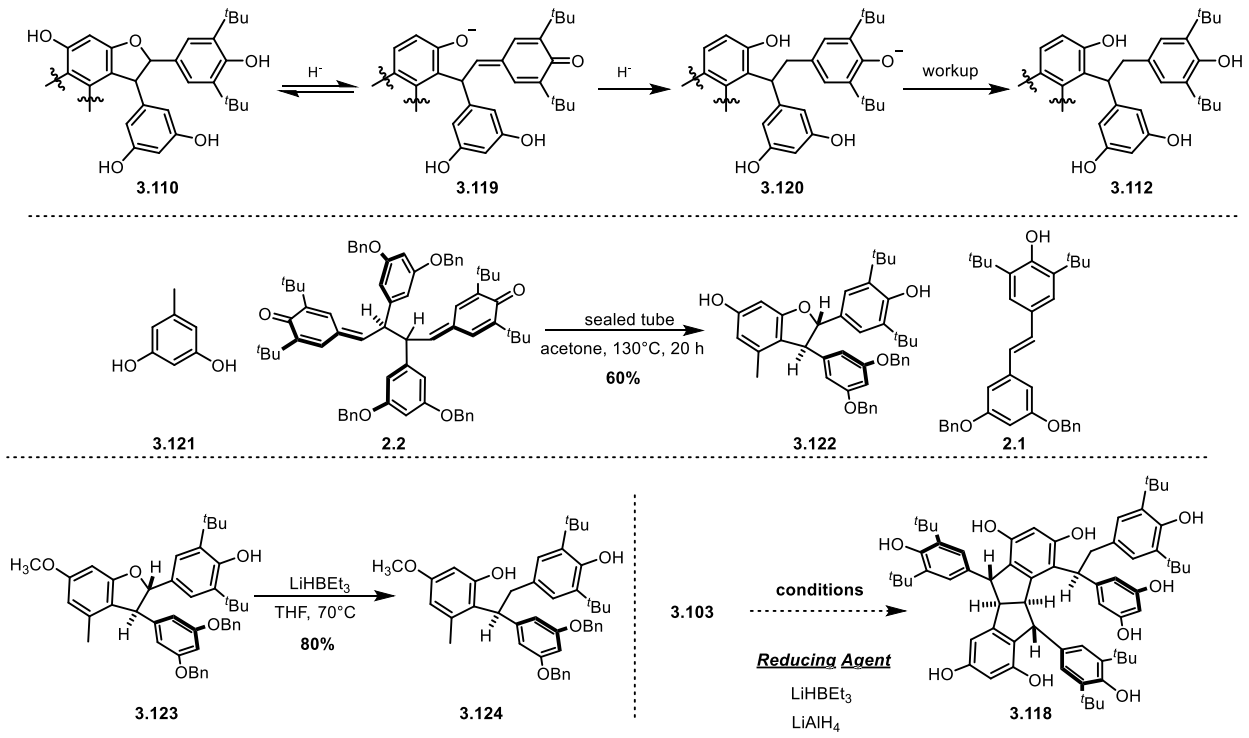

Figure 3.27. Proposed basic hydride strategy for reductively cleaving open the dihydrobenzofuran (Top). Synthesis of model substrate system for screening reductive cleavage conditions (Middle) Model substrate used for successful reductive cleavage. (Bottom, left) Screened conditions were unable to achieve reductive cleavage on the natural product system (Bottom, right)

model substrate (**3.122**) was synthesized by the persistent radical coupling of QMD **2.2** with orcinol (**3.121**) (**Figure 3.27**). With the failures of the $LiAlH_4$-mediated reductive cleavage attempts in hand, it was hypothesized that protection of the resorcinol groups was needed prior to treatment with a hydride source. To this end, (**3.122**) was methylated with methyl iodide and potassium carbonate. Temperature control was critical for this reaction to work as it was observed that higher temperatures resulted in complete methylation of both the resorcinol moieties and bis-tert-butyl phenol, a methylation that was believed to be improbable due to the steric constraints of the phenol. Gratifyingly, treatment of the orcinol-containing dihydrobenzofuran model substrate (**3.123**) with lithium triethylborohydride (super hydride) produced the desired reductive cleavage product (**3.124**). To apply this to the relevant C8 – C10 tBu_6 carasiphenol C system, the alkylated precursor (**3.103**) needed to be per-methylated using the same alkylating conditions used on the model system. With temperature control and using only slight excess of methyl iodide, the penta

methylated tBu6-carasiphenol was synthesized. With the methylated trimer in hand, it was time to apply the lithium triethylborohydride conditions on the relevant natural product scaffold. Unfortunately, the reaction would not convert the starting material to product when performed at room temperature. Even when performed at refluxing conditions with excess hydride (10 equivalents), the reductive cleavage product would not form and starting material was returned. This strategy was abandoned and replaced with a strategy to change the C3 tert-butyl groups to something more labile.

The need for harsh conditions to remove tert-butyl blocking groups and the stability of the natural product dihydrobenzofuran scaffold for reductive cleavage presents the need for an alternative C3 blocking group strategy. It has been acknowledged that trimethylsilyl groups can be removed easily but do not allow for the intermolecular persistent radical coupling needed to access the resveratrol trimers. Earlier efforts were made to replace the C3 blocking groups with alkylthioethers as they have been shown to be tolerated by the electrochemical oxidation and can

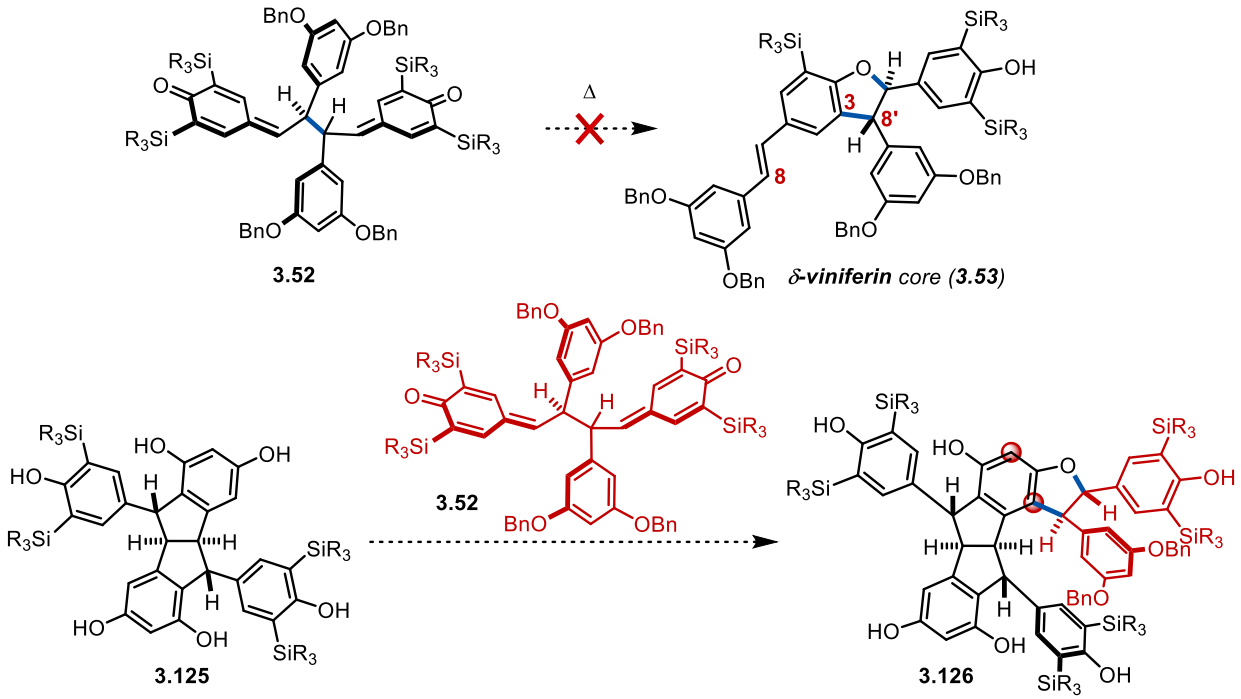

Figure 3.28. Current strategy for accessing trimer products requires finding a silyl group that is sufficiently hindered to deter intramolecular radical rearrangment while permitting intermolecular coupling.

be removed by reductive conditions (*i.e.* Raney nickel). It was found early on that these groups were very acid sensitive and would not be feasible in the construction of the dimeric scaffolds that require acidic conditions for the EAS cyclizations needed to furnish the carbon framework. Although trimethylsilyl groups at C3 have established shortcomings for the trimer synthetic routes (specifically the limitations in the persistent radical coupling), the use of larger silyl-based groups has not been explored. It can be reasoned that there exists a C3 silyl group that is sterically encumbered enough to permit dimerization and intermolecular persistent radical C8 – C10 coupling as well as preventing the undesired C8 – C3 rearrangement. This is an avenue that is currently being explored (**Figure 3.26**).

3.7 Experimental

General Procedures: Glassware was dried in a 150 °C oven or flame-dried under vacuum (~0.5 Torr) prior to use. Reaction vessels were equipped with Teflon/PTFE-coated magnetic stir bars and fitted with rubber septa, and reaction mixtures were maintained under a positive pressure of dry nitrogen unless otherwise noted. Air- and/or moisture-sensitive liquids were transferred using stainless steel needles or cannulae. Reaction progress was monitored by analytical thin–layer chromatography (TLC) using glass-backed plates pre-coated with 230–400 mesh silica gel (250 μm, Indicator F-254), available from Silicycle, Inc (cat #: TLG-R10011B-323). Thin layer chromatography plates were visualized by exposure to a dual short-wave/long-wave UV lamp and/or by exposure to ethanolic solutions of *p*-anisaldehyde or vanillin, or an aqueous solution of ceric ammonium molybdate (Hanessian's stain), and the stained plates were developed by warming with a heat gun. Flash column chromatography was performed according to the procedure described by Still et al.[1] either manually using 43-60 μm (230–400 mesh) silica gel or utilizing Redi*Sep*®*R*$_F$ Gold silica columns with a Teledyne Isco CombiFlash R$_F$ automated purification system. Upon reaction quenching and work up, organic solutions were dried over Na_2S_4 or $MgSO_4$ and concentrated on Büchi rotary evaporators at ~10 Torr/35 °C, then at ~0.5 Torr/25 °C using a Welch vacuum pump.

Materials: Commercially available starting materials were used as received without further purification unless otherwise noted. Organic solvents (acetonitrile, dichloromethane, diethyl ether, dimethylformamide, dimethyl sulfoxide, methanol, tetrahydrofuran, toluene) and amine bases (triethylamine, pyridine, *N,N*-diisopropylethylamine, and diisopropylamine) were purified

[1] Still, W. C.; Kahn, M.; Mitra, A. *J. Org. Chem.* **1978**, *43* (14), 2923–2925.

immediately prior to use by the method of Grubbs et al.[2] using a Phoenix Solvent Drying System (JC-Meyer Solvent Systems) or PureSolv Micro amine drying columns (Innovative Technology/Inert), respectively, and maintained under positive argon pressure. Solutions of organolithium reagents (*n*-BuLi, *t*-BuLi) and Grignard reagents were purchased from Acros Organics unless otherwise noted and titrated prior to use (1,10-phenanthroline/menthol) according to the method of Paquette.[3]

Product Analysis: Product names were generated using ChemDraw Ultra 21.0 (PerkinElmer). ^{1}H and ^{13}C NMR spectra were recorded at the indicated temperature at 117 kG and 176 kG (^{1}H 500 MHz, 700 MHz; ^{13}C 125 MHz and 175 MHz) using an internal deuterium lock on Varian Inova 500 or Varian VNMR 500 and 700 spectrometers. ^{1}H chemical shifts are expressed in parts per million (ppm) relative to the residual protio solvent resonance in $CDCl_3$ using δ 7.26 as standard for residual $CHCl_3$ or using the center line of the solvent signal as internal reference for acetone-d_6: δ 2.05, and DMSO-d_6: δ 2.50. Multiplicity is reported as follows: (br = broad, s = singlet, d = doublet, t = triplet, dd = doublet of doublets, ddd = doublet of doublet of doublets, m = multiplet), and the corresponding coupling constants are indicated as *J*-values in units of Hz. ^{13}C NMR spectra were completely ^{1}H-decoupled (broadband) and the center line of the solvent signal was used as internal reference: $CDCl_3$ δ 77.23; acetone-d_6 δ 29.92; DMSO-d_6 δ 39.51. ^{13}C chemical shifts are expressed in parts per million (ppm) to a single decimal place; in instances where multiple resonances approximate the same chemical shift value, two decimal places are used. For ^{1}H and ^{13}C assignments, the following resveratrol numbering scheme was used, and each successive resveratrol equivalent was denoted

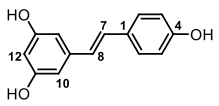

[2] Pangborn, A. B.; Giardello, M. A.; Grubbs, R. H.; Rosen, R. K.; Timmers, F. J. *Organometallics* **1996**, *15* (5), 1518–1520.
[3] Lin, H.S.; Paquette, L. A. *Synth. Commun.* **1994**, *24* (17), 2503–2506; Watson, S. C.; Eastham, J. F. *J. Organomet. Chem.* **1967**, *9* (1), 165–68.

with (a, b, c, etc.). Diastereotopic protons are denoted with (′), and protons found to exchange in the presence of D_2O are indicated with "exchangeable [D_2O]". Infrared data were obtained on a Perkin-Elmer Spectrum BX FT-IR spectrophotometer using an ATR mount with a ZnSe crystal and are reported as follows: [frequency of absorption (cm^{-1}), intensity of absorption (s = strong, m = medium, w = weak, br = broad)]. High-resolution mass spectra (HRMS) were obtained on a Micromass AutoSpec Ultima Magnetic Sector mass spectrometer using electrospray ionization (ESI), positive ion mode—we thank James Windak and Paul Lennon at the University of Michigan Department of Chemistry instrumentation facility for conducting these experiments. X-ray crystallographic data were collected on a Rigaku AFC10K Saturn 944+ CCD-based X-ray diffractometer—we thank Dr. Jeff W. Kampf for conducting these experiments.

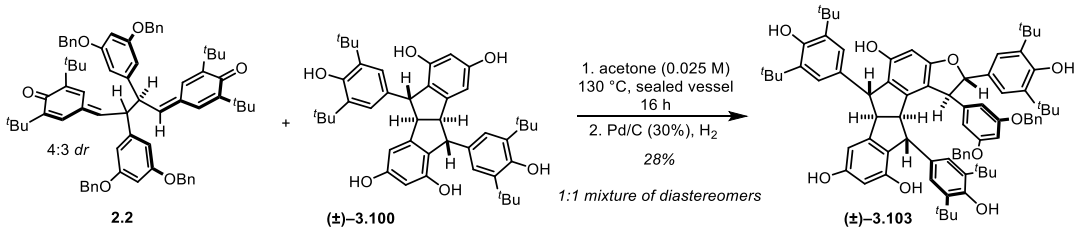

(1S,2S,6aR,11R,11aR)-2,6,11-tris(3,5-di-tert-butyl-4-hydroxyphenyl)-1-(3,5-dihydroxyphenyl)-1,2,6,6a,11,11a-hexahydroindeno[1',2':2,3]indeno[5,4-b]furan-5,8,10-triol (3.103):

A suspension of starting bis-*para*-quinone methide (2.2) (17 g, 17 mmol, 2.00 equiv) and starting [3.3.0] (3.100) (5.7 g, 8.4 mmol, 2.00 equiv) was prepared in degassed acetone (162 mL, 0.052 M) at room temperature in a 500 mL sealed vessel. The vessel was tightly sealed and the slowly stirring mixture heated to 130 °C behind a blast shield. At 16 h, the reaction was removed from the heated oil bath and allowed to cool to room temperature over the course of 0.5 h. TLC showed nearly complete consumption of [3.3.0] bicycle. Column chromatography was performed using a gradient of 1% acetone in DCM to 15% acetone to remove unreacted QMD however the isolated fractions contained various isomers. A slower gradient was performed to yield a fraction containing 3.5 grams of two trimer products that were inseparable from each other. This material was pushed forward with hydrogenolysis. The trimer material was dissolved in degassed methanol (300 mL) and 30% palladium on carbon (1 gram, 2.9 mmol, 1 equivalent) was added to the flask. The reaction mixture was charged with hydrogen gas and sparged for 30 min. TLC analysis at 12 h revealed full conversion to the desired product, and the reaction was sparged with argon. A slurry was made by adding celite which was then filtered off slowly and washed continuously with EtOAc (50 mL) so as to not let the filtrate go dry which creates a fire risk. The crude solution was then concentrated in vaccuo. The crude contained black residue from the Pd/C and was redissolved in 15% acetone in CH_2Cl_2 which was run through a silica plug and eluted with the same solvent

ratio. Column chromatography using a gradient of 1% acetone to 20% acetone in CH_2Cl_2 isolated the regiosiomer mixture with the above product as an inseparable mixture of diastereomers (1:1). Characterization data for the above regioisomer is provided below:

TLC (CH_2Cl_2/Acetone, 90:10), R_F:	0.75 (UV, *p*-anisaldehyde (red));
^{1}H NMR (700 MHz, acetone-D_6, 25 °C) δ:	δ 7.99 (s, exchangeable, 4H), 7.72 (s,, exchangeable 1H), 7.22 (s, 2H), 7.11 (s, 2H), 6.77 (s, 2H), 6.62 (d, 1H), 6.25 (s, 1H), 6.23 (t, J = 1.9 Hz, 1H), 6.19 (d, J = 2.0 Hz, exchangeable, 2H), 6.16 (d, J = 1.6 Hz, 1H), 6.08 (s, exchangeable, 1H), 5.76 (s, exchangeable, 1H), 5.61 (s, exchangeable, 1H), 5.30 (d, J = 5.4 Hz, 1H), 4.93 (d, J = 5.3 Hz, 1H), 4.67 (d, J = 8.0 Hz, 2H), 3.91 – 3.87 (m, J = 2.9 Hz, 2H), 3.82 (s, 1H), 1.40 (s, 36H), 1.25 (s, 18H).
^{13}C NMR (176 MHz, acetone-D_6, 25 °C) δ:	δ 161.8, 158.7, 158.1, 154.5, 154.3, 153.8, 151.9, 151.7, 149.0, 145.8, 144.4, 137.3, 136.8, 136.6, 136.4, 136.0, 133.2, 124.4, 123.8, 123.7, 123.3, 122.5, 116.0, 106.0, 102.4, 101.5, 101.3, 95.8, 94.5, 68.8, 59.8, 58.6, 55.0, 54.6, 53.2, 50.5, 34.3, 34.2, 34.0, 31.1, 29.9, 29.8, 29.7, 29.7, 29.4, 29.3, 29.2, 29.1, 29.0, 28.8, 28.7, 28.6;
FTIR (neat) cm^{-1}	3464.98 cm^{-1}, 2959.97 cm^{-1}, 1602.57 cm^{-1}, 1434.91 cm^{-1}, 1208.62 cm^{-1}, 1154.27 cm^{-1}, 1119.35 cm^{-1}, 1080.73 cm^{-1}, 995.02 cm^{-1}, 838.23 cm^{-1}, 770.31 cm^{-1}, 694.67 cm^{-1}
HRMS (APCI+)	*m/z* calculated for $C_{66}H_{80}O_9$ $[M+H]^+$: 1017.5875, found 1017.5883

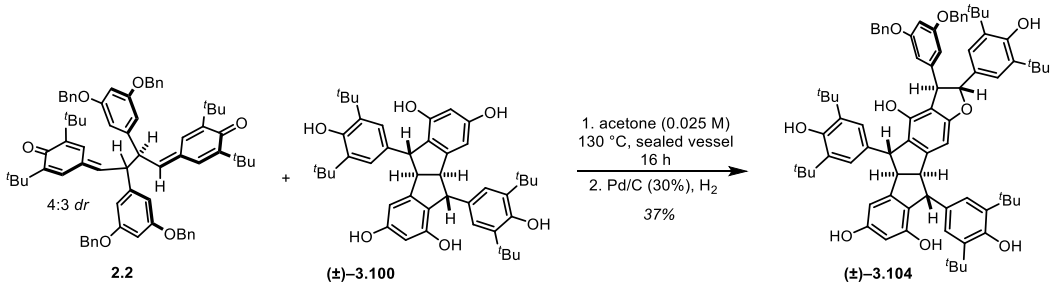

(2R,3R,5R,5aR,10R,10aR)-2,5,10-tris(3,5-di-tert-butyl-4-hydroxyphenyl)-3-(3,5-dihydroxyphenyl)-2,3,5,5a,10,10a-hexahydroindeno[1',2':2,3]indeno[5,6-b]furan-4,7,9-triol (3.104):

A suspension of starting bis-*para*-quinone methide (2.2) (17 g, 17 mmol, 2.00 equiv) and starting [3.3.0] (3.100) (5.7 g, 8.4 mmol, 2.00 equiv) was prepared in degassed acetone (162 mL, 0.052 M) at room temperature in a 500 mL sealed vessel. The vessel was tightly sealed and the slowly stirring mixture heated to 130 °C behind a blast shield. At 16 h, the reaction was removed from the heated oil bath and allowed to cool to room temperature over the course of 0.5 h. TLC showed nearly complete consumption of [3.3.0] bicycle. Column chromatography was performed using a gradient of 1% acetone in DCM to 15% acetone to remove unreacted QMD however the isolated fractions contained various isomers. A slower gradient was performed to yield a fraction containing 3.5 grams of two trimer products that were inseparable from each other. This material was pushed forward with hydrogenolysis. The trimer material was dissolved in degassed methanol (300 mL) and 30% palladium on carbon (1 gram, 2.9 mmol, 1 equivalent) was added to the flask. The reaction mixture was charged with hydrogen gas and sparged for 30 min. TLC analysis at 12 h revealed full conversion to the desired product, and the reaction was sparged with argon. A slurry was made by adding celite which was then filtered off slowly and washed continuously with EtOAc (50 mL) so as to not let the filtrate go dry which creates a fire risk. The crude solution was then concentrated in vaccuo. The crude contained black residue from the Pd/C and was redissolved

in 15% acetone in CH_2Cl_2 which was run through a silica plug and eluted with the same solvent ratio. Column chromatography using a gradient of 1% acetone to 20% acetone in CH_2Cl_2 isolated the regiosiomer mixture with the above product as an inseparable mixture of diastereomers (1:1). Characterization data for the above regioisomer is provided below:

TLC (CH_2Cl_2/Acetone, 90:10), R_F:	0.20 (UV, *p*-anisaldehyde (red));
^{1}H NMR (700 MHz, acetone-D_6, 25 °C) δ:	δ 8.1 (s, exchangeable, 2H), 8.0 (s, exchangeable, 1H), 8.0 (s, 1H), 7.3 (s, 2H), 7.0 (s, 2H), 6.8 (s, 2H), 6.7 (s, exchangeable, 1H), 6.6 (d, J = 1.2 Hz, 1H), 6.4 (s, 1H), 6.2 (t, J = 1.8 Hz, 1H), 6.1 (d, J = 1.7 Hz, 1H), 6.0 (s, exchangeable,1H), 5.8 (s, exchangeable, 1H), 5.6 (s, exchangeable, 1H), 5.4 (d, J = 1.2 Hz, 1H), 4.7 (s, 1H), 4.6 (d, J = 1.3 Hz, 1H), 4.4 (s, 1H), 3.92 – 3.88 (m, 2H), 1.4 (s, 18H), 1.4 (s, 18H), 1.34 (s, 18H).
^{13}C NMR (176 MHz, acetone-D_6, 25 °C) δ:	δ 162.5, 159.3, 158.1, 154.9, 154.3, 153.4, 151.8, 151.7, 149.0, 148.2, 144.1, 137.4, 137.2, 136.9, 136.6, 136.6, 133.6, 124.5, 123.6, 123.4, 122.7, 121.5, 115.3, 105.2, 101.9, 101.4, 101.3, 95.6, 93.3, 60.1, 59.8, 56.2, 53.6, 48.8, 34.3, 34.2, 34.2, 30.0, 29.9, 29.9, 29.8, 29.8, 29.7
FTIR (neat) cm^{-1}	3634.0 cm-1, 3510.7 cm-1, 2957.9 cm-1, 1601.9 cm-1, 1435.4 cm-1, 1234.3 cm-1, 1153.8 cm-1, 997.6 cm-1, 835.5 cm-1,768.8 cm-1
HRMS (APCI+)	*m/z* calculated for $C_{66}H_{80}O_9$ $[M+H]^+$: 1017.5875, found 1017.5892

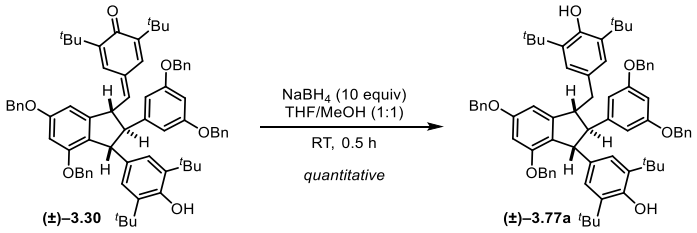

4-((1*R*,2*R*,3*R*)-5,7-bis(benzyloxy)-2-(3,5-bis(benzyloxy)phenyl)-3-(3,5-di-*tert*-butyl-4-hydroxybenzyl)-2,3-dihydro-1*H*-inden-1-yl)-2,6-di-*tert*-butylphenol (3.77a): The reaction vessel was charged with starting quinone methide (290 mg, 0.279 mmol, 1.00 equiv.) and $NaBH_4$ (106 mg, 2.79 mmol, 10.00 equiv). The mixture was taken up in THF (5.5 mL) at room temperature under inert atmosphere. To the faint yellow stirring solution was carefully added MeOH (5.5 mL), causing it to immediately become colorless with concomitant H_2-evolution. While the starting material and product have nearly identical R_F values, reaction progress can be monitored by the use of *p*-anisaldehyde stain, the action of which turns the starting material yellow-orange and the product pink. TLC analysis at 0.5 h indicated full conversion to **(3.77a)**, and the excess reductant was quenched by careful addition of sat. aq. NH_4Cl. MeOH was then removed from the heterogeneous mixture by rotary evaporation. The crude material was then dissolved into a mixture of EtOAc/H_2O, and transferred to a separatory funnel where the phases were separated. The aqueous layer was further extracted with additional portions of EtOAc. The organic layers were combined, washed with brine, dried over Na_2SO_4 and concentrated in vacuo to yield the desired **(3.77a)** (290 mg, 0.278 mmol, quantitative yield) as a white foam, which was carried on without further purification.

TLC (Hexanes/EtOAc, 85:15), R_F: 0.41 (UV, *p*-anisaldehyde (pink));

^{1}H NMR (500 MHz, $CDCl_3$, 25 °C) δ:	7.47 – 7.28 (m, 15H), 7.14 – 7.09 (m, 3H), 6.89 (s, 2H), 6.79 (s, 2H), 6.73 (m, 2H), 6.50 (d, *J* = 1.3 Hz, 1H), 6.41 (t, *J* = 2.0 Hz, 1H), 6.33 (d, *J* = 1.3 Hz, 1H), 6.19 (d, *J* = 2.0 Hz, 2H), 5.01 (d, *J* = 10.0 Hz, 1H), 4.99 (d, *J* = 10.0 Hz, 1H), 4.97 (d, *J* = 11.5 Hz, 1H), 4.95 (d, *J* = 11.5 Hz, 1H), 4.90 (d, *J* = 12.0 Hz, 1H), 4.88 (d, *J* = 11.7 Hz, 1H), 4.86 (d, *J* = 11.7 Hz, 1H), 4.82 (d, *J* = 12.0 Hz, 1H), 4.30 (d, *J* = 6.0 Hz, 1H), 3.59 (ddd [apparent quartet], *J* = 6.4, 7.3, 7.8 Hz, 1H), 3.02 (dd, *J* = 7.3, 13.9 Hz, 1H), 3.00 (dd [apparent triplet], *J* = 6.0, 6.4 Hz, 1H), 2.94 (dd, *J* = 7.8, 13.9 Hz, 1H), 1.35 (s, 18H), 1.33 (s, 18H);
^{13}C NMR (125 MHz, $CDCl_3$, 25 °C) δ:	160.0, 159.9, 156.0, 152.1, 152.0, 149.1, 148.6, 137.3, 137.18, 137.16, 136.15, 135.7, 135.4, 130.7, 128.8, 128.7, 128.3, 128.2, 128.1, 127.9, 127.8, 127.4, 126.5, 126.2, 125.2, 124.2, 106.8, 102.1, 99.8, 99.6, 70.4, 70.1, 69.5, 62.5, 57.5, 54.3, 41.9, 34.5, 34.4, 30.7, 30.6;
HRMS (ESI):	*m/z* calculated for $C_{72}H_{81}O_6$ $[M+H]^+$: 1041.6028, found 1041.6022;
FTIR (neat) cm^{-1}:	3629 (w), 2953 (m), 1593 (s), 1434 (s), 1374 (m), 1313 (m), 1232 (m), 1145 (s), 1047 (m).

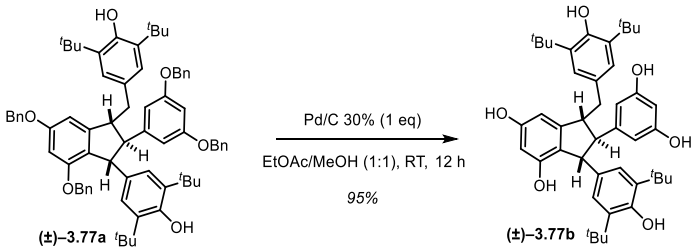

(1*R*,2*R*,3*R*)-1-(3,5-di-*tert*-butyl-4-hydroxybenzyl)-3-(3,5-di-*tert*-butyl-4-hydroxyphenyl)-2-(3,5-dihydroxyphenyl)-2,3-dihydro-1*H*-indene-4,6-diol (3.77b): A solution of starting indane (100 mg, 0.096 mmol, 1.00 equiv prepared in 1:1 EtOAc/MeOH (10.0 mL, 0.01 M) under inert atmosphere using solvents degassed prior to use. 30% Pd/C was added (34 mg, 0.96 mmol, 1 equiuivalent). The reaction was then charged with hydrogen gas and sparged continuously for 30 minutes. TLC analysis at 12 h revealed full conversion to the desired product, and the reaction was sparged with argon. A slurry was made by adding celite which was then filtered off slowly and washed continuously with EtOAc (50 mL) so as to not let the filtrate go dry which creates a fire risk. The crude solution was then concentrated in vaccuo. The crude contained black residue from the Pd/C and was redissolved in 1:9 acetone/CH2Cl2 which was run through a silica plug and eluted with the same solvent ratio. The desired **3.77b** (59 mg, 0.086 mmol, 90% yield) was isolated from the crude material as a white foam.

TLC (CH_2Cl_2/MeOH, 95:5), R_F:	0.17 (UV, *p*-anisaldehyde (red));
^{1}H NMR (500 MHz, acetone-d_6, 25 °C) δ:	8.00 (s, br, 1H, exchangeable [D_2O]), 7.97 (s, br, 1H, exchangeable [D_2O]), 7.21 (s, br, 1H, exchangeable [D_2O]), 6.90 (s, br, 2H), 6.82 (s, br, 2H), 6.29 (d, br, *J* = 1.5 Hz, 1H), 6.24 (d, br, *J* = 1.5 Hz, 1H), 6.15 (t, br, *J* = 1.5 Hz, 1H), 6.01

	(d, br, J = 1.5 Hz, 2H), 5.79 (s, br, 1H, exchangeable [D_2O]), 5.72 (s, br, 1H, exchangeable [D_2O]), 4.25 (d, J = 3.9 Hz, 1H), 3.37 (ddd, J = 4.2, 6.6, 8.1 Hz, 1H), 2.91 (dd [apparent triplet], J = 3.9, 4.2 Hz, 1H), 2.86 (dd, J = 6.6, 13.7 Hz, 1H), 2.79 (s, br, 1H, exchangeable [D_2O]), 2.77 (dd, J= 8.1, 13.7 Hz, 1H), 1.37 (s, 18H), 1.34 (s, 18H);
^{13}C NMR (175 MHz, acetone-d_6, 25 °C) δ:	159.3, 159.1, 155.3, 152.94, 152.86, 150.8, 150.5, 137.71, 137.69, 137.1, 131.8, 126.6, 124.7, 121.7, 106.3, 104.2, 102.2, 101.2, 61.8, 57.0, 55.6, 42.7, 35.2, 35.1, 30.90, 30.86;
HRMS (ESI):	*m/z* calculated for $C_{44}H_{57}O_6$ $[M+H]^+$: 681.4150, found 681.4148;
FTIR (neat) cm^{-1}:	3322 (m, br), 2957 (m), 1600 (s), 1434 (s), 1360 (s), 1230 (s), 1156 (m), 1134 (m), 1006 (w).

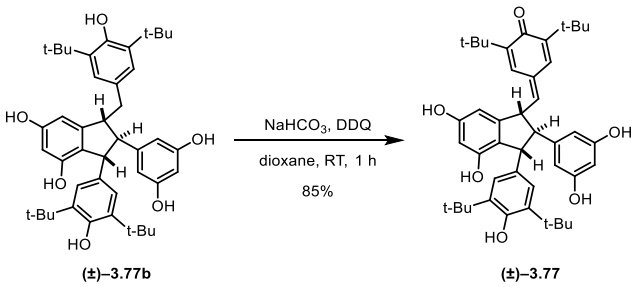

2,6-di-tert-butyl-4-(((1R,2R,3R)-3-(3,5-di-tert-butyl-4-hydroxyphenyl)-2-(3,5-dihydroxyphenyl)-4,6-dihydroxy-2,3-dihydro-1H-inden-1-yl)methylene)cyclohexa-2,5-dien-1-one (3.77): Starting phenol (3.77b) (37 mg, 0.055 mmol, 1.00 equiv) and $NaHCO_3$ (46 mg, 0.55 mmol, 10 equiv) were stirred in dioxane (1.0 mL) at 23 °C under inert atmosphere. In separate vessel, a solution of DDQ (14 mg, 0.061 mmol, 1.1 equiv) in dioxane (1.7 mL) was prepared. The solution of DDQ was added dropwise to the reaction mixture. Reaction progress was monitored by TLC and the reaction as quenched at 1 h with 10% aq. $Na_2S_2O_3$. The mixture was diluted with ethyl acetate and transferred to a separatory funnel containing sat. aq. Na_2CO_3 The aqueous phase was extracted with ethyl acetate (2x). Combined organic layers were washed with sat. aq. Na_2CO_3 (2x), dried over Na2SO4, and concentrated *in vacuo*. (NOTE: Do not expose material to alcoholic/nucleophilic solvents [e.g. iPrOH, MeOH, etc.], as the corresponding ether adduct forms readily). The resulting residue was purified by preparative TLC using 8% acetone in CH_2Cl_2 mobile phase to give quinone methide as a red amorphous solid (31 mg, 0.046 mmol, 85% yield). This material was then triterated by sonication in CH_2Cl_2 to yield a pale off white solid (NOTE: (3.77) is not stable to prolonged storage in solution and should be stored at –20 °C under inert atmosphere or used immediately).

TLC (Hexanes/EtOAc, 4:1), R_F:	0.57 (UV, *p*-anisaldehyde (yellow-orange));
^{1}H NMR (500 MHz, acetone-d_6, 25 °C) δ:	8.12 (br s, 3H), 7.28 (d, *J* = 2.2 Hz, 1H), 7.20 (br s, 1H), 7.03 (d, *J* = 2.2 Hz, 1H), 6.89 (s, 2H), 6.53 (d, *J* = 9.5 Hz, 1H), 6.33 (d, *J* = 2.0 Hz, 1H), 6.24 (d, *J* = 2.0 Hz, 1H), 6.23 (d, *J* = 2.0 Hz, 1H), 6.17 (d, *J* = 2.0 Hz, 1H), 5.83 (s, 1H), 4.63 (t, *J* = 9.5 Hz, 1H), 4.42 (d, *J* = 8.2 Hz, 1H), 3.02 (dd [apparent triplet], *J* = 8.2 Hz, 1H), 1.34 (s, 18 H), 1.26 (s, 9H), 1.22 (s, 9H);
^{13}C NMR (125 MHz, acetone-d_6, 25 °C) δ:	187.1, 159.7, 159.5, 155.6, 153.3, 150.3, 148.9, 148.1, 147.2, 145.5, 137.8, 135.9, 134.7, 133.3, 128.2, 124.9, 121.4, 107.5, 104.1, 103.2, 102.0, 66.4, 57.4, 52.9, 35.9, 35.5, 35.2, 30.8, 29.9, 29.8;

All characterization data consistent with that reported.[4]

[4] Li, W.; Li, H.; Li, Y.; Hou, Z. *Angew. Chem. Int. Ed.* **2006**, *45* (45), 7609–7611.

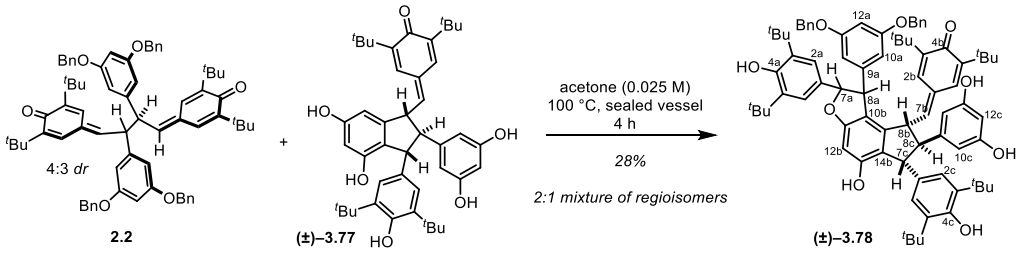

5-((1S,2S,6R,7R,8R)-1-(3,5-bis(benzyloxy)phenyl)-8-(3,5-di-tert-butyl-4-hydroxybenzyl)-2,6-bis(3,5-di-tert-butyl-4-hydroxyphenyl)-5-hydroxy-1,6,7,8-tetrahydro-2H-indeno[5,4-b]furan-7-yl)benzene-1,3-diol (3.78): A suspension of starting bis-*para*-quinone methide 2.2 (39 mg, 0.038 mmol, 1.00 equiv) and starting indane 3.77 (51 mg, 0.075 mmol, 2.00 equiv) was prepared in acetone (1.52 mL, 0.025 M) at room temperature in a 2 dram vial. The vessel was tightly sealed and the slowly stirring mixture heated to 100 °C. At 4 h, the reaction was removed from the heat and allowed to cool to room temperature over the course of 0.5 h. TLC confirmed full consumption of 3.77. Column chromatography using 20%, then 30% of a 3:1 EtOAc/acetone mixture in hexanes afforded the disproportionation product 3.71 (24 mg, 0.046 mmol, 123% yield),[5] four products of intermediate Rf (30 mg collectively), and recovered 2.2 (30 mg, 0.044 mmol, 59% recovery). The mixture of ≥4 compounds was further purified by preparative thin layer chromatography (plate developed 3x using 1% EtOH in CH_2Cl_2) and the desired product **3.78** was isolated as a tan amorphous solid (8.0 mg, 0.0067 mmol, 18% yield) along with an impure sample containing mostly a diastereomer of **3.78** (4.7 mg, 10% yield). Characterization data for the major diastereomer is provided below:

[5] Full disproportionation can generate 2 equiv. of stilbene**Error! Reference source not found.** relative to the starting indane, but only 1 equiv. i s theoretically needed, hence the yield >100%

TLC (CH_2Cl_2/Acetone, 95:5), R_F: 0.22 (UV, *p*-anisaldehyde (red));

^{1}H NMR (500 MHz, $CDCl_3$, 25 °C) δ: 7.42 – 7.28 (m, 10H, –$OCH_2C_6\underline{H}_5$), 7.13 (s, 2H, C_{2a}–$\underline{H}$), 6.92 (s, 2H, C_{2c}–$\underline{H}$), 6.56 (s, br, overlap, 2H, C_{10a}–$\underline{H}$), 6.55 (s, overlap, 1H, C_{12b}–$\underline{H}$), 6.45 (s, br, 1H, C_{12a}–$\underline{H}$), 6.43 (s, 2H, C_{2b}–$\underline{H}$), 6.02 (s, C_{12c}–$\underline{H}$), 5.57 (s, 2H, C_{10c}–$\underline{H}$), 5.51 (d, *J* = 2.9 Hz, 1H, C_{7a}–$\underline{H}$), 5.22 (s, 1H, –O$\underline{H}$, exchangeable [D_2O]), 5.10 (s, 1H, –O$\underline{H}$, exchangeable [D_2O]), 4.95 (d, *J* = 11.5 Hz, 2H, –OC$\underline{H}_2C_6H_5$), 4.92 (d, *J* = 11.5 Hz, 2H, –OC$\underline{H}_2C_6H_5$), 4.56 (s, br, 1H, –O$\underline{H}$, exchangeable [D_2O]), 4.48 (d, *J* = 2.9 Hz, 1H, C_{8a}–$\underline{H}$), 4.40 (s, br, 1H, –O$\underline{H}$, exchangeable [D_2O]), 4.25 (d, *J* = 2.0 Hz, 1H, C_{7c}–$\underline{H}$), 3.19 (ddd, br, *J* = 2.7, 3.4, 11.7 Hz, 1H, C_{8b}–$\underline{H}$), 2.90 (dd [apparent triplet], *J* = 2.0, 2.7 Hz, 1H, C_{8c}–$\underline{H}$), 2.47 (dd, *J* = 3.4, 13.5 Hz, 1H, C_{7b}–$\underline{H}$), 1.98 (dd, *J* = 11.7, 13.5 Hz, 1H, $C_{7b'}$–$\underline{H}$), 1.42 (s, 18H, C_{3a}–C(C$\underline{H}_3)_3$), 1.34 (s, 18H, C_{3c}–C(C$\underline{H}_3)_3$), 1.25 (s, 18H, C_{3b}–C(C$\underline{H}_3)_3$);

^{13}C NMR (125 MHz, $CDCl_3$, 25 °C) δ: 162.8 ($\underline{C}_{11b}$), 160.7 (br, $\underline{C}_{11a}$), 156.6 ($\underline{C}_{11c}$), 153.9 ($\underline{C}_{4a}$), 153.5 ($\underline{C}_{13b}$), 153.0 ($\underline{C}_{4c}$), 151.8 ($\underline{C}_{4b}$), 150.9 ($\underline{C}_{9c}$), 148.0 ($\underline{C}_{9a}$), 145.1 ($\underline{C}_{9b}$), 136.9 (–$OCH_2\underline{C}_6H_5$), 136.5 ($\underline{C}_{3c}$), 136.3 ($\underline{C}_{3a}$), 135.7 ($\underline{C}_{3b}$), 134.1 ($\underline{C}_{1c}$), 133.2 ($\underline{C}_{1a}$), 131.2 ($\underline{C}_{1b}$), 128.7 (–$OCH_2\underline{C}_6H_5$), 128.2 (–$OCH_2\underline{C}_6H_5$), 127.9 (–$OCH_2\underline{C}_6H_5$), 125.8 ($\underline{C}_{2b}$), 124.2 ($\underline{C}_{2c}$), 122.7 ($\underline{C}_{14b}$), 122.2 ($\underline{C}_{2a}$), 117.7 ($\underline{C}_{10b}$), 107.0 (br, $\underline{C}_{10a}$), 106.1 ($\underline{C}_{10c}$), 100.6 ($\underline{C}_{12a}$), 100.3 ($\underline{C}_{12c}$), 96.8 ($\underline{C}_{12b}$), 94.1 ($\underline{C}_{7a}$), 70.2 (–O$\underline{C}H_2C_6H_5$), 59.2 ($\underline{C}_{8c}$), 56.4 ($\underline{C}_{8a}$), 56.2 ($\underline{C}_{8b}$), 55.1 ($\underline{C}_{7c}$), 41.1 ($\underline{C}_{7b}$), 34.62 (C_{3a}–$\underline{C}(CH_3)_3$), 34.58 (C_{3c}–$\underline{C}(CH_3)_3$), 34.3 (C_{3b}–$\underline{C}(CH_3)_3$), 30.54 (C_{3c}–C($\underline{C}H_3)_3$), 30.52 (C_{3b}–C($\underline{C}H_3)_3$), 30.44 (C_{3a}–C($\underline{C}H_3)_3$);

HRMS (ESI): *m/z* calculated for $C_{44}H_{57}O_6$ $[M+H]^+$: 1199.6971, found 1199.6970;

FTIR (neat) cm^{-1}: 3638 (w), 2956 (m), 1594 (s), 1434 (s), 1365 (m), 1316 (m), 1234 (m), 1153 (s), 1082 (w), 1052 (m).

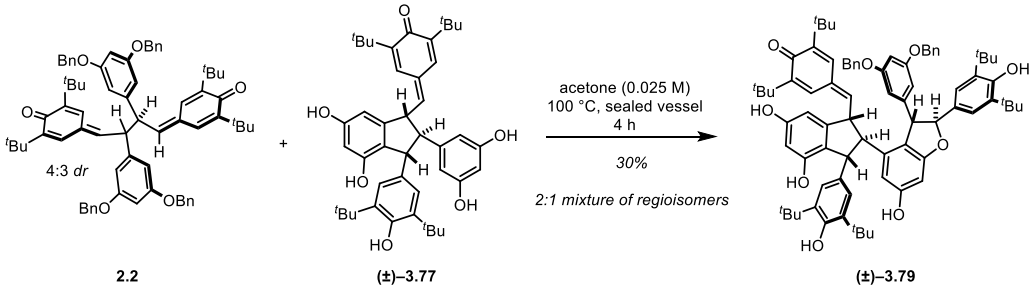

4-(((1S,2S,6R,7R,8R)-1-(3,5-bis(benzyloxy)phenyl)-2,6-bis(3,5-di-tert-butyl-4-hydroxyphenyl)-7-(3,5-dihydroxyphenyl)-5-hydroxy-1,6,7,8-tetrahydro-2H-indeno[5,4-b]furan-8-yl)methylene)-2,6-di-tert-butylcyclohexa-2,5-dien-1-one (3.79): A suspension of starting bis-*para*-quinone methide (2.2) (95 mg, 0.092 mmol, 2.00 equiv) and starting indane (31 mg, 0.046 mmol, 1.00 equiv) was prepared in acetone (400 μL) at room temperature in a 1 dram vial. The vessel was tightly sealed and the slowly stirring mixture heated to 100 °C. At 4 h, the reaction was removed from the heat and allowed to cool to room temperature over the course of 0.5 h. The solvent was removed *in vacuo* and the resultant residue was purified by preparative TLC (96:4 CH_2Cl_2/Acetone) to afford (3.79) as a pale pink amorphous solid (8.0 mg, 0.0067 mmol, 18% yield) as well an impure sample containing mostly a diastereomer of (3.78) (4.0 mg, 0.0034 mmol, 9% yield). (NOTE: these intermediates are not stable to prolonged storage in solution and should be stored at –20 °C under inert atmosphere or used immediately). Partial characterization data for the major diastereomer is provided below, but otherwise complete characterization was performed after the subsequent step (consult next page).

TLC (CH_2Cl_2/Acetone, 95:5), R_F: 0.48 (UV, vanillin (pale red));

^{1}H NMR (500 MHz, $CDCl_3$, 25 °C) δ:	7.41 – 7.29 (m, overlap, 6H), 7.09 (s, 2H), 6.89 (s, 2H), 6.75 (d, *J* = 2.0 Hz, 1H), 6.54 (s, 1H), 6.51 (t, *J* = 2.2 Hz, 1H), 6.32 (d, *J* = 2.2 Hz, 2H), 6.16 (t, *J* = 2.2 Hz, 1H), 6.11 (d, *J* = 2.2 Hz, 2H), 5.98 (d, *J* = 2.0 Hz, 1H), 5.64 (d, *J* = 10.5 Hz, 1H), 5.40 (d, *J* = 3.9 Hz, 1H), 5.21 (s, 1H), 5.17 (s, 1H), 4.91 (m br, 2H), 4.70 (m, br, 2H), 4.45 (dd, *J* = 8.3, 10.5 Hz, 1H), 4.33 (d, *J* = 8.3 Hz, 1H), 4.25 (d, *J* = 3.9 Hz, 1H), 2.88 (dd [apparent triplet], *J* = 8.3 Hz, 1H), 1.40 (s, 18H), 1.34 (s, 18H), 1.15 (s, 9H), 1.09 (s, 9H);
^{13}C NMR (125 MHz, $CDCl_3$, 25 °C) δ:	186.9, 163.0, 160.4, 157.0, 154.0, 153.8, 153.6, 148.1, 147.8, 147.4, 146.1, 144.7, 141.5, 136.9, 136.8, 136.3, 135.0, 132.8, 131.4, 131.1, 128.8, 128.3, 127.9, 126.4, 124.2, 122.1, 117.8, 107.8, 106.8, 101.6, 101.2, 97.8, 94.0, 70.1, 65.2, 56.4, 56.3, 54.0, 52.0, 35.3, 34.8, 34.62, 34.60, 30.45, 30.43, 29.6, 29.5.

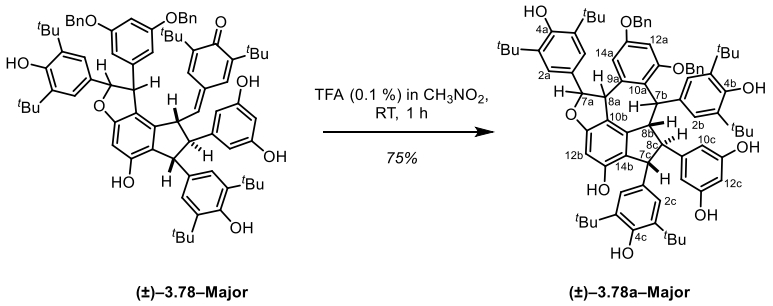

(±)–3.78–Major (±)–3.78a–Major

5-((3R,4R,4aS)-6,8-bis(benzyloxy)-3,5,10-tris(3,5-di-tert-butyl-4-hydroxyphenyl)-2-hydroxy-3,4,4a,5,9b,10-hexahydrobenzo[5,6]azuleno[7,8,1-cde]benzofuran-4-yl)benzene-1,3-diol (3.78a): The quinone methide intermediate 3.78 (8 mg, 0.0067 mmol, 1.00 equiv) was dissolved in 0.1% TFA in CH_3NO_2 (500 μL) and stirred at RT under inert atmosphere. After 1 hour, TLC showed full consumption of the starting material. A drop of Et_3N was added to quench the reaction and the solvent was removed *in vacuo*. The resulting residue was purified by preparative TLC (97:3 CH_2Cl_2/Acetone) to yield the cyclized product **3.78** (6 mg, 0.005 mmol, 75% yield) as a pale pink amorphous solid, determined to be a single diastereomer. The connectivity was rigorously assigned by 2D NMR, though the relative configuration at C_{7a}, C_{8a}, and C_{7b} could not be determined.

TLC (CH_2Cl_2/Acetone, 95:5), R_F:	0.22 (UV, vanillin (pale red));
^{1}H NMR (500 MHz, acetone-d_6, 25 °C) δ:	7.47 – 7.28 (m, 10H), 7.07 (s, 2H, C_{2a}–H), 6.90 (s, 1H, C_{14a}–H), 6.81 (s, 2H, C_{2c}–H), 6.73 (s, 2H, C_{2b}–H), 6.63 (s, 1H, C_{12a}–H), 6.17 (d, J = 3.4 Hz, 1H, C_{7a}–H), 6.16 (s, 1H, C_{12b}–H), 6.12 (t, J < 1.5 Hz, 1H, C_{12c}–H), 6.09 (d, J < 1.5 Hz, 2H, C_{10c}–H), 5.37 (s, 1H, C_{7b}–H), 5.13 (d, J = 11.7 Hz, 1H, –OC$H_2C_6H_5$), 5.12 (s, 1H, –OH), 5.09 (d, J = 11.7 Hz, 1H, –OC$H_2C_6H_5$), 4.99 (d, J = 11.3 Hz, 1H, –OC$H_2C_6H_5$), 4.95 (d, J = 11.3 Hz, 1H, –OC$H_2C_6H_5$), 4.87 (s, 1H, –OH),

4.43 (d, overlap, J = 3.4Hz, 1H, C_{8a}–H), 4.40 (d, J = 10.7 Hz, 1H, C_{7c}–H), 4.14 (br s, 2H, –OH), 4.01 (d, J = 11.2 Hz, 1H, C_{8b}–H), 2.97 (dd [apparent triplet], J = 10.7, 11.2 Hz, 1H, C_{8c}–H), 1.34 (s, 18H, C_{3a}–C(CH_3)$_3$), 1.32 (s, 18H, C_{3c}–C(CH_3)$_3$), 1.13 (s, 18H, C_{3b}–C(CH_3)$_3$);

^{13}C NMR (125 MHz, acetone-d_6, 25 °C) δ:

159.4 (C_{11b}), 159.3 (C_{11a}), 157.9 (C_{13a}), 156.7 (C_{11c}), 153.8 (C_{4a}), 153.5 (C_{13b}), 153.4 (C_{4c}), 151.5 (C_{4b}), 147.0 (C_{9a}), 143.4 (C_{9c}), 141.1 (C_{9b}), 137.4 (–OCH$_2$$C_6H_5$), 137.0 (–OCH$_2$$C_6H_5$), 136.6 ($C_{3c}$), 136.1 ($C_{3a}$), 135.1 ($C_{3b}$), 135.0 ($C_{1b}$), 132.9 ($C_{1a}$), 130.4 ($C_{1c}$), 128.90 (–OCH$_2$$C_6H_5$), 128.87(–OCH$_2$$C_6H_5$), 128.43 (–OCH$_2$$C_6H_5$), 128.37 (–OCH$_2$$C_6H_5$), 128.3 (–OCH$_2$$C_6H_5$), 127.9 (–OCH$_2$$C_6H_5$), 124.7 ($C_{2c}$), 124.5 ($C_{2b}$), 122.3 ($C_{2a}$), 120.2 ($C_{10a}$), 120.0 ($C_{10b}$), 118.8 ($C_{14b}$), 108.6 ($C_{10c}$), 104.3 ($C_{14a}$), 101.3 ($C_{12c}$), 98.4 ($C_{12a}$), 95.9 ($C_{12b}$), 86.7 ($C_{7a}$), 71.5 (–O$CH_2C_6H_5$), 70.4 (–O$CH_2C_6H_5$), 66.0 ($C_{8c}$), 55.3 ($C_{7c}$), 54.2 ($C_{8b}$), 51.3 ($C_{8a}$), 37.0 ($C_{7b}$), 34.6 (C–$C$(CH$_3$)$_3$), 34.5 (C–$C$(CH$_3$)$_3$), 34.4 (C–$C$(CH$_3$)$_3$), 30.51 (C–C($CH_3$)$_3$), 30.47 (C–C($CH_3$)$_3$), 30.4 (C–C($CH_3$)$_3$);

HRMS (ESI):

m/z calculated for $C_{80}H_{93}O_6$ $[M+H]^+$: 1197.6814, found 1197.6783;

FTIR (neat) cm^{-1}:

3178 (br), 2922 (s), 2855 (s), 1602 (s), 1452 (s), 1359 (m), 1211 (m), 1155 (s).

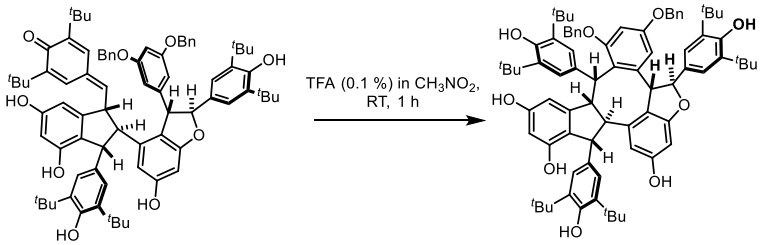

(±)–3.79–Minor (±)–3.79a–Minor

5-((3R,4R,4aS)-6,8-bis(benzyloxy)-3,5,10-tris(3,5-di-tert-butyl-4-hydroxyphenyl)-2-hydroxy-3,4,4a,5,9b,10-hexahydrobenzo[5,6]azuleno[7,8,1-cde]benzofuran-4-yl)benzene-1,3-diol (3.79a): Using the impure sample containing predominantly the minor diastereomer of quinone methide intermediate 3.79 (~5 mg), the acid-mediated *7-exo* Friedel–Crafts cyclization was performed as described in the previous entry. Isolation of the desired product was achieved by preparative TLC (97:3 CH_2Cl_2/Acetone) to yield the cyclized product 3.79a (~ 4 mg), determined to be a single diastereomer. The connectivity was rigorously assigned by 2D NMR, though the relative configuration at C_{7a}, C_{8a}, and C_{7b} could not be determined.

TLC (CH_2Cl_2/Acetone, 95:5), R_F:	0.22 (UV, vanillin (pale red));
^{1}H NMR (500 MHz, $CDCl_3$, 25 °C) δ:	7.37 – 7.27 (m, overlap, 8H, –OCH$_2$C$_6$H$_5$), 7.30 (s, 2H, C_{2a}–H), 7.21–7.19 (m, overlap, 2H, –OCH$_2$C$_6$H$_5$), 7.08 (s, 2H, C_{2b}–H), 6.92 (br s, 2H, C_{2c}–H), 6.54 (d, *J* = 2.2 Hz, 1H, C_{12a}–H), 6.38 (d, *J* = 2.2 Hz, 1H, C_{14a}–H), 6.30 (s, 1H, C_{12b}–H), 6.21 (t, *J* = 2.2 Hz, 1H, C_{12c}–H), 6.13 (d, *J* = 2.2 Hz, 2H, C_{10c}–H), 5.86 (d, *J* = 12.1 Hz, 1H, C_{7a}–H), 5.47 (d, *J* = 3.9 Hz, 1H, C_{7b}–H), 5.25 (s, 1H, C_{4a}–OH), 5.14 (s, 1H, C_{4c}–OH), 5.09 (d, *J* = 12.0 Hz, 1H, –OCH$_2$C$_6$H$_5$), 4.93 (d, *J* = 12.0 Hz, 1H, –OCH$_2$C$_6$H$_5$), 4.93 (s, 1H, C_{4b}–OH), 4.87 (d, *J* = 11.0 Hz, 1H, –OCH$_2$C$_6$H$_5$), 4.76 (d, *J* = 11.0 Hz, 1H, –OCH$_2$C$_6$H$_5$), 4.73 (br d, *J* = 12.1 Hz, 1H, C_{8a}–H), 4.67 (s, 1H, –OH), 4.22 (d, *J* = 10.3 Hz, 1H, C_{7c}–H), 3.80 (br dd, *J*

= 3.9, 11.5 Hz, 1H, C_{8b}–H), 3.37 (dd, *J* = 10.3, 11.5 Hz, 1H, C_{8c}–H), 1.36 (s, 18H, C_{3a}–C(CH_3)$_3$), 1.34 (s, 18H, C_{3c}–C(CH_3)$_3$), 1.21 (s, 18H, C_{3b}–C(CH_3)$_3$);

^{13}C NMR (125 MHz, $CDCl_3$, 25 °C) δ:

159.2 (C_{11b}), 157.7 (C_{13a}), 156.7 (C_{11a}), 156.6 (C_{11c}), 154.8 (C_{4a}), 153.5 (C_{4c}), 153.4 (C_{13b}), 151.8 (C_{4b}), 143.3 (C_{9c}), 142.6 (C_{9b}), 140.9 (C_{9a}), 137.2 (–$OCH_2C_6H_5$), 136.8 (–$OCH_2C_6H_5$), 136.7 (C_{3c}), 136.4 (C_{3a}), 135.3 (C_{3b}), 131.7 (C_{1b}), 129.7 (C_{1c}), 128.77 (–$OCH_2C_6H_5$), 128.75 (–$OCH_2C_6H_5$), 128.34 (–$OCH_2C_6H_5$), 128.31 (–$OCH_2C_6H_5$), 128.0 (–$OCH_2C_6H_5$), 127.8 (C_{10a}), 127.7 (–$OCH_2C_6H_5$), 126.7 (–$OCH_2C_6H_5$), 125.7 (C_{2b}), 125.3 (C_{2a}), 124.7 (C_{2c}—see footnote)[6], 118.0 (C_{14b}), 116.3 (C_{10b}), 108.5 (C_{10c}), 105.7 (C_{14a}), 101.4 (C_{12c}), 99.5 (C_{12a}), 96.5 (C_{12b}), 92.6 (C_{7a}), 70.7 (–$OCH_2C_6H_5$), 70.2 (–$OCH_2C_6H_5$), 62.3 (C_{8c}), 56.4 (C_{7c}), 50.7 (C_{8b}), 47.7 (C_{8a}), 37.9 (C_{7b}), 34.59 (C_{3c}–C(CH_3)$_3$), 34.55 (C_{3a}–C(CH_3)$_3$), 34.4 (C_{3b}–C(CH_3)$_3$), 30.6 (C_{3b}–C(CH_3)$_3$), 30.55 (C_{3c}–C(CH_3)$_3$), 30.45 (C_{3a}–C(CH_3)$_3$).

[6] Resonance for C_{2c} is broadened (presumably due to restricted rotation) to the point that it is not visible above the noise. This is consistent with broadening of C_{2c}–H in the ^{1}H-NMR spectrum. The existence of the ^{13}C–resonance at this frequency was confirmed by correlations in both the HSQC and HMBC spectra

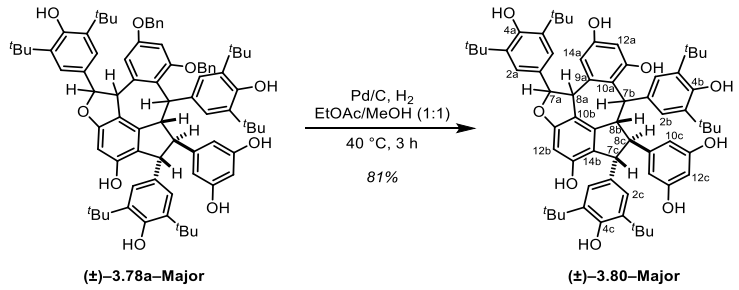

(3R,4R,4aS)-3,5,10-tris(3,5-di-tert-butyl-4-hydroxyphenyl)-4-(3,5-dihydroxyphenyl)-3,4,4a,5,9b,10-hexahydrobenzo[5,6]azuleno[7,8,1-cde]benzofuran-2,6,8-triol (3.80): A round bottom flask was charged with the major diastereomer of dibenzylated trimer X.X (6 mg, 0.005 mmol, 1.00 equiv) and Pd/C (30 wt%, 1 mg) and the flask was sealed and purged with N_2. EtOAc (HPLC grade, 500 μL) and MeOH (HPLC grade, 500 μL) were sequentially added and N_2 inlet was replaced with a H_2 balloon. The mixture was gently sparged with H_2 for 10 minutes at room temperature, at which point the vent needle was removed and the reaction mixture was warmed to 40 °C under H_2 (1 atm). After 3 h, the reaction was removed from the heat source, cooled to room temperature, and the contents filtered through a short plug of Celite, eluting with 1:1 EtOAc/MeOH. The filtrate was concentrated to dryness *in vacuo* and the resulting residue was purified by preparative TLC (90:10 CH_2Cl_2/Acetone) to afford **3.80** (4.1 mg, 0.004 mmol, 81% yield) as a single diastereomer. The connectivity was rigorously assigned by 2D NMR, though the relative configuration at C_{7a}, C_{8a}, and C_{7b} could not be determined.

TLC (CH_2Cl_2/Acetone, 95:5), R_F:	0.15 (UV, vanillin (pale red));
^{1}H NMR (500 MHz, $CDCl_3$, 25 °C) δ:	8.26 (br s, 1H), 8.11 (br s, 1H), 8.03 (br s, 1H), 7.16 (s, 2H, C_{2a}–H), 6.91 (s, 2H, C_{2b}–H), 6.81 (s, 2H, C_{2c}–H), 6.73 (d, *J* = 1.7 Hz, 1H, C_{14a}–H), 6.59 (br s, 1H), 6.53 (d, *J* = 2.0

Hz, 2H, C_{10c}–H), 6.42 (d, *J* = 1.7 Hz, 1H, C_{12a}–H), 6.24 (t, overlap *J* = 2.0 Hz, 1H, C_{12c}–H), 6.23 (d, overlap, *J* = 2.0 Hz, 1H, C_{7a}–H), 6.10 (s, 1H, C_{12b}–H), 5.95 (s, 1H, C_{4a}–OH), 5.74 (s, 1H, C_{4c}–OH), 5.58 (s, 1H, C_{4b}–OH), 5.34 (s, 1H, C_{7b}–H), 4.48 (d, *J* = 10.0 Hz, 1H, C_{7c}–H), 4.42 (d, *J* = 2.0 Hz, 1H, C_{8a}–H), 4.16 (d, *J* = 11.7 Hz, 1H, C_{8b}–H), 2.96 (dd [apparent triplet], *J* = 10.0, 11.7 Hz, 1H, C_{8c}–H), 1.35 (s, 18H, C_{3a}–C(CH_3)$_3$), 1.28 (s, 18H, C_{3c}–C(CH_3)$_3$), 1.16 (s, 18H, C_{3b}–C(CH_3)$_3$);

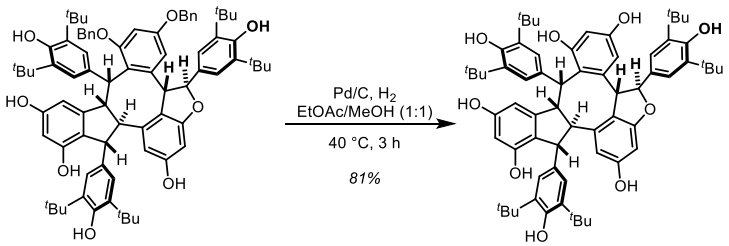

(±)–3.79a–Minor (±)–3.81–Minor

(3R,4R,4aS)-3,5,10-tris(3,5-di-tert-butyl-4-hydroxyphenyl)-4-(3,5-dihydroxyphenyl)-3,4,4a,5,9b,10-hexahydrobenzo[5,6]azuleno[7,8,1-cde]benzofuran-2,6,8-triol (3.81): A round bottom flask was charged with the major diastereomer of dibenzylated trimer 3.79a (6 mg, 0.005 mmol, 1.00 equiv) and Pd/C (30 wt%, 1 mg) and the flask was sealed and purged with N_2. EtOAc (HPLC grade, 500 μL) and MeOH (HPLC grade, 500 μL) were sequentially added and N_2 inlet was replaced with a H_2 balloon. The mixture was gently sparged with H_2 for 10 minutes at room temperature, at which point the vent needle was removed and the reaction mixture was warmed to 40 °C under H_2 (1 atm). After 3 h, the reaction was removed from the heat source, cooled to room temperature, and the contents filtered through a short plug of Celite, eluting with 1:1 EtOAc/MeOH. The filtrate was concentrated to dryness *in vacuo* and the resulting residue was purified by preparative TLC (90:10 CH_2Cl_2/Acetone) to afford **3.81** (4.1 mg, 0.004 mmol, 81% yield) as a single diastereomer. The connectivity was rigorously assigned by 2D NMR, though the relative configuration at C_{7a}, C_{8a}, and C_{7b} could not be determined.

TLC (CH_2Cl_2/Acetone, 95:5), R_F:	0.15 (UV, vanillin (pale red));
^{1}H NMR (500 MHz, $CDCl_3$, 25 °C) δ:	8.26 (br s, 1H), 8.11 (br s, 1H), 8.03 (br s, 1H), 7.16 (s, 2H, C_{2a}–H), 6.91 (s, 2H, C_{2b}–H), 6.81 (s, 2H, C_{2c}–H), 6.73 (d, *J* = 1.7 Hz, 1H, C_{14a}–H), 6.59 (br s, 1H), 6.53 (d, *J* = 2.0

Hz, 2H, C_{10c}–H), 6.42 (d, *J* = 1.7 Hz, 1H, C_{12a}–H), 6.24 (t, overlap *J* = 2.0 Hz, 1H, C_{12c}–H), 6.23 (d, overlap, *J* = 2.0 Hz, 1H, C_{7a}–H), 6.10 (s, 1H, C_{12b}–H), 5.95 (s, 1H, C_{4a}–OH), 5.74 (s, 1H, C_{4c}–OH), 5.58 (s, 1H, C_{4b}–OH), 5.34 (s, 1H, C_{7b}–H), 4.48 (d, *J* = 10.0 Hz, 1H, C_{7c}–H), 4.42 (d, *J* = 2.0 Hz, 1H, C_{8a}–H), 4.16 (d, *J* = 11.7 Hz, 1H, C_{8b}–H), 2.96 (dd [apparent triplet], *J* = 10.0, 11.7 Hz, 1H, C_{8c}–H), 1.35 (s, 18H, C_{3a}–C(CH_3)$_3$), 1.28 (s, 18H, C_{3c}–C(CH_3)$_3$), 1.16 (s, 18H, C_{3b}–C(CH_3)$_3$);

^{13}C NMR (125 MHz, $CDCl_3$, 25 °C) δ:

160.0 (C_{11b}), 159.3 (C_{11c}), 158.5 (C_{11a}), 156.9 (C_{13a}), 154.9 (C_{13b}), 154.6 (C_{4a}), 154.4 (C_{4a}), 153.2 (C_{4c}), 152.2 (C_{4b}), 147.8 (C_{9a}), 144.6 (C_{9c}), 143.4 (C_{9b}), 138.1 (C_{3a})[7], 137.4 (C_{3c})8, 137.1 (C_{3b})8, 136.6 (C_{1b}), 135.0 (C_{1a}), 133.3 (C_{1c}), 125.4 (C_{2c}), 125.0 (C_{2b}), 122.8 (C_{2a}), 121.1 (C_{14b}), 119.0 (C_{10b}), 116.9 (C_{10a}), 109.9 (C_{10c}), 104.2 (C_{14a}), 101.9 (C_{12c}), 101.6 (C_{12a}), 95.6 (C_{12b}), 86.8 (C_{7a}), 67.6 (C_{8c}), 56.7 (C_{7c}), 55.0 (C_{8b}), 52.3 (C_{8a}), 37.4 (C_{7b}), 35.2 (C–$C(CH_3)_3$), 35.1 (C–$C(CH_3)_3$), 30.9 (C–C(CH_3)$_3$), 30.78 (C–C(CH_3)$_3$), 30.75 (C–C(CH_3)$_3$).

[7] Each of the resonances for ^{t}Bu-bearing carbons (C_{3a}, C_{3b}, C_{3c}) had an accompanying minor resonance (approx. one-half the intensity) 0.1 ppm upfield of the major resonance, indicating restricted rotation of these sterically encumbered phenols

^{13}C NMR (125 MHz, $CDCl_3$, 25 °C) δ:	160.0 ($\underline{C}_{11b}$), 159.3 ($\underline{C}_{11c}$), 158.5 ($\underline{C}_{11a}$), 156.9 ($\underline{C}_{13a}$), 154.9 ($\underline{C}_{13b}$), 154.6 ($\underline{C}_{4a}$), 154.4 ($\underline{C}_{4a}$), 153.2 ($\underline{C}_{4c}$), 152.2 ($\underline{C}_{4b}$), 147.8 ($\underline{C}_{9a}$), 144.6 ($\underline{C}_{9c}$), 143.4 ($\underline{C}_{9b}$), 138.1 ($\underline{C}_{3a}$)[8], 137.4 ($\underline{C}_{3c}$)8, 137.1 ($\underline{C}_{3b}$)8, 136.6 ($\underline{C}_{1b}$), 135.0 ($\underline{C}_{1a}$), 133.3 ($\underline{C}_{1c}$), 125.4 ($\underline{C}_{2c}$), 125.0 ($\underline{C}_{2b}$), 122.8 ($\underline{C}_{2a}$), 121.1 ($\underline{C}_{14b}$), 119.0 ($\underline{C}_{10b}$), 116.9 ($\underline{C}_{10a}$), 109.9 ($\underline{C}_{10c}$), 104.2 ($\underline{C}_{14a}$), 101.9 ($\underline{C}_{12c}$), 101.6 ($\underline{C}_{12a}$), 95.6 ($\underline{C}_{12b}$), 86.8 ($\underline{C}_{7a}$), 67.6 ($\underline{C}_{8c}$), 56.7 ($\underline{C}_{7c}$), 55.0 ($\underline{C}_{8b}$), 52.3 ($\underline{C}_{8a}$), 37.4 ($\underline{C}_{7b}$), 35.2 (C–$\underline{C}$(CH_3)$_3$), 35.1 (C–$\underline{C}$(CH_3)$_3$), 30.9 (C–C($\underline{C}H_3$)$_3$), 30.78 (C–C($\underline{C}H_3$)$_3$), 30.75 (C–C($\underline{C}H_3$)$_3$).

[8] Each of the resonances for ^{t}Bu-bearing carbons (C_{3a}, C_{3b}, C_{3c}) had an accompanying minor resonance (approx. one-half the intensity) 0.1 ppm upfield of the major resonance, indicating restricted rotation of these sterically encumbered phenols

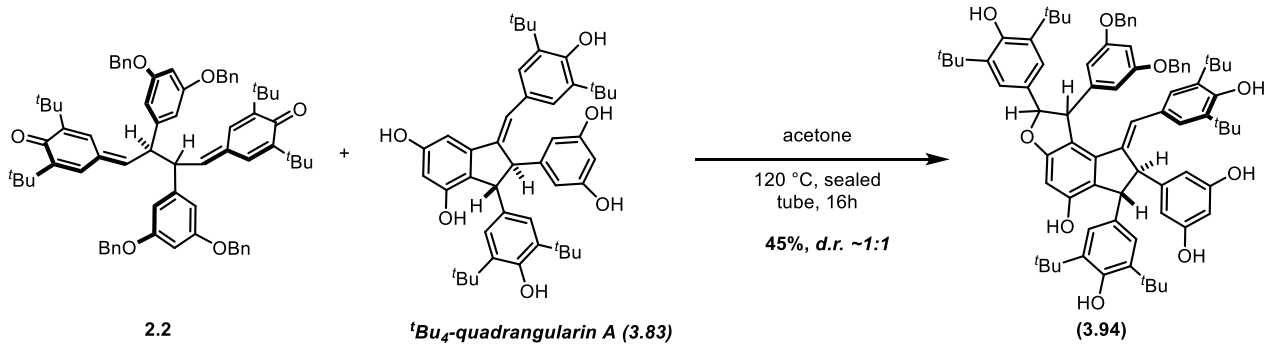

2.2 $^{t}Bu_4$-quadrangularin A (3.83) (3.94)

5-((6R,7R)-1-(3,5-bis(benzyloxy)phenyl)-8-((E)-3,5-di-tert-butyl-4-hydroxybenzylidene)-2,6-bis(3,5-di-tert-butyl-4-hydroxyphenyl)-5-hydroxy-1,6,7,8-tetrahydro-2H-indeno[5,4-b]furan-7-yl)benzene-1,3-diol (3.104): A suspension of starting bis-*para*-quinone methide 2.2 (266 mg, 0.256 mmol, 2.00 equiv) and starting indene 3.83 (87 mg, 0.128 mmol, 1.00 equiv) was prepared in acetone (2.48 mL, 0.025 M) at room temperature in a sealed tube. The vessel was tightly sealed and the slowly stirring mixture heated to 120 °C. At 12 h, the reaction was removed from the heat and allowed to cool to room temperature over the course of 0.5 h. TLC confirmed full consumption of 3.83. Column chromatography using 1%, to 15% of a acetone in dichloromethane afforded the mixture of diastereomers (1:1) which was subsequently separated by an additional column using the same gradient.

TLC (CH_2Cl_2/Acetone, 90:10), R_F:	0.20 (UV, *p*-anisaldehyde (red));
^{1}H NMR (500 MHz, acetone-D_6, 25 °C) δ:	δ 8.08 (s, 1H), 7.73 (s, 2H), 7.41 – 7.27 (m, 17H), 7.27 – 7.24 (m, 3H), 7.10 (s, 2H), 7.02 (s, 2H), 6.98 (d, J = 3.9 Hz, 1H), 6.74 (d, J = 2.2 Hz, 2H), 6.56 (t, J = 2.2 Hz, 1H), 6.40 (d, J = 4.7 Hz, 1H), 6.24 (d, J = 2.0 Hz, 2H), 6.15 (t, J = 2.0 Hz, 1H), 6.12 (s, 1H), 5.92 (s, 1H), 5.74 (s, 1H), 5.62 (s, 4H), 5.53 (d, J = 5.6 Hz, 1H), 5.09 – 4.99 (m, 7H), 4.38 (s, 1H), 4.30 (s, 1H), 1.45 (s, 18H), 1.35 (s, 18H), 1.23 (s, 18H)

^{13}C NMR (126 MHz, acetone-D_6, 25 °C) δ:	δ 162.49, 160.37, 158.40, 154.96, 153.76, 153.14, 152.00, 147.90, 146.27, 141.58, 140.15, 137.53, 137.28, 136.86, 136.74, 136.68, 133.39, 129.00, 128.57, 128.38, 128.25, 128.15, 127.76, 127.65, 125.78, 125.27, 123.50, 122.10, 112.98, 107.33, 106.23, 106.14, 100.95, 100.41, 96.36, 93.92, 69.95, 69.71, 59.27, 57.01, 56.94, 54.07, 34.39, 34.25, 34.14, 29.93, 29.82, 29.71, 29.70.
FTIR (neat) cm^{-1}	3626.46 cm-1, 2956.55 cm-1,1595.97 cm-1, 1435.72 cm-1, 1234.75 cm-1, 1149.29 cm-1, 1052.97 cm-1, 695.41 cm-1
HRMS (ESI):	*m/z* calculated for $C_{80}H_{92}O_9$ $[M+H]^+$: 1197.6820, found 1197.6841;

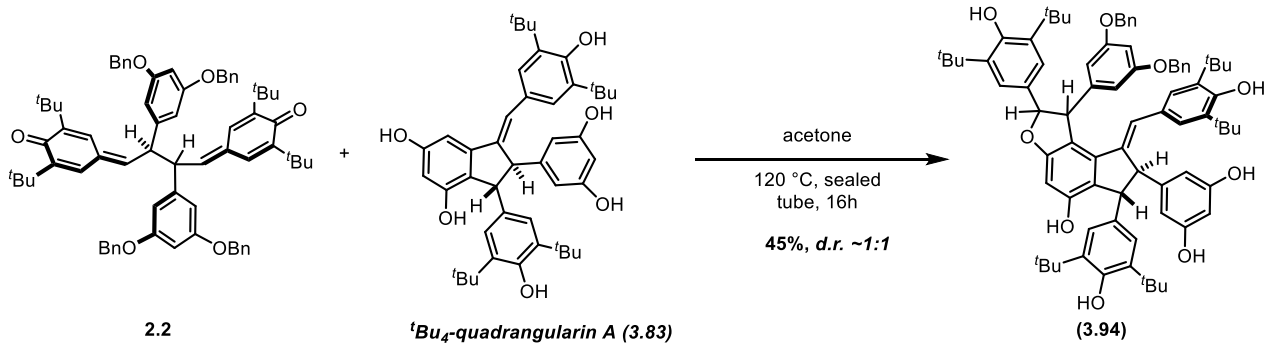

2.2 *$^tBu_4$-quadrangularin A (3.83)* **(3.94)**

5-((6R,7R)-1-(3,5-bis(benzyloxy)phenyl)-8-((E)-3,5-di-tert-butyl-4-hydroxybenzylidene)-2,6-bis(3,5-di-tert-butyl-4-hydroxyphenyl)-5-hydroxy-1,6,7,8-tetrahydro-2H-indeno[5,4-b]furan-7-yl)benzene-1,3-diol (3.104): A suspension of starting bis-*para*-quinone methide 2.2 (266 mg, 0.256 mmol, 2.00 equiv) and starting indene 3.83 (87 mg, 0.128 mmol, 1.00 equiv) was prepared in acetone (2.48 mL, 0.025 M) at room temperature in a sealed tube. The vessel was tightly sealed and the slowly stirring mixture heated to 120 °C. At 12 h, the reaction was removed from the heat and allowed to cool to room temperature over the course of 0.5 h. TLC confirmed full consumption of 3.83. Column chromatography using 1%, to 15% of a acetone in dichloromethane afforded the mixture of diastereomers (1:1) which was subsequently separated by an additional column using the same gradient.

TLC (CH_2Cl_2/Acetone, 90:10), R_F:	0.20 (UV, *p*-anisaldehyde (red));
^{1}H NMR (500 MHz, acetone-D_6, 25 °C) δ:	δ 8.06 (d, J = 4.1 Hz, 2H), 7.50 – 7.45 (m, 4H), 7.39 – 7.28 (m, 9H), 7.26 (s, 2H), 7.08 (s, 2H), 6.75 (d, J = 2.2 Hz, 1H), 6.71 (s, 2H), 6.68 (s, 1H), 6.65 (d, J = 2.2 Hz, 2H), 6.41 – 6.38 (m, 3H), 6.21 (d, J = 2.1 Hz, 1H), 6.06 (s, 1H), 5.91 (s, 1H), 5.66 (s, 1H), 5.50 (d, J = 4.2 Hz, 1H), 5.13 (d, J = 5.0 Hz, 4H), 4.74 (d, J = 4.3 Hz, 1H), 4.42 (s, 1H), 4.17 (s, 1H), 1.43 (s, 18H), 1.28 (s, 18H), 1.21 (s, 18H).

^{13}C NMR (126 MHz, acetone-D_6, 25 °C) δ:	δ 162.76, 161.06, 158.69, 154.92, 153.81, 153.04, 151.99, 148.05, 147.78, 141.80, 141.02, 137.57, 137.25, 136.86, 136.78, 133.69, 129.01, 128.57, 128.36, 128.25, 127.76, 127.72, 127.59, 125.70, 125.28, 123.44, 121.89, 112.56, 106.69, 106.13, 100.47, 99.40, 96.29, 93.65, 69.73, 59.44, 57.02, 54.07, 34.36, 34.18, 34.08, 29.89, 29.77, 29.70, 29.66.
FTIR (neat) cm^{-1}	3629.92 cm-1, 2958.37 cm-1,1595.06 cm-1, 1435.45 cm-1, 1151.54 cm-1, 1053.74 cm-1, 832.80 cm-1, 735.33 cm-1, 695.30 cm-1
HRMS (ESI):	*m/z* calculated for $C_{80}H_{92}O_9$ $[M+H]^+$: 1197.6820, found 1197.6841;

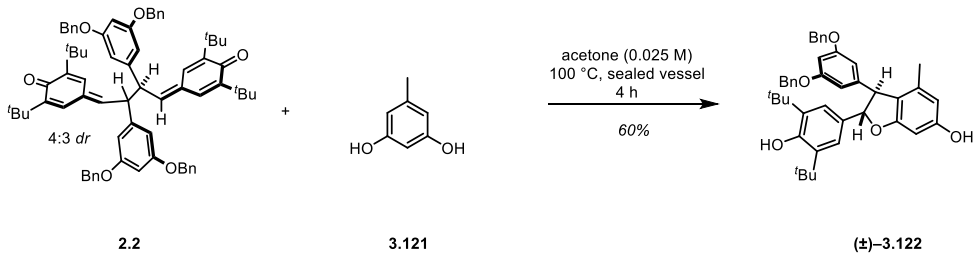

2.2 3.121 (±)–3.122

5-((2S,3S)-2-(3,5-di-tert-butyl-4-hydroxyphenyl)-6-hydroxy-4-methyl-2,3-dihydrobenzofuran-3-yl)benzene-1,3-diol (3.122): A suspension of starting bis-*para*-quinone methide **2.2** (1.55 g, 1.49 mmol, 2.00 equiv) and starting orcinol **3.121** (95.4 mg, 0.76 mmol, 1.00 equiv) was prepared in acetone (30 mL, 0.050 M) at room temperature in a sealed tube. The vessel was tightly sealed and the slowly stirring mixture heated to 130 °C. At 4 h, the reaction was removed from the heat and allowed to cool to room temperature over the course of 0.5 h. TLC confirmed full consumption of **3.121**. Column chromatography was performed using a gradient of 1% acetone in DCM to 15% acetone to remove unreacted QMD and delivered the product in 60% yield.

TLC (Hexanes/EtOAc, 70:30) R_F:	0.5 (UV, potassium permanganate);
^{1}H NMR (500 MHz, $(CD_3)_2CO$, 25 °C) δ:	8.23 (s, 1H), 7.44 (d, J = 8.8 Hz, 4H), 7.40 – 7.36 (m, 4H), 7.32 (d, J = 7.1 Hz, 2H), 7.18 (s, 2H), 6.61 (t, J = 2.3 Hz, 1H), 6.49 (s, 2H), 6.29 (s, 1H), 6.21 (s, 1H), 6.09 (s, 1H), 5.43 (d, J = 6.1 Hz, 1H), 5.12 – 5.04 (m, 4H), 4.40 (d, J = 6.1 Hz, 1H), 1.80 (s, 3H), 1.42 (s, 18H).;
^{13}C NMR (126 MHz, (CD3)2CO, 25 °C) δ:	162.1, 161.2, 159.4, 154.6, 146.9, 138.3, 138.2, 136.8, 133.6, 129.3, 128.6, 128.5, 123.0, 120.0, 110.1, 107.9, 101.1, 95.5, 94.3, 70.5, 57.4, 35.2, 30.6, 18.9.

HRMS (ESI):	*m/z calculated for C43H47O5+ ([M+H]+): 643.3418, found 643.3414*
FTIR (neat) cm^{-1}:	3626, 3387, 2956, 1703, 1593, 1452, 1360, 1290, 1233, 1153, 1055, 1028, 972, 881, 736, 696 cm-1

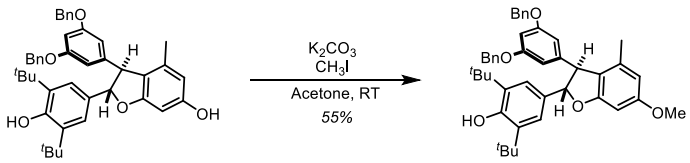

(±)–3.122 (±)–3.123

5-((2S,3S)-2-(3,5-di-tert-butyl-4-hydroxyphenyl)-6-hydroxy-4-methyl-2,3-dihydrobenzofuran-3-yl)benzene-1,3-diol (3.123): A suspension of dihydrobenzofuran **3.122** (66 mg, 0.10 mmol, 1 equiv.) and K2CO3 (71.0 mg, 0.51 mmol, 5.00 equiv) was prepared in acetone (1.0 mL, 0.10 M) at room temperature in a 2 dram vial. Iodomethane (19uL, 0.31 mmol, 3 equiv.) was added to the mixture via syringe. The vessel was left stirring at RT for 12 h at which time, the reaction was quenched by addition of aqueous bicarbonate. The crude was then extracted with ethyl acetate and washed with bicarbonate solution and brine then dried over Na2SO4 and concentrated under vacuum. Column chromatography was performed using a gradient of 1% ethyl acetate in hexanes to 30% ethyl acetate and delivered the product in 55% yield.

TLC (Hexanes/EtOAc, 80:20) R_F:	0.5 (UV, potassium permanganate);
^{1}H NMR (600 MHz, $CDCl_3$, 25 °C) δ:	7.40 – 7.28 (m, 10H), 7.11 (s, 2H), 6.53 (t, J = 2.2 Hz, 1H), 6.42 (d, J = 2.2 Hz, 2H), 6.39 (d, J = 2.2 Hz, 1H), 6.24 (d, J = 1.8 Hz, 1H), 5.43 (d, J = 6.2 Hz, 1H), 5.21 (s, 1H), 5.01 – 4.96 (m, 4H), 4.38 (d, J = 6.2 Hz, 1H), 3.81 (s, 3H), 1.84 (s, 3H), 1.41 (s, 18H)..;
^{13}C NMR (126 MHz, $CDCl^3$, 25 °C) δ:	161.04, 160.85, 160.18, 153.71, 145.71, 136.77, 136.18, 135.96, 132.05, 128.58, 128.53, 128.01, 127.76, 127.63,

	122.45, 120.22, 108.13, 107.14, 100.39, 93.82, 93.43, 70.06, 56.55, 55.46, 34.40, 30.25.
HRMS (APCI+):	*m/z calculated for $C_{44}H_{48}O_5$+ ([M+H]+): 657.3575, found 657.3566*
FTIR (neat) cm^{-1}:	2955.47, 1592.46, 1437.15, 1347.02, 1193.66, 1133.18, 1054.09, 830.04, 734.54, 694.95.

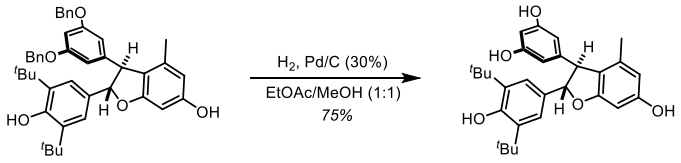

(±)–3.122 (±)–3.122a

5-((2S,3S)-2-(3,5-di-tert-butyl-4-hydroxyphenyl)-6-hydroxy-4-methyl-2,3-dihydrobenzofuran-3-yl)benzene-1,3-diol (3.123a): A suspension of dihydrobenzofuran **3.122** (60 mg, 0.09 mmol, 1 equiv.) and Pd/C (33.0 mg, 0.09 mmol, 1 equiv) was prepared in a degassed mixture of 1:1 ethyl acetate and methanol (4.7 mL, 0.02 M) at room temperature in a 2 dram vial. H2 was sparged through the mixture via balloon for 100 minutes at which time, the needle was pulled above solvent level and the reaction was left at RT over 12h. The crude was then sparged with argon after removal of hydrogen balloon. To the crude was added celite to form a slurry which was then filtered through a pad of celite and washed with ethyl acetate. The eluent was then concentrated under vacuum to deliver the crude product. This was further purified via silica plug using isocratic gradient of 50% ethyl acetate in hexanes delivering the product in 75% yield.

TLC (Hexanes/EtOAc, 70:30) R_F:	0.5 (UV, potassium permanganate);
^{1}H NMR (600 MHz, $CDCl_3$, 25 °C) δ:	7.09 (s, 2H), 6.30 (d, J = 2.1 Hz, 1H), 6.24 (dd, J = 4.8, 2.7 Hz, 1H), 6.21 (d, J = 2.1 Hz, 2H), 6.18 (d, J = 2.1 Hz, 1H), 5.40 (d, J = 5.9 Hz, 1H), 5.22 (s, 1H), 4.96 (s, 2H), 4.89 (s, 1H), 4.31 (d, J = 5.9 Hz, 1H), 1.89 (s, 3H), 1.40 (s, 18H).
^{13}C NMR (126 MHz, $CDCl_3$, 25 °C) δ:	161.01, 157.11, 156.61, 153.79, 146.36, 136.52, 136.03, 131.84, 122.44, 120.40, 109.25, 107.38, 101.37, 95.02, 93.87, 55.94, 34.39, 30.23, 18.82.

HRMS (APCI+):	*m/z calculated for $C_{29}H_{34}O_5$+ ([M+H]+): 463.2479, found 463.2497.*
FTIR (neat) cm^{-1}:	3628.91, 2953.17, 1728.90, 1594.13, 1437.13, 1225.23, 1146.81, 1054.57, 1033.23, 832.11, 734.64, 694.59

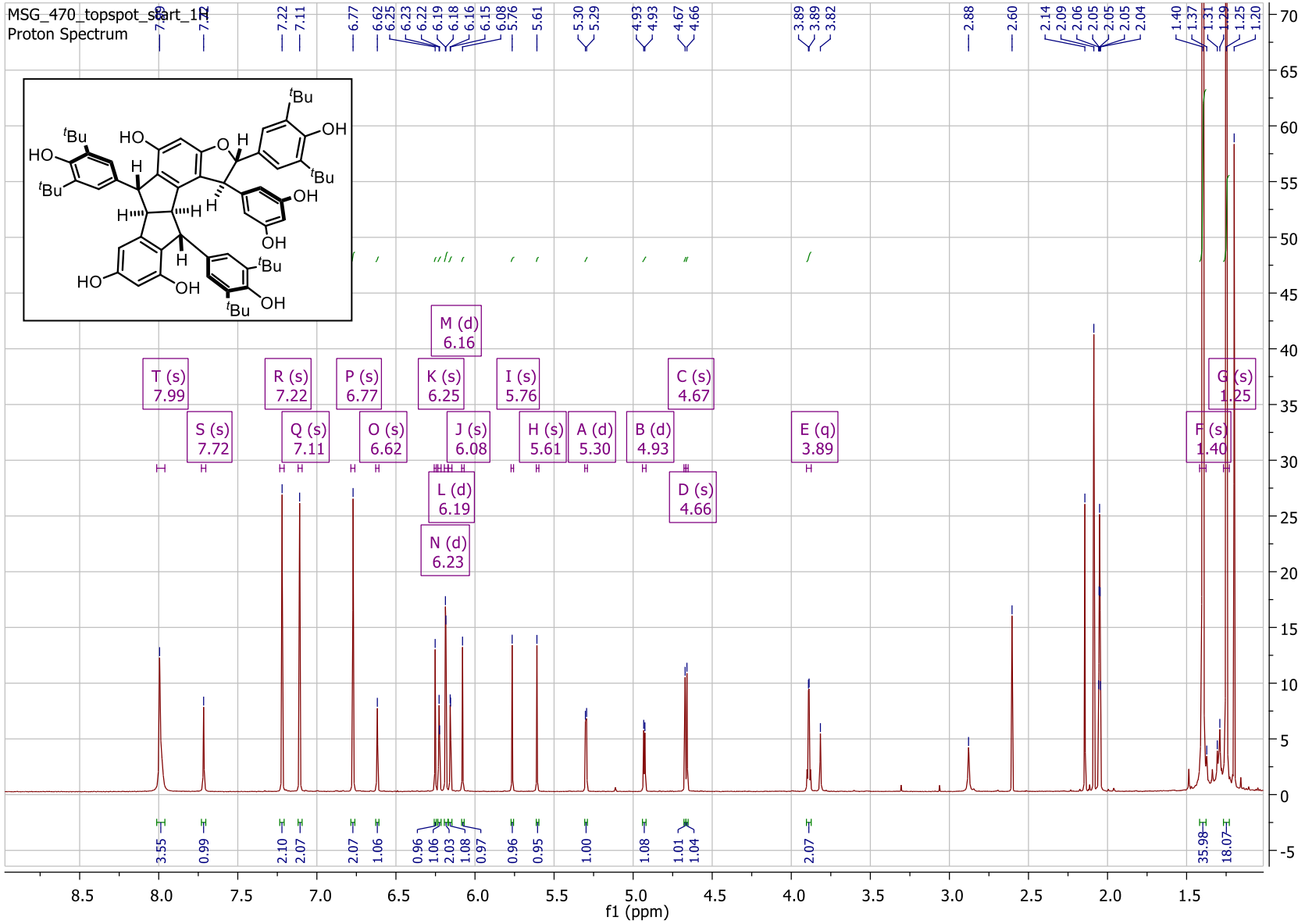
MSG_470_topspot_start_1H
Proton Spectrum
T (s) 7.99
S (s) 7.72
R (s) 7.22
Q (s) 7.11
P (s) 6.77
O (s) 6.62
M (d) 6.16
K (s) 6.25
J (s) 6.08
L (d) 6.19
N (d) 6.23
I (s) 5.76
H (s) 5.61
A (d) 5.30
C (s) 4.67
B (d) 4.93
D (s) 4.66
E (q) 3.89
G (s) 1.25
F (s) 1.40
f1 (ppm)

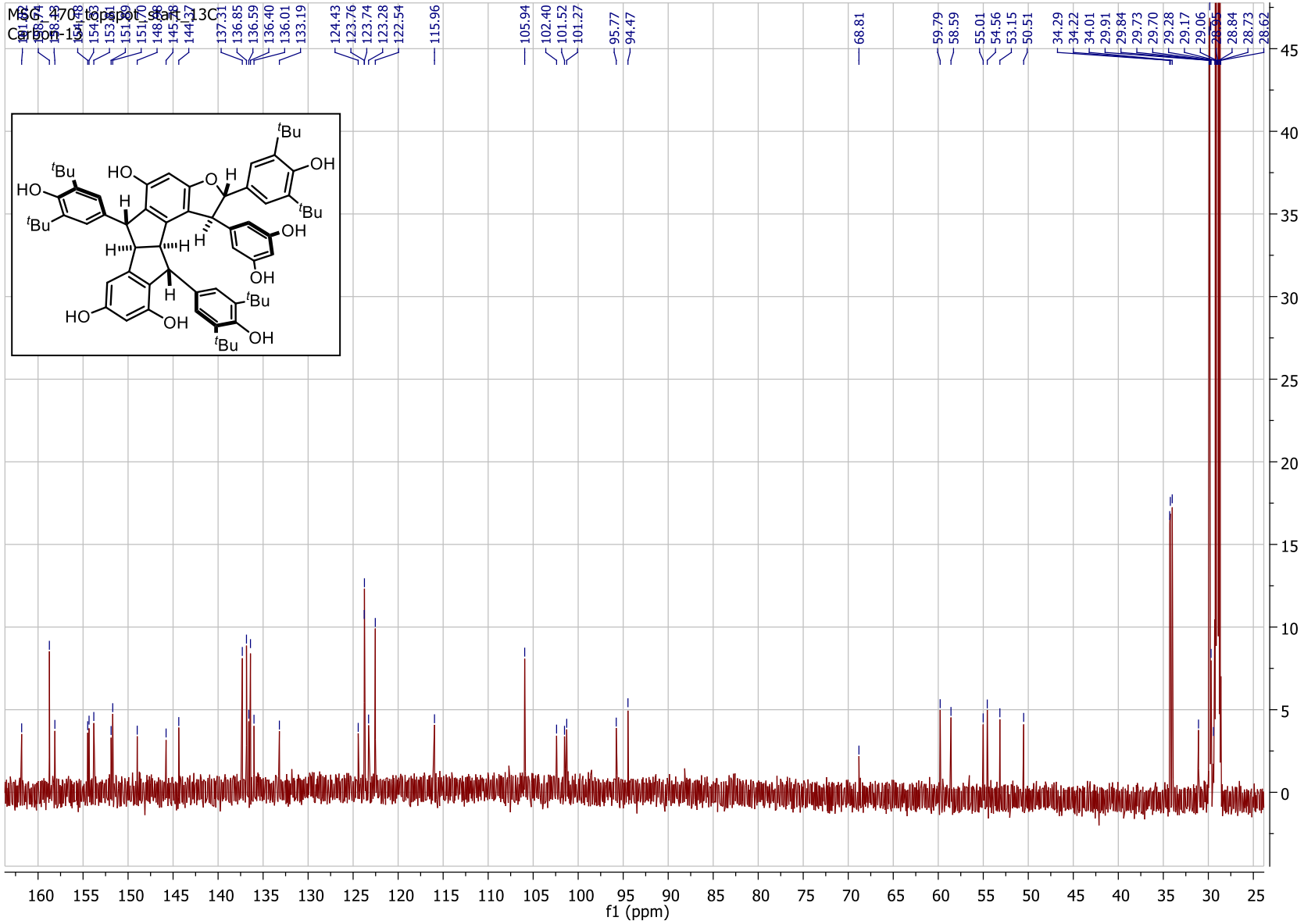
MSG-470-topspot-star-13C1
Carbon-13
f1 (ppm)

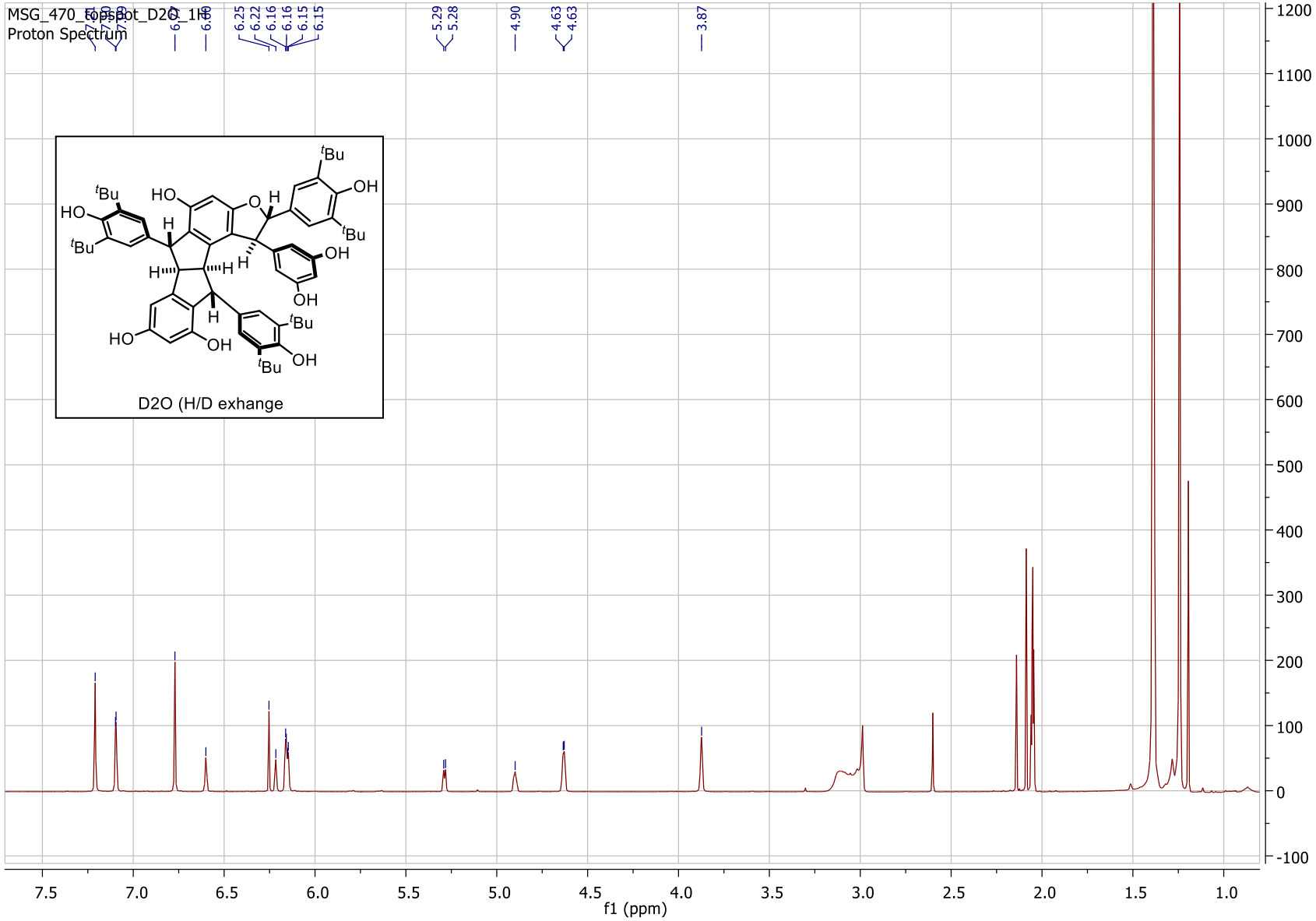
MSG_470_topspot_D2O_1H
Proton Spectrum
7.50
7.39
7.38
6.61
6.60
6.25
6.22
6.16
6.16
6.15
6.15
5.29
5.28
4.90
4.63
4.63
3.87
D2O (H/D exhange
f1 (ppm)

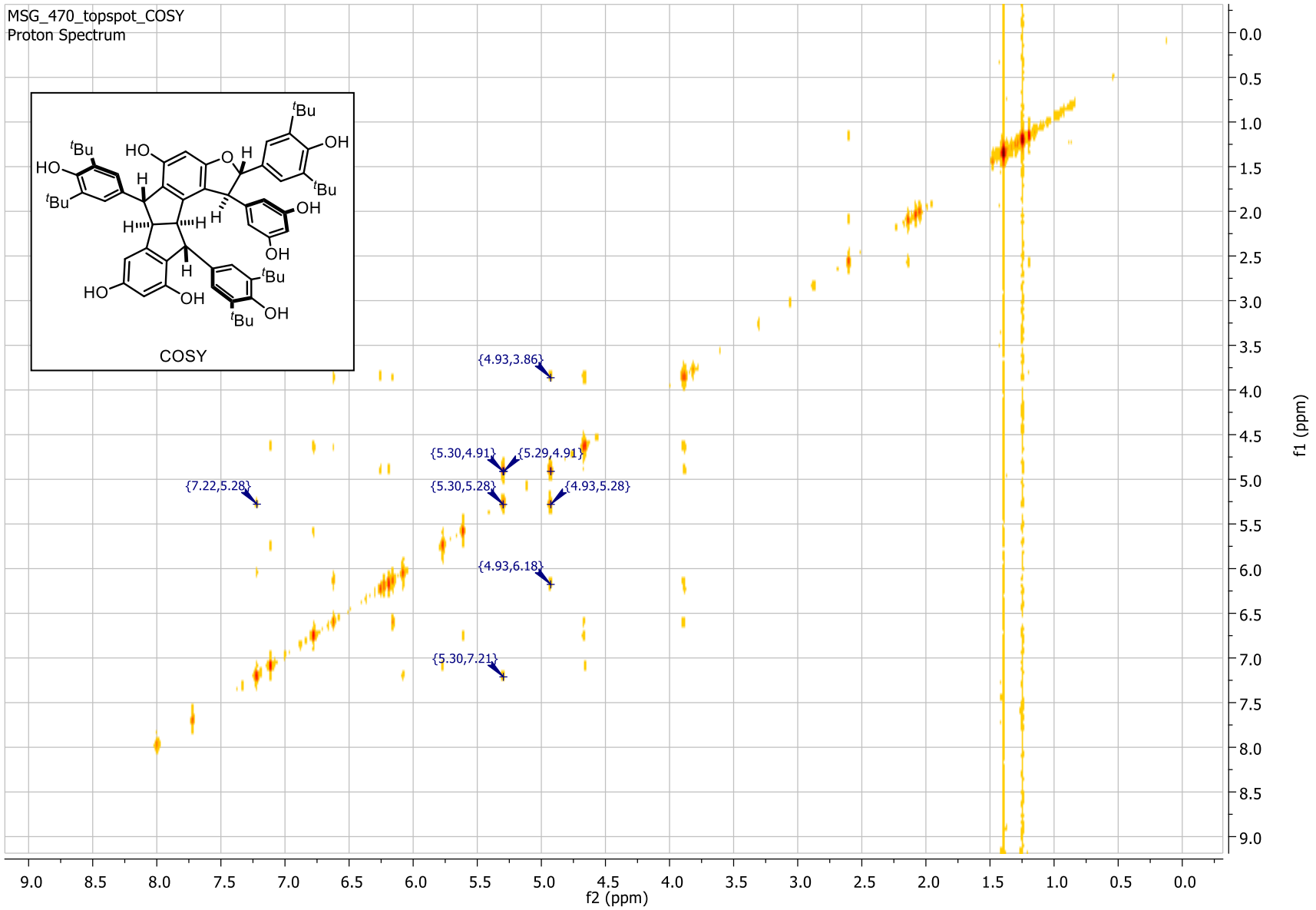
MSG_470_topspot_COSY
Proton Spectrum
COSY
{4.93,3.86}
{5.30,4.91}
{5.29,4.91}
{7.22,5.28}
{5.30,5.28}
{4.93,5.28}
{4.93,6.18}
{5.30,7.21}
f2 (ppm)
f1 (ppm)

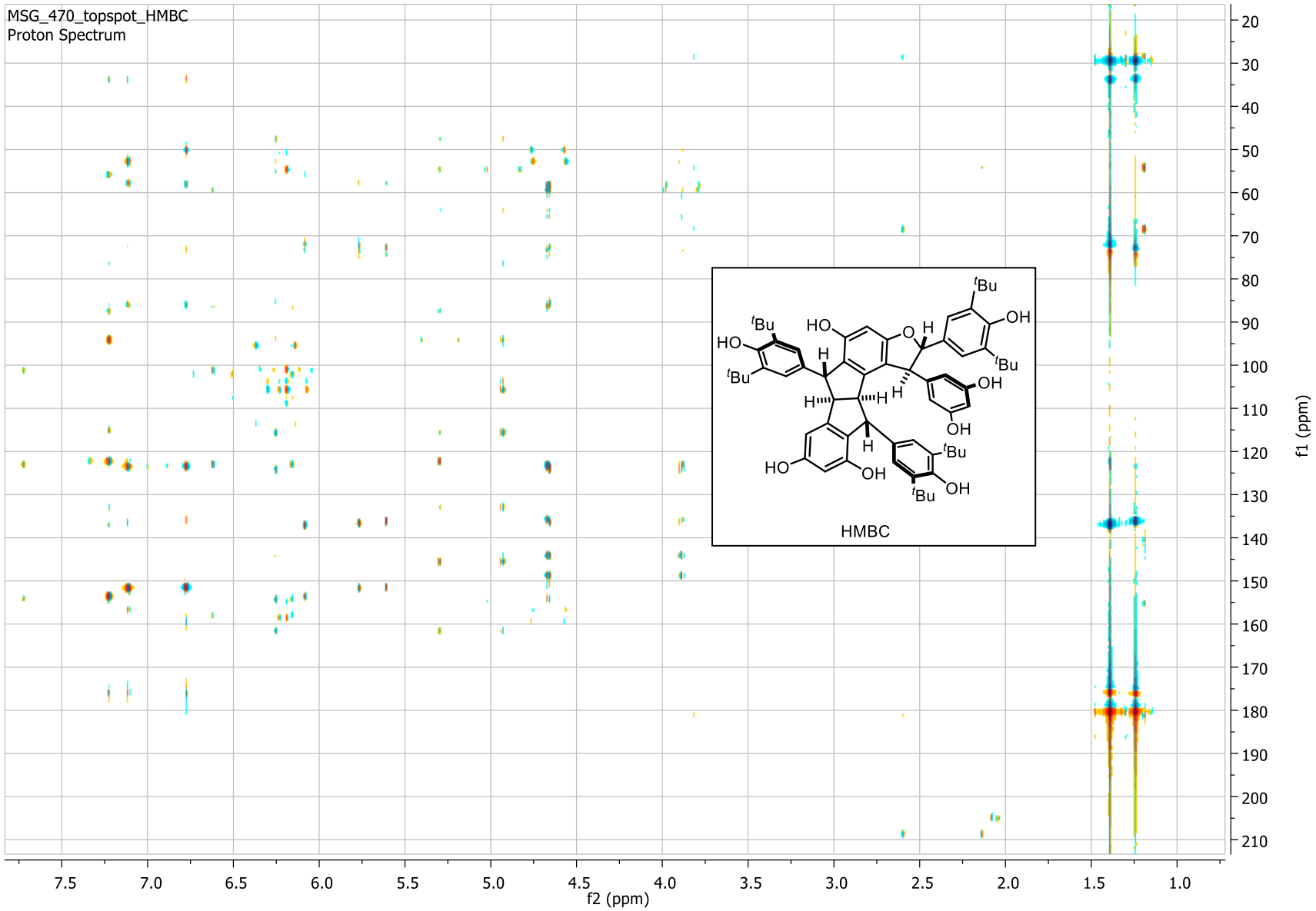
MSG_470_topspot_HMBC
Proton Spectrum
HMBC
f2 (ppm)
f1 (ppm)

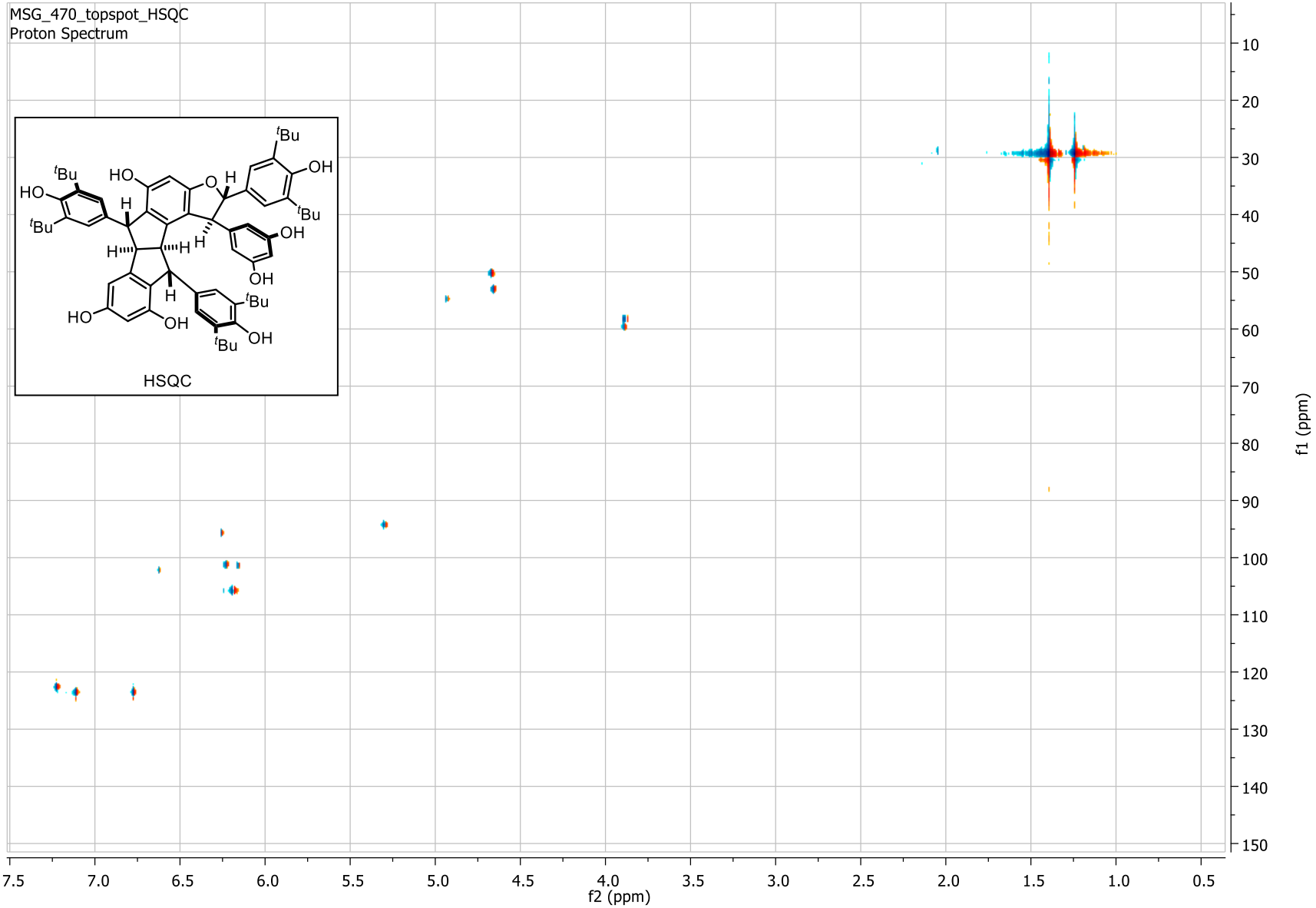
MSG_470_topspot_HSQC
Proton Spectrum
HSQC
f2 (ppm)
f1 (ppm)

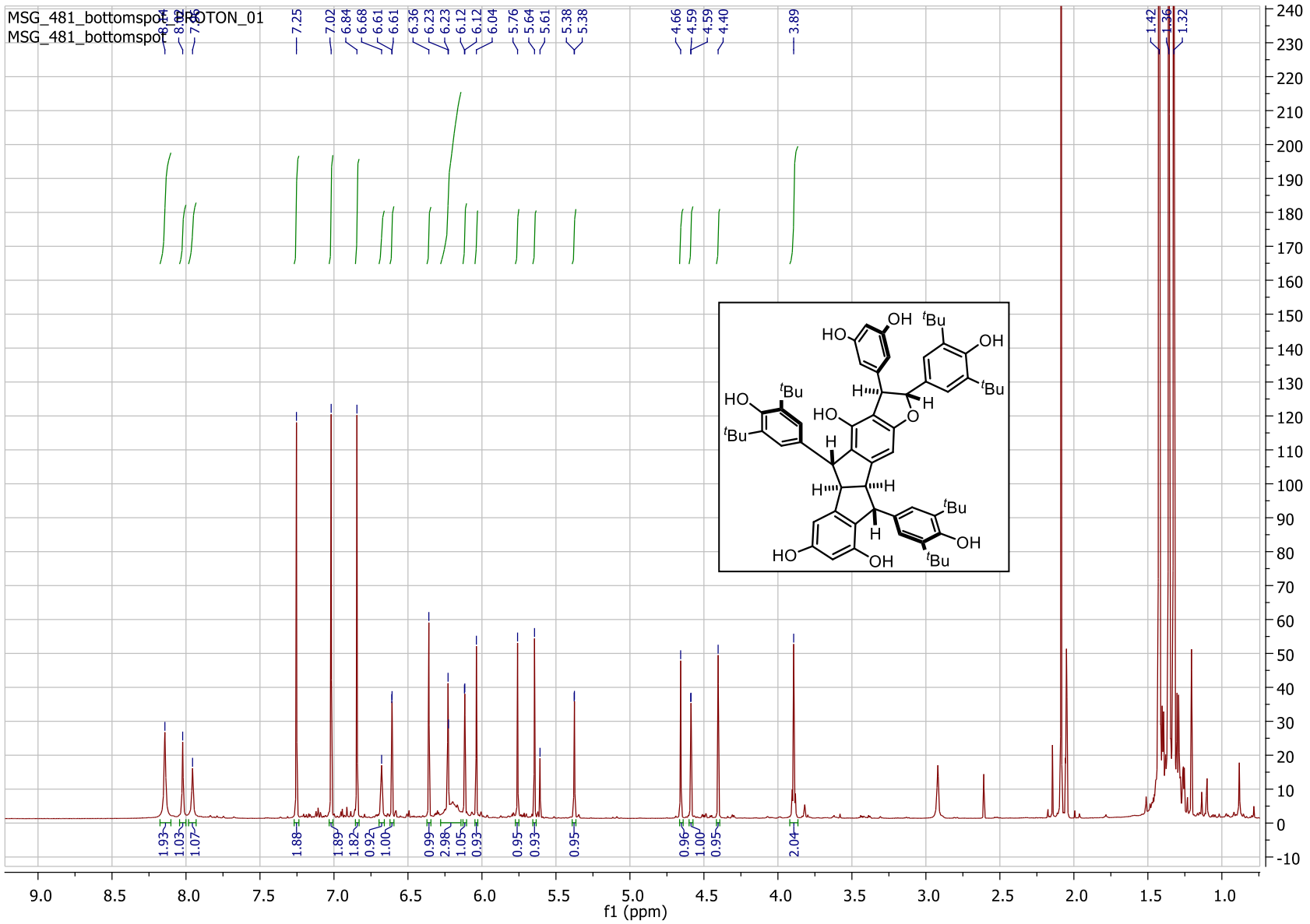
MSG_481_bottomspot-1 PROTON_01
MSG_481_bottomspot
8.04
8.02
7.98
7.25
7.02
6.84
6.68
6.61
6.61
6.36
6.23
6.23
6.12
6.12
6.04
5.76
5.64
5.61
5.38
5.38
4.66
4.59
4.59
4.40
3.89
1.42
1.36
1.32
1.93
1.03
1.07
1.88
1.89
1.82
0.92
1.00
0.99
2.98
1.05
0.93
0.95
0.93
0.95
0.96
1.00
0.95
2.04
f1 (ppm)

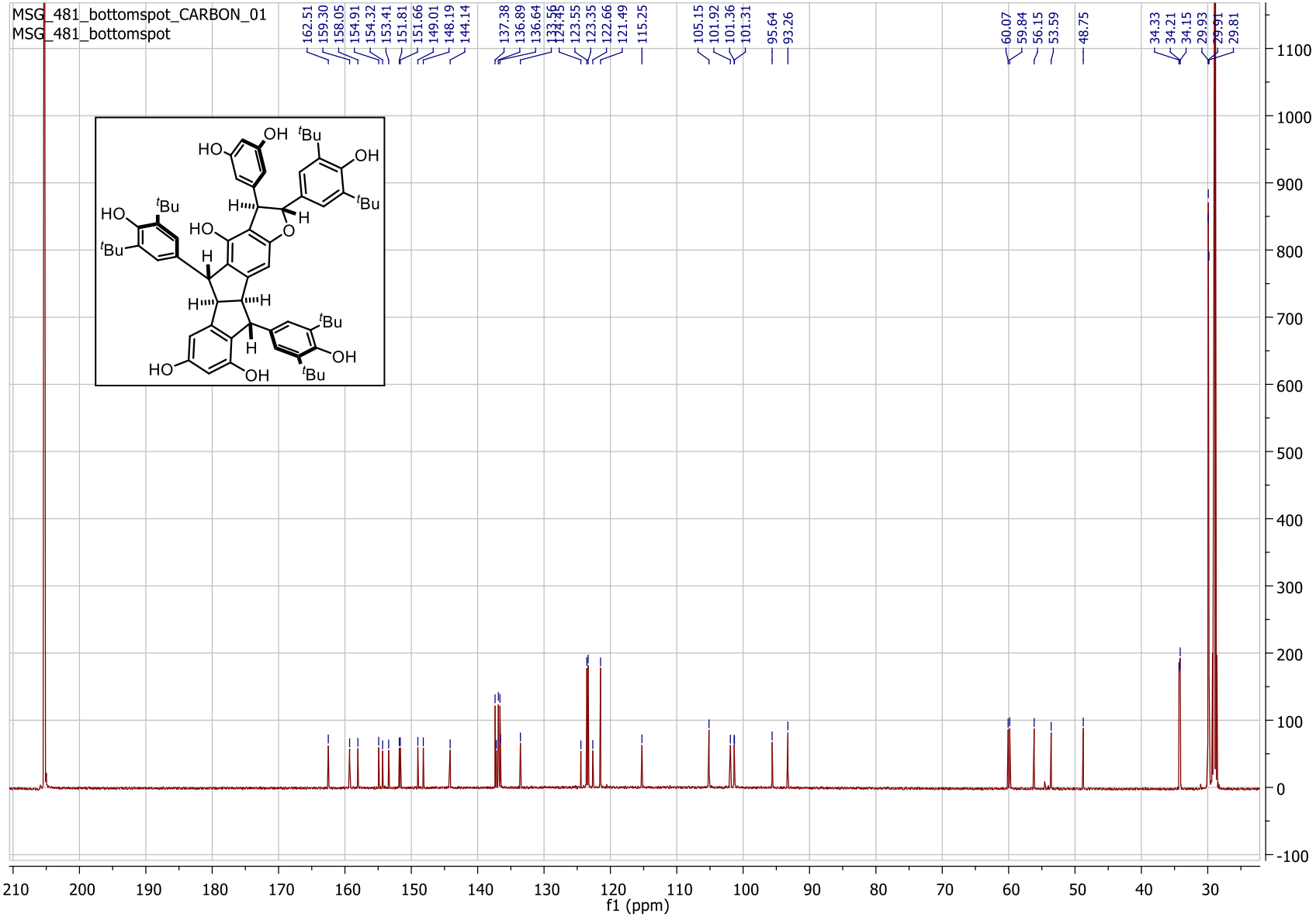
MSG_481_bottomspot_CARBON_01
MSG_481_bottomspot
162.51
159.30
158.05
154.91
154.32
153.41
151.81
151.66
149.01
148.19
144.14
137.38
136.89
136.64
133.56
124.45
123.55
123.35
122.66
121.49
115.25
105.15
101.92
101.36
101.31
95.64
93.26
60.07
59.84
56.15
53.59
48.75
34.33
34.21
34.15
29.93
29.91
29.81
f1 (ppm)

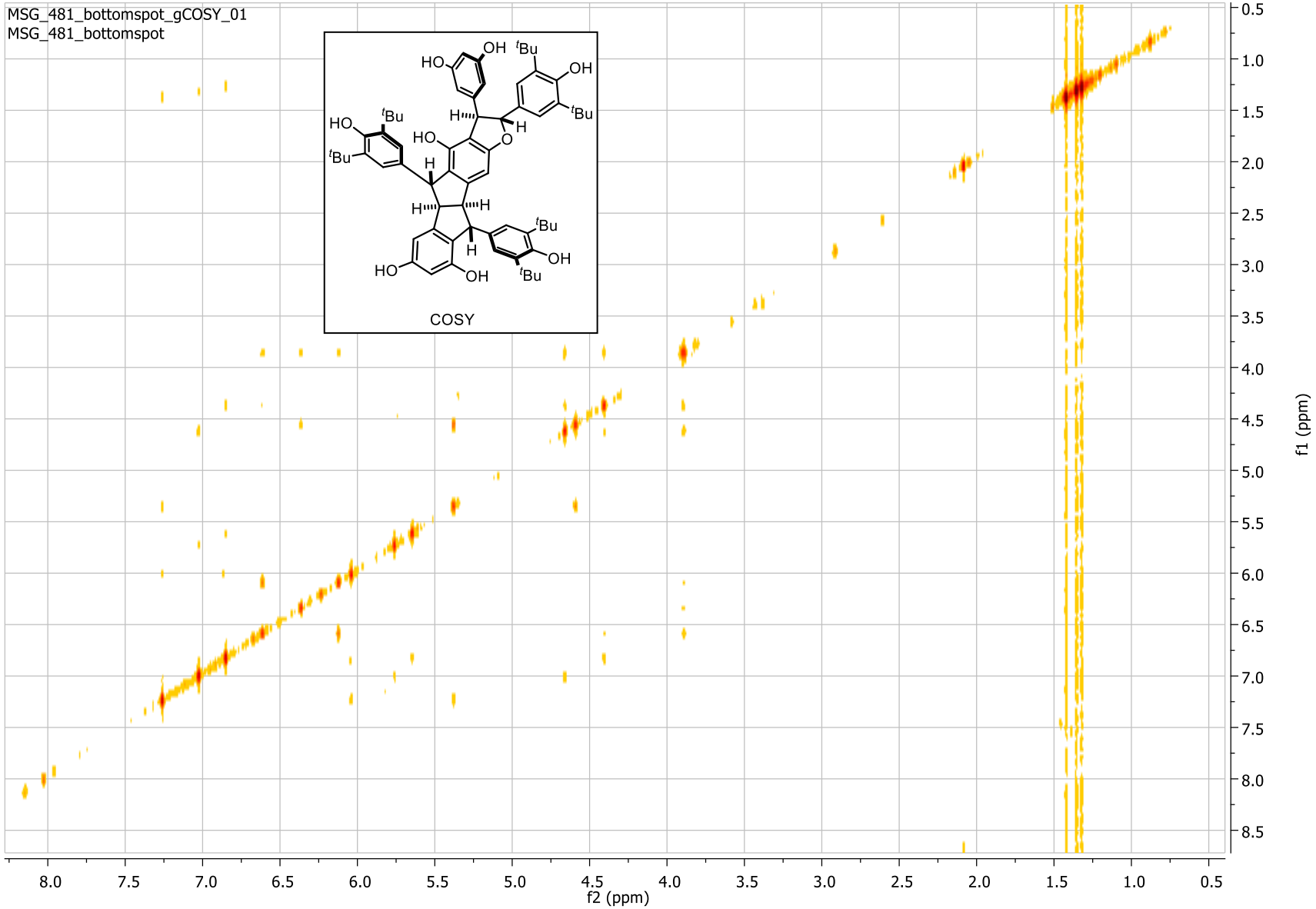
MSG_481_bottomspot_gCOSY_01
MSG_481_bottomspot
COSY
f2 (ppm)
f1 (ppm)

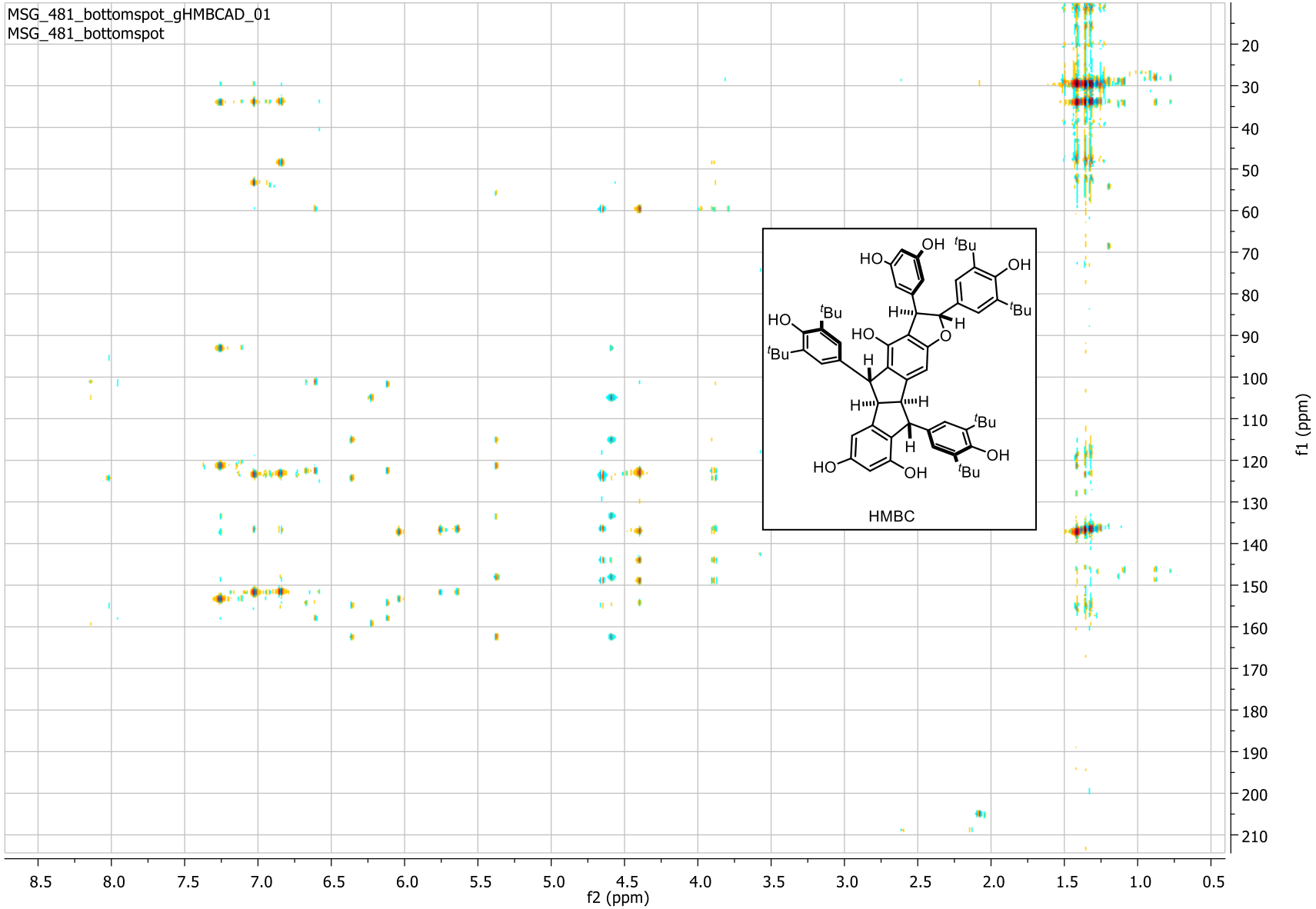
MSG_481_bottomspot_gHMBCAD_01
MSG_481_bottomspot
HMBC
f2 (ppm)
f1 (ppm)

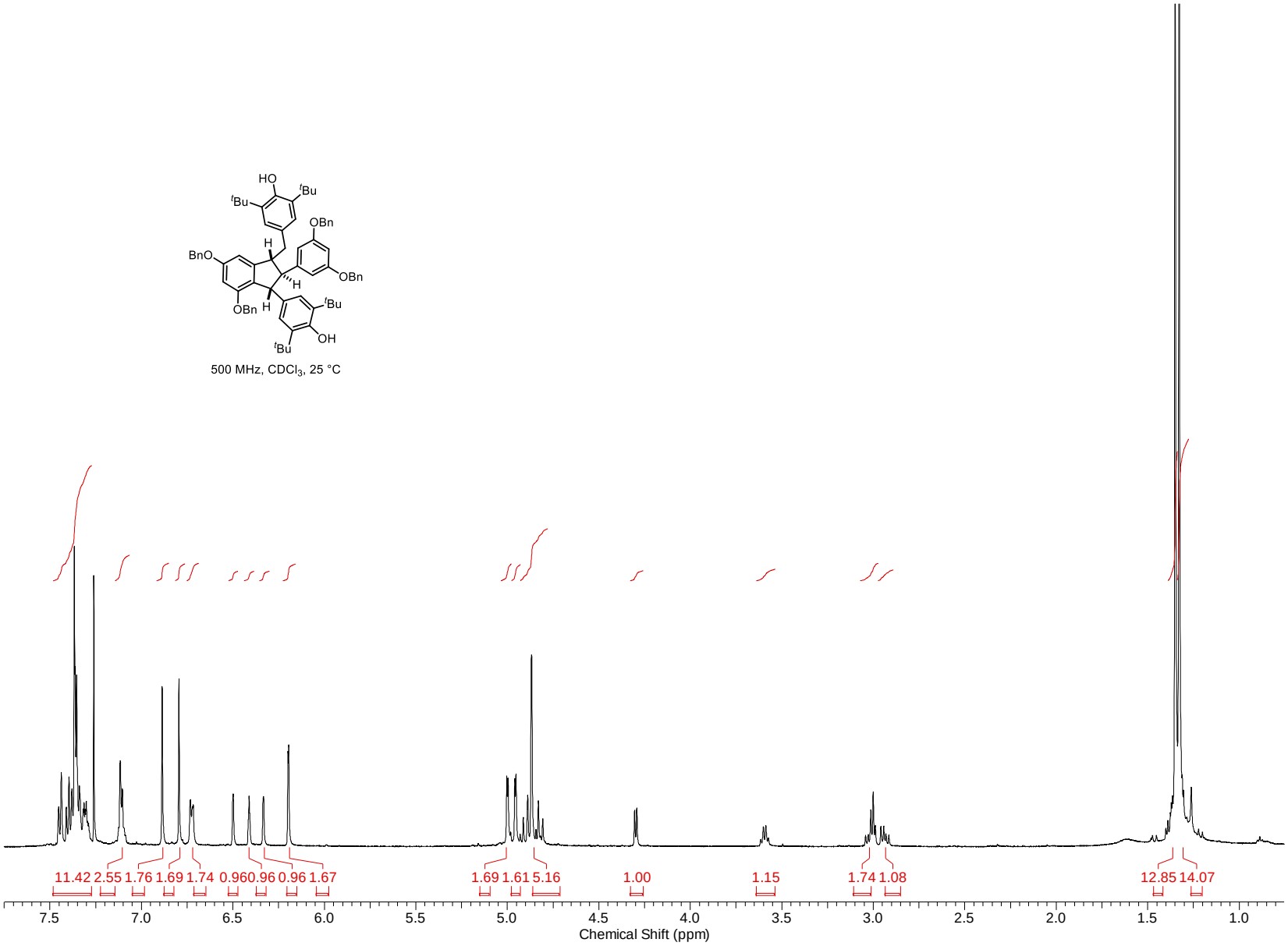
HO
tBu
tBu
OBn
H
BnO
OBn
H
H
OBn
tBu
H
OH
tBu
500 MHz, CDCl3, 25 °C
11.42 2.55 1.76 1.69 1.74 0.96 0.96 0.96 1.67
1.69 1.61 5.16
1.00
1.15
1.74 1.08
12.85 14.07
7.5 7.0 6.5 6.0 5.5 5.0 4.5 4.0 3.5 3.0 2.5 2.0 1.5 1.0
Chemical Shift (ppm)

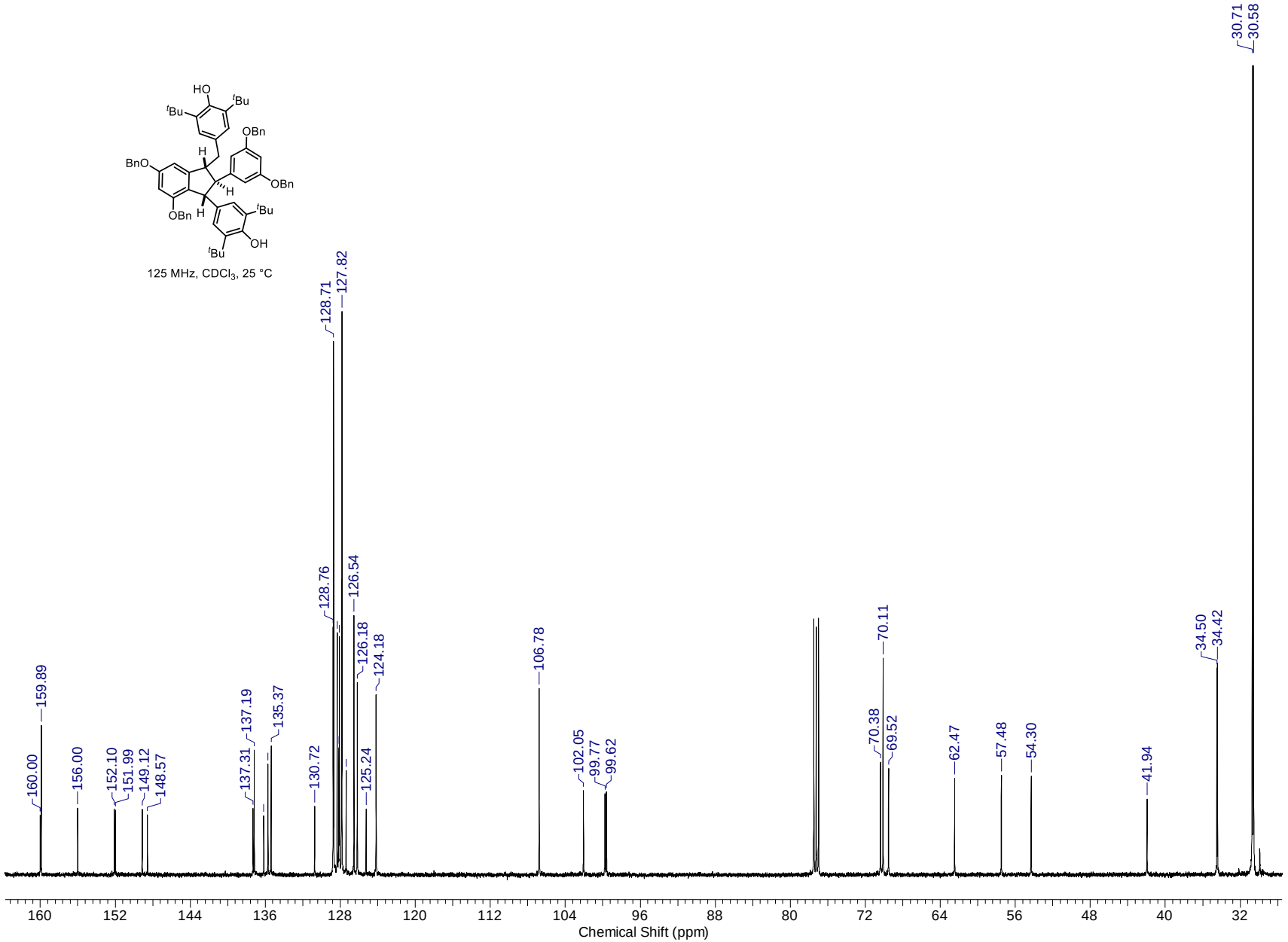
HO
tBu
tBu
OBn
H
BnO
OBn
H
OBn
H
tBu
tBu
OH
125 MHz, CDCl3, 25 °C
160.00
159.89
156.00
152.10
151.99
149.12
148.57
137.31
137.19
135.37
130.72
128.76
128.71
127.82
126.54
126.18
125.24
124.18
106.78
102.05
99.77
99.62
70.38
70.11
69.52
62.47
57.48
54.30
41.94
34.50
34.42
30.71
30.58
160
152
144
136
128
120
112
104
96
88
80
72
64
56
48
40
32
Chemical Shift (ppm)

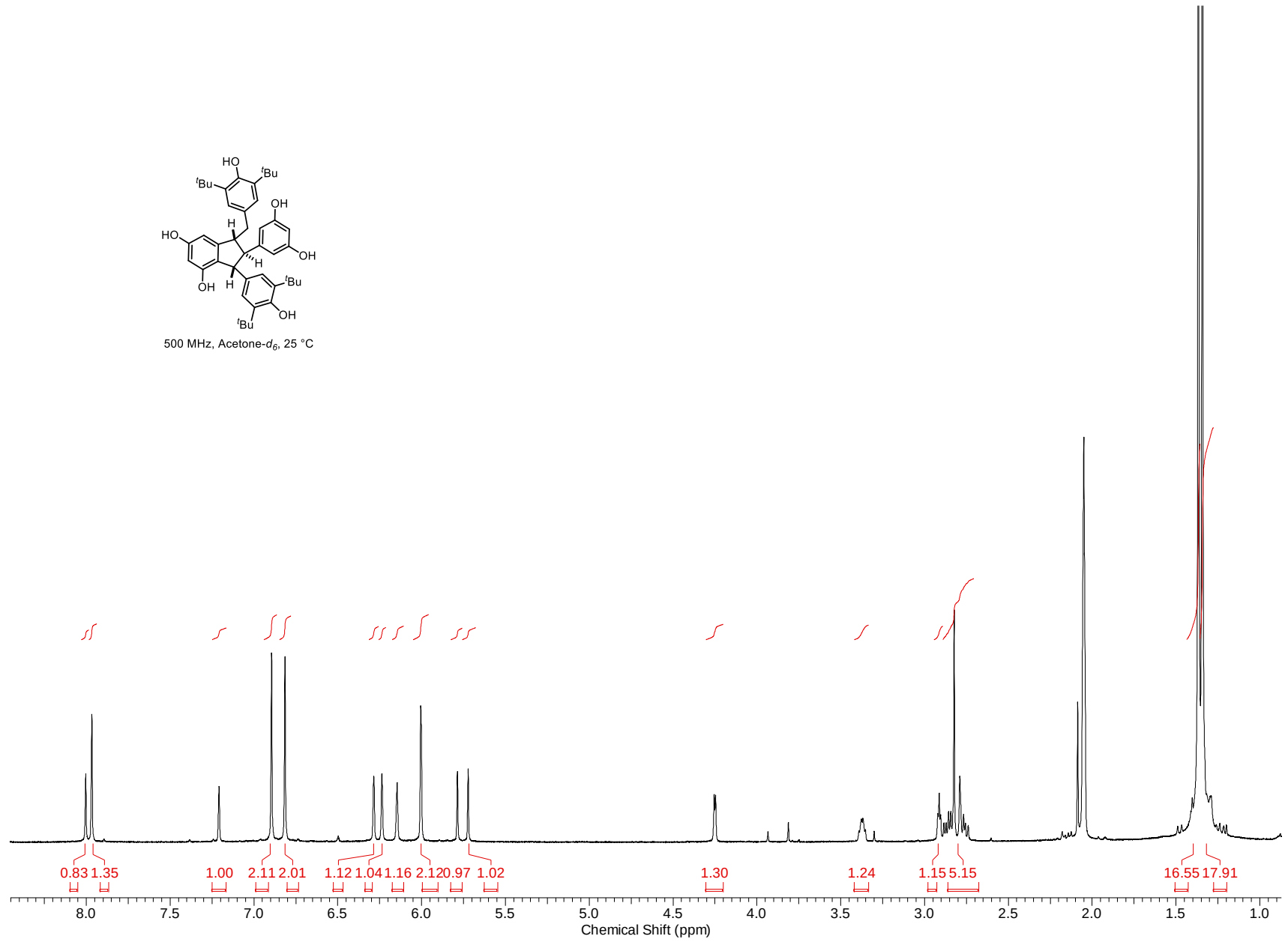
HO
tBu
tBu
OH
H
HO
OH
H
OH
H
tBu
tBu
OH
500 MHz, Acetone-d6, 25 °C
0.83 1.35
1.00
2.11 2.01
1.12 1.04 1.16 2.12 0.97 1.02
1.30
1.24
1.15 5.15
16.55 17.91
8.0 7.5 7.0 6.5 6.0 5.5 5.0 4.5 4.0 3.5 3.0 2.5 2.0 1.5 1.0
Chemical Shift (ppm)

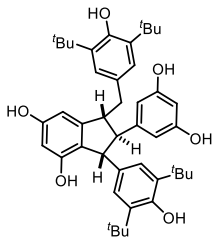

175 MHz, Acetone-d_6, 25 °C

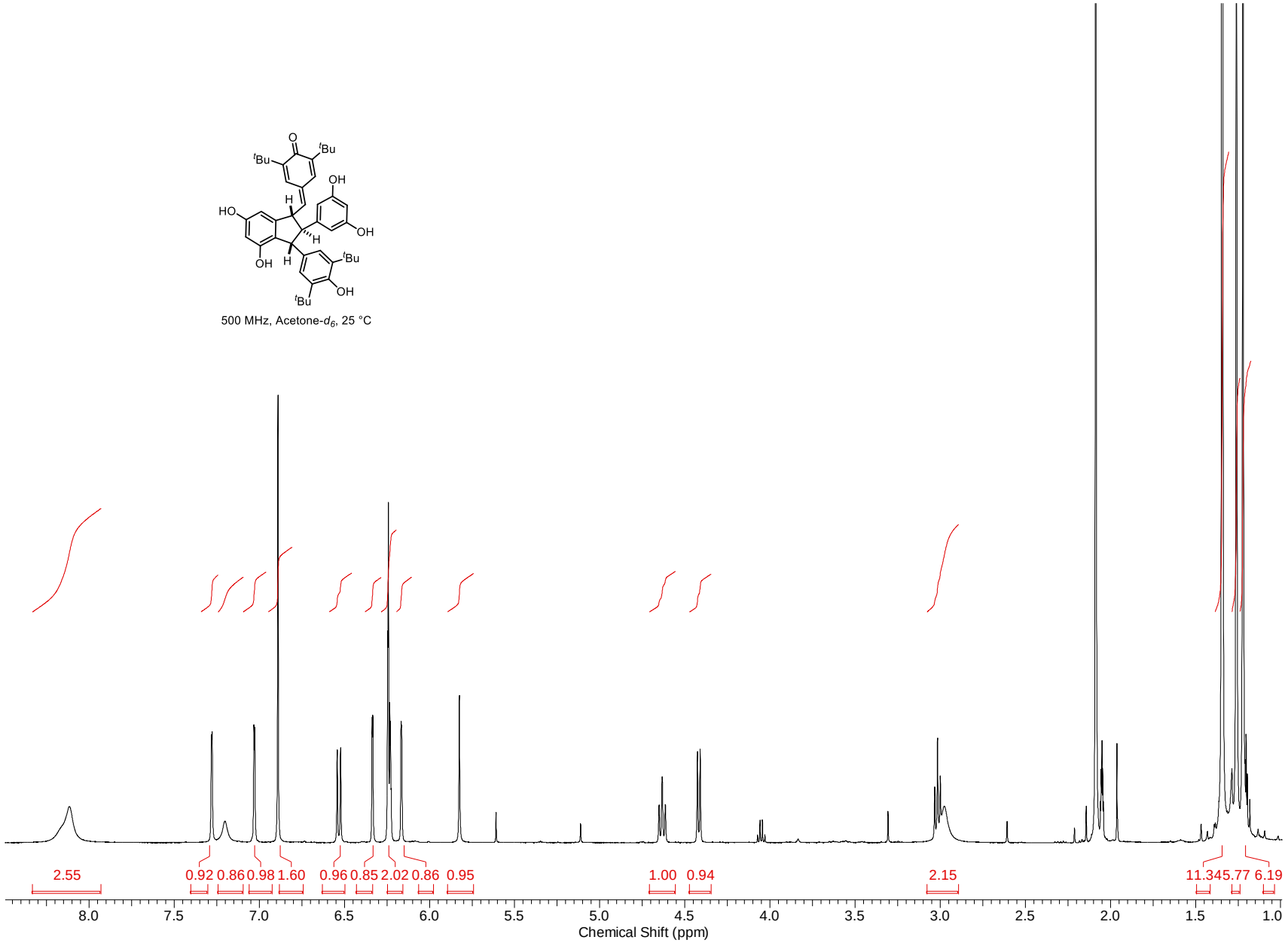
O
tBu
tBu
OH
HO
H
OH
H
H
OH
tBu
tBu
OH
500 MHz, Acetone-d6, 25 °C
2.55
0.92
0.86
0.98
1.60
0.96
0.85
2.02
0.86
0.95
1.00
0.94
2.15
11.34
5.77
6.19
8.0
7.5
7.0
6.5
6.0
5.5
5.0
4.5
4.0
3.5
3.0
2.5
2.0
1.5
1.0
Chemical Shift (ppm)

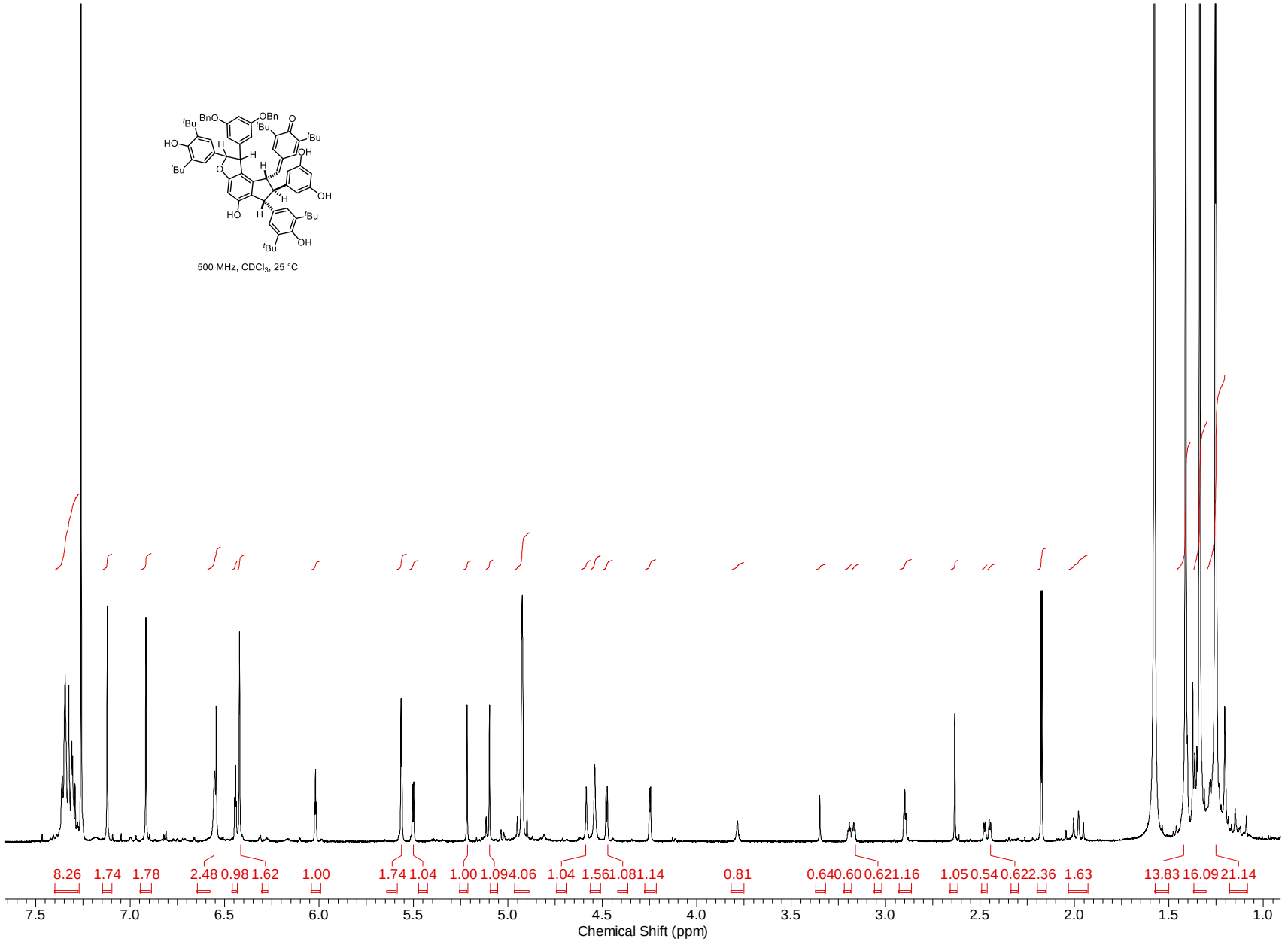
500 MHz, CDCl3, 25 °C
8.26 1.74 1.78 2.48 0.98 1.62 1.00 1.74 1.04 1.00 1.09 4.06 1.04 1.56 1.08 1.14 0.81 0.64 0.60 0.62 1.16 1.05 0.54 0.62 2.36 1.63 13.83 16.09 21.14
7.5 7.0 6.5 6.0 5.5 5.0 4.5 4.0 3.5 3.0 2.5 2.0 1.5 1.0
Chemical Shift (ppm)

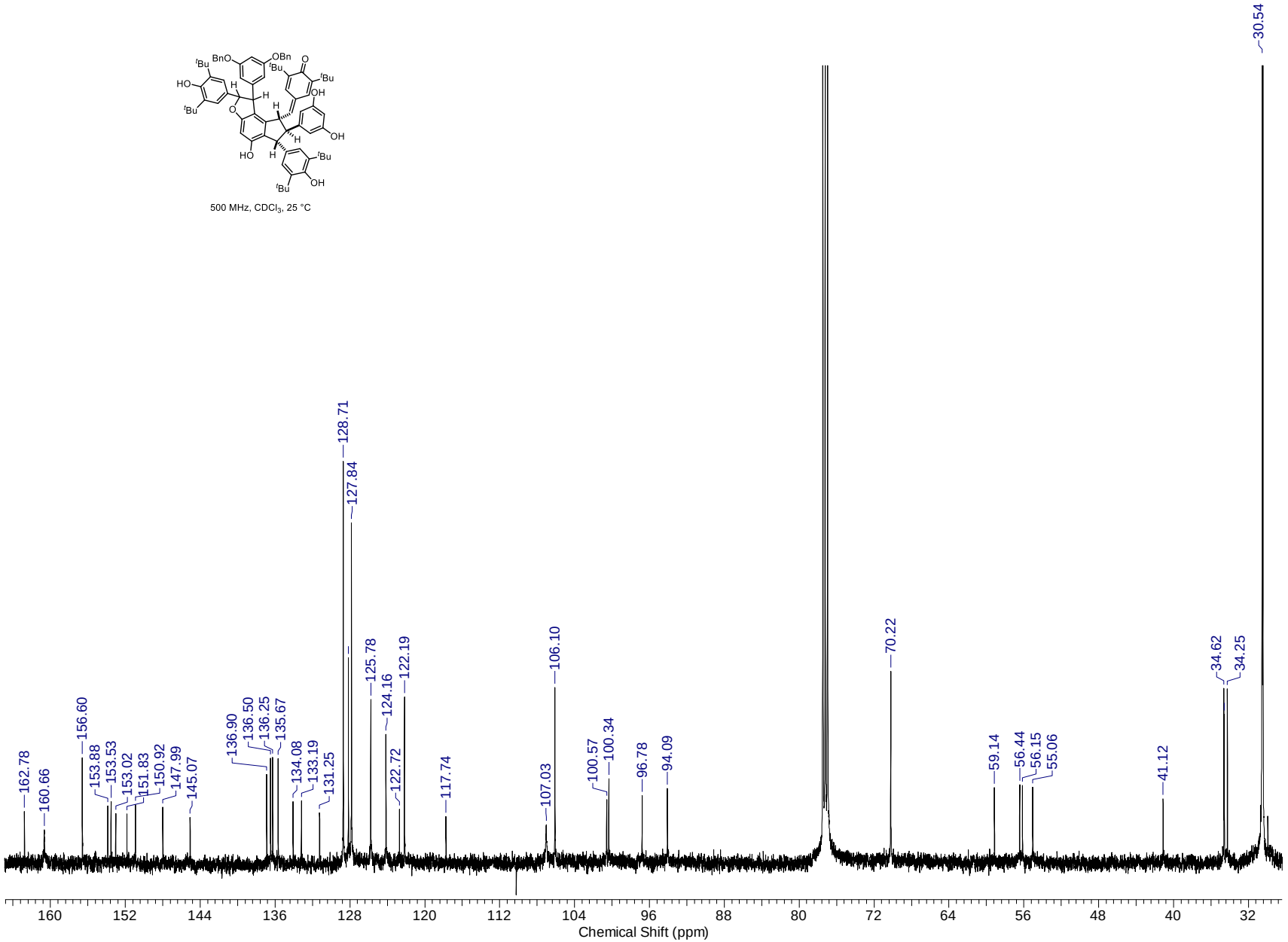
500 MHz, CDCl3, 25 °C
162.78
160.66
156.60
153.88
153.53
153.02
151.83
150.92
147.99
145.07
136.90
136.50
136.25
135.67
134.08
133.19
131.25
128.71
127.84
125.78
124.16
122.72
122.19
117.74
107.03
106.10
100.57
100.34
96.78
94.09
70.22
59.14
56.44
56.15
55.06
41.12
34.62
34.25
30.54
160
152
144
136
128
120
112
104
96
88
80
72
64
56
48
40
32
Chemical Shift (ppm)

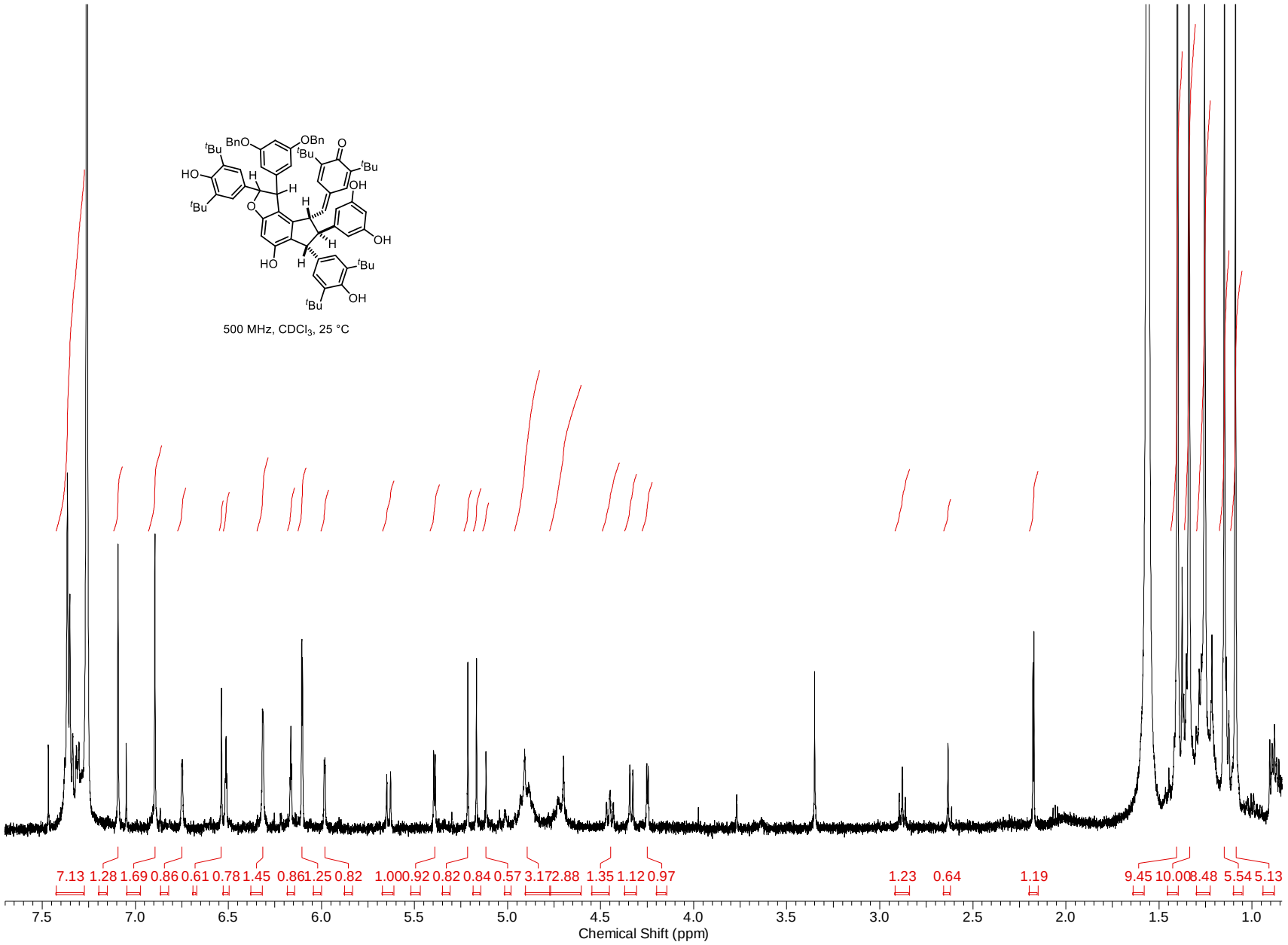
500 MHz, CDCl3, 25 °C
7.13 1.28 1.69 0.86 0.61 0.78 1.45 0.86 1.25 0.82 1.00 0.92 0.82 0.84 0.57 3.17 2.88 1.35 1.12 0.97 1.23 0.64 1.19 9.45 10.00 8.48 5.54 5.13
7.5 7.0 6.5 6.0 5.5 5.0 4.5 4.0 3.5 3.0 2.5 2.0 1.5 1.0
Chemical Shift (ppm)

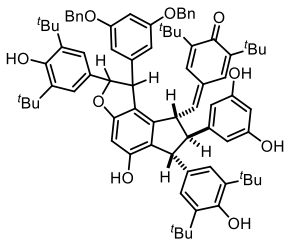

125 MHz, $CDCl_3$, 25 °C

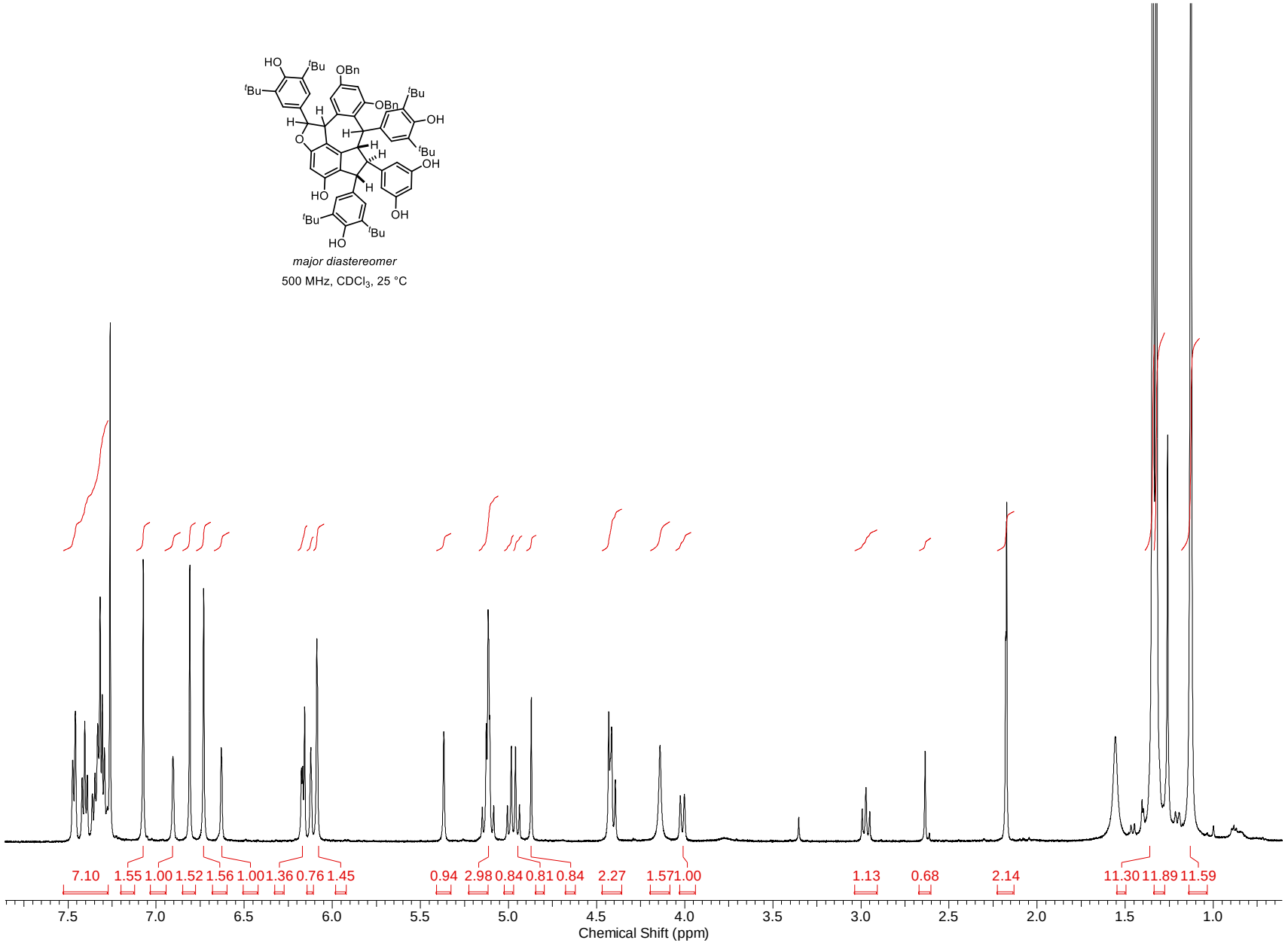
major diastereomer
500 MHz, CDCl3, 25 °C
7.10 1.55 1.00 1.52 1.56 1.00 1.36 0.76 1.45 0.94 2.98 0.84 0.81 0.84 2.27 1.57 1.00 1.13 0.68 2.14 11.30 11.89 11.59
7.5 7.0 6.5 6.0 5.5 5.0 4.5 4.0 3.5 3.0 2.5 2.0 1.5 1.0
Chemical Shift (ppm)

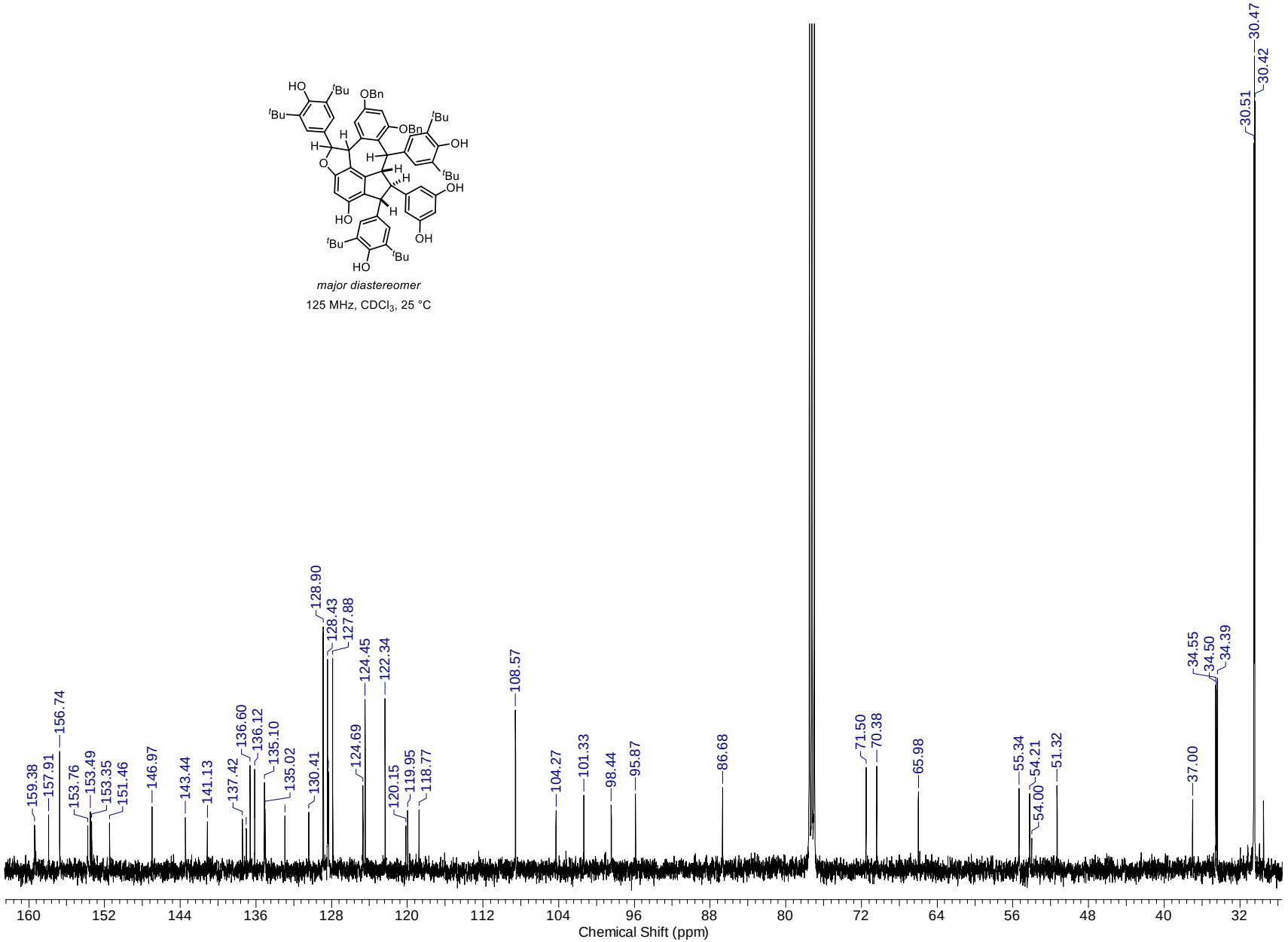
major diastereomer
125 MHz, CDCl3, 25 °C
159.38
157.91
156.74
153.76
153.49
153.35
151.46
146.97
143.44
141.13
137.42
136.60
136.12
135.10
135.02
130.41
128.90
128.43
127.88
124.69
124.45
122.34
120.15
119.95
118.77
108.57
104.27
101.33
98.44
95.87
86.68
71.50
70.38
65.98
55.34
54.21
54.00
51.32
37.00
34.55
34.50
34.39
30.51
30.47
30.42
160
152
144
136
128
120
112
104
96
88
80
72
64
56
48
40
32
Chemical Shift (ppm)

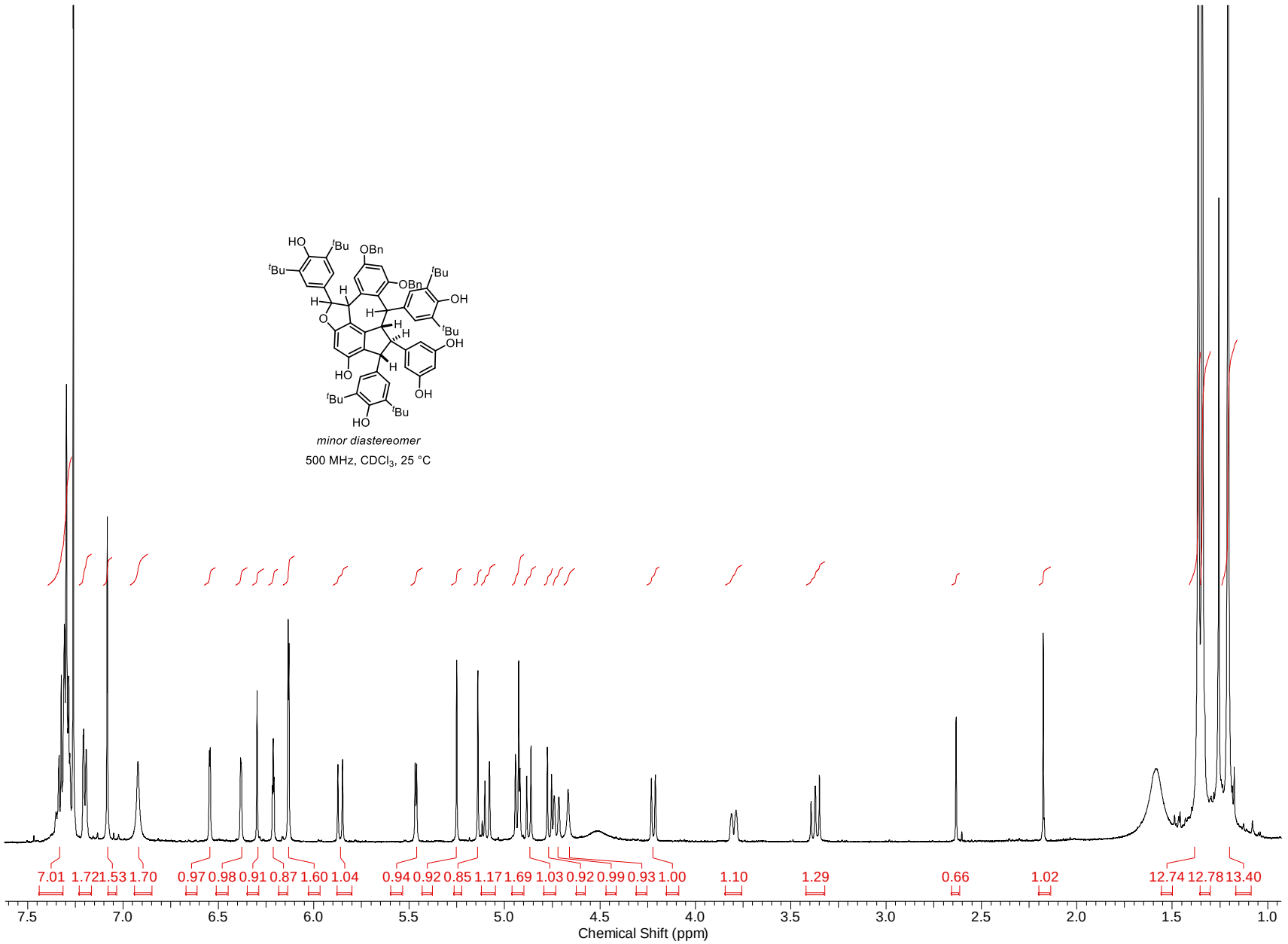
HO
tBu
tBu
OBn
OBn
tBu
OH
tBu
OH
HO
tBu
tBu
HO
OH
H
H
H
H
H
H
O
minor diastereomer
500 MHz, CDCl3, 25 °C
7.01 1.72 1.53 1.70 0.97 0.98 0.91 0.87 1.60 1.04 0.94 0.92 0.85 1.17 1.69 1.03 0.92 0.99 0.93 1.00 1.10 1.29 0.66 1.02 12.74 12.78 13.40
7.5 7.0 6.5 6.0 5.5 5.0 4.5 4.0 3.5 3.0 2.5 2.0 1.5 1.0
Chemical Shift (ppm)

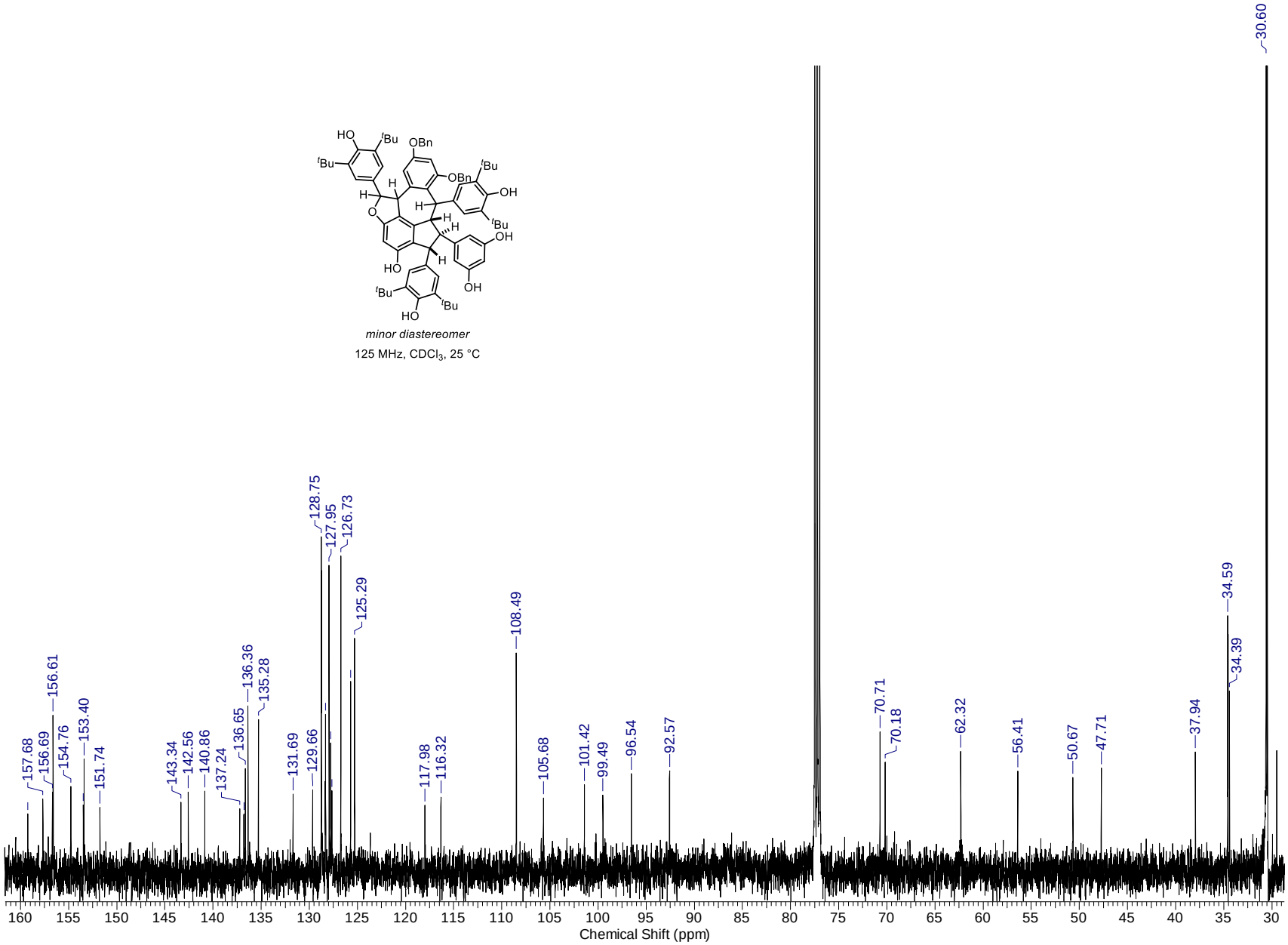
HO
tBu
OBn
tBu
OBn
tBu
OH
H
H
O
H
H
H
H
tBu
OH
OH
HO
H
tBu
OH
tBu
HO
minor diastereomer
125 MHz, CDCl3, 25 °C
30.60
34.59
34.39
128.75
127.95
126.73
125.29
108.49
136.36
135.28
156.61
157.68
156.69
154.76
153.40
151.74
143.34
142.56
140.86
137.24
136.65
131.69
129.66
117.98
116.32
105.68
101.42
99.49
96.54
92.57
70.71
70.18
62.32
56.41
50.67
47.71
37.94
160 155 150 145 140 135 130 125 120 115 110 105 100 95 90 85 80 75 70 65 60 55 50 45 40 35 30
Chemical Shift (ppm)

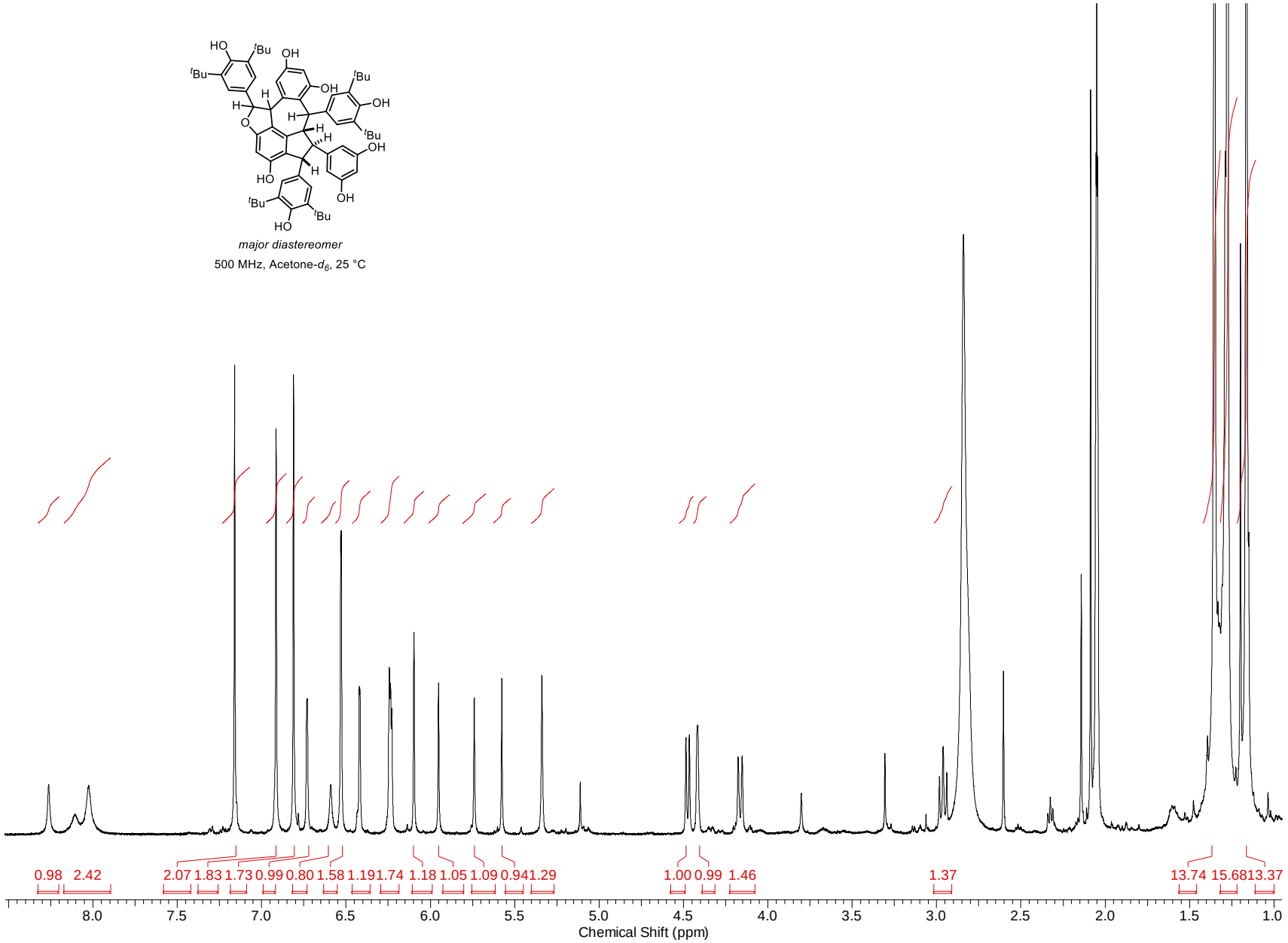
major diastereomer
500 MHz, Acetone-d_6, 25 °C
0.98 2.42 2.07 1.83 1.73 0.99 0.80 1.58 1.19 1.74 1.18 1.05 1.09 0.94 1.29 1.00 0.99 1.46 1.37 13.74 15.68 13.37
8.0 7.5 7.0 6.5 6.0 5.5 5.0 4.5 4.0 3.5 3.0 2.5 2.0 1.5 1.0
Chemical Shift (ppm)

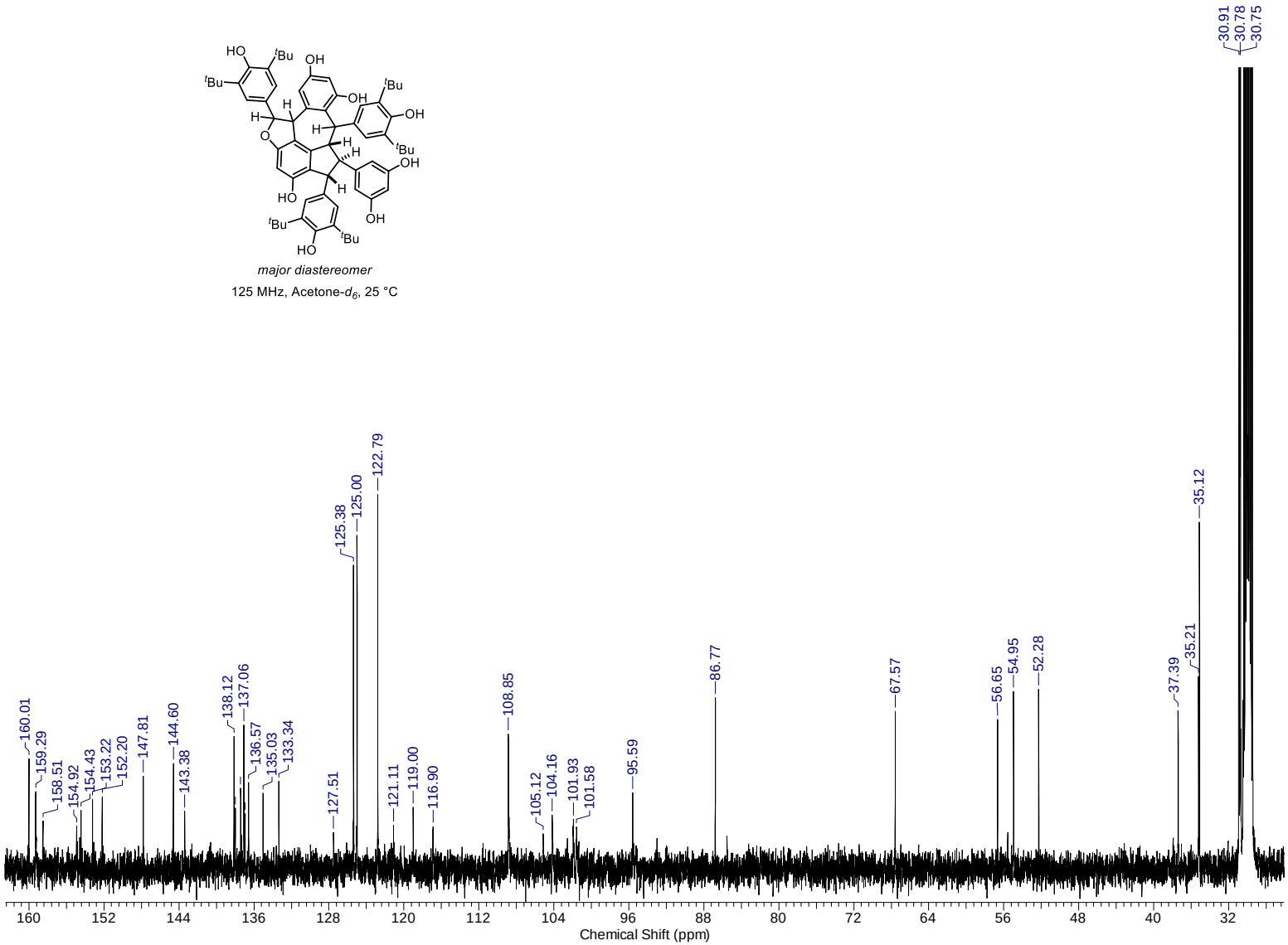
major diastereomer
125 MHz, Acetone-d_6, 25 °C
160.01
159.29
158.51
154.92
154.43
153.22
152.20
147.81
144.60
143.38
138.12
137.06
136.57
135.03
133.34
127.51
125.38
125.00
122.79
121.11
119.00
116.90
108.85
105.12
104.16
101.93
101.58
95.59
86.77
67.57
56.65
54.95
52.28
37.39
35.21
35.12
30.91
30.78
30.75
Chemical Shift (ppm)

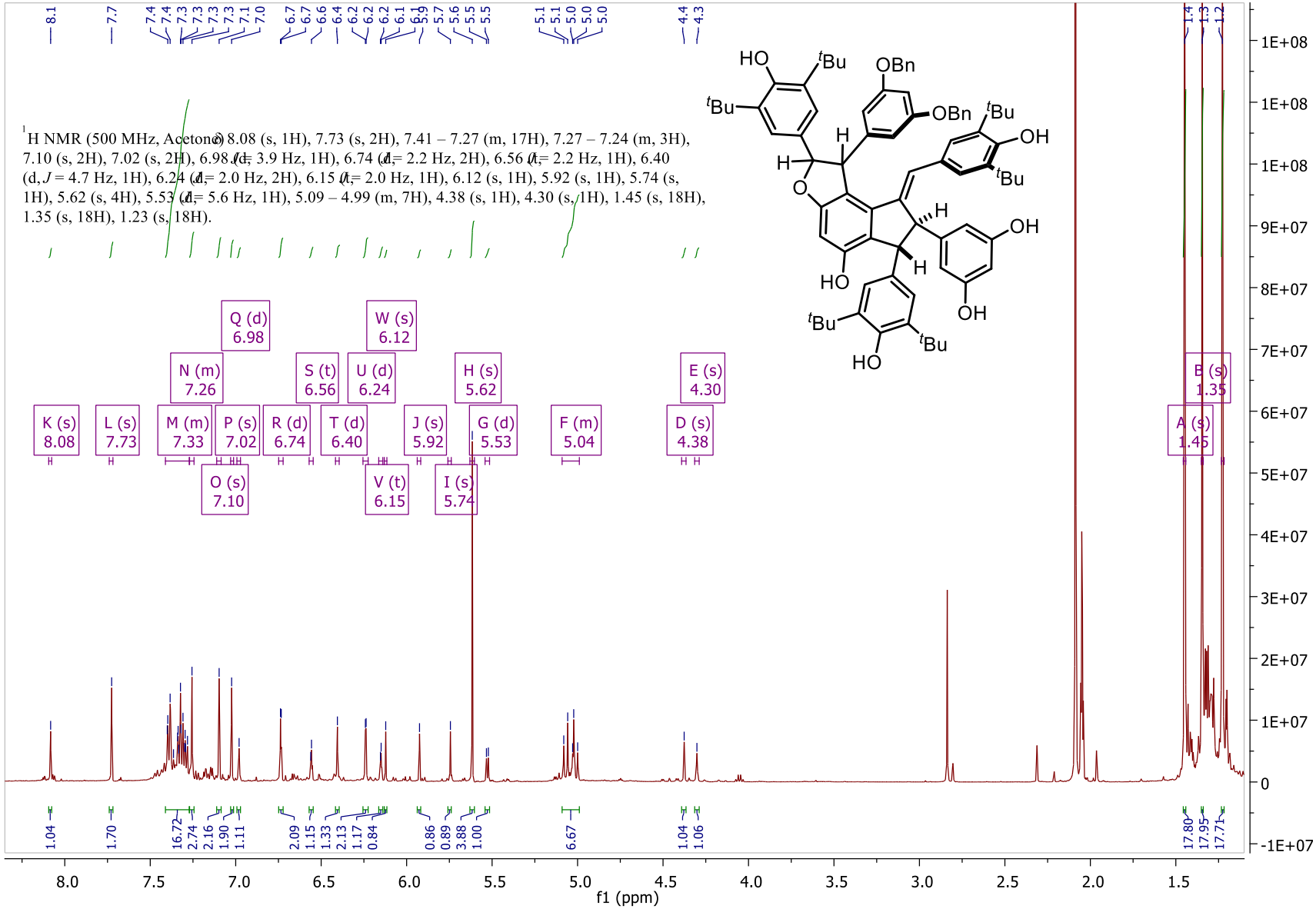
1H NMR (500 MHz, Acetone) δ 8.08 (s, 1H), 7.73 (s, 2H), 7.41 – 7.27 (m, 17H), 7.27 – 7.24 (m, 3H), 7.10 (s, 2H), 7.02 (s, 2H), 6.98 (d, J = 3.9 Hz, 1H), 6.74 (d, J = 2.2 Hz, 2H), 6.56 (t, J = 2.2 Hz, 1H), 6.40 (d, J = 4.7 Hz, 1H), 6.24 (d, J = 2.0 Hz, 2H), 6.15 (t, J = 2.0 Hz, 1H), 6.12 (s, 1H), 5.92 (s, 1H), 5.74 (s, 1H), 5.62 (s, 4H), 5.53 (d, J = 5.6 Hz, 1H), 5.09 – 4.99 (m, 7H), 4.38 (s, 1H), 4.30 (s, 1H), 1.45 (s, 18H), 1.35 (s, 18H), 1.23 (s, 18H).
Q (d) 6.98
W (s) 6.12
N (m) 7.26
S (t) 6.56
U (d) 6.24
H (s) 5.62
E (s) 4.30
B (s) 1.35
K (s) 8.08
L (s) 7.73
M (m) 7.33
P (s) 7.02
R (d) 6.74
T (d) 6.40
J (s) 5.92
G (d) 5.53
F (m) 5.04
D (s) 4.38
A (s) 1.45
O (s) 7.10
V (t) 6.15
I (s) 5.74
f1 (ppm)

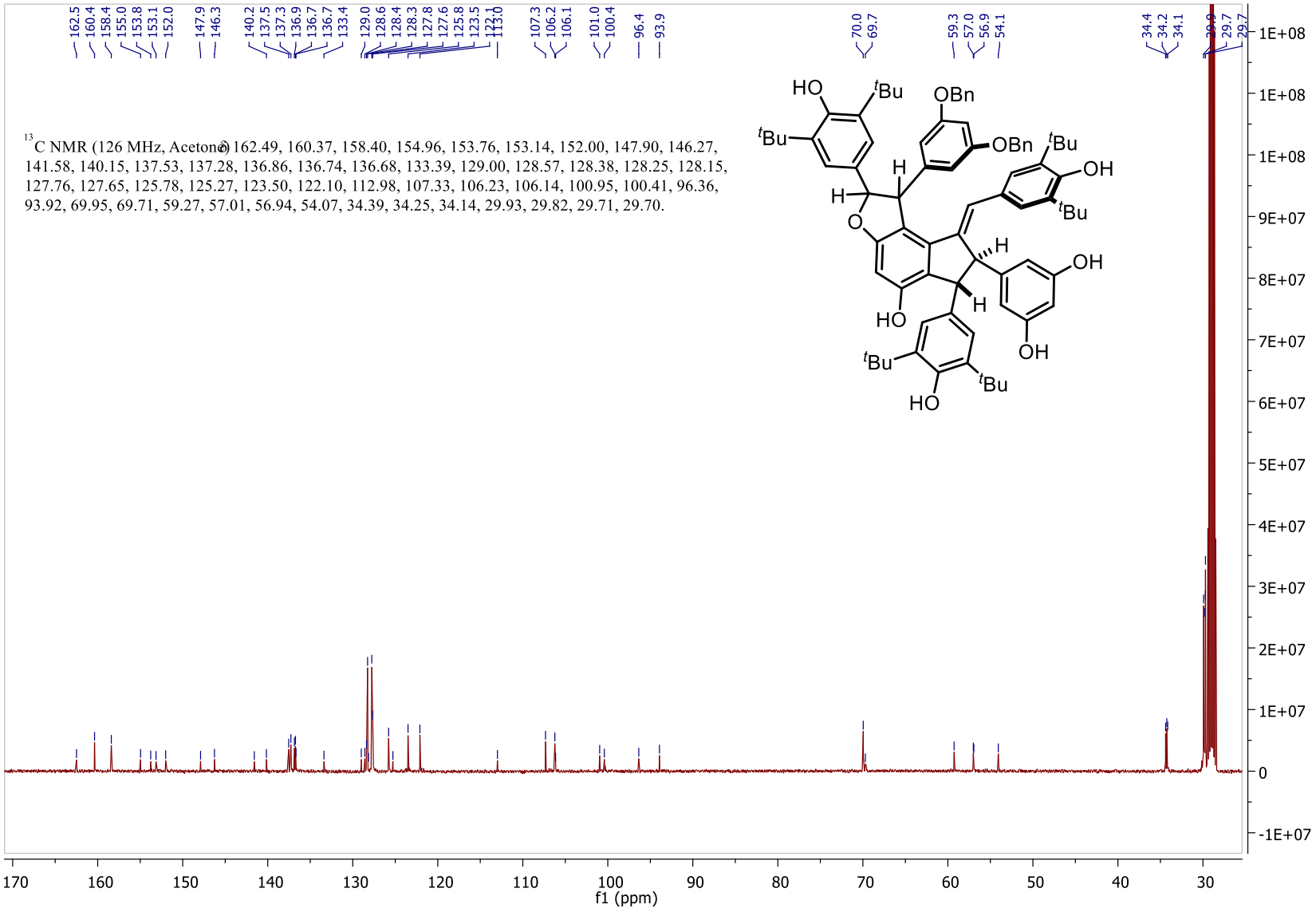

^{13}C NMR (126 MHz, Acetone-d_6) δ 162.49, 160.37, 158.40, 154.96, 153.76, 153.14, 152.00, 147.90, 146.27, 141.58, 140.15, 137.53, 137.28, 136.86, 136.74, 136.68, 133.39, 129.00, 128.57, 128.38, 128.25, 128.15, 127.76, 127.65, 125.78, 125.27, 123.50, 122.10, 112.98, 107.33, 106.23, 106.14, 100.95, 100.41, 96.36, 93.92, 69.95, 69.71, 59.27, 57.01, 56.94, 54.07, 34.39, 34.25, 34.14, 29.93, 29.82, 29.71, 29.70.

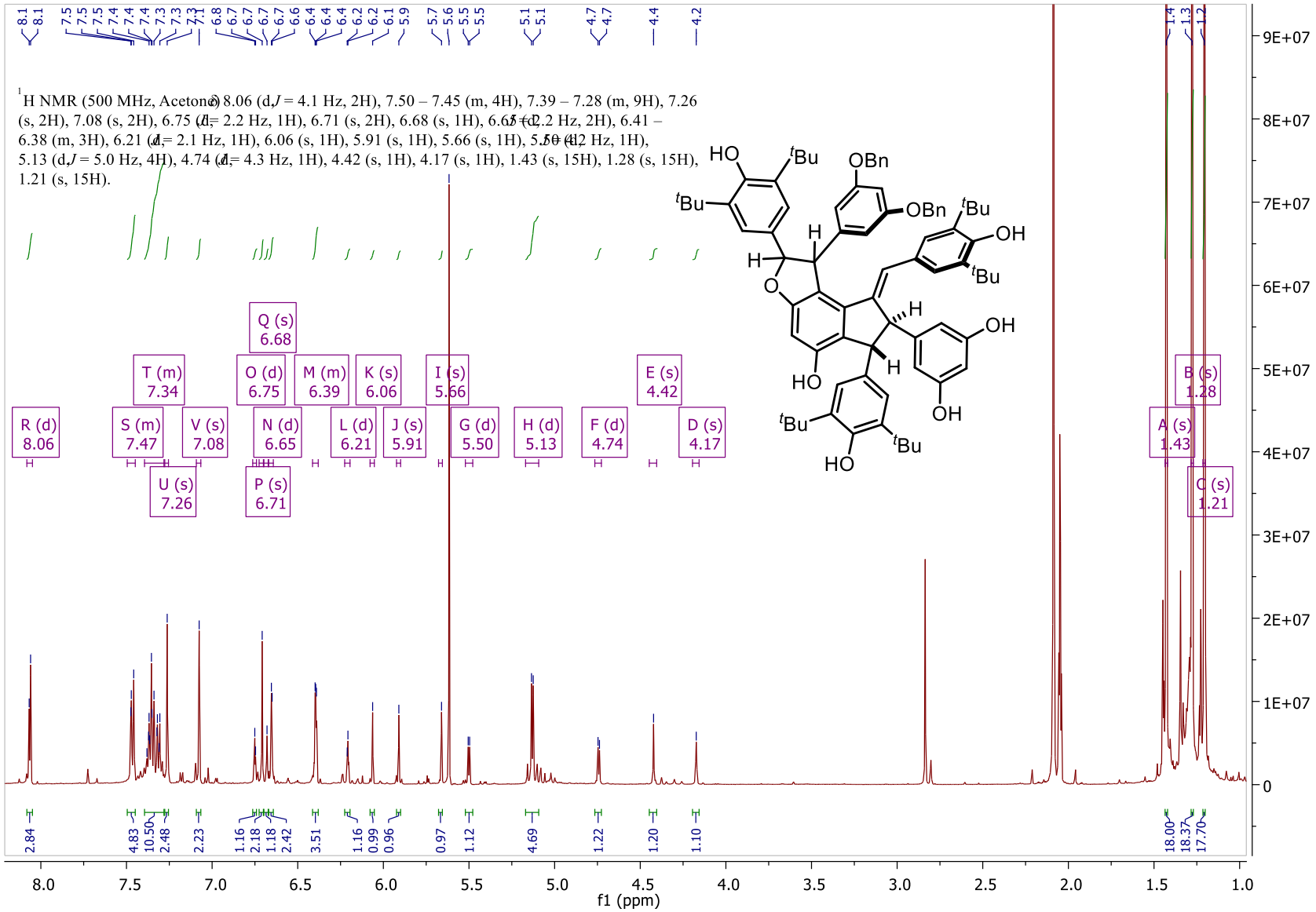
1H NMR (500 MHz, Acetone-d6) δ 8.06 (d, J = 4.1 Hz, 2H), 7.50 – 7.45 (m, 4H), 7.39 – 7.28 (m, 9H), 7.26 (s, 2H), 7.08 (s, 2H), 6.75 (d, J = 2.2 Hz, 1H), 6.71 (s, 2H), 6.68 (s, 1H), 6.65 (d, J = 2.2 Hz, 2H), 6.41 – 6.38 (m, 3H), 6.21 (d, J = 2.1 Hz, 1H), 6.06 (s, 1H), 5.91 (s, 1H), 5.66 (s, 1H), 5.50 (d, J = 4.2 Hz, 1H), 5.13 (d, J = 5.0 Hz, 4H), 4.74 (d, J = 4.3 Hz, 1H), 4.42 (s, 1H), 4.17 (s, 1H), 1.43 (s, 15H), 1.28 (s, 15H), 1.21 (s, 15H).
R (d) 8.06
S (m) 7.47
U (s) 7.26
V (s) 7.08
T (m) 7.34
N (d) 6.65
P (s) 6.71
O (d) 6.75
Q (s) 6.68
M (m) 6.39
L (d) 6.21
K (s) 6.06
J (s) 5.91
I (s) 5.66
G (d) 5.50
H (d) 5.13
F (d) 4.74
E (s) 4.42
D (s) 4.17
A (s) 1.43
B (s) 1.28
C (s) 1.21
HO
tBu
OBn
OH
H
O
f1 (ppm)

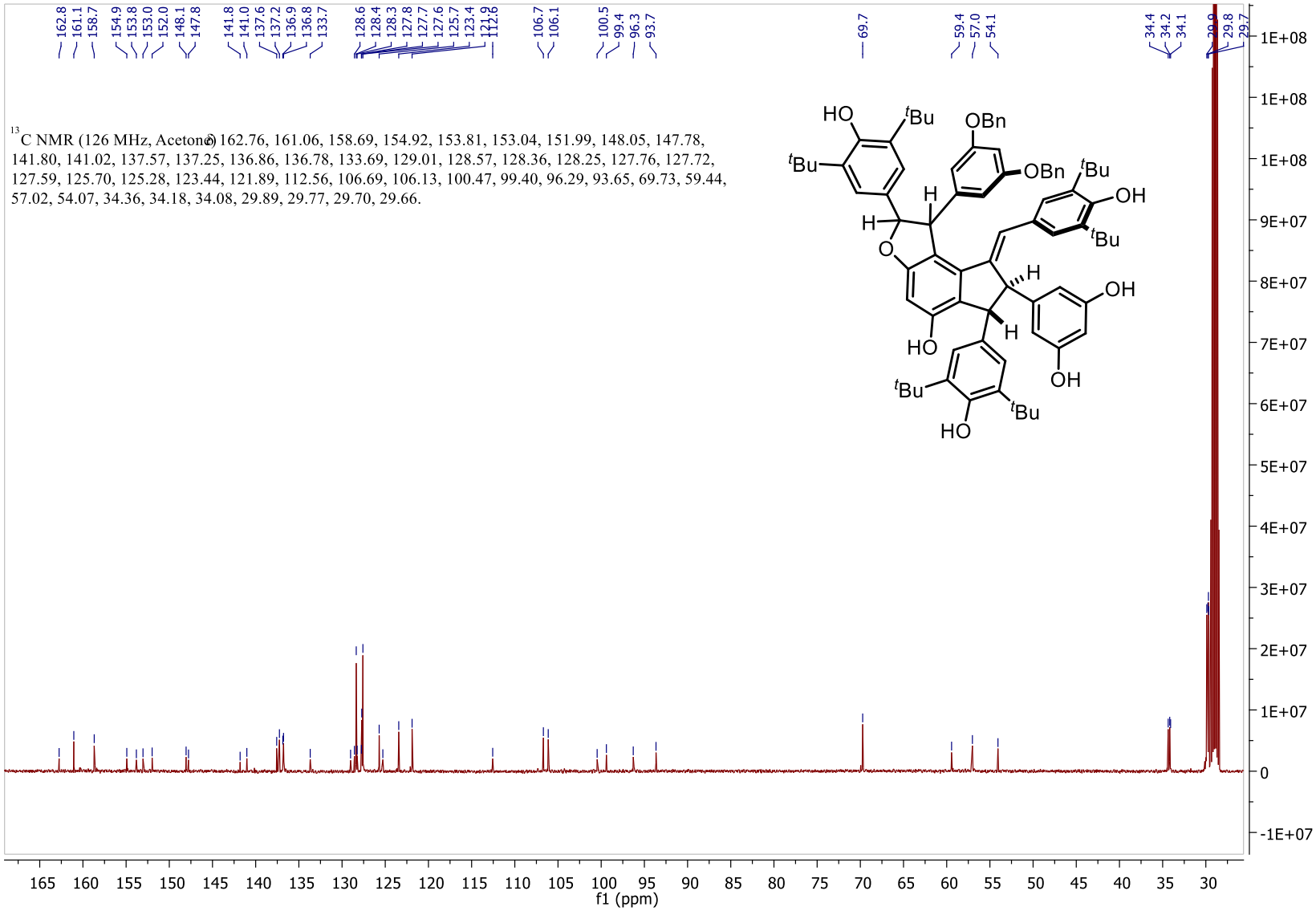

^{13}C NMR (126 MHz, Acetone) δ 162.76, 161.06, 158.69, 154.92, 153.81, 153.04, 151.99, 148.05, 147.78, 141.80, 141.02, 137.57, 137.25, 136.86, 136.78, 133.69, 129.01, 128.57, 128.36, 128.25, 127.76, 127.72, 127.59, 125.70, 125.28, 123.44, 121.89, 112.56, 106.69, 106.13, 100.47, 99.40, 96.29, 93.65, 69.73, 59.44, 57.02, 54.07, 34.36, 34.18, 34.08, 29.89, 29.77, 29.70, 29.66.

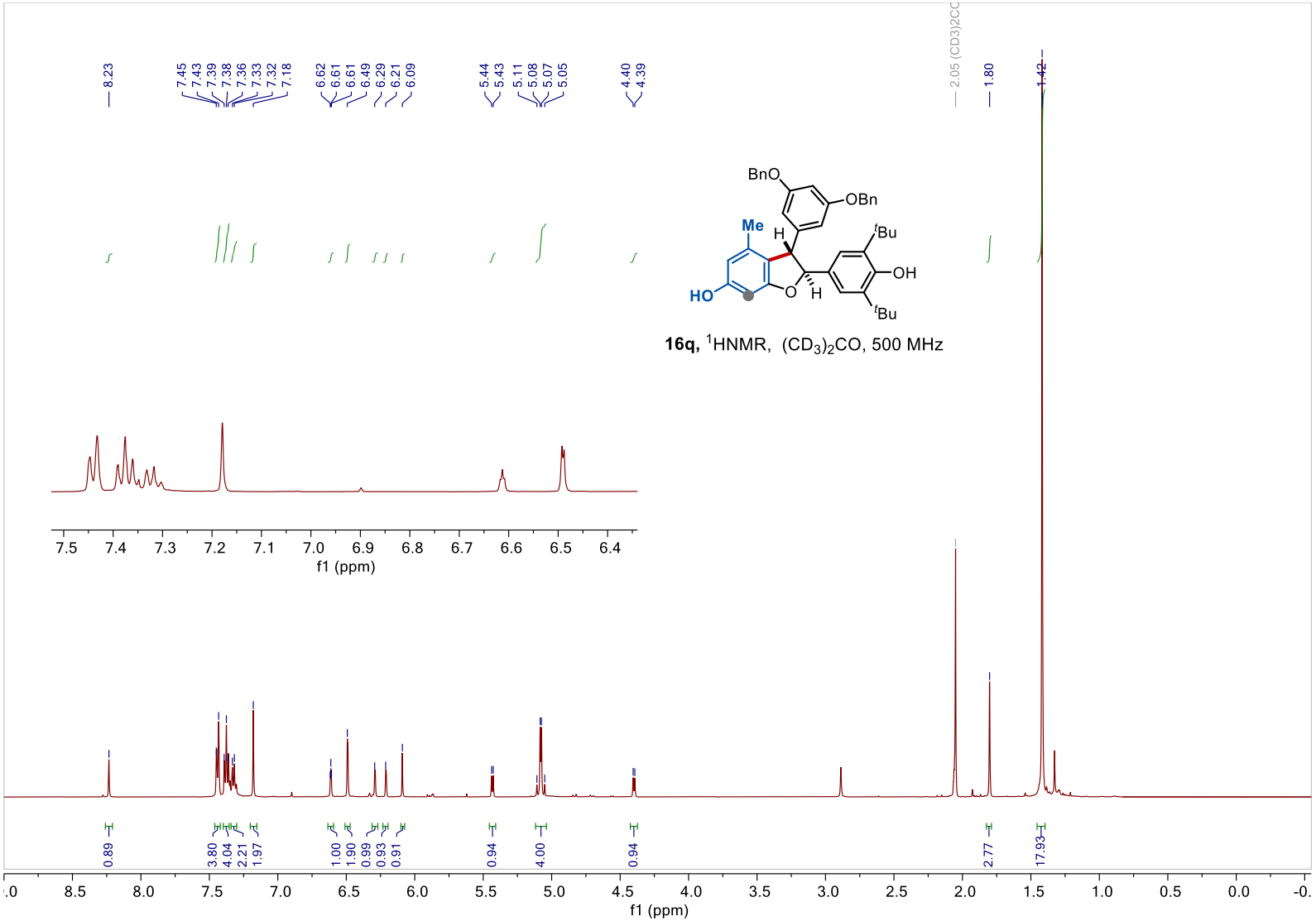
8.23
7.45
7.43
7.39
7.38
7.36
7.33
7.32
7.18
6.62
6.61
6.61
6.49
6.29
6.21
6.09
5.44
5.43
5.11
5.08
5.07
5.05
4.40
4.39
2.05 (CD3)2CO
1.80
1.42
BnO
OBn
Me
H
tBu
OH
HO
O
H
tBu
16q, 1HNMR, (CD3)2CO, 500 MHz
f1 (ppm)
0.89
3.80
4.04
2.21
1.97
1.00
1.90
0.99
0.93
0.91
0.94
4.00
0.94
2.77
17.93
f1 (ppm)

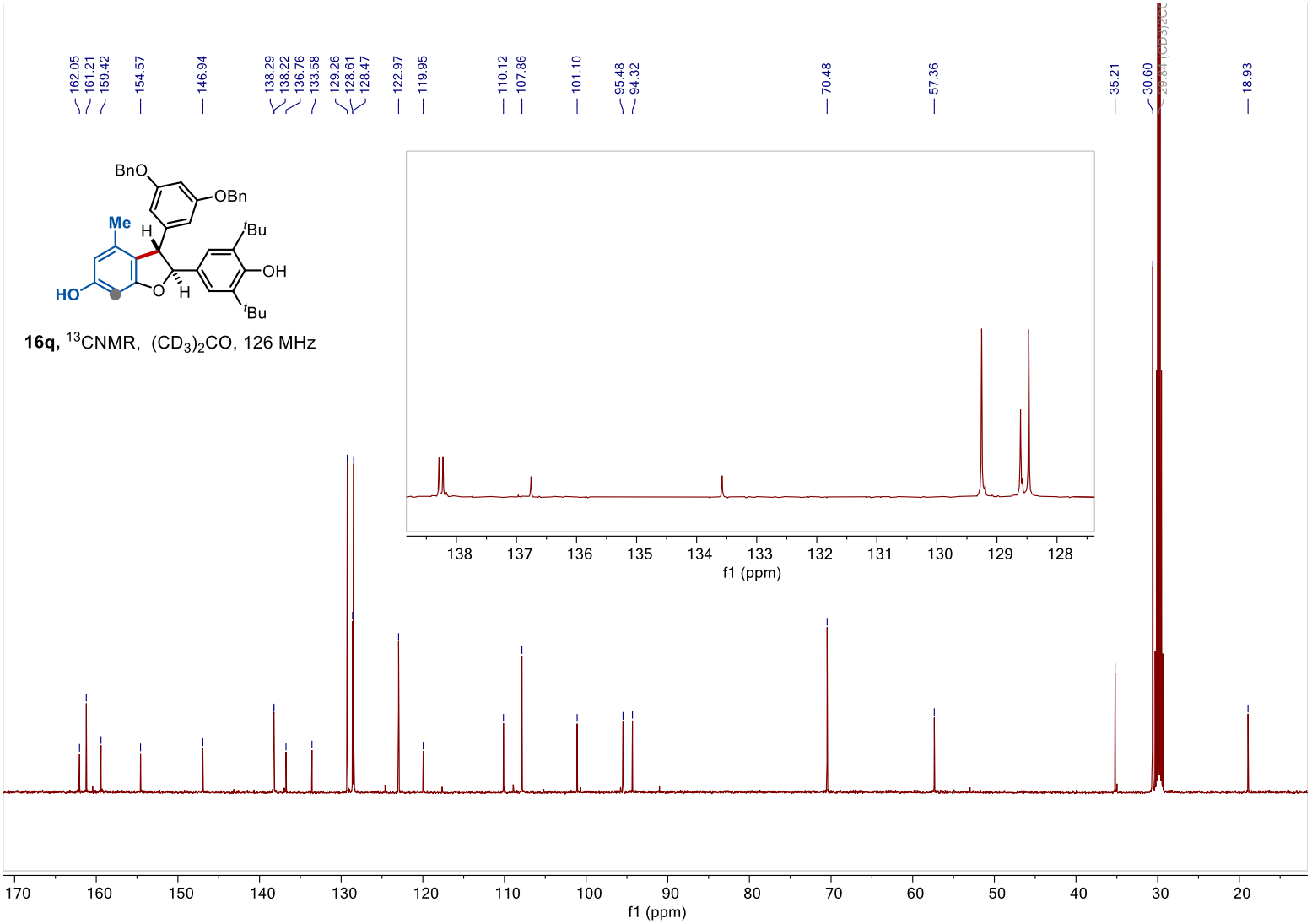
162.05
161.21
159.42
154.57
146.94
138.29
138.22
136.76
133.58
129.26
128.61
128.47
122.97
119.95
110.12
107.86
101.10
95.48
94.32
70.48
57.36
35.21
30.60
18.93
BnO
OBn
Me
H
tBu
OH
HO
O
H
tBu
16q, 13CNMR, (CD3)2CO, 126 MHz
138 137 136 135 134 133 132 131 130 129 128
f1 (ppm)
170 160 150 140 130 120 110 100 90 80 70 60 50 40 30 20
f1 (ppm)

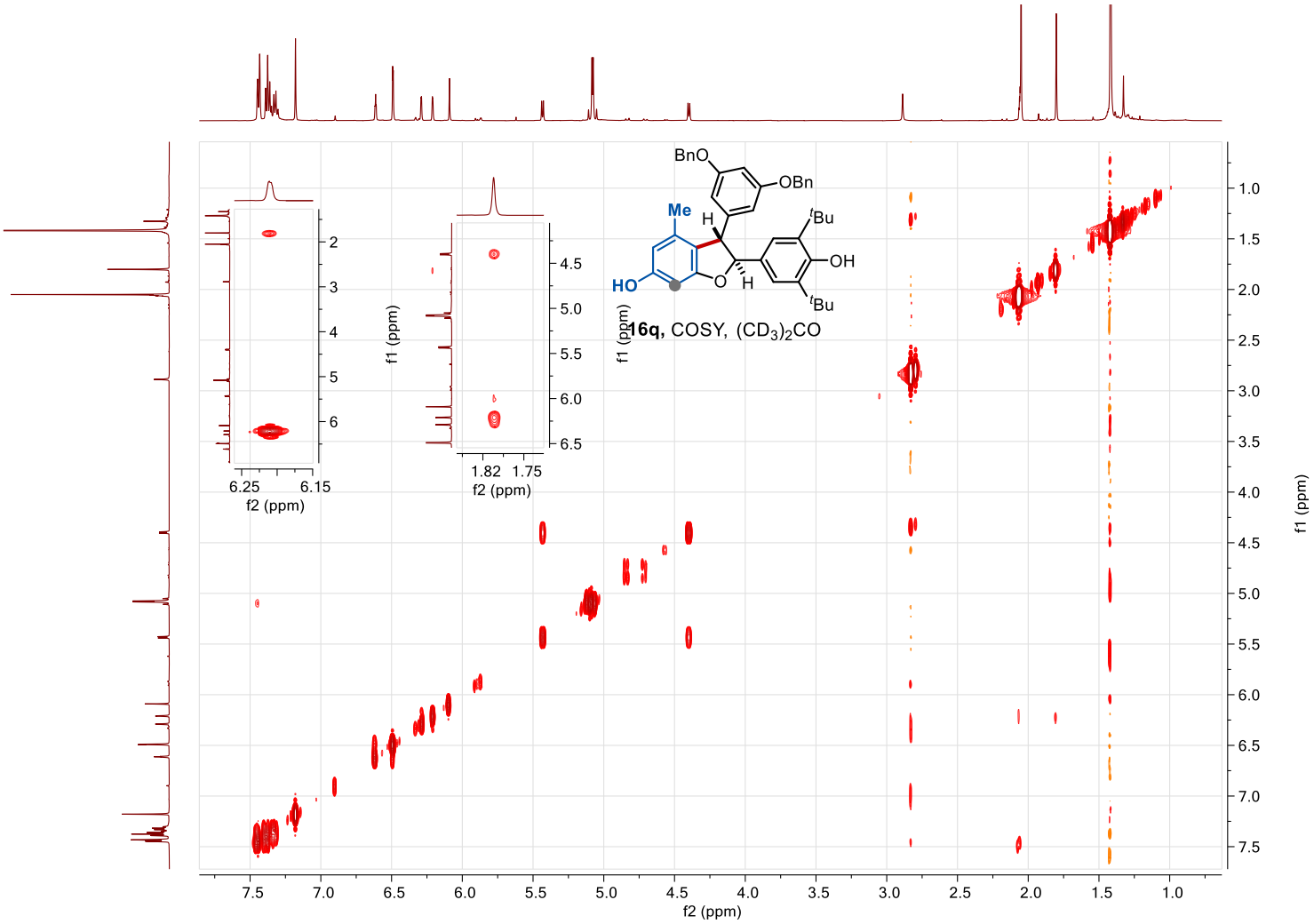
BnO
OBn
Me
H
tBu
OH
HO
O
H
tBu
16q, COSY, (CD3)2CO
f1 (ppm)
f2 (ppm)
6.25
6.15
1.82
1.75

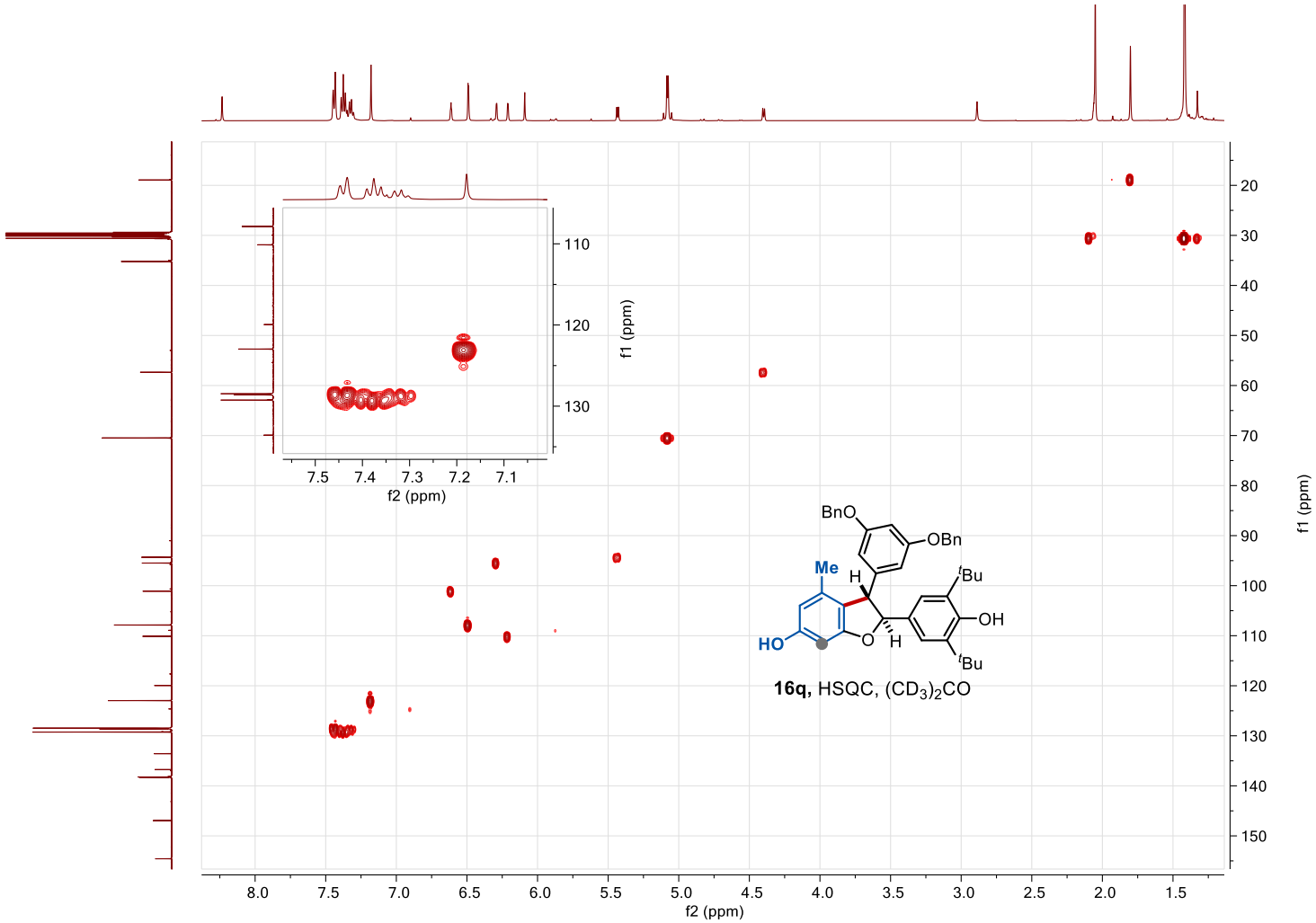
f1 (ppm)
f2 (ppm)
BnO
OBn
Me
H
tBu
OH
HO
O
H
tBu
16q, HSQC, (CD3)2CO

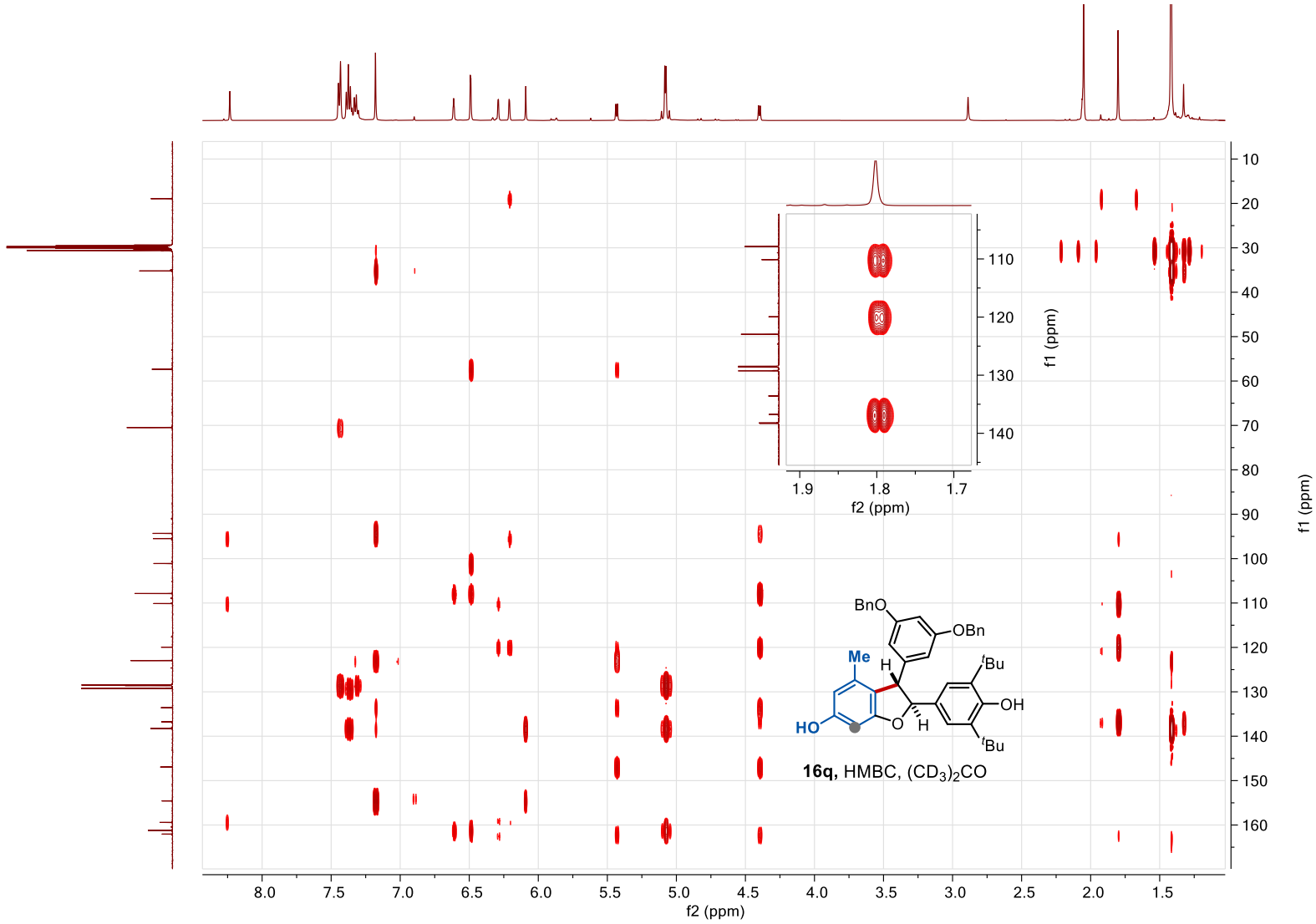
f2 (ppm)
f1 (ppm)
BnO
OBn
Me
H
tBu
OH
HO
O
H
tBu
16q, HMBC, (CD3)2CO

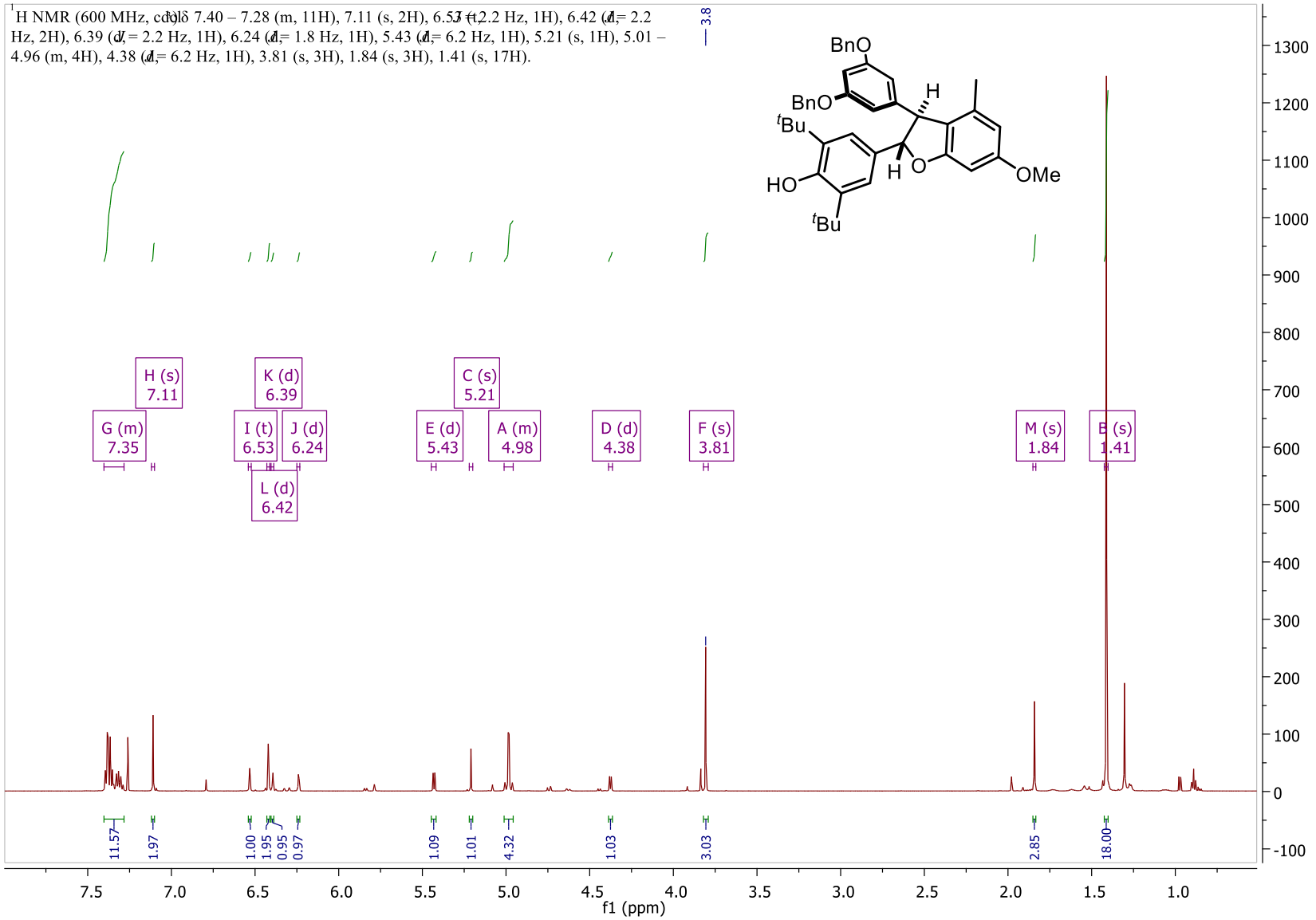
1H NMR (600 MHz, cdcl3) δ 7.40 – 7.28 (m, 11H), 7.11 (s, 2H), 6.53 (t, J = 2.2 Hz, 1H), 6.42 (d, J = 2.2 Hz, 2H), 6.39 (d, J = 2.2 Hz, 1H), 6.24 (d, J = 1.8 Hz, 1H), 5.43 (d, J = 6.2 Hz, 1H), 5.21 (s, 1H), 5.01 – 4.96 (m, 4H), 4.38 (d, J = 6.2 Hz, 1H), 3.81 (s, 3H), 1.84 (s, 3H), 1.41 (s, 17H).
BnO
BnO
tBu
HO
tBu
H
H
O
OMe
H (s) 7.11
K (d) 6.39
C (s) 5.21
G (m) 7.35
I (t) 6.53
J (d) 6.24
E (d) 5.43
A (m) 4.98
D (d) 4.38
F (s) 3.81
M (s) 1.84
B (s) 1.41
L (d) 6.42
11.57
1.97
1.00
1.95
0.95
0.97
1.09
1.01
4.32
1.03
3.03
2.85
18.00
f1 (ppm)

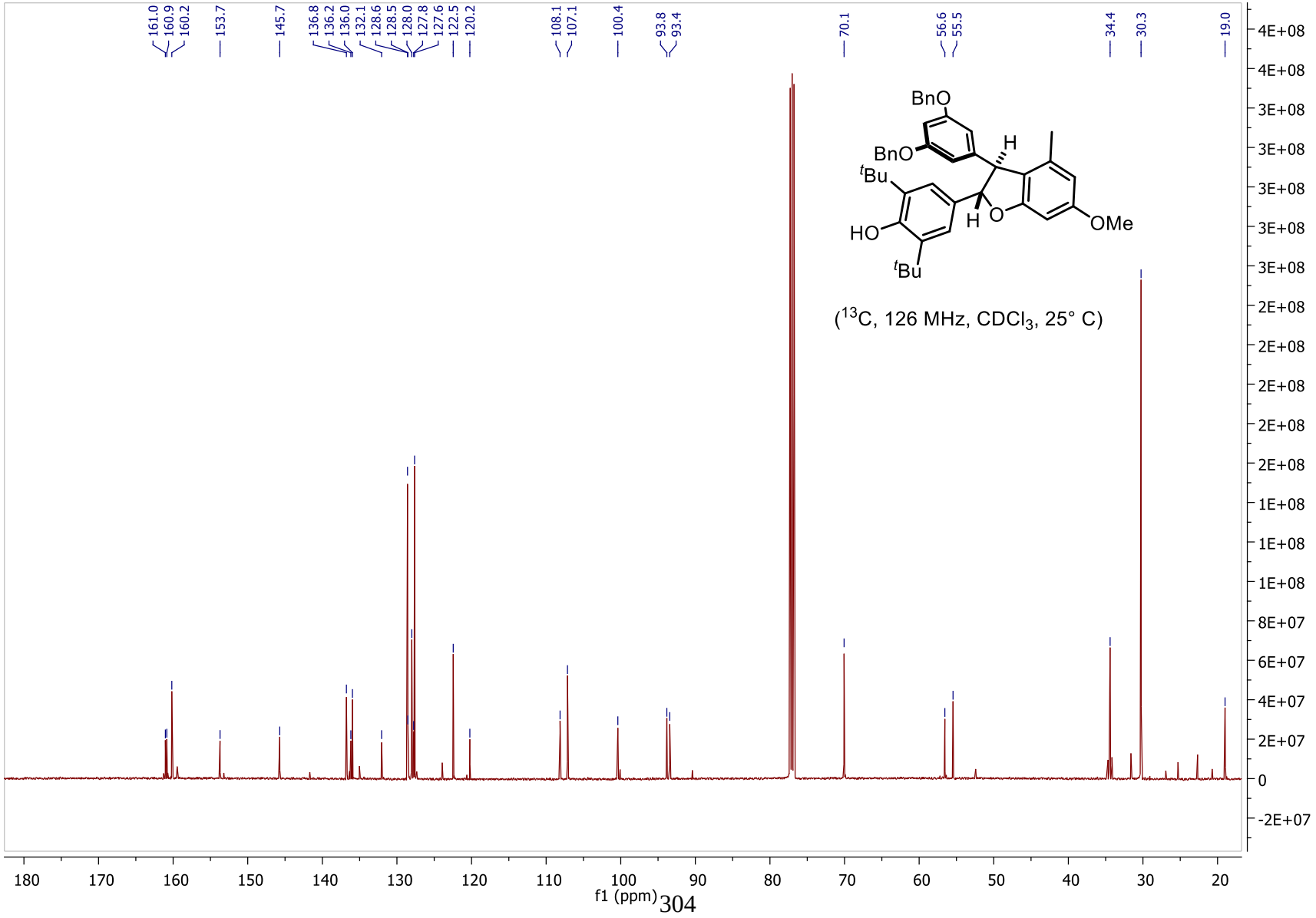
161.0
160.9
160.2
153.7
145.7
136.8
136.2
136.0
132.1
128.6
128.5
128.0
127.8
127.6
122.5
120.2
108.1
107.1
100.4
93.8
93.4
70.1
56.6
55.5
34.4
30.3
19.0
BnO
BnO
tBu
HO
tBu
H
H
O
OMe
(13C, 126 MHz, CDCl3, 25° C)
f1 (ppm)

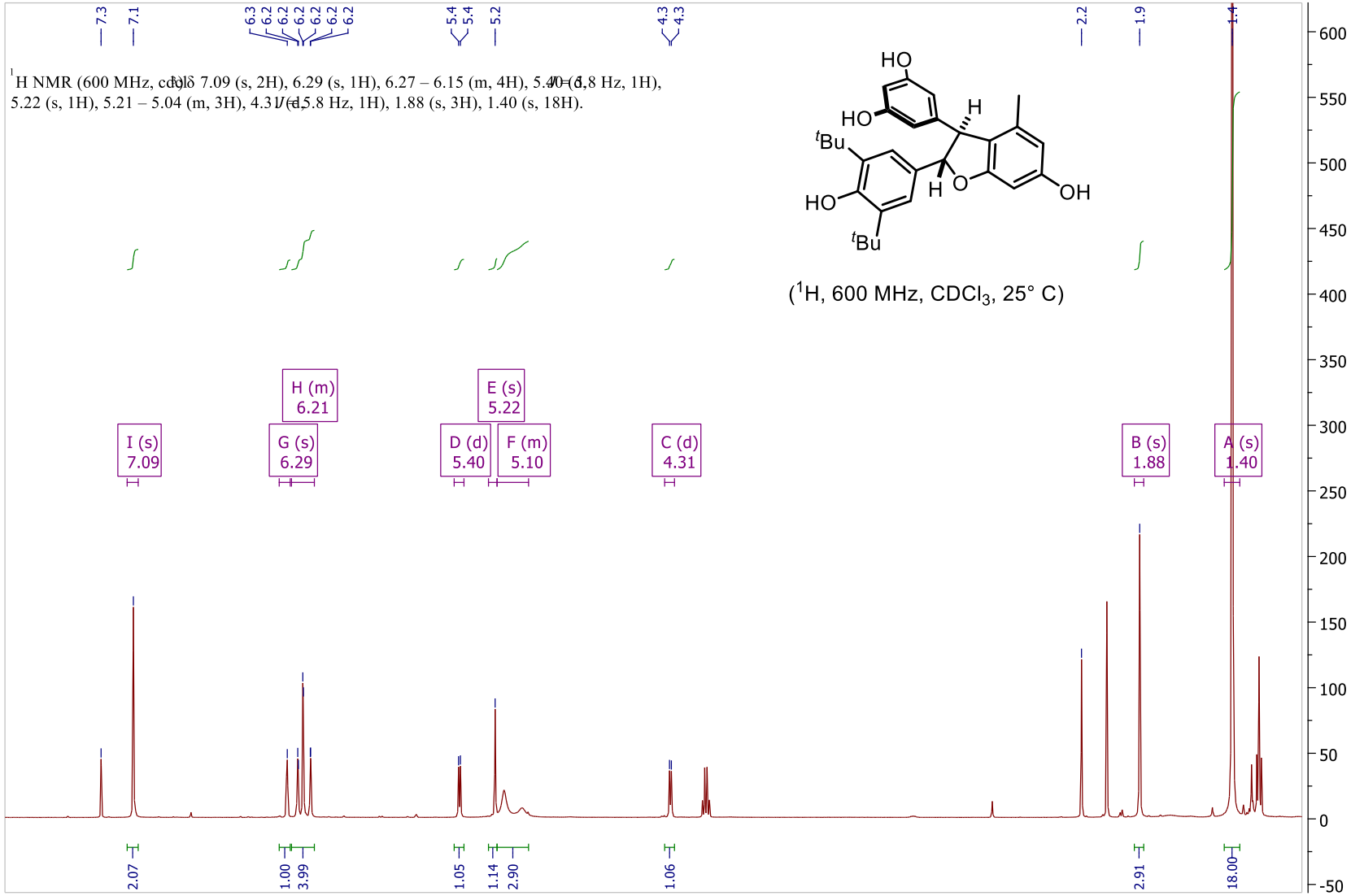

^{1}H NMR (600 MHz, cdcl3) δ 7.09 (s, 2H), 6.29 (s, 1H), 6.27 – 6.15 (m, 4H), 5.40 (d, *J* = 5.8 Hz, 1H), 5.22 (s, 1H), 5.21 – 5.04 (m, 3H), 4.31 (d, *J* = 5.8 Hz, 1H), 1.88 (s, 3H), 1.40 (s, 18H).

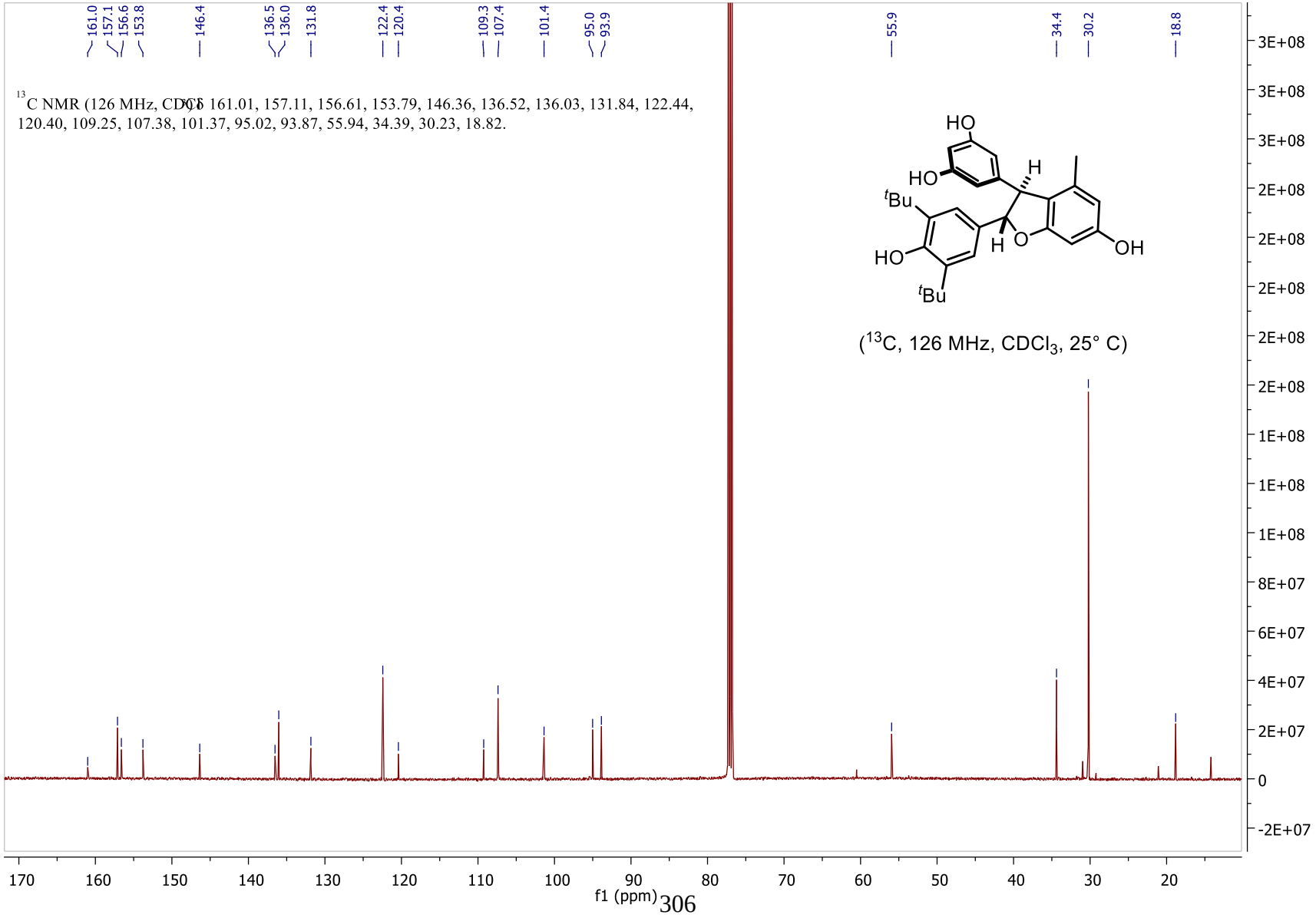
161.0
157.1
156.6
153.8
146.4
136.5
136.0
131.8
122.4
120.4
109.3
107.4
101.4
95.0
93.9
55.9
34.4
30.2
18.8
^{13}C NMR (126 MHz, CDCl3) δ 161.01, 157.11, 156.61, 153.79, 146.36, 136.52, 136.03, 131.84, 122.44, 120.40, 109.25, 107.38, 101.37, 95.02, 93.87, 55.94, 34.39, 30.23, 18.82.
HO
HO
H
^{t}Bu
H
O
OH
HO
^{t}Bu
(^{13}C, 126 MHz, $CDCl_3$, 25° C)
3E+08
3E+08
3E+08
2E+08
2E+08
2E+08
2E+08
2E+08
1E+08
1E+08
1E+08
8E+07
6E+07
4E+07
2E+07
0
-2E+07
170
160
150
140
130
120
110
100
90
80
70
60
50
40
30
20
f1 (ppm)

Chapter 4: Evaluation of the Radical Trapping Antioxidant Properties of Resveratrol-Related natural Products and Polyphenols

Portions of this chapter have been published in:

Romero, K. J.; Galliher, M. S.; Raycroft, M. A. R.; Chauvin, J.-P. R.; Bosque, I.; Pratt, D. A.; Stephenson, C. R. J., *Angewandte Chemie International Edition* **2018,** *57* (52), 17125-17129.[91]

4.1 Introduction

Phenols have long been studied for their radical-trapping antioxidant properties and have been utilized in various industries; most notable is the petroleum industry that uses hindered phenols as additives to petroleum products to prevent autooxidation and its breakdown. One of the more prominent examples is the industrial usage of bis-butylhydroxytoluene (BHT). Natural phenols are also utilized in biological systems to perform the same function as BHT. Nature's canonical RTA is alpha-tocopherol, one of the major isomers of vitamin E. Normal cellular functions generate reactive oxygen species (ROS) that must be sequestered as they can cause oxidation and subsequent breakdown of cellular machinery. Over time, these incidences of oxidation can result in cellular death via the non-apoptotic pathway, ferroptosis. RTAs within the cell are useful for terminating radical processes in which ROS help propagate.[4, 64, 79, 83, 86, 91, 102, 130-137]

Due to the far-reaching applications of antioxidants, numerous assays have been developed for the characterization of the antioxidant activity of chemical compounds to inhibit autoxidation (see **Figure 4.1** for an overview of autoxidation and its inhibition by phenols) over the years. The simplicity of the operation and the principles contribute to the popularity of an assay. Generally, these techniques are reliant on spectroscopic methods for determining the distribution of products for the equilibrium of an antioxidant of interest and an oxidant that can be spectroscopically detected.[79] Common assays include TROLOX equivalent antioxidant capacity (TEAC), ferric reducing antioxidant power (FRAP), cupric

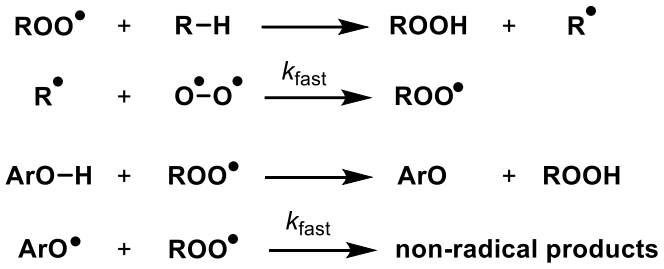

Figure 4.1. Overview of autoxidation and its inhibition by phenolic antioxidants.

TROLOX equivalent antioxidant capacity (TEAC)

Miller & Rice-Evans (**1993**)	Met-Myb	+	H_2O_2	→ HO•
	ABTS	+	HO•	→ $ABTS^{+\bullet}$
Re & Colleagues (**1999**)	ABTS	+	$(NH_4)_2S_2O_3$	→ $ABTS^{+\bullet}$

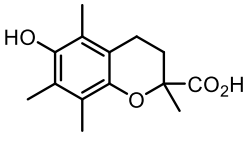

Trolox (4.3)

Mechanism:

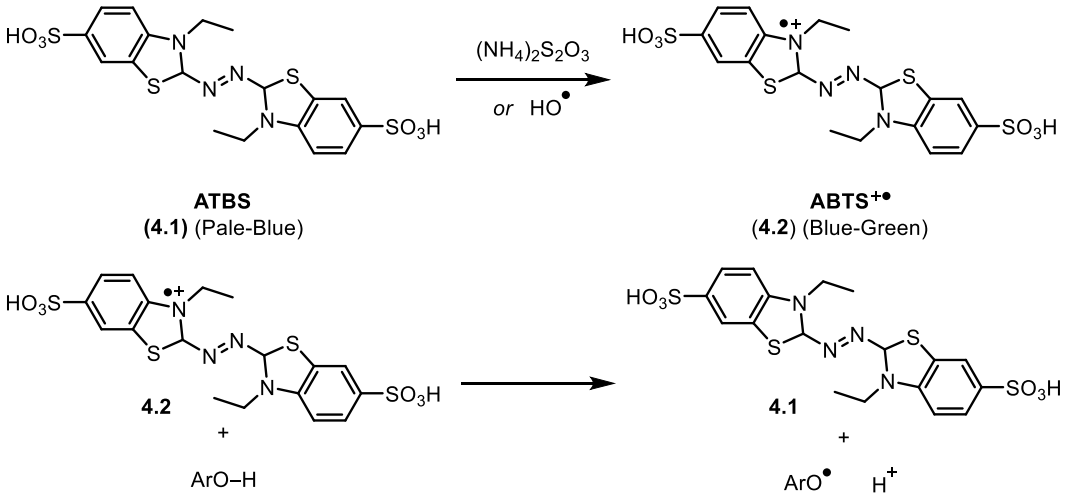

Figure 4.2: This presents an overview of the TROLOX equivalent antioxidant capacity (TEAC) in which ATBS is the main reagent of detection. Trolox is used as a benchmark to which antioxidants are compared.

reducing antioxidant capacity (CUPRAC), and DPPH$^{\bullet}$ quenching assays. These assays all share common characteristics: they all are available in kits, are widely available, they have well defined protocols, and are fast and easy to conduct. While a multitude of other assays that exist for the evaluation of radical-trapping antioxidants, they are less common and will not be discussed.

The TROLOX equivalent antioxidant capacity (TEAC) assay was originally developed in 1993 by Miller and Rice-Evans. This assay is outlined in scheme (**Figure 2**). In this protocol, hydroxyl radical is formed by treating metmyoglobin with hydrogen peroxide. Hydroxyl radical then oxidizes the ABTS (**4.2**) (initially pale blue in solution) reagent forming the radical cation species, ABTS$^{\bullet+}$ (blue-green) (**4.1**). In the presence of radical-trapping antioxidant, HAT of the antioxidant regenerates the ABTS reagent and phenoxyl radical. Results of this assay are compared against TROLOX (**4.3**), a synthetic vitamin E analog used as a benchmark standard.[138] Developments have been made towards the generation of ABTS$^{\bullet+}$ that directly oxidize the ABTS probe.[135] The strengths of this assay are as follows: the ABTS$^{\bullet+}$ intermediate is soluble in both organic and hydrophilic media which widens the scope of antioxidants that can be screened, ABTS$^{\bullet+}$ can be stored for up to 2 days when kept in the dark under ambient conditions, and the assay has good reproducibility. This assay is limited in that long reaction times (12 – 16 hours) are required to form the ABTS$^{\bullet+}$. More importantly, ABTS is unnatural and totally synthetic which makes conclusions about is relevance in biological systems questionable.[131]

The ferric reducing antioxidant power (FRAP) assay (**Figure 4.3**) was originally developed in in 1996 by Iris Benzie and J. J. Strain. In this assay, ferric tripyridyltriazine $[Fe^{III}(TPTZ)]^{3+}$ (**4.4**) starts off as a colorless solution. Antioxidant in solution reduces $[Fe^{III}(TPTZ)]^{3+}$ under acidic

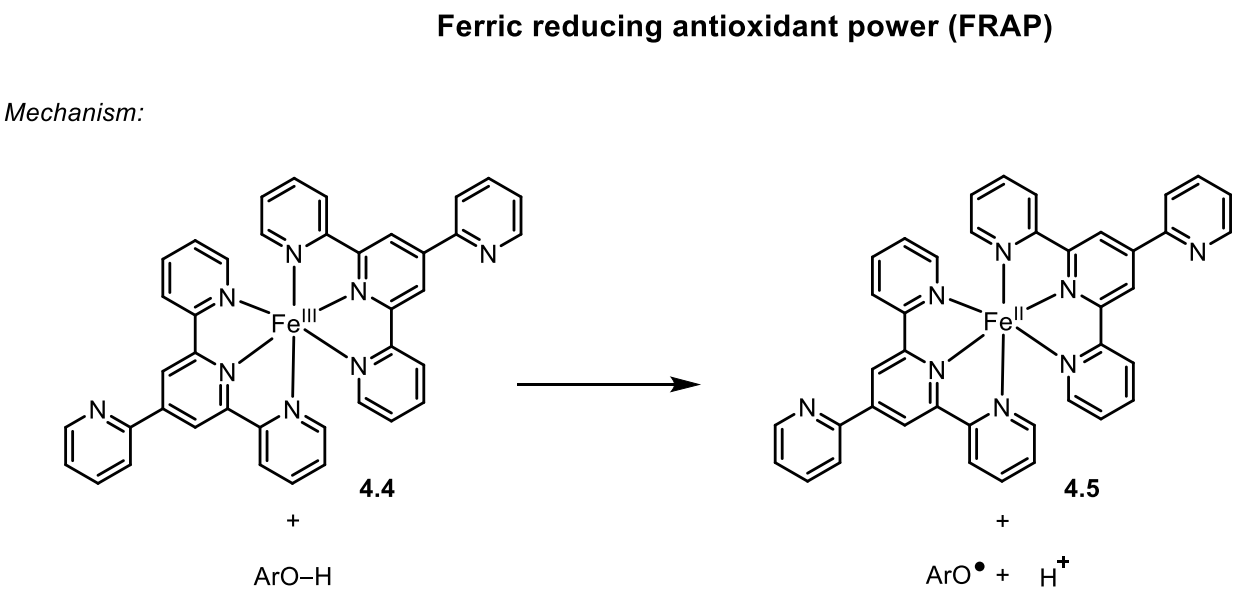

Figure 4.3: This presents an overview of the ferric reducing antioxidant power (FRAP) in which $[Fe^{III}(TPTZ)]^{3+}$ is the main reagent of detection following its reduction with an antioxidant.

conditions to $[Fe^{II}(TPTZ)]^{2+}$ (**4.5**) and turns an intense blue color. The iron-based indicator is formed *in situ*. This is accomplished by the addition of $FeCl_3$ to an acetate buffer solution followed by TPTZ. The order of addition is critical as $FeCl_3$ can be reduced by the TPTZ ligand.[139] The strengths of this assay is that it is easy to set up, requires inexpensive equipment, can be compared to various standards, and can be used to screen a variety of sample media however it is non-specific.[131] Due to the acidic nature of the media, this assay cannot be used to make biologically-relevant conclusions.

The cupric reducing antioxidant capacity (CUPRAC) was first developed by Apak and colleagues in 2004 as a means to determine the total antioxidant content for the nutritional index of foods (**Figure 4.4**). This assay was found to be very effective for polyphenols, thiols, synthetic antioxidants, vitamin C, and vitamin E. The setup for the CUPRAC is simple. Bis(neocuproine) copper (II) cation [$Cu(Nc)_2^{2+}$] in solution starts off as light blue color and upon undergoing reduction by the antioxidant to form the [$Cu(Nc)_2^{+}$] which turns the solution orange-yellow (Scheme X). This assay requires a blank of freshly prepared $CuCl_2$ as it is required to measure absorbance between 400 nm and 500 nm. The copper reagent is prepared *in situ* by mixing $CuCl_2$

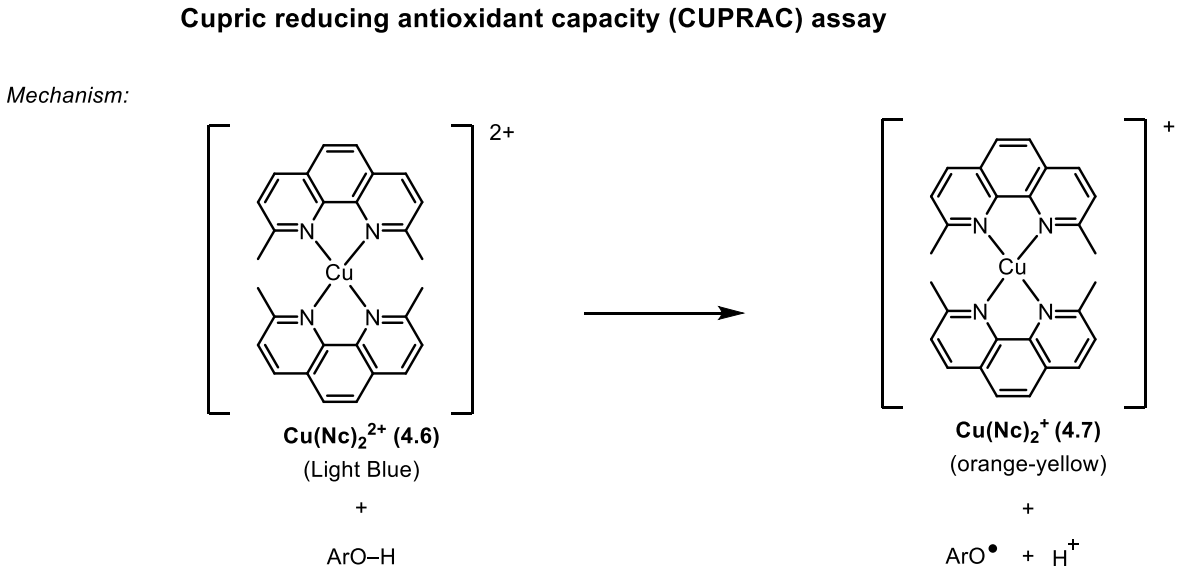

Figure 4.4: This presents an overview of the cupric reducing antioxidant capacity (CUPRAC) assay in which the formation of the copper-based reduced product is monitored spectroscopically.

with neocuproine in ammonium acetate buffer (pH=7).[130] This assay has many strengths including the ready availability of reagents, the rapid color change, and the ability to evaluate hydrophilic

DPPH• radical scavanging assay

Mechanism:

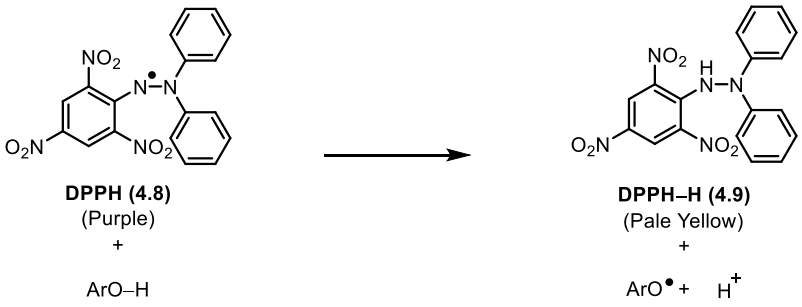

Figure 4.5: This presents an overview of the DPPH• radical scavanging assay in which the disappearance of DPPH• is monitored spectroscopically.

and lipophilic antioxidants. However, this assay is not able to evaluate antioxidant enzymes and can require extended periods of heating for full conversion of slower antioxidants.[131]

The DPPH• quenching assay (**Figure 4.5**) is considered to be the most popular of the aforementioned assays. Although the DPPH• radical was discovered by Goldschmidt and Ren in 1922[140] its use in an antioxidant assay was not realized until Blois developed the DPPH quenching assay in 1958.[132] The DPPH• radical is stabilized due to delocalization by the adjacent aromatic ring and because of this extreme stability, it is a shelf-stable free radical that is readily available for purchase by commercial venders. This mechanism of this assay can operate by two mechanisms: SET or HAT. In the SET mechanism, the antioxidant is oxidized by DPPH• radical and further deprotonated to give DPPH–H and the corresponding antioxidant-derived phenoxyl radical. For the HAT mechanism, the antioxidant under goes the simultaneous loss of proton and electron by the DPPH• radical. The assay starts off as purple in color and following quenching of DPPH• radical by the antioxidant, the solution decolorizes to pale yellow. There are many strengths that are associated with this assay. Due to the stability of the DPPH• radical, there is no need to generate it prior to the initiation of the assay compared to ABTS. The duration of the assay

is short (~30 minutes) even with weak antioxidants. The extreme sensitivity and ability of DPPH• radical to permeate cell membranes, make it seemingly ideal for complex biological systems.[131] However, due to the DPPH• radical being unlike any oxidized substrate that an antioxidant would quench in a biological system, the conclusions that can be made from the assay are not reliable as the antioxidant in question would terminate radical chain processes at a different rate.[79, 136] Additionally, the DPPH• radical is lipophilic and tends to react with Lewis bases and other radicals in solution.[131]

The aforementioned antioxidant assays have the same strengths in that they are all convenient, use readily available reagents, and have similar eases of operation. However, they all share the same limitations. These all fail to provide a kinetic assessment of the antioxidant and rely on a single endpoint measurement that represent the distribution of starting materials and products at equilibrium. Each assay relies on the use of synthetic radical probes that have stable oxidation states and are able to mimic oxidized substrates that are found in physiological conditions. As such, these artificially constructed systems fail to accurately portray real radical chain processes and the antioxidant is poised to undergo a very predictable reaction with the chromophore in solution, chromophores and radicals that are not found in biological systems. It has been discussed that radical chain reactions occur by lipids and sterols found in lipid membranes of the cell and these assays fail to recreate the amphiphilic nature of lipid membranes containing both hydrophilic (polar phosphate groups) and hydrophobic (polyunsaturated fatty acid side chains) which is essential for accurately portraying the efficacy of the transfer of hydrogens from an antioxidant to an oxidized substrate. Developments of new assays by the Pratt group at University of Ottawa have been made to interrogate the kinetics of radical processes that an antioxidant undergoes in

biomimetic and cellular systems which allows for more concrete conclusions about the efficacy of the antioxidant of interest.[134, 136]

4.2 Autoxidation assays in organic solution and liposomes

UV-vis instrumentation is a powerful tool that can be used for continuous detection of a chromophore making it ideal for kinetic measurements. In 2016, the Pratt group developed an assay for assessing the antioxidant activity in organic solutions. In this assay, two co-oxidants were examined individually in these assays based on the rate of inhibition of the antioxidant in chlorobenzene. Two co-oxidants were examined individually in these assays based on the rate of inhibition of the antioxidant in chlorobenzene. 1-hexadecene as a co-oxidant is useful for antioxidants having higher k_{inh} (>10^4 $M^{-1}s^{-1}$) as the rate of autoxidation is relatively fast. Cumene, alternatively, is a useful co-oxidant for antioxidants that have slower k_{inh} rates as this rate of oxidation is slower than 1-hexadecene. The choice of the oxidizable media influences the dye used in the assay. The use of 1-hexadecene requires PBD-DODIPY (**4.11**) (**Figure 4.6**) as this dye is highly reactive at rates needed to keep pace with the rate of autoxidation of the media. This high reactivity is a consequence of the extended conjugation. Cumene-based assays that work on slower

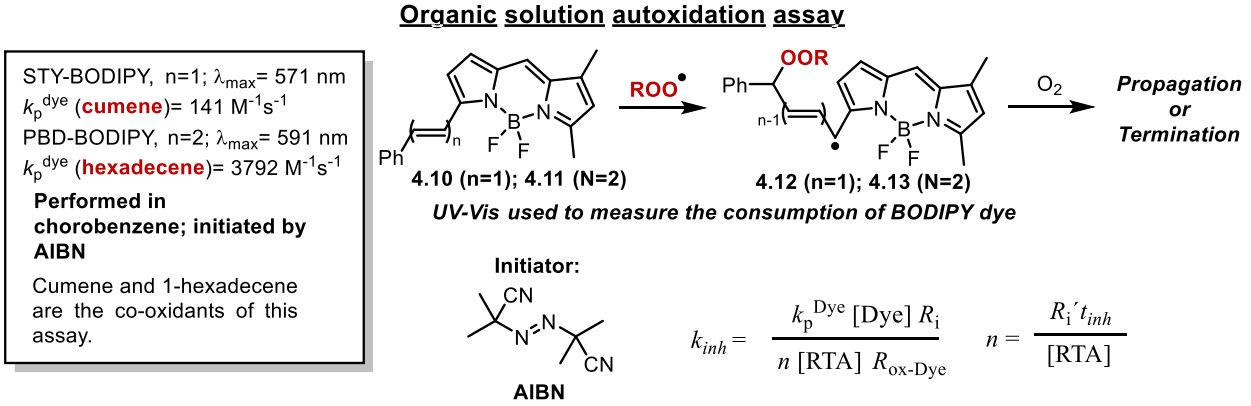

Figure 4.6: This presents an overview of the organic solution-based autoxidation assay in which cumene and 1-hexadecene are the co-oxidants and the consumption of Sty-BODIPY or PBD-BODIPY is measured by UV-vis spectrometry over time. PMC is used as a benchmark reference.

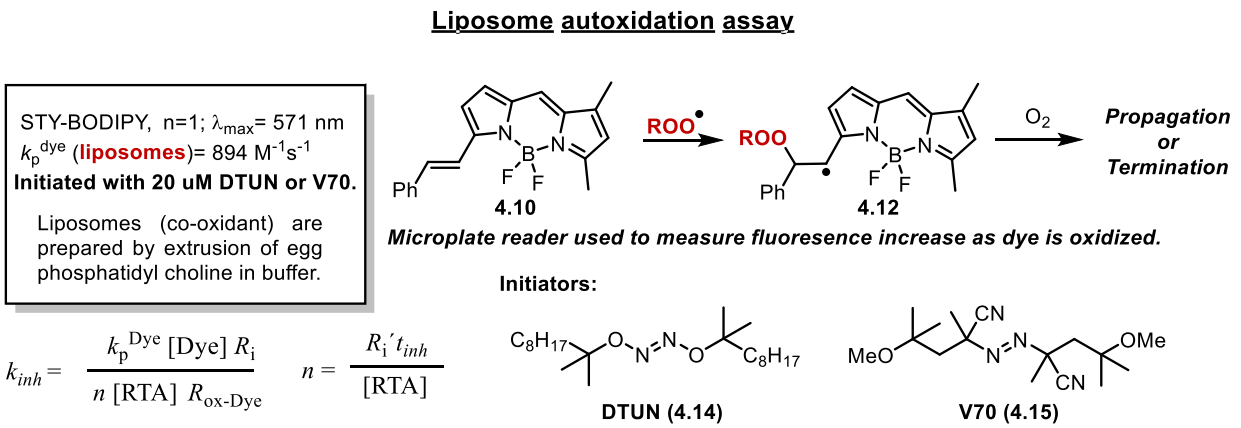

$$k_{inh} = \frac{k_p^{Dye}\,[Dye]\,R_i}{n\,[RTA]\,R_{ox\text{-}Dye}} \qquad n = \frac{R_i' t_{inh}}{[RTA]}$$

Figure 4.7: This presents an overview of the liposome autoxidation assay in which egg PC liposomes are the co-oxidant and the fluorescence of sty-BODIPY is measured over time. PMC is used as a benchmark reference.

antioxidants requires the use of Sty-BODIPY (**4.10**), a less reactive analog of PBD-BODIPY containing one styrenyl moiety in leu of a phenylbutadienyl functional group (PBD-BODIPY). The combination of dyes and oxidizable media is critical as the reactivities for oxidation need to be matched for the assay to work successfully. Azobisisobutyronitrile (AIBN) was chosen as the organically soluble radical initiator for the assays performed in chlorobenzene. Upon addition of the AIBN solution to a cuvette containing the oxidizable media (1-hexadecene or cumene) and dye in chlorobenzene heated to 37°C (biologically relevant), HAT of the organic substrate occurs along with rapid combination of molecular oxygen forming a peroxyl radical adduct. This adduct performs radical addition to the dye olefin forming a radical intermediate that can also combine with molecular oxygen. This oxidation of the dye destroys the conjugation thus leading to a disappearance in signal output at the indicated wavelength. When no antioxidant is added, the signal decreases at a linear rate as propagation is able to occur uninhibited. However, in the presence of antioxidant, peroxyl radicals can be sequestered with via the labile hydrogen of the antioxidant. The intermediate phenoxyl radical that forms can undergo an additional HAT step thus resulting in a non-radical product. One equivalent of phenol such as BHT sequesters 2

equivalents of peroxyl radicals. As a result, the signal output over time changes compared to the uninhibited curve. There are now two distinct regions. The first is the time of inhibition in which the antioxidant buffers the system against autoxidation. Once all of the antioxidant is consumed, the dye undergoes oxidation along with the organic substrate and the curve approaches a similar slope to the uninhibited graph.

In 2019, the Pratt group developed the Fluorescence-Enabled Inhibited Autoxidation (FENIX) assay in order to interrogate the radical trapping antioxidant properties of molecules within a liposome media. The liposome assays (**Figure 4.7**) inherently operate the same such that dye consumption over time is being recorded. Liposomal assays provide a means to ascertain the kinetics of the antioxidants in an environment that more closely resembles the lipid bilayer of cellular membranes. Unlike the organic solution assay, this environment is highly hydrogen bonding as the surfaces of the membrane contain the polar head phosphate group that interacts with aqueous buffer that comprises the bulk of the assay volume.

Reference molecules were needed to assess the trends of the assays as well as the relevant antioxidant activity. 2,2,5,7,8-pentamethyl-6-chromanol (PMC) (**4.16**), a synthetic analog of the biologically relevant α-tocopherol was used as a benchmark reference for antioxidant activity. As α-tocopherol is found intracellularly, it is reasoned that any antioxidant must be able to have competitive kinetics with α-tocopherol in order to be classified as biologically relevant. Additionally, PMC serves as an internal kinetic standard. PMC has a previously determined stoichiometry that can then be used to assess the integrity of the assay based on the rate of initiation (R_i) (R_i = 2.2 x 10^{-9} M s^{-1}). To assess the

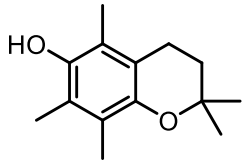

4.9 2,2,5,7,8-pentamethyl-6-chromanol (PMC) (4.16)

antioxidant properties of the phenols of interest, it was decided to subject each compound to several assays to determine the rate of inhibition (k_{inh}) and stoichiometry of sequestered peroxyl radicals in organic solutions (low hydrogen-bonding) and in liposomes (highly hydrogen bonding) followed by RTA cell assays. These assays are routinely used by the Pratt group for every potential new radical-trapping antioxidant. Organic solutions provide an environment in which the k_{inh} and stoichiometry may be accurately computed. The liposome media, is used as a cellular mimic in which all of the intercellular components and intramembrane components are absent.

4.3 Autoxidation assays of QMDs and quadrangularin A analogs

Through our previous collaborative efforts, the resveratrol, alkylated resveratrol, dimers and alkylated analogs were evaluated for their RTA propensity. The results of this study were that the alkylated analogs perform better than the natural products. This was due to the increased lipophilicity allowing the antioxidants to have better solubility in the organic media as well as better localization within cell membranes. Our synthetic efforts were again coupled with the antioxidant expertise of the Pratt lab in 2018 when the quadrangularin A analogs and QMDs synthesized as a result of our electrochemical methodology development were evaluated for their antixodant properties. With these derivatives in hand, we sought to extend our previous investigations of the radical-trapping antioxidant (RTA)[84] activities of resveratrol derivatives, which had revealed that the quadrangularin A scaffold was more potent than either the pallidol scaffold or the parent resveratrol scaffold.[64] Thus, the quadragularin A analogues were evaluated for their ability to inhibit co-autoxidations of PBD-BODIPY and 1-hexadecene in chlorobenzene at 37 °C (Figure 4).[134] PBD-BODIPY enables quantitative determination of the reaction progress of the autoxidation by UV-vis spectrophotometry; its consumption by reaction with chain-carrying

peroxyl radicals is associated with a loss of absorbance at 588 nm (Figure 4A). Kinetic analysis of the reaction progress data according to Eqs. 1 and 2 enables determination of the rate constant for the reaction of the RTA with peroxyl radicals (k_{inh}) as well as the reaction stoichiometry (n) (Figure 4B). Representative data are shown in Figure 4C and kinetic parameters are tabulated in Figure 4D.

The quadrangularin A analogues **30**–**33** are all good RTAs. Their inhibition rate constants are roughly one order of magnitude greater than BHT ($k_{inh} = 2\times10^4$ $M^{-1}s^{-1}$), the quintessential hindered phenolic RTA.[64] Substitution of the resorcinol ring has little impact on the reactivity of the quadrangularin A analogues; most k_{inh} values are within experimental error of each other, and the maximum difference is less than a factor of 2. These results are consistent with our expectation that quadrangularin A and its *tert*-butylated derivative inhibit autoxidation via H-atom transfer from the (hindered) phenolic moiety. The number (n) of peroxyl radicals trapped per molecule is *ca.* 4 for all four compounds. Since compounds **30**–**33** contain two hindered phenols per molecule, the maximum expected stoichiometry is 4, corresponding to double that of BHT and other hindered phenols (*e.g.* the parent phenols, see Table S2).[90]

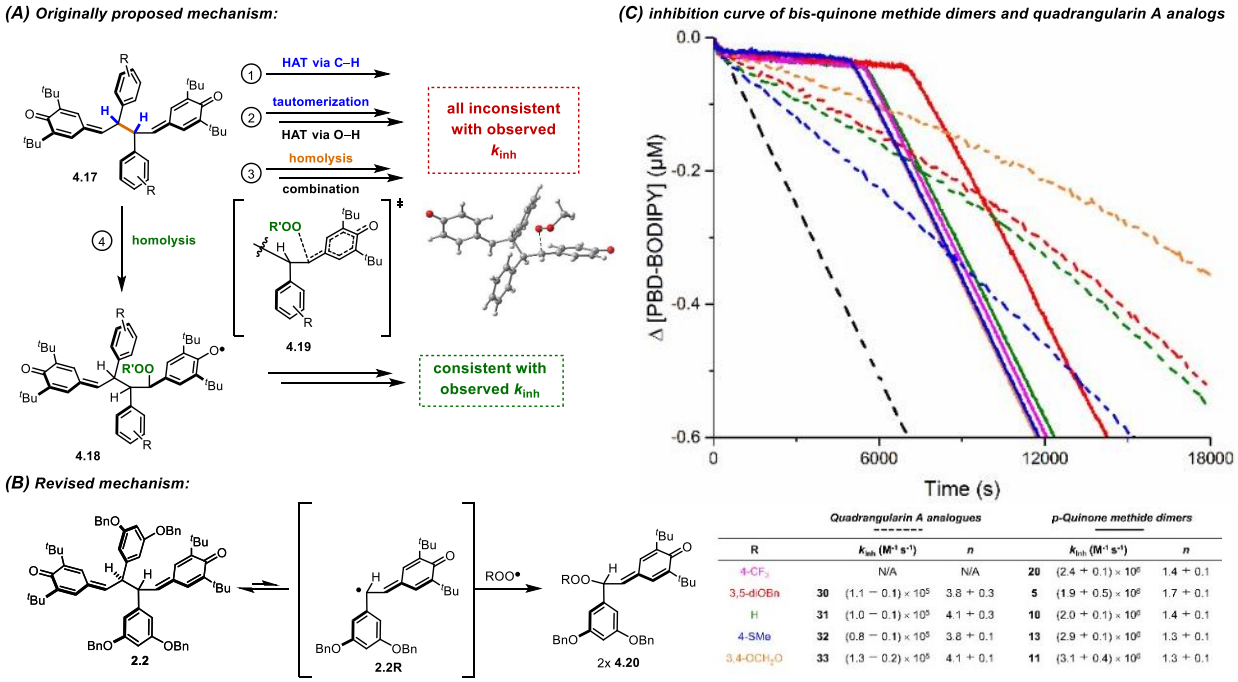

Figure 4.8. Mechanistic insight for the antioxidant potential of *bis*-quinone methides. A) the original proposed mechanistic hypotheses of BQMs based on k_{inh} B) Revised mechanism based on the loss of antioxidant activity when performed in liposomes. C) the inhibition curves comparing BQMs and quadrangularin A analogs.

To our great surprise, the QMDs from which the intermediates from which quadrangularin A analogues were synthesized are very good RTAs.[141] In fact, despite being devoid of phenolic moieties, the QMDs are >10-fold more reactive than the quadrangularin A derivatives (up to 36-fold more reactive for the 4-SMe derivative **32**). Interestingly, monomeric quinone methides have been reported to be – at best – poor RTAs,[142] suggesting that the QMD scaffold is special, perhaps due to the persistence of the quinone methide functionalities relative to those that have been previously studied.[143]

Mechanistic possibilities for the impressive reactivity of the QMDs are presented in Figure 4.8. At first glance, mechanism 1 can be excluded solely on the basis of the magnitude of k_{inh} determined from the inhibited autoxidations (k_{inh} = 2-3×10^6 $M^{-1}s^{-1}$). H-atom transfer from carbon is well known to be a relatively slow reaction, even when highly thermodynamically favorable.[144]

Indeed, the CBS-QB3-predicted[145] rate constants for HAT from a truncated form of the unsubstituted dimer to a model (methyl)peroxyl radical is a mere 6 $M^{-1}s^{-1}$ (see Supporting Information for the optimized structures, their energies, and the rate constants estimated therefrom). Mechanism 2 requires tautomerization of the QMD; however, upon exposing NMR samples of QMD to deuterated methanol (CD_3OD), no deuterium incorporation was observed. Furthermore, if tautomerization were to occur, the phenolic tautomer would be expected to exhibit similar reactivity to the monomeric resveratrol derivative from which the QMD is derived (k_{inh} ~10^5 $M^{-1}s^{-1}$). Mechanism 3 can be excluded solely on the basis of the magnitude of K_{eq} for the QMD dissociation/recombination equilibrium (1.8×10^{-10} M),[63] as it would necessitate the phenoxyl-peroxyl combination to proceed with a rate constant well in excess of the diffusion limit.

To the best of our knowledge, mechanism 4 has little precedent.[23] Although the addition of peroxyl radicals to carbon-carbon double bonds is well-known, it generally features in the propagation of autoxidation of unsaturated substrates (e.g. styrene), not in its inhibition! Of course, the primary difference in the current context is that the resultant radical (a hindered phenoxyl) is unreactive to O_2 and does not propagate the autoxidation. Moreover, not only does peroxyl radical addition produce a more stabilized phenoxyl radical, but the thermodynamics are greatly enhanced by aromatization of the quinone methide. Indeed, CBS-QB3 predicts $\Delta H = -31.5$ kcal/mol for the addition of a model (methyl)peroxyl radical to a truncated form of the unsubstituted dimer along with a rate constant of 4×10^6 $M^{-1}s^{-1}$, in excellent agreement with experiment.

It was later found that a different mechanism for the radical-trapping antioxidant properties of QMDs was in play. This conclusion was made following the performing of the liposome RTA assay. Although QMDs are excellent RTAs in organic solutions, it was found that this activity was

annihilated in the liposome media. Due to the lipophilicity of the alkylated and resorcinol-benzylated QMDs, it was unlikely that this was a result of the hydrogen bonding environment associated with the exterior (and interior) of the liposome space as they should have localization within the polyunsaturated fatty acid matrix. It was reasoned that the mechanism for QMD RTA activity was a result of persistent radical equilibrium in that dissociation of the QMD C8 – C8' bond forms the radical monomers which then undergo direct radical-radical combination with the peroxy radicals that form in the oxidizing samples (**Figure 4.8**).[146]

4.4 Autoxidation assays of phenols and resveratrol natural products

To assess the antioxidant properties of the phenols of interest, it was decided to subject each compound to both organic co-oxidation assays and liposome co-oxidation assays to determine the rate of inhibition (k_{inh}) and stoichiometry of sequestered peroxyl radicals in organic solutions (low hydrogen-bonding) and in liposomes (highly hydrogen bonding) followed by RTA cell assays.

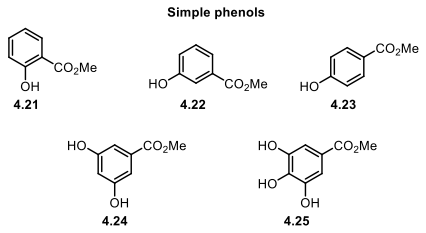

Figure 4.9. Simple phenol RTAs

The investigation of the antioxidant properties of these complex polyphenolic compounds and natural products began with a collection of simpler phenols, resorcinols, and catechols. As expected, the methylsalicylate (**4.21**) reference compound had no antioxidant activities in organic solution and liposomes. Methyl salicylate was chosen as a reference molecule for having poor antioxidant kinetics. This lack of activity is presumably due to the intramolecular hydrogen bond between the phenolic –OH group and the carbonyl oxygen. Previous work performed by the Pratt group supports that hydrogen bonding to the relevant H atoms for antioxidant related HAT significantly erodes activity. Because of this observation, it is typical that compounds behave worse in liposomes than in organic solutions due to the increased

hydrogen bonding within this media. On the contrary, PMC possesses very good antioxidant activity in both assays. When the phenol is moved away from the *ortho* position (methylsalicylate) to the *meta* position (**4.22**), antioxidant activity improves, albeit poorly. As the k_{inh} is low, a rate could only be ascertained using cumene as the oxidizable substrate. The *para* substituted analog (**4.23**) has a k_{inh} that was slightly less than the meta substituted substrate. Interestingly, the 3,5-dihydroxymethyl benzoate substrate (**4.24**) has a k_{inh} that is half of the mono *meta* substituted analog. When the assays are performed in liposomes, the antioxidant activities are non-existent. Collectively, these compounds were in the low to mid-range of 10^2 $M^{-1}s^{-1}$. The tri-hydroxy methyl benzoate (methyl gallate, **4.25**) substrate had the greatest antioxidant activity in both organic solution and liposomes amongst the methyl benzoate phenols. It is hypothesized that increasing the number of phenols improves the antioxidant activity in liposomes because it is statistically more likely to have a non-hydrogen bonded phenolic O–H to serve as an H atom source compared to the mono and di phenols. It should be noted that methyl gallate does not inhibit but rather retards autoxidation in liposomes. This is apparent based on the inhibition curve which does not contain the distinct inhibition period and the curve falling between uninhibited and inhibited when overlayed with PMC (See experimental).

When comparing the resorcinols and catechols (**Figure 4.10**), catechol **4.27** performs by an order of magnitude better than resorcinol **4.26** (7.3 ± 1.810^4 $M^{-1}s^{-1}$ vs $8.86 \pm 1.30x10^3$ $M^{-1}s^{-1}$). However, orcinol **4.27** and tBu_2-catechol **4.28** outperformed their un-alkylated analogs in organic solution and liposomes by an order of magnitude. Guiacol **4.26** showed very little activity in both media which is most likely due to intramolecular hydrogen bonding.

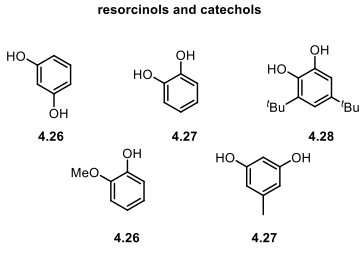

Figure 4.10. resorcinols and catechols

Adding conjugation to the catechols and O-methyl catechols (**Figure 11**) had a profound impact on the RTA potential of these motifs in that they witnessed an order of magnitude increase in activity. Interestingly, curcumin (**4.30**) is seen to have higher stoichiometry. This is due to the precedented intramolecular cyclization that occurs when oxidized.[147] Due to the methylation of the catechol, reduced activity would expected compared to free catechols. The performance of this molecule should in theory be equal to **4.29** but due to the long chain, intramolecular cyclization occurs after oxidation and subsequent oxidations occur to produce **4.31**.

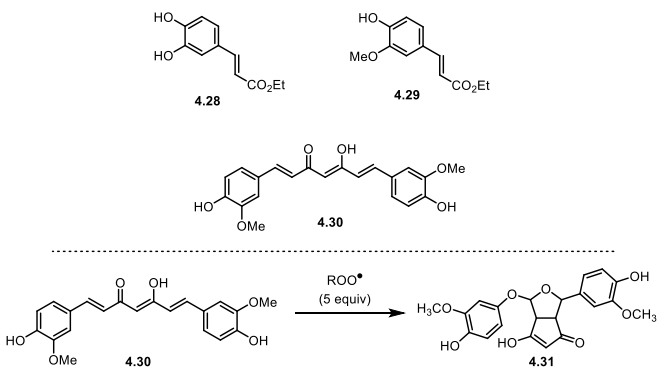

Figure 4.11. conjugated catechol and O-methyl catechols (Top); Reaction of curcumin when oxidized results in increased stoichiometry (Bottom).

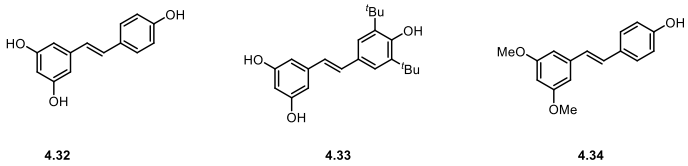

Figure 4.12. Resveratrol analogs

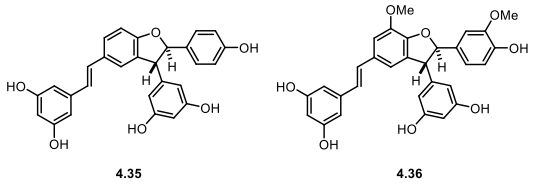

Figure 4.13. dihydrobenzofuran dimers of resveratrol and neolignan.

Comparing the resveratrol analogs (**Figure 12**) reveals surprising results. Resveratrol **4.32** performs as a good RTA in organic solution and works comparably to its alkylated analogs **4.33**

and **4.34** (10^5 $M^{-1}s^{-1}$). But in a highly hydrogen bonding environment like liposomes, the alkylated analogs perform much better, indicating that resveratrol would likely be a poor RTA in a cellular environment. **4.33** performs at an order of magnitude in liposomes and **4.34** has a k_{inh} that is double that of **4.32**. Surprisingly, **4.34** does not out-perform **4.33** substantially indicating the free resorcinols do not have as great of an effect in terms of lipophilicity as would be expected.

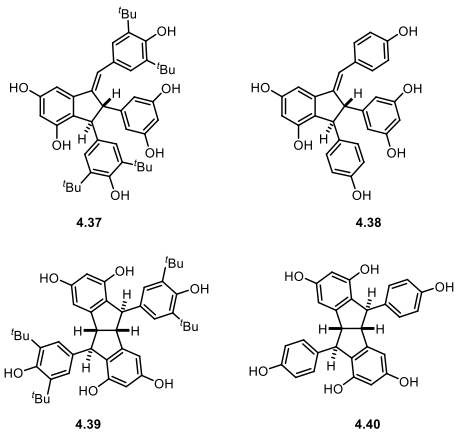

Figure 4.14. resveratrol dimers and alkylated dimer analogs.

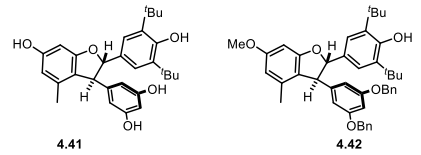

Figure 4.15. resveratrol/ orcinol dihydrobenzofurans

The dihydrobenzofuran-containing dimers of resveratrol (δ-viniferin, **4.35**) and neolignans (shegansu B, **4.36**) (**Figure 4.13**) both perform poorly in organic solutions and liposomes. They both inhibit at 10^3 $M^{-1}s^{-1}$ in cumene. **4.36** does not inhibit at all in liposomes whereas shegansu B retards autoxidation such that a rate constant cannot be ascertained due to lack of a distinct inhibition phase.

The resveratrol dimers provide a good example of how additional lipophilicty can increase RTA activity (**Figure 4.14**). **4.37** and **4.39** are better RTAs by an order of magnitude to their corresponding natural products **4.38** and **4.40** respectively. In liposomes, **4.38** and **4.40** are half an order of magnitude slower RTAs compared to their alkylated analogs.

The resveratrol-coupled orcinol dihydrobenzofurans present a break in trends (**Figure 4.15**). The unprotected analog **4.41**, although performing on par with the protected analog **4.42** in organic solution with respect to k_{inh}, has higher stoichiometry (n = 4 for **4.41**, and n= 2 for **4.42**). It is possible that an additional process than canonical hindered phenol RTA activity. Similarly, the alkylated trimers **4.43** and **4.44** containing dihydrobenzofurans have much higher stoichiometries than were expected (**4.43**, **4.34** n= 8). This confirms that having the free resorcinol ring adjacent to the DHB arene is playing a role in the extra equivalents of peroxyl radicals that are sequestered. The following mechanism for this observed stoichiometry is presented in **Figure 4.17**. While both mechanisms lead to a neutral product associated with n = 4 for peroxyl radicals that are sequestered, the top is most likely as it directly involves the resorcinol hydrogen that seems to be required (comparing stoichiometries of **4.41** and **4.42**).

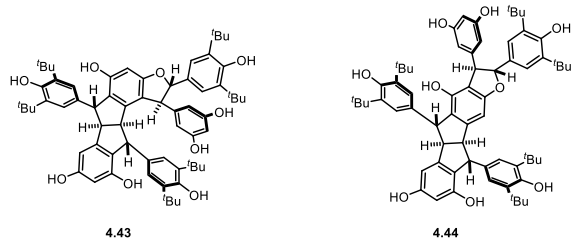

Figure 4.16. alkylated resveratrol trimers.

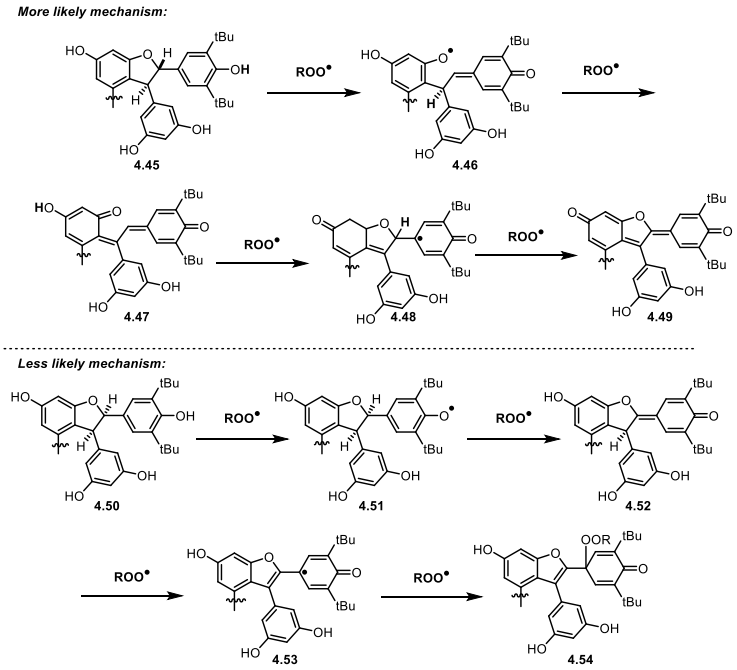

Figure 4.17. Proposed mechanism for observed additional stoichiometry in DHB-containing antioxidants.

The performance of both trimers in liposomes is very different. **4.43** is a good RTA in the highly hydrogen bonding environment whereas **4.44** does not inhibit at all. This may be due to the differences in polarity as **4.44** is very polar (by TLC) in comparison to **4.43**.

In comparing the vitisin resveratrol tetramers **4.55** and **4.56**, they behave the same in cumene while not inhibiting in hexadecane as they are slower antioxidants with typic phenolic stoichiometry. This is interesting because the last examples (except for delta viniferin and shegansu B) had much higher stoichiometry when the dihydrobenzofuran ring is present. This underscores that elevated stoichiometry only occurs when the phenols are hindered. These both behave mediocrely in liposomes with **4.55** performing slightly better by almost half an order of magnitude.

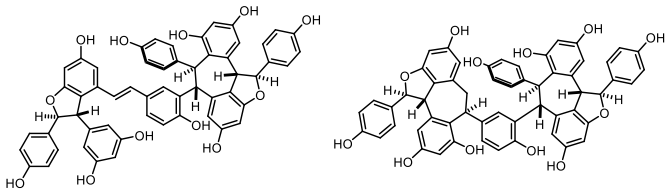

Figure 4.18. resveratrol tetramers.

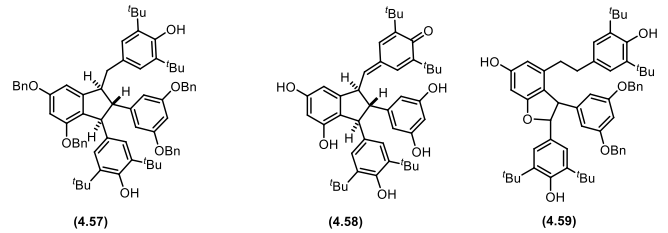

Figure 4.19 resveratrol synthetic dimer intermediates

The synthetic dimer intermediates (**Figure 4.19**) have very interesting RTA properties. **4.57** behaves moderately in hexadecane and has a stoichiometry that is close to 4 as expected for a compound containing two hindered phenols. **4.58** is a good RTA in hexadecane and has increased stoichiometry (n~5). Further, this RTA is good in liposomes, presumably a result of the lipophilicity. **4.59** also behaves as a good RTA in hexadecane and has increased stoichiometry that may be due to the dihydrobenzofuran.

The synthetic resveratrol intermediates **4.40** and **4.41** behave as equally good RTAs despite their differences in oxidation states and resorcinol protecting groups. Both are good RTAs in hexadecane and surprisingly have elevated stoichiometry in cumene (n~5).

Despite the good activities for several of these oligomers, they do not compare to PMC with the best of this set being an order of magnitude slower than PMC (10^6 $M^{-1}s^{-1}$). This suggests that these would not be able to be competitive with PMC in a cellular environment.

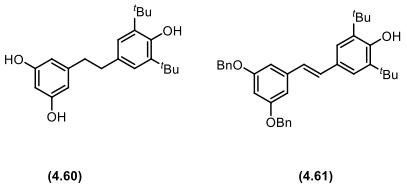

Figure 4.20. resveratrol synthetic intermediates

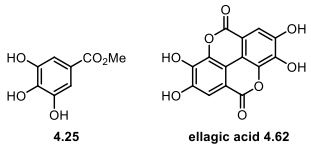

Figure 4.21. Gallate derivatives

Given the good RTA activities of methyl gallate (**4.25**), we sought to investigate its dimer ellagic acid **4.62** with the thought that we could investigate if there was an inherent drive for nature to oligomerize for the end goal of creating more potent antioxidants. Further, we expected ellagic acid to behave better as more phenols were masked by the fused cyclic core. This was not the case. Ellagic acid was 25-times slower at inhibiting autoxidation in cumene compared to methyl gallate. Additionally, ellagic acid had no inhibition in liposomes. This is thought to be the result of its poor solubility. Even making stock solutions in DMSO was unachievable at concentrations surpassing 10 mM. Due to this molecule being as planar as it is, this is unsurprising.

It has been found that vitamin E (**4.66**) and vitamin C (**4.68**) work in a synergistic manner within cells such that ascorbic acid (vitamin C) can increase the antioxidant properties of vitamin E. We sought to expand this study to polyphenols after finding increased activity when both a hindered phenol and a resorcinol component are present within the same molecule. Kinetically, the hindered phenol inhibits autooxidation and a faster rate compared to resorcinol. However, the

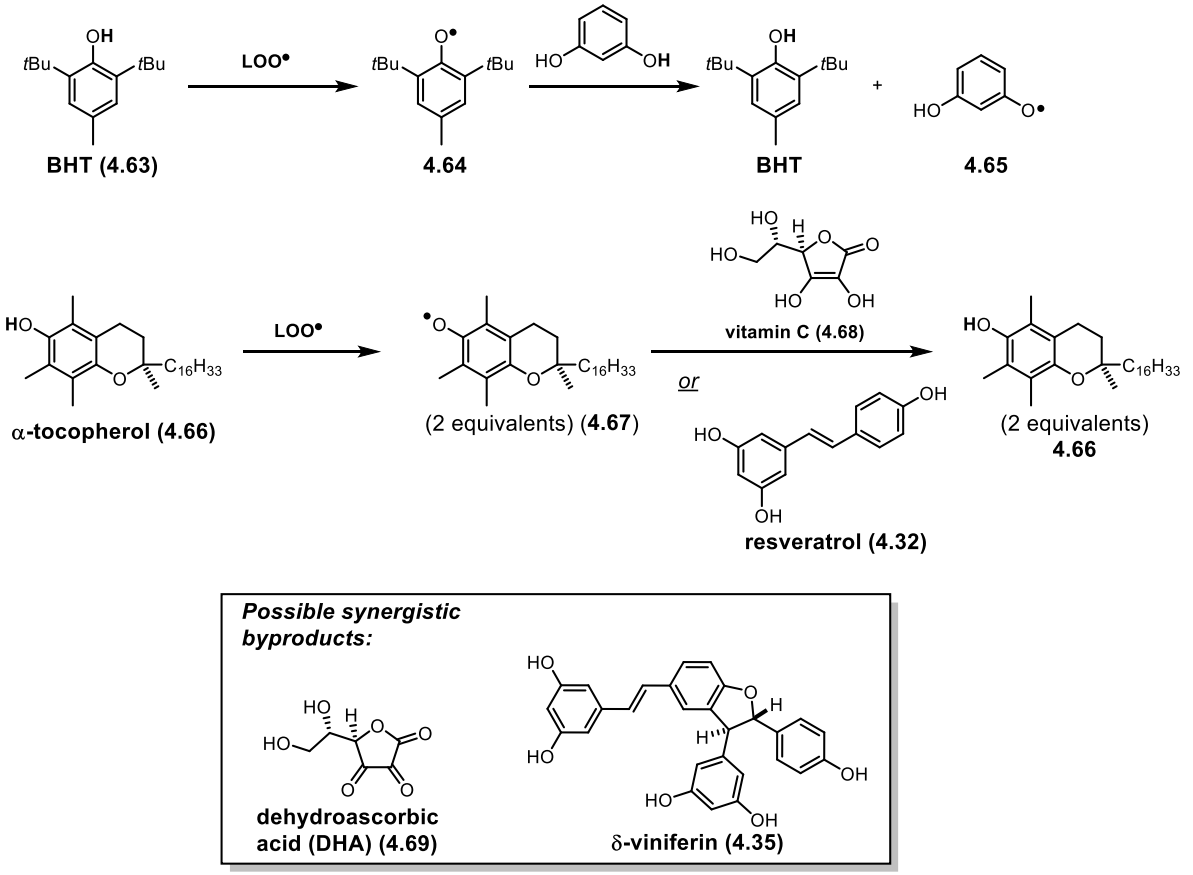

Figure 4.22. Synergistic effects between more reactive and less reactive phenols. (Top) BHT acts synergistically with resorcinol (slower antioxidant). (Bottom) vitamin C and resveratrol both have been observed to act synergistically with vitamin E.

increased stoichiometry found for the mixture of substrates suggests that the resorcinol ring is playing a role. A simple study was performed to interrogate possible synergy between these two motifs. This was done by taking BHT (a representative hindered phenol) and resorcinol and varying the relative concentrations of each within an autoxidizing environment. It was found that the 1:1 ratio of BHT and resorcinol corresponded to a higher peroxyl radical sequestering

stoichiometry than the BHT (5uM) alone. Based on this observation, it is ascertained that as the BHT becomes oxidized (kinetically favored), the resorcinol may act as a reducing agent to replenish the concentration of the active phenol in BHT which leads to a stoichiometry that is higher than the canonically reported value of 2.

This finding could allow for an alternative antioxidant role and mechanism for polyphenols that deviates from the previous conclusions that polyphenols act as independent antioxidants. In cells, vitamin E is the endogenous hindered phenol antioxidant. Assuming accumulation in the cell, polyphenols could play a supportive role working in synergy with vitamin E such that the oxidation and consumption of vitamin E can be reversed with the presence of polyphenol acting as a reducing agent and regenerating vitamin E. This synergy is precedented and has been observed between vitamin E and vitamin C *in vitro* and *in vivo*.[148] Oxidation of vitamin E (TH) forms the quinone species (TQ). This can be reduced by an equivalent of vitamin C to reform TH. This mechanism for synergy must occur at the lipid membrane – cytosol interface as vitamin C is a hydrophilic antioxidant that is found in the aqueous cytosol and vitamin E is a lipophilic antioxidant found within the lipid membrane. This process would produce the oxidized form of vitamin C as a byproduct. Additionally, it has been found that resveratrol can also have a synergistic effect with vitamin E.[149] Presumably, this occurs similarly to vitamin C in that resveratrol acts a reducing agent to regenerate vitamin E at the phase partition on the outside of the lipid membrane. Assuming HAT occurs at C4, the phenoxyl radical of resveratrol can be formed which ultimately may result in a dimerization process if concentrations permit (**Figure 4.22**). In the case of polyphenols like resveratrol, the unalkylated natural products have increased hydrophilicity therefore having larger concentrations in the cytosol of the cell. As a result, they

may be limited to the same vitamin E regeneration conditions as vitamin C. However, for the more lipophilic, alkylated polyphenols, it is reasoned that this synergy could be taking place within the confines of the lipid membrane.

4.5 Antioxidants as protecting agents in ferroptotic cells

To evaluate the antioxidant activity in these polyphenol natural products with respect to being able to rescue cells from ferroptotic cell death following treatment with a ferroptosis inducing agent (RSL-3), the mouse embryonic fibroblast cell line (pfa1), was chosen for the studies as this cell line is deficient in ACSL4 (**Figure 4.19**). ASCL4 is a gene responsible for the expression of the protein acyl-COA synthetase long chain family member 4, an enzyme that converts free long chain fatty acids into fatty acyl-COA esters. As a result of this function, ACSL4 is heavily responsible for lipid biosynthesis and fatty acid degradation. This later function has importance for the cell's management of oxidized fatty acids that contribute to ferroptosis. With this

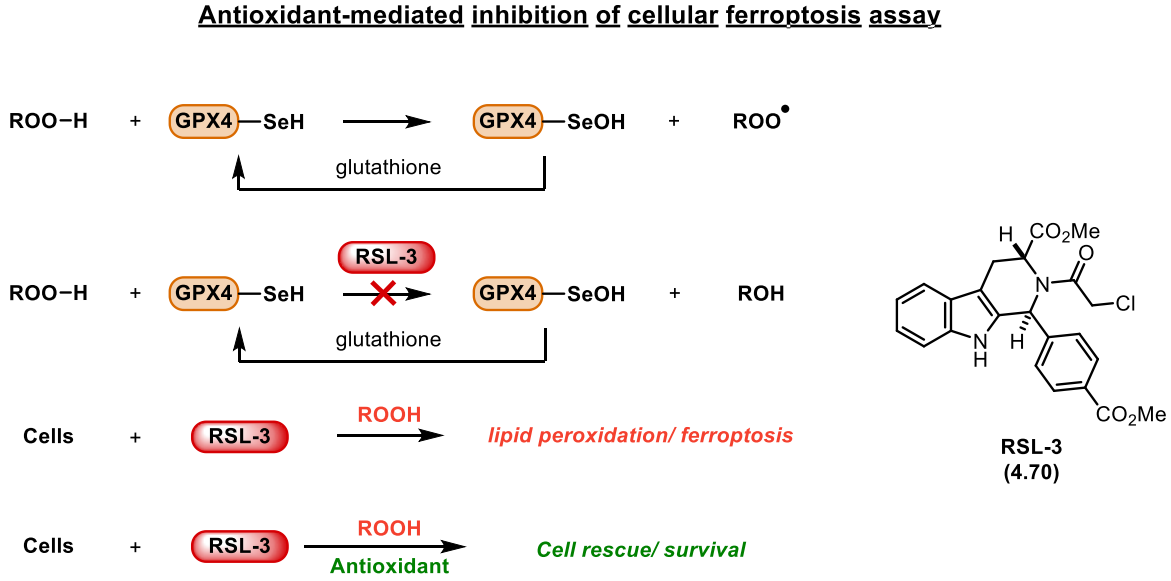

Figure 4.23: This presents an overview of theantioxidant-mediated inhibtioin of ferroptosis assay in which cells are treated with a ferroptosis inducer (RSL-3). The presence of a potent cellular antioxidant inhibits ferroptosis. Cellular viability was measured by Aquabluer assay.

mechanism for degrading oxidized fatty acids being disabled, the cell must rely solely on GPX4 (glutathione peroxidase 4) along with any other endogenous antioxidants that are already present to prevent ferroptosis. RSL-3 is a potent ferroptosis-inducer that acts via inhibition of the enzyme GPX4 via direct binding. This enzyme is responsible for reducing peroxyl fatty acid (product of autoxidation) to the corresponding alcohol. The mechanism for this enzymatic function is reliant on the seleno-serine active site residue that becomes oxidized to the corresponding selenic acid. Glutathione is used as a terminal reductant to regenerate the seleno-serine residue thus turning over the enzymatic catalytic cycle. Upon addition of ferroptosis-inducer RSL-3 that inhibits GPX4, the cell accumulates peroxyl fatty acids which then triggers ferroptosis. In the presence of a sufficiently potent antioxidant that has been pre-incubated with the cells prior to addition of RSL-3, the cells are be able to maintain an oxidative stress-free environment. PMC is a sufficiently potent antioxidant that can aid the cells in maintaining homeostasis and cell viability in the presence of the GPX4 inhibitor.

The natural products and their alkylated analogs were subjected to this cell assay. The results of the cell assay were consistent with the liposome assays. Compounds that performed well in liposomes, did the best in ferroptotic-induced cells. Surprisingly, alkylated resveratrol **4.23** did the best in cells (EC50 = 28.3 ± 3.0 nM), almost 200-fold more potent than resveratrol **4.22**. Second to that was tBu_6-carasiphenol **4.33** (EC50 = 106.1 ± 6.8 nM). As is consistent with liposome data, the unnatural alkylated trimer **4.34** was 16-fold less potent than the C8/C10 isomer (EC50 = 1.7 ± 0.3 μM). In comparing the dimers, alkylated quadrangularin A (**4.27**) was about 1.5 times more potent than alkylated pallidol (**4.29**). In both sets of dimers, the alkylated dimers were 40 times more potent than the natural product. The vitisin tetramers behaved similarly in cells as the dimer

natural products. These results suggest that there is no inherent increase in potency as a result of the oligomerization state. Lipophilicity, coupled with good radical trapping kinetics is what dictates if an antioxidant will be able to rescue the cells from ferroptosis.

4.6 Conclusions and Outlooks

It is apparent that the resveratrol-derived oligomers and resveratrol-like analogs perform underwhelmingly as radical-trapping antioxidants in comparison to the synthetic vitamin E analog, PMC. The long-standing attestation that resveratrol and its oligomers behave as antioxidants must no longer be attributed to their radical-trapping attributes as they have been shown herein to be insufficient to compete against vitamin E which is endogenous to mammalian cells. However, this is not to say that they do not have antioxidant properties in general. Earlier studies (consistent with these results) have shown that tBu_4-pallidol (**4.39**) has surprisingly good activity for preventing ferroptosis despite its radical-trapping antioxidant kinetics.[64] There is a potential for this molecule to have a protein-level mechanism for rescuing cells from ferroptosis such as activating genes controlled by the antioxidant response element (ARE). It is therefore possible that resveratrol and its oligomer natural products can have other mechanisms of action. There are a number of cellular pathways involved in the cellular antioxidant response to combat ROS production such as NRF2/Keap1.[150, 151] Therefore, it is necessary to analyze these natural products in a different context of antioxidant activity – specifically on the level of gene expression and cellular pathways. Additionally, as phytoalexins, it must be noted that plants have (presumably) evolved to synthesize these molecules to combat pathogenic stressors such as bacterial or fungal. With the ongoing research being conducted on bacteria that comprise the microbiome and the disease-relevance in the host organisms that result from the chemical interactions between the two organism types, it

may be possible that the asserted health benefits of these natural products can be acting on these simple bacteria organisms to produce a more complex antioxidant response that benefits the host.[152] Systematic accumulation of these natural products within a mammalian host (to levels needed for activity) seems improbable due to their poor lipid solubility and would certainly be excreted. Ingestion of these compounds through the consumption of wine or supplementation could potentially reach these organisms in the gut to elicit a positive antioxidant response for the host.[153] Certainly, more work is required before it can be concluded that these molecules are without any benefit. The main conclusion that can be made based on the cumulation of this research is that the natural products are too polar and not reactive enough to behave as biologically relevant antioxidants.

4.7 Experimental Procedures and Kinetic and Biological Data

General Procedures. All chemicals and solvents obtained from commercial suppliers were used as received unless indicated otherwise. 1-Hexadecene and cumene were purified and stored as previously described.[133, 134]

General Procedures for Inhibited Co-autoxidations.

The inhibited co-autoxidations were carried out following our reported methods.[134, 137] Autoxidations of 1-hexadecene (2.9 M) and PBD-BODIPY (10 μM) at 37 °C were initiated by AIBN (6 mM), 37 °C in chlorobenzene. A 3.5-mL quartz cuvette was charged with PhCl (0.44 mL) and 1-hexadecene (2.00 mL). The cuvette was preheated to the desired temperature in a thermostated sample holder of a UV-vis spectrophotometer and allowed to equilibrate for approximately 15 min. To the cuvette was added PBD-BODIPY (12.5 μL of a 2.00 mM stock solution in 1,2,4-trichlorobenzene) and initiator (50 μL of a 300 mM stock solution of AIBN in chlorobenzene). The solution was thoroughly mixed prior to monitoring the uninhibited co-autoxidation via the disappearance of the PBD-BODIPY probe at 588 nm (37 °C) for 5-10 min to ensure the reaction was proceeding at a constant rate. Finally, the antioxidant under investigation was added (5.0μL of a 2.5 mM solution in chlorobenzene), the solution was mixed thoroughly, and the absorbance readings were resumed. The resulting Abs vs time data were processed as previously reported. The rate of initiation (R_i = 1.30×10^{-9} Ms^{-1} (37 °C) and second order rate constant for propagation of the dye ($k_{PBD\text{-}BODIPY}$ = 3792 $M^{-1}s^{-1}$ (37 °C), 7633 $M^{-1}s^{-1}$ (70 °C), 8283 $M^{-1}s^{-1}$ (100 °C)) necessary to compute stoichiometric data (n) and inhibition rate constants (k_{inh})

were determined using PMC as a standard, which has an established stoichiometry of 2.[90] Similar experiments were conducted at 37 °C employing cumene (3.6 M) and STY-BODIPY (10 μM) initiated by AIBN (6 mM) in chlorobenzene. Reaction progress was monitored at 571 nm. The rate of initiation, also determined using PMC, was measured to be $R_i = 2.28\times10^{-9}$ Ms^{-1} and the second order rate constant for propagation of the dye had been determined previously ($k_{STY\text{-}BODIPY}$ = 141 $M^{-1}s^{-1}$) (37 °C). Inhibited autoxidation experiments involving liposomes were conducted at 37 °C employing egg-PC liposomes (1 mM), STY-BODIPY (10 μM), initiated by DTUN (0.2 mM) or V70 (0.2mM) in PBS buffer (10 mM). Reaction progress was monitored at 565 nm. The rate of initiation, determined using PMC, was measured to be $R_i = 2.29\times10^{-9}$ Ms^{-1} and the second order rate constant for propagation of the dye had been determined previously ($k_{STY\text{-}BODIPY}$ = 894 $M^{-1}s^{-1}$) (37 °C).

General Procedures for Ferroptosis-Rescue Assay. Pfa1 cells (3,000 in 100 mL) were seeded in 96-well plates and cultured overnight. The next day the media was removed, the cells were washed twice with PBS and the cells were suspended in new media for 30 minutes before addition of RTAs and LOX inhibitors. Ferroptosis was induced using (1S, 3R)-RSL3 (10 mM) 60 minutes after incubation of compounds. Cell viability was assessed 6 hours later using the AquaBluer assay (MultiTarget Pharmaceuticals, LLC) according to the manufacturer's instructions. Cell viability was calculated by normalizing the data to untreated controls. Experiments are carried out with six-technical replicates (n = 6 wells of a 96-well plate) and performed independently with a minimum of three biological replicates.

Analysis of Radical-Trapping Antioxidant Activity:

Kinetic Data

General Procedure for Inhibited Autoxidations

The inhibited autoxidations were carried out following our reported method.[9] All autoxidations of 1-hexadecene (2.9 M) and PBD-BODIPY (10 μM) were initiated by AIBN (6 mM) in chlorobenzene at 37 °C. A 3.5-mL quartz cuvette was charged with PhCl (0.44 mL), 1-hexadecene (2.00 mL). The cuvette was preheated to 37 °C in a thermostatted sample holder of a UV-vis spectrophotometer and allowed to equilibrate for approximately 15 min. To the cuvette was added PBD-BODIPY (12.5 μL of a 2.00 mM stock solution in 1,2,4-trichlorobenzene) and AIBN (50 μL of a 300 mM stock solution in chlorobenzene). The solution was thoroughly mixed prior to monitoring the uninhibited co-autoxidation via the disappearance of the PBD-BODIPY probe at 588 nm for 10 min to ensure the reaction was proceeding at a constant rate. Finally, the antioxidant under investigation was added (5.0 μL of a 2.5 mM solution in chlorobenzene), the solution was mixed thoroughly, and the absorbance readings were resumed. The resulting Abs vs time data were processed as previously reported.[9] The rate of initiation ($R_i = 1.3 \times 10^{-9}$ Ms^{-1}) and second order rate constant for propagation for the dye ($k_{PBD\text{-}BODIPY} = 3792$ $M^{-1}s^{-1}$) necessary to compute stoichiometric data (n) and inhibition rate constants (k_{inh}) were determined using PMC as a standard, which has an established stoichiometry of 2.[10,11]

Table 1. Comparison of inhibition rate constants (k_{inh}) and stoichiometry (n) during inhibited co-autoxidations of 1-hexadecene (2.9 M) and PBD-BODIPY (10 μM) initiated by AIBN (6 mM) in chlorobenzene at 37 °C.

X	*Quadrangularin A analogues*		*Quinone methide dimers*			*Parent phenols*	
	k_{inh} (10^5 $M^{-1}s^{-1}$)	*n*	k_{inh} (10^5 $M^{-1}s^{-1}$)	*n*		k_{inh} (10^5 $M^{-1}s^{-1}$)	*n*
4-CF3	N/A	N/A	24 ± 1	1.4 ± 0.1	**S14**	1.3 ± 0.1	2.3 ± 0.1
3,5-diOBn	1.1 ± 0.1	3.4 ± 0.1	19 ± 5	1.7 ± 0.1	**S10**	1.4 ± 0.1	2.3 ± 0.1
H	1.6 ± 0.3	2.0 ± 0.2	20 ± 1	1.4 ± 0.1	**S4**	1.6 ± 0.1	2.0 ± 0.1
4-SMe	0.75 ± 0.03	3.6 ± 0.1	29 ± 1	1.3 ± 0.1	**S7**	1.7 ± 0.1	2.2 ± 0.1
3,4-dioxyl	1.4 ± 0.1	1.9 ± 0.1	31 ± 4	1.3 ± 0.1	**S5**	1.9 ± 0.3	2.1 ± 0.1

Computational Data[12]

Table 2. Summary of enthalpies (ΔH, $\Delta H^{\ddagger}$), free energies (ΔG, $\Delta G^{\ddagger}$), and corresponding computed second order rate constants (*k*) for the addition of methyl peroxyl radical to or hydrogen atom transfer (HAT) from a truncated analogue of **14** in the gas phase at 37 °C.

Mechanism	***Position***	***ΔH, (kcal mol^{-1})***	***ΔG, (kcal mol^{-1})***	***$\Delta H^{\ddagger}$, (kcal mol^{-1})***	***$\Delta G^{\ddagger}$, (kcal mol^{-1})***	***k*** [a] **($M^{-1}s^{-1}$)**
HAT	C_{β}–H	-15.7	-15.3	7.5	19.0	6
Addition	C_{α}	-31.5	-19.4	-1.7	10.8	4×10^6

[a] Computed using $k = \frac{RT}{P} \cdot \frac{k_B T}{h} e^{\frac{-\Delta G^{TS}}{RT}}$ where T = 310.15 K.

Optimized Gaussian Structures and CBS-QB3[13] or DFT Energies (Hartree)

Methyl peroxyl radical

$H_3COO^{\bullet}$

CBS-QB3 Enthalpy = -189.954731 CBS-QB3 Free Energy = -189.985243

0 2

C	1.09605900	-0.18318300	0.00000000
H	1.87467700	0.57860700	-0.00001500
H	1.14885000	-0.80070400	0.89699800

H	1.14883700	-0.80072700	-0.89698300
O	-0.15733600	0.54388600	0.00000000
O	-1.18625300	-0.27864500	0.00000000

Methyl hydroperoxide

H_3COOH

CBS-QB3 Enthalpy = -190.589542 CBS-QB3 Free Energy = -190.620447

0 1

C	1.12961700	-0.22363900	0.02672600
H	1.97292100	0.47126800	0.02466400
H	1.14400500	-0.82582200	0.94203100
H	1.18954700	-0.87767200	-0.84877800
O	-0.01619300	0.60684200	-0.03138300
O	-1.16412600	-0.28550800	-0.09072600
H	-1.64161900	0.00339000	0.69859800

Truncated dimer

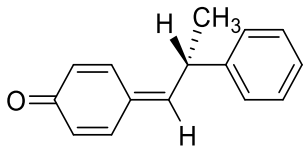

CBS-QB3 Enthalpy = -654.002976 CBS-QB3 Free Energy = -654.060994

0 1

C	-2.28497800	0.40886900	-1.38146900
C	-3.55270400	-0.03922500	-1.32815500
C	-4.13529300	-0.56092000	-0.07890600
C	-3.23865900	-0.55847700	1.09408900
C	-1.97179800	-0.10764000	1.02679200
H	-1.87418700	0.78842400	-2.31241000
H	-4.20081500	-0.03800300	-2.19697400
H	-3.66131800	-0.94226000	2.01572400
H	-1.34982200	-0.12439600	1.91411400
C	-1.40780200	0.40947300	-0.21456200
C	-0.14133100	0.88393400	-0.33638800
H	0.15649000	1.24391200	-1.31988600
O	-5.28793700	-0.97120500	-0.01361300
C	0.93072100	0.98559600	0.71399400
C	2.15417900	0.17948500	0.27509100
C	2.43091400	-1.05007100	0.87987500
C	3.00520900	0.62664700	-0.74224100
C	3.53098300	-1.81010100	0.48913600
H	1.77888600	-1.41666800	1.66618900
C	4.10408800	-0.13185400	-1.13742500
H	2.81702700	1.57620900	-1.23132600
C	4.37188000	-1.35298100	-0.52222200
H	3.72971200	-2.75869500	0.97523300
H	4.75316900	0.23292500	-1.92573000
H	5.22845900	-1.94234200	-0.82872500
C	1.25966000	2.46665200	1.00604200
H	1.57784500	2.99577200	0.10458500
H	0.38007500	2.98079300	1.40032500
H	2.06455800	2.53733300	1.74154700
H	0.57301500	0.54030300	1.64432900

C–H HAT radical product (truncated dimer)

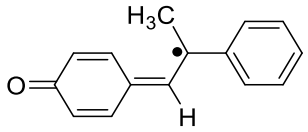

CBS-QB3 Enthalpy = -653.393246 CBS-QB3 Free Energy = -653.450284

0 2

C	1.52663700	-0.17878300	-0.06031300
C	2.26612700	1.04646900	-0.05163000
C	3.63125800	1.05609200	-0.05797800
C	4.41372500	-0.17389500	-0.07235200
C	3.64436100	-1.41088100	-0.11084300
C	2.28208000	-1.39605400	-0.11637600
H	1.74048500	1.98910300	-0.07297000
H	4.18983800	1.98508300	-0.06360700
H	4.20631700	-2.33724000	-0.13798000
H	1.73406700	-2.33262400	-0.14873300
C	0.09559100	-0.30235800	-0.05597100
H	-0.23773000	-1.30730800	-0.29735500
C	-0.90681300	0.59889900	0.18954500
C	-2.31412300	0.15072700	0.07608700
C	-3.30656300	1.03105100	-0.39201800
C	-2.71066100	-1.15268400	0.42751200
C	-4.62699500	0.61798900	-0.53178300
H	-3.03832200	2.04156900	-0.67632200
C	-4.03301100	-1.56037100	0.29989500
H	-1.98216700	-1.84097800	0.83868200
C	-4.99806500	-0.67954400	-0.18603900
H	-5.36792600	1.31206600	-0.91227100
H	-4.31363000	-2.56608300	0.59198900
H	-6.02906600	-0.99866600	-0.28584100
O	5.65560200	-0.16513300	-0.06495700
C	-0.67848700	2.04011600	0.58017800
H	0.15428900	2.12915000	1.27928800
H	-0.44885500	2.67090900	-0.28670000
H	-1.56247000	2.45544600	1.06398500

Addition radical product (truncated dimer)

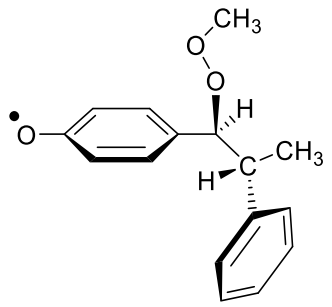

CBS-QB3 Enthalpy = -844.008115 CBS-QB3 Free Energy = -844.077218

0 2

C	1.68586100	-0.73545200	-0.94678200
C	2.03864400	-2.05690200	-1.04386900
C	1.65692100	-3.01393600	-0.01965400
C	0.89517400	-2.49267000	1.10074700
C	0.55651100	-1.16384100	1.17166500
H	1.98969400	-0.02773600	-1.70968300
H	2.61367700	-2.43783300	-1.87997300
H	0.61296200	-3.19839200	1.87314800
H	-0.01169700	-0.79243000	2.01765600
C	0.93550600	-0.26276200	0.15473600
O	1.97130500	-4.22160000	-0.09771200
O	1.58857600	2.04790200	-0.20443700
O	2.61138400	1.96629700	0.84596800
C	3.78537300	2.50236300	0.26894200
H	4.52260200	2.46789200	1.07383500
H	4.12979300	1.89716600	-0.57569200
H	3.63454500	3.53954000	-0.04808300
C	0.53023100	1.19587100	0.22243000
C	-0.67504300	1.54242800	-0.70021500
H	0.27533000	1.45818500	1.25591200
C	-1.89282900	0.70535500	-0.33377400
C	-2.36613100	-0.27753900	-1.20731200
C	-2.57489100	0.90298300	0.87332900
C	-3.48544600	-1.04383900	-0.88862100
H	-1.85000100	-0.44796500	-2.14632700
C	-3.69261200	0.13833500	1.19677100
H	-2.23685900	1.66374000	1.56895000
C	-4.15235100	-0.83895000	0.31597800

H	-3.83382500	-1.80139600	-1.58165800
H	-4.20687700	0.30800700	2.13631100
H	-5.02313000	-1.43390300	0.56681800
C	-0.98133300	3.05080000	-0.68657800
H	-1.22038800	3.40135600	0.32101200
H	-0.12719900	3.62451100	-1.04555200
H	-1.84128200	3.26025700	-1.32687200
H	-0.37898200	1.26472500	-1.71711200

C–H HAT TS (truncated dimer)

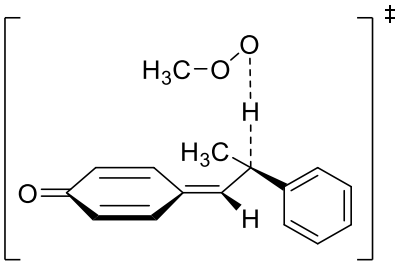

TS frequency: -1557.85 cm^{-1}
CBS-QB3 Enthalpy = -843.945793 CBS-QB3 Free Energy = -844.015840

0 2

C	2.25564500	-0.81459400	-1.31202000
C	3.59164400	-1.00867700	-1.27621500
C	4.34095000	-0.94392700	-0.01493100
C	3.53661400	-0.67398800	1.18686700
C	2.19873300	-0.47972300	1.13376700
H	1.72389600	-0.86184400	-2.25735800
H	1.65699900	-0.30200500	2.05014700
C	1.47427800	-0.52309700	-0.12151100
C	0.11527300	-0.32322000	-0.28906400
H	-0.22338500	-0.43776100	-1.31608500
O	5.55794900	-1.10835800	0.03910700
C	-0.95338200	0.11339200	0.59345900
H	-0.98829400	1.32936100	0.26126100
O	-0.99624200	2.63019100	-0.02807000
O	-0.04681900	2.76958300	-1.00881500
C	1.15191800	3.32650200	-0.45026100
H	1.58793500	2.64444600	0.28311000
H	1.82813900	3.45106200	-1.29669400
H	0.93127600	4.29146200	0.01023200
C	-0.78138600	0.19480600	2.11318300
H	-0.60022900	-0.79575900	2.54330900
H	0.03185600	0.86149900	2.40191900
H	-1.69744200	0.58282100	2.56083200
C	-2.32405400	-0.39026600	0.18827000
C	-3.44985900	0.43555600	0.30836200
C	-2.50351700	-1.70092100	-0.27188600
C	-4.71588900	-0.03568000	-0.02300300
H	-3.32776700	1.46076400	0.63874700
C	-3.77214400	-2.17439200	-0.60011000

H	-1.64639200	-2.36002900	-0.35910000
C	-4.88216500	-1.34322800	-0.47742900
H	-5.57354200	0.62163600	0.06581100
H	-3.89129700	-3.19433200	-0.94836100
H	-5.86931600	-1.70967500	-0.73514600
H	4.16560400	-1.21728600	-2.17165600
H	4.07690800	-0.64693800	2.12640000

Addition TS (truncated dimer)

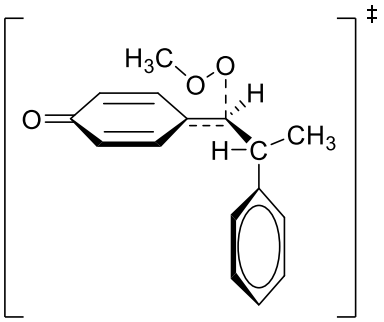

TS frequency: -343.37 cm^{-1}
CBS-QB3 Enthalpy = -843.960367 CBS-QB3 Free Energy = -844.028986

0 2

C	0.96314500	-0.76857400	-0.75517100
C	1.83634300	-1.75262400	-1.08048400
C	2.84270300	-2.24399300	-0.12820700
C	2.84016200	-1.60372700	1.19251200
C	1.96163900	-0.62042300	1.49770000
H	0.22717400	-0.43962100	-1.47830900
H	1.82743000	-2.22622800	-2.05555400
H	3.57672000	-1.95858700	1.90398000
H	1.98057100	-0.15155200	2.47654100
C	0.97599200	-0.15653500	0.55037100
O	3.63885800	-3.13567600	-0.42560300
O	1.35833300	2.52336000	0.56707000
O	1.45649800	2.81734500	-0.75543500
C	2.78161800	2.51858200	-1.22898300
H	2.79283600	2.84364900	-2.26985300
H	3.51406800	3.07645700	-0.64293800
H	2.97189500	1.44691100	-1.15775400
C	0.11111800	0.87785900	0.91263100
C	-1.10441000	1.33029600	0.13304000
H	-0.76303100	1.59726800	-0.87257200
H	0.14440000	1.17923200	1.95527200
C	-1.73255800	2.58771200	0.76472600
H	-2.57633300	2.93237100	0.16356300
H	-2.10800700	2.36997500	1.76906300
H	-0.99437700	3.38714100	0.83252300
C	-2.14961600	0.22465600	-0.01552300
C	-2.75441500	-0.00316100	-1.25515700

C	-2.56682600	-0.54188100	1.07849300
C	-3.74636600	-0.97085000	-1.40242800
H	-2.44737600	0.58550300	-2.11425100
C	-3.55574100	-1.51108400	0.93481700
H	-2.11460600	-0.38633700	2.05227600
C	-4.14944200	-1.72962700	-0.30691000
H	-4.20104800	-1.13240100	-2.37351500
H	-3.86193900	-2.09794800	1.79366400
H	-4.91795600	-2.48583000	-0.41895600

Addition TS (dimer)

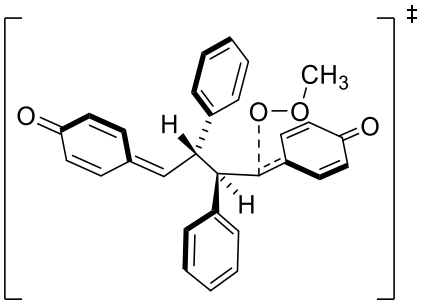

TS frequency: -398.43 cm^{-1}
DFT Enthalpy = -1420.677955 DFT Free Energy = -1420.774397

0 2

C	0.60031500	2.05824600	-0.77530600
C	0.75794700	2.68832800	-2.01173100
C	1.55020200	3.82910900	-2.13686000
C	2.19360300	4.35635900	-1.02139000
C	2.03749900	3.73949600	0.21969400
C	1.24612200	2.60228100	0.34237400
H	0.25358100	2.28765000	-2.88553500
H	1.65988900	4.30507700	-3.10482300
H	2.81086000	5.24239300	-1.11549500
H	2.53569300	4.14404000	1.09344200
H	1.12928000	2.13182200	1.31290800
C	-0.26601800	0.80745700	-0.65062800
H	-0.65354100	0.58365300	-1.64854100
C	0.58847600	-0.45477700	-0.21551700
H	0.70380600	-0.41268100	0.86323600
C	-0.09534900	-1.77858300	-0.56242100
C	-0.57209500	-2.61394400	0.45107800
C	-0.23990800	-2.19606200	-1.89276900
C	-1.18412900	-3.82841500	0.14669800
H	-0.48070200	-2.29802400	1.48299800
C	-0.85186000	-3.40854500	-2.19920000
H	0.12826900	-1.57519900	-2.70275000
C	-1.32742200	-4.23009800	-1.17855700
H	-1.55098700	-4.46020200	0.94790300
H	-0.95236300	-3.71394000	-3.23473300
H	-1.80262400	-5.17505700	-1.41541800
C	1.94713100	-0.42463400	-0.86423100
H	1.95496400	-0.26059900	-1.93908900

C	3.15304500	-0.61833900	-0.27149600
C	3.33403600	-0.85067100	1.15626800
C	4.36065200	-0.59801200	-1.09043500
C	4.55484800	-1.04107200	1.69126700
H	2.45971200	-0.87193200	1.79590100
C	5.58667100	-0.78537200	-0.56832200
H	4.23704300	-0.42258000	-2.15498300
C	5.78329600	-1.02375900	0.87262700
H	4.69372400	-1.21472500	2.75235800
H	6.48169800	-0.76914800	-1.17951300
C	-2.79696000	0.78924200	-0.00077400
C	-3.20596700	-0.26628500	-0.89096000
C	-3.83191900	1.52426900	0.68723200
C	-4.51622300	-0.55791500	-1.08332400
H	-2.44820900	-0.84131600	-1.40644800
C	-5.14645400	1.24916000	0.50544900
H	-3.52542700	2.32092700	1.35695700
C	-5.58433400	0.17857900	-0.39767200
H	-4.83088200	-1.34823500	-1.75490300
H	-5.92639000	1.80772700	1.00998700
O	6.89284500	-1.19451600	1.36391300
O	-6.77616500	-0.08491000	-0.57011800
C	-1.46158100	1.14673700	0.23837500
H	-1.33283400	2.05465700	0.81129200
O	-1.02977200	0.19349100	2.02623500
O	-1.67266300	0.82133800	3.05310100
C	-2.64791700	-0.06212400	3.63054900
H	-2.15070500	-0.94196400	4.04459000
H	-3.11966800	0.51642200	4.42559700
H	-3.38238700	-0.35591500	2.87988800

S1 – Methyl salicylate (summary and organic solution autoxidation)

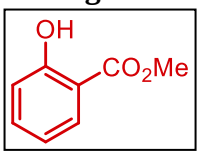

Table S1.1- Summary of kinetic and cell data for methyl salicylate

Compound	Organic Solutions		Liposomes		Cells
	k_{inh} (hexadecene) (M^{-1} s^{-1}); n	k_{inh} (cumene) (M^{-1} s^{-1}); n	k_{inh} (DTUN) (M^{-1} s^{-1}); n	k_{inh} (V70) (M^{-1} s^{-1}); n	EC_{50}
Methylsalicylate	DNI	DNI	N/A	N/A	N/A

Table S1.2 – Summary of hexadecane co-oxidation inhibition kinetics

Hexadecene	PMC	methyl-salicylate
Conc. (μM)	2	5
t_{inh} (s)	3391.406669	0
*k*p	3791.889263	3791.889263
Ri	1.18E-09	1.18E-09
[AOX] (M)	2.00E-06	5.00E-06
[Dye] (M)	1.00E-05	1.00E-05
n	2.00E+00	0.00E+00
log *k*	6.258417464	N/A
k_{inh} (M^{-1} s^{-1})	1.81E+06	N/A
Rate	6.16678E-12	0

Table S1.3 – Summary of cumene co-oxidation inhibition kinetics

Cumene	PMC	methylsalicylate	methylsalicylate
Conc. (μM)	2	5	50
t_{inh} (s)	1954	0	0
*k*p	141	141	141
Ri	2.05E-09	2.05E-09	2.05E-09
[AOX] (M)	2.00E-06	5.00E-06	5.00E-05
[Dye] (M)	1.00E-05	1.00E-05	1.00E-05
n	2.00E+00	0	0
log *k*	5.325059	N/A	N/A
k_{inh} (M^{-1} s^{-1})	2.11E+05	N/A	N/A
Rate	3.41E-12	0	0

Table S.4 – Summary of liposome autoxidation inhibition assay using DTUN initiator

Liposomes (DTUN)	PMC (E2)	PMC (F2)	PMC (G2)	methyl salicylate 1 (F6)	methyl salicylate 2 (F7)	methyl salicylate 3 (F8)
Conc. (μM)	5	5	5	5	5	5
t_{inh} (s)	18154.521	17323.0663	16289.0593	0	0	0
*k*p	894	894	894	894	894	894
Ri	5.51E-10	5.77E-10	6.14E-10	5.81E-10	5.81E-10	5.81E-10
[AOX] (M)	5.00E-06	5.00E-06	5.00E-06	5.00E-06	5.00E-06	5.00E-06
[Dye] (M)	1.00E-05	1.00E-05	1.00E-05	1.00E-05	1.00E-05	1.00E-05
n	2.00E+00	2.00E+00	2.00E+00	0.00E+00	0.00E+00	0.00E+00
k_{inh} (M^{-1} s^{-1})	9.55E+04	9.88E+04	1.04E+05	#DIV/0!	#DIV/0!	#DIV/0!
Rate	5.16E-12	5.2241E-12	5.27E-12	0.00E+00	0.00E+00	0.00E+00

Table S1.5 – Summary of liposome autoxidation inhibition assay using V70 initiator

Liposomes (V70)	PMC (E2)	PMC (F2)	PMC (G2)	methyl 3hydroxybenzoate 1 (F9)	methyl 3hydroxybenzoate 2 (F10)	methyl 3hydroxybenzoate 3 (F11)
Conc. (μM)	5	5	5	5	5	5
t_{inh} (s)	11154.635	13130.1844	12579.0861	0	0	0
*k*p	894	894	894	894	894	894
Ri	8.96E-10	7.62E-10	7.95E-10	8.18E-10	8.18E-10	8.18E-10
[AOX] (M)	5.00E-06	5.00E-06	5.00E-06	5.00E-06	5.00E-06	5.00E-06
[Dye] (M)	1.00E-05	1.00E-05	1.00E-05	1.00E-05	1.00E-05	1.00E-05
n	2.00E+00	2.00E+00	2.00E+00	0.00E+00	0.00E+00	0.00E+00
k_{inh} (M^{-1} s^{-1})	1.34E+05	1.21E+05	1.14E+05	#DIV/0!	#DIV/0!	#DIV/0!
Rate	6.00E-12	5.6295E-12	6.2361E-12	0.00E+00	0.00E+00	0.00E+00

S2 – 3-hydroxy methylbenzoate (summary and organic solution autoxidation)

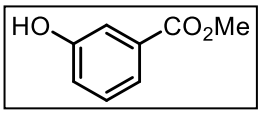

Table S2.1 - Summary of kinetic and cell data

Compound	Organic Solutions		Liposomes		Cells
	k_{inh} (hexadecene) (M^{-1} s^{-1}); n	k_{inh} (cumene) (M^{-1} s^{-1}); n	k_{inh} (DTUN) (M^{-1} s^{-1}); n	k_{inh} (V70) (M^{-1} s^{-1}); n	EC_{50}
3-hydroxy methylbenzoate	DNI	$6.1x10^2$; n=2	DNI	DNI	N/A

Table S2.2 – Summary of hexadecane co-oxidation inhibition kinetics

Hexadecene	PMC	3-hydroxy methylbenzoate
Conc. (μM)	2	5
t_{inh} (s)	3684.782702	0
*k*p	3791.889263	3791.889263
Ri	1.09E-09	1.09E-09
[AOX] (M)	2.00E-06	5.00E-06
[Dye] (M)	1.00E-05	1.00E-05
n	2.00E+00	0.00E+00
log *k*	6.167399821	N/A
k_{inh} (M^{-1} s^{-1})	1.47E+06	N/A
Rate	6.99913E-12	0

Table S2.3 – Summary of cumene co-oxidation inhibition kinetics

Cumene	PMC	3-hydroxy methylbenzoate	PMC	3-hydroxy methylbenzoate
Conc. (μM)	2	5	2	50
t_{inh} (s)	2001	0	1559	12668
*k*p	141	141	141	141
Ri	2.00E-09	2.05E-09	2.57E-09	2.57E-09
[AOX] (M)	2.00E-06	5.00E-06	2.00E-06	5.00E-05
[Dye] (M)	1.00E-05	1.00E-05	1.00E-05	1.00E-05
n	2.00E+00	0	2.00E+00	2.00E+00
log *k*	5.780031086	#DIV/0!	5.105928	2.785014391
k_{inh} (M^{-1} s^{-1})	6.03E+05	#DIV/0!	1.28E+05	6.10E+02
Rate	1.17E-12	0	7.09E-12	5.93548E-11

Table S2.4 – Summary of liposome autoxidation inhibition assay using DTUN initiator

Liposomes (DTUN)	PMC (E2)	PMC (F2)	PMC (G2)	methyl 3hydroxybenzoate 1 (F9)	methyl 3hydroxybenzoate 2 (F10)	methyl 3hydroxybenzoate 3 (F11)
Conc. (μM)	5	5	5	5	5	5
t_{inh} (s)	18154.521	17323.0663	16289.0593	0	0	0
*k*p	894	894	894	894	894	894
Ri	5.51E-10	5.77E-10	6.14E-10	5.81E-10	5.81E-10	5.81E-10
[AOX] (M)	5.00E-06	5.00E-06	5.00E-06	5.00E-06	5.00E-06	5.00E-06
[Dye] (M)	1.00E-05	1.00E-05	1.00E-05	1.00E-05	1.00E-05	1.00E-05
n	2.00E+00	2.00E+00	2.00E+00	0.00E+00	0.00E+00	0.00E+00
k_{inh} (M^{-1} s^{-1})	9.55E+04	9.88E+04	1.04E+05	#DIV/0!	#DIV/0!	#DIV/0!
Rate	5.16E-12	5.2241E-12	5.27E-12	0.00E+00	0.00E+00	0.00E+00

Table S2.5 – Summary of liposome autoxidation inhibition assay using V70 initiator

Liposomes (V70)	PMC (E2)	PMC (F2)	PMC (G2)	methyl 3hydroxybenzoate 1 (F9)	methyl 3hydroxybenzoate 2 (F10)	methyl 3hydroxybenzoate 3 (F11)
Conc. (μM)	5	5	5	5	5	5
t_{inh} (s)	11154.635	13130.1844	12579.0861	0	0	0
*k*p	894	894	894	894	894	894
Ri	8.96E-10	7.62E-10	7.95E-10	8.18E-10	8.18E-10	8.18E-10
[AOX] (M)	5.00E-06	5.00E-06	5.00E-06	5.00E-06	5.00E-06	5.00E-06
[Dye] (M)	1.00E-05	1.00E-05	1.00E-05	1.00E-05	1.00E-05	1.00E-05
n	2.00E+00	2.00E+00	2.00E+00	0.00E+00	0.00E+00	0.00E+00
k_{inh} (M^{-1} s^{-1})	1.34E+05	1.21E+05	1.14E+05	#DIV/0!	#DIV/0!	#DIV/0!
Rate	6.00E-12	5.6295E-12	6.2361E-12	0.00E+00	0.00E+00	0.00E+00

S3 – 4-hydroxy methylbenzoate (summary and organic solution autoxidation)

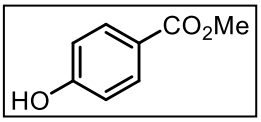

Table S3.1- Summary of kinetic and cell data

Compound	Organic Solutions		Liposomes		Cells
	k_{inh} (hexadecene) (M^{-1} s^{-1}); n	k_{inh} (cumene) (M^{-1} s^{-1}); n	k_{inh} (DTUN) (M^{-1} s^{-1}); n	k_{inh} (V70) (M^{-1} s^{-1}); n	EC_{50}
4-hydroxy methylbenzoate	DNI	4.8E+02; n=2	DNI	DNI	N/A

Table S3.2 – Summary of hexadecane co-oxidation inhibition kinetics

Hexadecene	PMC	4-hydroxy methylbenzoate
Conc. (μM)	2	5
t_{inh} (s)	3391.40667	0
*k*p	3791.88926	3791.889263
Ri	1.18E-09	1.18E-09
[AOX] (M)	2.00E-06	5.00E-06
[Dye] (M)	1.00E-05	1.00E-05
n	2.00E+00	0.00E+00
log *k*	6.25841746	N/A
k_{inh} (M^{-1} s^{-1})	1.81E+06	N/A
Rate	6.1668E-12	0

Table S3.3 – Summary of cumene co-oxidation inhibition kinetics

Cumene	PMC	4-hydroxy methylbenzoate	PMC	4-hydroxy methylbenzoate
Conc. (μM)	2	5	2	50
t_{inh} (s)	2001	0	1559	7207.308304
*k*p	141	141	141	141
Ri	2.00E-09	2.00E-09	2.57E-09	2.57E-09
[AOX] (M)	2.00E-06	5.00E-06	2.00E-06	5.00E-05
[Dye] (M)	1.00E-05	1.00E-05	1.00E-05	1.00E-05
n	2.00E+00	0.00E+00	2.00E+00	2.00E+00
log *k*	5.780031	#DIV/0!	5.105928	2.682452468
k_{inh} (M^{-1} s^{-1})	6.03E+05	#DIV/0!	1.28E+05	4.81E+02
Rate	1.17E-12	0	7.09E-12	7.51653E-11

Table S3.4 – Summary of liposome autoxidation inhibition assay using DTUN initiator

Liposomes (DTUN)	PMC (E2)	PMC (F2)	PMC (G2)	methyl 4hydroxybenzoate 1 (F9)	methyl 4hydroxybenzoate 2 (F10)	methyl 4hydroxybenzoate 3 (F11)
Conc. (μM)	5	5	5	5	5	5
t_{inh} (s)	18154.521	17323.0663	16289.0593	0	0	0
*k*p	894	894	894	894	894	894
Ri	5.51E-10	5.77E-10	6.14E-10	5.81E-10	5.81E-10	5.81E-10
[AOX] (M)	5.00E-06	5.00E-06	5.00E-06	5.00E-06	5.00E-06	5.00E-06
[Dye] (M)	1.00E-05	1.00E-05	1.00E-05	1.00E-05	1.00E-05	1.00E-05
n	2.00E+00	2.00E+00	2.00E+00	0.00E+00	0.00E+00	0.00E+00
k_{inh} (M^{-1} s^{-1})	1.34E+05	1.21E+05	1.14E+05	#DIV/0!	#DIV/0!	#DIV/0!
Rate	5.16E-12	5.2241E-12	5.27E-12	0.00E+00	0.00E+00	0.00E+00

Table S3.5 – Summary of liposome autoxidation inhibition assay using V70 initiator

Liposomes (V70)	PMC (E2)	PMC (F2)	PMC (G2)	methyl 4hydroxybenzoate 1 (F9)	methyl 4hydroxybenzoate 2 (F10)	methyl 4hydroxybenzoate 3 (F11)
Conc. (μM)	5	5	5	5	5	5
t_{inh} (s)	11154.635	13130.1844	12579.0861	0	0	0
*k*p	894	894	894	894	894	894
Ri	8.96E-10	7.62E-10	7.95E-10	8.18E-10	8.18E-10	8.18E-10
[AOX] (M)	5.00E-06	5.00E-06	5.00E-06	5.00E-06	5.00E-06	5.00E-06
[Dye] (M)	1.00E-05	1.00E-05	1.00E-05	1.00E-05	1.00E-05	1.00E-05
n	2.00E+00	2.00E+00	2.00E+00	0.00E+00	0.00E+00	0.00E+00
k_{inh} (M^{-1} s^{-1})	1.34E+05	1.21E+05	1.14E+05	#DIV/0!	#DIV/0!	#DIV/0!
Rate	6.00E-12	5.62948E-12	6.23606E-12	0.00E+00	0.00E+00	0.00E+00

S4 – Methyl-3,5-dihydroxybenzoate (summary and organic solution autoxidation)

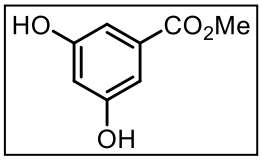

Table S4.1 - Summary of kinetic and cell data

Compound	Organic Solutions		Liposomes		Cells
	k_{inh} (hexadecene) (M^{-1} s^{-1}); n	k_{inh} (cumene) (M^{-1} s^{-1}); n	k_{inh} (DTUN) (M^{-1} s^{-1}); n	k_{inh} (V70) (M^{-1} s^{-1}); n	EC_{50}
Methyl-3,5-dihydroxybenzoate	DNI	(2.9 ± 0.2)E+02; n=2.88 ± 0.03	DNI	DNI	N/A

Table S4.2 – Summary of hexadecane co-oxidation inhibition kinetics

Hexadecene	PMC	Methyl-3,5dihydroxybenzoate
Conc. (μM)	2	5
t_{inh} (s)	3684.7827	0
*k*p	3791.88926	3791.88926
Ri	1.09E-09	1.09E-09
[AOX] (M)	2.00E-06	5.00E-06
[Dye] (M)	1.00E-05	1.00E-05
n	2.00E+00	0.00E+00
log *k*	6.16739982	N/A
k_{inh} (M^{-1} s^{-1})	1.47E+06	N/A
Rate	6.9991E-12	0

Table S4.3 – Summary of cumene co-oxidation inhibition kinetics

Cumene	PMC	methyl-3,5-dihydroxy benzoate	PMC	methyl-3,5-dihydroxy benzoate	PMC	methyl-3,5-dihydroxy benzoate
Conc. (μM)	2	5	2	5	2	5
t_{inh} (s)	2001	6709.103	1833	7410.637	2159	7360.447
*k*p	141	141	141	141	141	141
Ri	2.00E-09	2.00E-09	2.18E-09	2.18E-09	1.85E-09	1.85E-09
[AOX] (M)	2.00E-06	5.00E-06	2.00E-06	5.00E-06	2.00E-06	5.00E-06
[Dye] (M)	1.00E-05	1.00E-05	1.00E-05	1.00E-05	1.00E-05	1.00E-05
n	2.00E+00	2.68E+00	2.00E+00	3.23E+00	2.00E+00	2.73E+00
log *k*	5.780031	3.486829	5.322359	3.447402	4.837633	3.432213
k_{inh} (M^{-1} s^{-1})	6.03E+05	3.07E+03	2.10E+05	2.80E+03	6.88E+04	2.71E+03
Rate	1.17E-12	6.85E-11	3.66E-12	6.79E-11	9.49E-12	7.08E-11

Table S4.4 – Summary of liposome autoxidation inhibition assay using DTUN initiator

Liposomes (DTUN)	PMC (E2)	PMC (F2)	PMC (G2)	methyl-3,5-dihydroxy benzoate 1 (G6)	methyl-3,5-dihydroxy benzoate 2 (G7)	methyl-3,5-dihydroxy benzoate 3 (G8)
Conc. (μM)	5	5	5	5	5	5
t_{inh} (s)	18154.521	17323.0663	16289.0593	0	0	0
*k*p	894	894	894	894	894	894
Ri	5.51E-10	5.77E-10	6.14E-10	5.81E-10	5.81E-10	5.81E-10
[AOX] (M)	5.00E-06	5.00E-06	5.00E-06	5.00E-06	5.00E-06	5.00E-06
[Dye] (M)	1.00E-05	1.00E-05	1.00E-05	1.00E-05	1.00E-05	1.00E-05
n	2.00E+00	2.00E+00	2.00E+00	0.00E+00	0.00E+00	0.00E+00
k_{inh} (M^{-1} s^{-1})	9.55E+04	9.88E+04	1.04E+05	#DIV/0!	#DIV/0!	#DIV/0!
Rate	5.16E-12	5.22409E-12	5.27E-12	0.00E+00	0.00E+00	0.00E+00

Table S4.5 – Summary of liposome autoxidation inhibition assay using V70 initiator

Liposomes (V70)	PMC (E2)	PMC (F2)	PMC (G2)	methyl 4hydroxybenzoate 1 (F9)	methyl 4hydroxybenzoate 2 (F10)	methyl 4hydroxybenzoate 3 (F11)
Conc. (μM)	5	5	5	5	5	5
t_{inh} (s)	11154.635	13130.1844	12579.0861	0	0	0
*k*p	894	894	894	894	894	894
Ri	8.96E-10	7.62E-10	7.95E-10	8.18E-10	8.18E-10	8.18E-10
[AOX] (M)	5.00E-06	5.00E-06	5.00E-06	5.00E-06	5.00E-06	5.00E-06
[Dye] (M)	1.00E-05	1.00E-05	1.00E-05	1.00E-05	1.00E-05	1.00E-05
n	2.00E+00	2.00E+00	2.00E+00	0.00E+00	0.00E+00	0.00E+00
k_{inh} (M^{-1} s^{-1})	1.34E+05	1.21E+05	1.14E+05	#DIV/0!	#DIV/0!	#DIV/0!
Rate	6.00E-12	5.62948E-12	6.23606E-12	0.00E+00	0.00E+00	0.00E+00

S5 – orcinol (summary and organic solution autoxidation)

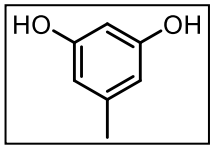

Table S5.1 - Summary of kinetic and cell data

Compound	Organic Solutions		Liposomes		Cells
	k_{inh} (hexadecene) (M^{-1} s^{-1}); n	k_{inh} (cumene) (M^{-1} s^{-1}); n	k_{inh} (DTUN) (M^{-1} s^{-1}); n	k_{inh} (V70) (M^{-1} s^{-1}); n	EC_{50}
orcinol	(2.96± 1.08)E+05; n=0.81± 0.4	(1.38 ± 0.19)E+04; n=2.15±0.14	DNI	DNI	N/A

Table S5.2– Summary of hexadecane co-oxidation inhibition kinetics

Hexadecene	PMC	orcinol	PMC	orcinol	PMC	orcinol
Conc. (μM)	2	5	2	5	2	5
t_{inh} (s)	4886	7798	4229	3159	4119	2804
*k*p	3791.88926	3791.88926	3791.88926	3791.88926	3791.88926	3791.88926
Ri	8.19E-10	8.19E-10	9.46E-10	9.46E-10	9.71E-10	9.71E-10
[AOX] (M)	2.00E-06	5.00E-06	2.00E-06	5.00E-06	2.00E-06	5.00E-06
[Dye] (M)	1.00E-05	1.00E-05	1.00E-05	1.00E-05	1.00E-05	1.00E-05
n	2.00E+00	1.28E+00	2.00E+00	5.98E-01	2.00E+00	5.44E-01
log *k*	6.12581094	5.21523085	6.24327873	5.43493373	6.4323787	5.65437807
k_{inh} (M^{-1} s^{-1})	1.34E+06	1.64E+05	1.75E+06	2.72E+05	2.71E+06	4.51E+05
Rate	5.8087E-12	2.9624E-11	5.1203E-12	4.4092E-11	3.4013E-12	2.9974E-11

Table S5.3 – Summary of cumene co-oxidation inhibition kinetics

Cumene	PMC	orcinol	PMC	orcinol	PMC	orcinol
Conc. (μM)	2	5	2	5	2	5
t_{inh} (s)	2343	6749.810328	2428	6196.781	2321	6078.149
*k*p	141	141	141	141	141	141
Ri	1.71E-09	1.71E-09	1.65E-09	1.65E-09	1.72E-09	1.72E-09
[AOX] (M)	2.00E-06	5.00E-06	2.00E-06	5.00E-06	2.00E-06	5.00E-06
[Dye] (M)	1.00E-05	1.00E-05	1.00E-05	1.00E-05	1.00E-05	1.00E-05
n	2.00E+00	2.30E+00	2.00E+00	2.04E+00	2.00E+00	2.09E+00
log *k*	5.531447	4.104835235	5.938324	4.104392	6.21875	4.203365
k_{inh} (M^{-1} s^{-1})	3.40E+05	1.27E+04	8.68E+05	1.27E+04	1.65E+06	1.60E+04
Rate	1.77E-12	1.64094E-11	6.69E-13	1.79E-11	3.67E-13	1.45E-11

Table S5.4 – Summary of liposome autoxidation inhibition assay using DTUN initiator

Liposomes (DTUN)	PMC (E2)	PMC (F2)	PMC (G2)	methyl-3,5-dihydroxy benzoate 1 (G6)	methyl-3,5-dihydroxy benzoate 2 (G7)	methyl-3,5-dihydroxy benzoate 3 (G8)
Conc. (μM)	5	5	5	5	5	5
t_{inh} (s)	4698.560591	4436.44094	4665.226286	0	0	0
*k*p	894	894	894	894	894	894
Ri	2.13E-09	2.25E-09	2.14E-09	5.81E-10	5.81E-10	5.81E-10
[AOX] (M)	5.00E-06	5.00E-06	5.00E-06	5.00E-06	5.00E-06	5.00E-06
[Dye] (M)	1.00E-05	1.00E-05	1.00E-05	1.00E-05	1.00E-05	1.00E-05
n	2.00E+00	2.00E+00	2.00E+00	0.00E+00	0.00E+00	0.00E+00
k_{inh} (M^{-1} s^{-1})	4.94E+05	4.78E+05	5.85E+05	#DIV/0!	#DIV/0!	#DIV/0!
Rate	3.85E-12	4.21E-12	3.28E-12	0.00E+00	0.00E+00	0.00E+00

Table S5.5 – Summary of liposome autoxidation inhibition assay using V70 initiator

Liposomes (V70)	PMC (E2)	PMC (F2)	PMC (G2)	orcinol 1 (A7)	orcinol 1 (A8)	orcinol 2 (A9)	orcinol 2 (A10)	orcinol 3 (B1)	orcinol 3 (B2)
Conc. (μM)	5	5	5	5	5	5	5	5	5
t_{inh} (s)	11154.635	13130.1844	12579.0861	0	0	0	0	0	0
*k*p	894	894	894	894	894	894	894	894	894
Ri	8.96E-10	7.62E-10	7.95E-10	5.17E-10	5.17E-10	5.17E-10	5.17E-10	5.17E-10	5.17E-10
[AOX] (M)	5.00E-06	5.00E-06	5.00E-06	5.00E-06	5.00E-06	5.00E-06	5.00E-06	5.00E-06	5.00E-06
[Dye] (M)	1.00E-05	1.00E-05	1.00E-05	1.00E-05	1.00E-05	1.00E-05	1.00E-05	1.00E-05	1.00E-05
n	2.00E+00	2.00E+00	2.00E+00	#DIV/0!	#DIV/0!	#DIV/0!	#DIV/0!	#DIV/0!	#DIV/0!
k_{inh} (M^{-1} s^{-1})	1.34E+05	1.21E+05	1.14E+05	7.06E-12	7.15E-12	8.29E-12	1.56E-11	1.61E-11	1.79E-11
Rate	6.00E-12	5.62948E-12	6.23606E-12	#DIV/0!	#DIV/0!	#DIV/0!	#DIV/0!	#DIV/0!	#DIV/0!

4.6 – Methyl gallate (summary and organic solution autoxidation)

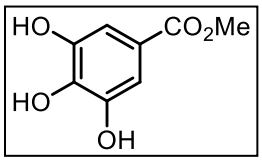

Table S6.1 - Summary of kinetic and cell data

Compound	Organic Solutions		Liposomes		Cells
	k_{inh} (hexadecene) (M^{-1} s^{-1}); n	k_{inh} (cumene) (M^{-1} s^{-1}); n	k_{inh} (DTUN) (M^{-1} s^{-1}); n	k_{inh} (V70) (M^{-1} s^{-1}); n	EC_{50}
Methyl gallate	(4.6 ± 0.1)E+05; n=1.5 ± 0.2	N/A	DNI	(3.11 ± 1.4)E+04; n=2*	5.3 ± 0.7 μM

Table S6.2 – Summary of hexadecane co-oxidation inhibition kinetics

Hexadecene	PMC	Methyl gallate	PMC	Methyl gallate	PMC	Methyl gallate
Conc. (μM)	2	5	2	5	2	5
t_{inh} (s)	3684.7827	7817.49145	4047.92216	6913.73042	4047.92216	7852.64006
*k*p	3791.88926	3791.88926	3791.88926	3791.88926	3791.88926	3791.88926
Ri	1.09E-09	1.09E-09	9.88E-10	9.88E-10	9.88E-10	9.88E-10
[AOX] (M)	2.00E-06	5.00E-06	2.00E-06	5.00E-06	2.00E-06	5.00E-06
[Dye] (M)	1.00E-05	1.00E-05	1.00E-05	1.00E-05	1.00E-05	1.00E-05
n	2.00E+00	1.70E+00	2.00E+00	1.37E+00	2.00E+00	1.55E+00
log *k*	6.16739982	5.67002263	6.23210736	5.65485194	6.23210736	5.65687063
k_{inh} (M^{-1} s^{-1})	1.47E+06	4.68E+05	1.71E+06	4.52E+05	1.71E+06	4.54E+05
Rate	6.9991E-12	1.037E-11	5.4893E-12	1.2142E-11	5.4893E-12	1.0641E-11

Table S6.3 – Summary of liposome autoxidation inhibition assay using DTUN initiator

Liposomes (DTUN)	PMC (E2)	PMC (F2)	PMC (G2)	methyl gallate 1 (G9)	methyl gallate 2 (G10)	methyl gallate 3 (G11)
Conc. (μM)	5	5	5	5	5	5
t_{inh} (s)	18154.521	17323.0663	16289.0593	0	0	0
*k*p	894	894	894	894	894	894
Ri	5.51E-10	5.77E-10	6.14E-10	5.81E-10	5.81E-10	5.81E-10
[AOX] (M)	5.00E-06	5.00E-06	5.00E-06	5.00E-06	5.00E-06	5.00E-06
[Dye] (M)	1.00E-05	1.00E-05	1.00E-05	1.00E-05	1.00E-05	1.00E-05
n	2.00E+00	2.00E+00	2.00E+00	0.00E+00	0.00E+00	0.00E+00
k_{inh} (M^{-1} s^{-1})	9.55E+04	9.88E+04	1.04E+05	#DIV/0!	#DIV/0!	#DIV/0!
Rate	5.16E-12	5.22409E-12	5.27E-12	0.00E+00	0.00E+00	0.00E+00

Table S6.4 – Summary of liposome autoxidation inhibition assay using V70 initiator

Liposomes (V70)	PMC (E2)	PMC (F2)	PMC (G2)	methyl gallate 1 (G9) 1st pahse	methyl gallate 1 (G9)	methyl gallate 2 (G10) 1st phase)	methyl gallate 3 (G11) 1st phase
Conc. (μM)	5	5	5	5	5	5	5
t_{inh} (s)	11154.635	13130.1844	12579.0861	11537.4228	11537.4228	11283.3716	9534.6651
*k*p	894	480	480	480	480	480	480
Ri	8.96E-10	7.62E-10	7.95E-10	8.18E-10	8.18E-10	8.18E-10	8.18E-10
[AOX] (M)	5.00E-06	5.00E-06	5.00E-06	5.00E-06	5.00E-06	5.00E-06	5.00E-06
[Dye] (M)	1.00E-05	1.00E-05	1.00E-05	1.00E-05	1.00E-05	1.00E-05	1.00E-05
n	2.00E+00	2.00E+00	2.00E+00	2.00E+00	1.89E+00	2.00E+00	2.00E+00
k_{inh} (M^{-1} s^{-1})	1.34E+05	6.49E+04	6.12E+04	2.52E+04	4.16E-07	2.50E+04	2.15E+04
Rate	6.00E-12	5.6295E-12	6.2361E-12	1.56E-11	1.00E+00	1.57E-11	1.83E-11

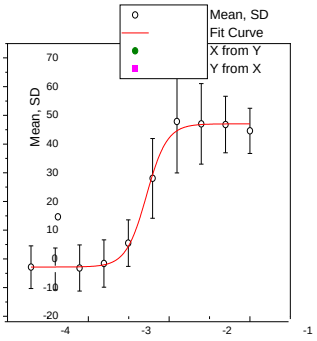

Dose responsive curve x axis = log(mM); y axis = % viability.

Table S6.5 – Dose response for ferroptosis inhibition

methyl gallate 1		methyl gallate 2		methyl gsllate 3	
Log(con)mM	% viability	Log(con)mM	% viability	Log(con)mM	% viability
-1	43.88517	-1	37.09273	-1	52.79916
-1.30103	37.59258	-1.30103	45.61638	-1.30103	57.19034
-1.60206	31.17556	-1.60206	52.12943	-1.60206	57.77583
-1.90309	30.03792	-1.90309	47.65995	-1.90309	65.91242
-2.20412	15.293	-2.20412	26.04428	-2.20412	42.82
-2.50515	-1.7272	-2.50515	3.934197	-2.50515	14.25152
-2.80618	-8.90857	-2.80618	-3.19192	-2.80618	7.328959
-3.10721	-10.7661	-3.10721	-3.98298	-3.10721	5.271134
-3.40824	-10.224	-3.40824	-4.4708	-3.40824	4.212085
-3.70927	-9.86846	-3.70927	-3.65996	-3.70927	4.935338

S7 – Resorcinol (summary and organic solution autoxidation)

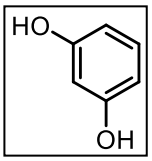

Table S7.1 - Summary of kinetic and cell data

Compound	Organic Solutions		Liposomes		Cells
	k_{inh} (hexadecene) (M^{-1} s^{-1}); n	k_{inh} (cumene) (M^{-1} s^{-1}); n	k_{inh} (DTUN) (M^{-1} s^{-1}); n	k_{inh} (V70) (M^{-1} s^{-1}); n	EC_{50}
resorcinol	DNI	(8.86 ± 1.30)E+03; n=2.36±0.18	DNI	DNI	N/A

Table S7.2 – Summary of hexadecane co-oxidation inhibition kinetics

Hexadecene	PMC	resorcinol
Conc. (μM)	2	5
t_{inh} (s)	2618.37872	0
*k*p	3791.88926	3791.88926
Ri	1.53E-09	1.53E-09
[AOX] (M)	2.00E-06	5.00E-06
[Dye] (M)	1.00E-05	1.00E-05
n	2.00E+00	0.00E+00
log *k*	6.25635524	N/A
k_{inh} (M^{-1} s^{-1})	1.80E+06	N/A
Rate	8.0254E-12	0

Table S7.3 – Summary of cumene co-oxidation inhibition kinetics

Cumene	PMC	resorcinol	resorcinol	PMC	resorcinol
Conc. (μM)	2	5	50	2	5
t_{inh} (s)	1954	5298	52742.1	2270	7564
*k*p	141	141	141	141	141
Ri	2.05E-09	2.05E-09	2.05E-09	1.76E-09	1.76E-09
[AOX] (M)	2.00E-06	5.00E-06	5.00E-05	2.00E-06	5.00E-06
[Dye] (M)	1.00E-05	1.00E-05	1.00E-05	1.00E-05	1.00E-05
n	2.00E+00	2.17E+00	2.16E+00	2.00E+00	2.67E+00
log *k*	5.325059	3.927606	3.290577	5.057172	3.867316
k_{inh} (M^{-1} s^{-1})	2.11E+05	8.46E+03	1.95E+03	1.14E+05	7.37E+03
Rate	3.41E-12	3.14E-11	1.37E-11	5.45E-12	2.53E-11

Table S7.4 – Summary of liposome autoxidation inhibition assay using DTUN initiator

Liposomes (DTUN)	PMC (E2)	PMC (F2)	PMC (G2)	resorcinol 1 (D3)	resorcinol 2 (D4)	resorcinol 3 (D5)
Conc. (μM)	5	5	5	5	5	5
t_{inh} (s)	18154.52099	17323.06628	16289.05931	0	0	0
*k*p	894	894	894	480	480	480
Ri	5.51E-10	5.77E-10	6.14E-10	5.81E-10	5.81E-10	5.81E-10
[AOX] (M)	5.00E-06	5.00E-06	5.00E-06	5.00E-06	5.00E-06	5.00E-06
[Dye] (M)	1.00E-05	1.00E-05	1.00E-05	1.00E-05	1.00E-05	1.00E-05
n	2.00E+00	2.00E+00	2.00E+00	0.00E+00	0.00E+00	0.00E+00
k_{inh} (M^{-1} s^{-1})	9.55E+04	9.88E+04	1.04E+05	#DIV/0!	#DIV/0!	#DIV/0!
Rate	5.16E-12	5.22409E-12	5.27E-12	0.00E+00	0.00E+00	0.00E+00

Table S7.5 – Summary of liposome autoxidation inhibition assay using V70 initiator

Liposomes (V70)	PMC (E2)	PMC (F2)	PMC (G2)	resorcinol 1 (D3)	resorcinol 2 (D4)	resorcinol 3 (D5)
Conc. (μM)	5	5	5	5	5	5
t_{inh} (s)	11154.63502	13130.18442	12579.08609	0	0	0
*k*p	894	894	894	480	480	480
Ri	8.96E-10	7.62E-10	7.95E-10	8.18E-10	8.18E-10	8.18E-10
[AOX] (M)	5.00E-06	5.00E-06	5.00E-06	5.00E-06	5.00E-06	5.00E-06
[Dye] (M)	1.00E-05	1.00E-05	1.00E-05	1.00E-05	1.00E-05	1.00E-05
n	2.00E+00	2.00E+00	2.00E+00	0.00E+00	0.00E+00	0.00E+00
k_{inh} (M^{-1} s^{-1})	1.34E+05	1.21E+05	1.14E+05	#DIV/0!	#DIV/0!	#DIV/0!
Rate	6.00E-12	5.62948E-12	6.23606E-12	0.00E+00	0.00E+00	0.00E+00

S8 – Catechol (summary and organic solution autoxidation)

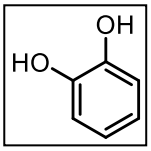

Table S8.1 - Summary of kinetic and cell data

Compound	Organic Solutions		Liposomes		Cells
	k_{inh} (hexadecene) (M^{-1} s^{-1}); n	k_{inh} (cumene) (M^{-1} s^{-1}); n	k_{inh} (DTUN) (M^{-1} s^{-1}); n	k_{inh} (V70) (M^{-1} s^{-1}); n	EC_{50}
catechol	(3.8 ± 0.8)E+05; n=1.9 ±0.2	(7.3 ± 1.8)E+04; n=1.61±0.26	DNI	DNI	N/A

Table S8.2 – Summary of hexadecane co-oxidation inhibition kinetics

Hexadecene	PMC	catechol	catechol	catechol	PMC	catechol	catechol
Conc. (μM)	2	5	5	5	2	5	5
t_{inh} (s)	2661	6482.31256	8095.98068	7816.24889	2618.37872	6453.89632	8130.71173
*k*p	3791.88926	3791.88926	3791.88926	3791.88926	3791.88926	3791.88926	3791.88926
Ri	1.50E-09	1.50E-09	1.50E-09	1.22E-09	1.53E-09	1.53E-09	1.53E-09
[AOX] (M)	2.00E-06	5.00E-06	5.00E-06	5.00E-06	2.00E-06	5.00E-06	5.00E-06
[Dye] (M)	1.00E-05	1.00E-05	1.00E-05	1.00E-05	1.00E-05	1.00E-05	1.00E-05
n	2.00E+00	1.95E+00	2.43E+00	1.91E+00	2.00E+00	1.97E+00	2.48E+00
log *k*	6.25223884	5.84823396	5.75169446	5.86288999	6.25635524	5.83898014	5.73867356
k_{inh} (M^{-1} s^{-1})	1.79E+06	7.05E+05	5.65E+05	7.29E+05	1.80E+06	6.90E+05	5.48E+05
Rate	7.9721E-12	8.2964E-12	8.2964E-12	6.6522E-12	8.0254E-12	8.5124E-12	8.5124E-12

Table S8.3 – Summary of cumene co-oxidation inhibition kinetics

Cumene	PMC	catechol	PMC	catechol	catechol
Conc. (μM)	2	5	2	5	5
t_{inh} (s)	2104	5017.446	1512	3815.152	3850.028
*k*p	141	141	141	141	141
Ri	1.90E-09	1.90E-09	2.65E-09	2.65E-09	2.65E-09
[AOX] (M)	2.00E-06	5.00E-06	2.00E-06	5.00E-06	5.00E-06
[Dye] (M)	1.00E-05	1.00E-05	1.00E-05	1.00E-05	1.00E-05
n	2.00E+00	1.91E+00	2.00E+00	2.02E+00	2.04E+00
log *k*	5.075041	4.774821	5.234955	4.967032	4.815906
k_{inh} (M^{-1} s^{-1})	1.19E+05	5.95E+04	1.72E+05	9.27E+04	6.54E+04
Rate	5.64E-12	4.72E-12	5.43E-12	3.99E-12	5.6E-12

Table S8.4 – Summary of liposome autoxidation inhibition assay using DTUN initiator

Liposomes (DTUN)	PMC (E2)	PMC (F2)	PMC (G2)	catechol 1 (C3)	catechol 2 (C4)	catechol 3 (C5)
Conc. (μM)	5	5	5	5	5	5
t_{inh} (s)	18154.521	17323.0663	16289.0593	0	0	0
*k*p	480	480	480	480	480	480
Ri	5.51E-10	5.77E-10	6.14E-10	5.81E-10	5.81E-10	5.81E-10
[AOX] (M)	5.00E-06	5.00E-06	5.00E-06	5.00E-06	5.00E-06	5.00E-06
[Dye] (M)	1.00E-05	1.00E-05	1.00E-05	1.00E-05	1.00E-05	1.00E-05
n	2.00E+00	2.00E+00	2.00E+00	0.00E+00	0.00E+00	0.00E+00
k_{inh} (M^{-1} s^{-1})	5.13E+04	5.30E+04	5.59E+04	#DIV/0!	#DIV/0!	#DIV/0!
Rate	5.16E-12	5.2241E-12	5.2687E-12	0.00E+00	0.00E+00	0.00E+00

Table S8.5 – Summary of liposome autoxidation inhibition assay using V70 initiator

Liposomes (V70)	PMC (E2)	PMC (F2)	PMC (G2)	catechol 1 (C3)	catechol 2 (C4)	catechol 3 (C5)
Conc. (μM)	5	5	5	5	5	5
t_{inh} (s)	11154.635	13130.1844	12579.0861	0	0	0
*k*p	894	480	480	480	480	480
Ri	8.96E-10	7.62E-10	7.95E-10	8.18E-10	8.18E-10	8.18E-10
[AOX] (M)	5.00E-06	5.00E-06	5.00E-06	5.00E-06	5.00E-06	5.00E-06
[Dye] (M)	1.00E-05	1.00E-05	1.00E-05	1.00E-05	1.00E-05	1.00E-05
n	2.00E+00	2.00E+00	2.00E+00	0.00E+00	0.00E+00	0.00E+00
k_{inh} (M^{-1} s^{-1})	1.34E+05	6.49E+04	6.12E+04	#DIV/0!	#DIV/0!	#DIV/0!
Rate	6.00E-12	5.6295E-12	6.2361E-12	0.00E+00	0.00E+00	0.00E+00

S9 – Di-tBu catechol (summary and organic solution autoxidation)

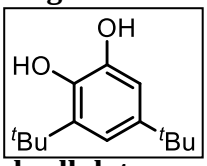

Table S9.1 - Summary of kinetic and cell data

Compound	Organic Solutions		Liposomes		Cells
	k_{inh} (hexadecene) (M^{-1} s^{-1}); n	k_{inh} (cumene) (M^{-1} s^{-1}); n	k_{inh} (DTUN) (M^{-1} s^{-1}); n	k_{inh} (V70) (M^{-1} s^{-1}); n	EC_{50}
di-tertbutyl catechol	(9.5 ± 2.1)E+05; n=2.05 ± 0.19	N/A	(1.87 ± 0.04)E+04; n=2*	(3.71 ± 0.47)E+04; n=2*	N/A

Table S9.2 – Summary of hexadecane co-oxidation inhibition kinetics

Hexadecene	PMC	di-tertbutyl catechol	PMC	di-tertbutyl catechol	PMC	di-tertbutyl catechol
Conc. (μM)	2	5	2	5	2	5
t_{inh} (s)	3473.54565	9412.44527	3315.55272	8882.18934	3195.54853	7314.06383
*k*p	3791.88926	3791.88926	3791.88926	3791.88926	3791.88926	3791.88926
Ri	1.15E-09	1.15E-09	1.21E-09	1.21E-09	1.25E-09	1.25E-09
[AOX] (M)	2.00E-06	5.00E-06	2.00E-06	5.00E-06	2.00E-06	5.00E-06
[Dye] (M)	1.00E-05	1.00E-05	1.00E-05	1.00E-05	1.00E-05	1.00E-05
n	2.00E+00	2.17E+00	2.00E+00	2.14E+00	2.00E+00	1.83E+00
log *k*	6.13412338	5.91390988	6.21600307	5.92802146	6.23611343	6.07691688
k_{inh} (M^{-1} s^{-1})	1.36E+06	8.20E+05	1.64E+06	8.47E+05	1.72E+06	1.19E+06
Rate	8.016E-12	4.9118E-12	6.955E-12	5.0386E-12	6.8896E-12	4.3429E-12

Table S9.3 – Summary of liposome autoxidation inhibition assay using DTUN initiator

Liposomes (DTUN)	PMC (E2)	PMC (F2)	PMC (G2)	di-tBu catechol 1 (C9)	di-tBu catechol 2 (C10)	di-tBu catechol 3 (C11)
Conc. (μM)	5	5	5	5	5	5
t_{inh} (s)	18154.52099	17323.06628	16289.05931	14111.65161	12230.16875	11888.60105
*k*p	894	894	894	894	894	894
Ri	5.51E-10	5.77E-10	6.14E-10	5.81E-10	5.81E-10	5.81E-10
[AOX] (M)	5.00E-06	5.00E-06	5.00E-06	5.00E-06	5.00E-06	5.00E-06
[Dye] (M)	1.00E-05	1.00E-05	1.00E-05	1.00E-05	1.00E-05	1.00E-05
n	2.00E+00	2.00E+00	2.00E+00	2.00E+00	2.00E+00	2.00E+00
k_{inh} (M^{-1} s^{-1})	9.55E+04	9.88E+04	1.04E+05	1.92E+04	1.87E+04	1.83E+04
Rate	5.16E-12	5.22409E-12	5.27E-12	2.70E-11	2.78E-11	2.83E-11

Table S9.4 – Summary of liposome autoxidation inhibition assay using V70 initiator

Liposomes (V70)	PMC (E2)	PMC (F2)	PMC (G2)	di-tBu catechol 1 (C9)	di-tBu catechol 2 (C10)	di-tBu catechol 3 (C11)
Conc. (μM)	5	5	5	5	5	5
t_{inh} (s)	11154.635	13130.1844	12579.0861	847.539457	336.089359	508.6800034
*k*p	894	480	480	894	894	894
Ri	8.96E-10	7.62E-10	7.95E-10	8.18E-10	8.18E-10	8.18E-10
[AOX] (M)	5.00E-06	5.00E-06	5.00E-06	5.00E-06	5.00E-06	5.00E-06
[Dye] (M)	1.00E-05	1.00E-05	1.00E-05	1.00E-05	1.00E-05	1.00E-05
n	2.00E+00	2.00E+00	2.00E+00	2.00E+00	2.00E+00	2.00E+00
k_{inh} (M^{-1} s^{-1})	1.34E+05	6.49E+04	6.12E+04	4.21E+04	3.64E+04	3.28E+04
Rate	6.00E-12	5.6295E-12	6.2361E-12	1.74E-11	2.01E-11	2.23E-11

S10 – Guiacol (summary and organic solution autoxidation)

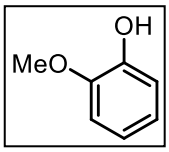

Table S10.1 - Summary of kinetic and cell data

Compound	Organic Solutions		Liposomes		Cells
	k_{inh} (hexadecene) (M^{-1} s^{-1}); n	k_{inh} (cumene) (M^{-1} s^{-1}); n	k_{inh} (DTUN) (M^{-1} s^{-1}); n	k_{inh} (V70) (M^{-1} s^{-1}); n	EC_{50}
guiacol	DNI	(6.4 ± 2.7)E+03; n=2.4 ± 0.4	DNI	DNI	N/A

Table S10.2 – Summary of hexadecane co-oxidation inhibition kinetics

Hexadecene	PMC	guiacol	PMC	guiacol	PMC	guiacol
Conc. (μM)	2	5	2	5	2	5
t_{inh} (s)	3473.54565	0	3315.55272	0	3195.54853	0
*k*p	3791.88926	3791.88926	3791.88926	3791.88926	3791.88926	3791.88926
Ri	1.15E-09	1.15E-09	1.21E-09	1.21E-09	1.25E-09	1.25E-09
[AOX] (M)	2.00E-06	5.00E-06	2.00E-06	5.00E-06	2.00E-06	5.00E-06
[Dye] (M)	1.00E-05	1.00E-05	1.00E-05	1.00E-05	1.00E-05	1.00E-05
n	2.00E+00	0.00E+00	2.00E+00	0.00E+00	2.00E+00	0.00E+00
log *k*	6.13412338	#DIV/0!	6.21600307	#DIV/0!	6.23611343	#DIV/0!
k_{inh} (M^{-1} s^{-1})	1.36E+06	#DIV/0!	1.64E+06	#DIV/0!	1.72E+06	#DIV/0!
Rate	8.016E-12	1.6825E-11	6.955E-12	1.6825E-11	6.8896E-12	0

Table S10.3 – Summary of cumene co-oxidation inhibition kinetics

Cumene	PMC	guiacol	guiacol
Conc. (μM)	2	5	50
t_{inh} (s)	1665	4495	34812.46
*k*p	141	141	141
Ri	2.40E-09	2.40E-09	2.40E-09
[AOX] (M)	2.00E-06	5.00E-06	5.00E-05
[Dye] (M)	1.00E-05	1.00E-05	1.00E-05
n	2.00E+00	2.16E+00	1.67E+00
log *k*	5.046748	3.699076	3.307158
k_{inh} (M^{-1} s^{-1})	1.11E+05	5.00E+03	2.03E+03
Rate	7.6E-12	6.27E-11	2E-11

Table S10.4 – Summary of liposome autoxidation inhibition assay using DTUN initiator

Liposomes (DTUN)	PMC (E2)	PMC (F2)	PMC (G2)	guaiacol 1 (C6)	guaiacol 2 (C7)	guaiacol 3 (C8)
Conc. (μM)	5	5	5	5	5	5
t_{inh} (s)	18154.521	17323.0663	16289.0593	0	0	0
*k*p	894	894	894	894	894	894
Ri	5.51E-10	5.77E-10	6.14E-10	5.81E-10	5.81E-10	5.81E-10
[AOX] (M)	5.00E-06	5.00E-06	5.00E-06	5.00E-06	5.00E-06	5.00E-06
[Dye] (M)	1.00E-05	1.00E-05	1.00E-05	1.00E-05	1.00E-05	1.00E-05
n	2.00E+00	2.00E+00	2.00E+00	0.00E+00	0.00E+00	0.00E+00
k_{inh} (M^{-1} s^{-1})	9.55E+04	9.88E+04	1.04E+05	#DIV/0!	#DIV/0!	#DIV/0!
Rate	5.16E-12	5.22409E-12	5.27E-12	0.00E+00	2.00E+00	3.00E+00

Table S10.5 – Summary of liposome autoxidation inhibition assay using V70 initiator

Liposomes (V70)	PMC (E2)	PMC (F2)	PMC (G2)	guaiacol 1 (C6)	guaiacol 2 (C7)	guaiacol 3 (C8)
Conc. (μM)	5	5	5	5	5	5
t_{inh} (s)	11154.63502	13130.18442	12579.08609	0	0	0
*k*p	894	894	894	480	480	480
Ri	8.96E-10	7.62E-10	7.95E-10	8.18E-10	8.18E-10	8.18E-10
[AOX] (M)	5.00E-06	5.00E-06	5.00E-06	5.00E-06	5.00E-06	5.00E-06
[Dye] (M)	1.00E-05	1.00E-05	1.00E-05	1.00E-05	1.00E-05	1.00E-05
n	2.00E+00	2.00E+00	2.00E+00	0.00E+00	0.00E+00	0.00E+00
k_{inh} (M^{-1} s^{-1})	1.34E+05	6.49E+04	6.12E+04	#DIV/0!	#DIV/0!	#DIV/0!
Rate	6.00E-12	5.6295E-12	6.2361E-12	0.00E+00	0.00E+00	0.00E+00

S11 – 3,4-dihydroxy ethyl cinnamate (summary and organic solution autoxidation)

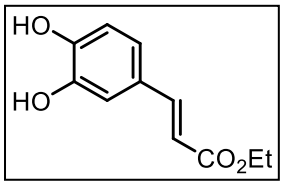

Table S11.1 – Summary of kinetic and cell data

Compound	Organic Solutions		Liposomes		Cells
	k_{inh} (hexadecene) (M^{-1} s^{-1}); n	k_{inh} (cumene) (M^{-1} s^{-1}); n	k_{inh} (DTUN) (M^{-1} s^{-1}); n	k_{inh} (V70) (M^{-1} s^{-1}); n	EC_{50}
3,4-dihydroxy ethyl cinnamate	(7.1 ± 0.6)E+05; n=2.01 ± 0.01	DNI	(9.47 ± 0.2)E+03; n=2*	(6.51 ± 0.84)E+04; n=2*	N/A

Table S11.2 – Summary of hexadecane co-oxidation inhibition kinetics

Hexadecene	PMC	3,4-dihydroxy ethyl cinnamate	PMC	3,4-dihydroxy ethyl cinnamate	3,4-dihydroxy ethyl cinnamate
Conc. (μM)	2	5	2	5	5
t_{inh} (s)	3473.54565	8287.62006	3315.55272	8371.6807	11176.2209
*k*p	3791.88926	3791.88926	3791.88926	3791.88926	3791.88926
Ri	1.15E-09	1.15E-09	1.21E-09	1.21E-09	1.21E-09
[AOX] (M)	2.00E-06	5.00E-06	2.00E-06	5.00E-06	5.00E-06
[Dye] (M)	1.00E-05	1.00E-05	1.00E-05	1.00E-05	1.00E-05
n	2.00E+00	1.91E+00	2.00E+00	2.02E+00	2.70E+00
log *k*	6.13412338	5.83023342	6.21600307	5.8308056	5.70532328
k_{inh} (M^{-1} s^{-1})	1.36E+06	6.76E+05	1.64E+06	6.77E+05	5.07E+05
Rate	8.016E-12	6.7638E-12	6.955E-12	6.6871E-12	6.6871E-12

Table S11.3 – Summary of liposome autoxidation inhibition assay using DTUN initiator

Liposomes (DTUN)	PMC (E2)	PMC (F2)	PMC (G2)	ethyl 34dihyroxy cinnamate 1 (E3)	ethyl 34dihyroxy cinnamate 2 (E4)	ethyl 34dihyroxy cinnamate 3 (E5)
Conc. (μM)	5	5	5	5	5	5
t_{inh} (s)	18154.521	17323.0663	16289.0593	5440.283364	5155.728262	5176.590787
*k*p	894	894	894	894	894	894
Ri	5.51E-10	5.77E-10	6.14E-10	5.81E-10	5.81E-10	5.81E-10
[AOX] (M)	5.00E-06	5.00E-06	5.00E-06	5.00E-06	5.00E-06	5.00E-06
[Dye] (M)	1.00E-05	1.00E-05	1.00E-05	1.00E-05	1.00E-05	1.00E-05
n	2.00E+00	2.00E+00	2.00E+00	2.00E+00	2.00E+00	2.00E+00
k_{inh} (M^{-1} s^{-1})	9.55E+04	9.88E+04	1.04E+05	9.63E+03	9.54E+03	9.24E+03
Rate	5.16E-12	5.22409E-12	5.27E-12	5.39E-11	5.44E-11	5.62E-11

Table S11.4 – Summary of liposome autoxidation inhibition assay using V70 initiator

Liposomes (V70)	PMC (E2)	PMC (F2)	PMC (G2)	ethyl 34dihyroxy cinnamate 1 (E3)	ethyl 34dihyroxy cinnamate 2 (E4)	ethyl 34dihyroxy cinnamate 3 (E5)
Conc. (μM)	5	5	5	5	5	5
t_{inh} (s)	11154.635	13130.1844	12579.0861	5125.054954	4440.580566	4760.406454
*k*p	894	894	894	894	894	894
Ri	8.96E-10	7.62E-10	7.95E-10	8.18E-10	8.18E-10	8.18E-10
[AOX] (M)	5.00E-06	5.00E-06	5.00E-06	5.00E-06	5.00E-06	5.00E-06
[Dye] (M)	1.00E-05	1.00E-05	1.00E-05	1.00E-05	1.00E-05	1.00E-05
n	2.00E+00	2.00E+00	2.00E+00	2.00E+00	2.00E+00	2.00E+00
k_{inh} (M^{-1} s^{-1})	1.34E+05	6.49E+04	6.12E+04	5.54E+04	6.94E+04	7.06E+04
Rate	6.00E-12	5.6295E-12	6.2361E-12	1.32E-11	1.05E-11	1.04E-11

S12 – 4-hydroxy-3-methoxy ethyl cinnamate (summary and organic solution autoxidation)

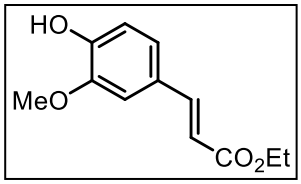

Table S12.1 – Summary of kinetic and cell data

Compound	Organic Solutions		Liposomes		Cells
	k_{inh} (hexadecene) (M^{-1} s^{-1}); n	k_{inh} (cumene) (M^{-1} s^{-1}); n	k_{inh} (DTUN) (M^{-1} s^{-1}); n	k_{inh} (V70) (M^{-1} s^{-1}); n	EC_{50}
4-hydroxy-3-methoxy ethyl cinnamate	DNI	(7.94 ± 0.03)E+03; n=2.63 ± 0.08	DNI	DNI	N/A

Table S12.2 – Summary of hexadecane co-oxidation inhibition kinetics

Hexadecene	PMC	4-hydroxy-3-methoxy ethyl cinnamate	PMC	4-hydroxy-3-methoxy ethyl cinnamate	PMC	4-hydroxy-3-methoxy ethyl cinnamate
Conc. (μM)	2	5	2	5	2	5
t_{inh} (s)	3473.54565	0	3315.55272	0	3195.54853	0
*k*p	3791.88926	3791.889263	3791.88926	3791.889263	3791.88926	3791.88926
Ri	1.15E-09	1.15E-09	1.21E-09	1.21E-09	1.25E-09	1.25E-09
[AOX] (M)	2.00E-06	5.00E-06	2.00E-06	5.00E-06	2.00E-06	5.00E-06
[Dye] (M)	1.00E-05	1.00E-05	1.00E-05	1.00E-05	1.00E-05	1.00E-05
n	2.00E+00	0.00E+00	2.00E+00	0.00E+00	2.00E+00	0.00E+00
log *k*	6.13412338	#DIV/0!	6.21600307	#DIV/0!	6.23611343	#DIV/0!
k_{inh} (M^{-1} s^{-1})	1.36E+06	#DIV/0!	1.64E+06	#DIV/0!	1.72E+06	#DIV/0!
Rate	8.016E-12	0	6.955E-12	1.6825E-11	6.8896E-12	0

Table S12.3 – Summary of cumene co-oxidation inhibition kinetics

Cumene	PMC	4-hydroxy-3-methoxy ethyl cinnamate	PMC	4-hydroxy-3-methoxy ethyl cinnamate	4-hydroxy-3-methoxy ethyl cinnamate
Conc. (μM)	2	5	2	5	50
t_{inh} (s)	2378	6575.279376	1665	5365.347	50036.65
*k*p	141	141	141	141	141
Ri	1.68E-09	2.05E-09	2.40E-09	2.40E-09	2.40E-09
[AOX] (M)	2.00E-06	5.00E-06	2.00E-06	5.00E-06	5.00E-05
[Dye] (M)	1.00E-05	1.00E-05	1.00E-05	1.00E-05	1.00E-05
n	2.00E+00	2.69E+00	2.00E+00	2.58E+00	2.40E+00
log *k*	5.102765	3.901215411	5.046748	3.898938	3.390562
k_{inh} (M^{-1} s^{-1})	1.27E+05	7.97E+03	1.11E+05	7.92E+03	2.46E+03
Rate	4.68E-12	2.69209E-11	7.6E-12	3.32E-11	1.15E-11

Table S12.4 – Summary of liposome autoxidation inhibition assay using DTUN initiator

Liposomes (DTUN)	PMC (E2)	PMC (F2)	PMC (G2)	ethyl 4hydroxy3methoxy cinnamate 1 (D9)	ethyl 4hydroxy3methoxy cinnamate 2 (D10)	ethyl 4hydroxy3methoxy cinnamate 3 (D11)
Conc. (μM)	5	5	5	5	5	5
t_{inh} (s)	18154.521	17323.0663	16289.0593	0	0	0
*k*p	894	894	894	480	480	480
Ri	5.51E-10	5.77E-10	6.14E-10	5.81E-10	5.81E-10	5.81E-10
[AOX] (M)	5.00E-06	5.00E-06	5.00E-06	5.00E-06	5.00E-06	5.00E-06
[Dye] (M)	1.00E-05	1.00E-05	1.00E-05	1.00E-05	1.00E-05	1.00E-05
n	2.00E+00	2.00E+00	2.00E+00	0.00E+00	0.00E+00	0.00E+00
k_{inh} (M^{-1} s^{-1})	9.55E+04	9.88E+04	1.04E+05	#DIV/0!	#DIV/0!	#DIV/0!
Rate	5.16E-12	5.22409E-12	5.27E-12	0.00E+00	2.00E+00	3.00E+00

Table S12.5 – Summary of liposome autoxidation inhibition assay using V70 initiator

Liposomes (V70)	PMC (E2)	PMC (F2)	PMC (G2)	ethyl 4hydroxy3methoxy cinnamate 1 (D9)	ethyl 4hydroxy3methoxy cinnamate 2 (D10)	ethyl 4hydroxy3methoxy cinnamate 3 (D11)
Conc. (μM)	5	5	5	5	5	5
t_{inh} (s)	11154.635	13130.1844	12579.0861	0	0	0
*k*p	894	894	894	480	480	480
Ri	8.96E-10	7.62E-10	7.95E-10	8.18E-10	8.18E-10	8.18E-10
[AOX] (M)	5.00E-06	5.00E-06	5.00E-06	5.00E-06	5.00E-06	5.00E-06
[Dye] (M)	1.00E-05	1.00E-05	1.00E-05	1.00E-05	1.00E-05	1.00E-05
n	2.00E+00	2.00E+00	2.00E+00	0.00E+00	0.00E+00	0.00E+00
k_{inh} (M^{-1} s^{-1})	1.34E+05	6.49E+04	6.12E+04	#DIV/0!	#DIV/0!	#DIV/0!
Rate	6.00E-12	5.6295E-12	6.2361E-12	0.00E+00	0.00E+00	0.00E+00

S13 – curcumin (summary and organic solution autoxidation)

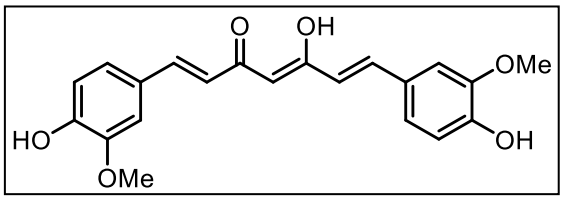

Table S13.1 – Summary of kinetic and cell data

Compound	Organic Solutions		Liposomes		Cells
	k_{inh} (hexadecene) (M^{-1} s^{-1}); n	k_{inh} (cumene) (M^{-1} s^{-1}); n	k_{inh} (DTUN) (M^{-1} s^{-1}); n	k_{inh} (V70) (M^{-1} s^{-1}); n	EC_{50}
curcumin	(6.5 ± 0.6)E+04; n= 4.0 ± 0. 1	(9.55 ± 1.66)E+03; n= 5.3 ± 0.7	(1.14 ± 0.04)E+03; n= 4*	(3.76 ± 0.36)E+03; n=4*	N/A

Table S13.2 – Summary of hexadecane co-oxidation inhibition kinetics

Hexadecene	PMC	curcumin	PMC	curcumin	curcumin
Conc. (μM)	2	5	2	5	5
t_{inh} (s)	3391.40667	16168.1613	2640.83673	18602.8015	18634.7798
*k*p	3791.88926	3791.88926	3791.88926	3791.88926	3791.88926
Ri	1.18E-09	1.18E-09	1.51E-09	1.08E-09	1.08E-09
[AOX] (M)	2.00E-06	5.00E-06	2.00E-06	5.00E-06	5.00E-06
[Dye] (M)	1.00E-05	1.00E-05	1.00E-05	1.00E-05	1.00E-05
n	2.00E+00	3.81E+00	2.00E+00	4.04E+00	4.04E+00
log *k*	6.25841746	4.85278573	6.23852281	4.77072397	4.81432178
k_{inh} (M^{-1} s^{-1})	1.81E+06	7.13E+04	1.73E+06	5.90E+04	6.52E+04
Rate	6.1668E-12	3.2916E-11	8.2907E-12	3.4558E-11	3.1204E-11

Table S13.3 – Summary of cumene co-oxidation inhibition kinetics

Cumene	PMC	curcumin	PMC	curcumin	PMC	curcumin
Conc. (μM)	2	5	2	5	2	5
t_{inh} (s)	1594	10664.94	1559	11682.77	2159	12444
*k*p	141	141	141	141	141	141
Ri	2.51E-09	2.51E-09	2.57E-09	2.57E-09	1.85E-09	1.85E-09
[AOX] (M)	2.00E-06	5.00E-06	2.00E-06	5.00E-06	2.00E-06	5.00E-06
[Dye] (M)	1.00E-05	1.00E-05	1.00E-05	1.00E-05	1.00E-05	1.00E-05
n	2.00E+00	5.35E+00	2.00E+00	5.99E+00	2.00E+00	4.61E+00
log *k*	5.60601	3.984353	5.247065	4.045523	4.837633	3.897772
k_{inh} (M^{-1} s^{-1})	4.04E+05	9.65E+03	1.77E+05	1.11E+04	6.88E+04	7.90E+03
Rate	2.19E-12	1.37E-11	5.12E-12	1.09E-11	9.49E-12	1.43E-11

Table S13.4 – Summary of liposome autoxidation inhibition assay using DTUN initiator (approx. n = 2)

Liposomes (DTUN)	PMC (E2)	PMC (F2)	PMC (G2)	curcumin 1 (D6)	curcumin 2 (D7)	curcumin 3 (D8)
Conc. (μM)	5	5	5	5	5	5
t_{inh} (s)	18154.521	17323.0663	16289.0593	10489.1354	8011.53531	9469.5781
*k*p	894	894	894	480	480	480
Ri	5.51E-10	5.77E-10	6.14E-10	5.81E-10	5.81E-10	5.81E-10
[AOX] (M)	5.00E-06	5.00E-06	5.00E-06	5.00E-06	5.00E-06	5.00E-06
[Dye] (M)	1.00E-05	1.00E-05	1.00E-05	1.00E-05	1.00E-05	1.00E-05
n	2.00E+00	2.00E+00	2.00E+00	2.00E+00	2.00E+00	2.00E+00
k_{inh} (M^{-1} s^{-1})	9.55E+04	9.88E+04	1.04E+05	1.27E+04	1.21E+04	1.19E+04
Rate	5.16E-12	5.22409E-12	5.27E-12	2.20E-11	2.30E-11	2.33E-11

Table S13.5 – Summary of liposome autoxidation inhibition assay using V70 initiator (approx. n = 2)

Liposomes (V70)	PMC (E2)	PMC (F2)	PMC (G2)	curcumin 1 (D6)	curcumin 2 (D7)	curcumin 3 (D8)
Conc. (μM)	5	5	5	5	5	5
t_{inh} (s)	11154.635	13130.1844	12579.0861	4129.90146	4219.35128	3848.18255
*k*p	894	480	480	480	480	480
Ri	8.96E-10	7.62E-10	7.95E-10	8.18E-10	8.18E-10	8.18E-10
[AOX] (M)	5.00E-06	5.00E-06	5.00E-06	5.00E-06	5.00E-06	5.00E-06
[Dye] (M)	1.00E-05	1.00E-05	1.00E-05	1.00E-05	1.00E-05	1.00E-05
n	2.00E+00	2.00E+00	2.00E+00	2.00E+00	2.00E+00	2.00E+00
k_{inh} (M^{-1} s^{-1})	1.34E+05	6.49E+04	6.12E+04	3.89E+04	3.75E+04	4.49E+04
Rate	6.00E-12	5.6295E-12	6.2361E-12	1.01E-11	1.05E-11	8.75E-12

Table S13.6 – Summary of liposome autoxidation inhibition assay using DTUN initiator (approximated n = 4)

Liposomes (DTUN)	PMC (E2)	PMC (F2)	PMC (G2)	curcumin 1 (D6)	curcumin 2 (D7)	curcumin 3 (D8)
Conc. (μM)	5	5	5	5	5	5
t_{inh} (s)	18154.521	17323.0663	16289.0593	10489.1354	8011.53531	9469.5781
*k*p	894	894	894	480	480	480
Ri	5.51E-10	5.77E-10	6.14E-10	5.81E-10	5.81E-10	5.81E-10
[AOX] (M)	5.00E-06	5.00E-06	5.00E-06	5.00E-06	5.00E-06	5.00E-06
[Dye] (M)	1.00E-05	1.00E-05	1.00E-05	1.00E-05	1.00E-05	1.00E-05
n	2.00E+00	2.00E+00	2.00E+00	4.00E+00	4.00E+00	4.00E+00
k_{inh} (M^{-1} s^{-1})	9.55E+04	9.88E+04	1.04E+05	6.34E+03	6.07E+03	5.97E+03
Rate	5.16E-12	5.22409E-12	5.27E-12	2.20E-11	2.30E-11	2.33E-11

Table S13.7 – Summary of liposome autoxidation inhibition assay using V70 initiator (approx. n = 4)

Liposomes (V70)	PMC (E2)	PMC (F2)	PMC (G2)	curcumin 1 (D6)	curcumin 2 (D7)	curcumin 3 (D8)
Conc. (μM)	5	5	5	5	5	5
t_{inh} (s)	11154.635	13130.1844	12579.0861	4129.901459	4219.35128	3848.182555
*k*p	894	480	480	480	480	480
Ri	8.96E-10	7.62E-10	7.95E-10	8.18E-10	8.18E-10	8.18E-10
[AOX] (M)	5.00E-06	5.00E-06	5.00E-06	5.00E-06	5.00E-06	5.00E-06
[Dye] (M)	1.00E-05	1.00E-05	1.00E-05	1.00E-05	1.00E-05	1.00E-05
n	2.00E+00	2.00E+00	2.00E+00	4.00E+00	4.00E+00	4.00E+00
k_{inh} (M^{-1} s^{-1})	1.34E+05	6.49E+04	6.12E+04	1.94E+04	1.88E+04	2.24E+04
Rate	6.00E-12	5.6295E-12	6.2361E-12	1.01E-11	1.05E-11	8.75E-12

S14 – Resveratrol (summary and organic solution autoxidation)

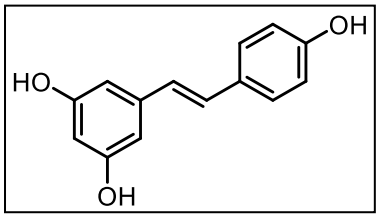

Table S14.1 – Summary of kinetic and cell data

Compound	Organic Solutions		Liposomes		Cells
	k_{inh} (hexadecene) (M^{-1} s^{-1}); n	k_{inh} (cumene) (M^{-1} s^{-1}); n	k_{inh} (DTUN) (M^{-1} s^{-1}); n	k_{inh} (V70) (M^{-1} s^{-1}); n	EC_{50}
resveratrol	(3.3 ± 0.3)E+05; n=0.7 ± 0.2	(4.6 ± 0.4)E+04; n=1.840 ± 0.004	(1.7 ± 0.1)E+03; n=2*	(3.9 ± 0.3)E+04; n=2*	5.3 ± 2.7 μM

Table S14.2 – Summary of hexadecane co-oxidation inhibition kinetics

Hexadecene	PMC	resveratrol	resveratrol	PMC	resveratrol
Conc. (μM)	2	10	10	2	10
t_{inh} (s)	3649.313835	5846.08334	5625.74695	3391.40667	7503
*k*p	3791.889263	3791.88926	3791.88926	3791.88926	3791.889263
Ri	1.10E-09	1.10E-09	1.10E-09	1.18E-09	1.18E-09
[AOX] (M)	2.00E-06	1.00E-05	1.00E-05	2.00E-06	1.00E-05
[Dye] (M)	1.00E-05	1.00E-05	1.00E-05	1.00E-05	1.00E-05
n	2.00E+00	6.41E-01	6.17E-01	2.00E+00	8.85E-01
log *k*	6.13203931	5.52996775	5.55690817	6.25841746	5.477270471
k_{inh} (M^{-1} s^{-1})	1.36E+06	3.39E+05	3.61E+05	1.81E+06	3.00E+05
Rate	7.6666E-12	1.9144E-11	1.8697E-11	6.1668E-12	1.684E-11

Table S14.3 – Summary of cumene co-oxidation inhibition kinetics

Cumene	PMC	Resveratrol 1st pahse	Resveratrol 2nd phase	Resveratrol Δ phases
Conc. (μM)	2	5	5	5
t_{inh} (s)	2378	4497.511	8663.62386	2452.036593
*k*p	141	141	141	141
Ri	1.68E-09	1.68E-09	1.68E-09	1.68E-09
[AOX] (M)	2.00E-06	5.00E-06	5.00E-06	5.00E-06
[Dye] (M)	1.00E-05	1.00E-05	1.00E-05	1.00E-05
n	2.00E+00	1.51E+00	2.91E+00	1.40E+00
log *k*	5.102765	4.63669	4.35196273	3.823107125
k_{inh} (M^{-1} s^{-1})	1.27E+05	4.33E+04	2.25E+04	6.65E+03
Rate	4.68E-12	7.24E-12	7.237E-12	5.08605E-11

Table S14.4 – Summary of liposome autoxidation inhibition assay using DTUN initiator

Cumene	PMC	Resveratrol 1st phase	Resveratrol 2nd phase	Resveratrol Δ phases
Conc. (μM)	2	5	5	5
t_{inh} (s)	2378	4511.519	8536.347	2644.385
*k*p	141	141	141	141
Ri	1.68E-09	1.68E-09	1.68E-09	1.68E-09
[AOX] (M)	2.00E-06	5.00E-06	5.00E-06	5.00E-06
[Dye] (M)	1.00E-05	1.00E-05	1.00E-05	1.00E-05
n	2.00E+00	1.52E+00	2.87E+00	1.35E+00
log *k*	5.102765	4.688932	4.411983	3.825503
k_{inh} (M^{-1} s^{-1})	1.27E+05	4.89E+04	2.58E+04	6.69E+03
Rate	4.68E-12	6.4E-12	6.4E-12	5.24E-11

Table S14.5 – Summary of liposome autoxidation inhibition assay using DTUN initiator (approximated n = 2)

Liposomes (DTUN)	PMC (E2)	PMC (F2)	PMC (G2)	RSV 1 (E9)	RSV 2 (E10)	RSV 3 (E11)
Conc. (μM)	5	5	5	5	5	5
t_{inh} (s)	18154.521	17323.0663	16289.0593	13626.1196	13873.744	12106.8932
*k*p	894	894	894	894	894	894
Ri	5.51E-10	5.77E-10	6.14E-10	5.81E-10	5.81E-10	5.81E-10
[AOX] (M)	5.00E-06	5.00E-06	5.00E-06	5.00E-06	5.00E-06	5.00E-06
[Dye] (M)	1.00E-05	1.00E-05	1.00E-05	1.00E-05	1.00E-05	1.00E-05
n	2.00E+00	2.00E+00	2.00E+00	2.00E+00	2.00E+00	2.00E+00
k_{inh} (M^{-1} s^{-1})	9.55E+04	9.88E+04	1.04E+05	9.15E+03	9.38E+03	8.16E+03
Rate	5.16E-12	5.22409E-12	5.27E-12	3.05E-11	2.97E-11	3.42E-11

Table S14.6 – Summary of liposome autoxidation inhibition assay using V70 initiator

Liposomes (V70)	PMC (E2)	PMC (F2)	PMC (G2)	RSV 1 (E9)	RSV 2 (E10)	RSV 3 (E11)
Conc. (μM)	5	5	5	5	5	5
t_{inh} (s)	11154.635	13130.1844	12579.0861	5582.66862	5606.65978	5719.09391
*k*p	894	894	894	894	894	894
Ri	8.96E-10	7.62E-10	7.95E-10	8.18E-10	8.18E-10	8.18E-10
[AOX] (M)	5.00E-06	5.00E-06	5.00E-06	5.00E-06	5.00E-06	5.00E-06
[Dye] (M)	1.00E-05	1.00E-05	1.00E-05	1.00E-05	1.00E-05	1.00E-05
n	2.00E+00	2.00E+00	2.00E+00	2.00E+00	2.00E+00	2.00E+00
k_{inh} (M^{-1} s^{-1})	1.34E+05	6.49E+04	6.12E+04	2.18E+04	2.17E+04	1.88E+04
Rate	6.00E-12	5.6295E-12	6.2361E-12	1.80E-11	1.81E-11	2.09E-11

Table S14.7 – Dose response for ferroptosis inhibition

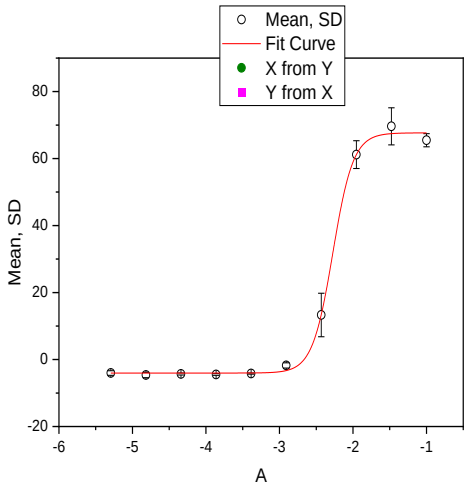

Dose responsive curve x axis = log(mM); y axis = % viability.

RSV1		RSV2		RSV3	
Log(con)mM	% viability	Log(con)mM	% viability	Log(con)mM	% viability
-1	22.09859098	-1	33.57281051	-1	51.30099361
-1.301029996	5.548871573	-1.301029996	27.84877201	-1.301029996	41.829829
-1.602059991	-10.61326658	-1.602059991	9.179410714	-1.602059991	17.44588521
-1.903089987	-10.98146877	-1.903089987	1.132484689	-1.903089987	10.23057981
-2.204119983	-11.91166377	-2.204119983	-3.969241765	-2.204119983	5.116150919
-2.505149978	-13.1906819	-2.505149978	-4.049341335	-2.505149978	4.952558075
-2.806179974	-13.57826315	-2.806179974	-3.907626711	-2.806179974	4.83201598
-3.10720997	-12.78372159	-3.10720997	-5.152250798	-3.10720997	3.824628472
-3.408239965	-14.19839315	-3.408239965	-4.560746282	-3.408239965	4.728694185
-3.709269961	-12.68682627	-3.709269961	-4.061664346	-3.709269961	4.496220144

S15 – tBu_2-resveratrol (summary and organic solution autoxidation)

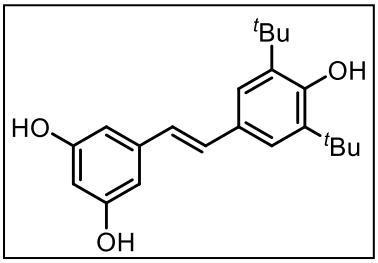

Table S15.1 – Summary of kinetic and cell data

Compound	Organic Solutions		Liposomes		Cells
	k_{inh} (hexadecene) (M^{-1} s^{-1}); n	k_{inh} (cumene) (M^{-1} s^{-1}); n	k_{inh} (DTUN) (M^{-1} s^{-1}); n	k_{inh} (V70) (M^{-1} s^{-1}); n	EC_{50}
tBu2-resveratrol	(2.2 ± 0.2)E+05; n=1.7 ± 0.2	(1.6 ± 0.3)E+04; n=2.7 ± 0.5	(5.9 ± 0.2)E+04; n=1.9 ± 0.1	(8.68 ± 0.12)E+04; n=1.82 ± 0.03	28.3 ± 3.0 nM

Table S15.2 – Summary of hexadecane co-oxidation inhibition kinetics

Hexadecene	PMC	tBu2-resveratrol	PMC	tBu2-resveratrol	PMC	tBu2-resveratrol
Conc. (μM)	2	5	2	5	2	5
t_{inh} (s)	4216	8894	3375	8103	3137	5936
*k*p	3791.88926	3791.88926	3791.88926	3791.88926	3791.88926	3791.88926
Ri	9.49E-10	9.49E-10	1.19E-09	1.19E-09	1.28E-09	1.28E-09
[AOX] (M)	2.00E-06	5.00E-06	2.00E-06	5.00E-06	2.00E-06	5.00E-06
[Dye] (M)	1.00E-05	1.00E-05	1.00E-05	1.00E-05	1.00E-05	1.00E-05
n	2.00E+00	1.69E+00	2.00E+00	1.92E+00	2.00E+00	1.51E+00
log *k*	7.11907598	5.37200118	6.20070513	5.30768502	6.30357825	5.37048292
k_{inh} (M^{-1} s^{-1})	1.32E+07	2.36E+05	1.59E+06	2.03E+05	2.01E+06	2.35E+05
Rate	6.8369E-13	1.8103E-11	7.0785E-12	2.3042E-11	6.0089E-12	2.7221E-11

Table S15.3 – Summary of cumene co-oxidation inhibition kinetics

Cumene	PMC	tBu2-resveratrol	tBu2-resveratrol	PMC	tBu2-resveratrol
Conc. (μM)	2	5	5	2	5
t_{inh} (s)	2104	7667.237	8117.942	1512	5610.447
*k*p	141	141	141	141	141
Ri	1.90E-09	1.90E-09	1.90E-09	2.65E-09	2.65E-09
[AOX] (M)	2.00E-06	5.00E-06	5.00E-06	2.00E-06	5.00E-06
[Dye] (M)	1.00E-05	1.00E-05	1.00E-05	1.00E-05	1.00E-05
n	2.00E+00	2.91E+00	3.09E+00	2.00E+00	2.97E+00
log *k*	5.075041	4.170351	4.190648	5.234955	4.213612
k_{inh} (M^{-1} s^{-1})	1.19E+05	1.48E+04	1.55E+04	1.72E+05	1.64E+04
Rate	5.64E-12	1.24E-11	1.12E-11	5.43E-12	1.54E-11

Table S15.4 – Summary of liposome autoxidation inhibition assay using DTUN initiator

Liposomes (DTUN)	PMC (E2)	PMC (F2)	PMC (G2)	tBu 2 RSV 1 (F3)	tBu 2 RSV 2 (F4)	tBu 2 RSV 3 (F5)
Conc. (μM)	5	5	5	5	5	5
t_{inh} (s)	18154.521	17323.0663	16289.0593	15286.133	17748.7197	16535.6885
*k*p	894	894	894	894	894	894
Ri	5.51E-10	5.77E-10	6.14E-10	5.81E-10	5.81E-10	5.81E-10
[AOX] (M)	5.00E-06	5.00E-06	5.00E-06	5.00E-06	5.00E-06	5.00E-06
[Dye] (M)	1.00E-05	1.00E-05	1.00E-05	1.00E-05	1.00E-05	1.00E-05
n	2.00E+00	2.00E+00	2.00E+00	1.78E+00	2.06E+00	1.92E+00
k_{inh} (M^{-1} s^{-1})	9.55E+04	9.88E+04	1.04E+05	5.82E+04	5.66E+04	6.08E+04
Rate	5.16E-12	5.22409E-12	5.27E-12	1.01E-11	8.90E-12	8.90E-12

Table S15.5 – Summary of liposome autoxidation inhibition assay using V70 initiator

Liposomes (V70)	PMC (E2)	PMC (F2)	PMC (G2)	tBu 2 RSV 1 (F3)	tBu 2 RSV 2 (F4)	tBu 2 RSV 3 (F5)
Conc. (μM)	5	5	5	5	5	5
t_{inh} (s)	11154.635	13130.1844	12579.0861	11353.1023	11013.1647	10978.7519
*k*p	894	480	480	480	480	480
Ri	8.96E-10	7.62E-10	7.95E-10	8.18E-10	8.18E-10	8.18E-10
[AOX] (M)	5.00E-06	5.00E-06	5.00E-06	5.00E-06	5.00E-06	5.00E-06
[Dye] (M)	1.00E-05	1.00E-05	1.00E-05	1.00E-05	1.00E-05	1.00E-05
n	2.00E+00	2.00E+00	2.00E+00	1.86E+00	1.80E+00	1.80E+00
k_{inh} (M^{-1} s^{-1})	1.34E+05	6.49E+04	6.12E+04	8.79E+04	8.55E+04	8.70E+04
Rate	6.00E-12	5.6295E-12	6.2361E-12	8.95E-12	9.49E-12	9.36E-12

Table S15.6 – Dose response for ferroptosis inhibition

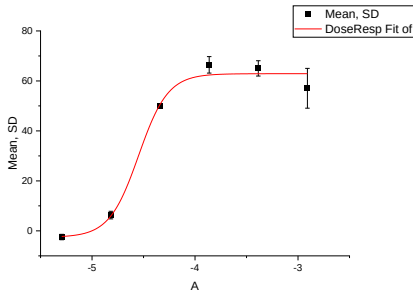

Dose responsive curve x axis = log(mM); y axis = % viability.

tBu2 RSV1		tBu2 RSV2		tBu2 RSV3	
Log(con)mM	% viability	Log(con)mM	% viability	Log(con)mM	% viability
-2.90833	71.02355	-2.90833	62.39075	-2.90833	34.81819
-3.20936	64.10274	-3.20936	64.6128	-3.20936	52.66131
-3.51039	27.78631	-3.51039	31.70827	-3.51039	30.77024
-3.81142	2.6835	-3.81142	5.439444	-3.81142	15.99597
-4.11245	-8.50634	-4.11245	-2.92366	-4.11245	6.818672
-4.41348	-9.89763	-4.41348	-3.93576	-4.41348	4.071329
-4.71451	-11.1938	-4.71451	-4.9859	-4.71451	3.735218
-5.01554	-12.5494	-5.01554	-5.81536	-5.01554	4.217464
-5.31657	-10.9084	-5.31657	-5.00873	-5.31657	3.720604
-5.6176	-10.1355	-5.6176	-5.97517	-5.6176	4.480507

S16 – Pterostilbene (summary and organic solution autoxidation)

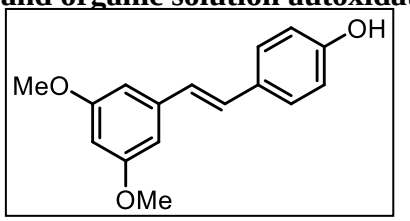

Table S16.1 – Summary of kinetic and cell data

Compound	Organic Solutions		Liposomes		Cells
	k_{inh} (hexadecene) (M^{-1} s^{-1}); n	k_{inh} (cumene) (M^{-1} s^{-1}); n	k_{inh} (DTUN) (M^{-1} s^{-1}); n	k_{inh} (V70) (M^{-1} s^{-1}); n	EC_{50}
pterostilbene	(3.0 ± 0.2)E+05; n= 2.1 ± 0.2	(4.1 ± 0.3)E+04; n= 1.6 ± 0.2	(6.1 ± 0.2)E+03; n= 2*	(2.0 ± 0.2)E+04; n= 2*	1.4 ± 0.3 μM

Table S16.2 – Summary of hexadecane co-oxidation inhibition kinetics

Hexadecene	PMC	pterostilbene	PMC	pterostilbene	PMC	pterostilbene
Conc. (μM)	2	5	2	5	2	5
t_{inh} (s)	2661	7238	3277.85399	7667	2618.37872	7100
*k*p	3791.88926	3791.889263	3791.88926	3791.88926	3791.88926	3791.88926
Ri	1.50E-09	1.50E-09	1.22E-09	1.22E-09	1.53E-09	1.53E-09
[AOX] (M)	2.00E-06	5.00E-06	2.00E-06	5.00E-06	2.00E-06	5.00E-06
[Dye] (M)	1.00E-05	1.00E-05	1.00E-05	1.00E-05	1.00E-05	1.00E-05
n	2.00E+00	2.18E+00	2.00E+00	1.87E+00	2.00E+00	2.17E+00
log *k*	6.25223884	5.453310855	6.20797236	5.48717492	6.25635524	5.50163897
k_{inh} (M^{-1} s^{-1})	1.79E+06	2.84E+05	1.61E+06	3.07E+05	1.80E+06	3.17E+05
Rate	7.9721E-12	1.84462E-11	7.1663E-12	1.6108E-11	8.0254E-12	1.6825E-11

Table S16.3 – Summary of cumene co-oxidation inhibition kinetics

Cumene	PMC	pterostilbene	PMC	pterostilbene	PMC	pterostilbene
Conc. (μM)	2	5	2	5	2	5
t_{inh} (s)	2159	4851.205	2104	4574	1512	3677
*k*p	141	141	141	141	141	141
Ri	1.85E-09	1.85E-09	1.90E-09	1.90E-09	2.65E-09	2.65E-09
[AOX] (M)	2.00E-06	5.00E-06	2.00E-06	5.00E-06	2.00E-06	5.00E-06
[Dye] (M)	1.00E-05	1.00E-05	1.00E-05	1.00E-05	1.00E-05	1.00E-05
n	2.00E+00	1.80E+00	2.00E+00	1.74E+00	2.00E+00	1.95E+00
log *k*	4.837633	4.591924	5.075041	4.644455	5.234955	4.585124
k_{inh} (M^{-1} s^{-1})	6.88E+04	3.91E+04	1.19E+05	4.41E+04	1.72E+05	3.85E+04
Rate	9.49E-12	7.44E-12	5.64E-12	6.99E-12	5.43E-12	9.97E-12

Table S16.4 – Summary of liposome autoxidation inhibition assay using DTUN initiator

Liposomes (DTUN)	PMC (E2)	PMC (F2)	PMC (G2)	pterostilbene 1 (E6)	pterostilbene 2 (E7)	pterostilbene 3 (E8)
Conc. (μM)	5	5	5	6126.81858	4759.658695	5307.322072
t_{inh} (s)	18154.521	17323.0663	16289.0593	894	894	894
*k*p	894	894	894	5.81E-10	5.81E-10	5.81E-10
Ri	5.51E-10	5.77E-10	6.14E-10	5.00E-06	5.00E-06	5.00E-06
[AOX] (M)	5.00E-06	5.00E-06	5.00E-06	1.00E-05	1.00E-05	1.00E-05
[Dye] (M)	1.00E-05	1.00E-05	1.00E-05	2.00E+00	2.00E+00	2.00E+00
n	2.00E+00	2.00E+00	2.00E+00	6126.81858	4759.658695	5307.322072
k_{inh} (M^{-1} s^{-1})	9.55E+04	9.88E+04	1.04E+05	9.87E+03	8.65E+03	8.66E+03
Rate	5.16E-12	5.22409E-12	5.27E-12	5.26E-11	6.00E-11	5.99E-11

Table S16.5 – Summary of liposome autoxidation inhibition assay using V70 initiator

Liposomes (V70)	PMC (E2)	PMC (F2)	PMC (G2)	pterostilbene 1 (E6)	pterostilbene 2 (E7)	pterostilbene 3 (E8)
Conc. (μM)	5	5	5	5	5	5
t_{inh} (s)	11154.63502	13130.18442	12579.08609	705.771948	830.407123	734.155694
*k*p	894	894	894	894	894	894
Ri	8.96E-10	7.62E-10	7.95E-10	8.18E-10	8.18E-10	8.18E-10
[AOX] (M)	5.00E-06	5.00E-06	5.00E-06	5.00E-06	5.00E-06	5.00E-06
[Dye] (M)	1.00E-05	1.00E-05	1.00E-05	1.00E-05	1.00E-05	1.00E-05
n	2.00E+00	2.00E+00	2.00E+00	2.00E+00	2.00E+00	2.00E+00
k_{inh} (M^{-1} s^{-1})	1.34E+05	1.21E+05	1.14E+05	1.31E+04	1.43E+04	1.42E+04
Rate	6.00E-12	5.62948E-12	6.23606E-12	2.99E-11	2.75E-11	2.77E-11

Table S16.6 – Dose response for ferroptosis inhibition

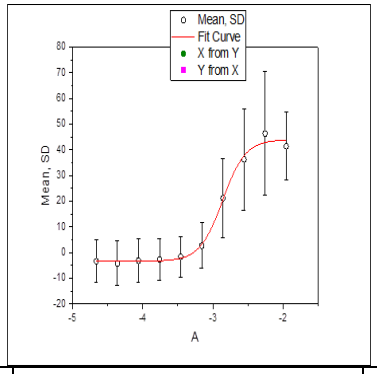

Dose responsive curve x axis = log(mM); y axis = % viability.

Pterostilbene 1		Pterostilbene 2		Pterostilbene 2	
Log(con)mM	% viability	Log(con)mM	% viability	Log(con)mM	% viability
-1.95425	46.43869	-1.95425	26.36385	-1.95425	51.28377
-2.25528	58.49247	-2.25528	18.63116	-2.25528	61.74511
-2.55631	26.32323	-2.55631	23.32623	-2.55631	59.00708
-2.85734	10.77153	-2.85734	13.63418	-2.85734	39.07458
-3.15837	-4.45072	-3.15837	-0.01972	-3.15837	12.52949
-3.4594	-8.93698	-3.4594	-2.89714	-3.4594	6.941503
-3.76043	-10.2451	-3.76043	-3.75975	-3.76043	5.779132
-4.06146	-10.8749	-4.06146	-4.32661	-4.06146	5.779132
-4.36249	-12.5706	-4.36249	-4.89347	-4.36249	4.900897
-4.66352	-11.2043	-4.66352	-4.16025	-4.66352	5.228083

S17 – (±)-δ-viniferin (summary and organic solution autoxidation)

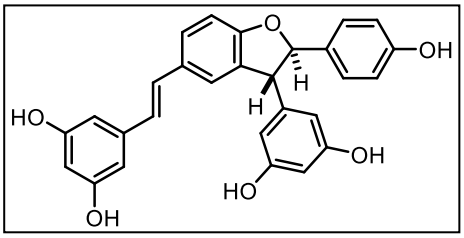

Table S17.1 – Summary of kinetic and cell data

Compound	Organic Solutions		Liposomes		Cells
	k_{inh} (hexadecene) (M^{-1} s^{-1}); n	k_{inh} (cumene) (M^{-1} s^{-1}); n	k_{inh} (DTUN) (M^{-1} s^{-1}); n	k_{inh} (V70) (M^{-1} s^{-1}); n	EC_{50}
delta-viniferin	DNI	(4.6 ± 0.3)E+03; n= 4.7 ± 0.2	DNI	N/A	22.9 ± 3.8 μM

Table S17.2 – Summary of hexadecane co-oxidation inhibition kinetics

Hexadecene	PMC	delta-viniferin	PMC	delta-viniferin	PMC	delta-viniferin
Conc. (μM)	2	5	2	5	2	5
t_{inh} (s)	4223	0	4390	18419	4631	0
*k*p	3791.88926	3791.88926	3791.88926	3791.88926	3791.88926	3791.88926
Ri	9.47E-10	9.47E-10	9.11E-10	9.11E-10	8.64E-10	8.64E-10
[AOX] (M)	2.00E-06	5.00E-06	2.00E-06	5.00E-06	2.00E-06	5.00E-06
[Dye] (M)	1.00E-05	1.00E-05	1.00E-05	1.00E-05	1.00E-05	1.00E-05
n	2.00E+00	0.00E+00	2.00E+00	3.36E+00	2.00E+00	0.00E+00
log *k*	6.38394506	#DIV/0!	6.47642889	4.75641129	6.49596142	#DIV/0!
k_{inh} (M^{-1} s^{-1})	2.42E+06	#DIV/0!	3.00E+06	5.71E+04	3.13E+06	#DIV/0!
Rate	3.7093E-12	3.6072E-11	2.8835E-12	3.6072E-11	2.6134E-12	3.6072E-11

Table S17.3 – Summary of cumene co-oxidation inhibition kinetics

Cumene	PMC	delta-viniferin	PMC	delta-viniferin	PMC	delta-viniferin
Conc. (μM)	2	5	2	5	2	5
t_{inh} (s)	2343	14543.63	2428	14059.03	2321	13519.65
*k*p	141	141	141	141	141	141
Ri	1.71E-09	1.71E-09	1.65E-09	1.65E-09	1.72E-09	1.72E-09
[AOX] (M)	2.00E-06	5.00E-06	2.00E-06	5.00E-06	2.00E-06	5.00E-06
[Dye] (M)	1.00E-05	1.00E-05	1.00E-05	1.00E-05	1.00E-05	1.00E-05
n	2.00E+00	4.96E+00	2.00E+00	4.63E+00	2.00E+00	4.66E+00
log *k*	5.531447	3.64968	5.938324	3.692617	6.21875	3.654773
k_{inh} (M^{-1} s^{-1})	3.40E+05	4.46E+03	8.68E+05	4.93E+03	1.65E+06	4.52E+03
Rate	1.77E-12	2.17E-11	6.69E-13	2.04E-11	3.67E-13	2.31E-11

Table S17.4 – Summary of liposome autoxidation inhibition assay using DTUN initiator

Liposomes (DTUN)	PMC (E2)	PMC (F2)	PMC (G2)	delta-viniferin 1 (E9)	delta-viniferin 1 (E10)	delta-viniferin 2 (F1)	delta-viniferin 2 (F2)	delta-viniferin 3 (F3)	delta-viniferin 3 (F4)
Conc. (μM)	5	5	5	5	5	5	5	5	5
t_{inh} (s)	4698.560591	4436.44094	4665.226286	0	0	0	0	0	0
*k*p	894	894	894	894	894	894	894	894	894
Ri	2.13E-09	2.25E-09	2.14E-09	2.18E-09	2.18E-09	2.18E-09	2.18E-09	2.18E-09	2.18E-09
[AOX] (M)	5.00E-06	5.00E-06	5.00E-06	5.00E-06	5.00E-06	5.00E-06	5.00E-06	5.00E-06	5.00E-06
[Dye] (M)	1.00E-05	1.00E-05	1.00E-05	1.00E-05	1.00E-05	1.00E-05	1.00E-05	1.00E-05	1.00E-05
n	2.00E+00	2.00E+00	2.00E+00	2.00E+00	2.00E+00	2.00E+00	2.00E+00	2.00E+00	2.00E+00
k_{inh} (M^{-1} s^{-1})	4.94E+05	4.78E+05	5.85E+05	4.86E-07	3.89E-07	3.24E-07	2.78E-07	2.43E-07	2.16E-07
Rate	3.85E-12	4.21E-12	3.28E-12	4.00E+00	5.00E+00	6.00E+00	7.00E+00	8.00E+00	9.00E+00

Table S17.5 – Dose response for ferroptosis inhibition

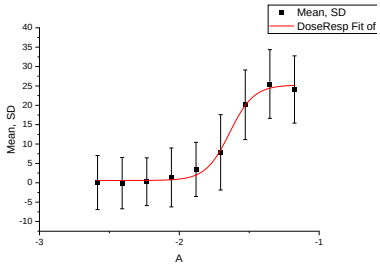

Dose responsive curve x axis = log(mM); y axis = % viability.

delta-viniferin 1		delta-viniferin 2		delta-viniferin 3	
Log(con)mM	% viability	Log(con)mM	% viability	Log(con)mM	% viability
-1	-1.46057	-1	6.538098	-1	17.15314
-1.17609	-1.86052	-1.17609	17.93593	-1.17609	30.21474
-1.35218	-7.05102	-1.35218	19.23459	-1.35218	31.76456
-1.52827	-6.35777	-1.52827	13.78947	-1.52827	26.49515
-1.70437	-8.7397	-1.70437	0.980912	-1.70437	14.73369
-1.88046	-10.0196	-1.88046	-1.48455	-1.88046	8.405228
-2.05655	-10.8372	-2.05655	-3.99616	-2.05655	6.752079
-2.23264	-11.4416	-2.23264	-4.07527	-2.23264	4.625372
-2.40873	-11.486	-2.40873	-4.77404	-2.40873	4.590932
-2.58482	-11.7793	-2.58482	-4.86633	-2.58482	4.995609

S18 – (±)-shegansu B (summary and organic solution autoxidation)

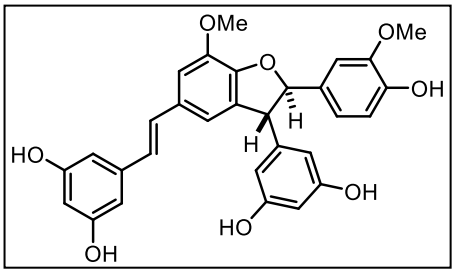

Table S18.1 – Summary of kinetic and cell data

Compound	Organic Solutions		Liposomes		Cells
	k_{inh} (hexadecene) (M^{-1} s^{-1}); n	k_{inh} (cumene) (M^{-1} s^{-1}); n	k_{inh} (DTUN) (M^{-1} s^{-1}); n	k_{inh} (V70) (M^{-1} s^{-1}); n	EC_{50}
shegansu B	DNI	(6.7 ± 0.5)E+03; n= 4.1 ± 0.3	Retards	N/A	33.0 ± 10.5 μM

Table S18.2 – Summary of hexadecane co-oxidation inhibition kinetics

Hexadecene	PMC	shegansu B	PMC	shegansu B	PMC	shegansu B
Conc. (μM)	2	5	2	5	2	5
t_{inh} (s)	4573	0	4692	0	4265	0
*k*p	3791.88926	3791.88926	3791.88926	3791.88926	3791.88926	3791.88926
Ri	8.75E-10	8.75E-10	8.52E-10	8.52E-10	9.38E-10	9.38E-10
[AOX] (M)	2.00E-06	5.00E-06	2.00E-06	5.00E-06	2.00E-06	5.00E-06
[Dye] (M)	1.00E-05	1.00E-05	1.00E-05	1.00E-05	1.00E-05	1.00E-05
n	2.00E+00	0.00E+00	2.00E+00	0.00E+00	2.00E+00	0.00E+00
log *k*	6.15961906	#DIV/0!	6.19640331	#DIV/0!	6.34134974	#DIV/0!
k_{inh} (M^{-1} s^{-1})	1.44E+06	#DIV/0!	1.57E+06	#DIV/0!	2.19E+06	#DIV/0!
Rate	5.7412E-12	2.785E-11	5.1411E-12	2.785E-11	4.0514E-12	7.6963E-11

Table S18.3 – Summary of cumene co-oxidation inhibition kinetics

Cumene	PMC	shegansu B	PMC	shegansu B	PMC	shegansu B
Conc. (μM)	2	5	2	5	2	5
t_{inh} (s)	2343	12936.83	2428	11792.09	2321	11759.44
*k*p	141	141	141	141	141	141
Ri	1.71E-09	1.71E-09	1.65E-09	1.65E-09	1.72E-09	1.72E-09
[AOX] (M)	2.00E-06	5.00E-06	2.00E-06	5.00E-06	2.00E-06	5.00E-06
[Dye] (M)	1.00E-05	1.00E-05	1.00E-05	1.00E-05	1.00E-05	1.00E-05
n	2.00E+00	4.42E+00	2.00E+00	3.88E+00	2.00E+00	4.05E+00
log *k*	5.531447	3.794772	5.938324	3.862187	6.21875	3.814612
k_{inh} (M^{-1} s^{-1})	3.40E+05	6.23E+03	8.68E+05	7.28E+03	1.65E+06	6.53E+03
Rate	1.77E-12	1.75E-11	6.69E-13	1.64E-11	3.67E-13	1.84E-11

Table S18.4 – Summary of liposome autoxidation inhibition assay using DTUN initiator

Liposomes (DTUN)	PMC (E2)	PMC (F2)	PMC (G2)	shegansu B 1 (F5)	shegansu B 1 (F6)	shegansu B 2 (F7)	shegansu B 2 (F8)	shegansu B 3 (F9)	shegansu B 3 (F10)
Conc. (μM)	5	5	5	5	5	5	5	5	5
t_{inh} (s)	4698.560591	4436.44094	4665.226286	0	0	0	0	0	0
*k*p	894	894	894	894	894	894	894	894	894
Ri	2.13E-09	2.25E-09	2.14E-09	2.18E-09	2.18E-09	2.18E-09	2.18E-09	2.18E-09	2.18E-09
[AOX] (M)	5.00E-06	5.00E-06	5.00E-06	5.00E-06	5.00E-06	5.00E-06	5.00E-06	5.00E-06	5.00E-06
[Dye] (M)	1.00E-05	1.00E-05	1.00E-05	1.00E-05	1.00E-05	1.00E-05	1.00E-05	1.00E-05	1.00E-05
n	2.00E+00	2.00E+00	2.00E+00	2.00E+00	2.00E+00	2.00E+00	2.00E+00	2.00E+00	2.00E+00
k_{inh} (M^{-1} s^{-1})	4.94E+05	4.78E+05	5.85E+05	4.86E-07	3.89E-07	3.24E-07	2.78E-07	2.43E-07	2.16E-07
Rate	3.85E-12	4.21E-12	3.28E-12	4.00E+00	5.00E+00	6.00E+00	7.00E+00	8.00E+00	9.00E+00

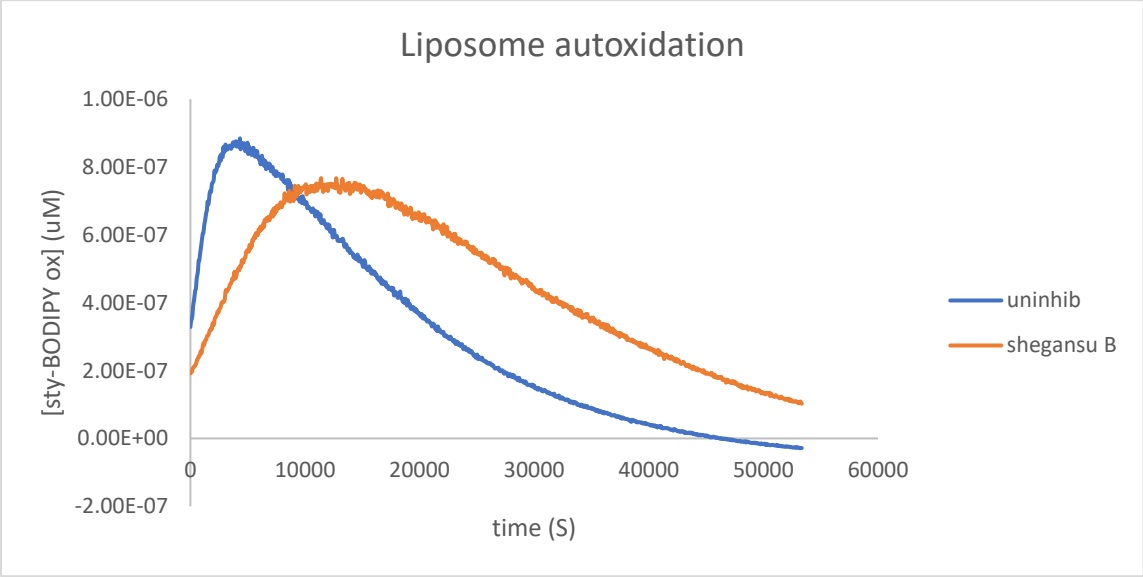

Shegansu B is seen to retard autoxidation as the slope of the curve is different from uninhibited. However, a rate constant and stoichiometric data can be be generated from this inhibition profile.

Table S18.5 – Dose response for ferroptosis inhibition

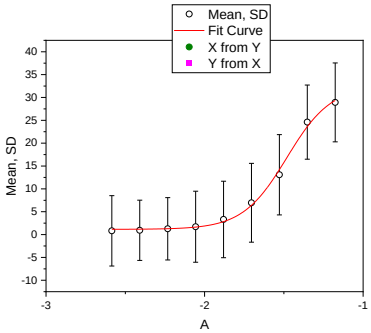

Dose responsive curve x axis = log(mM); y axis = % viability.

Shegansu B 1		Shegansu B 2		Shegansu B 3	
Log(con)mM	% viability	Log(con)mM	% viability	Log(con)mM	% viability
-1	-2.99816	-1	4.49453	-1	11.78041
-1.17609	6.876222	-1.17609	22.82072	-1.17609	35.02781
-1.35218	10.20916	-1.35218	18.87202	-1.35218	30.34389
-1.52827	5.738579	-1.52827	6.874298	-1.52827	19.29707
-1.70437	-0.26071	-1.70437	0.855662	-1.70437	13.05471
-1.88046	-6.19778	-1.88046	-2.61181	-1.88046	9.223192
-2.05655	-8.62416	-2.05655	-3.77203	-2.05655	7.217027
-2.23264	-9.80625	-2.23264	-3.56108	-2.23264	6.089098
-2.40873	-10.8461	-2.40873	-3.71929	-2.40873	5.598319
-2.58482	-10.384	-2.58482	-4.62901	-2.58482	6.261301

S19 – (±)-tBu$_4$-quadrangularin A (summary and organic solution autoxidation)

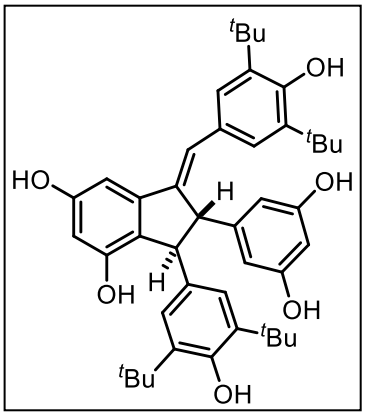

Table S19.1 – Summary of kinetic and cell data

Compound	Organic Solutions		Liposomes		Cells
	k_{inh} (hexadecene) (M^{-1} s^{-1}); n	k_{inh} (cumene) (M^{-1} s^{-1}); n	k_{inh} (DTUN) (M^{-1} s^{-1}); n	k_{inh} (V70) (M^{-1} s^{-1}); n	EC_{50}
tBu4-quadrangularin A	(1.5 ± 0.1)E+05; n=4.5 ± 0.2	N/A	(1.8 ± 0.2)E+04; n=4*	(2.53 ± 0.07)E+04; n=3.86 ± 0.05	172.4 ± 17.2 nM

Table S19.2 – Summary of hexadecane co-oxidation inhibition kinetics

Hexadecene	PMC	tBu4-quadrangularin A	PMC	tBu4-quadrangularin A	PMC	tBu4-quadrangularin A
Conc. (μM)	2	5	2	5	2	5
t_{inh} (s)	4216	23549.5553	3375	19728.5348	3137	17112.9501
*k*p	3791.88926	3791.88926	3791.88926	3791.88926	3791.88926	3791.88926
Ri	9.49E-10	9.49E-10	1.19E-09	1.19E-09	1.28E-09	1.28E-09
[AOX] (M)	2.00E-06	5.00E-06	2.00E-06	5.00E-06	2.00E-06	5.00E-06
[Dye] (M)	1.00E-05	1.00E-05	1.00E-05	1.00E-05	1.00E-05	1.00E-05
n	2.00E+00	4.47E+00	2.00E+00	4.68E+00	2.00E+00	4.36E+00
log *k*	7.11907598	5.16215902	6.20070513	5.21389527	6.30357825	5.16417929
k_{inh} (M^{-1} s^{-1})	1.32E+07	1.45E+05	1.59E+06	1.64E+05	2.01E+06	1.46E+05
Rate	6.8369E-13	1.1084E-11	7.0785E-12	1.1745E-11	6.0089E-12	1.5183E-11

Table S19.3 – Summary of liposome autoxidation inhibition assay using DTUN initiator

Liposomes (DTUN)	PMC (C3)	PMC (D3)	PMC (E3)	tBu quad A (C4)	tBu quad A (D4)	tBu quad A (E4)
Conc. (μM)	5	5	5	5	5	5
t_{inh} (s)	18154.521	17323.0663	16289.0593	20121.29357	22021.25441	18793.1036
*k*p	894	894	894	894	894	894
Ri	5.51E-10	5.77E-10	6.14E-10	5.43E-10	5.43E-10	5.43E-10
[AOX] (M)	5.00E-06	5.00E-06	5.00E-06	5.00E-06	5.00E-06	5.00E-06
[Dye] (M)	1.00E-05	1.00E-05	1.00E-05	1.00E-05	1.00E-05	1.00E-05
n	2.00E+00	2.00E+00	2.00E+00	4.00E+00	4.00E+00	4.00E+00
k_{inh} (M^{-1} s^{-1})	9.55E+04	9.88E+04	1.04E+05	3.44E+04	3.39E+04	2.93E+04
Rate	5.16E-12	5.22409E-12	5.27E-12	7.06E-12	7.15E-12	8.29E-12

Table S19.4 – Summary of liposome autoxidation inhibition assay using V70 initiator

Liposomes (V70)	PMC (C3)	PMC (D3)	PMC (E3)	tBu quad A (C4)	tBu quad A (D4)	tBu quad A (E4)
Conc. (μM)	5	5	5	5	5	5
t_{inh} (s)	11154.63502	13130.18442	12579.08609	24643.8392	25147.44666	24574.3018
*k*p	894	894	894	894	894	894
Ri	8.96E-10	7.62E-10	7.95E-10	7.79E-10	7.79E-10	7.79E-10
[AOX] (M)	5.00E-06	5.00E-06	5.00E-06	5.00E-06	5.00E-06	5.00E-06
[Dye] (M)	1.00E-05	1.00E-05	1.00E-05	1.00E-05	1.00E-05	1.00E-05
n	2.00E+00	2.00E+00	2.00E+00	3.84E+00	3.92E+00	3.83E+00
k_{inh} (M^{-1} s^{-1})	1.34E+05	1.21E+05	1.14E+05	4.71E+04	4.84E+04	4.57E+04
Rate	6.00E-12	5.62948E-12	6.23606E-12	7.70E-12	7.35E-12	7.96E-12

Table S19.5 – Dose response for ferroptosis inhibition

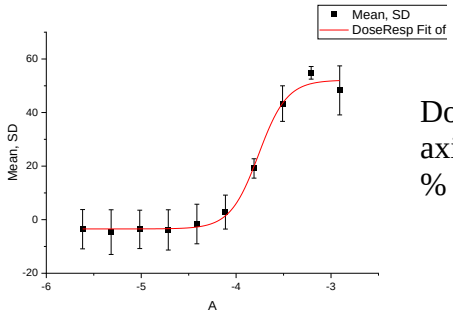

Dose responsive curve x axis = log(mM); y axis = % viability.

tBu quad A1		tBu quad A2		tBu quad A3	
Log(con)mM	% viability	Log(con)mM	% viability	Log(con)mM	% viability
-2.90833	58.58512	-2.90833	45.18513	-2.90833	41.08009
-3.20936	52.11618	-3.20936	55.97574	-3.20936	56.38776
-3.51039	37.32324	-3.51039	42.23255	-3.51039	50.46928
-3.81142	15.74029	-3.81142	18.74127	-3.81142	22.93009
-4.11245	-1.53796	-4.11245	-0.03957	-4.11245	10.09941
-4.41348	-8.09014	-4.41348	-3.20522	-4.41348	6.431413
-4.71451	-10.8846	-4.71451	-4.64346	-4.71451	4.078635
-5.01554	-9.73115	-5.01554	-5.39683	-5.01554	4.268611
-5.31657	-12.5019	-5.31657	-5.54902	-5.31657	4.107862
-5.6176	-9.89763	-5.6176	-5.24463	-5.6176	4.473201

S20 – (±)-Quadrangularin A (summary and organic solution autoxidation)

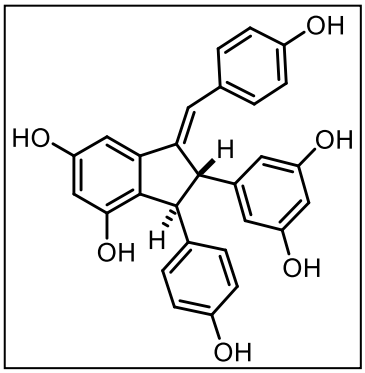

Table S20.1 – Summary of kinetic and cell data

Compound	Organic Solutions		Liposomes		Cells
	k_{inh} (hexadecene) (M^{-1} s^{-1}); n	k_{inh} (cumene) (M^{-1} s^{-1}); n	k_{inh} (DTUN) (M^{-1} s^{-1}); n	k_{inh} (V70) (M^{-1} s^{-1}); n	EC_{50}
quadrangularin A	DNI	(2.9 ± 0.5)E+04; n=3.34 ± 0.40	(6.13 ± 0.16)E+03; n=4*	(7.80 ± 0.32)E+03; n=4*	7.6 ± 0.8 μM

Table S20.2 – Summary of hexadecane co-oxidation inhibition kinetics

Hexadecene	PMC	quadrangularin A
Conc. (μM)	2	5
t_{inh} (s)	4216	0
*k*p	3791.88926	3791.88926
Ri	9.49E-10	9.49E-10
[AOX] (M)	2.00E-06	5.00E-06
[Dye] (M)	1.00E-05	1.00E-05
n	2.00E+00	0.00E+00
log *k*	7.11907598	#DIV/0!
k_{inh} (M^{-1} s^{-1})	1.32E+07	#DIV/0!
Rate	6.8369E-13	#DIV/0!

Table S20.3 – Summary of cumene co-oxidation inhibition kinetics

Cumene	PMC	quadrangularin A	PMC	quadrangularin A	PMC	quadrangularin A
Conc. (μM)	2	5	2	5	2	5
t_{inh} (s)	2001	7389.389	1559	6500.21	1833	8556
*k*p	141	141	141	141	141	141
Ri	2.00E-09	2.00E-09	2.57E-09	2.57E-09	2.18E-09	2.18E-09
[AOX] (M)	2.00E-06	5.00E-06	2.00E-06	5.00E-06	2.00E-06	5.00E-06
[Dye] (M)	1.00E-05	1.00E-05	1.00E-05	1.00E-05	1.00E-05	1.00E-05
n	2.00E+00	2.95E+00	2.00E+00	3.34E+00	2.00E+00	3.73E+00
log *k*	5.780031	4.518995	5.105928	4.496482	5.322359	4.367674
k_{inh} (M^{-1} s^{-1})	6.03E+05	3.30E+04	1.28E+05	3.14E+04	2.10E+05	2.33E+04
Rate	1.17E-12	5.78E-12	7.09E-12	6.92E-12	3.66E-12	7.07E-12

Table S20.4 – Summary of liposome autoxidation inhibition assay using DTUN initiator (approximated n = 4)

Liposomes (DTUN)	PMC (C3)	PMC (D3)	PMC (E3)	quad A (C6)	quad A (D6)	quad A (E6)
Conc. (μM)	5	5	5	5	5	5
t_{inh} (s)	18154.521	17323.0663	16289.0593	5222.946988	5941.301646	11888.60105
*k*p	894	894	894	894	894	894
Ri	5.51E-10	5.77E-10	6.14E-10	5.43E-10	5.43E-10	5.43E-10
[AOX] (M)	5.00E-06	5.00E-06	5.00E-06	5.00E-06	5.00E-06	5.00E-06
[Dye] (M)	1.00E-05	1.00E-05	1.00E-05	1.00E-05	1.00E-05	1.00E-05
n	2.00E+00	2.00E+00	2.00E+00	4.00E+00	4.00E+00	4.00E+00
k_{inh} (M^{-1} s^{-1})	9.55E+04	9.88E+04	1.04E+05	1.16E+04	1.15E+04	1.11E+04
Rate	5.16E-12	5.22409E-12	5.27E-12	2.09E-11	2.10E-11	2.19E-11

Table S20.5 – Summary of liposome autoxidation inhibition assay using V70 initiator (approximated n = 4)

Liposomes (V70)	PMC (C3)	PMC (D3)	PMC (E3)	quad A (C6)	quad A (D6)	quad A (E6)
Conc. (μM)	5	5	5	5	5	5
t_{inh} (s)	11154.63502	13130.18442	12579.08609	5222.946988	5941.301646	11888.60105
*k*p	894	894	894	894	894	894
Ri	8.96E-10	7.62E-10	7.95E-10	7.79E-10	7.79E-10	7.79E-10
[AOX] (M)	5.00E-06	5.00E-06	5.00E-06	5.00E-06	5.00E-06	5.00E-06
[Dye] (M)	1.00E-05	1.00E-05	1.00E-05	1.00E-05	1.00E-05	1.00E-05
n	2.00E+00	2.00E+00	2.00E+00	4.00E+00	4.00E+00	4.00E+00
k_{inh} (M^{-1} s^{-1})	1.34E+05	1.21E+05	1.14E+05	1.46E+04	1.50E+04	1.39E+04
Rate	6.00E-12	5.62948E-12	6.23606E-12	2.38E-11	2.32E-11	2.51E-11

Table S20.6 – Dose response for ferroptosis inhibition

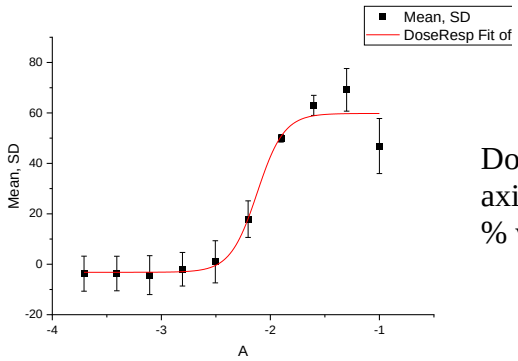

Dose responsive curve x axis = log(mM); y axis = % viability.

quad A1		quad A2		quad A3	
Log(con)mM	% viability	Log(con)mM	% viability	Log(con)mM	% viability
-1	57.96676	-1	46.55488	-1	36.11149
-1.30103	77.4806	-1.30103	69.42215	-1.30103	60.56722
-1.60206	67.09938	-1.60206	59.11856	-1.60206	62.78117
-1.90309	48.6201	-1.90309	51.57731	-1.90309	49.68015
-2.20412	11.38803	-2.20412	16.56489	-2.20412	25.69935
-2.50515	-5.74753	-2.50515	-1.66045	-2.50515	10.31861
-2.80618	-7.54313	-2.80618	-3.77595	-2.80618	5.393853
-3.10721	-11.3246	-3.10721	-5.58707	-3.10721	3.969034
-3.40824	-9.81439	-3.40824	-4.90981	-3.40824	3.713297
-3.70927	-9.95709	-3.70927	-5.02395	-3.70927	3.764445

S21 – (±)-tBu$_4$-pallidol (summary and organic solution autoxidation)

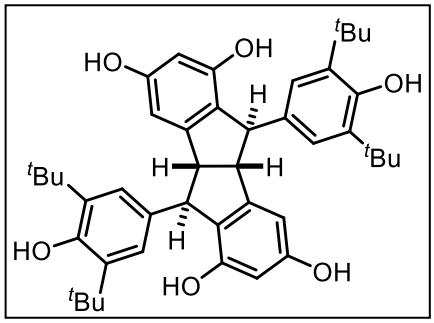

Table S21.1 – Summary of kinetic and cell data

Compound	Organic Solutions		Liposomes		Cells
	k_{inh} (hexadecene) (M^{-1} s^{-1}); n	k_{inh} (cumene) (M^{-1} s^{-1}); n	k_{inh} (DTUN) (M^{-1} s^{-1}); n	k_{inh} (V70) (M^{-1} s^{-1}); n	EC_{50}
tBu4-pallidol	(7.31 ± 0.91)E+04; n=3.1 ± 0.3	(1.3 ± 0.4)E+04; n= 5.63 ± 0.31	(1.59 ± 0.03)E+04; n= 1.98 ± 0.12	(2.05 ± 0.02)E+03; n= 1.78 ± 0.02	280.9 ± 32.4 nM

Table S21.2 – Summary of hexadecane co-oxidation inhibition kinetics

Hexadecene	PMC	tBu4-pallidol	tBu4-pallidol	PMC	tBu4-pallidol
Conc. (μM)	2	5	5	2	5
t_{inh} (s)	4352	15286.3618	18696	4385	16975
*k*p	3791.88926	3791.88926	3791.88926	3791.88926	3791.88926
Ri	9.19E-10	9.19E-10	9.19E-10	9.12E-10	9.12E-10
[AOX] (M)	2.00E-06	5.00E-06	5.00E-06	2.00E-06	5.00E-06
[Dye] (M)	1.00E-05	1.00E-05	1.00E-05	1.00E-05	1.00E-05
n	2.00E+00	2.81E+00	3.44E+00	2.00E+00	3.10E+00
log *k*	6.23241057	4.90471206	4.88085587	6.09813476	4.79885259
k_{inh} (M^{-1} s^{-1})	1.71E+06	8.03E+04	7.60E+04	1.25E+06	6.29E+04
Rate	5.1018E-12	3.0892E-11	2.6684E-11	6.8978E-12	3.5496E-11

Table S21.3 – Summary of cumene co-oxidation inhibition kinetics

Cumene	PMC	tBu4-pallidol	tBu4-pallidol	PMC	tBu4-pallidol	tBu4-pallidol
Conc. (μM)	2	5	5	2	5	5
t_{inh} (s)	2432	17333	17203	2396	16123	15867
*k*p	141	141	141	141	141	141
Ri	1.64E-09	1.64E-09	1.64E-09	1.67E-09	1.67E-09	1.67E-09
[AOX] (M)	2.00E-06	5.00E-06	5.00E-06	2.00E-06	5.00E-06	5.00E-06
[Dye] (M)	1.00E-05	1.00E-05	1.00E-05	1.00E-05	1.00E-05	1.00E-05
n	2.00E+00	5.70E+00	5.66E+00	2.00E+00	5.38E+00	5.30E+00
log *k*	5.158239	3.929261	3.927955	5.761271	4.208229	4.223463
k_{inh} (M^{-1} s^{-1})	1.44E+05	8.50E+03	8.47E+03	5.77E+05	1.62E+04	1.67E+04
Rate	4.03E-12	9.57E-12	9.68E-12	1.02E-12	5.41E-12	5.31E-12

Table S21.4 – Summary of liposome autoxidation inhibition assay using DTUN initiator

Liposomes (DTUN)	PMC (C3)	PMC (D3)	PMC (E3)	tBu pallidol (C5)	tBu pallidol (D5)	tBu pallidol (E5)
Conc. (μM)	5	5	5	5	5	5
t_{inh} (s)	18154.521	17323.0663	16289.0593	19275.27076	18351.81371	17098.02429
*k*p	894	894	894	894	894	894
Ri	5.51E-10	5.77E-10	6.14E-10	5.43E-10	5.43E-10	5.43E-10
[AOX] (M)	5.00E-06	5.00E-06	5.00E-06	5.00E-06	5.00E-06	5.00E-06
[Dye] (M)	1.00E-05	1.00E-05	1.00E-05	1.00E-05	1.00E-05	1.00E-05
n	2.00E+00	2.00E+00	2.00E+00	2.09E+00	1.99E+00	1.86E+00
k_{inh} (M^{-1} s^{-1})	9.55E+04	9.88E+04	1.04E+05	2.97E+04	3.02E+04	2.92E+04
Rate	5.16E-12	5.22409E-12	5.27E-12	1.56E-11	1.61E-11	1.79E-11

Table S21.5 – Summary of liposome autoxidation inhibition assay using V70 initiator

Liposomes (V70)	PMC (C3)	PMC (D3)	PMC (E3)	tBu pallidol (C5)	tBu pallidol (D5)	tBu pallidol (E5)
Conc. (μM)	5	5	5	5	5	5
t_{inh} (s)	11154.63502	13130.18442	12579.08609	11440.83445	11566.64298	11343.6505
*k*p	894	894	894	894	894	894
Ri	8.96E-10	7.62E-10	7.95E-10	7.79E-10	7.79E-10	7.79E-10
[AOX] (M)	5.00E-06	5.00E-06	5.00E-06	5.00E-06	5.00E-06	5.00E-06
[Dye] (M)	1.00E-05	1.00E-05	1.00E-05	1.00E-05	1.00E-05	1.00E-05
n	2.00E+00	2.00E+00	2.00E+00	1.78E+00	1.80E+00	1.77E+00
k_{inh} (M^{-1} s^{-1})	1.34E+05	1.21E+05	1.14E+05	3.83E+04	3.85E+04	3.76E+04
Rate	6.00E-12	5.62948E-12	6.23606E-12	2.04E-11	2.01E-11	2.09E-11

Table S21.6 – Dose response for ferroptosis inhibition

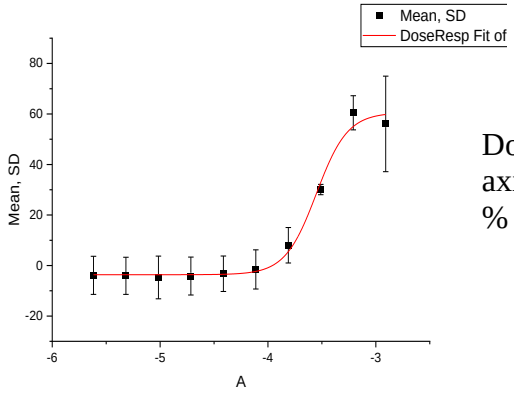

Dose responsive curve x axis = log(mM); y axis = % viability.

tBu pallidol 1		tBu pallidol 2		tBu pallidol 3	
Log(con)mM	% viability	Log(con)mM	% viability	Log(con)mM	% viability
-2.90833	71.02355	-2.90833	62.39075	-2.90833	34.81819
-3.20936	64.10274	-3.20936	64.6128	-3.20936	52.66131
-3.51039	27.78631	-3.51039	31.70827	-3.51039	30.77024
-3.81142	2.6835	-3.81142	5.439444	-3.81142	15.99597
-4.11245	-8.50634	-4.11245	-2.92366	-4.11245	6.818672
-4.41348	-9.89763	-4.41348	-3.93576	-4.41348	4.071329
-4.71451	-11.1938	-4.71451	-4.9859	-4.71451	3.735218
-5.01554	-12.5494	-5.01554	-5.81536	-5.01554	4.217464
-5.31657	-10.9084	-5.31657	-5.00873	-5.31657	3.720604
-5.6176	-10.1355	-5.6176	-5.97517	-5.6176	4.480507

S22 – (±)-Pallidol (summary and organic solution autoxidation)

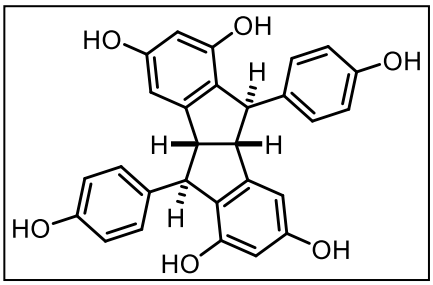

Table S22.1 – Summary of kinetic and cell data

Compound	Organic Solutions		Liposomes		Cells
	k_{inh} (hexadecene) (M^{-1} s^{-1}); n	k_{inh} (cumene) (M^{-1} s^{-1}); n	k_{inh} (DTUN) (M^{-1} s^{-1}); n	k_{inh} (V70) (M^{-1} s^{-1}); n	EC_{50}
pallidol	DNI	(7.0 ± 1.4)E+03; n= 4.27 ± 0.66	(3.13 ± 0.14)E+03; n= 4*	(4.97 ± 0.18)E+03; n= 4*	11.6 ± 1.3 μM

Table S22.2 – Summary of hexadecane co-oxidation inhibition kinetics

Hexadecene	PMC	Pallidol
Conc. (μM)	2	5
t_{inh} (s)	4216	0
*k*p	3791.88926	3791.88926
Ri	9.49E-10	9.49E-10
[AOX] (M)	2.00E-06	5.00E-06
[Dye] (M)	1.00E-05	1.00E-05
n	2.00E+00	0.00E+00
log *k*	7.11907598	#DIV/0!
k_{inh} (M^{-1} s^{-1})	1.32E+07	#DIV/0!
Rate	6.8369E-13	0

Table S22.3 – Summary of cumene co-oxidation inhibition kinetics

Cumene	PMC	Pallidol	PMC	Pallidol	PMC	Pallidol
Conc. (μM)	2	5	2	5	2	5
t_{inh} (s)	2001	9286.654	1559	7978.647	1833	11466.21
*k*p	141	141	141	141	141	141
Ri	2.00E-09	2.00E-09	2.57E-09	2.57E-09	2.18E-09	2.18E-09
[AOX] (M)	2.00E-06	5.00E-06	2.00E-06	5.00E-06	2.00E-06	5.00E-06
[Dye] (M)	1.00E-05	1.00E-05	1.00E-05	1.00E-05	1.00E-05	1.00E-05
n	2.00E+00	3.71E+00	2.00E+00	4.09E+00	2.00E+00	5.00E+00
log *k*	5.780031	3.828948	5.105928	3.926341	5.322359	3.752917
k_{inh} (M^{-1} s^{-1})	6.03E+05	6.74E+03	1.28E+05	8.44E+03	2.10E+05	5.66E+03
Rate	1.17E-12	2.25E-11	7.09E-12	2.09E-11	3.66E-12	2.17E-11

Table S22.4 – Summary of liposome autoxidation inhibition assay using DTUN initiator (approximating n = 2)

Liposomes (DTUN)	PMC (C3)	PMC (D3)	PMC (E3)	pallidol (C7)	pallidol (D7)	pallidol (E7)
Conc. (μM)	5	5	5	5	5	5
t_{inh} (s)	18154.521	17323.0663	16289.0593	0	0	0
*k*p	894	894	894	480	480	480
Ri	5.51E-10	5.77E-10	6.14E-10	5.43E-10	5.43E-10	5.43E-10
[AOX] (M)	5.00E-06	5.00E-06	5.00E-06	5.00E-06	5.00E-06	5.00E-06
[Dye] (M)	1.00E-05	1.00E-05	1.00E-05	1.00E-05	1.00E-05	1.00E-05
n	2.00E+00	2.00E+00	2.00E+00	2.00E+00	2.00E+00	2.00E+00
k_{inh} (M^{-1} s^{-1})	9.55E+04	9.88E+04	1.04E+05	6.52E+03	6.31E+03	5.95E+03
Rate	5.16E-12	5.22409E-12	5.27E-12	4.00E-11	4.13E-11	4.38E-11

Table S22.5 – Summary of liposome autoxidation inhibition assay using V70 initiator

Liposomes (V70)	PMC (C3)	PMC (D3)	PMC (E3)	pallidol (C7)	pallidol (D7)	pallidol (E7)
Conc. (μM)	5	5	5	5	5	5
t_{inh} (s)	11154.63502	13130.18442	12579.08609	0	0	0
*k*p	894	894	894	480	480	480
Ri	8.96E-10	7.62E-10	7.95E-10	7.79E-10	7.79E-10	7.79E-10
[AOX] (M)	5.00E-06	5.00E-06	5.00E-06	5.00E-06	5.00E-06	5.00E-06
[Dye] (M)	1.00E-05	1.00E-05	1.00E-05	1.00E-05	1.00E-05	1.00E-05
n	2.00E+00	2.00E+00	2.00E+00	2.00E+00	2.00E+00	2.00E+00
k_{inh} (M^{-1} s^{-1})	1.34E+05	1.21E+05	1.14E+05	9.81E+03	1.03E+04	9.65E+03
Rate	6.00E-12	5.62948E-12	6.23606E-12	3.81E-11	3.62E-11	3.88E-11

Stoichiometry was assumed to equal 2 as t_{inh} cannot be gathered from the curve as pallidol retards autoxidation.

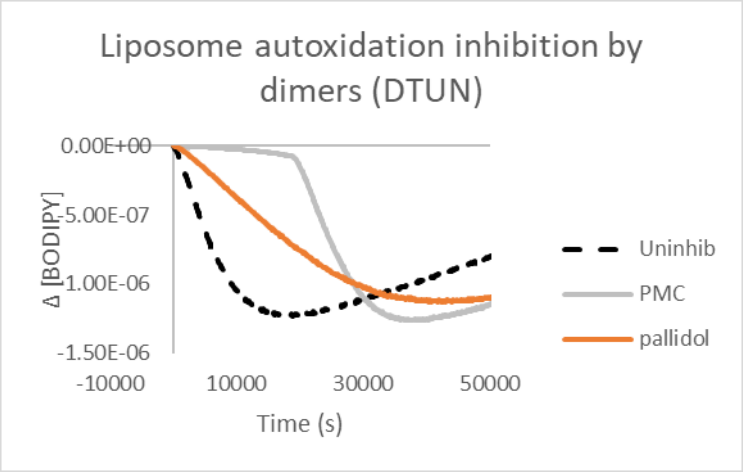

Table S22.6 – Summary of liposome autoxidation inhibition assay using DTUN initiator (approximating n = 4)

Liposomes (DTUN)	PMC (C3)	PMC (D3)	PMC (E3)	pallidol (C7)	pallidol (D7)	pallidol (E7)
Conc. (μM)	5	5	5	5	5	5
t_{inh} (s)	17620.5231	19182.3888	18540.4586	0	0	0
*k*p	480	480	480	480	480	480
Ri	5.68E-10	5.21E-10	5.39E-10	5.43E-10	5.43E-10	5.43E-10
[AOX] (M)	5.00E-06	5.00E-06	5.00E-06	5.00E-06	5.00E-06	5.00E-06
[Dye] (M)	1.00E-05	1.00E-05	1.00E-05	1.00E-05	1.00E-05	1.00E-05
n	2.00E+00	2.00E+00	2.00E+00	4.00E+00	4.00E+00	4.00E+00
k_{inh} (M^{-1} s^{-1})	7.77E+04	8.09E+04	6.79E+04	3.26E+03	3.16E+03	2.98E+03
Rate	3.51E-12	3.0927E-12	3.8143E-12	4.00E-11	4.13E-11	4.38E-11

Table S22.7 – Summary of liposome autoxidation inhibition assay using V70 initiator

Liposomes (V70)	PMC (C3)	PMC (D3)	PMC (E3)	pallidol (C7)	pallidol (D7)	pallidol (E7)
Conc. (μM)	5	5	5	5	5	5
t_{inh} (s)	11154.63502	13130.18442	12579.08609	0	0	0
*k*p	894	894	894	480	480	480
Ri	8.96E-10	7.62E-10	7.95E-10	7.79E-10	7.79E-10	7.79E-10
[AOX] (M)	5.00E-06	5.00E-06	5.00E-06	5.00E-06	5.00E-06	5.00E-06
[Dye] (M)	1.00E-05	1.00E-05	1.00E-05	1.00E-05	1.00E-05	1.00E-05
n	2.00E+00	2.00E+00	2.00E+00	4.00E+00	4.00E+00	4.00E+00
k_{inh} (M^{-1} s^{-1})	1.34E+05	1.21E+05	1.14E+05	4.90E+03	5.17E+03	4.83E+03
Rate	6.00E-12	5.62948E-12	6.23606E-12	3.81E-11	3.62E-11	3.88E-11

Stoichiometry was assumed to equal 2 as t_{inh} cannot be gathered from the curve as pallidol retards autoxidation.

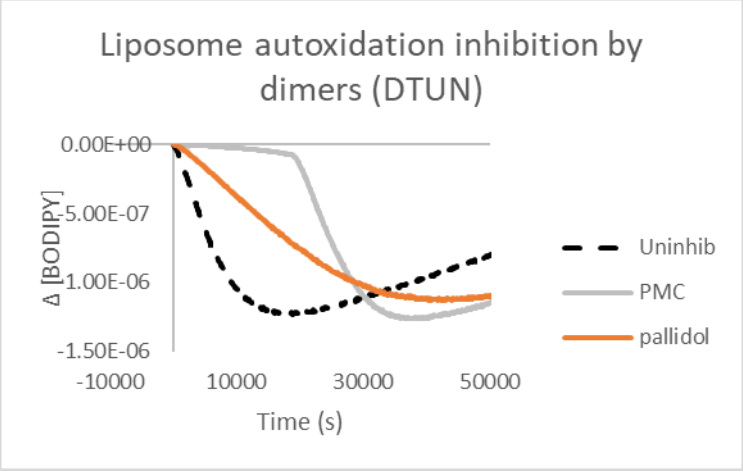

Table S22.8 – Dose response for ferroptosis inhibition

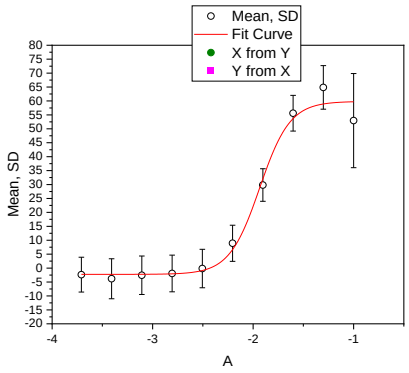

pallidol 1		pallidol 2		pallidol 3	
Log(con)mM	% viability	Log(con)mM	% viability	Log(con)mM	% viability
-1	68.96634	-1	54.57555	-1	35.30774
-1.30103	73.19969	-1.30103	57.67271	-1.30103	63.73105
-1.60206	58.03811	-1.60206	48.33556	-1.60206	60.4284
-1.90309	26.20475	-1.90309	26.69345	-1.90309	36.57912
-2.20412	3.539683	-2.20412	7.067928	-2.20412	16.12749
-2.50515	-6.37777	-2.50515	-1.35606	-2.50515	7.264384
-2.80618	-7.89987	-2.80618	-3.01498	-2.80618	5.123503
-3.10721	-8.57769	-3.10721	-4.09556	-3.10721	4.962754
-3.40824	-10.3495	-3.40824	-4.97068	-3.40824	3.866739
-3.70927	-7.51935	-3.70927	-4.126	-3.70927	4.590109

S23 – (±)-orcinol/tBuRSV DHB (summary and organic solution autoxidation)

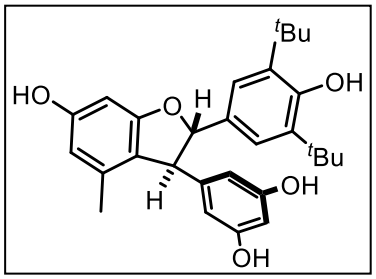

Table S23.1 – Summary of kinetic and cell data

Compound	Organic Solutions		Liposomes		Cells
	k_{inh} (hexadecene) (M^{-1} s^{-1}); n	k_{inh} (cumene) (M^{-1} s^{-1}); n	k_{inh} (DTUN) (M^{-1} s^{-1}); n	k_{inh} (V70) (M^{-1} s^{-1}); n	EC_{50}
orcinol/tBuRSV DHB	(8.90 ± 0.57)E+04; n=2.3 ± 0.1	(6.91 ± 0.01)E+04; n= 3.83 ± 0.36	DNI	N/A	N/A

Table S23.2 – Summary of hexadecane co-oxidation inhibition kinetics

Hexadecene	PMC	orcinol/tBuRSV DHB	PMC	orcinol/tBuRSV DHB	PMC	orcinol/tBuRSV DHB
Conc. (μM)	2	5	2	5	2	5
t_{inh} (s)	4573	12673.0929	4692	12983.5381	4265	13086.8774
*k*p	3791.88926	3791.88926	3791.88926	3791.88926	3791.88926	3791.88926
Ri	8.75E-10	8.75E-10	8.52E-10	8.52E-10	9.38E-10	9.38E-10
[AOX] (M)	2.00E-06	5.00E-06	2.00E-06	5.00E-06	2.00E-06	5.00E-06
[Dye] (M)	1.00E-05	1.00E-05	1.00E-05	1.00E-05	1.00E-05	1.00E-05
n	2.00E+00	2.22E+00	2.00E+00	2.21E+00	2.00E+00	2.45E+00
log *k*	6.15961906	4.93258711	6.19640331	4.93361935	6.34134974	4.98040064
k_{inh} (M^{-1} s^{-1})	1.44E+06	8.56E+04	1.57E+06	8.58E+04	2.19E+06	9.56E+04
Rate	5.7412E-12	3.4945E-11	5.1411E-12	3.4029E-11	4.0514E-12	3.0312E-11

Table S23.3 – Summary of cumene co-oxidation inhibition kinetics

Cumene	PMC	orcinol/tBuRSV DHB	PMC	orcinol/tBuRSV DHB	PMC	orcinol/tBuRSV DHB
Conc. (μM)	2	5	2	5	2	5
t_{inh} (s)	2532	10954.53	2357	11326.57	2231	11682.74
*k*p	141	141	141	141	141	141
Ri	1.58E-09	1.58E-09	1.70E-09	1.70E-09	1.79E-09	1.79E-09
[AOX] (M)	2.00E-06	5.00E-06	2.00E-06	5.00E-06	2.00E-06	5.00E-06
[Dye] (M)	1.00E-05	1.00E-05	1.00E-05	1.00E-05	1.00E-05	1.00E-05
n	2.00E+00	3.46E+00	2.00E+00	3.84E+00	2.00E+00	4.19E+00
log *k*	5.034121	3.840168	6.057932	3.838928	5.114031	3.839856
k_{inh} (M^{-1} s^{-1})	1.08E+05	6.92E+03	1.14E+06	6.90E+03	1.30E+05	6.92E+03
Rate	5.15E-12	1.86E-11	5.23E-13	1.8E-11	4.86E-12	1.75E-11

Table S23.4 – Summary of liposome autoxidation inhibition assay using DTUN initiator

Liposomes (DTUN)	PMC (A4)	PMC (A5)	PMC (A6)	orcinol/tBu RSV 1 (D7)	orcinol/tBu RSV 1 (D8)	orcinol/tBu RSV 2 (D9)	orcinol/tBu RSV 2 (D10)	orcinol/tBu RSV 3 (E1)	orcinol/tBu RSV 3 (E2)
Conc. (μM)	5	5	5	5	5	5	5	5	5
t_{inh} (s)	4698.56059	4436.44094	4665.22629	0	0	0	0	0	0
*k*p	894	894	894	894	894	894	894	894	894
Ri	2.13E-09	2.25E-09	2.14E-09	2.18E-09	2.18E-09	2.18E-09	2.18E-09	2.18E-09	2.18E-09
[AOX] (M)	5.00E-06	5.00E-06	5.00E-06	5.00E-06	5.00E-06	5.00E-06	5.00E-06	5.00E-06	5.00E-06
[Dye] (M)	1.00E-05	1.00E-05	1.00E-05	1.00E-05	1.00E-05	1.00E-05	1.00E-05	1.00E-05	1.00E-05
n	2.00E+00	2.00E+00	2.00E+00	0.00E+00	0.00E+00	0.00E+00	0.00E+00	0.00E+00	0.00E+00
k_{inh} (M^{-1} s^{-1})	4.94E+05	4.78E+05	5.85E+05	#DIV/0!	#DIV/0!	#DIV/0!	#DIV/0!	#DIV/0!	#DIV/0!
Rate	3.85E-12	4.21E-12	3.28E-12	0.00E+00	0.00E+00	0.00E+00	0.00E+00	0.00E+00	0.00E+00

S24 – (±)-orcinol/tBuRSV DHB (OBn_2)/(OMe) (summary and organic solution autoxidation)

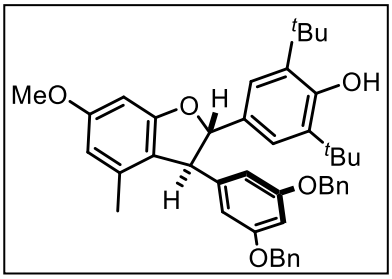

Table S24.1 – Summary of kinetic and cell data

Compound	Organic Solutions		Liposomes		Cells
	k_{inh} (hexadecene) (M^{-1} s^{-1}); n	k_{inh} (cumene) (M^{-1} s^{-1}); n	k_{inh} (DTUN) (M^{-1} s^{-1}); n	k_{inh} (V70) (M^{-1} s^{-1}); n	EC_{50}
orcinol(OMe)/ tBuRSV(OBn)DHB	(5.65 ± 0.30)E+04; n=3.96 ± 1.32	(5.29 ± 0.25)E+04; n= 2.31 ± 0.23	DNI	N/A	N/A

Table S24.2 – Summary of hexadecane co-oxidation inhibition kinetics

Hexadecene	PMC	orcinol(OMe)/ tBuRSV(OBn)DHB	PMC	orcinol(OMe)/ tBuRSV(OBn)DHB	PMC	orcinol(OMe)/ tBuRSV(OBn)DHB
Conc. (µM)	2	5	2	5	2	5
t_{inh} (s)	4573	27330.72167	4692	27330.72167	4265	12958.78866
*k*p	3791.889263	3791.889263	3791.889263	3791.889263	3791.889263	3791.889263
Ri	8.75E-10	8.75E-10	8.52E-10	8.52E-10	9.38E-10	9.38E-10
[AOX] (M)	2.00E-06	5.00E-06	2.00E-06	5.00E-06	2.00E-06	5.00E-06
[Dye] (M)	1.00E-05	1.00E-05	1.00E-05	1.00E-05	1.00E-05	1.00E-05
n	2.00E+00	4.78E+00	2.00E+00	4.66E+00	2.00E+00	2.43E+00
log *k*	6.159619057	4.738391287	6.19640331	4.738391287	6.341349735	4.777307482
k_{inh} (M^{-1} s^{-1})	1.44E+06	5.48E+04	1.57E+06	5.48E+04	2.19E+06	5.99E+04
Rate	5.74117E-12	2.53404E-11	5.14114E-12	2.53404E-11	4.05145E-12	4.88634E-11

Table S24.3 – Summary of cumene co-oxidation inhibition kinetics

Cumene	PMC	Orcinol (OMe)/ tBuRSV(OBn) DHB	PMC	Orcinol (OMe)/ tBuRSV(OBn) DHB	PMC	Orcinol (OMe)/ tBuRSV(OBn) DHB
Conc. (μM)	2	5	2	5	2	5
t_{inh} (s)	2532	6581.141293	2357	6766.510374	2231	7084.265793
*k*p	141	141	141	141	141	141
Ri	1.58E-09	1.58E-09	1.70E-09	1.70E-09	1.79E-09	1.79E-09
[AOX] (M)	2.00E-06	5.00E-06	2.00E-06	5.00E-06	2.00E-06	5.00E-06
[Dye] (M)	1.00E-05	1.00E-05	1.00E-05	1.00E-05	1.00E-05	1.00E-05
n	2.00E+00	2.08E+00	2.00E+00	2.30E+00	2.00E+00	2.54E+00
log *k*	5.034121028	3.746025925	6.057932398	3.718917525	5.114031085	3.705190189
k_{inh} (M^{-1} s^{-1})	1.08E+05	5.57E+03	1.14E+06	5.24E+03	1.30E+05	5.07E+03
Rate	5.14875E-12	3.84496E-11	5.23403E-13	3.98049E-11	4.85972E-12	3.92405E-11

Table S24.4 – Summary of liposome autoxidation inhibition assay using DTUN initiator

Liposomes (DTUN)	PMC (A4)	PMC (A5)	PMC (A6)	orcinol (OMe)/tBu RSV (OBn) 1 (E3)	orcinol (OMe)/tBu RSV (OBn) 1 (E4)	orcinol (OMe)/tBu RSV (OBn) 2 (E5)	orcinol (OMe)/tBu RSV (OBn) 2 (E6)	orcinol (OMe)/tBu RSV (OBn) 3 (E7)	orcinol (OMe)/tBu RSV (OBn) 3 (E8)
Conc. (μM)	5	5	5	5	5	5	5	5	5
t_{inh} (s)	4698.56059	4436.44094	4665.22629	0	0	0	0	0	0
*k*p	894	894	894	894	894	894	894	894	894
Ri	2.13E-09	2.25E-09	2.14E-09	2.18E-09	2.18E-09	2.18E-09	2.18E-09	2.18E-09	2.18E-09
[AOX] (M)	5.00E-06	5.00E-06	5.00E-06	5.00E-06	5.00E-06	5.00E-06	5.00E-06	5.00E-06	5.00E-06
[Dye] (M)	1.00E-05	1.00E-05	1.00E-05	1.00E-05	1.00E-05	1.00E-05	1.00E-05	1.00E-05	1.00E-05
n	2.00E+00	2.00E+00	2.00E+00	0.00E+00	0.00E+00	0.00E+00	0.00E+00	0.00E+00	0.00E+00
k_{inh} (M^{-1} s^{-1})	4.94E+05	4.78E+05	5.85E+05	#DIV/0!	#DIV/0!	#DIV/0!	#DIV/0!	#DIV/0!	#DIV/0!
Rate	3.85E-12	4.21E-12	3.28E-12	0.00E+00	0.00E+00	0.00E+00	0.00E+00	0.00E+00	0.00E+00

S25 – ellagic acid (summary and organic solution autoxidation)

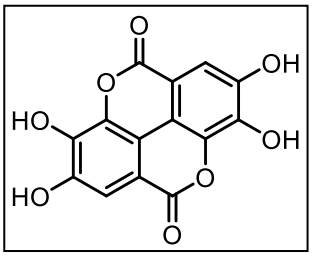

Table S25.1 – Summary of kinetic and cell data

Compound	Organic Solutions		Liposomes		Cells
	k_{inh} (hexadecene) (M^{-1} s^{-1}); n	k_{inh} (cumene) (M^{-1} s^{-1}); n	k_{inh} (DTUN) (M^{-1} s^{-1}); n	k_{inh} (V70) (M^{-1} s^{-1}); n	EC_{50}
ellagic acid	DNI	(1.84 ± 0.14)E+04; n=1.10 ± 0.03	DNI	N/A	25.2 ± 1.4 μM

Table S25.2 – Summary of hexadecane co-oxidation inhibition kinetics

Hexadecene	PMC	ellagic acid	PMC	ellagic acid	PMC	ellagic acid
Conc. (μM)	2	5	2	5	2	5
t_{inh} (s)	4631	0	4028	0	4078	0
*k*p	3791.88926	3791.88926	3791.88926	3791.88926	3791.88926	3791.88926
Ri	8.64E-10	8.64E-10	9.93E-10	9.93E-10	9.81E-10	9.81E-10
[AOX] (M)	2.00E-06	5.00E-06	2.00E-06	5.00E-06	2.00E-06	5.00E-06
[Dye] (M)	1.00E-05	1.00E-05	1.00E-05	1.00E-05	1.00E-05	1.00E-05
n	2.00E+00	0.00E+00	2.00E+00	0.00E+00	2.00E+00	0.00E+00
log *k*	6.49596142	#DIV/0!	6.42826022	#DIV/0!	6.39151125	#DIV/0!
k_{inh} (M^{-1} s^{-1})	3.13E+06	#DIV/0!	2.68E+06	#DIV/0!	2.46E+06	#DIV/0!
Rate	2.6134E-12	3.6072E-11	3.5115E-12	3.6072E-11	3.7746E-12	3.6072E-11

Table S25.3 – Summary of cumene co-oxidation inhibition kinetics

Cumene	PMC	ellagic acid	PMC	ellagic acid	PMC	ellagic acid
Conc. (μM)	2	5	2	5	2	5
t_{inh} (s)	2343	3287	2428	3224	2321	3223
*k*p	141	141	141	141	141	141
Ri	1.71E-09	1.71E-09	1.65E-09	1.65E-09	1.72E-09	1.72E-09
[AOX] (M)	2.00E-06	5.00E-06	2.00E-06	5.00E-06	2.00E-06	5.00E-06
[Dye] (M)	1.00E-05	1.00E-05	1.00E-05	1.00E-05	1.00E-05	1.00E-05
n	2.00E+00	1.12E+00	2.00E+00	1.06E+00	2.00E+00	1.11E+00
log *k*	5.531447	4.250013	5.938324	4.299972	6.21875	4.239098
k_{inh} (M^{-1} s^{-1})	3.40E+05	1.78E+04	8.68E+05	2.00E+04	1.65E+06	1.73E+04
Rate	1.77E-12	2.41E-11	6.69E-13	2.19E-11	3.67E-13	2.52E-11

Table S25.4 – Summary of liposome autoxidation inhibition assay using DTUN initiator

Liposomes (DTUN)	PMC (A4)	PMC (A5)	PMC (A6)	ellagic acid 1 (G1)	ellagic acid 1 (G2)	ellagic acid 2 (G3)	ellagic acid 2 (G4)	ellagic acid 3 (G5)	ellagic acid 3 (G6)
Conc. (μM)	5	5	5	5	5	5	5	5	5
t_{inh} (s)	4698.56059	4436.44094	4665.22629	0	0	0	0	0	0
*k*p	894	894	894	894	894	894	894	894	894
Ri	2.13E-09	2.25E-09	2.14E-09	2.18E-09	2.18E-09	2.18E-09	2.18E-09	2.18E-09	2.18E-09
[AOX] (M)	5.00E-06	5.00E-06	5.00E-06	5.00E-06	5.00E-06	5.00E-06	5.00E-06	5.00E-06	5.00E-06
[Dye] (M)	1.00E-05	1.00E-05	1.00E-05	1.00E-05	1.00E-05	1.00E-05	1.00E-05	1.00E-05	1.00E-05
n	2.00E+00	2.00E+00	2.00E+00	0.00E+00	0.00E+00	0.00E+00	0.00E+00	0.00E+00	0.00E+00
k_{inh} (M^{-1} s^{-1})	4.94E+05	4.78E+05	5.85E+05	#DIV/0!	#DIV/0!	#DIV/0!	#DIV/0!	#DIV/0!	#DIV/0!
Rate	3.85E-12	4.21E-12	3.28E-12	0.00E+00	0.00E+00	0.00E+00	0.00E+00	0.00E+00	0.00E+00

Table S22.5 – Dose response for ferroptosis inhibition

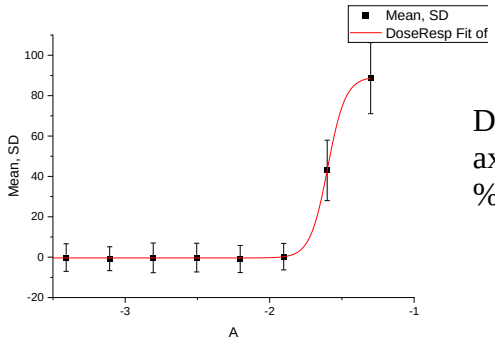

Dose responsive curve x axis = log(mM); y axis = % viability.

ellagic acid1		ellagic acid2		ellagic acid3	
Log(con)mM	% viability	Log(con)mM	% viability	Log(con)mM	% viability
-1	63.36730462	-1	53.54015116	-1	70.51884762
-1.301029996	87.39112401	-1.301029996	76.22375087	-1.301029996	101.093489
-1.602059991	18.5192866	-1.602059991	32.38593103	-1.602059991	53.53963252
-1.903089987	-0.509569236	-1.903089987	-4.398284722	-1.903089987	4.892287028
-2.204119983	2.165669254	-2.204119983	-5.67057032	-2.204119983	3.841848771
-2.505149978	3.64104995	-2.505149978	-5.235488198	-2.505149978	4.814795681
-2.806179974	11.15127096	-2.806179974	-5.545319406	-2.806179974	4.866456579
-3.10720997	15.84404811	-3.10720997	-4.958617757	-3.10720997	3.428561588
-3.408239965	9.889198317	-3.408239965	-5.017947138	-3.408239965	4.633982539
-3.709269961	8.173846063	-3.709269961	-4.345547495	-3.709269961	4.745914484

S26 – (±)-tBu$_6$-carasiphenol C/ wilsonol A (summary and organic solution autoxidation)

Synthesis of this molecule is described in Chapter 3 of this dissertation. See Experimental for details.

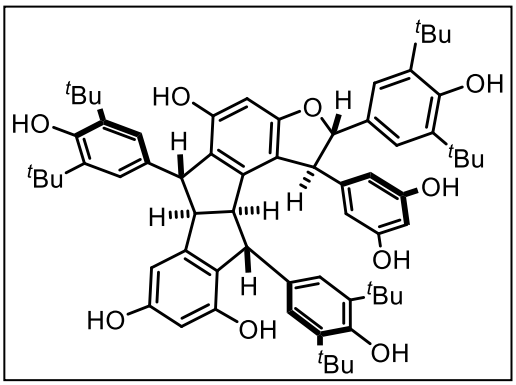

Table S26.1 – Summary of kinetic and cell data

Compound	Organic Solutions		Liposomes		Cells
	k_{inh} (hexadecene) (M^{-1} s^{-1}); n	k_{inh} (cumene) (M^{-1} s^{-1}); n	k_{inh} (DTUN) (M^{-1} s^{-1}); n	k_{inh} (V70) (M^{-1} s^{-1}); n	EC_{50}
tBu6 carasiphenol C/ tBu6 wilsonol A	(7.31 ± 0.44)E+04; n=5.73 ± 0.41	(8.30 ± 1.38)E+03; n= 8.23 ± 0.31	(3.68 ± 0.15)E+04; n= 7.60 ± 0.42	N/A	106.1 ± 6.8 nM

Table S26.2 – Summary of hexadecane co-oxidation inhibition kinetics

Hexadecene	PMC	tBu6 carasiphenol C/ tBu6 wilsonol A	PMC	tBu6 carasiphenol C/ tBu6 wilsonol A acid	PMC	tBu6 carasiphenol C/ tBu6 wilsonol A
Conc. (μM)	2	5	2	5	2	5
t_{inh} (s)	4886	33280.8373	4229	32754.768	4625	31989.1757
*k*p	3791.88926	3791.88926	3791.88926	3791.88926	3791.88926	3791.88926
Ri	8.19E-10	8.19E-10	9.46E-10	9.46E-10	8.65E-10	8.65E-10
[AOX] (M)	2.00E-06	5.00E-06	2.00E-06	5.00E-06	2.00E-06	5.00E-06
[Dye] (M)	1.00E-05	1.00E-05	1.00E-05	1.00E-05	1.00E-05	1.00E-05
n	2.00E+00	5.45E+00	2.00E+00	6.20E+00	2.00E+00	5.53E+00
log *k*	6.12581094	4.85167585	6.24327873	4.84622658	6.20428119	4.89310539
k_{inh} (M^{-1} s^{-1})	1.34E+06	7.11E+04	1.75E+06	7.02E+04	1.60E+06	7.82E+04
Rate	5.8087E-12	1.6032E-11	5.1203E-12	1.6495E-11	5.1227E-12	1.5162E-11

Table S26.3 – Summary of cumene co-oxidation inhibition kinetics

Cumene	PMC	tBu6 carasiphenol C/ tBu6 wilsonol A	PMC	tBu6 carasiphenol C/ tBu6 wilsonol A	PMC	tBu6 carasiphenol C/ tBu6 wilsonol A
Conc. (μM)	2	5	2	5	2	5
t_{inh} (s)	2532	25111	2357	24154	2231	23858
*k*p	141	141	141	141	141	141
Ri	1.58E-09	1.58E-09	1.70E-09	1.70E-09	1.79E-09	1.79E-09
[AOX] (M)	2.00E-06	5.00E-06	2.00E-06	5.00E-06	2.00E-06	5.00E-06
[Dye] (M)	1.00E-05	1.00E-05	1.00E-05	1.00E-05	1.00E-05	1.00E-05
n	2.00E+00	7.94E+00	2.00E+00	8.20E+00	2.00E+00	8.55E+00
log *k*	5.034121	3.83361	6.057932	3.980125	5.114031	3.930687
k_{inh} (M^{-1} s^{-1})	1.08E+05	6.82E+03	1.14E+06	9.55E+03	1.30E+05	8.52E+03
Rate	5.15E-12	8.24E-12	5.23E-13	6.11E-12	4.86E-12	6.93E-12

Table S26.4 – Summary of liposome autoxidation inhibition assay using DTUN initiator

Liposomes (DTUN)	PMC (A4)	PMC (A5)	PMC (A6)	tBu6 carasiphenol C/ tBu6 wilsonol A 1 (B9)	tBu6 carasiphenol C/ tBu6 wilsonol A 1 (B10)	tBu6 carasiphenol C/ tBu6 wilsonol A 2 (C1)	tBu6 carasiphenol C/ tBu6 wilsonol A 2 (C2)	tBu6 carasiphenol C/ tBu6 wilsonol A 3 (C3)	tBu6 carasiphenol C/ tBu6 wilsonol A 3 (C4)
Conc. (μM)	5	5	5	5	5	5	5	5	5
t_{inh} (s)	4698.56059	4436.44094	4665.22629	18171.9382	15724.1444	17012.4678	18469.7523	16545.7448	17385.3267
*k*p	894	894	894	894	894	894	894	894	894
Ri	2.13E-09	2.25E-09	2.14E-09	2.18E-09	2.18E-09	2.18E-09	2.18E-09	2.18E-09	2.18E-09
[AOX] (M)	5.00E-06	5.00E-06	5.00E-06	5.00E-06	5.00E-06	5.00E-06	5.00E-06	5.00E-06	5.00E-06
[Dye] (M)	1.00E-05	1.00E-05	1.00E-05	1.00E-05	1.00E-05	1.00E-05	1.00E-05	1.00E-05	1.00E-05
n	2.00E+00	2.00E+00	2.00E+00	7.91E+00	6.84E+00	7.40E+00	8.04E+00	7.20E+00	7.56E+00
k_{inh} (M^{-1} s^{-1})	4.94E+05	4.78E+05	5.85E+05	3.89E+04	3.22E+04	3.50E+04	4.00E+04	3.74E+04	3.73E+04
Rate	3.85E-12	4.21E-12	3.28E-12	1.26E-11	1.77E-11	1.50E-11	1.21E-11	1.45E-11	1.38E-11

Table S26.5 – Dose response for ferroptosis inhibition

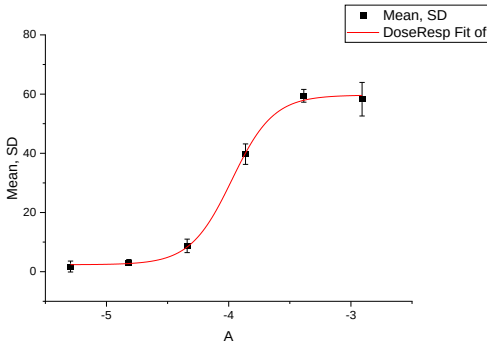

Dose responsive curve x axis = log(mM); y axis = % viability.

tBu6 carasiphenol C/ tBu6 wilsonol A 1		tBu6 carasiphenol C/ tBu6 wilsonol A 2		tBu6 carasiphenol C/ tBu6 wilsonol A 3	
Log(con)mM	% viability	Log(con)mM	% viability	Log(con)mM	% viability
-1.95425	4.657231	-1.95425	18.23878	-1.95425	22.4185
-2.25528	10.05879	-2.25528	34.03471	-2.25528	36.77779
-2.55631	17.3565	-2.55631	55.4468	-2.55631	49.85316
-2.85734	18.85347	-2.85734	56.04021	-2.85734	55.85957
-3.15837	21.24862	-3.15837	60.20112	-3.15837	56.39084
-3.4594	11.25636	-3.4594	43.85418	-3.4594	43.01294
-3.76043	9.703257	-3.76043	34.41618	-3.76043	33.76721
-4.06146	2.711174	-4.06146	13.40676	-4.06146	15.81441
-4.36249	-6.25815	-4.36249	1.651649	-4.36249	6.214489
-4.66352	-7.568	-4.66352	-1.14584	-4.66352	4.709199

S27 – (±)-tBu$_6$-C8/C12 trimer (summary and organic solution autoxidation)

Synthesis of this molecule is described in Chapter 3 of this dissertation. See Experimental for details.

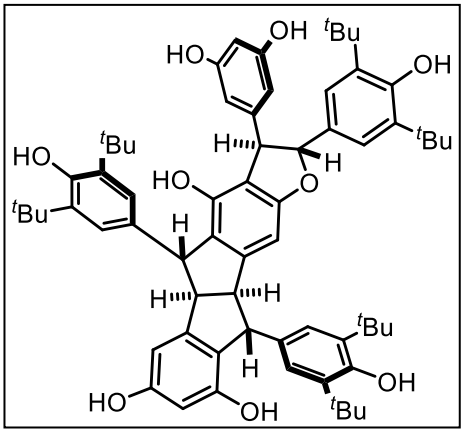

Table S27.1 – Summary of kinetic and cell data

Compound	Organic Solutions		Liposomes		Cells
	k_{inh} (hexadecene) (M^{-1} s^{-1}); n	k_{inh} (cumene) (M^{-1} s^{-1}); n	k_{inh} (DTUN) (M^{-1} s^{-1}); n	k_{inh} (V70) (M^{-1} s^{-1}); n	EC_{50}
tBu6 C8/C12 trimer	(5.68 ± 0.33)E+04; n=5.27 ± 0.49	(7.53 ± 1.78)E+03; n= 7.95 ± 0.31	DNI	N/A	1.7 ± 0.3 μM

Table S27.2 – Summary of hexadecane co-oxidation inhibition kinetics

Hexadecene	PMC	tBu6 C8/C12 trimer	PMC	tBu6 C8/C12 trimer	PMC	tBu6 C8/C12 trimer
Conc. (μM)	2	5	2	5	2	5
t_{inh} (s)	4886	33027.0874	4119	29258.0059	4625	27330.7217
*k*p	3791.88926	3791.88926	3791.88926	3791.88926	3791.88926	3791.88926
Ri	8.19E-10	8.19E-10	9.71E-10	9.71E-10	8.65E-10	8.65E-10
[AOX] (M)	2.00E-06	5.00E-06	2.00E-06	5.00E-06	2.00E-06	5.00E-06
[Dye] (M)	1.00E-05	1.00E-05	1.00E-05	1.00E-05	1.00E-05	1.00E-05
n	2.00E+00	5.41E+00	2.00E+00	5.68E+00	2.00E+00	4.73E+00
log *k*	6.12581094	4.74098043	6.4323787	4.78318712	6.20428119	4.73839129
k_{inh} (M^{-1} s^{-1})	1.34E+06	5.51E+04	2.71E+06	6.07E+04	1.60E+06	5.48E+04
Rate	5.8087E-12	2.0845E-11	3.4013E-12	2.1351E-11	5.1227E-12	2.534E-11

Table S27.3 – Summary of cumene co-oxidation inhibition kinetics

Cumene	PMC	tBu6 C8/C12 trimer	PMC	tBu6 C8/C12 trimer	PMC	tBu6 C8/C12 trimer
Conc. (μM)	2	5	2	5	2	5
t_{inh} (s)	2532	24141.21	2357	23493.01	2231	22977.27
*k*p	141	141	141	141	141	141
Ri	1.58E-09	1.58E-09	1.70E-09	1.70E-09	1.79E-09	1.79E-09
[AOX] (M)	2.00E-06	5.00E-06	2.00E-06	5.00E-06	2.00E-06	5.00E-06
[Dye] (M)	1.00E-05	1.00E-05	1.00E-05	1.00E-05	1.00E-05	1.00E-05
n	2.00E+00	7.63E+00	2.00E+00	7.97E+00	2.00E+00	8.24E+00
log *k*	5.034121	3.849867	6.057932	3.97725	5.114031	3.77977
k_{inh} (M^{-1} s^{-1})	1.08E+05	7.08E+03	1.14E+06	9.49E+03	1.30E+05	6.02E+03
Rate	5.15E-12	8.25E-12	5.23E-13	6.32E-12	4.86E-12	1.02E-11

Table S27.4 – Summary of liposome autoxidation inhibition assay using DTUN initiator

Liposomes (DTUN)	PMC (A4)	PMC (A5)	PMC (A6)	tBu6 carasiphenol C/ tBu6 wilsonol A 1 (B9)	tBu6 carasiphenol C/ tBu6 wilsonol A 1 (B10)	tBu6 carasiphenol C/ tBu6 wilsonol A 2 (C1)	tBu6 carasiphenol C/ tBu6 wilsonol A 2 (C2)	tBu6 carasiphenol C/ tBu6 wilsonol A 3 (C3)	tBu6 carasiphenol C/ tBu6 wilsonol A 3 (C4)
Conc. (μM)	5	5	5	5	5	5	5	5	5
t_{inh} (s)	4698.56059	4436.44094	4665.22629	0	0	0	0	0	0
*k*p	894	894	894	894	894	894	894	894	894
Ri	2.13E-09	2.25E-09	2.14E-09	2.18E-09	2.18E-09	2.18E-09	2.18E-09	2.18E-09	2.18E-09
[AOX] (M)	5.00E-06	5.00E-06	5.00E-06	5.00E-06	5.00E-06	5.00E-06	5.00E-06	5.00E-06	5.00E-06
[Dye] (M)	1.00E-05	1.00E-05	1.00E-05	1.00E-05	1.00E-05	1.00E-05	1.00E-05	1.00E-05	1.00E-05
n	2.00E+00	2.00E+00	2.00E+00	0.00E+00	0.00E+00	0.00E+00	0.00E+00	0.00E+00	0.00E+00
k_{inh} (M^{-1} s^{-1})	4.94E+05	4.78E+05	5.85E+05	#DIV/0!	#DIV/0!	#DIV/0!	#DIV/0!	#DIV/0!	#DIV/0!
Rate	3.85E-12	4.21E-12	3.28E-12	3.77E-11	3.71E-11	4.07E-11	1.00E+00	2.00E+00	3.00E+00

Table S27.5 – Dose response for ferroptosis inhibition

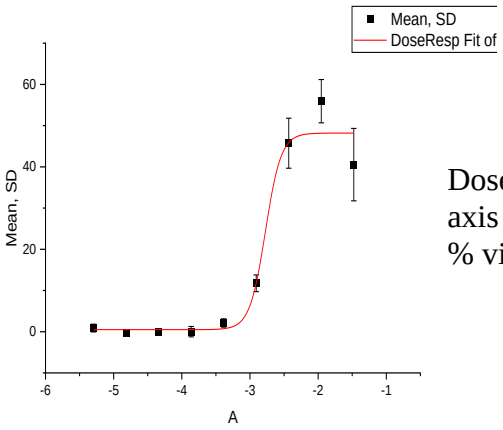

Dose responsive curve x axis = log(mM); y axis = % viability.

tBu C8/C12 trimer 1		tBu C8/C12 trimer 2		tBu C8/C12 trimer 3	
Log(con)mM	% viability	Log(con)mM	% viability	Log(con)mM	% viability
-1.954246852	27.14916133	-1.954246852	35.92089322	-1.954246852	38.57085934
-2.255276848	22.73310844	-2.255276848	36.50017131	-2.255276848	51.49864967
-2.556306844	10.43926628	-2.556306844	21.55197078	-2.556306844	44.85028261
-2.857336839	-0.619578042	-2.857336839	10.7858755	-2.857336839	25.41432387
-3.158366835	-5.840250742	-3.158366835	2.245055826	-3.158366835	12.49391243
-3.459396831	-8.877846447	-3.459396831	-1.421350636	-3.459396831	7.889493957
-3.760426826	-9.925723404	-3.760426826	-2.911932069	-3.760426826	5.233098685
-4.061456822	-11.26051905	-4.061456822	-4.529672107	-4.061456822	2.244654005
-4.362486818	-11.32289268	-4.362486818	-3.477081427	-4.362486818	2.539809035
-4.663516813	-10.92993882	-4.663516813	-4.28948363	-4.663516813	2.44388365

S28 – (±)-vitisin A (summary and organic solution autoxidation)

Synthesis of this molecule is described in some detail in Chapter 3 of this dissertation. See the published literature for details.[101]

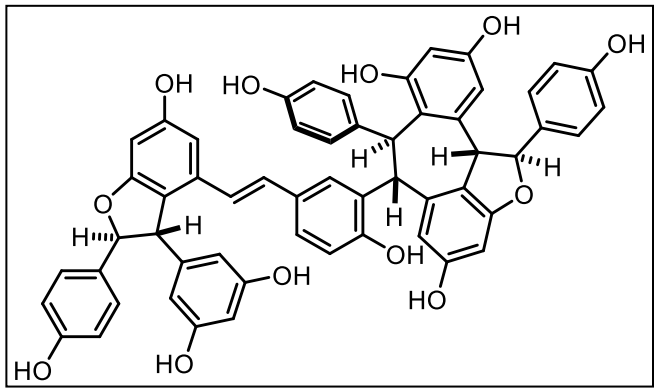

Table S28.1 – Summary of kinetic and cell data

Compound	Organic Solutions		Liposomes		Cells
	k_{inh} (hexadecene) (M^{-1} s^{-1}); n	k_{inh} (cumene) (M^{-1} s^{-1}); n	k_{inh} (DTUN) (M^{-1} s^{-1}); n	k_{inh} (V70) (M^{-1} s^{-1}); n	EC_{50}
vitisin A	DNI	(5.45 ± 0.36)E+03; n= 1.70 ± 0.39	(1.29 ± 0.04)E+04; n= 2*	(1.58 ± 0.06)E+04; n= 2*	11.9 ± 2.2 μM

Table S28.2 – Summary of hexadecane co-oxidation inhibition kinetics

Hexadecene	PMC	vitisin A	vitisin A	PMC	vitisin A
Conc. (μM)	2	5	5	2	5
t_{inh} (s)	2551.41369	0	0	3159.20393	0
*k*p	3791.88926	3791.88926	3791.88926	3791.88926	3791.88926
Ri	1.57E-09	1.57E-09	1.57E-09	1.27E-09	1.27E-09
[AOX] (M)	2.00E-06	5.00E-06	5.00E-06	2.00E-06	5.00E-06
[Dye] (M)	1.00E-05	1.00E-05	1.00E-05	1.00E-05	1.00E-05
n	2.00E+00	0.00E+00	0.00E+00	2.00E+00	0.00E+00
log *k*	6.43542711	#DIV/0!	#DIV/0!	6.26208005	#DIV/0!
k_{inh} (M^{-1} s^{-1})	2.73E+06	#DIV/0!	#DIV/0!	1.83E+06	#DIV/0!
Rate	5.4532E-12	0	0	6.5644E-12	0

Table S28.3 – Summary of cumene co-oxidation inhibition kinetics

Cumene	PMC	vitisin A	PMC	vitisin A	PMC	vitisin A
Conc. (μM)	2	5	2	5	2	5
t_{inh} (s)	1594	2772	1516	2975	1559	4170
*k*p	141	141	141	141	141	141
Ri	2.51E-09	2.51E-09	2.64E-09	2.64E-09	2.57E-09	2.57E-09
[AOX] (M)	2.00E-06	5.00E-06	2.00E-06	5.00E-06	2.00E-06	5.00E-06
[Dye] (M)	1.00E-05	1.00E-05	1.00E-05	1.00E-05	1.00E-05	1.00E-05
n	2.00E+00	1.39E+00	2.00E+00	1.57E+00	2.00E+00	2.14E+00
log *k*	5.60601	3.768356	5.274804	3.719703	5.247065	3.718414
k_{inh} (M^{-1} s^{-1})	4.04E+05	5.87E+03	1.88E+05	5.24E+03	1.77E+05	5.23E+03
Rate	2.19E-12	8.67E-11	4.94E-12	9.04E-11	5.12E-12	6.47E-11

Table S28.4 – Summary of liposome autoxidation inhibition assay using DTUN initiator

Liposomes (DTUN)	PMC (A4)	PMC (A5)	PMC (A6)	vitisin A (C8)	vitisin A (D8)	vitisin A(E8)
Conc. (μM)	5	5	5	5	5	5
t_{inh} (s)	4698.56059	4436.44094	4665.22629	10489.1354	8011.53531	9469.5781
*k*p	894	894	894	894	894	894
Ri	2.13E-09	2.25E-09	2.14E-09	5.43E-10	5.43E-10	5.43E-10
[AOX] (M)	5.00E-06	5.00E-06	5.00E-06	5.00E-06	5.00E-06	5.00E-06
[Dye] (M)	1.00E-05	1.00E-05	1.00E-05	1.00E-05	1.00E-05	1.00E-05
n	2.00E+00	2.00E+00	2.00E+00	2.00E+00	2.00E+00	2.00E+00
k_{inh} (M^{-1} s^{-1})	4.94E+05	4.78E+05	5.85E+05	2.48E+04	2.41E+04	2.31E+04
Rate	3.85E-12	4.21E-12	3.28E-12	1.96E-11	2.01E-11	2.10E-11

Table S28.5 – Summary of liposome autoxidation inhibition assay using V70 initiator

Liposomes (V70)	PMC (C3)	PMC (D3)	PMC (E3)	vitisin A (C8)	vitisin A (D8)	vitisin A(E8)
Conc. (μM)	5	5	5	5	5	5
t_{inh} (s)	11154.63502	13130.18442	12579.08609	10489.1354	8011.53531	9469.5781
*k*p	894	894	894	894	894	894
Ri	8.96E-10	7.62E-10	7.95E-10	7.79E-10	7.79E-10	7.79E-10
[AOX] (M)	5.00E-06	5.00E-06	5.00E-06	5.00E-06	5.00E-06	5.00E-06
[Dye] (M)	1.00E-05	1.00E-05	1.00E-05	1.00E-05	1.00E-05	1.00E-05
n	2.00E+00	2.00E+00	2.00E+00	2.00E+00	2.00E+00	2.00E+00
k_{inh} (M^{-1} s^{-1})	1.34E+05	1.21E+05	1.14E+05	2.88E+04	3.08E+04	2.86E+04
Rate	6.00E-12	5.62948E-12	6.23606E-12	2.42E-11	2.27E-11	2.44E-11

Table S28.6 – Dose response for ferroptosis inhibition

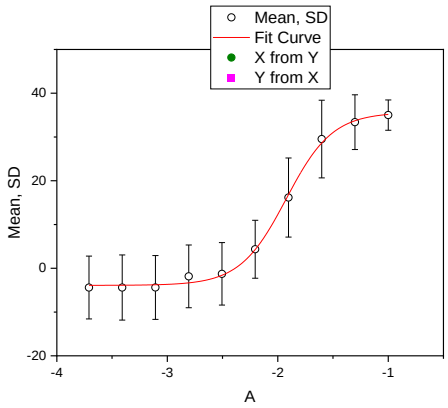

Dose responsive curve x axis = log(mM); y axis = % viability.

vitisin A 1		vitisin A 2		vitisin A 3	
Log(con)mM	% viability	Log(con)mM	% viability	Log(con)mM	% viability
-1	31.04751	-1	37.48212	-1	36.48264
-1.30103	28.77088	-1.30103	30.89813	-1.30103	40.49675
-1.60206	19.30256	-1.60206	35.10849	-1.60206	34.18781
-1.90309	5.93589	-1.90309	19.54569	-1.90309	23.03833
-2.20412	-2.61553	-2.20412	5.084931	-2.20412	10.56803
-2.50515	-8.64706	-2.50515	-0.77143	-2.50515	5.602042
-2.80618	-9.28328	-2.80618	-1.273	-2.80618	5.019111
-3.10721	-12.0714	-3.10721	-3.49121	-3.10721	2.414368
-3.40824	-12.1899	-3.40824	-3.6325	-3.40824	2.628356
-3.70927	-11.7782	-3.70927	-3.94333	-3.70927	2.539809

S29 – (±)-vitisin B (summary and organic solution autoxidation)

Synthesis of this molecule is described in some detail in Chapter 3 of this dissertation. See the published literature for details.[101]

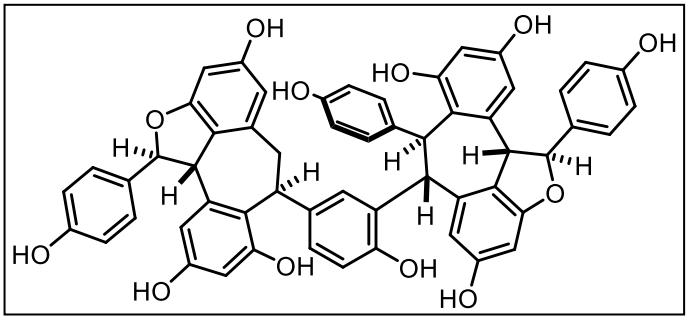

Table S29.1 – Summary of kinetic and cell data

Compound	Organic Solutions		Liposomes		Cells
	k_{inh} (hexadecene) (M^{-1} s^{-1}); n	k_{inh} (cumene) (M^{-1} s^{-1}); n	k_{inh} (DTUN) (M^{-1} s^{-1}); n	k_{inh} (V70) (M^{-1} s^{-1}); n	EC_{50}
vitisin D	DNI	(5.80 ± 0.06)E+03; n= 1.51 ± 0.19	(6.78 ± 0.03)E+03; n= 2*	(8.11 ± 0.03)E+03; n= 2*	12.1 ± 2.5 μM

Table S29.2 – Summary of hexadecane co-oxidation inhibition kinetics

Hexadecene	PMC	vitisin D	PMC	vitisin D	vitisin D
Conc. (μM)	2	5	5	5	5
t_{inh} (s)	2551.41369	0	0	0	0
*k*p	3791.88926	3791.88926	3791.88926	3791.88926	3791.88926
Ri	1.57E-09	1.57E-09	1.57E-09	1.27E-09	1.27E-09
[AOX] (M)	2.00E-06	5.00E-06	5.00E-06	5.00E-06	5.00E-06
[Dye] (M)	1.00E-05	1.00E-05	1.00E-05	1.00E-05	1.00E-05
n	2.00E+00	0.00E+00	0.00E+00	0.00E+00	0.00E+00
log *k*	6.43542711	#DIV/0!	#DIV/0!	6.26208005	#DIV/0!
k_{inh} (M^{-1} s^{-1})	2.73E+06	#DIV/0!	#DIV/0!	1.83E+06	#DIV/0!
Rate	5.4532E-12	0	0	6.5644E-12	0

Table S29.3 – Summary of cumene co-oxidation inhibition kinetics

Cumene	PMC	vitisin D	PMC	vitisin D	PMC	vitisin D
Conc. (μM)	2	5	2	5	2	5
t_{inh} (s)	1594	2714.167	1516	2739.381	1559	3360.509
*k*p	141	141	141	141	141	141
Ri	2.51E-09	2.51E-09	2.64E-09	2.64E-09	2.57E-09	2.57E-09
[AOX] (M)	2.00E-06	5.00E-06	2.00E-06	5.00E-06	2.00E-06	5.00E-06
[Dye] (M)	1.00E-05	1.00E-05	1.00E-05	1.00E-05	1.00E-05	1.00E-05
n	2.00E+00	1.36E+00	2.00E+00	1.45E+00	2.00E+00	1.72E+00
log *k*	5.60601	3.78867	5.274804	3.707307	5.247065	3.789378
k_{inh} (M^{-1} s^{-1})	4.04E+05	6.15E+03	1.88E+05	5.10E+03	1.77E+05	6.16E+03
Rate	2.19E-12	8.45E-11	4.94E-12	1.01E-10	5.12E-12	6.81E-11

Table S29.4 – Summary of liposome autoxidation inhibition assay using DTUN initiator

Liposomes (DTUN)	PMC (A4)	PMC (A5)	PMC (A6)	vitisin D (C10)	vitisin D (D10)	vitisin D (E10)
Conc. (μM)	5	5	5	5	5	5
t_{inh} (s)	4698.56059	4436.44094	4665.22629	5440.283364	5155.72826	5176.59079
*k*p	894	894	894	894	894	894
Ri	2.13E-09	2.25E-09	2.14E-09	5.43E-10	5.43E-10	5.43E-10
[AOX] (M)	5.00E-06	5.00E-06	5.00E-06	5.00E-06	5.00E-06	5.00E-06
[Dye] (M)	1.00E-05	1.00E-05	1.00E-05	1.00E-05	1.00E-05	1.00E-05
n	2.00E+00	2.00E+00	2.00E+00	2.00E+00	2.00E+00	2.00E+00
k_{inh} (M^{-1} s^{-1})	4.94E+05	4.78E+05	5.85E+05	1.29E+04	1.31E+04	1.19E+04
Rate	3.85E-12	4.21E-12	3.28E-12	3.77E-11	3.71E-11	4.07E-11

Table S29.5 – Summary of liposome autoxidation inhibition assay using V70 initiator

Liposomes (V70)	PMC (C3)	PMC (D3)	PMC (E3)	vitisin D (C10)	vitisin D (D10)	vitisin D (E10)
Conc. (μM)	5	5	5	5	5	5
t_{inh} (s)	11154.63502	13130.18442	12579.08609	5440.283364	5155.72826	5176.59079
*k*p	894	894	894	894	894	894
Ri	8.96E-10	7.62E-10	7.95E-10	7.79E-10	7.79E-10	7.79E-10
[AOX] (M)	5.00E-06	5.00E-06	5.00E-06	5.00E-06	5.00E-06	5.00E-06
[Dye] (M)	1.00E-05	1.00E-05	1.00E-05	1.00E-05	1.00E-05	1.00E-05
n	2.00E+00	2.00E+00	2.00E+00	2.00E+00	2.00E+00	2.00E+00
k_{inh} (M^{-1} s^{-1})	1.34E+05	1.21E+05	1.14E+05	1.55E+04	1.53E+04	1.46E+04
Rate	6.00E-12	5.62948E-12	6.23606E-12	4.50E-11	4.56E-11	4.7798E-11

Table S29.6 – Dose response for ferroptosis inhibition

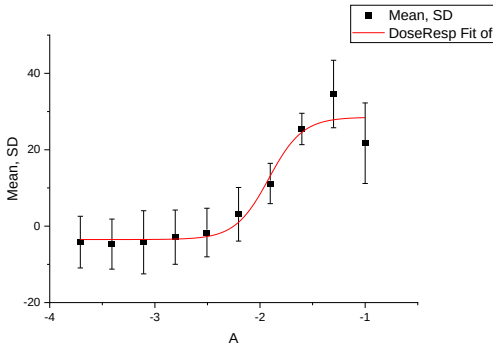

Dose responsive curve x axis = log(mM); y axis = % viability.

vitisin D 1		vitisin D 2		vitisin D 3	
Log(con)mM	% viability	Log(con)mM	% viability	Log(con)mM	% viability
-1	31.04751	-1	37.48212	-1	36.48264
-1.30103	28.77088	-1.30103	30.89813	-1.30103	40.49675
-1.60206	19.30256	-1.60206	35.10849	-1.60206	34.18781
-1.90309	5.93589	-1.90309	19.54569	-1.90309	23.03833
-2.20412	-2.61553	-2.20412	5.084931	-2.20412	10.56803
-2.50515	-8.64706	-2.50515	-0.77143	-2.50515	5.602042
-2.80618	-9.28328	-2.80618	-1.273	-2.80618	5.019111
-3.10721	-12.0714	-3.10721	-3.49121	-3.10721	2.414368
-3.40824	-12.1899	-3.40824	-3.6325	-3.40824	2.628356
-3.70927	-11.7782	-3.70927	-3.94333	-3.70927	2.539809

S30 – (±)-tBu$_4$-reduced quadrangularin A (OBn$_4$) (summary and organic solution autoxidation)

Synthesis of this molecule is described in Chapter 3 of this dissertation. See Experimental for details.

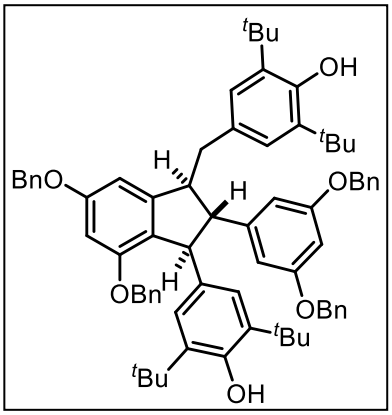

Table S30.1 – Summary of kinetic and cell data

Compound	Organic Solutions		Liposomes		Cells
	k_{inh} (hexadecene) (M^{-1} s^{-1}); n	k_{inh} (cumene) (M^{-1} s^{-1}); n	k_{inh} (DTUN) (M^{-1} s^{-1}); n	k_{inh} (V70) (M^{-1} s^{-1}); n	EC_{50}
tBu4-reduced quadrangularin A (OBn4)	reduced tBu-CPQM-OBn	(5.43 ± 0.30)E+04; n=3.09 ± 0.32	(9.53 ± 1.11)E+03; n= 3.75 ± 0.29	DNI	N/A

Table S30.2 – Summary of hexadecane co-oxidation inhibition kinetics

Hexadecene	PMC	tBu4-reduced quadrangularin A (OBn4)	PMC	tBu4-reduced quadrangularin A (OBn4)	PMC	tBu4-reduced quadrangularin A (OBn4)
Conc. (μM)	2	5	2	5	2	5
t_{inh} (s)	4573	16854	4692	16751	4265	18419
*k*p	3791.88926	3791.88926	3791.88926	3791.88926	3791.88926	3791.88926
Ri	8.75E-10	8.75E-10	8.52E-10	8.52E-10	9.38E-10	9.38E-10
[AOX] (M)	2.00E-06	5.00E-06	2.00E-06	5.00E-06	2.00E-06	5.00E-06
[Dye] (M)	1.00E-05	1.00E-05	1.00E-05	1.00E-05	1.00E-05	1.00E-05
n	2.00E+00	2.95E+00	2.00E+00	2.86E+00	2.00E+00	3.46E+00
log *k*	6.15961906	4.70815935	6.19640331	4.73741634	6.34134974	4.75641129
k_{inh} (M^{-1} s^{-1})	1.44E+06	5.11E+04	1.57E+06	5.46E+04	2.19E+06	5.71E+04
Rate	5.7412E-12	4.4055E-11	5.1411E-12	4.1437E-11	4.0514E-12	3.6072E-11

Table S30.3 – Summary of cumene co-oxidation inhibition kinetics

Cumene	PMC	tBu6 C8/C12 trimer	PMC	tBu6 C8/C12 trimer	PMC	tBu6 C8/C12 trimer
Conc. (μM)	2	5	2	5	2	5
t_{inh} (s)	2508	10734	2337	11630	2379	11455
*k*p	141	141	141	141	141	141
Ri	1.59E-09	1.59E-09	1.71E-09	1.71E-09	1.68E-09	1.68E-09
[AOX] (M)	2.00E-06	5.00E-06	2.00E-06	5.00E-06	2.00E-06	5.00E-06
[Dye] (M)	1.00E-05	1.00E-05	1.00E-05	1.00E-05	1.00E-05	1.00E-05
n	2.00E+00	3.42E+00	2.00E+00	3.98E+00	2.00E+00	3.85E+00
log *k*	5.338556	3.930685	5.724708	3.970862	5.698546	4.030089
k_{inh} (M^{-1} s^{-1})	2.18E+05	8.52E+03	5.31E+05	9.35E+03	5.00E+05	1.07E+04
Rate	2.58E-12	1.54E-11	1.14E-12	1.3E-11	1.19E-12	1.15E-11

S31 – (±)-tBu$_4$-cyclized paraquinone methide dimer (tBu$_4$-CPQM-OH) (summary and organic solution autoxidation)

Synthesis of this molecule is described in Chapter 3 of this dissertation. See Experimental for details.

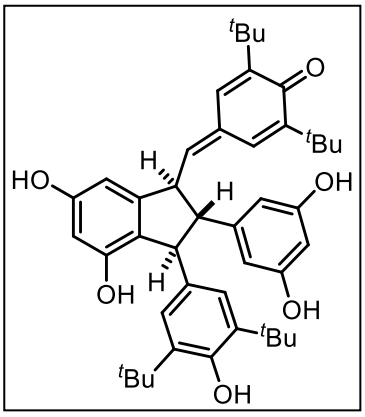

Table S31.1 – Summary of kinetic and cell data

Compound	Organic Solutions		Liposomes		Cells
	k_{inh} (hexadecene) (M^{-1} s^{-1}); n	k_{inh} (cumene) (M^{-1} s^{-1}); n	k_{inh} (DTUN) (M^{-1} s^{-1}); n	k_{inh} (V70) (M^{-1} s^{-1}); n	EC_{50}
tBu4-CPQM-OH	(1.09 ± 0.14)E+05; n=2.52 ± 0.13	(5.51 ± 0.96)E+03; n= 5.24 ± 0.21	(8.31 ± 0.38)E+04; n= 2.40 ± 0.04	N/A	N/A

Table S31.2 – Summary of hexadecane co-oxidation inhibition kinetics

Hexadecene	PMC	tBu4-CPQM-OH	PMC	tBu4-CPQM-OH	PMC	tBu4-CPQM-OH
Conc. (μM)	2	5	2	5	2	5
t_{inh} (s)	4886	33027.0874	4119	29258.0059	4625	27330.7217
*k*p	3791.88926	3791.88926	3791.88926	3791.88926	3791.88926	3791.88926
Ri	8.19E-10	8.19E-10	9.71E-10	9.71E-10	8.65E-10	8.65E-10
[AOX] (M)	2.00E-06	5.00E-06	2.00E-06	5.00E-06	2.00E-06	5.00E-06
[Dye] (M)	1.00E-05	1.00E-05	1.00E-05	1.00E-05	1.00E-05	1.00E-05
n	2.00E+00	5.41E+00	2.00E+00	5.68E+00	2.00E+00	4.73E+00
log *k*	6.12581094	4.74098043	6.4323787	4.78318712	6.20428119	4.73839129
k_{inh} (M^{-1} s^{-1})	1.34E+06	5.51E+04	2.71E+06	6.07E+04	1.60E+06	5.48E+04
Rate	5.8087E-12	2.0845E-11	3.4013E-12	2.1351E-11	5.1227E-12	2.534E-11

Table S31.3 – Summary of cumene co-oxidation inhibition kinetics

Cumene	PMC	tBu4-CPQM-OH	PMC	tBu4-CPQM-OH	PMC	tBu4-CPQM-OH
Conc. (μM)	2	5	2	5	2	5
t inh (s)	4886	18006.4401	4229	12981.5102	4119	13719.0785
kp	3791.88926	3791.88926	3791.88926	3791.88926	3791.88926	3791.88926
Ri	8.19E-10	8.19E-10	9.46E-10	9.46E-10	9.71E-10	9.71E-10
[AOX] (M)	2.00E-06	5.00E-06	2.00E-06	5.00E-06	2.00E-06	5.00E-06
[Dye] (M)	1.00E-05	1.00E-05	1.00E-05	1.00E-05	1.00E-05	1.00E-05
n	2.00E+00	2.95E+00	2.00E+00	2.46E+00	2.00E+00	2.66E+00
log k	6.12581094	4.96100944	6.24327873	5.02751798	6.4323787	5.09714759
kinh	1.34E+06	9.14E+04	1.75E+06	1.07E+05	2.71E+06	1.25E+05
Rate	5.8087E-12	2.3037E-11	5.1203E-12	2.7417E-11	3.4013E-12	2.21E-11

Table S31.4 – Summary of liposome autoxidation inhibition assay using DTUN initiator

Liposomes (DTUN)	PMC (A4)	PMC (A5)	PMC (A6)	CPQM-OH 1 (B3)	CPQM-OH 1 (B4)	CPQM-OH 2 (B5)	CPQM-OH 2 (B6)	CPQM-OH 3 (B7)	CPQM-OH 3 (B8)
Conc. (μM)	5	5	5	5	5	5	5	5	5
t_{inh} (s)	4698.56059	4436.44094	4665.22629	5627.220047	5570.579817	5452.93389	5576.924309	5527.062401	5343.687549
*k*p	894	894	894	894	894	894	894	894	894
Ri	2.13E-09	2.25E-09	2.14E-09	2.18E-09	2.18E-09	2.18E-09	2.18E-09	2.18E-09	2.18E-09
[AOX] (M)	5.00E-06	5.00E-06	5.00E-06	5.00E-06	5.00E-06	5.00E-06	5.00E-06	5.00E-06	5.00E-06
[Dye] (M)	1.00E-05	1.00E-05	1.00E-05	1.00E-05	1.00E-05	1.00E-05	1.00E-05	1.00E-05	1.00E-05
n	2.00E+00	2.00E+00	2.00E+00	2.45E+00	2.42353245	2.37E+00	2.43E+00	2.40E+00	2.32E+00
k_{inh} (M^{-1} s^{-1})	4.94E+05	4.78E+05	5.85E+05	8.08E+04	8.62E+04	8.17E+04	7.97E+04	8.07E+04	8.92E+04
Rate	3.85E-12	4.21E-12	3.28E-12	1.97E-11	1.86E-11	2.01E-11	2.01E-11	2.00E-11	1.87E-11

S32 – tBu_2-reduced resveratrol (tBu_2-RSV [sat]) (summary and organic solution autoxidation)

Synthesis of this molecule is described in Chapter 3 of this dissertation. See Experimental for details.

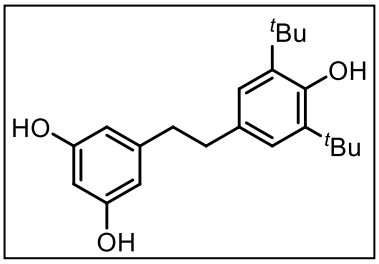

Table S32.1 – Summary of kinetic and cell data

Compound	Organic Solutions		Liposomes		Cells
	k_{inh} (hexadecene) (M^{-1} s^{-1}); n	k_{inh} (cumene) (M^{-1} s^{-1}); n	k_{inh} (DTUN) (M^{-1} s^{-1}); n	k_{inh} (V70) (M^{-1} s^{-1}); n	EC_{50}
tBu2-RSV [sat]	(1.08 ± 0.19)E+05; n=2.26 ± 0.21	(7.21 ± 0.94)E+03; n=4.38 ± 0.79	N/A	N/A	N/A

Table S32.2 – Summary of hexadecane co-oxidation inhibition kinetics

Hexadecene	PMC	tBu2-RSV [sat]	PMC	tBu2-RSV [sat]	PMC	tBu2-RSV [sat]
Conc. (μM)	2	5	2	5	2	5
t_{inh} (s)	4152	12582	4529	11442	4307	12634
*k*p	3791.88926	3791.88926	3791.88926	3791.88926	3791.88926	3791.88926
Ri	9.63E-10	9.63E-10	8.83E-10	8.83E-10	9.29E-10	9.29E-10
[AOX] (M)	2.00E-06	5.00E-06	2.00E-06	5.00E-06	2.00E-06	5.00E-06
[Dye] (M)	1.00E-05	1.00E-05	1.00E-05	1.00E-05	1.00E-05	1.00E-05
n	2.00E+00	2.42E+00	2.00E+00	2.02E+00	2.00E+00	2.35E+00
log *k*	6.31801889	4.98804638	6.05190124	4.98829058	6.33257852	5.11451258
k_{inh} (M^{-1} s^{-1})	2.08E+06	9.73E+04	1.13E+06	9.73E+04	2.15E+06	1.30E+05
Rate	4.3915E-12	3.0978E-11	7.4294E-12	3.4045E-11	4.0931E-12	2.3056E-11

Table S33.3 – Summary of cumene co-oxidation inhibition kinetics

Cumene	PMC	tBu6 C8/C12 trimer	PMC	tBu6 C8/C12 trimer	PMC	tBu6 C8/C12 trimer
Conc. (μM)	2	5	2	5	2	5
t_{inh} (s)	1955	12764	2242	11948	3063	13972
*k*p	141	141	141	141	141	141
Ri	2.05E-09	2.05E-09	1.78E-09	1.78E-09	1.31E-09	1.31E-09
[AOX] (M)	2.00E-06	5.00E-06	2.00E-06	5.00E-06	2.00E-06	5.00E-06
[Dye] (M)	1.00E-05	1.00E-05	1.00E-05	1.00E-05	1.00E-05	1.00E-05
n	2.00E+00	5.22E+00	2.00E+00	4.26E+00	2.00E+00	3.65E+00
log *k*	5.231785	3.917972	5.018134	3.83735	5.593158	3.811736
k_{inh} (M^{-1} s^{-1})	1.71E+05	8.28E+03	1.04E+05	6.88E+03	3.92E+05	6.48E+03
Rate	4.23E-12	1.33E-11	6.03E-12	1.72E-11	1.17E-12	1.56E-11

S33 – (±) tBu_4-reduced ε-veniferin (tBu_4- ε-veniferin [sat]) (summary and organic solution autoxidation)

Synthesis of this molecule is described in Chapter 3 of this dissertation. See Experimental for details.

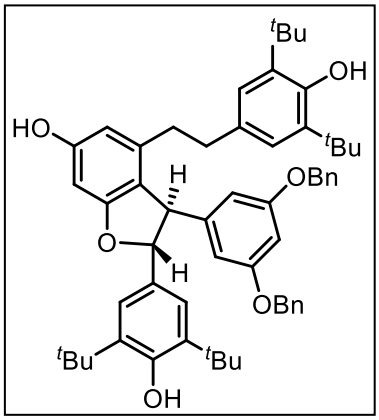

Table S33.1 – Summary of kinetic and cell data

Compound	Organic Solutions		Liposomes		Cells
	k_{inh} (hexadecene) (M^{-1} s^{-1}); n	k_{inh} (cumene) (M^{-1} s^{-1}); n	k_{inh} (DTUN) (M^{-1} s^{-1}); n	k_{inh} (V70) (M^{-1} s^{-1}); n	EC_{50}
tBu4-epsi-veniferin (OBn) [sat]	(1.21 ± 0.40)E+05; n=2.05 ± 0.24	(6.39 ± 0.57)E+03; n=5.03 ± 0.46	N/A	N/A	N/A

Table S33.2 – Summary of hexadecane co-oxidation inhibition kinetics

Hexadecene	PMC	tBu4-epsi-veniferin (OBn) [sat]	PMC	tBu4-epsi-veniferin (OBn) [sat]	PMC	tBu4-epsi-veniferin (OBn) [sat]
Conc. (μM)	2	5	2	5	2	5
t_{inh} (s)	4152	9743.85294	4529	11001.7366	4307	12532.3978
*k*p	3791.88926	3791.88926	3791.88926	3791.88926	3791.88926	3791.88926
Ri	9.63E-10	9.63E-10	8.83E-10	8.83E-10	9.29E-10	9.29E-10
[AOX] (M)	2.00E-06	5.00E-06	2.00E-06	5.00E-06	2.00E-06	5.00E-06
[Dye] (M)	1.00E-05	1.00E-05	1.00E-05	1.00E-05	1.00E-05	1.00E-05
n	2.00E+00	5.22265253	2.00E+00	1.94E+00	2.00E+00	2.33E+00
log *k*	6.31801889	1.67E+05	6.05190124	5.00419659	6.33257852	4.9825819
k_{inh} (M^{-1} s^{-1})	2.08E+06	2.3306E-11	1.13E+06	1.01E+05	2.15E+06	9.61E+04
Rate	4.3915E-12	5.22265253	7.4294E-12	3.4135E-11	4.0931E-12	3.1495E-11

Table S33.3 – Summary of cumene co-oxidation inhibition kinetics

Cumene	PMC	tBu4-epsi-veniferin (OBn) [sat]	PMC	tBu4-epsi-veniferin (OBn) [sat]	PMC	tBu4-epsi-veniferin (OBn) [sat]
Conc. (μM)	2	5	2	5	2	5
t_{inh} (s)	1955	13517	2242	13827	3063	17721
*k*p	141	141	141	141	141	141
Ri	2.05E-09	2.05E-09	1.78E-09	1.78E-09	1.31E-09	1.31E-09
[AOX] (M)	2.00E-06	5.00E-06	2.00E-06	5.00E-06	2.00E-06	5.00E-06
[Dye] (M)	1.00E-05	1.00E-05	1.00E-05	1.00E-05	1.00E-05	1.00E-05
n	2.00E+00	5.53E+00	2.00E+00	4.93E+00	2.00E+00	4.63E+00
log *k*	5.231785	3.848346	5.018134	3.777929	5.593158	3.787661
k_{inh} (M^{-1} s^{-1})	1.71E+05	7.05E+03	1.04E+05	6.00E+03	3.92E+05	6.13E+03
Rate	4.23E-12	1.48E-11	6.03E-12	1.7E-11	1.17E-12	1.3E-11

S34 – tBu_2-resveratrol $(OBn)_2$ (tBu_2-RSV-OBn_2) (summary and organic solution autoxidation)

Synthesis of this molecule is described in Chapter 2 of this dissertation. See Experimental for details.

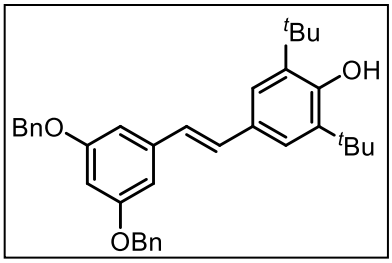

Table S34.1 – Summary of kinetic and cell data

Compound	Organic Solutions		Liposomes		Cells
	k_{inh} (hexadecene) (M^{-1} s^{-1}); n	k_{inh} (cumene) (M^{-1} s^{-1}); n	k_{inh} (DTUN) (M^{-1} s^{-1}); n	k_{inh} (V70) (M^{-1} s^{-1}); n	EC_{50}
tBu2- RSV-OBn2	(1.35 ± 0.35)E+05; n=2.63 ± 0.13	(7.96 ± 1.69)E+03; n=5.19 ± 0.73	N/A	N/A	N/A

Table S34.2 – Summary of hexadecane co-oxidation inhibition kinetics

Hexadecene	PMC	tBu4-epsi-veniferin (OBn) [sat]	PMC	tBu4-epsi-veniferin (OBn) [sat]	PMC	tBu4-epsi-veniferin (OBn) [sat]
Conc. (μM)	2	5	5	5	2	5
t_{inh} (s)	4152	14400	14337	11001.7366	4307	13829
*k*p	3791.88926	3791.88926	3791.88926	3791.88926	3791.88926	3791.88926
Ri	9.63E-10	9.63E-10	8.83E-10	8.83E-10	9.29E-10	9.29E-10
[AOX] (M)	2.00E-06	5.00E-06	5.00E-06	5.00E-06	2.00E-06	5.00E-06
[Dye] (M)	1.00E-05	1.00E-05	1.00E-05	1.00E-05	1.00E-05	1.00E-05
n	2.00E+00	2.77E+00	2.53E+00	1.94E+00	2.00E+00	2.57E+00
log *k*	6.31801889	5.1321516	4.99534095	5.00419659	6.33257852	5.22795159
k_{inh} (M^{-1} s^{-1})	2.08E+06	1.36E+05	9.89E+04	1.01E+05	2.15E+06	1.69E+05
Rate	4.3915E-12	1.9425E-11	2.6733E-11	3.4135E-11	4.0931E-12	1.6222E-11

Table S34.3 – Summary of cumene co-oxidation inhibition kinetics

Cumene	PMC	tBu6 C8/C12 trimer	PMC	tBu6 C8/C12 trimer	PMC	tBu6 C8/C12 trimer
Conc. (μM)	2	5	2	5	2	5
t_{inh} (s)	1955	14407	2242	14652	3063	16972
*k*p	141	141	141	141	141	141
Ri	2.05E-09	2.05E-09	1.78E-09	1.78E-09	1.31E-09	1.31E-09
[AOX] (M)	2.00E-06	5.00E-06	2.00E-06	5.00E-06	2.00E-06	5.00E-06
[Dye] (M)	1.00E-05	1.00E-05	1.00E-05	1.00E-05	1.00E-05	1.00E-05
n	2.00E+00	5.89E+00	2.00E+00	5.23E+00	2.00E+00	4.43E+00
log *k*	5.231785	3.995222	5.018134	3.860133	5.593158	3.829019
k_{inh} (M^{-1} s^{-1})	1.71E+05	9.89E+03	1.04E+05	7.25E+03	3.92E+05	6.75E+03
Rate	4.23E-12	9.9E-12	6.03E-12	1.33E-11	1.17E-12	1.23E-11

S35 – *bis*-butylhydroxytoluene (BHT) (summary and organic solution autoxidation)

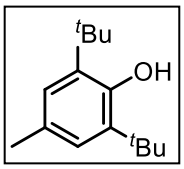

Table S35.1 – Summary of kinetic and cell data

Compound	Organic Solutions		Liposomes		Cells
	k_{inh} (hexadecene) (M^{-1} s^{-1}); n	k_{inh} (cumene) (M^{-1} s^{-1}); n	k_{inh} (DTUN) (M^{-1} s^{-1}); n	k_{inh} (V70) (M^{-1} s^{-1}); n	EC_{50}
BHT	N/A	(8.34 ± 0.69)E+03; n=2.30 ± 0.72	N/A	N/A	N/A

Table S35.2 – Summary of cumene co-oxidation inhibition kinetics

Cumene	PMC	BHT	PMC	BHT	PMC	BHT
Conc. (μM)	2	5	2	5	2	5
t_{inh} (s)	1998	7343	3994	7563	2407	7387
*k*p	141	141	141	141	141	141
Ri	2.00E-09	2.00E-09	1.00E-09	1.00E-09	1.66E-09	1.66E-09
[AOX] (M)	2.00E-06	5.00E-06	2.00E-06	5.00E-06	2.00E-06	5.00E-06
[Dye] (M)	1.00E-05	1.00E-05	1.00E-05	1.00E-05	1.00E-05	1.00E-05
n	2.00E+00	2.94E+00	2.00E+00	1.51E+00	2.00E+00	2.46E+00
log *k*	5.520901	3.955941	5.538634	3.883363	6.452746	3.920433
k_{inh} (M^{-1} s^{-1})	3.32E+05	9.04E+03	3.46E+05	7.64E+03	2.84E+06	8.33E+03
Rate	2.13E-12	2.13E-11	1.02E-12	2.44E-11	2.07E-13	2.29E-11

S36 – BHT/ Rescorcinol Synergy Experiments (constant resorcinol concentration)

Procedure. This experiment was set as the previously described cumene co-ocidation reactions. BHT and resorcinol were prepared as a 2.5mM stock solution. Equal volumes were added to make the 1:1 sample. Resorcinol was kept constant and decreasing aliquots of BHT were added to obtain the (1:5), (1:10) while maintaining a total antioxidant concentration of 5μM. Experiments were conducted at 37 °C employing cumene (3.6 M) and STY-BODIPY (10 μM) initiated by AIBN (6 mM) in chlorobenzene. Reaction progress was monitored at 571 nm. The rate of initiation, also determined using PMC, was measured to be $R_i = 2.28\times10^{-9}$ Ms^{-1} and the second order rate constant for propagation of the dye had been determined previously ($k_{STY\text{-}BODIPY}$ = 141 $M^{-1}s^{-1}$) (37 °C).

Table S36.1 – Summary of cumene co-oxidation inhibition kinetics

Cumene	PMC	BHT	BHT + resorcinol (1:1) (5uM)	BHT + resorcinol (1:5) (5uM)	BHT + resorcinol (1:10) (5uM)	BHT + resorcinol (1:1) (5uM)
Conc. (μM)	2	5				
t_{inh} (s)	1998	7343	5	3	2.75	5
*k*p	141	141	12738	6892	6762	12738
Ri	2.00E-09	2.00E-09	141	141	141	141
[AOX] (M)	2.00E-06	5.00E-06	2.00E-09	2.00E-09	2.00E-09	2.00E-09
[Dye] (M)	1.00E-05	1.00E-05	5.00E-06	3.00E-06	2.75E-06	5.00E-06
n	2.00E+00	2.94E+00	1.00E-05	1.00E-05	1.00E-05	1.00E-05
log *k*	5.520901	3.955941	3.95173269	4.013043	4.00632	3.95173269
k_{inh} (M^{-1} s^{-1})	3.32E+05	9.04E+03	8.95E+03	1.03E+04	1.01E+04	8.95E+03
Rate	2.13E-12	2.13E-11	1.23709E-11	1.99E-11	2.06E-11	1.23709E-11

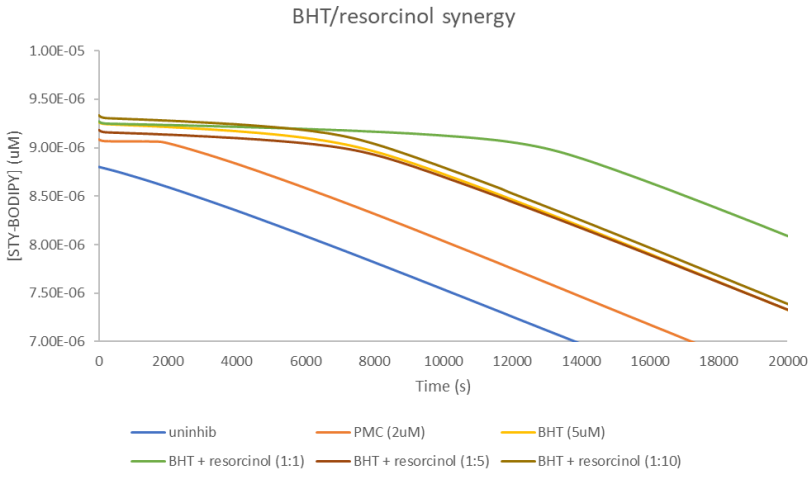

S37 – BHT/ Rescorcinol Synergy Experiments (constant BHT concentration)

Procedure. This experiment was set as the previously described cumene co-ocidation reactions. BHT and resorcinol were prepared as a 2.5mM stock solution. Equal volumes were added to make the 1:1 sample. BHT was kept constant and decreasing aliquots of resorcinol were added to obtain the (1:5), (1:10) while maintaining a total antioxidant concentration of 5μM. Experiments were conducted at 37 °C employing cumene (3.6 M) and STY-BODIPY (10 μM) initiated by AIBN (6 mM) in chlorobenzene. Reaction progress was monitored at 571 nm. The rate of initiation, also determined using PMC, was measured to be $R_i = 2.28\times10^{-9}$ Ms^{-1} and the second order rate constant for propagation of the dye had been determined previously ($k_{STY\text{-}BODIPY}$ = 141 $M^{-1}s^{-1}$) (37 °C).

Table S37.1 – Summary of cumene co-oxidation inhibition kinetics

Cumene	PMC	BHT	BHT + resorcinol (1:1) (5uM)	BHT + resorcinol (5:1) (5uM)	BHT + resorcinol (10:1) (5uM)
Conc. (μM)	2	5	5	3	2.75
t_{inh} (s)	3994	7563	11717	8656	7960
*k*p	141	141	141	141	141
Ri	1.00E-09	1.00E-09	1.00E-09	1.00E-09	1.00E-09
[AOX] (M)	2.00E-06	5.00E-06	5.00E-06	3.00E-06	2.75E-06
[Dye] (M)	1.00E-05	1.00E-05	1.00E-05	1.00E-05	1.00E-05
n	2.00E+00	1.51E+00	2.35E+00	2.89E+00	2.90E+00
log *k*	5.538633858	3.8833633	4.157335336	3.966759481	3.976778825
k_{inh} (M^{-1} s^{-1})	3.46E+05	7.64E+03	1.44E+04	9.26E+03	9.48E+03
Rate	1.02126E-12	2.4387E-11	8.3766E-12	1.7585E-11	1.86872E-11

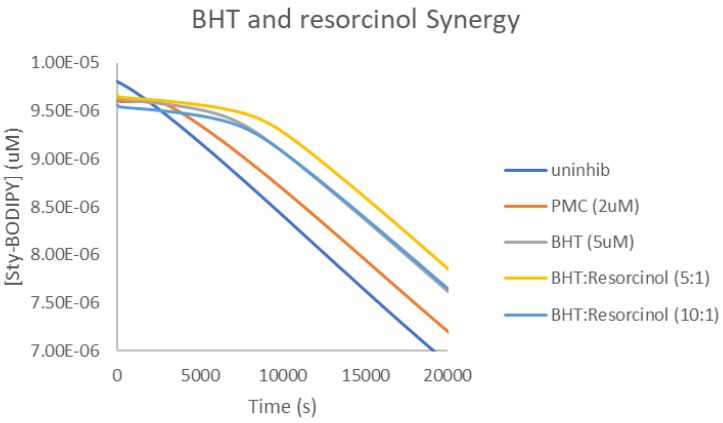
BHT and resorcinol Synergy
1.00E-05
9.50E-06
9.00E-06
8.50E-06
8.00E-06
7.50E-06
7.00E-06
[Sty-BODIPY] (uM)
0
5000
10000
15000
20000
Time (s)
uninhib
PMC (2uM)
BHT (5uM)
BHT:Resorcinol (5:1)
BHT:Resorcinol (10:1)

REFERENCES

1. Galliher, M. S.; Roldan, B. J.; Stephenson, C. R. J., Evolution towards green radical generation in total synthesis. *Chemical Society Reviews* **2021,** *50* (18), 10044-10057.
2. Romero, K. J.; Galliher, M. S.; Pratt, D. A.; Stephenson, C. R. J., Radicals in natural product synthesis. *Chemical Society Reviews* **2018,** *47* (21), 7851-7866.
3. Li, A.-N.; Li, S.; Zhang, Y.-J.; Xu, X.-R.; Chen, Y.-M.; Li, H.-B. Resources and Biological Activities of Natural Polyphenols *Nutrients* [Online], 2014, p. 6020-6047.
4. Neha, K.; Haider, M. R.; Pathak, A.; Yar, M. S., Medicinal prospects of antioxidants: A review. *European Journal of Medicinal Chemistry* **2019,** *178*, 687-704.
5. Renaud, S.; de Lorgeril, M., Wine, alcohol, platelets, and the French paradox for coronary heart disease. *The Lancet* **1992,** *339* (8808), 1523-1526.
6. Law, M.; Stampfer, M.; Barker, D. J. P.; Mackenbach, J. P.; Wald, N.; Rimm, E.; Kunst, A. E., Why heart disease mortality is low in France: the time lag explanation. *BMJ* **1999,** *318* (7196), 1471.
7. Resveratrol market by product type (natural resveratrol and synthetic resveratrol), form (powder and liquid), application (neutraceuticals, pharmaceuticals, cosmetic and others): Global Analysis and Industry Forecast, 2021-2030. https://www.alliedmarketresearch.com/resveratrol-market-A14242.
8. Resveratrol. clinicaltrials.gov.
9. Patel, K. R.; Scott, E.; Brown, V. A.; Gescher, A. J.; Steward, W. P.; Brown, K., Clinical trials of resveratrol. *Annals of the New York Academy of Sciences* **2011,** *1215* (1), 161-169.
10. Keylor, M. H.; Matsuura, B. S.; Stephenson, C. R. J., Chemistry and Biology of Resveratrol-Derived Natural Products. *Chemical Reviews* **2015,** *115* (17), 8976-9027.
11. Vogt, T., Phenylpropanoid Biosynthesis. *Molecular Plant* **2010,** *3* (1), 2-20.
12. Schöppner, A.; Kindl, H., Purification and properties of a stilbene synthase from induced cell suspension cultures of peanut. *Journal of Biological Chemistry* **1984,** *259* (11), 6806-6811.
13. Vannozzi, A.; Dry, I. B.; Fasoli, M.; Zenoni, S.; Lucchin, M., Genome-wide analysis of the grapevine stilbene synthase multigenic family: genomic organization and expression profiles upon biotic and abiotic stresses. *BMC Plant Biology* **2012,** *12* (1), 130.
14. Langcake, P.; Pryce, R. J., The production of resveratrol by Vitis vinifera and other members of the Vitaceae as a response to infection or injury. *Physiological Plant Pathology* **1976,** *9* (1), 77-86.
15. Flamini, R.; Mattivi, F.; Rosso, M. D.; Arapitsas, P.; Bavaresco, L. Advanced Knowledge of Three Important Classes of Grape Phenolics: Anthocyanins, Stilbenes and Flavonols *International Journal of Molecular Sciences* [Online], 2013, p. 19651-19669.
16. Regev-Shoshani, G.; Shoseyov, O.; Bilkis, I.; Kerem, Z., Glycosylation of resveratrol protects it from enzymic oxidation. *Biochemical Journal* **2003,** *374* (1), 157-163.

17. Sako, M.; Hosokawa, H.; Ito, T.; Iinuma, M., Regioselective Oxidative Coupling of 4-Hydroxystilbenes: Synthesis of Resveratrol and ε-Viniferin (E)-Dehydrodimers. *The Journal of Organic Chemistry* **2004,** *69* (7), 2598-2600.
18. Solomon, E. I.; Sundaram, U. M.; Machonkin, T. E., Multicopper Oxidases and Oxygenases. *Chemical Reviews* **1996,** *96* (7), 2563-2606.
19. Breuil, A.-C.; Adrian, M.; Pirio, N.; Meunier, P.; Bessis, R.; Jeandet, P., Metabolism of stilbene phytoalexins by Botrytis cinerea: 1. Characterization of a resveratrol dehydrodimer. *Tetrahedron Letters* **1998,** *39* (7), 537-540.
20. Pezet, R., Purification and characterization of a 32-kDa laccase-like stilbene oxidase produced by Botrytis cinerea Pers.:Fr. *FEMS Microbiology Letters* **1998,** *167* (2), 203-208.
21. Cichewicz, R. H.; Kouzi, S. A.; Hamann, M. T., Dimerization of Resveratrol by the Grapevine Pathogen Botrytis cinerea. *Journal of Natural Products* **2000,** *63* (1), 29-33.
22. Isaac, I. S.; Dawson, J. H., Haem iron-containing peroxidases. *Essays in Biochemistry* **1999,** *34*, 51-69.
23. Langcake, P.; Pryce, R. J., Oxidative dimerisation of 4-hydroxystilbenes in vitro: production of a grapevine phytoalexin mimic. *Journal of the Chemical Society, Chemical Communications* **1977,** (7), 208-210.
24. Langcake, P.; Pryce, R. J., A new class of phytoalexins from grapevines. *Experientia* **1977,** *33* (2), 151-152.
25. Takaya, Y.; Terashima, K.; Ito, J.; He, Y.-H.; Tateoka, M.; Yamaguchi, N.; Niwa, M., Biomimic transformation of resveratrol. *Tetrahedron* **2005,** *61* (43), 10285-10290.
26. Li, C.; Lu, J.; Xu, X.; Hu, R.; Pan, Y., pH-switched HRP-catalyzed dimerization of resveratrol: a selective biomimetic synthesis. *Green Chemistry* **2012,** *14* (12), 3281-3284.
27. Lamb, C.; Dixon, R. A., THE OXIDATIVE BURST IN PLANT DISEASE RESISTANCE. *Annual Review of Plant Physiology and Plant Molecular Biology* **1997,** *48* (1), 251-275.
28. Davin, L. B.; Wang, H.-B.; Crowell, A. L.; Bedgar, D. L.; Martin, D. M.; Sarkanen, S.; Lewis, N. G., Stereoselective Bimolecular Phenoxy Radical Coupling by an Auxiliary (Dirigent) Protein Without an Active Center. *Science* **1997,** *275* (5298), 362-367.
29. Kim, K.-W.; Smith, C. A.; Daily, M. D.; Cort, J. R.; Davin, L. B.; Lewis, N. G., Trimeric Structure of (+)-Pinoresinol-forming Dirigent Protein at 1.95 Å Resolution with Three Isolated Active Sites*. *Journal of Biological Chemistry* **2015,** *290* (3), 1308-1318.
30. Gomberg, M., AN INSTANCE OF TRIVALENT CARBON: TRIPHENYLMETHYL. *Journal of the American Chemical Society* **1900,** *22* (11), 757-771.
31. Griller, D.; Ingold, K. U., Persistent carbon-centered radicals. *Accounts of Chemical Research* **1976,** *9* (1), 13-19.
32. van den Bergh, H. E.; Callear, A. B., Experimental determination of the oscillator strength of the B(2B1)—X(2A2) transition of the free allyl radical. *Transactions of the Faraday Society* **1970,** *66* (0), 2681-2684.
33. Claridge, R. F. C.; Fischer, H., Self-termination and electronic spectra of substituted benzyl radicals in solution. *The Journal of Physical Chemistry* **1983,** *87* (11), 1960-1967.

34. Schreiner, K.; Berndt, A., ESR Spectrum of a Perpendicular Benzyl Radical. *Angewandte Chemie International Edition in English* **1974,** *13* (2), 144-145.
35. M .A. R. Raycroft, D. A. P., unpublished.
36. Soper, J. D.; Mayer, J. M., Slow Hydrogen Atom Self-Exchange between Os(IV) Anilide and Os(III) Aniline Complexes: Relationships with Electron and Proton Transfer Self-Exchange. *Journal of the American Chemical Society* **2003,** *125* (40), 12217-12229.
37. Blanksby, S. J.; Ellison, G. B., Bond Dissociation Energies of Organic Molecules. *Accounts of Chemical Research* **2003,** *36* (4), 255-263.
38. Ciriminna, R.; Ghahremani, M.; Karimi, B.; Pagliaro, M., Electrochemical Alcohol Oxidation Mediated by TEMPO-like Nitroxyl Radicals. *ChemistryOpen* **2017,** *6* (1), 5-10.
39. Mahoney, L. R.; Mendenhall, G. D.; Ingold, K. U., Calorimetric and equilibrium studies on some stable nitroxide and iminoxy radicals. Approximate oxygen-hydrogen bond dissociation energies in hydroxylamines and oximes. *Journal of the American Chemical Society* **1973,** *95* (26), 8610-8614.
40. Fischer, H., Unusual selectivities of radical reactions by internal suppression of fast modes. *Journal of the American Chemical Society* **1986,** *108* (14), 3925-3927.
41. Fischer, H., The Persistent Radical Effect: A Principle for Selective Radical Reactions and Living Radical Polymerizations. *Chemical Reviews* **2001,** *101* (12), 3581-3610.
42. Giese, B.; Rupaner, R., A Convenient Synthesis of exo-Brevicomin via a Radical C-C Bond Forming Reaction. *Synthesis* **1988,** *1988* (03), 219-221.
43. Koteswar Rao, Y.; Nagarajan, M., Synthesis of (±) silphinene. *Tetrahedron Letters* **1988,** *29* (1), 107-108.
44. Engel, P. S., Mechanism of the thermal and photochemical decomposition of azoalkanes. *Chemical Reviews* **1980,** *80* (2), 99-150.
45. Jasperse, C. P.; Curran, D. P.; Fevig, T. L., Radical reactions in natural product synthesis. *Chemical Reviews* **1991,** *91* (6), 1237-1286.
46. Giese, B.; Meister, J., Die Addition von Kohlenwasserstoffen an Olefine Eine neue synthetische Methode. *Chemische Berichte* **1977,** *110* (7), 2588-2600.
47. Giese, B.; Heuck, K., Carbon-carbon bond formation between alkylated alkenes and acrylic ester via 2-methoxyalkyl radicals. *Tetrahedron Letters* **1980,** *21* (19), 1829-1832.
48. Nicolaou, K. C.; Ellery, S. P.; Chen, J. S., Samarium Diiodide Mediated Reactions in Total Synthesis. *Angewandte Chemie International Edition* **2009,** *48* (39), 7140-7165.
49. Edmonds, D. J.; Johnston, D.; Procter, D. J., Samarium(II)-Iodide-Mediated Cyclizations in Natural Product Synthesis. *Chemical Reviews* **2004,** *104* (7), 3371-3404.
50. Anastas, P.; Eghbali, N., Green Chemistry: Principles and Practice. *Chemical Society Reviews* **2010,** *39* (1), 301-312.
51. Le Grognec, E.; Chrétien, J.-M.; Zammattio, F.; Quintard, J.-P., Methodologies Limiting or Avoiding Contamination by Organotin Residues in Organic Synthesis. *Chemical Reviews* **2015,** *115* (18), 10207-10260.
52. Botte, G. G., Electrochemical Manufacturing in the Chemical Industry. *Interface magazine* **2014,** *23* (3), 49-55.
53. Frankland, E.; Brodie, B. C., XIX. On a new series of organic bodies containing metals. *Philosophical Transactions of the Royal Society of London* **1852,** *142*, 417-444.

54. Gray, G. A.; Jackson, W. R., Sodium borohydride reduction of oxymercury compounds. *Journal of the American Chemical Society* **1969,** *91* (22), 6205-6207.
55. Kuivila, H. G., Organotin hydrides and organic free radicals. *Accounts of Chemical Research* **1968,** *1* (10), 299-305.
56. Davies, A. G., Recent Advances in the Chemistry of the Organotin Hydrides. *Journal of Chemical Research* **2006,** *2006* (3), 141-148.
57. Zard, S. Z., On the Trail of Xanthates: Some New Chemistry from an Old Functional Group. *Angewandte Chemie International Edition in English* **1997,** *36* (7), 672-685.
58. Barton, D. H. R.; McCombie, S. W., A new method for the deoxygenation of secondary alcohols. *Journal of the Chemical Society, Perkin Transactions 1* **1975,** (16), 1574-1585.
59. Curran, D. P.; McFadden, T. R., Understanding Initiation with Triethylboron and Oxygen: The Differences between Low-Oxygen and High-Oxygen Regimes. *Journal of the American Chemical Society* **2016,** *138* (24), 7741-7752.
60. Crossley, S. W. M.; Obradors, C.; Martinez, R. M.; Shenvi, R. A., Mn-, Fe-, and Co-Catalyzed Radical Hydrofunctionalizations of Olefins. *Chemical Reviews* **2016,** *116* (15), 8912-9000.
61. Kochi, J. K., Mechanisms of Organic Oxidation and Reduction by Metal Complexes. *Science* **1967,** *155* (3761), 415.
62. Fantin, M.; Lorandi, F.; Gennaro, A.; Isse, A. A.; Matyjaszewski, K., Electron Transfer Reactions in Atom Transfer Radical Polymerization. *Synthesis* **2017,** *49* (15), 3311-3322.
63. Keylor, M. H.; Matsuura, B. S.; Griesser, M.; Chauvin, J.-P. R.; Harding, R. A.; Kirillova, M. S.; Zhu, X.; Fischer, O. J.; Pratt, D. A.; Stephenson, C. R. J., Synthesis of resveratrol tetramers via a stereoconvergent radical equilibrium. *Science* **2016,** *354* (6317), 1260.
64. Matsuura, B. S.; Keylor, M. H.; Li, B.; Lin, Y.; Allison, S.; Pratt, D. A.; Stephenson, C. R. J., A Scalable Biomimetic Synthesis of Resveratrol Dimers and Systematic Evaluation of their Antioxidant Activities. *Angewandte Chemie International Edition* **2015,** *54* (12), 3754-3757.
65. Kagan, H. B., Twenty-five years of organic chemistry with diiodosamarium: an overview. *Tetrahedron* **2003,** *59* (52), 10351-10372.
66. Gansäuer, A.; Pierobon, M.; Bluhm, H., Catalytic, Highly Regio- and Chemoselective Generation of Radicals from Epoxides: Titanocene Dichloride as an Electron Transfer Catalyst in Transition Metal Catalyzed Radical Reactions. *Angewandte Chemie International Edition* **1998,** *37* (1-2), 101-103.
67. Wipf, P.; Maciejewski, J. P., Titanocene(III)-Catalyzed Formation of Indolines and Azaindolines. *Organic Letters* **2008,** *10* (19), 4383-4386.
68. Shatskiy, A.; Lundberg, H.; Kärkäs, M. D., Organic Electrosynthesis: Applications in Complex Molecule Synthesis. *ChemElectroChem* **2019,** *6* (16), 4067-4092.
69. Bohn, M. A.; Paul, A.; Hilt, G., Electrochemically Initiated Radical Reactions. *Encyclopedia of Radicals in Chemistry, Biology and Materials* **2012**.
70. Little, R. D., A Perspective on Organic Electrochemistry. *The Journal of Organic Chemistry* **2020,** *85* (21), 13375-13390.

71. Okamoto, K.; Chiba, K., Electrochemical Total Synthesis of Pyrrolophenanthridone Alkaloids: Controlling the Anodically Initiated Electron Transfer Process. *Organic Letters* **2020,** *22* (9), 3613-3617.
72. McAtee, R. C.; McClain, E. J.; Stephenson, C. R. J., Illuminating Photoredox Catalysis. *Trends in Chemistry* **2019,** *1* (1), 111-125.
73. Nicholls, T. P.; Leonori, D.; Bissember, A. C., Applications of visible light photoredox catalysis to the synthesis of natural products and related compounds. *Natural Product Reports* **2016,** *33* (11), 1248-1254.
74. Shaw, M. H.; Twilton, J.; MacMillan, D. W. C., Photoredox Catalysis in Organic Chemistry. *The Journal of Organic Chemistry* **2016,** *81* (16), 6898-6926.
75. Sears, J. E.; Boger, D. L., Total Synthesis of Vinblastine, Related Natural Products, and Key Analogues and Development of Inspired Methodology Suitable for the Systematic Study of Their Structure–Function Properties. *Accounts of Chemical Research* **2015,** *48* (3), 653-662.
76. Vukovic, J.; Goodbody, A. E.; Kutney, J. P.; Misawa, M., Production of 3', 4'-anhydrovinblastine: a unique chemical synthesis. *Tetrahedron* **1988,** *44* (2), 325-331.
77. Beatty, J. W.; Stephenson, C. R. J., Synthesis of (−)-Pseudotabersonine, (−)-Pseudovincadifformine, and (+)-Coronaridine Enabled by Photoredox Catalysis in Flow. *Journal of the American Chemical Society* **2014,** *136* (29), 10270-10273.
78. Lovering, F.; Bikker, J.; Humblet, C., Escape from Flatland: Increasing Saturation as an Approach to Improving Clinical Success. *Journal of Medicinal Chemistry* **2009,** *52* (21), 6752-6756.
79. Li, B.; Pratt, D. A., Methods for determining the efficacy of radical-trapping antioxidants. *Free Radical Biology and Medicine* **2015,** *82*, 187-202.
80. Bolland, J. L.; Gee, G., Kinetic studies in the chemistry of rubber and related materials. III. Thermochemistry and mechanisms of olefin oxidation. *Transactions of the Faraday Society* **1946,** *42* (0), 244-252.
81. Russell, G. A., Deuterium-isotope effects in the autoxidation of aralkyl hydrocarbons. mechanism of the interaction of peroxy radicals1. *Journal of the American Chemical Society* **1957,** *79* (14), 3871-3877.
82. Ingold, K. U., Inhibition of the Autoxidation of Organic Substances in the Liquid Phase. *Chemical Reviews* **1961,** *61* (6), 563-589.
83. Valgimigli, L.; Pratt, D. A., Antioxidants in chemistry and biology. *Encyclopedia of Radicals in Chemistry, Biology and Materials* **2012,** *3*, 1623-1677.
84. Ingold, K. U.; Pratt, D. A., Advances in Radical-Trapping Antioxidant Chemistry in the 21st Century: A Kinetics and Mechanisms Perspective. *Chemical Reviews* **2014,** *114* (18), 9022-9046.
85. Burton, G. W.; Ingold, K. U., Vitamin E: application of the principles of physical organic chemistry to the exploration of its structure and function. *Accounts of Chemical Research* **1986,** *19* (7), 194-201.
86. Niki, E., Antioxidants in relation to lipid peroxidation. *Chemistry and Physics of Lipids* **1987,** *44* (2), 227-253.
87. Foti, M. C. In *Antioxidant properties of phenols*, Journal of Pharmacy and Pharmacology, 2007; pp 1673-1685.

88. Howard, J. A.; Ingold, K. U., THE INHIBITED AUTOXIDATION OF STYRENE: PART III. THE RELATIVE INHIBITING EFFICIENCIES OF ORTHO-ALKYL PHENOLS. *Canadian Journal of Chemistry* **1963,** *41* (11), 2800-2806.
89. Pratt, D. A.; Dilabio, G. A.; Mulder, P.; Ingold, K. U., Bond strengths of toluenes, anilines, and phenols: To hammett or not. *Accounts of Chemical Research* **2004,** *37* (5), 334-340.
90. Burton, G. W.; Doba, T.; Gabe, E.; Hughes, L.; Lee, F. L.; Prasad, L.; Ingold, K. U., Autoxidation of biological molecules. 4. Maximizing the antioxidant activity of phenols. *Journal of the American Chemical Society* **1985,** *107* (24), 7053-7065.
91. Romero, K. J.; Galliher, M. S.; Raycroft, M. A. R.; Chauvin, J.-P. R.; Bosque, I.; Pratt, D. A.; Stephenson, C. R. J., Electrochemical Dimerization of Phenylpropenoids and the Surprising Antioxidant Activity of the Resultant Quinone Methide Dimers. *Angewandte Chemie International Edition* **2018,** *57* (52), 17125-17129.
92. Li, W.; Dong, T.; Chen, P.; Liu, X.; Liu, M.; Han, X., Concise synthesis of several oligostilbenes from the enzyme-promoted oxidation of brominated resveratrol. *Tetrahedron* **2017,** *73* (21), 3056-3065.
93. Li, W.; Li, H.; Li, Y.; Hou, Z., Total Synthesis of (±)-Quadrangularin A. *Angewandte Chemie International Edition* **2006,** *45* (45), 7609-7611.
94. Li, W.; Li, H.; Luo, Y.; Yang, Y.; Wang, N., Biosynthesis of Resveratrol Dimers by Regioselective Oxidative Coupling Reaction. *Synlett* **2010,** *2010* (08), 1247-1250.
95. Chi, H. M.; Cole, C. J. F.; Hu, P.; Taylor, C. A.; Snyder, S. A., Total syntheses of spiroviolene and spirograterpene A: a structural reassignment with biosynthetic implications. *Chemical Science* **2020,** *11* (40), 10939-10944.
96. Jepsen, T. H.; Thomas, S. B.; Lin, Y.; Stathakis, C. I.; de Miguel, I.; Snyder, S. A., Harnessing Quinone Methides: Total Synthesis of (±)-Vaticanol A. *Angewandte Chemie International Edition* **2014,** *53* (26), 6747-6751.
97. Snyder, S. A.; Gollner, A.; Chiriac, M. I., Regioselective reactions for programmable resveratrol oligomer synthesis. *Nature* **2011,** *474* (7352), 461-466.
98. Snyder, S. A.; Thomas, S. B.; Mayer, A. C.; Breazzano, S. P., Total Syntheses of Hopeanol and Hopeahainol A Empowered by a Chiral Brønsted Acid Induced Pinacol Rearrangement. *Angewandte Chemie International Edition* **2012,** *51* (17), 4080-4084.
99. Snyder, S. A.; Wright, N. E.; Pflueger, J. J.; Breazzano, S. P., Total Syntheses of Heimiol A, Hopeahainol D, and Constrained Analogues. *Angewandte Chemie International Edition* **2011,** *50* (37), 8629-8633.
100. Wright, N. E.; Snyder, S. A., 9-Membered Carbocycle Formation: Development of Distinct Friedel–Crafts Cyclizations and Application to a Scalable Total Synthesis of (±)-Caraphenol A. *Angewandte Chemie International Edition* **2014,** *53* (13), 3409-3413.
101. Romero, K. J.; Keylor, M. H.; Griesser, M.; Zhu, X.; Strobel, E. J.; Pratt, D. A.; Stephenson, C. R. J., Synthesis of Vitisins A and D Enabled by a Persistent Radical Equilibrium. *Journal of the American Chemical Society* **2020,** *142* (14), 6499-6504.
102. Quideau, S.; Deffieux, D.; Douat-Casassus, C.; Pouységu, L., Plant Polyphenols: Chemical Properties, Biological Activities, and Synthesis. *Angewandte Chemie International Edition* **2011,** *50* (3), 586-621.

103. For simplicity and consistency, we have chosen to denote the carbon involved in the dihydrobenzofuran formation as C3 throughout this report, though we recognize that for the mono-methoxylated species (3, 26, 28, and 29) this carbon is actually denoted as C5.
104. Snyder, S. A.; Zografos, A. L.; Lin, Y., Total Synthesis of Resveratrol-Based Natural Products: A Chemoselective Solution. *Angewandte Chemie International Edition* **2007,** *46* (43), 8186-8191.
105. Nicolaou, K. C.; Wu, T. R.; Kang, Q.; Chen, D. Y. K., Total Synthesis of Hopeahainol A and Hopeanol. *Angewandte Chemie International Edition* **2009,** *48* (19), 3440-3443.
106. Jeffrey, J. L.; Sarpong, R., Concise Synthesis of Pauciflorol F Using a Larock Annulation. *Organic Letters* **2009,** *11* (23), 5450-5453.
107. Klotter, F.; Studer, A., Cover Picture: Total Synthesis of Resveratrol-Based Natural Products Using a Palladium-Catalyzed Decarboxylative Arylation and an Oxidative Heck Reaction (Angew. Chem. Int. Ed. 9/2014). *Angewandte Chemie International Edition* **2014,** *53* (9), 2253-2253.
108. Soldi, C.; Lamb, K. N.; Squitieri, R. A.; González-López, M.; Di Maso, M. J.; Shaw, J. T., Enantioselective Intramolecular C–H Insertion Reactions of Donor–Donor Metal Carbenoids. *Journal of the American Chemical Society* **2014,** *136* (43), 15142-15145.
109. Ward, R. S., The synthesis of lignans and neolignans. *Chemical Society Reviews* **1982,** *11* (2), 75-125.
110. Sefkow, M., The Stereoselective Synthesis of Neolignans. *Synthesis* **2003,** *2003* (17), 2595-2625.
111. Pan, J.-Y.; Chen, S.-L.; Yang, M.-H.; Wu, J.; Sinkkonen, J.; Zou, K., An update on lignans: natural products and synthesis. *Natural Product Reports* **2009,** *26* (10), 1251-1292.
112. Mihelcic, J.; Moeller, K. D., Anodic Cyclization Reactions: The Total Synthesis of Alliacol A. *Journal of the American Chemical Society* **2003,** *125* (1), 36-37.
113. Sperry, J. B.; Wright, D. L., The application of cathodic reductions and anodic oxidations in the synthesis of complex molecules. *Chemical Society Reviews* **2006,** *35* (7), 605-621.
114. Frontana-Uribe, B. A.; Little, R. D.; Ibanez, J. G.; Palma, A.; Vasquez-Medrano, R., Organic electrosynthesis: a promising green methodology in organic chemistry. *Green Chemistry* **2010,** *12* (12), 2099-2119.
115. Tabakovic, I.; Gunic, E.; Juranic, I., Anodic Fragmentation of Catharanthine and Coupling with Vindoline. Formation of Anhydrovinblastine. *The Journal of Organic Chemistry* **1997,** *62* (4), 947-953.
116. Tobinaga, S., A review: synthesis of alkaloids by oxidative phenol and nonphenol coupling reactions. *Bioorganic Chemistry* **1975,** *4* (1), 110-125.
117. Grimshaw, J., CHAPTER 6 - OXIDATION OF AROMATIC RINGS. In *Electrochemical Reactions and Mechanisms in Organic Chemistry*, Grimshaw, J., Ed. Elsevier Science B.V.: Amsterdam, 2000; pp 187-238.

118. Yan, M.; Kawamata, Y.; Baran, P. S., Synthetic Organic Electrochemical Methods Since 2000: On the Verge of a Renaissance. *Chemical Reviews* **2017,** *117* (21), 13230-13319.
119. Miller, A. K.; Hughes, C. C.; Kennedy-Smith, J. J.; Gradl, S. N.; Trauner, D., Total Synthesis of (−)-Heptemerone B and (−)-Guanacastepene E. *Journal of the American Chemical Society* **2006,** *128* (51), 17057-17062.
120. Rosen, B. R.; Werner, E. W.; O'Brien, A. G.; Baran, P. S., Total Synthesis of Dixiamycin B by Electrochemical Oxidation. *Journal of the American Chemical Society* **2014,** *136* (15), 5571-5574.
121. Hong, F.-J.; Low, Y.-Y.; Chong, K.-W.; Thomas, N. F.; Kam, T.-S., Biomimetic Oxidative Dimerization of Anodically Generated Stilbene Radical Cations: Effect of Aromatic Substitution on Product Distribution and Reaction Pathways. *The Journal of Organic Chemistry* **2014,** *79* (10), 4528-4543.
122. Chong, K.-W.; Thomas, N. F.; Low, Y.-Y.; Kam, T.-S., Reactivity of Anodically Generated 4-Methoxystilbene Cation Radicals: The Influence of Ortho-Substituted Hydroxymethyl, Aminomethyl, and Carboxylic Acid Groups. *The Journal of Organic Chemistry* **2018,** *83* (24), 15087-15100.
123. Mori, N.; Furuta, A.; Watanabe, H., Electochemical asymmetric dimerization of cinnamic acid derivatives and application to the enantioselective syntheses of furofuran lignans. *Tetrahedron* **2016,** *72* (51), 8393-8399.
124. Yamamura, S.; Shizuri, Y.; Shigemori, H.; Okuno, Y.; Ohkubo, M., Natural products syntheses using anodic oxidation of phenols as a key step. *Tetrahedron* **1991,** *47* (4), 635-644.
125. LI Wen-Ling, H. K.-K., LI Ying,HOU Zi-Jie*, Total Synthesis of (±)-Shegansu B, Gnetuhainin F, (±)-Maackin A and (±)-Cassigarol E. *Acta Chimica Sinica* **2005,** *63* (17), 1607-1612.
126. Meyers, C. Y.; Malte, A. M.; Matthews, W. S., Ionic reactions of carbon tetrachloride. Survey of reactions with ketones, alcohols, and sulfones. *Journal of the American Chemical Society* **1969,** *91* (26), 7510-7512.
127. Becker, H. D., New stable phenoxy radicals. Oxidation of hydroxystilbenes. *The Journal of Organic Chemistry* **1969,** *34* (5), 1211-1215.
128. Studer, A.; Curran, D. P., The electron is a catalyst. *Nature Chemistry* **2014,** *6* (9), 765-773.
129. Narayanan, S.; Murthy, K. V. V. S. B. S. R., Montmorillonite as a versatile solid acid catalyst for tert.-butylation of resorcinol. *Applied Catalysis A: General* **2001,** *213* (2), 273-278.
130. Apak, R.; Güçlü K Fau - Ozyürek, M.; Ozyürek M Fau - Karademir, S. E.; Karademir, S. E., Novel total antioxidant capacity index for dietary polyphenols and vitamins C and E, using their cupric ion reducing capability in the presence of neocuproine: CUPRAC method. (0021-8561 (Print)).
131. Bibi Sadeer, N.; Montesano, D.; Albrizio, S.; Zengin, G.; Mahomoodally, M. F., The Versatility of Antioxidant Assays in Food Science and Safety—Chemistry, Applications, Strengths, and Limitations. *Antioxidants* **2020,** *9* (8), 709.

132. Blois, M. S., Antioxidant Determinations by the Use of a Stable Free Radical. *Nature* **1958,** *181* (4617), 1199-1200.
133. Chauvin, J.-P. R.; Griesser, M.; Pratt, D. A., The antioxidant activity of polysulfides: it's radical! *Chemical Science* **2019,** *10* (19), 4999-5010.
134. Haidasz, E. A.; Van Kessel, A. T. M.; Pratt, D. A., A Continuous Visible Light Spectrophotometric Approach To Accurately Determine the Reactivity of Radical-Trapping Antioxidants. *The Journal of Organic Chemistry* **2016,** *81* (3), 737-744.
135. Re, R.; Pellegrini, N.; Proteggente, A.; Pannala, A.; Yang, M.; Rice-Evans, C., Antioxidant activity applying an improved ABTS radical cation decolorization assay. *Free Radical Biology and Medicine* **1999,** *26* (9), 1231-1237.
136. Shah, R.; Farmer, L. A.; Zilka, O.; Van Kessel, A. T. M.; Pratt, D. A., Beyond DPPH: Use of Fluorescence-Enabled Inhibited Autoxidation to Predict Oxidative Cell Death Rescue. *Cell Chemical Biology* **2019,** *26* (11), 1594-1607.e7.
137. Stockwell, B. R., Dawn of a New Era of Targeted Antioxidant Therapies. *Cell Chemical Biology* **2019,** *26* (11), 1483-1485.
138. Miller, N. J.; Rice-Evans, C. A.; Davies, M. J.; Gopinathan, V.; Milner, A. D., A novel method for measuring antioxidant capacity and its application to monitoring the antioxidant status in premature neonates. *Clinical science* **1993,** *84 4*, 407-12.
139. Benzie, I. F. F.; Strain, J. J., The ferric reducing ability of plasma (FRAP) as a measure of "antioxidant power": the FRAP assay. *Analytical biochemistry* **1996,** *239 1*, 70-6.
140. Goldschmidt, S.; Renn, K., Zweiwertiger Stickstoff: Über das α, α-Diphenyl-β-trinitrophenyl-hydrazyl. (IV. Mitteilung über Amin-Oxydation). *Berichte der deutschen chemischen Gesellschaft (A and B Series)* **1922,** *55* (3), 628-643.
141. The analyses of RTA activity for the QMDs were carried out using the mixture of diastereomers arising from the dimerization protocol.
142. N. V. Zolotova, F. A. G., M. B. Tokareva, E. T. Denisov, A. A. Volod'kin,, *Kinetika i Kataliz (Engl. Transl.)* **1979,** *20*, 48.
143. Volod'kin, A. A.; Ershov, V. V., Stable Methylenequinones. *Russian Chemical Reviews* **1988,** *57* (4), 336-349.
144. Zavitsas, A. A., Comment on "Identity Hydrogen Abstraction Reactions, X• + H−X' → X−H + X'• (X = X' = CH3, SiH3, GeH3, SnH3, PbH3): A Valence Bond Modeling". *The Journal of Physical Chemistry A* **2002,** *106* (19), 5041-5042.
145. Montgomery, J. A.; Frisch, M. J.; Ochterski, J. W.; Petersson, G. A., A complete basis set model chemistry. VI. Use of density functional geometries and frequencies. *The Journal of Chemical Physics* **1999,** *110* (6), 2822-2827.
146. Raycroft, M. A. R.; Chauvin, J.-P. R.; Galliher, M. S.; Romero, K. J.; Stephenson, C. R. J.; Pratt, D. A., Quinone methide dimers lacking labile hydrogen atoms are surprisingly excellent radical-trapping antioxidants. *Chemical Science* **2020,** *11* (22), 5676-5689.
147. Griesser, M.; Pistis, V.; Suzuki, T.; Tejera, N.; Pratt, D. A.; Schneider, C., Autoxidative and Cyclooxygenase-2 Catalyzed Transformation of the Dietary Chemopreventive Agent Curcumin*. *Journal of Biological Chemistry* **2011,** *286* (2), 1114-1124.

148. Liu, J.; Lee, Y. W., Vitamin C supplementation restores the impaired vitamin E status of guinea pigs fed oxidized frying oil. *The Journal of nutrition* **1998,** *128 1*, 116-22.
149. Timoshnikov, V. A.; Kobzeva, T. V.; Polyakov, N. A.-O.; Kontoghiorghes, G. A.-O., Redox Interactions of Vitamin C and Iron: Inhibition of the Pro-Oxidant Activity by Deferiprone. LID - 10.3390/ijms21113967 [doi] LID - 3967. (1422-0067 (Electronic)).
150. Huchzermeyer, B. A.-O.; Menghani, E. A.-O.; Khardia, P.; Shilu, A., Metabolic Pathway of Natural Antioxidants, Antioxidant Enzymes and ROS Providence. LID - 10.3390/antiox11040761 [doi] LID - 761. (2076-3921 (Print)).
151. Taguchi, K.; Yamamoto, M., The KEAP1–NRF2 System in Cancer. *Frontiers in Oncology* **2017,** *7*.
152. Silpe, J. E.; Balskus, E. P., Deciphering Human Microbiota-Host Chemical Interactions. (2374-7943 (Print)).
153. Riaz Rajoka, M. A.-O.; Thirumdas, R.; Mehwish, H. M.; Umair, M. A.-O. X.; Khurshid, M. A.-O.; Hayat, H. F.; Phimolsiripol, Y. A.-O.; Pallarés, N. A.-O.; Martí-Quijal, F. A.-O.; Barba, F. A.-O., Role of Food Antioxidants in Modulating Gut Microbial Communities: Novel Understandings in Intestinal Oxidative Stress Damage and Their Impact on Host Health. LID - 10.3390/antiox10101563 [doi] LID - 1563. (2076-3921 (Print)).